Studies in Sedimentary Provenance of the Intramontane Granada Basin, Southern Spain

John James Hughes B.Sc.(Edinburgh)

A thesis presented for the degree of Ph.D.

University of Glasgow
Department of Geology and Applied Geology

October 1995

ProQuest LLC.
789 East Eisenhower Parkway
P.O. Box 1346
Ann Arbor, MI 48106 – 1346

Abstract

The Granada Basin is an intramontane basin situated within the Betic Orogen of southern Spain, at the westernmost extension of the Alpine Orogenic Belt. The Basin was initiated in the early-mid Miocene and is still active today. The Granada Basin rests upon rocks of the metamorphic Internal Zones of the Betic Orogen, which have evolved in core-complex style, extending and uplifting since the late Miocene, a process which has profoundly affected the evolution of the Eastern margin of the Granada Basin. The sediments of the basin record some of this history, both in conglomerate clast composition and in syn and post-sedimentary deformation of the basin. Sediment was derived from the rocks of the Internal Zone rocks in the Sierra Nevada region. The basin flank has been uplifted progressively during the rise of the Internal Zones core-complex. This has resulted in the westward migration of the depocentre of the basin and the recycling of the eastern basin margin. The Granada Basin is therefore an ideal place to study the evolution of sediment composition, in relation to recycling during a single orogenic phase, and the evolution of maturity and the progressive loss of provenance signature during recycling.

Three conglomeratic fan formations are found on the eastern flank of the basin, which record a transition from marine to terrestrial deposition. In order of decreasing age these are the Dudar, Pinos Genil and Alhambra Formations. Despite a constant provenance, the maturity of the sediments increases with decreasing age. Conglomerate clasts become increasingly rounded and clast composition becomes more mature into the younger Pinos Genil and Alhambra Formations. Quartzose clasts become more common and labile schistose clasts increasingly confined to the smaller grain sizes. Sandstone composition, however, does not become more mature, but marginally less mature. Quartz content does not increase, and lithic component grains do not diminish, despite the increased effects of terrestrial weathering in the younger formations. This disparity between the different grain sizes may be explained by the continuing break-down of conglomerate clasts within the sediment, providing a primary source of sand-size detritus. Provenance indications from sandstone detrital modes are generally confirmed using established discrimination schemes, but in detail, the nature of the Granada Basin sands derived from a high grade metamorphic core-complex source may require the recognition of a distinct provenance type.

Major and trace element geochemistry indicates a general increase in compositional maturity with sandstones, as the quantity of SiO_2 and other more immobile elements increase at the expense of mobile elements. These changes are generally consistent with weathering differences between the marine Dudar and terrestrial Alhambra Formations, but also with the possibility of sedimentary recycling. This increase in compositional maturity occurs in the sandstones despite the detrital mode maintaining its immaturity. SiO_2 increase is not obviously related to increased quartz content. The geochemical provenance indication given by the sediments is a passive margin regime, incorrect in the present tectonic setting but, perhaps

related to the depositional setting of the protoliths to the metasedimentary rocks in the Sierra Nevada source region.

Heavy minerals record an increase in stable species into the younger formations, consistent with increased maturity. Zircon, apatite, tourmaline and, surprisingly, epidote increase in abundance at the expense of garnet and amphiboles. However, for garnet and tourmaline intra-species chemistry reveals no compositional bias that can be related to sedimentary recycling or erosional and depositional weathering differences between formations. Epidote alone shows an increase in Fe poor examples in the Pinos Genil and Alhambra Formations compared with the Dudar Formation.

Isotopic dating of conglomerate clasts and basement rocks from the Sierra Nevada reveals a cooling history for the Internal Zones that reaches back to the late Cretaceous. Most ages fall between 30 and 10 Ma, with the peak of cooling between 18-13Ma. Cooling rates range up to 100°C/Ma. The Alpujarride Complex, structurally above the Nevado Filabride Complex records an earlier (25Ma , ^{40}Ar-^{39}Ar) and slower cooling rate (35.7°C/Ma.). There is a complex relationship between cooling in the Internal Zones and sedimentation in the Granada Basin. During the most rapid cooling, sedimentation in the Granada basin had either not begun or was shallow marine carbonate deposition, indicating that there was no relief in the Internal zones at the time. The coarse sedimentation in the Dudar Formation records the uplift and evolution of the Sierra Nevada core-complex, with rapid generation of relief and the exposure of the Nevado Filabride Complex to form the dominant sediment source for the eastern Granada Basin. However, the uplift recorded by the coarse sediments of the Dudar Formation is not directly related to the isotopic cooling ages recorded by this detritus. The cooling ages preserved in the detritus pre-date uplift and sedimentation by up to 10Ma. There is, in this case, a significant lag between source cooling, which was not directly associated with the production of sediment, and the uplift and erosion of the rocks in the Internal Zones of the Sierra Nevada.

On a wider scale, the prolonged history of Betic Evolution and the dominantly left-lateral movement at the boundary between the Iberian and African plates since the Jurassic, suggests that the Orogen may be best explained by invoking an important role for strike-slip tectonics. This may even account for the emplacement of the Internal Zones into the region, and the subsequent deformation of the External Zones.

Acknowledgements

I would like to thank the N.E.R.C. for providing financial support for this project under grant GT4/90/GS/50. The Dept. of Geology and Applied Geology here in the University of Glasgow have been very tolerant in providing facilities, initially during my stay under the leadership of Prof. B. E. Leake and more recently under Dr. C.D. Gribble. Out in East Kilbride the S.U.R.R.C. have also been extremely helpful. In Spain Drs. Fernandez and Visares provided invaluable guidance in the field.

Prof. Brian Bluck was my supervisor, without whom I would never have come to Glasgow, and could not have finished this project. I would like to thank Brian for being patient with me and for always bringing enthusiasm into the subject, but above all for his intelligence in always seeing the productive problems. Dr. Tim Dempster has been a great help, in practical ways, but in also providing an alternative voice and for being so generous with his time. Dr. Jeff Harris must be thanked profusely for allowing many of my samples to be included for analysis by Dr. Dave Phillips (of Anglo-American) who also was extremely patient in explaining aspects of analysis and providing information.

At the S.U.R.R.C., Dr. Graeme Rogers was extremely helpful, encouraging, and always willing to listen. Dr Tony Fallick helped greatly in paving the way for analyses to be done, and brought some much needed clarity when things went a bit wrong! Dr. Ray Burgess was tremendous in introducing me to the laser probe. I thank him for the time he spent packing and then analysing my samples, and for the quality of the work done. Dr. Paul McConville also spent a great deal of time with my samples, and strove to produce the best under difficult circumstances. Anne Kelly and Vincent Gallagher helped make trips to East Kilbride more than bearable, as well as being invaluable in providing support and instruction in the right thing to do with Rb-Sr analyses. Jim Imlach must be thanked too for the K-Ar analyses and for all the right information. Andrew Tait also spent many hours analysing my samples. Thanks also to Vinnie, Dr. Adrian Boyce, Susan and Vojta for the lifts out there.

In the department I must thank Roddy Morrison for supplies of anything and everything, and for being interested in what I was doing. Murdo Macleod provided constant support and advice, and interesting tales about Knightswood! Dugald Turner was always there to provide ideas and not least some wit, especially where mineral separations were concerned. Bill Higginson too, brought relief to the less than exciting moments in the geochemistry lab. Jim Gallacher helped greatly in providing the right information and advice, not least about Irish citizenship!. Jim Kavanagh helped in desperate moments when the printers wouldn't work or when I needed copies very quickly. Robert Macdonald was always willing to help. His expertise in operating the probe was irreplaceable, but I thank him especially for introducing me to the guitar music sites on the internet, and for the advice on maintaining my bike! Pete Ainsworth made the SEM painless, even though I dont think I ever knew exactly what to do next. The thin section people, Alan, Andrew and Suzanne did great work, and have a thankfully wide taste in loud music. Lastly, Douglas Maclean never ceased to amaze me by the speed with which he does things at, and the photos look so good too. All these people deserve the greatest thanks.

Thanks to all my postgraduate friends too. Thanks to Chris for all the computer advice and bringing a great deal of comic light to the place. To Dave for being calm, eloquent and never too busy to pass the time of day. To Gary for comradely support and for good moans! To Carolyn for things on weathering and on how to deal with Brian! To Tim for his incisive wit, and hilarious stories. To Jeremy for the beer, the conversation, and that wonderful cation exel thingy. And Vojta for assistance, lifts and for being Czech!. To Andy especially for the rediculous conversations in that wee room of ours, taking me up a snow-storm-bound mountain for the first time in my life and getting me back safely, and the memory of the Spanish brandy! And to Robbie for being a good and constant friend, and for all the great music and books he's lent me too. Also to Mark, Orla, Thomas and Ken, the high earning postdoc people, who have been very generous with their time and (oh dear) in buying drinks! Special thanks to Ken for all the invaluable statistical advice and especially for his time when he was clearly far too busy. The discriminant analyses are all his work. These people made the whole experience utterly worthwhile, and provided continuous support and encouragement, by sharing the experience. I hope I did the same for them.

At the S.R.C. thanks must go to Margaret Meechan and her staff for giving me work and also connections to the outside world.

Thanks to Angus and Dave, my long suffering flatmates, present and ex., who provided friendship constantly and made a warm home. And also to Dave again, in the past year for providing a very comfortable place to live, though I'll never forget our flitting to Anniesland!

And to the Barton family, who have never compromised on their complete generosity to me over the past four years, and have welcomed me in and made their home my home too.

I must thank, (though it is a completely inadequate gesture), my parents, Ann and Pat for support that it is impossible to describe, let alone match. I thank them for their prayers. They have given selflessly for my entire life, I could not be here writing this today without them. I thank God for them especially, but also for everyone mentioned here

And Finally.....

She wanted a page to herself. So here it is.

Thank you Margaret.

For supporting me through all of this, for constant companionship, for encouraging me, for being a great friend.

John,

9th October 1995

Contents

List of Figures, Tables and Plates

Figures

Chapter 7

Tables

Chapter 1

Chapter 4

Plates

Chapter 4

Chapter 6

1. Introduction and Geological Setting

1.1 Rationale

This work is concerned primarily with the evolution of the composition of sedimentary basin infill in continental syn/post orogenic settings. The Granada Basin of S.E. Spain, is an internal basin within the Betic Cordillera, the westernmost extension of the Tertiary age Alpine orogenic belt. The basin was initiated in the Neogene and is still active today. Though forming in a post tectonic time it is still taken here to represent the earliest stages of sedimentation and sedimentary flux away from an orogenic zone.

The original idea for this project was to apply the $^{40}Ar/^{39}Ar$ dating method, using laser ablation to the age characterisation of detritus within the Granada basin. This would allow source evolution to be tied to sedimentation, and the age patterns within first cycle orogenic deposits to be fingerprinted. This has since been expanded to include other dating methods and much detailed sedimentary petrography. This work has shed some light upon the tectonics of the Betic orogen, and as will be seen ideas of orogenesis in this region are also changing through insights provided by plate movement and crustal seismic studies.

1.2 Objectives

The objectives of this study are:

1. To document the compositional characteristics of sediment in the deposits of the Eastern Granada Basin, from conglomerates to sandstones. Furthermore to describe properties of the heavy mineral population and the bulk and grain size dependant geochemistry of sediment in the Granada Basin.

2. To document isotopic age data of detritus in the deposits of the Eastern Granada Basin, on single grain and conglomerate clast scale along with data on the isotopic ages of in-situ source regions.

To achieve these objectives conventional petrographic means were applied, in the field and laboratory, to the measurement of clast and grain compositions. Conglomerates were subdivided on clast type, and sandstones were point counted to obtain modal analyses. Bulk sandstone major and trace element geochemistry was measured by X-Ray Fluorescence, and heavy mineral chemistry was investigated using electron microprobe analysis.

$^{40}Ar/^{39}Ar$ was applied to bulk detrital muscovite concentrates from the sandstones of the Granada Basin, along with conglomerate clast muscovites and basement rocks from the Sierra Nevada source region. K-Ar and Rb-Sr dating methods were also applied to muscovites separated from conglomerate clasts and basement source rocks.

Then to use this data to:

3. Draw conclusions about the local history of the evolution of the Granada Basin in the context of its regional geology.

4. Draw conclusions about *sediment dynamics* and sources within the Granada Basin, especially concerning sediment recycling, and the effects of this on provenance information carried by sediment.

5. Draw conclusions about *source dynamics* from the isotopic data. Especially how source signatures are recorded in sedimentary basins in proximal orogenic settings.

6. Draw conclusions about sediment recycling and dispersal from orogenic zones.

In the next section the characteristics of sedimentary basins are be reviewed with special emphasis upon basins formed in collisional megasutures, and their role in tectonic syntheses. After this issues of sedimentary provenance will be discussed. This detailed discussion is necessary in order to put the provenance and dating work into the correct context. Plate Tectonics is a unifying concept and allows the full interdependency of different elements to be understood. Basin classification is related to plate tectonic setting, through the mechanisms of crustal behaviour, which is determined by crustal type, which in turn determines provenance type and sediment composition.

1.3 Sedimentary basins

The definition of sedimentary basins is best given by Bally and Snelson (1980) as "Realms of subsidence with thicknesses of sediments commonly exceeding 1km that are today still preserved in a more or less coherent form." Basins exist spatially, but also temporally as they contain distinctive stratigraphies that record in the changing ages of sediment, the history of depositional style and environment and of basin formation and evolution. To paraphrase Friend (1985) "The sedimentary fill defines the basin". The composition of sediment within the basin (the major concern of this thesis) contains a signature of sediment source evolution, which can be linked to basin forming tectonics once combined with flow direction data. This information can be vital in palaeogeographic studies and tectonic syntheses, as sometimes sediments are all that is left of tectonic elements such as island arcs and orogenic belts (e.g.. Houghton 1988, Kelly and Bluck 1989). This is the basis and the importance of sedimentary provenance studies. It is the purpose of the following sections to review the factors controlling the genesis of sedimentary basins and the way basins are classified, in order to lay a foundation for a discussion of basins formed within convergent, and more specifically basins in collisional settings.

1.3.1 Controls on basin formation

Basin analysis has flourished since the advent of plate tectonic theory, and has benefited from the interdisciplinary approach that a wider view has encouraged. There are two main frameworks in which basins can be classified. The first is largely mechanistic, presenting the physical controls of basin formation, derived from an understanding of the physical properties of the crust. This relies heavily upon insights derived from geophysical techniques.

The second framework for subdivision is purely plate tectonic, placing basins within their different settings. Any basin model or classification that does not explain how a basin forms cannot be useful as it will be of little genetic and consequent predictive importance (Allen and Allen 1990). Any competent basin model has to integrate information drawn from several sub-disciplines.

Dickinson (1974) discussed the conditions required for sedimentation to take place. Vertical crustal motions are clearly necessary to generate subsiding basins and relative uplifting source areas. However, plate tectonics emphasises horizontal movements. At convergent and divergent plate margins vertical crustal movements are produced due to changes in; (Dickinson op.cit.) 1) crustal thickness, 2) the thermal state of the crust and 3) the isostatic balance of the crust. (related to 1 and 2).

Each of these factors is different for different types of crust. Additionally to the normal division of oceanic from continental crust, Dickinson defines 5 types of transitional and anomalous crust variously generated in divergent and convergent settings. In divergent settings continental crust is thinned as plates separate and a new ocean begins to form. Attenuated continental crust is one transitional crustal type. Another is the interfingering of sediments and volcanics in the earliest stages of ocean spreading, generating a crustal profile thicker than true ocean crust and thinner than its neighbouring attenuated and normal continental crust. Transitional crustal types of this sort are found at passive or Atlantic type margins. In convergent systems, in arc-trench settings the formation of a volcanic system above the subducting plate, plus attendant plutonism and compressional deformation produces crust of "abnormal" composition and thickness. Two types are recognised; crust produced when material is added magmatically or volcanically and crust produced in subduction complexes by the tectonic stacking of ocean crust and offscraping of pelagic sediments off the downgoing plate.

To summarise this, divergent settings produce thinner, hotter continental and normal oceanic crust, areas of subsidence that can act as sediment sinks. Convergent settings produce thicker crust of either oceanic or continental affinities which due to isostatic forces can uplift providing sediment source areas, but also weaker zones that can respond to gravitational or tensile instabilities.

According to Allen and Allen (1990) there are three dominant controls on basin subsidence; 1) thermal, 2) crustal thinning and 3) crustal loading. These can be further generalised into two dominant mechanisms of basin origin. (Miall 1990, Allen and Allen 1990);

1. Lithospheric stretching

2. Lithospheric loading and flexure.

However, a third special tectonic environment often allows these disparate controls to operate together. Transform plate boundaries exhibit complex structural evolution that is not purely extensional or compressional. Either behaviour is possible along a transform boundary

depending on the local geometry of the fault. A dominant tectonic transpression or transtension will operate normally, often due to oblique plate convergence or divergence. This is important as transform boundaries are often the settings for sedimentary basin development. The Granada Basin is probably a basin formed in this context.

Lithospheric stretching

Lithospheric stretching has been successfully modelled in the past two decades (for example McKenzie 1978, Keen 1985, Kuznir and Parks 1987). The strength of the lithosphere is critical, it determines rheology which is in turn controlled by the geothermal gradient and the composition of the lithosphere. Stretching initiates rifting by causing brittle extension in the upper crust accompanied by ductile deformation in the lower crust, as evidenced by the absence of brittle structures on the lower crustal seismic profiles (for example Allmendinger et.al. 1987). The lithosphere is weakened as the geothermal gradient is raised when hot asthenosphere moves in to fill the space created by thinning. *Active rifting* occurs when a heat source in the mantle, for example a hot spot, impinges on the base of the crust causing uplift, crustal thinning and heating before rifting. *Passive rifting* occurs when intraplate stresses generated by larger plate tectonic forces are such that a relatively weak area of crust is pulled apart, letting in hot athenospheric material to ever higher portions of the crust, and causing heating *because* of rifting.

Quartz and feldspar are weaker than olivine, imparting a strength deficiency upon crust compared to the subcrustal lithosphere (Kuznir and Parks 1987, Dewey 1988). This compositional control is important in determining the position of lithospheric stretching and thinning, as it will clearly have a preference for olivine poor continental crust, and potentially for overthickened and strain weakened orogenic zones.

In the McKenzie (1978) model, cooling results in the lithosphere returning to normal thickness and density causing subsidence, which is observed in actual cases to be below the original pre-stretch surface level. This subsidence is proportional to the square root of time since rifting began and is a major control upon sedimentation upon the rifted margin. Thicknesses of up to 10km of sediment can accumulate on rifted continental margins, a significant load that contributes to subsidence through lithospheric flexure.

Lithospheric Loading

Supracrustal loading is caused by fold and thrust belts, and also by seamounts and rifted margin clastic wedges, as just discussed. Loading causes the lithosphere to flex and downwarp adjacent to the load, creating a depression that can act as a sink for sediment. The elastic thickness and flexural rigidity of the crust determine the response to the applied load. Miall (1990) and Allen et.al. (1986) discuss the continuing debate on the alternative elastic or viscoelastic models for the crust. The viscoelastic model appears to predict stratigraphic patterns in the Alberta foreland basin better than an elastic model (Beaumont 1981). Allen et. al. also give reasons for preferring the viscoelastic over the elastic model though Jordan (1981) proposed an elastic rheology that fitted observations of the Cretaceous western United States foreland basin. Again the response of the lithosphere to loading is controlled by its thermal

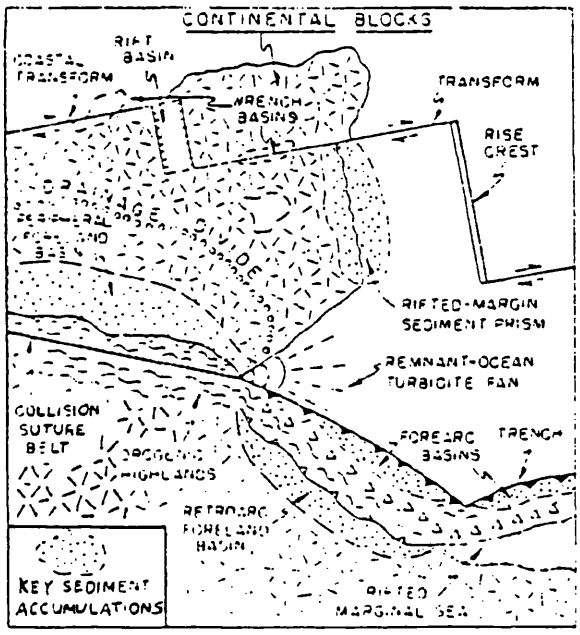

Fig. 1.1 The main plate tectonic settings of sedimentation. From Ingersoll (1988),

state, thickness and composition. The previous history of lithosphere is of paramount importance in determining these. Often overthrust loads at convergent margins rest upon attenuated passive margin crust, that may or may not have thermally stabilised and their associated sedimentary wedges, forming peripheral foreland basins. Retroarc foreland (Dickinson 1974) depressions form on the continental side of active continental subduction margins, as a result of landward thrusting and also of the increased crustal thickness due to compression and magmatic addition of material in the arc itself. Retroarc basins form upon continental crust of normal thickness.

1.3.2. Plate tectonic settings of basin formation

The principles of plate tectonics are familiar to most earth scientists, and several good reviews and introductions to the subject are available (e.g. Brown and Mussett 1981, Cox and Hart 1986, Windley 1988). It is not necessary to reiterate these here. However, plate tectonic setting does influence the type of basin forming mechanism and types of crust involved. **Fig 1.1** is taken from Ingersoll (1988) and summarises the major plate tectonic sites of sedimentation. It is possible to establish a general basin classification of basins formed in either divergent, convergent or transform settings. Lithospheric stretching and thermal subsidence are the major controls on basin development of passive margin, continental rift and oceanic basins. Basins generated in divergent settings are dominantly controlled by lithospheric thinning and thermal subsidence. Convergent settings produce shortening and thickening of crust favouring the formation of basins due to supracrustal loading. Extension is not uncommon in convergent settings, especially in a backarc environment, as thermal effects or subduction rollback can cause tension and lithospheric stretching.

Transform Settings

Transform settings are an often complex hybrid of compression and extension. Which predominates is a function of local fault geometries superimposed upon large scale plate interaction. Crustal types are not so clearly prescribed as they are for simple divergent and convergent environments, though they are most often formed within continental crust. Basins are often relatively small and may suffer wrenching and deformation themselves. Pull-aparts formed at "releasing" bends (Crowell 1974) on faults are common, but basins formed by crustal loading due to overthrusting at "restraining" bends in faults can occur. These basins are a result of the brittle behaviour of the upper crust and form as a result of shallow phenomena linked to a deeper crustal mechanism. Compared with the general classes of basin in macroscopic convergent and divergent settings the overall rheology and thermal state of the crust may not be as critical in their formation as the strength and type of supracrustal materials that they form upon.

It can be appreciated from the previous discussion that a purely mechanistic or plate tectonic classification may not be fully satisfactory. A combination of both allows a full explanation of any basin in both genetic and descriptive terms.

1.3.3 Sedimentary basin fill

The stratigraphy and the depositional sequence architecture are controlled by tectonics and eustatic sea level changes. Differences occur due to different combinations of tectonic and erosional rates, that are controlled ultimately by the properties of the crust and regional stress fields induced by plate interaction (Allen and Allen 1990). As the sedimentary fill is the key response to basin formation and local tectonism it acts as a powerful record of events. The age of sediment gives the time of basin forming events and the accumulation rate of sediment gives the subsidence pattern for the basin (Friend 1985). Sediment composition records the temporal evolution and subaerial exposure of source regions.

Depositional style is determined again by sea level, and rate of tectonism which affects sediment supply and the calibre of sediment produced and transported. Drainage patterns are important in controlling depositional patterns (Miall 1984, Leeder and Gawthorpe 1987), and are controlled by base level, either local or eustatic but also local tectonic movements that may generate physical barriers to sediment dispersal patterns (for example advancing thrust faults in the Pyrenees, Hirst and Nichols, 1986)

1.3.4 Classification schemes

Classification schemes for sedimentary basins differ largely upon the emphasis between basin forming mechanism and tectonic setting, combined with the degree of detail in distinguishing the tectonic setting. The following is a summary of the some of the more important basin classification schemes available.

Dickinson (1974)

Dickinson (1974) was the earliest to discuss sedimentation in relation to plate tectonics and to attempt a classification of sedimentary basins consistent with its tenets. He proposed to classify basins using 3 characteristics;

1. The type of substratum the basin rests upon.

2. The proximity of the basin to a plate margin.

3. The type of plate margin nearest to the basin. That is to say the type of plate interaction that controls basin development.

This basis for classification incorporates the important variables in plate tectonics; the type of crust involved (oceanic or continental) and the type of plate interaction occurring at plate margins (divergent or convergent). It is at plate margins that most important activity takes place, though intraplate settings are not inherently inactive, any activity can usually be linked to plate margin processes. So proximity to a plate margin determines the strength of the effects of divergent or convergent motions on basin development.

Table 1.1 is a summary of Dickinsons classification. He distinguishes basins formed due to rifting of continental crust, those associated with subduction at arc-trench systems and peripheral or foreland basins, formed as a result of continental collision. Here basins are

Table 1.1 Basin classification of Dickinson (1974).

Rifted continental Margins
- Prerift arch
- Rift Valley
- Proto-Oceanic gulf
- Narrow Ocean
- Open Ocean
- Aulacogens

Arc-Trench Systems
- Trenches
- Forearc
- Intra-arc
- Inter-arc or Retro-arc

Peripheral Basins (Foreland Basins)

Intracontinental

Table 1.2 Basin classification of Bally and Snelson (1980).

1. Basins located on the rigid Lithosphere, not associated with formation of Megasutures

11. Related to formation of oceanic crust
    - 111. Rifts
    - 112. Oceanic transform associated basins
    - 113. Oceanic absyssal plains
    - 114. Atlantic type passive margins (shelf, slope & rise) which straddle continental and oceanic crust
        - 1141. Overlying earlier rift systems
        - 1142. Overlying earlier transform systems
        - 1143. Overlying earlier backarc basins of (321) and (322) type

12. Located on pre-Mesozoic continental lithosphere
    - 121. Cratonic basins
        - 1211. Located on earlier rifted grabens
        - 1212. Located on former backarc basins of (321) type

2. Perisutural basins on rigid lithosphere associated with the formation of compressional megasuture

21. Deep sea trench or moat on oceanic crust adjacent to B-subduction margin
22. Foredeep and underlying platform sediments, or moat on continental crust adjacent to A-subduction margin
    - 221. Ramp with buried grabens, but little or no block faulting
    - 222. Dominated by block faulting
23. Chinese type basins associated with distal blockfaulting related to compressional or megasuture and without associated A-subduction margin (sic.)

3. Episutural basins located and mostly contained in compressional megasuture

31. Associated with B-subduction zone
    - 311. Forearc basins
    - 312. Circum pacific backarc basins
        - 3121. Backarc basins floored by oceanic crust and associated with B-subduction (marginal sea sensu stricto)
        - 3122. Backarc basins floored by continental or intermediate crust, associated with B-subduction
32. Backarc basins, associated with continental colloision and on concave side of A-subduction arc
    - 321. On continental crust or Pannonian type basins
    - 322. On transitional and oceanic crust or W.Mediterranean-type basins
33. Basins related to Episutural megashear systems
    - 331. Great basin-type basins
    - 332. California-type basins

clearly classified by placing them in plate tectonic settings. His classification is influenced by the mechanics of basin formation as discussed above, and the conditions required for sedimentation.

Bally and Snelson (1980)

Dickinsons three criteria for classifying basins have generally been adopted as the basis for most later classification schemes. Bally and Snelson (1980) offer a very thorough basin classification developed from Dickinsons earlier suggestions (**Table 1.2**). Central to their interpretation is the idea of the Megasuture, defined as the total products of convergent tectonics, including all metamorphic, igneous and sedimentary rocks (**Fig 1.2**). Subduction is an important part of the classification. They differentiate B-subduction (subduction of oceanic crust) from A-subduction (subduction of continental crust). Basins are subdivided on their position relative to megasutures and to rigid crust. Crust within megasutures has been remobilised by deformation, intrusion and thrust faulting, making it "pervasively plastically deformed" (Bally and Snelson, op. cit.). Rigid crust then does not exist within megasutures. Despite this the effects of megasuture processes on basin development can still be seen on adjacent rigid crust. They acknowledge this in creating the Perisutural basin classes, for foreland and Chinese type basins. Some doubt has been shed upon the validity or uniqueness of some basin classes, especially the latter and the Pannonian type back-arc basins. Klein (1987) (commented upon by Miall (1990)) considered that they could be included in more general basin classes. They successfully differentiate all other basins in a plate tectonic scheme, by including sufficient detail of different tectonic settings (for example backarc floored by oceanic crust from those floored by continental crust).

Kingston et.al. (1983)

The petroleum industry has long attempted basin classification for its specific requirements, mainly for predictive purposes. Typical of these schemes is that by Kingston et.al. (1983), presented in **Table 1.3**. They proposed a classification based upon;

1. Basin forming tectonics.
2. Depositional sequences.
3. Basin modifying tectonics.

Emphasis is put on the sedimentary sequences contained in basins. Plate setting can change during basin evolution so affecting basin forming and modifying tectonics. Basins can typically go through many cycles of tectonism and sedimentation. Kingston et.al. devised a way of concisely describing a complete sequence of basin forming and modifying events. Again as a major criteria they used the type of crust involved, and the nature of the nearest plate boundary movement to affect basin development so basins are placed clearly within general plate tectonic environments. However, foreland, or peripheral basins, either in arc or collision settings are omitted, except perhaps as Trench Associated (TA) basins. Overall this classification is successful in describing basin fill and modifiers in a simple way. It was

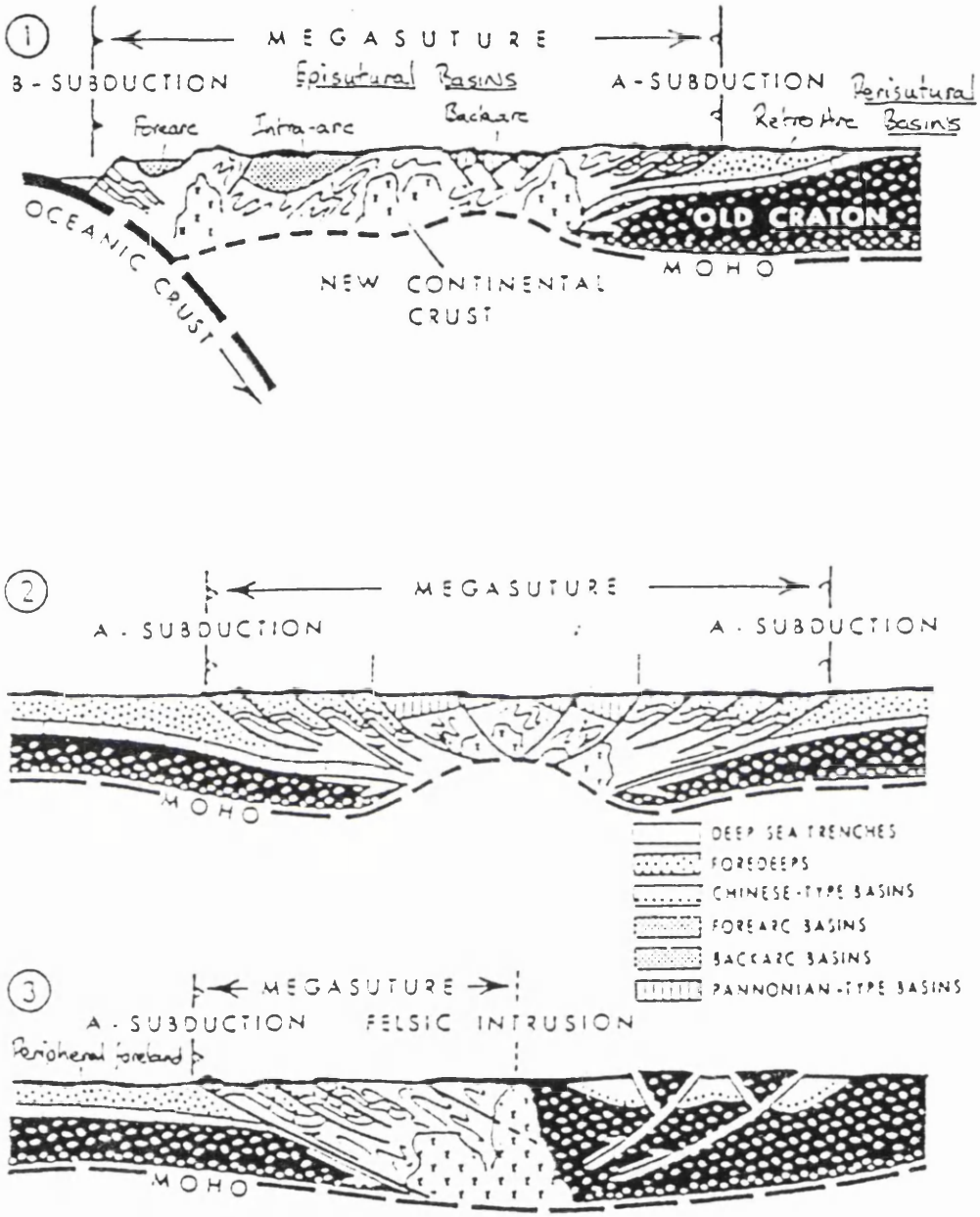

Fig. 1.2 Definition of megasuture types, and the locations of sedimentary basins. Modified from Baily and Snelson (1980).

Table 1.3 Basin classification of Kingston et.al. (1983).

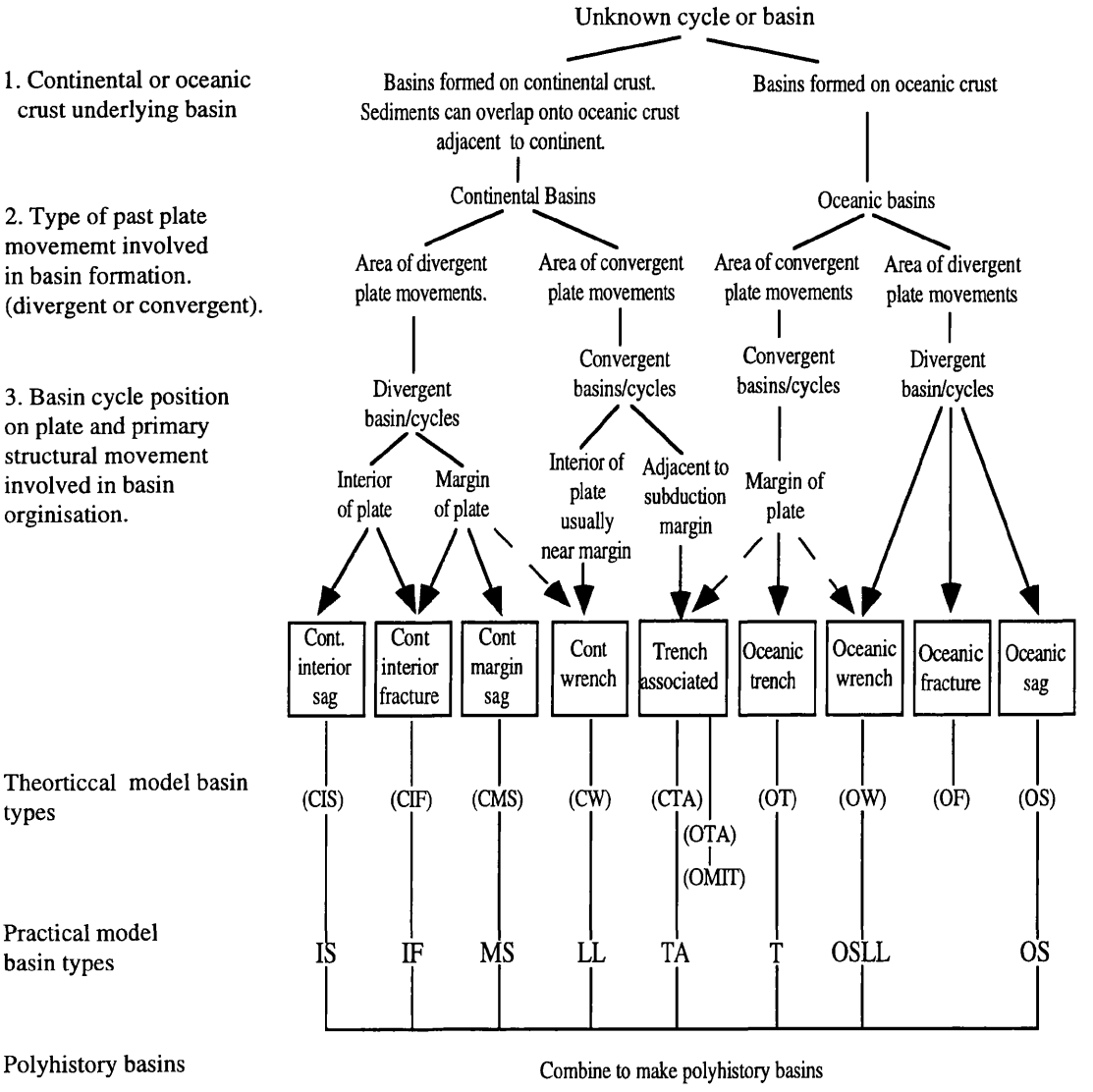

Continental margin	Basin type	Basin position on or within plate.	Crustal type	Geodynamic model of formation.
Plate interior	interior cratonic basin	interior	C	rifting, stretching and thermal subsidence
	cratonic margin basin	edge	C	rifting, stretching and thermal subsidence
Passive margin	rift basin	interior and edge	C,T	rifting and stretching
	aulacogen	edge to interior	T,C	rifting and stretching
	flexure basin	edge	C	loading ,flexure: elastic and viscoelastic
Active margin	trench basin	edge	O	convergence; compression
	trench slope basin	edge	O, or older sediment	compression-extension, folding
	fore-arc basin	off edge	O, or older sediment	compression
	intra-arc basin	arc	C-magmatic	extension-rifting
	back-arc (interarc) basin	interior	O	rifting, stretching
	retro-arc basin	interior	C	compression
Transform margin	pull apart basin	transform edge	C/T or O	rifting, translation, thermal subsidence
	transform basin	transform edge	C/T or O	rifting, translation, thermal subsidence
Collision margin	foreland basin	interior	Annealed C&O or C&C	compressional folding, flexure
	superposed (or collage) basin	suture	C/T or O	compression
Margin independant	Polyhistory basin	interior or edge	C/T or O	multiple
	successor basin	interior or edge	C/T or O	multiple
	resurgent basin	interior or edge	C/T or O	multiple

Table 1.4 Basin classification of Klein (1987).

Table 1.5 Basin classification of Ingersoll (1988).

Divergent Settings

Terrestrial rift valleys, rifts within continental crust, comonly associated with bimodal volcanism

Proto-oceanic rift troughs: incipient oceanic basins floored by new oceanic crust and flanked by young continental margins.

Continental rises and terraces: mature rifted continental margins in intraplate settings at continental-oceanic interfaces.

Continental embankments: progradational sediment piles constructed off edges of rifted continental margins.

Faied rifts and aulacogens: inactive terrestrial rift valleys, which may be reactivated during convergeny tectonics and become aulacogensat high angles to orogenic belts.

Intracrsatonic basins: broad cratonic basins floored by failed rifts in axial zones.

Oceanic basins: basins floored by oceanic crust formed at divergent plate boundaries unrelated to arc-trench systems.

Oceanic islands, aseismic ridges, and plateus: sedimentary aprons and platforms formed in intraoceanic settings other than magmatic arcs

Convergent settings

Trenches: deep troughs formed by subduction of oceanic lithosphere.

Trench-slope basins: local structural depressionsdeveloped upon subduction complexes.

Forearc basins: basins developed between subduction complexes and magmatic arcs.

Intra-arc basins: local basins within magmatic arcs.

Interarc and backarc basins: oceanic basins between and behind intraoceanic magmatic arcs, and continental basins behind continental-margin magmatic aarcs without foreland fold thrust belts.

Retroarc foreland basins: foreland basins on continental sides of continental-margin arc-trench systems.

Remnant ocean basins: shrinking ocean basins caught between colliding continental margins and/or arc-trench systems and ultimately subducted or deformed within suture belts.

Peripheral foreland basins: foreland basins above rifted continental margins that have been pulled into subduction zones during crustal collision.

Piggyback basins: basins formed and moved atop moving thrust sheets.

Foreland intermontane basins: basins formed among basement cored uplifts in foreland settings.

Transform settings

Transtensional basins: basins formed by extension along strike-slip fault systems.

Transpressional basins: basins formed by compression along strike-slip fault systems.

Transrotantional basins: basins formed by rotation of crustal blocks about vertical axeswithin strike-slip fault systems.

Hybrid settings

Intracontinental wrench basins: diverse basins formed within and on continental crust due to distant collisional processes.

Successor basin: basins formed in intermontane settings following cessation of local orogenic activity.

intended as a means of characterisation to allow comparisons, for petroleum exploration and emphasises differences between basins, and systematically highlights details of evolution.

Klein (1988)

After reviewing previous classifications Klein presented his own (**Table 1.4**). Basins are explained in terms of the type of plate margin interaction affecting basin tectonics, basin position within its plate and the type of crust the basin is formed upon. Additionally to this he included the mechanism of basin formation as a major part of the scheme. This is an important difference from the schemes of Dickinson and Bally and Snelson, who considered basin forming mechanisms as being important but did not include them as explicit parts of their classifications.

Ingersoll (1988)

Ingersoll (1988) reviewed basin types in light of the tectonics of their formation, and produced a classification (**Table 1.5**). These are actualistic basin types, presented by reference to real basins, placed within the broad scope of Dickinsons (1974) three criteria for classification. His major subdivisions are based simply upon plate tectonic settings and owe much to Dickinsons scheme, but represent a more detailed, and combined with Miall (1990) the beginnings of a comprehensive basin model approach.

Miall (1990)

In this important textbook Miall discusses a thorough scheme of basin models subdivided into general tectonic settings as divergent margin, convergent margin, transform and transcurrent, basins formed during continental collision and suturing and cratonic basins. Each model includes the plate setting, basin forming mechanisms, structure of the basin and the evolution of the depositional systems within the basin. Basins are typed on largely tectonic and structural grounds but each model integrates details of evolution and the associated sedimentary response.

In conclusion, each classification scheme has it merits, but none is perfect. Sedimentary basins are each rather unique entities that contain a distinctive stratigraphy, deposited in a distinct tectonic setting formed because of a distinct set of local causes and mechanisms (though linked to large scale plate processes). Each basin should perhaps be considered and characterised on its own. The usefulness of classification is that it sets up models that highlight characteristics but invite constant re-evaluation.

It is also clear, especially when considering Dickinsons (1974) scheme, that crustal type varies with plate setting and therefore basin classification. The sediments contained within a basin will therefore have a composition consistent with the plate tectonic environment, and by inference the basin classification. Thus provenance and basin classification are tied through plate tectonics.

The following section will focus on basins formed within convergent and especially collisional settings, as such basins are most relevant to the Granada Basin.

1.4 Basins in convergent and collisional settings

1.4.1 Origin of extension in convergent settings

Basins may form in continental collision zones by both lithospheric loading and stretching mechanisms. They can be fitted generally into the episutural and perisutural classes of Bally and Snelson (1980, see **Table 1.2.**). Foreland basins are the case for loading, forming peripherally (perisutural) to developing orogenic zones and may be the most significant sites of sediment accumulation associated with collisional megasutures. Basins caused by stretching are common, forming within a megasuture (episutural), for example in the Mediterranean region and in the Basin and Range province. Their explanation though is more complex and debate still continues. This overview will concentrate upon this latter class of basin due to stretching as it is the relevant type for evaluating the Granada Basin. There are two general causes of crustal stretching in convergent settings that produce episutural basins, back-arc extension and extensional collapse, each will be discussed in turn. However, oblique convergence can produce transform movements, with transpressional components of movement, that can exhibit local compression or extension, that can also allow basins to form.

Back-arc extension

There are two ways that back-arc extension is thought to take place (Royden et.al. 1982) though there is some debate as to the relative importance of each. Back arc extension is common in oceanic subduction settings like the Western Pacific, where marginal basins floored by oceanic crust exist inboard of island arcs. Actively induced extension is the result of increased heat flow to the base of the crust above a subduction zone, beyond the arc, due perhaps to convection induced by the subducting plate. The second cause may be subduction rollback, where the leading edge of the overriding plate advances over the trench causing tension and perhaps rifting behind. The age and the angle of decent of the subducting plate are important factors in determining which mechanism predominates. In the W Pacific subducting ocean crust is old, thick and dense and so descends steeply into the mantle. This pulls the trench position oceanwards, causing extension behind the arc or even within the arc (Karig 1971). It is conceivable that both rollback and induced convection operate together to create back-arc extension.

Back arc extension has also been suggested to be operating within continental collision zones. The Aegean and Tyrrhenian seas have been explained this way (McKenzie 1978, Le Pichon 1983) as has the Pannonian basin of eastern central Europe (Bally and Snelson 1980). These basins formed late in the process of continental collision but also contemporaneously with thrusting at their margins, suggesting that an alternative model of formation may be appropriate. The Basin and Range extension is in a typically back arc position with reference to the consuming margin of the western US. However extension postdates the onset of transform tectonics and the end of subduction in the region, and the early Tertiary core complex evolution corresponds to a phase of reduced rate convergence of the Pacific and American plates (Coney 1987) also supporting an alternative mode of extension.

Extensional collapse

Continental collision zones are areas of anomalously thick crust. This causes an increase in the vertical compressional stress due to gravity. If horizontal compression across the orogen eases or stops completely then the vertical stress may dominate and cause thinning and extension. This is commonly termed extensional collapse (Dewey 1988). The consequences of this can be dramatic thinning and contemporaneous thrusting in external zones, directed away from the centre of the previously thickened crustal welt (Platt and Vissers 1989). But equally less catastrophic extension occurs in thrust belts that rise above 3km (Dewey 1988), as seen in the Himalayas and the Andes (Cabrera et.al. 1987).

Another important contributing factor may be the removal of the thickened portion of the subcrustal lithosphere. It may become unstable and drop off into the less dense asthenosphere below, or it may be removed by convective forces. The remnant subducting slab beneath a collision edifice may play a similar role, acting partly like a detaching mass from the base of the orogen. Or as it drops away it can let hot material enter beneath the orogen thus creating conditions better suited to the removal of a lithospheric root. On losing a root zone, the isostatic balance of the lithosphere is changed as the lower density material fills the space left, analogous in some ways to the way asthenosphere is drawn in under thinning lithosphere. The result is uplift and an increase in the vertical compressive stress and gravitational instability. The lower crust is heated by the hot asthenosphere that is emplaced against it, which further tends to weaken the crust. Spreading ensues by outward directed thrusting.

Extensional collapse has also been invoked as the cause of extension in the Mediterranean region (Dewey 1988) in contrast to the models of McKenzie (1978), Channell (1986) and Le Pichon (1983) who favoured back-arc processes. It has also been causally linked to lithospheric delamination (Nelson 1992). Extension in the western U.S. Cordillera and the Tibetan Plateau has been explained by extensional collapse following uplift caused by lithospheric delamination. Thinner than expected crust, high heat flow and low gravity anomalies are all consistent with the presence of hot asthenosphere at the base of the crust (Coney 1987). The Basin and Range extension is commonly linked to the cessation of compression at the western margin of the American plate in the Oligocene when the east pacific triple junction was subducted, establishing a continental transform setting in California. A widening window with no subduction has been forming ever since, and the absence of a compressional regime may have allowed stress relaxation and extension.

1.4.2 Extensional style and basin formation

Half graben basins

Crustal thinning and extension produces a characteristic upper crustal response as a result of the brittle behaviour of this cold portion of the crust. Commonly half graben basins form as steep normal faults cut the crust. Basins form atop the hanging wall and adjacent to the footwall scarp. High angle faulting of this sort is characteristic of the Basin and Range blockfaulting. This form of extension clearly has a powerful control over the dispersal paths for sediment and consequently upon the facies architecture in the basin. Coarse fan deposits

are common adjacent to the footwall fault scarp while broad fan deposits may form upslope upon the hanging wall (Leeder and Gawthorpe 1986). In the centre of the basin finer grained fluvial or lacustrine deposits can form, and through drainage rivers will tend to the axis of maximum subsidence. As extension proceeds the hangingwall will deform and drop away as blocks rotate along often listric faults, generating growth sequences, that thicken towards the footwall, and the deposits will assume a dip direction also towards the footwall. These basins are characteristic of the early stages of continental rifting, and can be found under thick thermal subsidence controlled Atlantic type margin sequences. They appear to be typical for the Aegean sea and the Basin and Range.

Core complex extension

The formation of basins around core complexes is depicted in theoretical models to be in the half graben style (for example Gautier, 1993), though things are complicated by problems of uplift and the rotation of hanging wall blocks. Extension manifested as core complexes was first recognised in the Western U.S. Cordillera (Davis and Coney 1979, Coney 1980 and refs therein), but also subsequently in the Aegean (Lister et.al. 1984, Gautier and Brun 1993) and in Indonesia (Hill 1992). High grade metamorphics are brought to the surface in domal uplifts, juxtaposed next to lower grade metamorphics or unmetamorphosed upper plate rocks along low angle normal detachments. Core complexes often form the highest ground in their vacinity. Massive shearing and evidence for ductile deformation is present in core zones, where thick mylonites are characteristically present.

The origin of the low angle detachments has been debated. Some workers regard them to be rotated high angle normal faults (Buck, 1988, Wernicke and Axen, 1988), while others argue that these faults originate and operate at a low angle throughout their history.(e.g.. Scott and Lister, 1992). However, to exhume large portions of crust, as is evident in core complexes, high angle normal faults offer the best means of raising subcrustal rocks to the surface as rapidly as suggested by isotopic data on cooling rates (Buck, 1988). Low angle faults, to achieve the same, require extremely large horizontal displacements. All of this has important consequences for the development of sedimentary basins and sediment sources. Domino style faulting and the development of half grabens is contingent on the development of high angle normal faults and will favour the formation of small basins either side of an evolving core complex. Uplift can be large, allowing the formation of ample sediment source regions. Low angle faulting will stifle the adequate formation of basins, and causes potential space problems in accommodating large displacements. Despite this the absence of significant sedimentation adjacent to core complexes perhaps demonstrates the importance of low angle movements in crustal exhumation.

Recently Brun et.al. (1994) discussed an analogue model for the development of detachment faults and core complexes. The geometry of the extension produced two potential sites for the formation of sedimentary basins; one associated with accommodation faults unconnected to the major detachment fault, and the other in the hanging wall of the main detachment fault. This not only predicts the development of depocentres but also of the

massive rotation of crustal blocks and the probable deformation and uplift of deposits as the detachment evolves and the core uplifts.

Transform basins

Extension and basin formation in California has also been linked to transform tectonics through a large scale crustal megashear (Atwater. 1970). The role of strike slip movements (*senu stricto*) in convergent and collisional settings has perhaps not been fully recognised, though clearly has a considerable influence on the assembly of such areas, as evidenced by the terrane accretion of the U.S. Cordillera and the Caledonides. Continental convergence is rarely orthogonal and oblique motions induce lateral stresses parallel to plate margins that cause strike-slip inboard of a subduction zone. Pieces of crust can be transported 1000's km along strike slip zones creating a mosaic of unrelated palaeogeographic domains. Strike slip can also be seen at some distance from collisional areas due to the accommodation of compressional motions by 'extrusion tectonics' (Molnar and Tapponier 1980) and also proximally within orogenic zones, again as a result of accommodation of compression (Cronin, 1989).

Strike slip movements in continental crust result in zones of complex deformation, compression, extension and basin formation largely depend on the local geometry of the fault zone (Crowell, 1974, Sylvester, 1988). Simple shear causes movement to be concentrated along a principle displacement zone that is complicated by synthetic shear zones. Related folding, thrust and normal faulting takes place to accommodate displacements, that complicate the structural pattern around the fault further. The shape of the fault trace determines the predominance of compression or extension on a local scale and therefore also the location of sedimentary basins. Transpression or transtension may predominate and generate thrust or pull apart basins. Subsidence can be extremely rapid and large thicknesses of sediment can accumulate (12km Ridge basin, Crowell, 1974) controlled by internal drainage. Transcurrent movements can also laterally stretch basins, generating large stratigraphic thicknesses with little vertical thickness as the depocentre moves past the source area causing overlap of sequences. The Old Red Sandstone of the Midland Valley of Scotland (Bluck 1978) and the similar age Hornelen basin of Norway (Steel and Gloppen 1980) have been explained in this way.

The tectonic scenario of the Betic Cordillera indicates that transform tectonics have been very important in the development of sedimentary basins. Strike-slip may even be related to the core-complex style of evolution seen in the Internal Zones in the Sierra Nevada (see below for more details). The sedimentation in the Eastern Granada Basin (the object of this thesis) may be controlled by faulting and uplift in the source region related to a dominant right-lateral shear zone that runs through the Betic Cordillera.

Synsedimentary extension and basin deformation

Many more basins are now recognised as having formed contemporaneously with extensional deformation within the basin sediments. Serranne and Seguret (1987) described an extensional detachment and deformation at the base of the Devonian basins of W Norway. Pebbles in conglomerates are deformed and imbrication angles are decreased near the detachment, along with C-S shear fabrics. Malavielle et. al. (1990) discuss the development of

asymmetrical half graben basins within the French Massif Central. Again low angle detachments have deformed sediments at the contact between basement and the sediments. Pebbles are stretched and fractured, syn-sedimentary normal faults are common and 'extensional decollemonts' are found in phyllites and coals. Extensionally related recumbent folds are seen in south dipping sediments, that collapsed down slope towards the footwall, under gravity. Not only do basins subside but they often continue to extend, involving the sedimentary fill in extension even when relatively unconsolodated, as is seen in the Granada Basin (Munro, 1995). As noted above the rotation of initially high angle faults and the uplift and evolution of core complexes can deform depositing sediments. The modelling study of Brun *et. al.* (1994) highlights the possibility of hanging wall rotation during core-complex extension and core uplift. Syn-depositional extension is also observed in the basinal areas developed on either side of the core-complex uplift.

The first part of this introduction has discussed the controls of basin formation and the classifications of basins that arise from the operation of these controls. This leads to specific types of crust being involved in basin formation, and therefore specific types of crust are associated with basin classifications. Sediments generated in different tectonic settings will have distinct compositions determined by the types of crust involved. In this way provenance, basin type and tectonic setting are all related. The next section discusses provenance, concentrating on tectonic discrimination and the use of sediment composition in tectonic reconstruction. This is important as the bulk of this thesis is concerned with how provenance signature in the sediments of the eastern Granada Basin changes depending on depositional conditions and/or sediment reworking. Of equal importance is how the sediments studied in this work reflect their source as understood, and classified by established provenance discrimination schemes.

1.5 Sedimentary provenance

This section discusses issues in provenance discrimination utilising the compositional properties of sedimentary detritus. An important part of this thesis discusses the evolution of sediment composition within the proximal, intra-montane setting of the Granada Basin, and attempts to discuss generalities that may be more widely applicable to orogenically derived sediment. A brief summary of the principles of provenance work and its role in constructing tectonic histories is required.

1.5.1 Scope of Provenance studies

Sedimentary rocks compositionally reflect their source regions. This is the basic premise of sedimentary provenance studies. However, various processes scramble the signature, but they do represent a record of something that no longer exists intact. Sediments act like a temporal probe into the past nature of source terrains. Therefore provenance studies have an important role in tectono-magmatic and palaeogeographic reconstructions. Provenance is also important in the construction of basin models. Plate tectonics determine plate boundary interactions and therefore the types of crust to be found in different settings. Plate Tectonics

also determine the types of crustal movements that generate sedimentary basins, and form the basis for basin classification. In this way sediment composition is related to plate tectonic setting and to basin type.

The scope of provenance studies is wide. Haughton et.al. (1991) review new techniques being applied in provenance work and discuss the areas of application of such work. Not only can provenance information be used for source reconstruction and to make inferences about tectonics, but also for investigating sediment dispersal systems and even crustal evolution. A widening range of techniques is being applied in provenance studies. The fundamental measurements are made upon the total attributes of the sediment, in bulk and down to the single grain. It is in this latter field that recent advances have been made, with the advent of single grain dating using laser probe, and electron microprobe chemical analysis that allows the study of intra-sample mineral chemical variation. Additionally palaeoflow information is absolutely essential, in order to fix source positions and to investigate depositional systems.

In summary, provenance involves techniques of sedimentary petrography, geochemistry, isotopic dating, palaeoflow measurements and micro-chemical analysis. It also touches on aspects of sedimentary diagenesis to constrain post depositional alteration and loss of compositional provenance information.

1.5.2 Tectonic discrimination using sandstone composition

Dickinson (1970) defined grain categories for the analysis of detrital framework modes, which have been generally adopted by later workers. Using these categories he constructed ternary diagrams to enable sandstone compositions to be plotted and compared. Dickinson and Suczek (1979) demonstrated how provenance types are defined by plate tectonics. The spatial arrangement of crustal types is determined by plate tectonics and interactions at plate margins. Provenance areas will produce sediments that compositionally directly reflect the types of crust they contain, so it should be possible to link sediment to provenance types, to tectonic setting and to integrate this with basin classification.

The principle of the approach is uniformitarian. Dickinson and Suczek (1979) took published analyses of sediments from constrained tectonic settings, recast the data in common grain categories and took averages for entire sandstone suites, rejecting analyses with standard deviations from the mean greater than 10%. They then plotted the data onto four ternary diagrams to establish if sands from different tectonic settings would plot separately, providing a method of discriminating between tectonic regimes, and providing a basis for comparison of sands of unknown tectonic setting. Three major tectonic provenance groupings were utilised 1) Continental block, 2) Magmatic arc and 3) Recycled orogen. The diagrams appear to successfully discriminate these three provenance types and 9 sub provenance divisions (see **Fig.1.3**).

That tectonically related sandstones that have been sampled and analysed by disparate workers using different methods and criteria should group together on these diagrams is a fair vindication of the approach taken by Dickinson and Suczek. They specify the criteria invoked to include published analyses but it is not clear how they dealt with grain size variation control of composition, or the variance of counting methods and grain recognition employed.

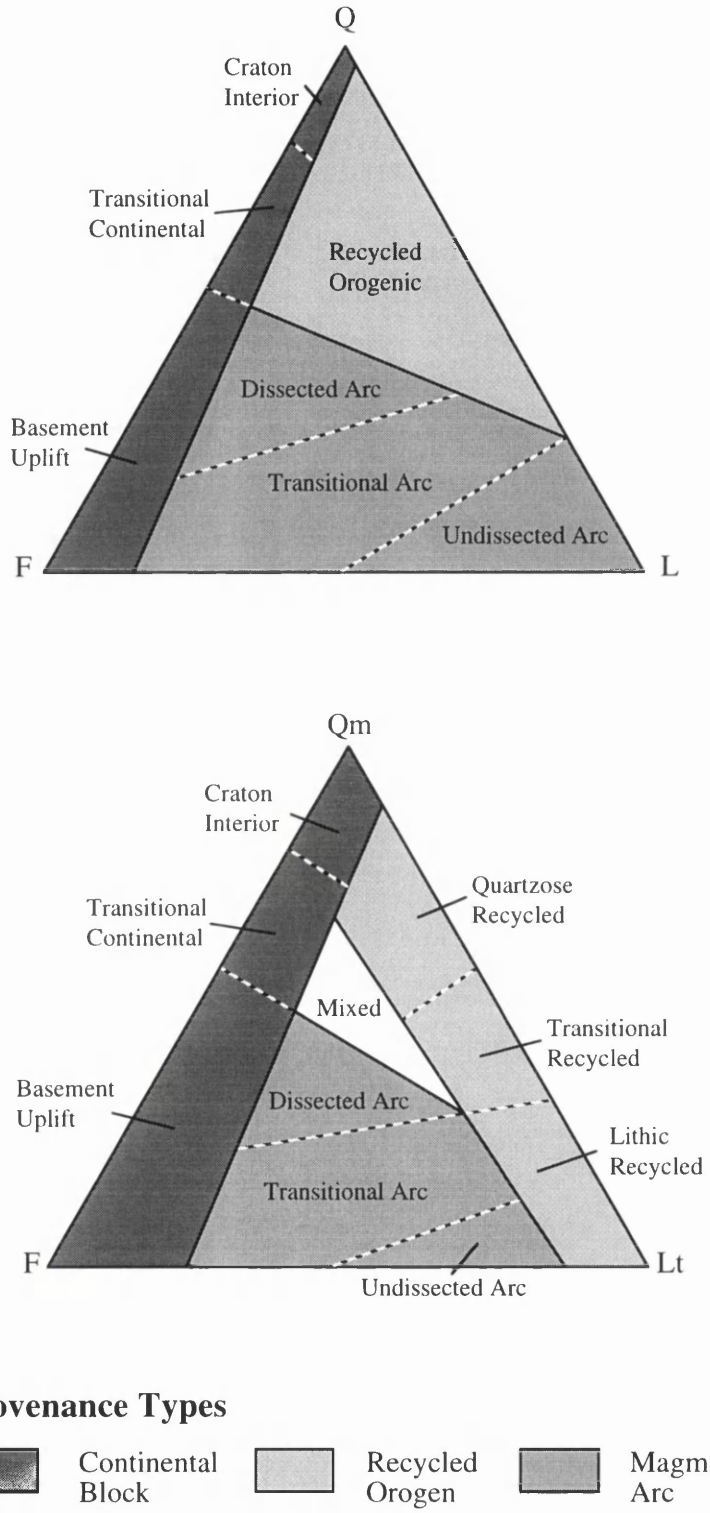

Fig. 1.3 QFL and QmFLt ternary provenance discrimination plots as derived by Dickinson et.al. (1983).

However, Dickinson et.al. (1983) develop the theme and refine the two most discriminating ternary plots (QFL and QmFLt, **Fig 1.3**). They caution against the use of these diagrams to place individual samples into tectonic settings, as the domains on the plots have been defined by the means of large numbers of analyses.

These discrimination methods are often applied to sandstones often deposited a great distance from source, that may have been through several phases of reworking and that may also be a mixture of sediment from several sources. However, the conclusions reached about provenance may, on a large scale, be correct. The degree of accuracy is difficult to asses, but the information provided by provenance studies *is* positive evidence for something, that is unfortunately poorly constrained. Further work on the dynamics of provenance signatures in sandstones is required to clarify the confidence that tectonic workers can put on provenance indications from sandstones. The next section discusses deficiencies in our understanding of the application of provenance information in tectonic reconstructions.

1.5.3 Applicability of provenance discrimination by sandstone frameworks

Anomalies to the normal perceived relationship between tectonic setting, provenance type and sandstone composition as suggested by Dickinson and Suczek (1979) and Dickinson et.al. (1983), have been encountered. Mack (1984) reviewed possible causes of sandstones giving erroneous tectonic settings. Sandstones could be deposited in the transition between shifting tectonic regimes allowing them to become structurally misplaced. Weathering and reworking can affect compositions, pushing framework modes towards the quartz pole and continental block provenance type. There is also the strong possibility of provenance types that have not been fully recognised. Lastly Mack (1984) suggested the possibility of the poor classification and the unresolved role of carbonate clasts.

In this discussion it is important to distinguish between sandstones that are truly anomalous in a particular tectonic setting, that may have been transported across tectonic boundaries, from those that are in context with their setting, but are not accommodated by present provenance models or classifications. The discrimination diagrams of Dickinson and Suczek (1979) are not necessarily all encompassing and require constant revising, and need to be checked for accuracy against as many real examples as possible. This also applies to geochemical and other provenance discrimination schemes. New provenance types need to be sought out wherever possible.

Girty et.al. (1988) encountered problems with the application of the Dickinson et.al. (1983) discrimination models to Holocene sands of known tectonic setting, from southern California and northern Mexico. The area is a dissected Mesozoic magmatic arc, of four drainage areas composed of plutonic rocks, metasediments and metavolcanics. Sand from each drainage area correctly reflects the composition of the rocks in its provenance. However when plotted on a QFL diagram each sample set does not plot within the magmatic arc provenance area, but around it. If the sediment were mixed together, say in a marine shelf or trench, the framework mode would fall within the magmatic arc zone. The sediment is from local source areas which are each attributed correctly, but erroneously for the megascopic tectonic regime. In essence this is a scale problem.

The inheritance of crustal types complicates the provenance picture especially in convergent regimes. The cyclic nature of plate tectonics ensures that tectonic regimes and associated crustal types and sites of deposition change with time. Atlantic type margin sequences derived from continental block provenance areas can become involved in convergent tectonics, suffering folding and uplift and metamorphism, becoming a new sediment source. Old continental blocks can become involved too, being uplifted and eroded also. It is possible to have separate domains within a particular tectonic setting with disparate crustal compositions, that can be recognised as distinctive provenance types formed during previous tectonic regimes.

Velbel (1985) described mature quartzose sandstones from accretionary prisms in Indonesia and Barbados. For the given tectonic regime and the discrimination diagrams of Dickinson et. al. (1979 and 1983) immature sands with feldspars and volcanic lithic fragments are expected. The unexpected mature sandstone modes are explained by the introduction of sediment to the arc region by tectonic and sedimentary processes. The sands reflect their actual provenance but have been transported across tectono-sedimentary boundaries, to be deposited in a setting unrelated to their provenance. In the Indonesian arc, sands of recycled orogen provenance have been brought south from the Himalayas via the Bengal fan to be incorporated into the prism by movement along the trench and by offscraping from the downgoing plate. The anomalous terrane composition of the Sumatra arc also contributes.

The existence of sands of a provenance unrelated to their depositional setting indicates that caution should be exercised when interpreting detrital modes of sandstones in order to reconstruct palaeogeography and make tectonic inferences.

Zuffa (1980 and 1991) made the point that framework modes of arenites were open to misinterpretation because the temporal and spatial origin of grains is often unconstrained. Four grain classes were proposed; 1) carbonate extrabasinal, 2) non-carbonate extrabasinal, 3) carbonate intrabasinal and 4) non-carbonate intrabasinal. Proper recognition of these grain types can separate provenance control of composition from the control exerted by intrabasinal sources (for example biogenic shell production and evaporites). Otherwise erroneous provenance assignment could take place. The recognition of syndepositional intrabasinal and extrabasinal (for example volcanic) material provides much insight into basin environments and conditions. This information improves basin models and further constrains tectonic and palaeogeographic models.

The factors discussed in this section deal with the characterisation of the primary control of sediment composition, that is provenance, and its correct identification through sandstone detrital modes. However, external factors can modify sediment composition and make it less than ideally representative of the source region, diminishing the utility of sand composition as a provenance indicator. The next section considers the two main factors.

1.5.4 Other factors affecting detrital modes

Once surface outcrops erode the sediment produced begins a long process of change. Similarity to parent rock fades as it is weathered, transported, reworked, deposited, buried and subjected to diagenesis. Information carried about ultimate sources is diminished, but

sometimes information about sedimentary processes is acquired. In the following sections the more important variables that control sandstone detrital modes other than provenance, climate and diagenesis, are reviewed.

Climate

The major factors that determine the effect of climate upon sandstone composition are the intensity and duration of weathering (Johnson et.al. 1988). Suttner and Dutta (1986) looked at the climate dependant composition of sandstone sequences, when provenance and depositional dynamics remained unchanged for the sequences considered. Humidity and temperature are the main controlling factors. For the Gondwana sequence in India, they found that as the climate during erosion and deposition changed from arid glacial to warm humid, QFL quartz percentages increased from 54% to 99%. A log-log plot of total Q/ total feldspar + rock fragments against total poly quartz/ total feldspar + rock fragments discriminates well between sediments from arid, semi-arid, semi-humid and humid climates. Work carried out by Girty (1991) generally confirms this result for plutonic derived sands from Southern California. However little degradation of feldspar and lithic grains occurred in the climate zones he considered. This suggests there exists a 'climactic threshold' for the onset of feldspar and lithic fragment breakdown that lies between humid temperate mesothermal and humid microthermal climate types.

Johnson et. al. (1988) describe first cycle quartz arenites from the Orinoco river, South America, that are generated from a complex, mainly metamorphic drainage area. Two ways of producing mature sediments in a first cycle of erosion and transportation are suggested. Intense chemical weathering combined with a long period for weathering to occur are common to both. Sediment is stored for long periods in alluvial plains, near source, while in other areas protracted residence in soil profiles due to slow erosion rates occurs. Sands generated in this way can be from various types of provenance, but as all but the most stable grains have been dissolved, little useful source signature is left making them of no apparent use in source reconstruction. Despite this the fact that quartz arenites can be generated in a first cycle of sedimentation by the action of climate could *actually help* in constraining tectonic models. If no evidence of recycling, such as sedimentary lithic grains or mineral overgrowths are seen then ancient quartz arenites may point to climactic considerations previously unconstrained. Tectonic models that accommodate recycling may be reconsidered.

Slope and discharge are also important in controlling weathering intensity (Grantham and Velbel 1988). High slope gradients increase erosion rates and thus reduce the time available to weather source rocks and sediment (Leeder 1991).

Diagenesis

Subsurface alteration of sandstone detrital modes can reduce provenance information. It works to the same end as weathering, increasing the content of stable minerals especially quartz (Velbel and Saad 1991) reducing feldspar and unstable lithic grains. Milliken (1988) demonstrated that grain dissolution can take place even in young relatively shallow buried sediments at low temperatures (<100°C) without major meteoric water flow. Plagioclase was

albitised, and potassium feldspar and unstable heavy minerals dissolved. Alteration increases with depth.

Studies by Morton (1984, 1985, 1987) describe how heavy mineral populations in subsurface sandstones have been altered by diagenetic processes. Dissolution increases with depth, evidenced by the strength of etching and faceting of grains. Such evidence for the diagenetic alteration of the framework modes of sandstones has important implications for provenance work. For all provenance studies, the diagenetic state of the sediments under investigation must be constrained in order to properly interpret petrographic data.

1.5.5. Conglomerates

Conglomerates have long been favourites for provenance work, for the obvious reason that they preserve complete hand-specimen sized samples of *actual* source rocks. The value of having intact examples of source rocks is immeasurable, but the size of the detritus itself places a constraint upon the utility of using conglomerate clasts. Conglomerates tend to be relatively proximal deposits with identifiable sources nearby, and compared to sandstones deposited in large river systems, they sample only a relatively small area. Where source is apparently missing, conglomerate clasts can be the only surviving remnants, and their proximal deposition can be a positive help in source positioning. Conglomerates can record the unroofing (and therefore the lithostratigraphy) of their source region, but more importantly clasts also retain information about the conditions of evolution of the source region, for example pressure and temperature conditions, information which is largely lost on disagregation to form sand. Examples of the use of conglomerates in reaching inferences concerning tectonics include work by Bluck (1980), Dempster and Bluck (1989), Haughton (1988), Haughton and Halliday (1991), Graham et.al. (1991) and Cuthbert (1991).

Haughton (1988) recognised the presence of a terrane in the Midland valley of Scotland that fed detritus north westwards to the Lower ORS during the Devonian, that has since been removed. From the conglomerate clasts he recognised this 'cryptic' terrane as a sedimentary and metasedimentary flysch terrane cut by granodioritic and tonalitic intrusions. Dating of the clasts revealed an age of intrusion from 443 Ma to 420 Ma. (Haughton and Halliday, 1991), which helps to constrain models of Midland Valley evolution during the early Palaeozoic. This highlights the potential for tectonic reconstruction using conglomerates utilising the age information carried by clasts.

Metamorphic information can also be preserved in conglomerate clasts. This can be used to constrain evolution in source regions, and possibly link tectonism recorded by metamorphism to sedimentation, or at least clarify the relationship between the two. For example, Cuthbert (1991) looked at clasts in the Hornelen basin of western Norway, and compared their metamorphic evolution with the basement to the basin, and the surrounding Western Gneiss Region. The evolution of the clasts and basement is distinct from the Western Gneiss rocks, suggesting a source in the basin basement rocks where evolution linked to sedimentation in the basin. However, the basin was brought to lower structural levels along a basin-sole fault zone, during crustal extension, and juxtaposed against higher grade material that was not the source for the conglomerate detritus in the basin.

In Western Ireland the Derryveeny Formation records the stripping of a Metamorphic block, presumed to be part of the Connemara Dalradian exposed nearby (Graham et. al. 1991). Uniformity of source with the Connemara Dalradian is suggested by common Nd model ages. Differences in the lithologies recorded suggests preservation in the Derryveeny formation of the original cover to the presently exposed Dalradian rocks. This places constraints on the 'docking' of the Connemara Terrane to have been by the Ordovician deposition of the Derryveeny formation. This shows the power of combining isotopic and metamorphic studies of sedimentary detritus with tectonic reconstructions.

Dempster and Bluck (1989) dated metamorphic boulders from the Highland Border Complex to the south of the Dalradian block in Scotland, in order to clarify the provenance of the detritus. A North American provenance is ruled out, as is a Dalradian source, because Grenville age (1.2-0.9 Ma) events have reworked the crust in this area, compared to the 1.9-1.7 Ma age of the clasts. Other sources, including African crust are considered in an overall right-lateral sense of shear. This highlights the ability of such conglomerate based provenance studies to constrain the timing and style of terrane movement, utilising the pressure and temperature information carried by conglomerate clasts.

It can be appreciated that conglomerates offer much to provenance workers, in preserving a very detailed record of source rock type. However, most studies have not utilised conglomerates to examine the evolution of provenance signature, perhaps because they appear to faithfully reflect source composition. Conglomerates are an important part of the starting point of the evolution of sedimentary detritus. Sands can be generated by the breakdown of conglomerates, even though at the point of erosion the complete range of grain sizes are generated from muds to conglomerate clasts. This thesis focuses in some detail upon the relationship between the evolution of conglomerate clast assemblage composition and the evolution of sandstone composition. This is important as it may highlight important points about the way sandstones in particular, carry and modify provenance signature. This is done in this work using a well constrained provenance area.

The final part of this introduction introduces the Geology of the Betic Cordillera, the macroscopic setting of the Granada Basin, before Chapter 2 discusses the geology of the study area in more detail.

1.6 Geological Setting - The Betic Cordillera

1.6.1 Introduction

This thesis centres around the deposits of the eastern border of the Granada Basin and the adjacent metamorphic basement source rocks in the Sierra Nevada.

Details of the geological setting of the south of Spain are presented in this section. This is necessary in order to clearly interpret aspects of provenance and palaeogeography. The isotopic data, presented in **Chapter 7** is particularly crucial in constraining models of tectonic and palaeogeographic evolution, and a clear understanding of the nature and past history of the rocks dated is needed.

1.6.2 Location

The Granada basin is located in the Betic Cordillera of southern Spain (**Fig 1.4**). It is one of several small intramontane basins that lie upon this complex thrust faulted, folded and recently extended region, that were initiated, probably by strike-slip tectonics, during the early-mid Neogene. The Betic Cordillera taken together with the Rif in Morocco and the Tellirides of northern Africa form an arcuate mountain belt surrounding the Western Mediterranean. The westernmost part of the Mediterranean is the Alboran Sea, which is floored by thinned continental crust, extended also during the early-mid Neogene. The Alboran sea is surrounded by thrust-thickened crust, that forms the mountain ranges of southern Spain and northern Africa. The direction of tectonic transport is radially away from the Alboran basin in Spain and Africa (for example Platt and Vissers 1989). This region is at the most westerly part of the Alpine Orogenic belt, formed as a consequence of the closure of the Mesozoic ocean, from the late Cretaceous to the present day.

1.6.3. Plate Tectonic setting

Present motions

The Betic Orogen lies at the boundary between the African and Iberia plates. At present Iberia moves as part of the Eurasian plate, but this has not always been the case, as is explained below. Studies of movement vectors of recent earthquakes along the Eurasian-African plate boundary running from the Mid-Atlantic ridge near the Azores, to the Straits of Gibraltar show the comtempory state of movement (Burfon et. al. 1988). The most westerly part is in extension along a NE axis at a slip rate of 0.76cm/yr. The central sector shows E-W trending right-lateral slip at 3.39cm/yr. Finally for the most easterly part, up to the Straits of Gibraltar, the movement is compressional, oriented along a NNW axis. Africa is being thrust under Iberia at the present.

Past Plate Motions

Plate motion reconstructions have been attempted by using magnetic anomalies in the Atlantic (Srivastava et. al. 1990, Roest and Srivastava 1991), from P-T-t data and structural information from the Internal zones of the Cordillera (De Jong 1990) and from other general

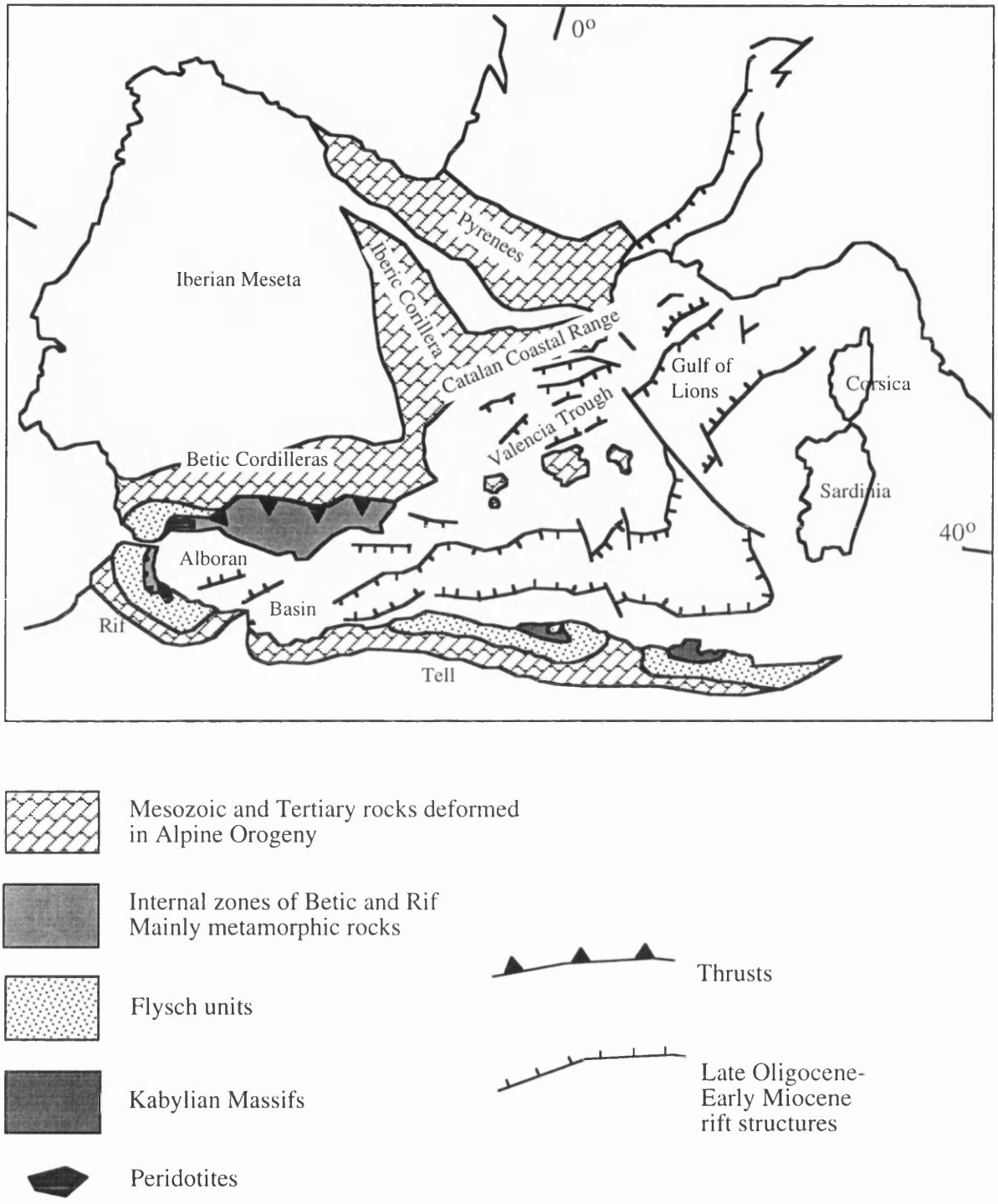

Fig. 1.4 General tectonic components and major stuctures of the Western Mediterranean

geological considerations integrating tectonics, structure and sedimentology (for example Dewey 1989, Sanz De Galdeano 1990).

Srivastava et. al. (1990) examined magnetic lineation patterns in the Atlantic, on both sides of the mid ocean ridge. From this they were able to reconstruct the relative motion of Iberia, Eurasia and Africa and locate rotation pole positions. From the onset of spreading in the North Atlantic, in the Late Jurassic, until the late Eocene (~37Ma) Iberia moved as part of the African plate. The plate boundary between Eurasia and Africa was located in the Bay of Biscay, and across the present trace of the Pyrenees, which formed as a result of compression and transcurrent motion across this plate boundary. In the late Eocene a second boundary formed between Africa and Iberia, establishing the present relative plate motions along its length. Both the southern and northern plate boundaries operated at the same time, so Iberia moved independently. At the end of the Oligocene the Bay of Biscay plate boundary stopped operating, and Iberia become part of Eurasia.

The present plate motions involving compression and dextral strike slip motion between Africa and Iberia, were established by the Late Eocene, around 37Ma. The magnitude of this motion is not great, as the West Mediterranean lies at the 'hinge' of movement and closure of Tethys. Dewey et.al. (1989) present a reconstruction of the movement of Africa relative to Europe, in which there is a dominant left lateral strike slip movement from 175Ma until 74Ma. From this time onwards Africa moves northwards into Europe, but at the Straits of Gibraltar the distance covered is small compared with the compression in the East Mediterranean. Dewey et.al. (1989) portray the relative motion of Africa against a Europe that contains Iberia, as opposed to the Srivastava et.al. (1990) model that has Iberia moving as part of Africa until 37Ma.

De Jong (1990) using P-T-t data and stretching lineation directions from the Internal Zones and the positions of rotation poles for Iberia and Africa produced a scenario that is in general agreement with the plate model of Srivastava et.al.(1990), and the tectonic evolution of the Betics and the Pyrenees. Early Cretaceous (116Ma tourmaline K-Ar) high pressure metamorphism is attributed to burial of up to 37 km during continental collision. A period of thrusting followed in the Betics between 99-83Ma before movement between Africa and Iberia ceased and transferred to the Pyrenees. Oblique convergence continued though, indicating the *non-rigid* character of the Alboran-Betic area. At the end of the Oligocene the present Betic-African plate boundary reformed, during a time of extension and increased heat flow, related to extension and ocean spreading in the western Mediterranean. Compression resumed at around 20 Ma. The relative sequence of major events are in agreement with Srivastava et.al. (1990), but there is no exact agreement of timing. De Jong (1990) only really lacks good geochronological control, which Srivastava offers using well constrained ocean magnetic lineations.

The Betic Cordillera can be divided into four zones or domains; the Mesozoic sedimentary External Zones, the metamorphic Internal Zones, the Neogene to recent intramontane sedimentary basins and the Oligocene age Flysch units of the Gibraltar Arc region. The intramontane sedimentary basins rest in unconformable contact upon the Internal

and External Zones. The Granada Basin is located on the contact between the Internal and External Zones in the centre of the Cordillera (see **Fig.1.5**). The following sections will outline the general characteristics of lithology and structure for each of the major constituents

1.6.4 External Zones

The External zones constitute a linear belt some 600km by 100km that runs across southern Spain, north of the Internal Zones, and into the Balearic Islands (**Fig. 1.5**). They consist of unmetamorphosed sediments that were deposited upon the southern continental margin of Iberia from the Triassic to Lower Miocene in shallow to deep marine conditions in a stable shelf environment. Two subdivisions are recognised (**see Fig. 1.5**), the Prebetic, in the NE, and the Subbetic, in the SW.

The Prebetic

The Prebetic is predominantly shallow marine in character. The earliest Triassic deposits are red beds with evaporites in a characteristic early rift type sequence. Jurassic rocks are marine dolomites, marls and limestones. In the Cretaceous thin dolomite was deposited along with lagoonal deposits in a landward position. Basinward, pelagic conditions became established during the Cretaceous, but a continental signature remained (Garcia-Hernandez et. al. 1980). In the Palaeogene regression exposed the northern deposits, and established coastal and shallow marine conditions in the southern Prebetic. Sea level rose during the Early Miocene and calc-arenites and marls were deposited.

The Subbetic

The Subbetic is located to the south of the Prebetic, deposited downslope in a deeper marine environment. Three units have been recognised on facies and palaeogeographic grounds (Garcia-Hernandez et.al. 1980); the External, Median and Internal Subbetic, arranged from north to south respectively. In the External Subbetic carbonate platform conditions predominated. Upper Jurassic rocks are oolitic and nodular limestones. The Median Subbetic is formed of pelagic marls and limestones with interbedded volcanics. Mid Jurassic rocks are marly limestones interbedded with volcanics. Upper Jurassic deposits include pelagic radiolarites and marls. The very latest Jurassic includes breccias and micritic limestones, again with interbedded volcanics. The Internal Subbetic is composed of further carbonates deposited in a platform setting.

Structure

The External Zones are a complex thin skinned thrust belt, resting upon crystalline basement of Palaeozoic age. This basement has suffered thinning during the Mesozoic deposition of the external zones upon an Atlantic type margin, especially during the early Jurassic when the Prebetic and Subbetic became differentiated. Compression began stacking the elements of the External zone extended margin in the late Palaeogene as the Internal zones impinged from the south. Extension in the Internal Zones during the early Miocene was contemporaneous with thrusting in the External Zones. The main thrusting direction is to the NW (Banks and Warburton 1991) slightly oblique to the trend of the orogen, indicating a

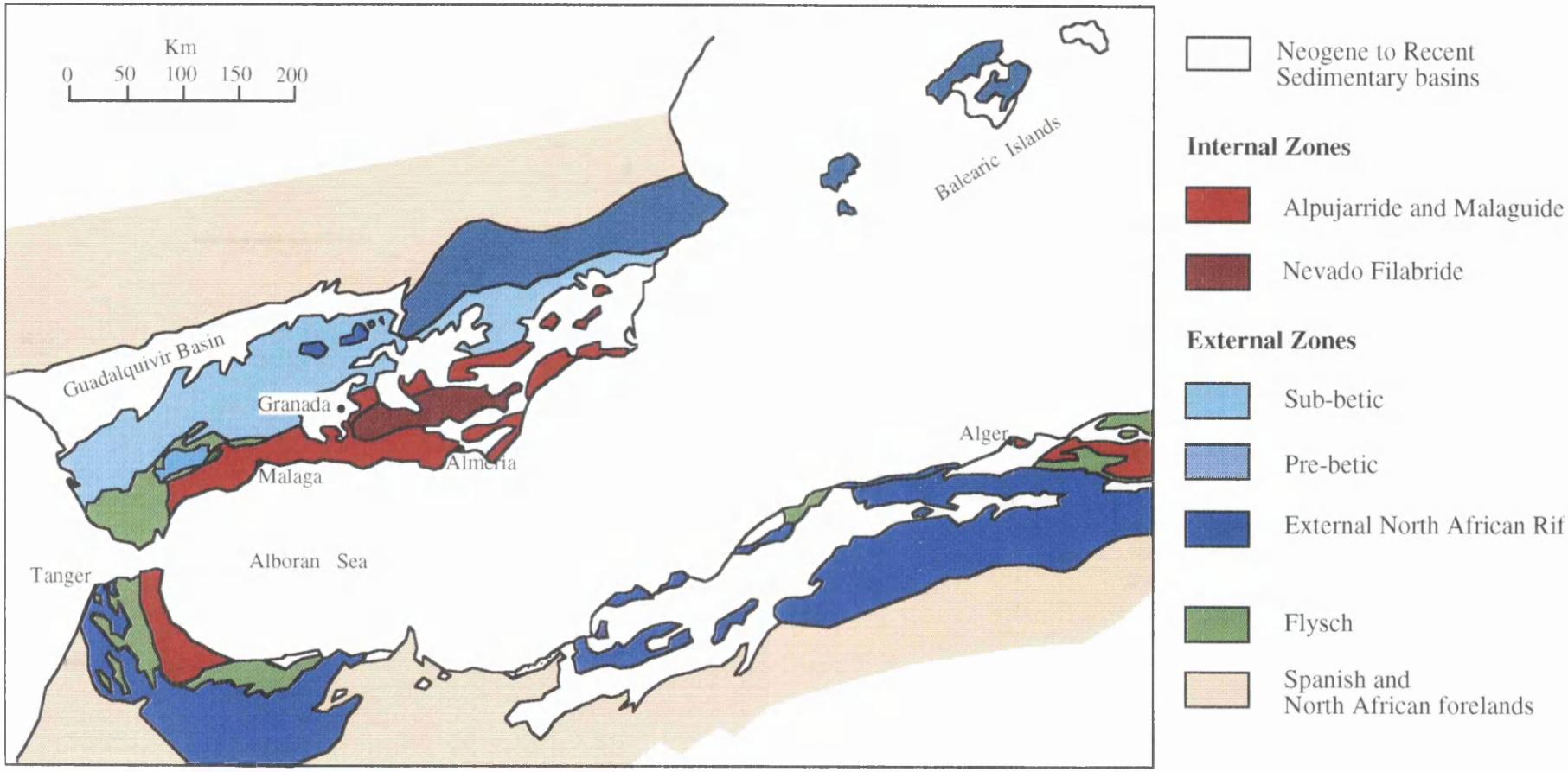

Fig 1.5 Map showing Main Tectonic units of the Betic- North African Orogen redrawn from Torres-Roldan (1979)

dextral component of compressive movement. Important clockwise rotations of Jurassic and Cretaceous rocks support early Tertiary dextral transpression (Platzman 1992).

The structure is a wide imbricate thrust stack with the Subbetic thrust over the Prebetic in a northwards direction. Important backthrusts exist in the southern Prebetic and Subbetic, especially where the latter is underthrust by the internal zones. Thrusts are mainly accommodated on Triassic Evaporites.

Palaeogeography

Garcia-Hernandez et.al. (1980) proposed a basin initiated in the Triassic with a single main depocentre. The early Prebetic was deposited nearshore and the early Subbetic downslope in deeper water. In the mid Jurassic pelagic conditions became established as extension ensued, causing basin subsidence and the break up of the inshore carbonate platform. This time sees the proper differentiation of the Prebetic from the Subbetic. The Prebetic remained a marginal facies of lagoonal, shallow marine and carbonate platform deposits separated from the pelagic Subbetic to the south by an elevated, isolated fragment of the previous thicker crust. The Subbetic persisted in accumulating in deep water, but shallowed in the south to another carbonate platform. However this platform area was not subaerially exposed and influenced deposition in the external zones only until the mid Cretaceous.

Blankenship (1992) analysed the structure of the external zones, using published maps, seismic profiles and well data, and concluded that the degree of shortening across the zone is much greater than previously thought. This forced a change in the palaeogeographic interpretation. The new model consists of a single basin with platform margins on either side. The previously identified central platform area that separated the Prebetic and the Subbetic is recognised by Blankenship as bounded by a major low angle detachment. It is proposed that the rocks above this detachment are far travelled and are the same platform sequence that formed at the southern margin of the External zones in the Mesozoic. The previously accepted model by Garcia-Hernandez et. al. (1980) restored thrust slices only a short distance and therefore took their present relative positions to represent their original relative positions pre-thrusting. However, Blankenship (1992) shows considerable shortening of up to 200km, as opposed to previous estimates of only 15km, allowing rocks to be moved considerably out of sequence. This model has lately been brought into question (, 1993).

Implications of External Zone Palaeogeography

An important point can be made about the Mesozoic and early Tertiary palaeogeography of the External Zones. It is clear that any continental influence that is seen in the External Zones is derived from the North, from the Iberian Meseta, or foreland. Facies in the External Zones demonstrate how water deepened to the south, and the persistence of the southern carbonate platform shows there to be little continental influence in this region in the Cretaceous and perhaps for longer. This is important in our interpretation of the relation between the External and Internal zones, now just to the south. Clearly during the Mesozoic the Internal Zones were not immediately to the south as they are now, but in some other relative position. The timing of thrusting in the External Zones is controlled by the impingement of

the Internal Zones during the late Palaeogene. However the peak of metamorphism in the highest grade parts of the Internal zones is now considered to be Cretaceous in age, requiring a great thickness of crust and presumably a considerable amount of subaerial relief, and sediment production. No sediment of this calibre or source is seen in Cretaceous age External Zone deposits, so the Internal Zones were in some distal position before the Late Palaeogene.

1.6.5. Internal Zones

The Internal Zones (see **Fig. 1.5**) of the Betic Cordillera are a thrust stack of three nappe complexes, arranged in the following structural order (lowest first): The Nevado Filabride (poorly defined and often subdivided), the Alpujarride and the Malaguide. The lowest two units are Metamorphic in character and the Malaguides are non metamorphic. Metamorphic grade generally decreases with ascending structural order. The Nevado Filabride unit comprises the core of the internal zones, surrounded in thrust contact by the lower grade metamorphic rocks of the Alpujarride complex arranged in an E-W trending antiformal structure, comparable to the Metamorphic Core Complexes of the Western United States. The Nevado-Filabride despite being the structurally lowest tectonic unit in the Internal Zones, forms the highest ground in mainland Spain. In the following sections details of each unit in the Internal Zones will be presented. Special attention will be paid to the Nevado Filabride and Alpujarride units, as these form the basement and source rocks of the Granada Basin.

Nevado Filabride

The Nevado Filabride is often subdivided into two component units. The lower is the Veleta unit, which is overthrust by the Mulhacen unit. The Veleta unit is at the lowest tectonic level of the Betic orogen. Six kilometres of graphitic mica schists, sometimes with garnet and chloritiod (Diaz de Federico et.al. 1990) contain only a few intercalations of non graphitic mica schist and marble. These schists are thought to be derived from the metamorphism of Palaeozoic age pelitic sediments, though some have even been attributed to the Pre-Cambrian (Gomez-Pugnaire et.al. 1982). The metamorphism is recognised as having progressed through initial low pressure- low temperature up to amphibolite grade.

The Mulhacen is lithologically more diverse than the Veleta, and protoliths are considered to range up to Mesozoic in age. Essentially a 'basement' of Palaeozoic graphitic schists, like the Veleta complex, are overlain by a cover of Mesozoic carbonates and clastic rocks. Six thrust slices are recognised in the Sierra Nevada in the source area for the Granada Basin sediments (Diaz de Federico et.al. 1990). The units are from top to bottom:

Sabinas - Graphitic mica schists, Rhyolitic Gneiss and Micaceous marbles

Ophiolite - Various mafic rocks ; harzburgites, serpentinites, rodingites, gabbros, volcanics. Metamorphosed to form in places eclogites, that are now retrogressed.

Caldera - this has a 'basement' of granitic gneiss and graphitic mica schists, similar to the Veleta complex and attributed to the Palaeozoic, overlain by a 'cover' of Triassic graphitic and non graphitic micaschists, rhylolitic gneiss and marble

San Francisco - Graphitic and non-graphitic mica schists.

The metamorphism in the Mulhacen unit has long been recognised as plurifacial (Egeler and Nijhaus 1966) in contrast to the Veleta unit. Two events are generally recognised for which there is no evidence in the Veleta unit. The interthrust and intruded metabasic rocks, typified by the ophiolite sequence in the Sierra Nevada, are often the best indicators of metamorphic grade. Gomez-Pugnaire and Fernandez-Soler (1987) document the formation of eclogites in basic and ultra-basic rocks from the eastern internal zones, during early 'alpine' HP eclogitic and blueschist grade metamorphism. Following this, retrogression followed the path through amphibolite facies to greenschist facies. Morten et.al. (1987) describe eclogitic metagabbros that have retrogressed to amphibolite grade near Lubrin. Metabasites in the Sierra Nevada were first metamorphosed in a HP event (640°C and 16kb) followed by retrogression and then involvement in a lower P event (Puga et.al. 1989). The metamorphic evolution finished in greenschist facies. Puga et.al. attribute this evolution to two phases of subduction, or overthrusting, the first in the late Cretaceous and the second in the late Eocene-early Oligocene. This late stage decrease in P-T conditions runs from 6-8kb at 550-600°C to 3-4kb at 450-500°C.

In the east, in the Sierra De Los Filabres, three units are recognised by Bakker et.al. (1989). They are generally similar to the units to the west described by Diaz De Federico et. al. (1990), and are composed of a basement unit of Palaeozoic age schists with a cover of Triassic schists, quartzites, and marbles. One unit is intruded by a granite in its lower Palaeozoic portion, which is now deformed to an augen gneiss. This granite has yielded a Rb/Sr whole rock age of 269Ma (Preim et.al. 1966), confirming the Palaeozoic age for the older schists.

Bakker et. al. (1989) determined the P-T path of the Mulhacen Unit in the Sierra de los Filabres using a combination of mineral chemistry and structural data. Six phases of deformation and metamorphism are recognised, beginning with a HP/LT event indicating initial burial up to 37Km (P 10Kb and T=300°C), despite the lack of structural evidence for this event. The following event occurred at similar pressures but at higher temperatures, and represents the establishment of increasingly intermediate conditions. Following this temperatures peaked at around 550°C during decompression to 8-9kb and the formation of the most pervasive deformation structures. Pressures and temperatures continued to drop to 3-4kb and 400-450°C, conditions which have been related to thinning and the development of extensional crenulation cleavage as rock was excised by up to 6km. After this temperatures rose, with falling pressures, to peak at 500°C, related again to the crustal thinning event. Structures at this time are first S-SW vergent followed by N-NE vergent in the next deformation event. This is a similar metamorphic evolution to that previously described (see above), as two main events are seen. However, it differs as P drops continuously throughout, and the last event is attributed to late crustal thinning, not thickening as in the model of Puga et.al. (1989).

In summary the Nevado Filabride records in the higher nappes of the Mulhacen complex, HP metamorphism followed by retrogression through Amphibolite facies to late Greenschist conditions. The early HP phase is usually attributed to subduction related

processes (Loomis 1975, Puga et.al. 1989, Bakker et.al. 1989), but the late reheating event in greenschist facies could be due to more thrusting or even crustal thinning (Van Wees et. al., 1992).

Alpujarride

The Alpujarride overlies the Nevado Filabride in thrust contact, completely surrounding the latter (see **Fig. 1.5**). Akin to the Nevado Filabride, it consists of a series of distinct thrust nappes with varying metamorphic characteristics. In the west and central areas three nappe units are distinguished (Moine et.al., 1991). The lowest consists of phyllites and quartzites of Late Palaeozoic age overlain by Triassic carbonates. The second unit is made up of graphitic schists and quartzites of presumed Palaeozoic age. The final unit, and highest structurally, is composed of mica schists, gneiss, migmatites, granulites and peridotites. These peridotites are the largest outcrops of mantle derived ultramafic rocks on earth, and are emplaced as detached thrust slices, involved in thrusting during the Palaeogene and exposed due to late extension in the early Miocene. The Ronda peridotite mass has an equivalent in the Beni Bousera mass of Morocco.

Three structural events can be recognised in the Alpujarride, the first two being compressional, with WSW-ENE shear sense and stretching lineations, perhaps associated with the emplacement of the Ronda Peridotites. This is overprinted by brittle N directed thrusting and SW oriented extension.

Metamorphic grade increases up the structural section. As with the Mulhacen unit of the Nevado Filabride complex plurifacial metamorphism is seen. The highest nappes record early HP/HT granulite facies conditions, as seen in the rocks beneath the Ronda peridotite. Following this, LP assemblages were superimposed on the HP rocks. Conditions in the HP event ranged from 7-8kb and from 300-330°C. Tubia et.al. (1991) also studied the Ronda ultramafics and the rocks beneath them, and found eclogites interbedded with amphibolites and migmatites. Initial conditions of >15kb at 730°C were followed by a retrogression to amphibolite facies conditions of 5-8kb at 650°C. It is clear that this HP metamorphism recognised in the highest Alpujarride nappes occurred prior to the superposition of the complete Alpujarride thrust stack, as the metamorphic 'pile' is presently inverted. This is possibly the result of late structural inversion due to compression (Van Wees et. al., 1992)

Malaguides

The Malaguides rest structurally above the Alpujarride complex in thrusted contact, and do not come into contact with the Nevado Filabride. In **Fig 1.5** they are grouped with the Alpujarride, but can be found in a strip along the northern border of the Internal Zones at the contact with the External Zones. They are largely unmetamorphosed, except perhaps for their lowest portion (Torres-Roldan, 1979), but this is poorly documented. Longeran and Mange-Rajetzky (1994) summarise the salient features of the Malaguides, especially those in the eastern Betics. They comprise a continuous sequence of sediments ranging in age from the Silurian to the Miocene. Early deposits are conglomerates, shales and greywackes. Permo-Triassic sediments include dolomites and shallow marine limestones. Carbonates continued to

dominate until the lower Miocene when deep water conditions took over. Sedimentation terminated in the early Miocene due to thrusting, causing basin inversion, driven by extension in the lower units of the Internal Zones.

Longeran and Mange-Rajetzky (1994) found a record of unroofing of a metamorphic block in the detritus of the Tertiary section of the eastern Malaguides. The source of the sediment is implied to be the lower units of the Internal Zones. They propose that the Malaguides, during the Tertiary, were the foreland basin caused by crustal loading due to the orogenic activity and crustal thickening in the Internal Zones. The lower Miocene time deepening of water in the Malaguide basin and calculated subsidence curves from the sediment are consistent with crustal loading and induced subsidence. However, this combined with the unroofing sequence preserved in the sedimentary detritus is all the evidence available for the Malaguides being a foreland basin, an issue which is open to question.

1.6.6 Neogene Intramontane Sedimentary Basins

The intramontane basins of the Betic Cordillera occupy a much larger area than similar basins found in other orogenic areas, and their infill can reach considerable thicknesses. They are the result of extensional and strike slip tectonics that have affected the Betics from the late Oligocene to the present. They rest unconformably upon the External and Internal Zones and straddle the contact between the two, most notably in the case of the Granada and Guadix-Baza basins.

The Neogene basins are important in constraining the tectonic evolution of the Betics. They overlie tectonic contacts thus helping to date events. They record in facies types and patterns along with deformation structures, the evolution of structural episodes. The composition of the sediment contains evidence of source area evolution in lithological detail which can help to date tectonic events, for instance those responsible for unroofing. Thermal evolution data is contained also in specific detrital metamorphic minerals and rock fragments.

Structure and tectonic origin of basins

Two models have been suggested for the structural setting and origin of the basins. Doblas and Oyarzon (1989) and Platt and Vissers (1989) suggest extension driven by gravity spreading from thickened crust making up the Internal Zone from the Oligocene onwards. Montenat et.al. (1987), Sanz de Galdeano (1992), prefer strike slip tectonics and describe the Betics in the context of a crustal scale shear zone. Montenat et.al.(1987) suggest that the eastern Betics are part of a NE-SW trending left-lateral shear zone, and movements on a complex set of faults are responsible for the formation of wrench furrows and graben type basins, like the formation of basins in the western US Strike slip margin. Both of these models are consistent with the two main models of Betic evolution, the first with extensional collapse and the second with a westward moving Alboran microplate. However, both models are not incompatible.

An extensional phase is recognised during the Tortonian-early Pleistocene, oriented in E-W and NE-SW directions, due perhaps to perpendicular compression, followed by compression from the early Pleistocene to the present in a N-S direction. This occurred in the

general framework of a Betic scale right-lateral shear zone. Horizontal movements were oriented N-S, SE-NW and E-W (Dabrio 1992). According to Montenat (1987) the orientation of compression shifted during the late Neogene from NW-SE in the Tortonian, through N-S in the late Tortonian back to NW-SE in the late Pliocene. These movements are generally consistent with the plate tectonic reconstructions discussed above (section 2.3.2) and the late (9Ma) change in plate motion direction when Africa started to move westwards relative to Europe (Dewey et.al. 1989). This is the geodynamic context in which the intramontane basins of the Betic Cordillera evolved. The faults that control basin formation are oriented E-W, NW-SE and NNE-SSW (Montenat et.al 1987, Montenat et.al. 1990), often with important late Neogene vertical components that were important in controlling the location of subsidence.

The possibility of transpression as the dominant building force of the Betics is not incompatible with basin formation. As presented in an earlier discussion on the formation of transform basins, the dynamics of detailed fault geometries and local variations in compression and extension that result, may allow the formation of basins in an largely compressional setting. Rotations have taken place as a result of transform tectonics in the Betics (Platzman 1992), and these may have played an important role in the formation of basins, especially along the suture between the Internal and External Zones, where the Granada and Guadix Baza basins lie. It is possible that in the early stages of transpression local irregularities in fault geometries may favour the formation of small localised basins such as the Neogene Intramontane basins of the Betics. Later development of the orogen and the persistence of transpression may smooth out these irregularities, resulting in the loss of these basins and the reworking of their sedimentary fill.

Sedimentation

The earliest post metamorphic deposits are shallow marine detrital sediments of Oligocene and early Miocene age, deposited unconformably upon the Malaguide complex (Sanz de Galdeano 1992). Marine detrital deposition, including turbidites, continued in the Internal Zones during the late Aquitainian and Burdigalian. At this time the basins had not yet become the individual entities we see today, sedimentation was more widespread and continuous across the orogen, and sub basins were connected.

Late Burdigalian and Langhian sediments are marls, conglomerates and turbidites. Sea level rose in the late Langhian, resulting in the deposition of marls upon the Alpujarride complex. It is this time that we see the first deposits of Calcareous arenites that are recognisable at the base of the Granada basin, and in more widespread basins, as the present basin layout began to form. The earliest deposits of the linear strike-slip related Alpujarride basin are also of this age.

Basin sequences began to form at the beginning of the Tortonian. Sedimentation is mainly detrital, and becomes increasingly sub-aerial, two factors indicating the increase in erosional relief in the Internal Zones from the Tortonian onwards. It is at this time that we see the first detritus sourced from the Nevado Filabride complex entering the basins surrounding the Sierra Nevada and ranges to the east.

Sanz de Galdeano (1992) distinguishes two phases in the evolution of Neogene sedimentation upon the External and Internal zones. Sedimentation occurred over a large area, and was continuous and connected across the orogen in the early Neogene. The intramontane basins we see today had not become separated. Relief in the Internal zones was subdued, indeed it was mostly submarine, as sedimentation was dominated by carbonates, and often pelagic. Following this, around the beginning of the Tortonian at 11Ma, relief in the Internal Zones was rejuvenated and large amounts of coarse sediment began accumulating in smaller basins, as tectonic movements subdivided depocentres and built up source areas.

Important Neogene sedimentation also took place in the Guadilquivir Basin, which straddles the contact between the Betic Cordillera and the Spanish foreland. It has been considered to be the foreland basin to the Betic orogen (Sanz de Galdeano 1992), caused by the crustal loading resulting from the thrusting of the Internal Zones upon the External Zones. The basin rests on rocks of the External Zones, which are deformed in a thin skinned fold and thrust belt (Section 2.4.1.3). Sediment in the basin is thin and often shallow marine, testifying that the basin did not undergo the degree of subsidence expected in foreland type basins. The existence of a foreland basin in the Guadilquivir, as 'classically' understood (for example Beaumont 1981, Allen et.al. 1986) has recently been debated (Stromberg, 1994, Stromberg and Bluck, *in preparation*).

In summary, the Neogene basins that rest unconformably upon the Internal and External zones, have an early phase of generally marine carbonate deposition beginning in the late Oligocene that continued until the early Tortonian. At this time tectonic movements caused uplift, the creation of sub-aerial erosional relief and the break up of the previous basinal entities. A second event is recognised in the Pleistocene when basin edges were redefined. Strike slip motions were important and control movements on many faults until the late Miocene, when N-S compression and dextral movement becomes dominant in the relative motion between Africa and Iberia.

1.6.7 Models of Betic Evolution

Several models have been suggested to explain the macroscopic evolution of the Betic Cordillera, especially the behaviour of the Internal Zones and their effect on the currently observed features in the orogen. A consensus view that makes sense of all observations has yet to be reached, and debate still continues. The following is a brief summary.

In very general terms there are two views that predominate;

1. The Betic Orogen is the result of compressional tectonics between Africa and Iberia, and subsequent extension centred around the thinned crust of the Alboran Sea.

2. The Betic Orogen is the result of dominant strike-slip tectonics with an important component of transpression.

The former viewpoint involves orthogonal compression between Africa and Iberia, and invokes mechanisms of extensional collapse, as in the models of Platt and Vissers (1989) and Doblas and Oyarzon (1989), and as also suggested by Dewey (1988). **Figure 1.6** shows the evolutionary model of Platt and Vissers (1989). A crustal 'welt' formed during the Oligocene, by compression, that became over thickened and gravitationally unstable. The root to this thick

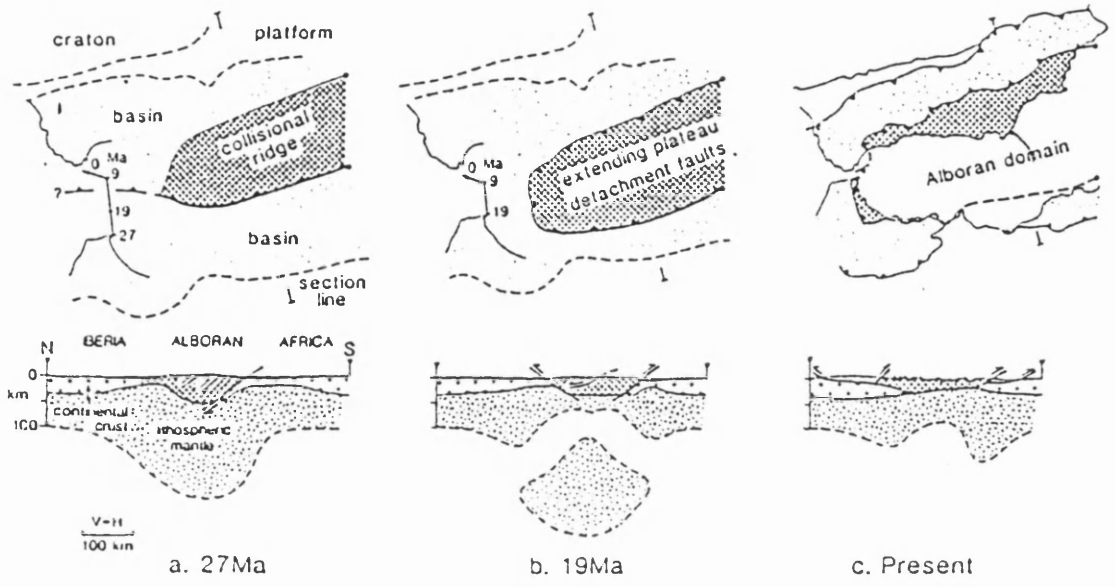

Fig. 1.6 Taken from Platt and Vissers (1989) to show the extensional collapse model suggested by these authors for the evolution of the Betic orogen from the late Oligocene onwards. In (a) a collisional ridge forms due to Africa-Iberia collision, generating a substantial root in the lithospheric mantle. In (b) this root falls off into the mantle, and extension ensues in the collisional ridge along large detachment faults. (c) shows the present arrangement of Internal Zones andthe main detachment thrust faults, which have a radial sense of movement arranged around the Alboran Sea. The line on the left with ages shows the relative movement of Africa relativeto Iberia.

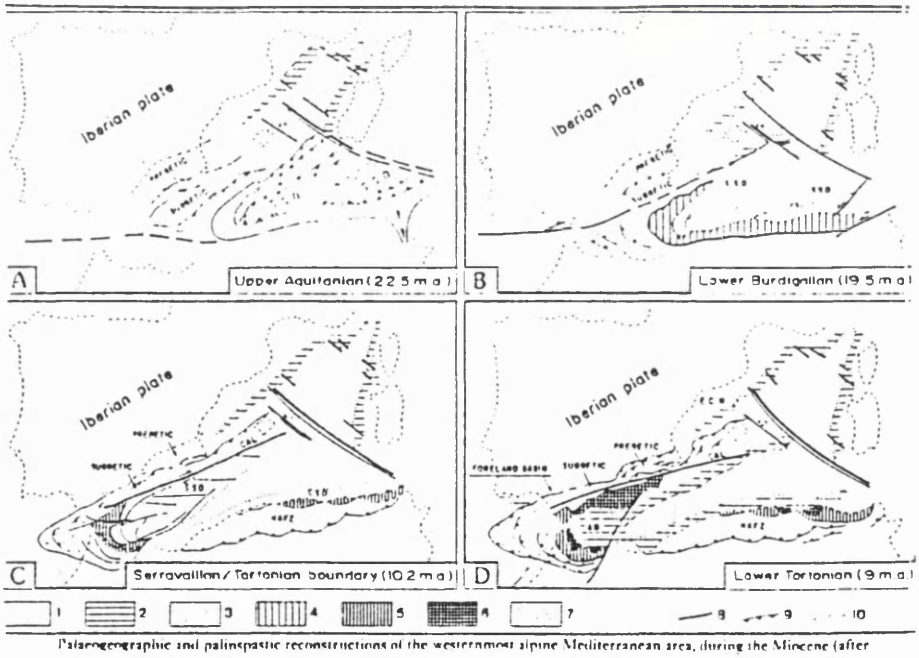

Palaeogeographic and palinspastic reconstructions of the westernmost alpine Mediterranean area, during the Miocene (after Martin-Algarra, 1987; Sanz de Galdeano, 1990; modified). *Key*: 1 = Oceanic crust, 2 = Thin continental crust, 3 = North African Flysch Trough, 4 = Units from North African Flysch Trough displaced partially, 5 = Campo de Gibraltar units and similar units in North Africa, 6 = Internal Zones, 7 = Olistostromes, 8 = Main faults, 9 = Front of the olistostromes, 10 = Present coast line; S.S.D. = South Sardinian Domain, CAL = Cadiz Alicante line, NAEZ = North African External Zones, E.C.M = Ebro continental margin, VT = Valencia trough, and AB = Alboran basin.

Fig. 1.7 The model proposed by Sanz de Galeano and Vera (1992) for the evolution of the western Mediterranean, showing the westwards movement of the Alboran microplate that includes the Internal Zones of the Betics. Transpression is important at the northern boundary of the Alboran plate, with a right-lateral sense of movement. Thrusting took place at the contact between the Internal and External Zones and within the External Zones.

crust became thermally unstable also, and may have dropped off into the asthenosphere. Isostatic uplift ensued and horizontal tensile forces driven by gravity became dominant. Extension proceeded by outward directed thrusting, to the north in the Betics and to the south in North Africa. This is consistent with observed thrusting directions, the thinned crust in the Alboran Sea and the presence of a detached mass in the asthenosphere beneath the Betics (Blanco and Spakman, 1991). However, collision and crustal thickening are attributed to a single phase, ending in the early Miocene, which does not sit easily with the fact of disparate metamorphic evolution in different units of the Internal Zones.

The removal of a portion of the lithospheric mantle beneath the Betics is also invoked by Zeck et. al. (1992), who record very high cooling rates in the Alpujarride Complex. Cooling has certainly taken place, but there is little evidence for uplift until the late Tortonian, at the earliest. In contrast Van Wees et. al. (1992) explain rapid cooling in the Internal Zones, by the inversion of a previously extended region, resulting in the underthrusting of cold crust under warm. Thus cooling proceeded from beneath, was rapid, and did not involve uplift. Uplift associated with extension, as happens in the extensional collapse model, would raise isotherms, and need not lead to such rapid cooling either.

The contrast in character of Internal Zone crust compared to the External Zones passive-margin rocks and the Iberian Meseta crust to the north, suggests that the Internal Zones are exotic and have been emplaced by some mechanism into the area. The predominance of strike slip faults in the Betics, and their role in the formation of the intramontane basins, such as the Granada Basin, suggest to many workers the possibility of strike slip as the mechanism of emplacement of the Internal Zones. This features in the models of Sanz de Galdeano (1990) and Sanz de Galdeano and Vera (1992, see also **Fig. 1.7**). The Internal Zones moved westwards into the Straits of Gibraltar due to ocean floor spreading further east in the Mediterranean. Moving westwards the Alboran 'microplate' collided with the External Zones in a right-lateral strike-slip environment. Palaeomagnetic rotations in the Gibraltar arc are consistent with a westwards moving Alboran Microplate according to Platzman (1992), though he prefers an extending collisional ridge, with some obliquity of convergence.

Evidence exists to support both modelling approaches. Tectonic evolutionary models of these sort are next discussed in **Chapter 7** along with evidence for the role of strike-slip in the evolution of the Betics. The extensional collapse models become less credible in this light, and the concept of terrane tectonism as suggested for the westwards moving Alboran microplate becomes a more likely possibility.

1.7 Layout of Thesis

The following chapters present the results of field work and laboratory studies of sediment composition and sediment and source age dating from the Granada Basin. Firstly the Geology of the Granada Basin is introduced, concentrating on features of the study area at the eastern edge of the Basin. Following this, data is presented in order of 'size'; conglomerates first, then sandstones, in both petrography and geochemistry chapters. Following this heavy minerals are discussed, for variety, abundance and detailed geochemistry. Finally the results of isotopic age dating of detritus and source rocks are presented, and interpreted in terms of the

evolution of the Internal Zones in the immediate vacinity of the Granada Basin, but also with implications for the whole orogen.

Throughout this discussion the full range of evidence including sediment depositional age and cooling time/rate of source rocks is combined to constrain tectonics. Sediment dynamics are considered in relation to source dynamics as far as possible.

2 The Granada Basin

2.1 Stratigraphy and Sedimentology

The Granada Basin rests upon the suture between the Mesozoic sedimentary External Zones and the metamorphic Internal Zones, in the central part of the Betic Cordillera (see **Fig. 1.5**). Rodriguez-Fernandez et.al. (1989) consider that the basin formed in an overall dextral shear context at this boundary, as the internal zones were emplaced against the External Zones by westward motion. Three major dextral-slip faults intersect creating the conditions for block movements and the creation of depocentres.

The sedimentary sequence begins in the very latest Serravalian, continuing to the present day. Recent siesmicity indicates that the basin is still active in its central portion, and on some normal faults at the south-east margin (Montenat et.al., 1990). The area covered in this study is located at the eastern margin of the basin, east of the city of Granada (See **Figs. 2.1** and **2.2**). This area is no longer a site of active deposition, these flank areas are subject to erosion and reworking into the centre of the basin. Similar areas to the south of the basin with predominantly Miocene age deposits are seen to be caught up in faulted contact with the basement rocks of the Internal Zone (see **Fig. 2.1**).

The late Miocene to Pliocene sequence represents a complete marine transgression-regression cycle (Fernandez, 1989). Five distinct sedimentary sequences are observed throughout the basin (Rodriguez-Fernandez et.al., 1989, Montenat et.al., 1990), separated by unconformable contacts. These unconformities are angular at the basin margins, testifying to tectonic control and progressive basement uplift throughout sedimentation. Towards the centre of the basin the contacts become paraconformities. In general coarse fans feed sediment from the fault controlled basin margins, which laterally, towards the basin centre, give way to finer grained shallow marine, evaporitic and lacustrine deposits in the central areas of the basin. Rodriguez-Fernandez et.al. (1989) identify five distinct depocentres controlled by the complex fault system in the basement.

Of the five depositional sequences, the oldest two are marine in character, and the youngest three are continental. The following section outlines the details of the five sequences, oldest first.

Late Serravalian-Early Tortonian. - ***La Peza and Quentar Formations***

Marine conditions. Conglomerates and sands deposited at basin margins, shallow marine calc-arenites and planktonic marls deposited in basin centre. Conglomerates and beach deposits sourced from the Alpujarride complex. In the south of the basin, near Alhama de Granada, nearshore deposits document the transgression onto the Internal zones during the early Tortonian (Fernandez and Rodriguez-Fernandez 1991). Rapid vertical facies changes

Fig. 2.1 Geological map of the Granada Basin showing the distribution of the main basement units of the External and Internal zones, and the ditribution of the main basin sedimentary sequences. The study area, depicted in Fig. 2.2, is indicated. Taken from Rodriguez-Fernandez et.al. (1989)

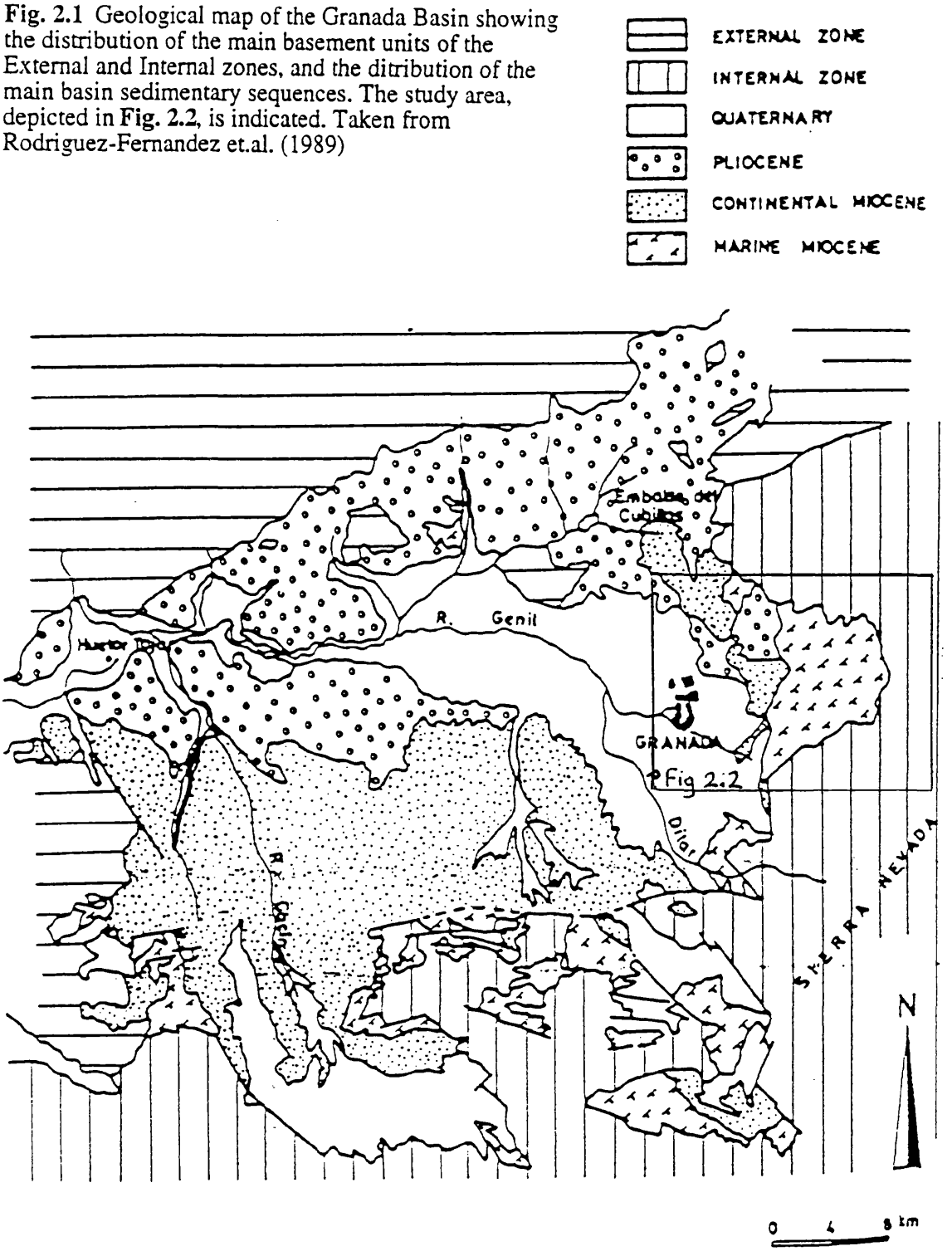

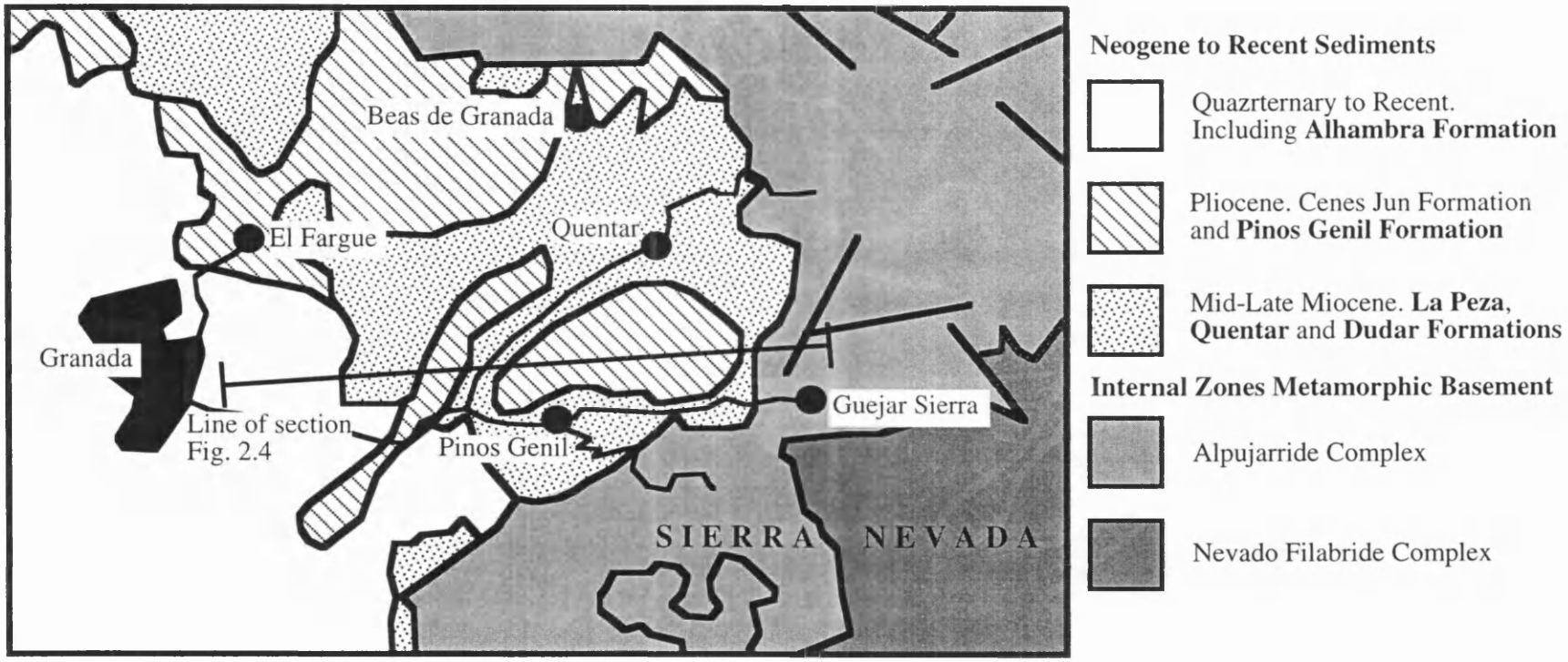

Fig. 2.2 Sketch map of the eastern flank of the Granada Basin, showing the main Internal Zone units of the basin substrate, and the main sedimentary formations.

indicate rapid early subsidence of the basin. Bioclastic sedimentation progressively took over from siliciclastic deposits, as subsidence slowed.

In the eastern margin of the basin the earliest sediments are shallow marine conglomerates composed of rounded dolomite clasts sourced in the Alpujarride complex. This rapidly gives way to calc-arenites, composed of dominantly bioclastic materials (bivalves, gastropods, foraminifera). Two formations are present; the **La Peza Formation** and the younger **Quentar Formation.**

*Late Tortonian. - **Dudar Formation***

Resting on the earlier sequence in unconformable contact. Coarse marine fan-deltas prograded from the edge of the basin towards a rapidly subsiding basin centre. According to Montenat et.al. (1990), the unconformity is discordant at the edge of the basin, becoming less angular towards the basin centre. Close examination of the contact near Pinos Genil is inconclusive about the nature of the contact between the fan-deltas and the underlying calc-arenite. It does not appear discordant, though it is the locus of shearing and sediment deformation. The onset of coarse clastic sedimentation marks the beginning of the end of the transgressive episode in the Granada Basin. Marls were deposited in the basin centre. As sea level dropped patch reefs formed in the north and south of the basin, and eventually evaporites in the centre. The sequence of fan-delta deposits at the eastern margin of the basin is known as the **Dudar Formation.**

*Pliocene. - **Pinos Genil Formation***

Alluvial Fans replaced fan deltas at the margins, and lacustrine conditions replaced marine in the basin centre. Continental deposition became fully established. The lacustrine sedimentation began with carbonate stromatolites, followed by laminated sands with important detrital gypsum (Rodriguez-Fernandez and Fernandez 1989).

The alluvial fan system dominates at the eastern margin and onlaps the basement, according to Rodriguez-Fernandez and Fernandez (1989). However, no evidence of this onlap has been seen at the eastern margin of the basin in the study area. This sequence rests in angular unconformity with the lower sediments at the basin margin next to the Sierra Nevada, indicating uplift of the earlier sequence prior to deposition of the Pliocene sediment. This sequence is known as the **Pinos Genil Formation.**

At the top of the Pinos Genil Formation a sequence of lacustrine silts and sandstones is developed. These are (tentatively) the **Cenes Jun Formation** deposits. They are grouped with the Pinos Genil Formation in a tectono-sedimentary unit as the contact between the two is conformable (Montenat et.al. 1990). The deposits correlate with the Messinian sea level drop in the Mediterranean. It was found to be difficult to establish clearly their distribution in the field. It was also decided to concentrate from the beginning on conglomerate grade material and interbedded sands, and as conglomerates are missing from the Cenes Jun Formation they are considered no further. This is not because they are not worthy of attention, but because resources for sampling and analysis had to be prioritised.

Late Pliocene-early Pleistocene. - ***Alhambra Formation***

Conglomerate deposition continued in alluvial fans prograding basinwards that formed a transverse drainage system. Lacustrine conditions persisted in the central area. In the study area alluvial conglomerates and sands are characteristic of this sequence, and are known as the **Alhambra Formation.**

Early-Mid Pleistocene

Conglomerates were deposited along the N border of the basin in a broad alluvial plain, and are not developed in the study area.

Each successive sequence occupies an increasingly smaller area, so the oldest deposits cover the largest area, and are now exposed well outside the active margin of the present day basin. The active Granada Basin has become smaller through time, a process that has incorporated earlier basin deposits into the flank areas, which become source areas for sediment. The active margin at the eastern edge of the basin in the study area, beyond which sedimentation takes place, is now located not in the metamorphic basement of the internal zones, but in the 'new' basement of previous basin sediments, which are now being reworked by the Rio Genil. The general geometry of the deposits at the eastern edge is of sequences separated by unconformities, with increasing dip towards the metamorphic basement rocks of the Internal Zones, that documents continued uplift of the basin edge throughout sedimentation. This suggests that this process has been continuous since the late Miocene. More evidence for basin uplift will be presented later.

2.2 Sedimentology of study area

Figure 2.3 is a graphical log representing the stratigraphy of the eastern border of the Granada Basin showing the generally course grained nature of the sediments. All sediments studied were from fan deposits, flowing transversely away from the source region in the Sierra Nevada. The following section briefly presents details of sedimentology in the study area, especially from the Dudar fan-delta formation, and also for those specific areas sampled for petrographic and geochemical analysis.

Figure 2.4 is a schematic cross section across the eastern border of the Granada Basin, the rough line of which is indicated on **Fig. 2.2**. Unfortunately a detailed published geological map of the areas south of Guejar Sierra, including Pinos Genil was not available to allow the precise drawing of a cross-section. The drawing was based on observations made whilst sampling. No mapping of the area was undertaken, so this section must be viewed with some caution. It shows the general stratigraphic and structural relationships between the different formations and the relative positions of the samples taken for petrographic and geochemical analysis.

La Peza and Quentar Formations

This is the first formation deposited in the east of the basin. At the unconformity with the Alpujarride substrate, there is a nearshore conglomerate composed of rounded Alpujarride dolomite clasts. Many of these clasts show borings, indicating deposition in a shallow marine to

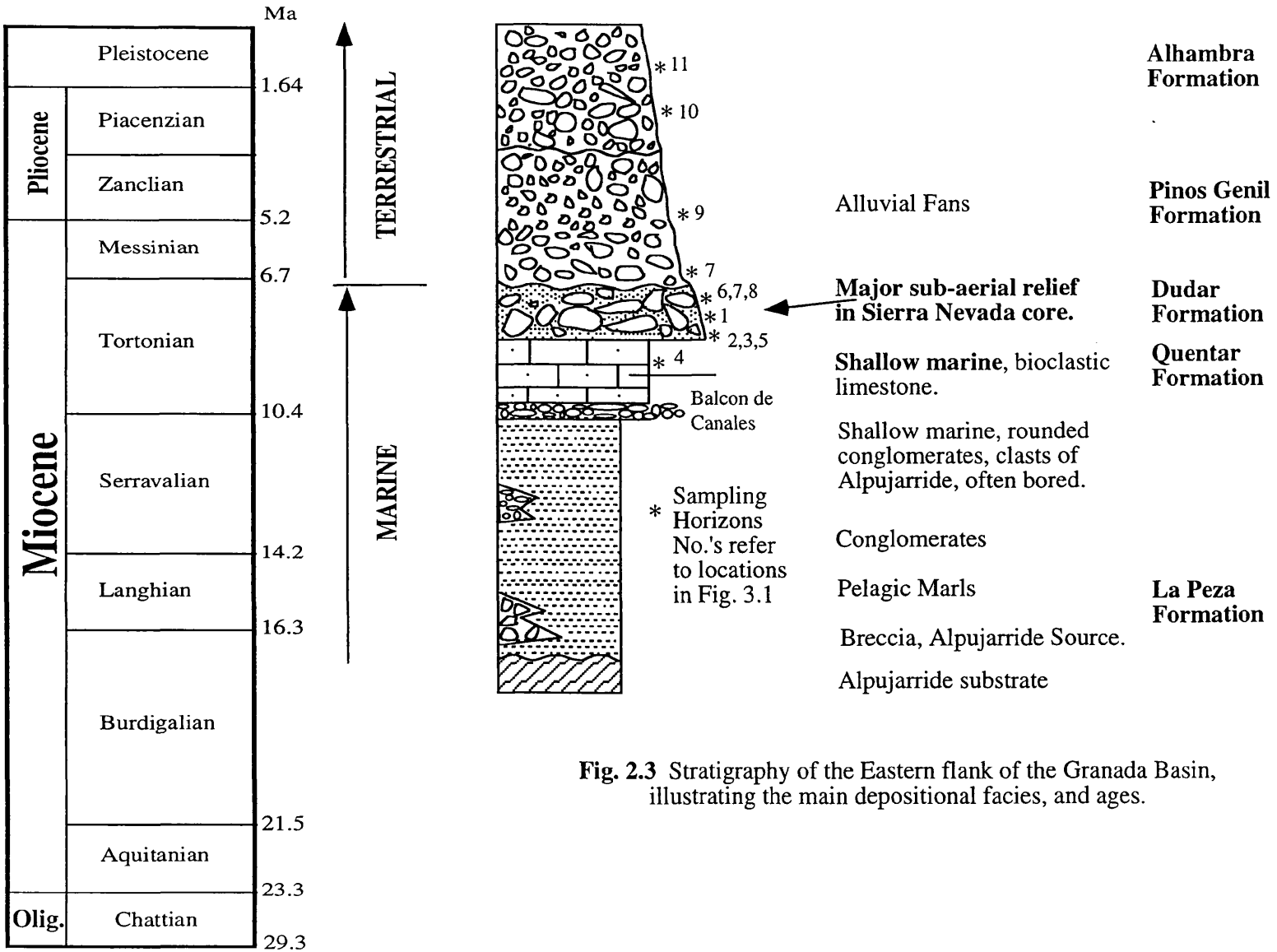

Fig. 2.3 Stratigraphy of the Eastern flank of the Granada Basin, illustrating the main depositional facies, and ages.

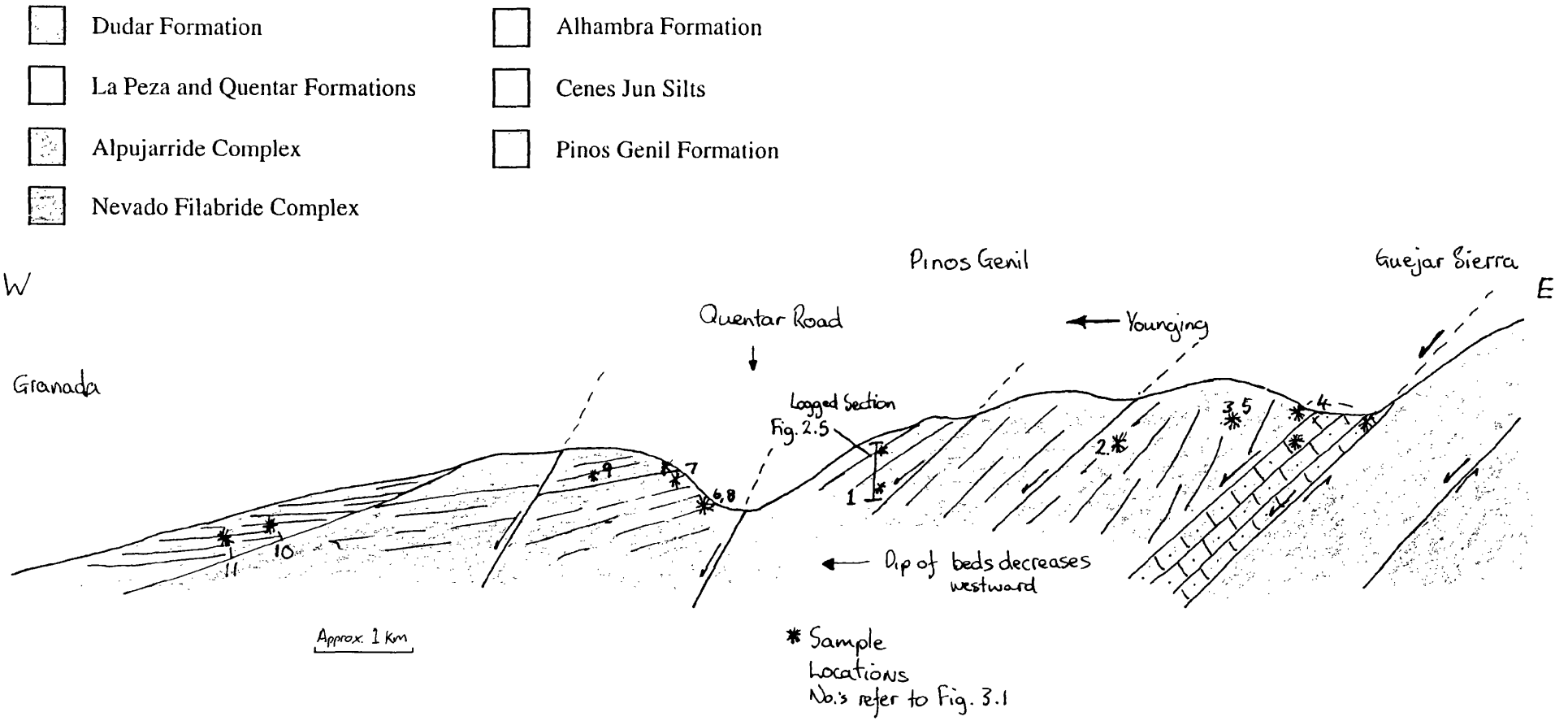

Fig. 2.4 Schematic cross-section through the eastern border of the Granada Basin. The approximaterefrence line for the section is shown on Fig. 2.2. The main features to note are the relative stratigraphic and structural positions of the different formations and the increasing dip of the deposits to the east, towards the basement. The positions of some of the faults and their angles of dip are speculative, they are shown hereto illustrate the general structure.

littoral environment. Water must have deepened soon after as thick bioclastic limestones, or calc-arenite, is found above the conglomerates. The calc-arenite forms the Quentar Formation, which often overlaps the La Peza formation onto the basement. It is a pale orange, resistant rock, that forms cliffs that exhibit thick bedding and dip steeply away from the basement concentrically around the edge of the basin, dipping northwards in the south and dipping west at the north-east margin, at an angle of 50°. It is composed mainly of coarse bioclastic material but also contains a significant component of siliciclastic detrital material, including much dolomite from the underlying Alpujarride. Up the section however, more quartzose material and fragments of mica-schist and other metamorphic rocks from the deeper Internal Zone units gradually appear. At the top of the section a blue and white marl unit marks the transition to the next formation

Dudar Formation

Just above the marl unit the first conglomerate clasts of Nevado Filabride rocks appear. This records the onset of uplift in the core zone of the Internal Zones in the Sierra Nevada, and the beginning of fan deposition in the Granada Basin. The Dudar formation is a marine fan-delta deposit, covering and area of around 100km^2. It consists of a sequence of grey-blue conglomerates, sands and silts, that thicken away from the basin margin. Conglomerates are more extensive in proximal areas in the south and east towards Pinos Genil and Guejar Sierra, with sediment fining towards the distal north west. The area around Dudar consists of sand and silt units. Most samples for petrographic, geochemical and isotopic work were taken from a section near Pinos Genil, in the proximal fan area.

A detailed sedimentary log was taken through this proximal part of the fan (**Fig. 2.5**), which shows the main features of the fan sedimentology. Coarsening upwards units are obvious, though in general sediment becomes finer towards the top of the fan, culminating in a 20m thick unit of blue-grey siltstones. Conglomerates were deposited in laterally continuous sheets sometimes traceable for 100's m laterally (**Plate 2.1**). They often have sharp, sometimes erosive bases (**Plate 2.2**) or can grade from, and to sand and silt units. This suggests rapid deposition in unconstrained sheet floods that spread out and cover large areas of fan surface. Conglomerate beds can be up to 20m or more thick, have no internal structure, are matrix supported and are poorly sorted. Imbrication is common in the conglomerates indicating a flow direction from the south and east .

Fine to coarse sand is dominant throughout the fan delta, in marked contrast to the conglomerate units. The transition between the two is often sharp, representing a change in sediment depositional regime. Sometimes sand beds fine upwards from pebbly units that can be directly above conglomerates, or within thick sand units. Bed thicknesses are typically less than 1m, usually around 10-50cm. Occasionally a sand unit shows some channels and truncation of underlying beds, and can sometimes interfinger with conglomerate beds. Fluidisation structures are common, especially in finer grained units and in silt beds. Rare cross laminations are the only flow direction structures visible. Fine ripple laminations are common in the sand and silt units.

Pinos Genil Formation.

This is composed of red conglomerates and sands, deposited in a sub-aerial alluvial environment. The contact with the Dudar formation is sudden, and clearly erosive in parts (**Plate 2.3**), where it is seen, but not demonstrably angular. Here it also represents a change from fine sediment deposition of silts with minor conglomerates, to coarse sands and increased amounts of conglomerate, which dominate the formation. The conglomerates are poorly sorted and matrix supported by coarse sand. They exhibit lens shaped geometry interfingering with less common sand lenses, and a crude bedding, suggesting deposition in channels of a braided system. Maximum clast size is smaller than the Dudar Formation, despite the general conglomeratic nature of the Pinos Genil Formation.

Alhambra Formation.

This rests above the silts and lacustrine sediments of the Cenes Jun Formation, in unconformable contact. It consists of red sands and conglomerates, deposited in an extensive sub-aerial alluvial setting, perhaps by a system of braided streams. Conglomerate clast imbrication indicates flow from the south east, but with an important flow component from the north east (**Fig. 2.6**). Conglomerates are generally massive, poorly bedded with little internal structure and are matrix supported. Compared with the Pinos Genil formation the Alhambra Formation has a higher proportion of sand.

The sediment in the Alhambra Formation is compositionally immature, though it is texturally more mature than the Dudar or Pinos Genil Deposits. It is much more weathered than the other formations at the eastern flank of the Granada Basin, and exhibits increased grain and clast break-up and dissolution, and extensive iron oxide grain and clast coating.

2.3 Structures in the study area

Deposits at the margin of the study area, at the unconformity with the Alpujarride basement dip basinward at angles up to 50°. Up section in younger rocks and in towards the basin centre, dip angles decrease and soon become near horizontal. Also dipping towards the centre of the basin there is a series of high angle normal faults, that cut the basin deposits and drop higher level deposits to lower levels (see **Plate 2.4**). The present erosion level would have removed them from view had the normal faults not been operating. **Fig. 2.4** illustrates in a schematic form the general structure of the deposits in a cross section running east-west including the large scale faults and the decreasing dip of the sediments to the east.

Elevation decreases away from the basin edge, so older deposits not only dip at a higher angle towards the basin centre, but are at a greater elevation. These observations indicate that the edge of the basin has been uplifted as the Internal Zones in the Sierra Nevada have risen. This is indicated also by the transition to terrestrial depositional conditions at the top of the Dudar Formation at the unconformity with the Pinos Genil Formation.

Throughout the Dudar Formation there is considerable evidence for soft sediment deformation, and the effects of syn-sedimentary extension. At the base of the fan, deposits at the contact above the calc-arenite, and also within the fan-delta itself, shearing has taken place producing a tectonic fabric, and sometimes reorienting imbrication. Small thrust detachment

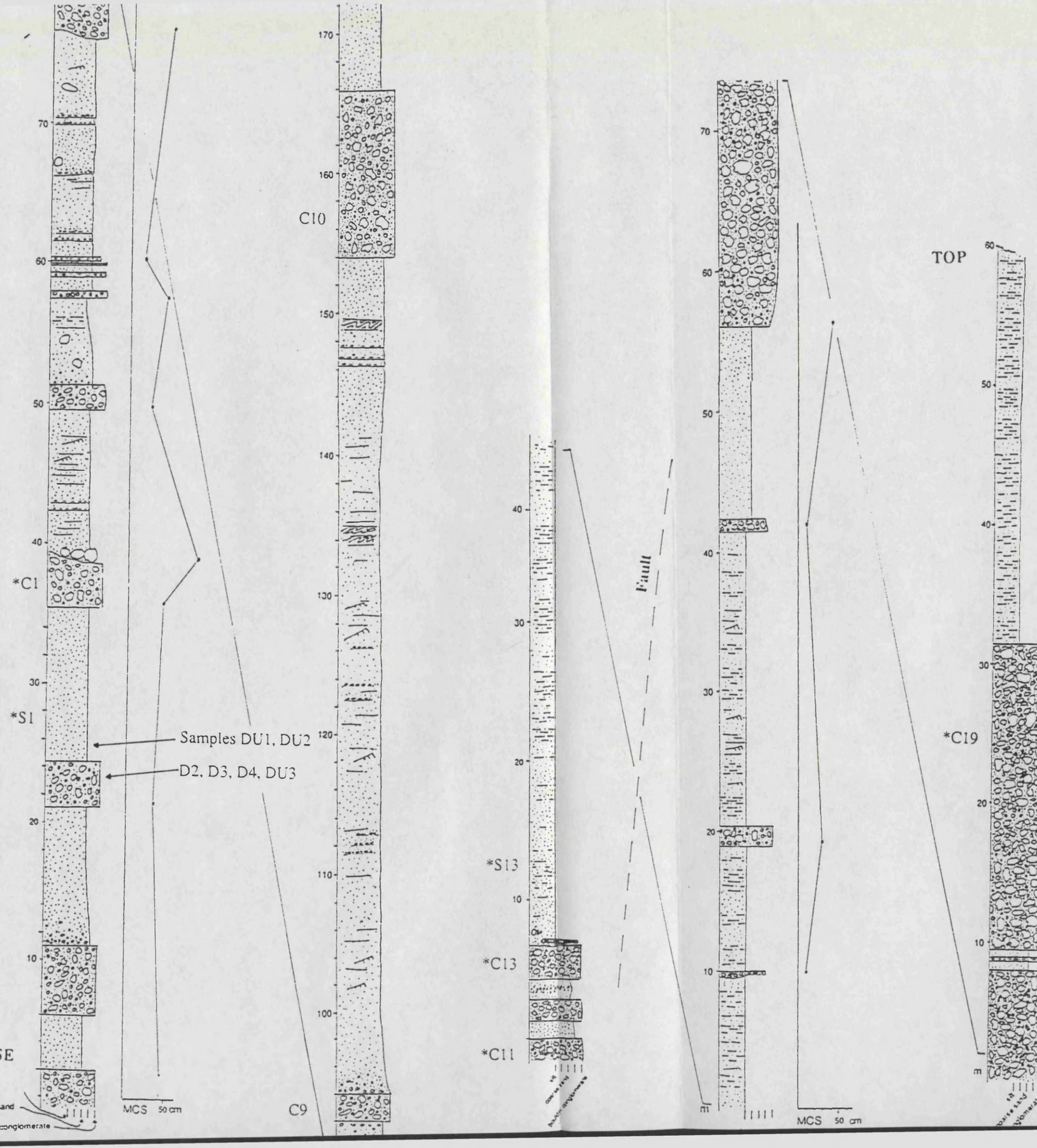

Fig. 2.5 Sedimentary logs through the central and upper part of the proximal fan-delta deposits of the Dudar Formation, immediately north of Pinos Genil town. This section of fan is extensively faulted, which makes the following of a continuous sedimentary section difficult. Attempts were made to correlate distinctive sand bodies where possible. Silt and sand dominate the fan deposits. Coarsening upwards trends are just visible in the lower sections of the log.

Key

MCS Maximum Clast Size.

Erosive base.

Cross lamination.

Sediment slumping and dewatering structures.

Pebbly bed bases to fining upwards beds.

* Sample sites for conglomerate clasts and detrital micas for dating work, and sandstones for petrography, heavy mineral analysis and geochemistry.

planes with slickenside development are abundant, often with stepped geometry and en-echelon arrangement (**Plate 2.5**). Extensional cleavage is incipient in several places, forming in near unconsolodated sediment. Mud diapirs and other evidence of fluid diseqilibrium can also be found (Munro, 1995). Altogether there is abundant evidence for sediment instability, related to basin instability. The uplift of the marginal deposits is testified to by the increasing dip towards the basement. This uplift may have created gravitational instabilities in the marine fan-delta deposits causing movement away from the source area which extended the whole deposit. This point is developed in the next chapter.

Plate 2.1 Laterally continuous sheets of conglomerate as part of a coarsening upwards unit in the Dudar Formation. Looking west at Location 1, **Fig. 3.1**.

Plate 2.2 Sharp erosive base to pebbly conglomerate bed in Dudar Formation at Location 1 (see **Fig 3.1**).

Plate 2.3 Unconformable erosive contact of the Pinos Genil Formation (Upper pale red deposits) on top of the grey marine deposits of the Dudar Formation at location 6 (Fig. 3.1). Lower planar beds are truncated by channels of the Pinos Genil Formation.

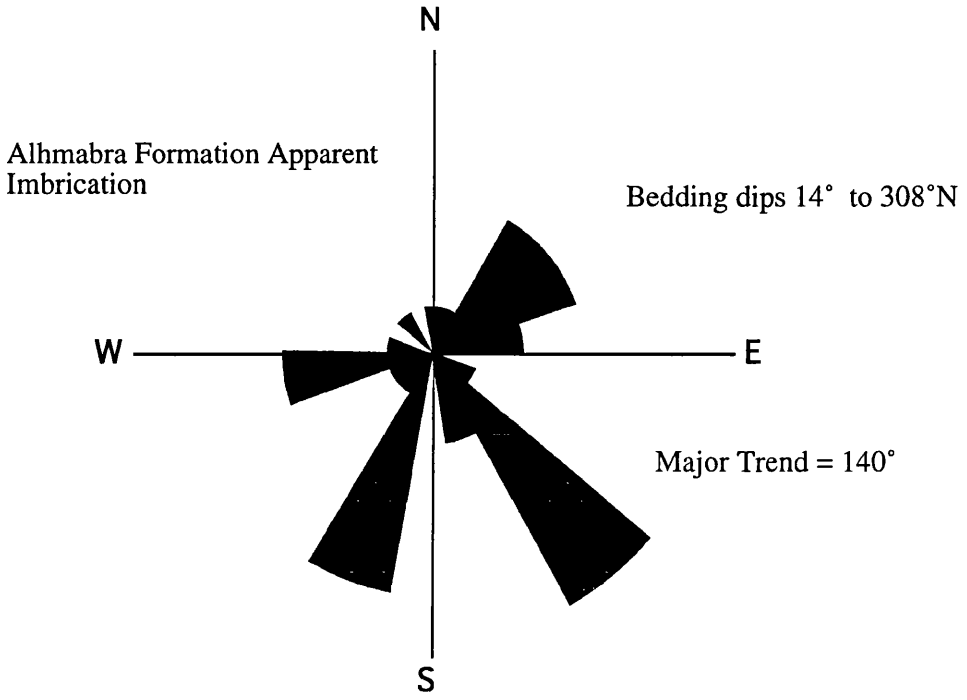

Fig. 2.6 Apparent imbrication from Alhambra Formation Conglomerates indicating flow from the south dominantly, but also a source in the north-east. The dip of the beds is low so measurements are uncorrected, as the dip of the beds makes no significant difference to indicated palaeoflow.

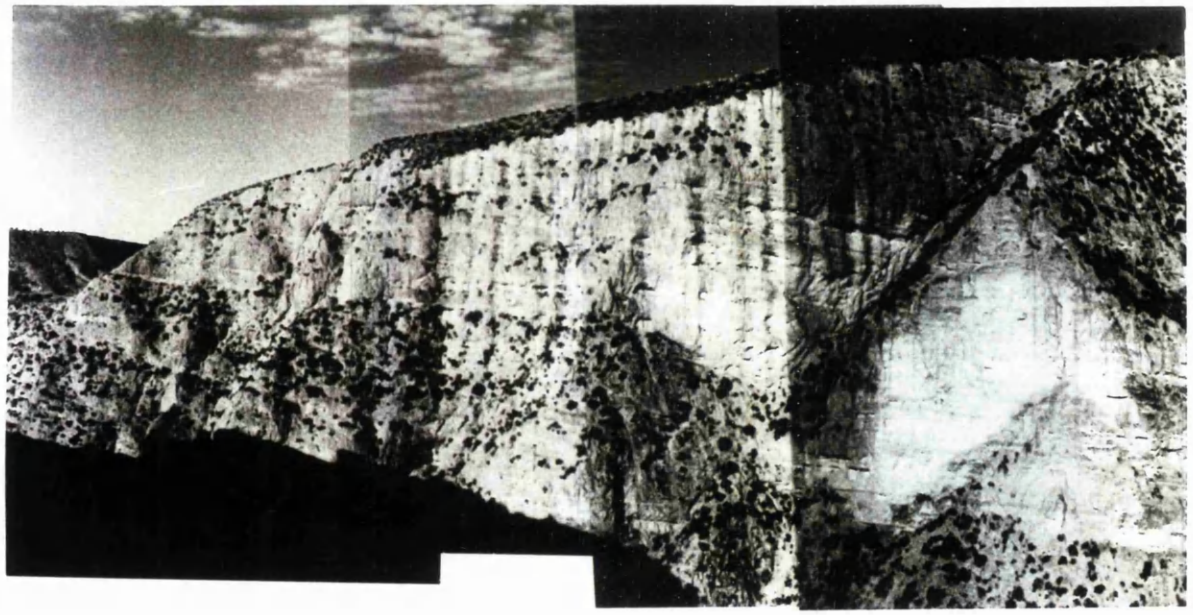

Plate 2.4 Large scale high-angle normal faults in the upper Dudar Formation. West is to the left, towards the basin. These faults are angled basinward and drop higher levels of deposits to succesively lower levels.

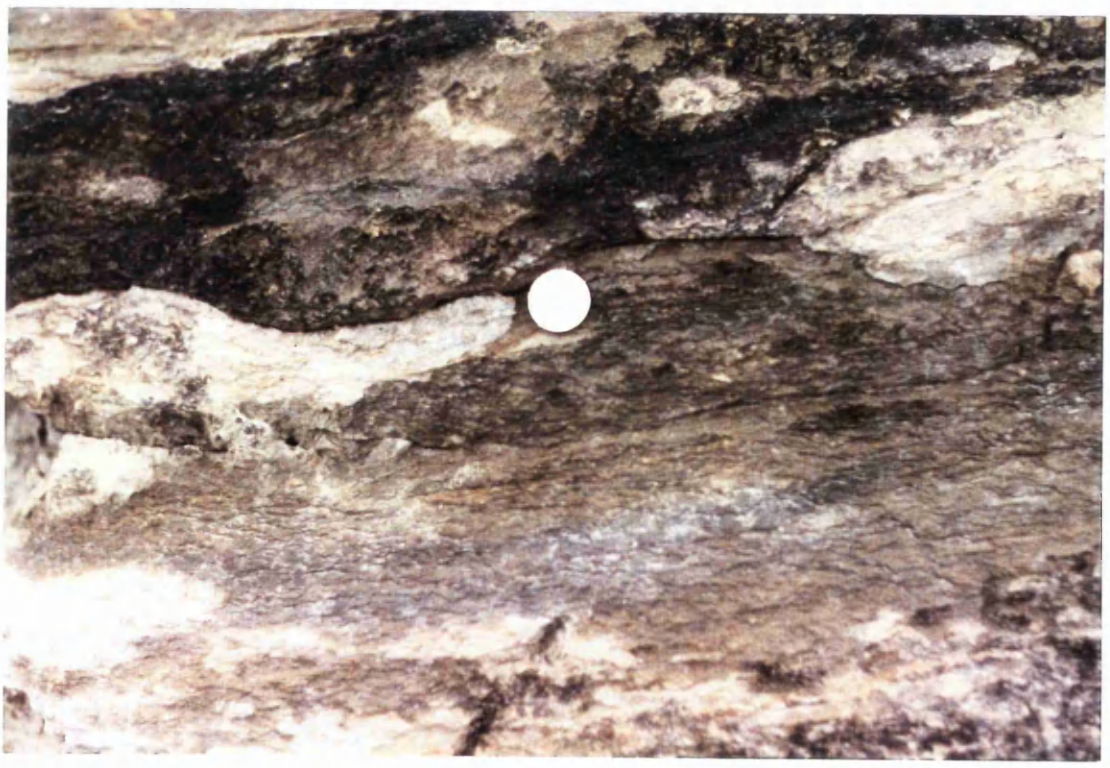

Plate 2.5 Small scale deformation features in silts of the Dudar Formation fan-delta. Top photograph shows en-echelon arrangement of detachment planes that exhibit polished surfaces and slikenside development. Lower photgraph shows tectonic fabric that runs bottom right to mid-left transversely acrross bedding laminations that go from bottom left to mid-right. This fabric may be cleavage that is developing in response to pervasive extension of these mostly poorly conmsolidated and non-cemented sandstones.

3. Granada Basin Conglomerate Petrography

3.1 Introduction

The main aim of this project is to study the evolution of the composition of sedimentary basin infill in continental intramontane settings. A stated objective, presented in section 1.2, is to document the compositional characteristics of the sediment in each basin included in this study. This section presents details of conglomerate composition and texture for each of the three Miocene to Pleistocene fan formations at the eastern edge of the Granada Basin. The sedimentology and stratigraphy of these have been described in section 2.5.

The range of clast types is given in detail, and then stratigraphic variations are presented. Following this, variations of clast composition with size is discussed for selected conglomerate horizons from the three formations. From these data conclusions are drawn about the evolution of the source of the sediment in the Granada Basin, but also about *sediment dynamics* within the basin, especially concerning the possibility of sediment recycling, and the effects this has on provenance information carried by sediment.

The Eastern flank of the Granada basin is ideal for considering sediment dynamics, and the effects of sediment recycling in particular, for the following reasons:

1. Source Variation

Each formation has the same ultimate source region; the Internal Zones within the Sierra Nevada. This is constrained by palaeocurrent measurements. Variations in lithologies exposed within a source region over time during progressive erosion may be expected to be manifest as stratigraphic variations of composition in sediment derived from such a source. However, the lithologies currently exposed in the Sierra Nevada source region are the same as those observed *throughout* the fan formations of the adjoining Granada Basin. All clasts in the Dudar Formation (the oldest detrital formation, at the base of the stratigraphic sequence) can be matched to lithologies exposed currently within the source region. As the present erosion level of the Sierra Nevada is lower than the erosion level that was the source of material for the Dudar Formation, the vertical lithological variability of the Sierra Nevada must be small, and no significant stratigraphic variation in clast composition of conglomerates sourced from the Sierra Nevada should be expected. Thus with such a consistent source through time, any significant variations in composition and textural maturity within the conglomerates of the Eastern Granada Basin cannot easily be related to changes within the source region, but are more likely to be related to variations in erosional and depositional processes (i.e.. *sediment dynamics*) within the basin. Another possibility is that any compositional and textural differences may be related to processes of sedimentary recycling. This would perpetuate the appearance of a non varying source whilst increasing textural maturity. The next reason

provides additional evidence for the possibility of sediment recycling within the Granada Basin.

2. Depositional Geometry and Syn-Sedimentary Tectonism

The geometry of the sedimentary formations indicate syn-depositional tectonism, and strongly suggest the possibility of reworking of older sediments into younger deposits. The oldest formations, the *marine* La Peza, Quentar and Dudar formations, dip at angles between 35-50° away from the Internal Zone basement outcrops, towards the centre of the basin. Overlying these, younger deposits, the *terrestrial* Pinos Genil and Alhambra Formations dip at significantly shallower angles or are near horizontal. Thus angles of dip increase with age in formations progressively nearer the source region. Older deposits are also at a higher elevation at the edge of the Basin at the contact with the Internal Zones basement.

All this indicates progressive uplift of the oldest deposits at the edge of the basin *during or before* deposition of the younger sediments. Formations are separated from each other by unconformities, and each formation offlaps towards the basin centre, indicating a *shift of depocentre* away from the basin edge. This shift of depocentre would have been forced by the uplift of the basin edge area. Because of the uplift, this area ceased to be a centre of deposition, and would have been liable to erosion as it was at a greater elevation than the active depocentre. The older deposits could have been incorporated into the source area ready to be eroded into subsequent deposits in the basin. In this way deposit can become source and sediment can be recycled. As the main drainage from the source region feeding sediment to the basin must have passed through the uplifted sedimentary deposits, it is reasonable to suggest that erosion may have been greater in these softer, relatively unconsolodated sediments, compared with a hard, primary metamorphic source in the Sierra Nevada.

Three formations with different depositional facies formed as a result of these syn-depositional tectonics and changing sea level (probably also tectonic). Each has a different apparent textural and compositional maturity, but as argued they all share the same source. The eastern Granada Basin is therefore suited to the examination of sedimentary dynamics as they affect the composition and source signature of intramontane sediments.

Data is presented below on conglomerate texture and composition. This chapter aims to use these data to constrain any variation in source characteristics with time and also to constrain the possibility of sedimentary recycling as a result of the uplift, and inclusion into the source region, of the oldest deposits at the basin edge.

3.2 Sampling Locations

Sampling locations are depicted in **Fig. 3.1**. These are the places that all the samples analysed in this thesis were taken from; for sandstone petrography, geochemistry, heavy mineral analysis and isotopic dating. The same samples are used throughout, for consistency when detailing compositional parameters. All locations are listed with the samples that were taken from those locations. **Fig. 3.1** is relevant to all chapters and is often referred back to. The relative stratigraphic positions of the samples are referred to in **Fig. 3.1**, but they are better

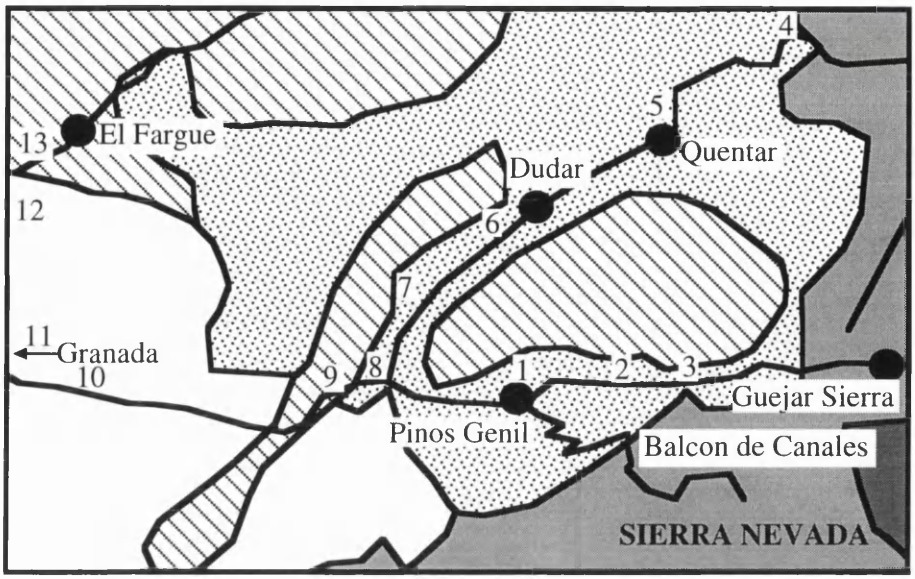

Fig. 3.1 Locations of sediment sample sites for petrographic and geochemical analysis.

Sample Sites:

1. DU1, DU2, S13. Also location of logged section through proximal mid-upper fan delta.

2. Base Dudar Formation, white marls, sandstones. Samples 4.1, 4.2.

3. Top Quentar Formation calc-arenite, transition to base Dudar Formation fan delta. Samples CA 1.1, CA 1.2, FD 1.3, FD 2.1, FD 2.2, FD 2.3, FD 2.4, FD 3. All samples in approximate ascending stratigraphic order.

4. Basin unconformity with internal zones Alpujarride complex. La Peza Formation calc-arenites. Samples QR1 (Alpujarride) and QR2.

5. Quentar formation calc-arenites. Samples QR3 and QR4.

6. Distal fan-delta deposits of Dudar Formation. Fine grained sands and silts. Sample D1.

7. Distal fan-delta deposits of Dudar Formation, and earliest alluvial deposits of Pinos-Genil Formation. Samples FD 6.1, FD 6.3 and PG 6.2.

8. Distal fan-delta deposits of Dudar Formation. Sample FD 5.8.

9. Conglomeratic alluvial deposits of Pinos Genil Formation. Samples PG 5.1, 5.2, 5.3, 5.4, 5.5, 5.6, 5.7. Sample spread over 200m lateral area, and 20m stratigraphic section.

10. Alhambra formation, at extensive Roman Gold Mines. Samples A. 9.1, 9.2, 9.3, 9.4, 9.5, 9.6.

11. Alhambra formation conglomeratic alluvial deposits. Samples A. 8.1, 8.2, 8.3.

12. Alhambra formation. Sample A. 12.1.

13. Silts of the Cenes Jun Formation. Samples 10.1, 10.2.

appreciated on **Figs. 2.3** and **2.4**, the schematic stratigraphic log and cross section of the eastern Granada Basin.

For this chapter, conglomerates were sampled at locations 1 , 7, 9 and 10.

3.3 Conglomerate Texture and Clast Roundness

Roundness has been qualitatively measured for each of the three formations examined in this study, using the visual comparison charts of Pettijohn et.al.(1973). **Figure 3.2** presents the data collected from selected conglomerate horizons within each formation. Around 30-35 clasts were considered from each sample, and as can be seen the differences between formations are small. These roundness data are qualitative only and inferences drawn from them can carry only a small significance, and cannot be used in isolation as evidence for increased conglomerate maturity in the younger formations.

Dudar Formation

The sediment of the Dudar Formation is compositionally and texturally immature. Conglomerate clasts are fresh and unweathered, and the marine deposits are free from a coating of red iron oxide. The conglomerates are massive, with no internal sedimentary structures and are mostly matrix supported (**Plate 3.3**). **Figure 3.2a** presents the measurements from two conglomerate horizons in the Dudar Formation. The largest single mode is sub-rounded, and the range extends from angular to rounded clasts. For C1 there is a skew towards subrounded and rounded clasts. In C12 the skew is towards angular and sub-angular clasts. In each, and for the clast size interval measured (up to 50cm across for these examples) no very angular or well rounded clasts are seen (see **Plates 3.4**).

The clast size in the Dudar Formation is extremely variable, and the formation as a whole is poorly sorted. Common average maximum clast size of conglomerate horizons are between 20-45cm with some clasts over 1m. The maximum size of clast observed was upwards of 3m, composed of Nevado Filabride, Veleta Complex graphitic schist (**Plate 3.6**). These mega-clasts appear often to be sub-rounded to sub-angular, though this depends on the exact lithology. Schistose lithologies with a strong planar fabric can be angular to very angular in large blocks (**Plates 3.8, 3.9**), contrasting with the less angular nature of smaller clasts.

Pinos Genil Formation

Again the conglomerates in this formation are matrix supported. However they are better sorted than the Dudar Formation deposits and have some sedimentary structures, cross bedding and channel features. **Fig 3.2b** depicts roundness for two conglomerate horizons at sample site No. 9 on **Fig. 3.1**. For PG1 the distribution is quite even around a mode of sub-rounded clasts. In PG2 the distribution is tighter, around rounded clasts as a maximum mode. The spread of values is greater then for the Dudar Formation, and well rounded clasts appear for the first time. Angular clasts are not present in PG2 The Pinos Genil formation is marginally more texturally mature than the Dudar Formation.

Alhambra Formation

Conglomerates in the Alhambra Formation are matrix and sometimes clast supported

c) Alhambra Formation

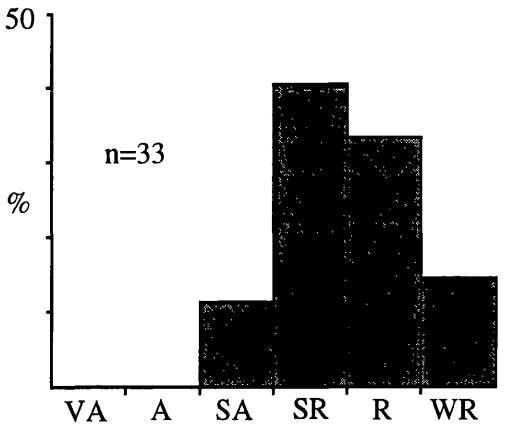

b) Pinos Genil Formation

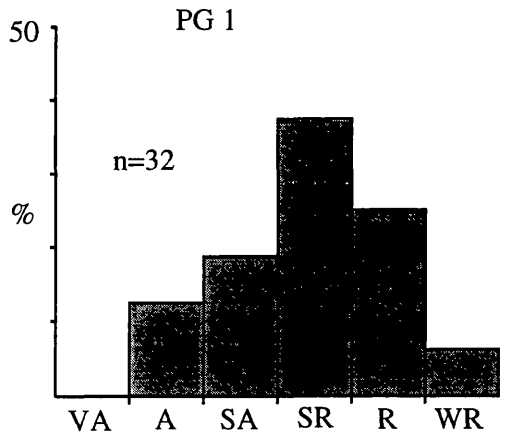

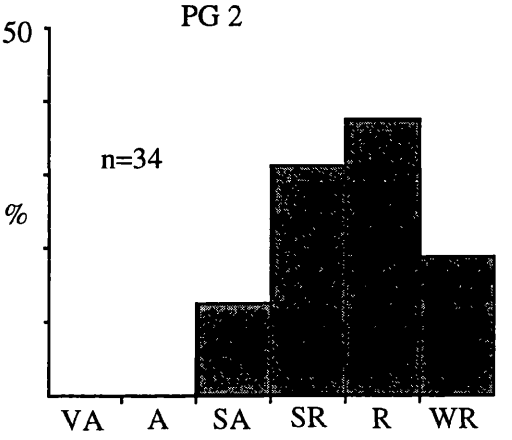

a) Dudar Formation

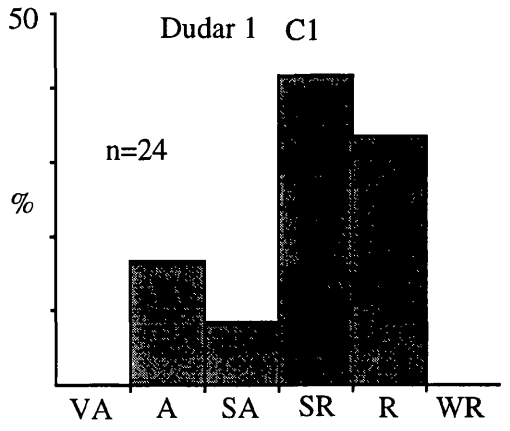

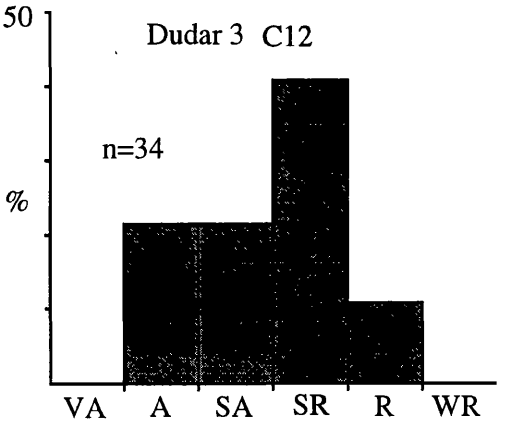

Fig. 3.2 Estimates of clast roundness in selected conglomerates from each of the three sampled formations from the eastern edge of the Granada Basin. The graphs are arranged above in ascending stratigraphic order.

Plate 3.1 Outcrop of Feldspar-Tourmaline Mylonite in detachment in Mulhacen Unit of the Nevado Filabride Complex within the Sierra Nevada source region at 2000m approx. Note high strain fabric and high angle brittle normal faults running top left to bottom right. These faults can control the break-down of the rock into large angular rectilinear blocks.

Plate 3.2 Schist outcrop some 1m below **Plate 3.1**. Illustrates how schist lithologies break into platy clasts controlled by the priminant schistose planar fabric.

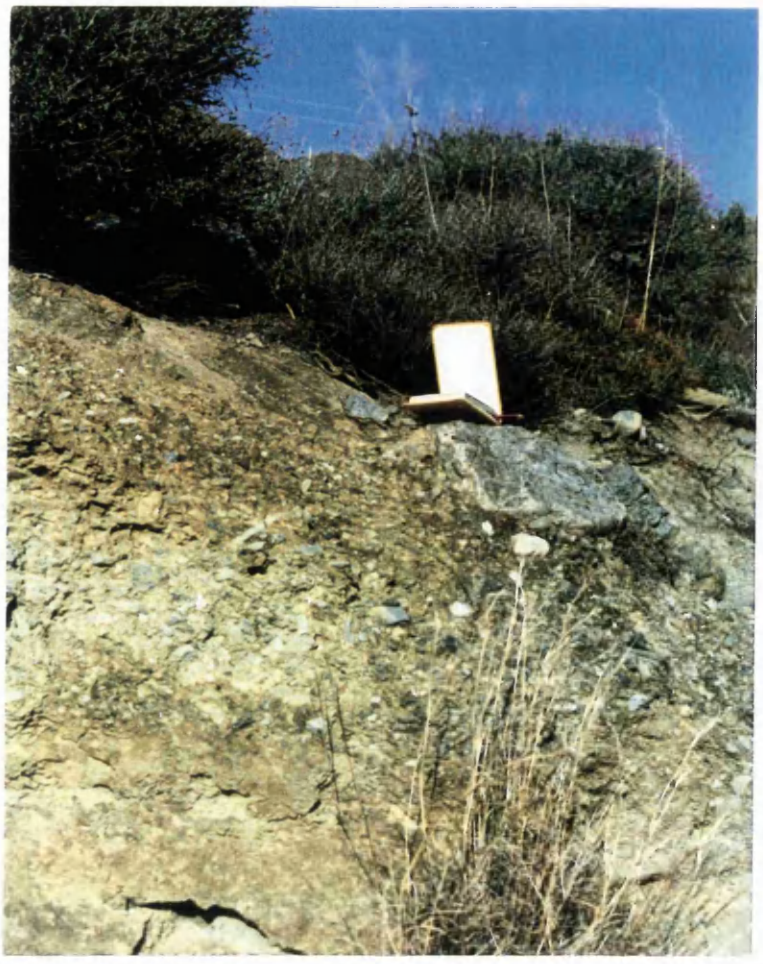

Plate 3.3 Conglomerate texture of horizon C3 within logged section (location 1, and Fig 2.4). Matrix supported

Plate 3.4 Conglomerate texture. Horizon C1 Dudar Formation location 1 (**Fig.3.1**, and **2.6**) matrix support

Plate 3.5 Poorly sorted matrix supported conglomerate, horizon C8 Dudar Formation, location 1 (Fig. 3.1). Note large angular clasts. At the top is a large clast of amphibolite. Most clasts are sub-rounded to sub-angular.

Plate 3.6 Mega Clasts in the Dudar Formation, location 1 (Fig. 3.1) above Pinos Genil Town. Tape measure scale is 1m.

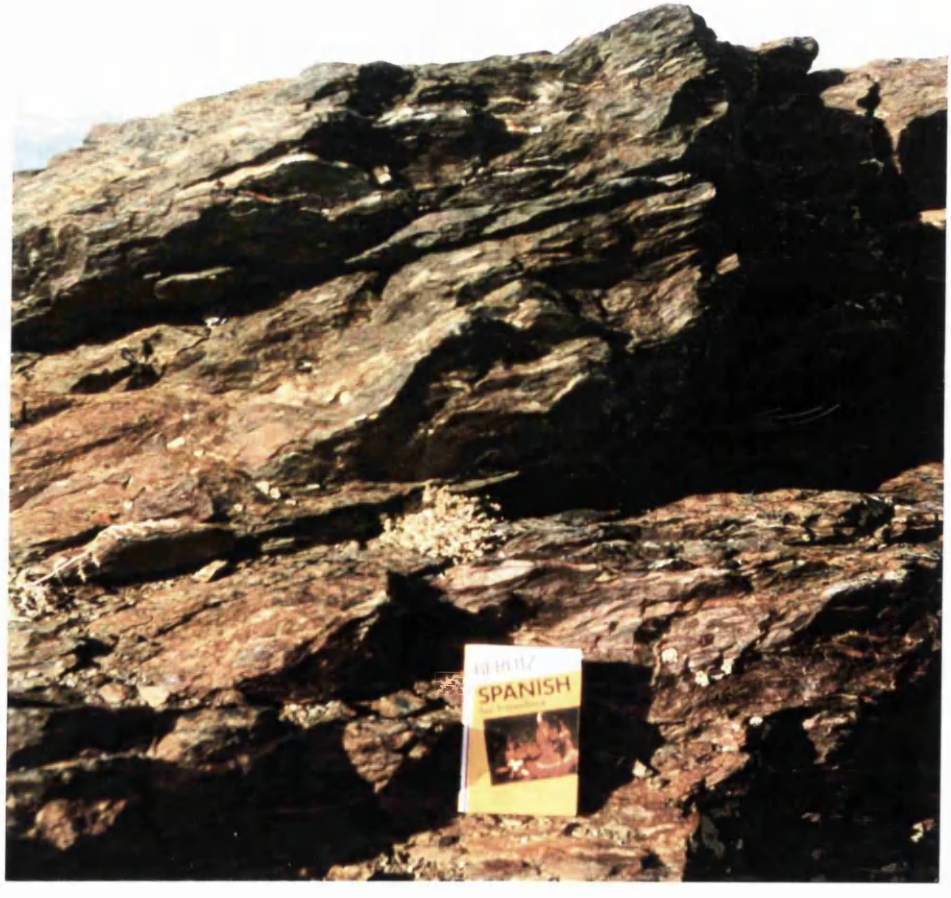

Plate 3.7 In-situ exposure of Veleta Unit schists in the Sierra Nevada at 2500m elevation, for comparison with the clast in Plate 3.6 above. Phrase-book is 14cm tall.

Plates 3.8 and 3.9 Large 1m size clasts in the Dudar Formation at approximately location 3 (**Fig. 3.1**). Some are sub-rounded to rounded, but others are very angular, defined by strong schistocity. These are high grade metamorphic rocks derived from the Veleta and Mulhacen Units of the Nevado Filabride Complex.

Plate 3.10 Typical texture of Alhambra Formation conglomerate, showing a mixture of matrix and clast support. Clasts are dominantly rounded or sub-rounded. Compared with the Dudar Formation this represents a measurable increase in textural maturity in detritus derived from the same source.

Plate 3.11 Mega-clast of Veleta Unit schist in the Alhambra Formation at location 10. For such a large clast there is a (tentative) suggestion of a rounded outline.

and poorly sorted. **Fig. 3.2c** shows a qualitative estimate of the roundness distribution of clasts in the conglomerate horizon shown in **Plate 3.10,** at sample site No.10 on **Fig. 3.1**. The largest single class are subrounded clasts, with a distribution ranging from subangular to well rounded. No very angular and, for the first time, no angular clasts are present. Some 3-4m long clasts of Veleta complex schists are found in the formation (**Plate 3.11**) something which is difficult to explain.

3.4 Clast types

Ten clast categories were used for counting clast type abundances. These subdivisions evolved after examination of the complete clast assemblage, and represent the best subdivision possible without sacrificing useful compositional and provenance information. Details of each are presented below. Often clast types are brought together under genetically linked categories, such as the amphibolites, marbles and the tourmaline rich gneisses and mylonites. In these cases it was impractical to subdivide and count a statistically significant number of each sub-category. The general range of lithological variation is described for each. The abundant schists are a case apart, as it was possible to subdivide the group and count enough clasts of each type.

For each clast type firstly the lithology is described including any variations present. After this the provenance of the rock type is presented. Following this a qualitative description, were possible, of the characteristic form of rock breakdown at the point of erosion within the source is presented. This is to give some idea of how each lithology reduces in size through breakage.

Vein Quartz

Description: Hard, 'milky' white and yellow, vitreous crystalline quartz. Pure examples only, if found with fragments of country rock attached attributed to vein quartz category only when more than 70 to 80 % of clast was vein quartz. Otherwise categorised by the rock type attached.

Provenance: Veins occur throughout the Internal Zone rocks, noticeably in the schists of the Veleta unit, where they are often folded into late foliations. The Alpujarride is extensively veined, some of which are quartz.

Quartzite:

Description: Grey crystalline type.

Provenance: Found in some units of the Alpujarride basement in the western Sierra Nevada.

Dolomite

Description: Grey-blue brecciated fine grained, muddy carbonate, often with veining between fragments of breccia. The veins consist of coarse crystalline carbonate and quartz. Some clasts exhibit a tectonic foliation and evidence of shearing, and small scale folding of veins.

Provenance: Typical of Alpujarride in the north and west of the Sierra Nevada,

beneath tertiary sediments of the basin, where it is up to 1km thick. Here it weathers sometimes an orange colour, and breaks easily along brecciation surfaces. The blocks so produced are often small and angular. Much brittle faulting appears to have caused this brecciation and perhaps facilitated veining.

Marble

Description: Seen in two forms, as angular fragments of coarse crystalline type with thick bands of mica in schistose fabric, and as small rounded orange clasts with finer grain size and homogeneously distributed 1mm (approx.) size muscovite grains, also in a schistose fabric.

Provenance: Marble is only found in the Sierra Nevada in the Mulhacen Unit of the Nevado Filabride Complex, in a 10m thick section (see below).

Serpentinite:

Description: Fine grained, pale green with concentrations of chromite. Some examples show evidence of shearing, as the chromite inclusions are streaked out, compared to their usual equant shape.

Provenance: The source for serpentinites is in the Ophiolite unit of the Mulhacen Unit within the Nevado Filabride Complex. It forms small flat clasts, controlled by a slight foliation in the rock.

Amphibolites

Description: A group of related rock types that show variation in texture and mineralogy. Some are coarse grained, with dominant amphibole and interstitial feldspar while some have a similar colour and mineralogy but can be finer grained and exhibit a tectonic fabric. Others are fine grained and consist entirely of dark green amphibole. One variety has greater than 50% leucocratic minerals in a medium grained non-foliated texture, and often appears badly weathered. Garnet amphibolites are common, often exhibiting a crenulated and folded foliation with muscovite. The garnets are 1-2mm maximum size and are predominantly almandines.

Provenance: The source for meta-igneous rocks in the Sierra Nevada area is the ophiolite unit of the Mulhacen Complex within the Nevado-Filabride. In the source, similar rock types weather badly, and do not produce large blocks on erosion, unlike the blocks seen in the Granada Basin conglomerates.

Tourmaline Mylonite

Description: This is again a group of similar rock types. Typically they occur as coarse grained granitic augen gneisses. The main foliation consists of muscovites, often of a greenish type, and quartz. Porphyroblasts of black-dark blue tourmaline are common, in sizes up to 2mm. The main augen are of white alkali feldspar, sometimes up to 1cm across. Some examples show a highly deformed mylonitic texture, with much stretching of grains, and extensional breaking of tourmaline augen (**Plate 3.1**).

Provenance: Clearly from thrust or detachment zones, probably from within the

Mulhacen complex, which contains several interthrust rock sequences, and in particular the Caldera unit (Diaz de Federico 1990). One notable exposure on the roadside within the Mulhacen complex exhibits a tourmaline mylonite with a stingily stretched fabric of quartz and feldspar, in contact with a dark, pelitic mica-schist, which is also strongly foliated (**Plate 3.1**). The whole outcrop is cut by high angle normal faults, perpendicular to the thrust plane and the foliations in the rocks. As a consequence of this at this exposure, the tourmaline mylonite is breaking into large, square angular blocks, but also small thin flakes, braking up along the mylonitic foliation.

Schist Group:

This includes a wide variety of lithologies, and in reality represents a probable continuum of rock types. Subdivision was based on provenance characteristics and the perceived resistance of the rock type to breakdown. For example the higher the quartz content the more resistant the rock is to abrasion. The development of foliations that encourage rock splitting may also be inhibited by higher quartz contents. The graphitic schists are less resistant to abrasion and breakdown and also exhibit a strong schistosity. They are more likely to show early size reduction and maintain an angular shape. The descriptions given here are characteristic of the range of rock types, and are representative in as much as they classify all schists present in the conglomerates. Provenance is a more difficult to specify. However, the focus of this story is predominantly on sedimentary dynamic processes, so the most important aspect of these descriptions is their ability to allow a consistent recognition of rock types that can facilitate comparisons of compositional range between formations.

At the outcrop within the source, schists produce angular blocks, sometimes equant but more often tabular. They are liable to brake along cleavages but also joints. Also produced is sand sized material especially rich in mica, akin to the actual composition of the sand found within the Granada Basin. **Plate 3.2** shows in-situ brake down of schist within the Mulhacen unit of the Nevado Filabride, below the contact with a tourmaline mylonite outcrop, this schist itself is highly strained. However, it demonstrates the break down of schistose rock into angular plate and blade shaped clasts, along with much sandy material. Also found at this outcrop were angular, equant blocks as mentioned above.

Mica Schist

Description: This is non-graphitic, with no garnet and <50% quartz. It can be medium to coarse grained (0.25-2mm approx.).

Provenance: Non graphitic schists originate within the Mulhacen unit of the Nevado Filabride complex, as part of the sequence of meta-sediments attributed to the Mesozoic.

Quartz-Mica Schist

Description: Includes several variations. All have significant (>50%) quartz content and are by definition non-graphitic.

Provenance: Again from the Mesozoic sequence within the Mulhacen Complex of the Nevado-Filabride.

Graphitic mica schist and graphitic garnet-mica schist.

Description: Course grained dark grey/black, with phyllitic 'sheen' on graphitic surfaces. Often shows red oxidation, and alteration of muscovites. Coarse folded foliations with important quartz layers and veining, and often large almandine garnets.

Provenance: Predominantly from the Veleta Unit of the Nevado-Filabride complex. This contains up to 6km of graphitic schists, so is the prime provenance for these clasts. The lower parts of sub-units within the Mulhacen unit are composed of graphitic schists of the same type, forming a Palaeozoic 'basement' to the diverse Mesozoic 'cover' sequence of schists, marbles, quartzites and ophiolite rocks (Diaz de Federico 1990).

Garnet-Mica schist

Description: Some variation in type, but commonly coarse grained with micas 2-3mm in size, and euhedral garnet porphyroblasts up to 5-7mm in diameter in folded and crenulated schistocity. Quartz content can be high, up to 50%. Other examples are finer grained with 1-2mm diameter garnets, and can be slightly graphitic.

Provenance: Coarse, non-graphitic muscovite schists are not present in the Veleta unit, but only within the higher, 'cover', parts of the units within the Mulhacen complex. At outcrop these rocks break along their schistocity to form angular, blade shape blocks. They also produce a coarse muscovite rich sand, found at outcrops often in large amounts.

Phyllite

Description: A fine grained, low grade metamorphic rock with a weak planar foliation. Dark in colour due to high graphite content.

Provenance: Within the Alpujarride complex. Outcrops are seen below the extensive grey dolomites. Also from the upper units of the Mulhacen group within the Nevado Filabride complex (Diaz de Federico et. al., 1990).

3.5 Clast Provenance

Palaeocurrents in the fan deposits of the eastern border of the Granada Basin indicate flow from the south and east (**Fig. 2.4**), in which direction lies the Sierra Nevada with its outcrops of the Alpujarride and Nevado Filabride complexes of the Internal Zones. The clast composition of the Granada Basin sediments resembles closely the metamorphic rocks exposed within the Sierra Nevada. Sometimes clast lithologies can be identified with a high degree of certainty, and even related to a particular level within the Sierra Nevada. For most lithologies, however, it is difficult to assign, in more than general terms, a specific horizon in the Sierra Nevada.

In general the graphitic schists can be traced to the Veleta unit of the Nevado Filabride complex. However, graphitic schists also form the lower parts of some of the Mulhacen units (Diaz de Federico et.al. 1990) and so could also have their source here. The quartz-mica schists and the garnet-mica schists, especially the coarse micaceous non-graphitic types, must come from the upper, Mesozoic age portions of the Mulhacen units. This includes specifically the San Francisco, Caldera, Sabinas and the upper portion of the Ophiolite unit which contains

a meta-sedimentary cover to the meta-igneous rocks.

Marble clasts have a very precise source, in the top of the Caldera Unit within the Mulhacen group, which contains a 10m thick section of marble (Diaz de Federico et. al. 1990). No marble is seen in any other unit in the Internal Zones. The Amphibolites and the Serpentinites also have a precise source, in the Ophiolite unit of the Mulhacen group. The tourmaline granite gneisses and mylonites also originate in the Mulhacen complex, probably partly at the base of the Caldera sub-unit. As these rocks have suffered high degrees of strain, they may have been the locus of extensional deformation in the Internal Zones of the Sierra Nevada. Their inclusion as clasts into the sediments of the Granada Basin is important in documenting the timing of the exposure of these detachments within the source area. They are among the first clasts seen at the base of the Dudar Formation.

The Dolomite clasts are clearly derived from the Alpujarride Complex. Some quartzite clasts may be from the Alpujarride, as quartzite can be found within the higher parts of the complex, and only in one small part of the Ophiolite unit within the Nevado Filabride. Some low grade schists, and phyllites are also available in the Alpujarride at the edge of the Sierra Nevada (Montesinos, Morenos and Tonosa Formations, Diaz de Federico et. al. 1990). However, some phyllites are present in the upper parts of the higher units in the Mulhacen Group. Considering the preponderance of clasts derived from the Mulhacen Group, it is more likely that phyllite clasts are also, or even mainly, derived from here. If numbers phyllite clasts increase as numbers of Alpujarride dolomite clasts increase, then it would be more likely that the phyllite is sourced from the Alpujarride complex.

In summary, clasts come from the Internal Zones of the Betic Cordillera, in the Alpujarride and Nevado Filabride complexes. Most clasts have their source within the Nevado-Filabride complex, specifically from the diverse Mulhacen Group. Some clasts can be tied to a specific horizon within the Sierra Nevada source region, but most can only be attributed to one of the three main sources in the Alpujarride complex, Mulhacen group or Veleta Unit.

3.6 Stratigraphic variations of clast types

The ten conglomerate clast categories that evolved after studying the range of clast types in the fan formations at the eastern edge of the Granada Basin are described in **section 3.4** above. They were used to analyse the clast composition of conglomerates in the Dudar, Pinos Genil and Alhambra Formations. Type was noted against the size of each clast. The method used for counting is presented in **Appendix 1**. As the sampling sites are spread vertically through the stratigraphy of the fan deposits, they provide an insight into vertical changes in the numbers of different conglomerate clast types. This is important as it is linked to temporal changes in the lithologies exposed within the source region, that were available for erosion and inclusion into the fan deposits during the late Miocene. It is also important as stratigraphic variability constrains the possibility of clast recycling from formation to formation. If clasts remain the same then recycling is not excluded. If clast types vary considerably then recycling is not the dominant control on sediment maturity.

Figures 3.3, 3.4 and **3.5** present the data in graphical form. The size information contained in these plots will not be considered here, but in **section 3.7**.

La Peza and Quentar Formations

The earliest deposits of the Granada Basin, the La Peza and Quentar Formations (not shown on the clast v's size diagrams) derive their terrigenous detrital materials from the local Alpujarride. In the region east of Quentar the sequence of shallow marine carbonates contains fragments of the black staurolite schist that forms the Alpujarride basement in that area, along with the grey dolomite and vein quartz beneath the schist. At the Balcon de Canales (**Fig. 3.1**) the conglomerate at the base of the sequence contains almost only Alpujarride dolomite clasts, and minor amounts of Alpujarride schists. Only Alpujarride rocks contributed sediment to the early Granada Basin (see **Plate 3.12**).

Dudar Formation

The conglomerate compositions for the Dudar Formation were measured within the logged section presented in Fig. 2.5, that is located at location 1 (Fig. 3.1) at the village of Pinos Genil. These deposits are proximal fan deposits at the mid to upper reaches of the Dudar Formation. Further up the sequence in the Dudar Formation, the fan deposits, as well as indicating a dramatic change in sedimentary regime, mark the first influx of detritus with a source in the Nevado Filabride complex. Some clasts of dolomite continue to be present throughout the Dudar Formation, but in reduced amounts, indicating the waning of the Alpujarride as an important detrital source, relative to the Nevado Filabride (**Fig. 3.3a-d**).

This change in source is the general trend. However, there are some detailed changes which are significant. Near the bottom of the Dudar Formation amphibolite and marble clasts are found in large numbers (**Fig 3.3c, samples Dudar 5 and Dudar 6**). These clast types then decrease in proportion in younger sediments, but are still present in significant numbers. In the logged section in the Dudar Formation near Pinos Genil town (at sample site 3 **Fig. 3.1**), that ranges from the centre to the top of the fan, there are variations in relative numbers of different schist clasts. This logged section is presented in **Fig. 2.3** and has the positions of measured and sampled conglomerates marked. In the lower conglomerate horizons there are few graphitic schist clasts. This number increases in higher deposits, but decreases in still higher deposits. This pattern is inversely mirrored by increases and decreases in the number of garnet-mica schist clasts and quartz-mica schist clasts. Numbers of dolomite, marble and quartzite clasts also vary in number in this measured section, though by smaller amounts. For example C8, near the middle of the measured section, (see **Fig. 2.3**) contains no marble clasts, but a significant number of quartzite clasts. Stratigraphically a few metres below, C1 (near the base of the logged section, probably near the middle of the Dudar Formation) contains marble clasts, no dolomite or tourmaline gneiss clasts, and only a small number of quartzite clasts. Numbers of clasts of vein quartz remain constant throughout the Dudar Formation.

Near the top of the preserved sequence of the Dudar Formation the number of clasts sourced from the Alpujarride complex increases significantly (**Plate 3.13**, and **Fig 3.3d**). This occurs a few 10's of metres beneath the erosional unconformity with the Pinos Genil formation, above which level the Dudar Formation may have existed. Much possible detail of provenance changes in Dudar Formation time has thus been lost.

Plate 3.12 Conglomerates of the La Peza Formation at the Balcon de Canales, 10-20m above the unconformity with the Alpujarride Complex at the base of the Granada Basin sedimentary sequence. Note rounded clasts of Alpujarride Dolomite, some showing borings, indicating deposition in shallow marine conditions.

Plate 3.13 Conglomerates at the very top of the preserved Dudar Formation, 10-20m below unconformity with the Pinos Genil Formation. This shows the abundance of angular clasts of dolomite with provenance in the Alpujarride Formation in the Sierra Nevada source region. This indicates the re-exposure of the complex in the late Tortonian.

Pinos Genil Formation

The conglomerates measured in the Pinos Genil Formation are located in the mid reaches of the fan. The Pinos Genil Formation shows some compositional differences from the underlying Dudar Formation (see **Fig. 3.4a-b**). Graphitic phyllite appears for the first time in significant amounts, coupled with a decrease in the amount of graphitic schist and garnet-mica schist. There is very little of the tourmaline gneiss and mylonite group of rocks in these alluvial fan deposits. The quantity of vein quartz appears to increase, particularly into coarser clast sizes. Amphibolite clasts become more common as do marble clasts, quite considerably in the case of PG3 (**Fig. 3.4b**). Overall the abundance of schist clasts of all kinds is smaller compared with the Dudar Formation.

Alhambra Formation

The conglomerates measured in the Alhambra Formation are located in the mid stratigraphic level of the Formation. For these conglomerates there are little or no marble clasts present, though this should not be taken as uniform for the whole formation, if the magnitude of the variations seen in the Dudar and Pinos Genil Formations is typical for all formations. In the examples presented in **Fig. 3.5**, variations in the numbers of tourmaline gneiss and mylonite, amphibolite and marble clasts between individual conglomerates can be seen. Dolomite clasts persist throughout, and can be observed in several locations in the Alhambra formation. There is a decrease in the number of schist clasts, and an increase in the number of vein quartz clasts compared with the Dudar Formation.

Overall, observed variations in clast composition do not indicate significant changes in the source, from the inception of fan sedimentation to the present day. The same lithologies persist throughout the stratigraphy of the three fan formations, and can be related to lithologies exposed currently in the Sierra Nevada. However, phyllite clasts are introduced into the Pinos Genil Formation, originating possibly from the Alpujarride complex, but also possibly from the Mulhacen Complex, indicating the unroofing of another lithology within the complex.

This is supported by the late increase in the number of dolomite clasts in the Dudar formation, indicating the uncovering of the Alpujarride complex. This could have occurred during the uplift of the Nevado Filabride core. This uplift, as mentioned above, is recorded in the increasing dip angles of sedimentary deposits as they near the metamorphic basement. However the number of dolomite clasts in the Pinos Genil and Alhambra Formations is not as large as that seen in the late Dudar Formation, suggesting the covering of this source by the time of deposition of the Pinos Genil Formation. This may have been achieved by onlap of fan deposits onto the basin margin. The late increase in dolomite clasts in the upper Dudar Formation may also relate to recycling of the early La Peza Formation. However, there is no evidence for the re-sedimentation of abundant carbonate material.

The source region for the fan deposits in the Sierra Nevada remained lithologically similar throughout the deposition of the fan deposits at the Eastern edge of the Granada Basin. Small variations of clast abundances are clear, but the range of composition remains essentially unchanged. However, as the compositional range changes little, the relative proportions of

clasts sourced from the Alpujarride and Nevado-Filabride complexes does vary. Early clasts are all from the Alpujarride, which is later swamped by abundant material from the Nevado-Filabride Complex. Late in the Dudar Formation there is an increase in the number of clasts of Alpujarride dolomite. Then in the Pinos Genil formation there is the introduction of phyllite clasts perhaps derived from the Alpujarride formation, but also likely from some units of the Mulhacen unit. Tectonic implications are drawn from this pattern in **section 3.7**.

3.7 Clast type variation with size

Figures 3.3 to **3.5** present graphs of clast type plotted against clast size. The use of this type of graph allows the recognition of those lithologies that are proximal to the source. More importantly it allows the recognition of those lithologies that most readily reduce in size, that break up the easiest. This type of size/composition analysis can furnish a more complete description of sediment maturity than merely percentage abundances of different clast types, combined with roundness and textural maturity indicators. These diagrams have been presented in the past (Bluck 1980) but utilised in quantifying stratigraphic variations in clast abundance, to enable source reconstruction to be attempted. They have not been used to date for the information they include on sedimentary composition evolution, and how this may effect provenance signatures. They can also be used to constrain the provenance signatures and reconstructions they support along with more conventional modal analyses. Aspects of their specific use are discussed below, especially with respect to how such data presentation constrains models of sedimentary recycling.

Inspection of **Figs. 3.3-3.5** shows that schists dominate the clast petrography of the sediments of the Eastern Granada Basin, thus reflecting the lithostratigraphy of the source regions in the Sierra Nevada. The clast types presented in **section 3.3** evolved after consideration of the complete range of clast types, and were used as classification criteria for quantitatively recording the clast compositions of the selected conglomerates of each fan formation.

Dudar Formation

In the Dudar Formation the abundance of schist type clasts increases with increasing grain size. In the smallest clast size interval (>5cm and 2-4cm) schist clasts make up between 55 and 70% approximately. This increases to up to 100% in some larger size classes (**Fig. 3.3b** C12). In the largest clast sizes (15 to 128cm) schist clasts make up between 75-90% of clasts. In general there is an increase in numbers of schist clasts in intermediate clast sizes where the numbers of schist clasts reach a maximum (10cm in Dudar 1 -C1, and Dudar 2 -C8 and 128cm in Dudar 6). This is followed by a decrease in numbers of schist clasts from this maximum in coarser clast sizes.

Other rock types occupy the smaller clast sizes, with a slight increase in the larger sizes also. Most of these other rock types are distributed across the clast size spectrum, most notably marble. Quartzite covers the entire range in C1, C8, C19 and Dudar 6, but is restricted to <15cm in C1 and C12. Amphibolite clasts can be present in all size classes (as in C1, C8, Dudar 5, Dudar 7), but also in smaller sizes (<20cm in C12, <15cm in C19) and *especially* in larger

Dudar Formation, Marine fan-delta

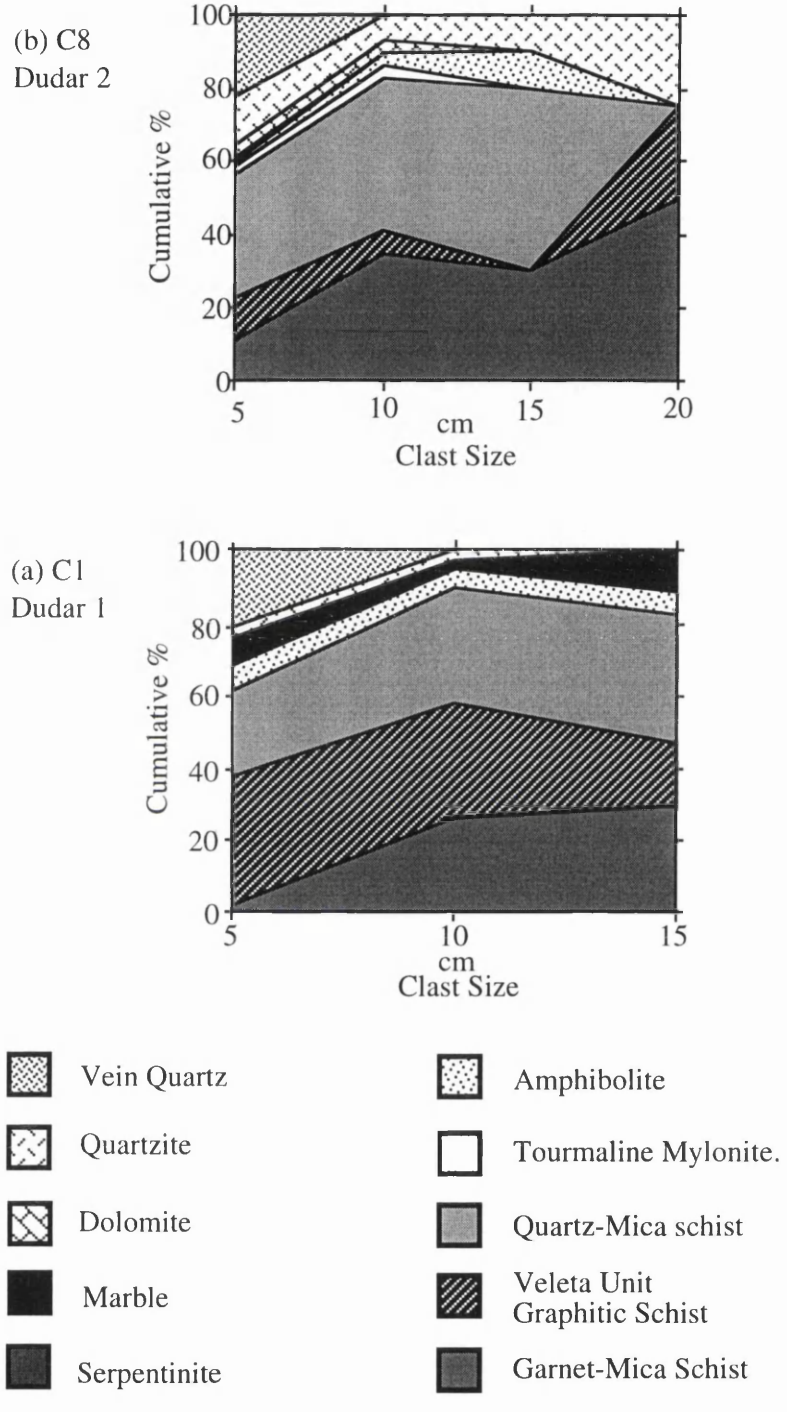

Fig. 3.3 a Conglomerate composition versus size for two conglomerate horizons in the Dudar Formation marine fan-delta, towards the base of the measured section in **Fig. 2.5**. C1 is stratigaphically below C8, and so on. These sampled horizons are in the mid to upper reaches of the proximal fan deposits of the Dudar Formation.

Dudar Formation, marine fan-delta

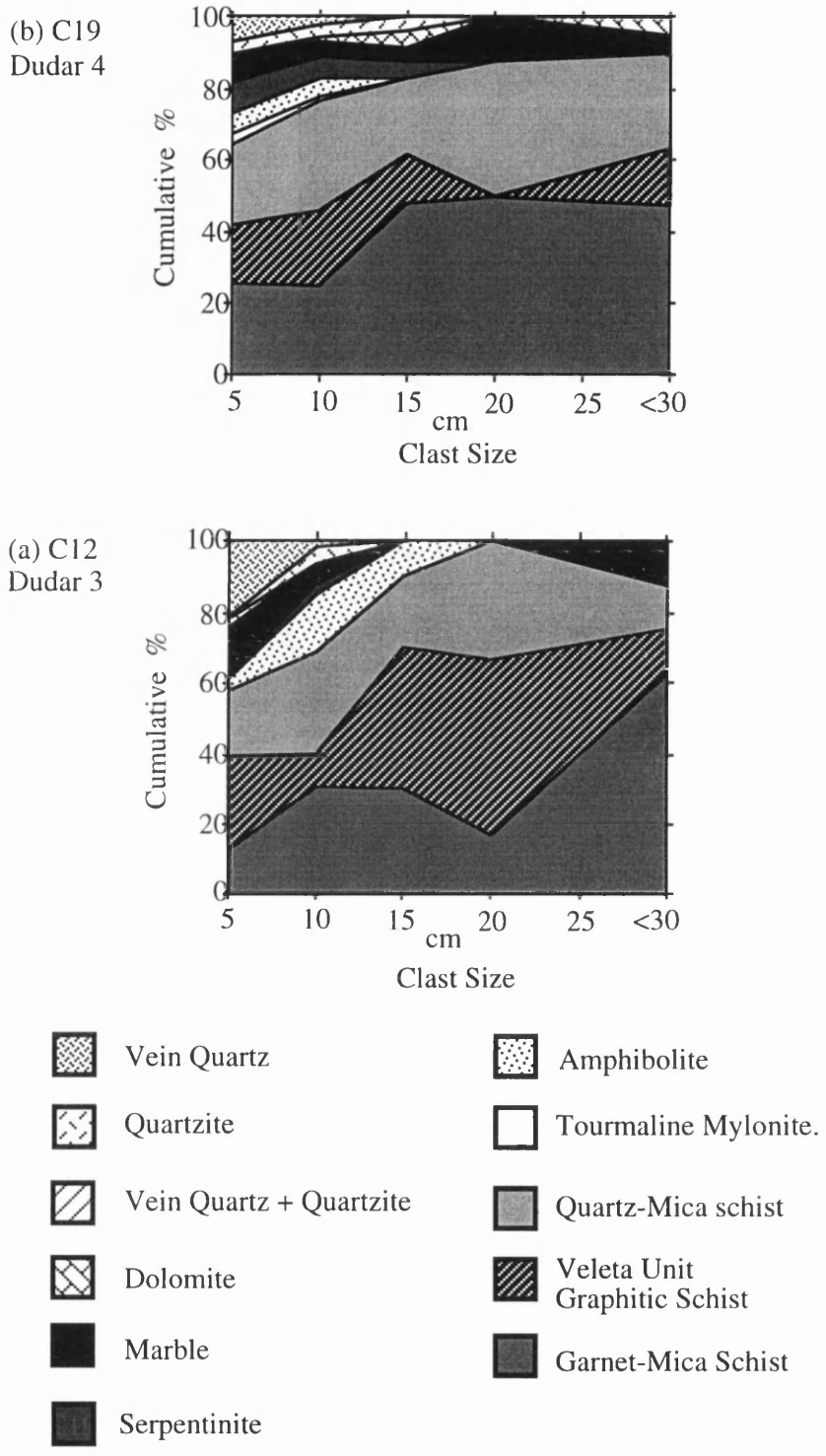

Fig. 3.3 b Conglomerate composition versus clast size for two locations in the Dudar Formation, marine Fan Delta. Locations of C12 and C19 are on the sample logs in **Fig. 2.3**., at location 1 at Pinos Genil Villag, and are part of the mid to upper stratigraphic levels of the proximal Dudar Formation fan deposits.

Dudar Formation, marine fan-delta

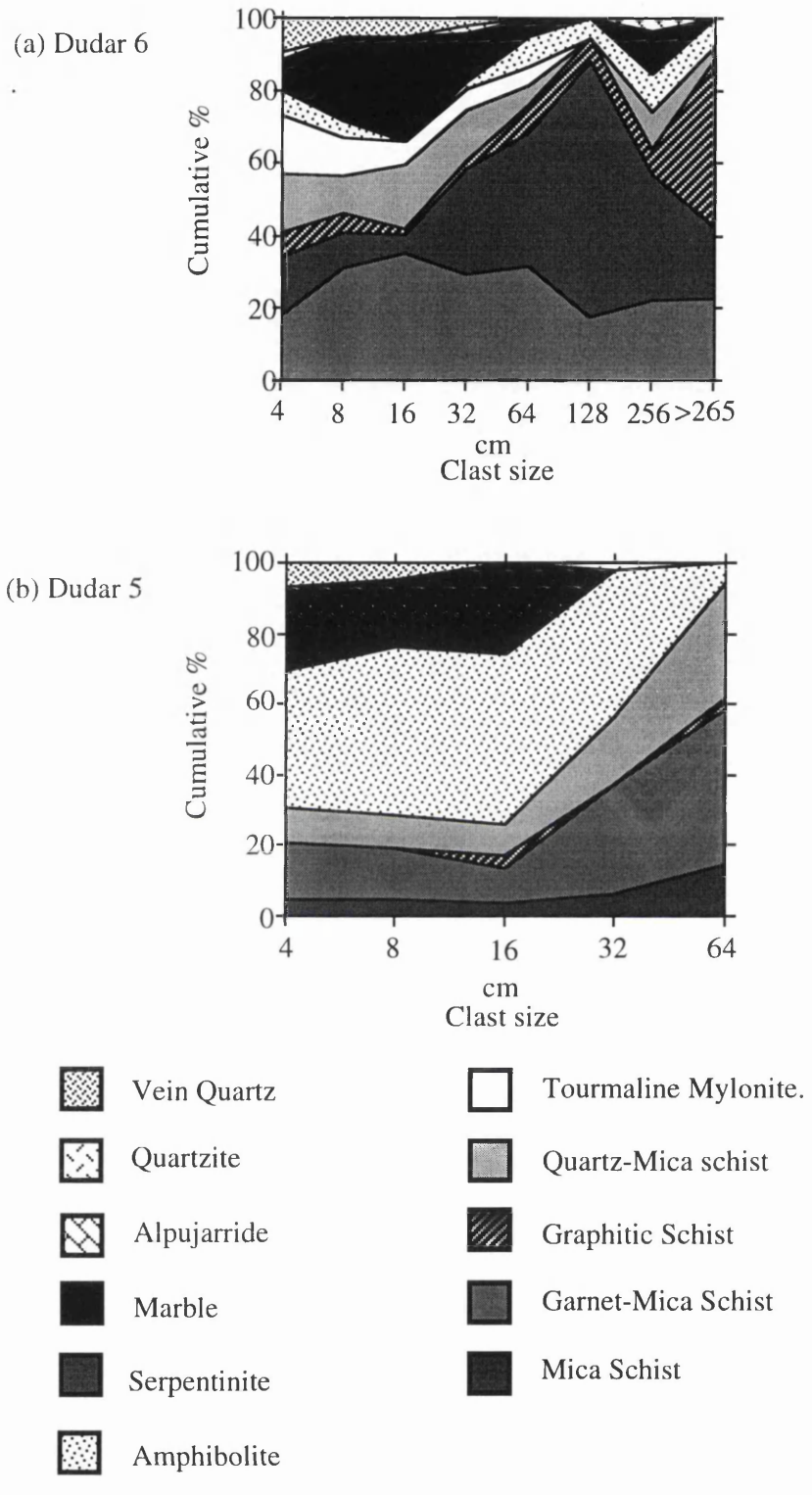

Fig. 3.3 c Conglomerate composition versus size for two horizons both near the base of the Dudar Formation. Dudar 5 and 6 are located near the town of Quentar near the contact with the Alpujarride basement, and the contact with the shallow marine La Peza and Quentar Formation carbonates.

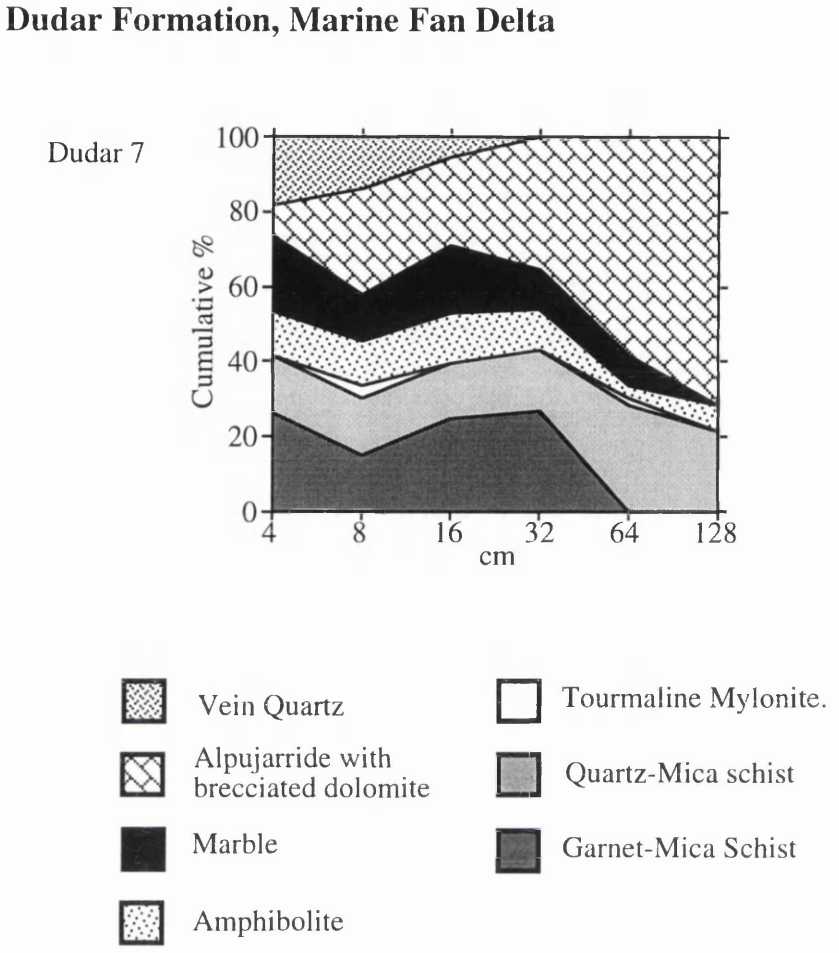

Fig. 3. 3d Conglomerate clast composition versus size for the very top of the Dudar Formation, at location 7 (**Fig. 3.1**). Note the dominance of dolomite clasts, many brecciated, sourced from the Alpujarride complex, compared with the conglomerates lower in the Formation. They increase in number in the coarsest clast sizes. Clasts of graphitic schist characteristic of the Veleta unit of the Nevado Filabride complex are missing.

Pinos Genil Formation, Subaerial Alluvial Deposits

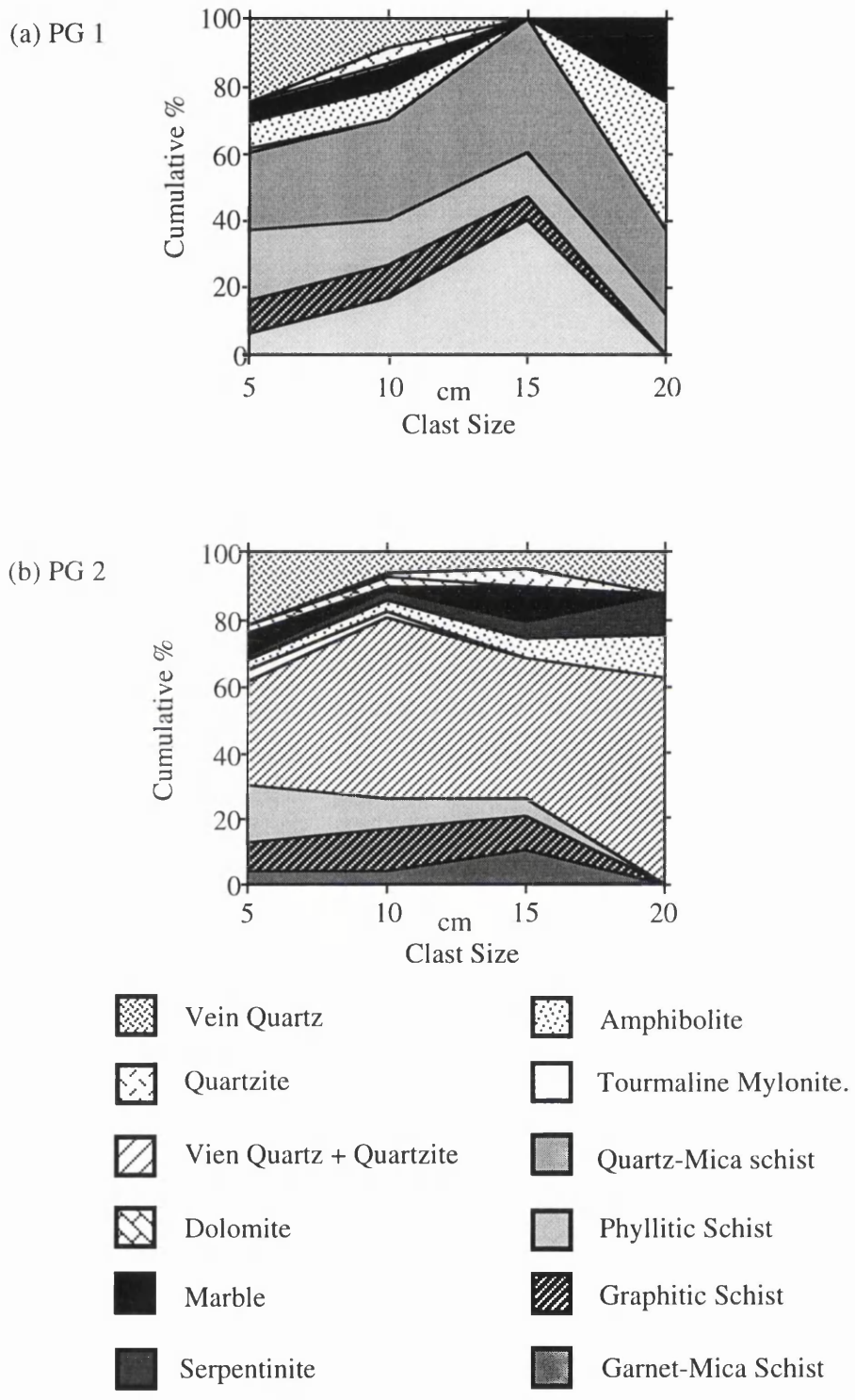

Fig. 3.4a Conglomerate composition versus size for two adjacent locations in the Pinos Genil formation, both at the same approximate stratigraphic level at the middle of the Formation, at location 9 **Fig. 3.1**.

Pinos Genil Formation, Subaerial Alluvial Deposits

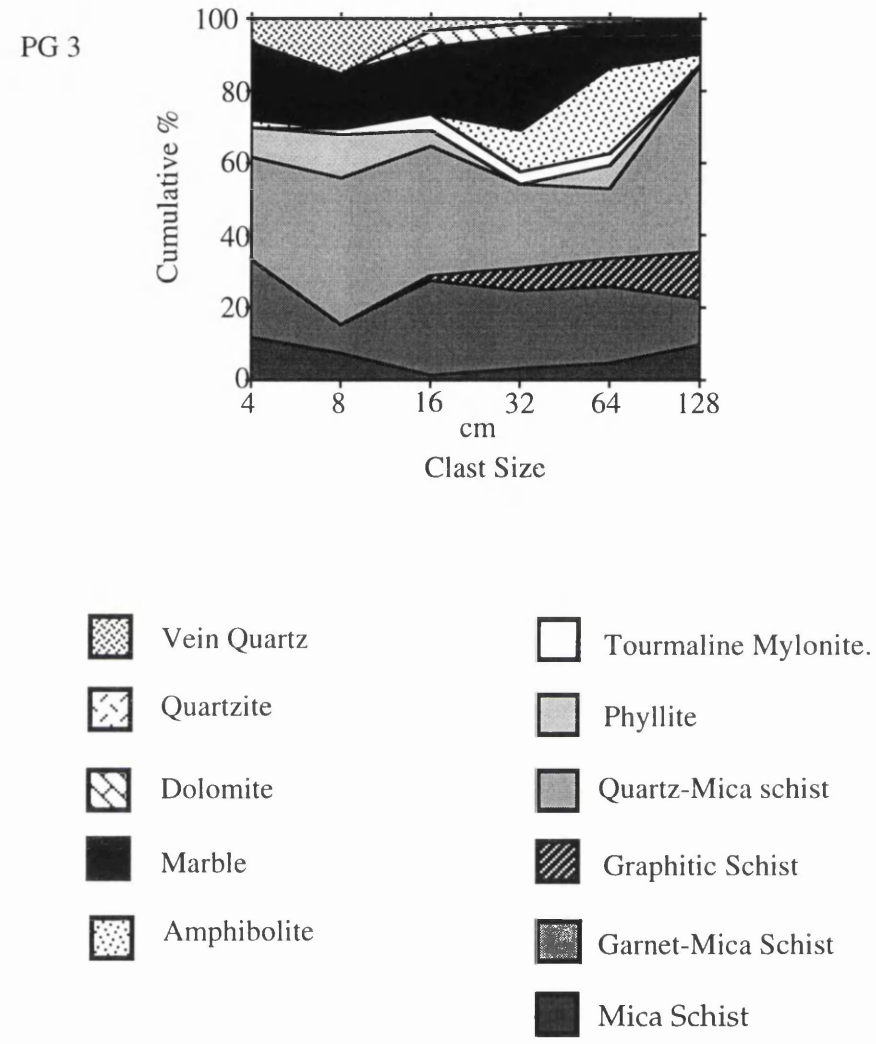

Fig. 3.4b Conglomerate composition versus size for the third selected conglomerate from the Pinos Genil Formation, alluvial fan deposit. This horizon is located near the base of the fan deposit just above the unconformity with the Dudar Formation, at location no. 7, **Fig. 3.1**.

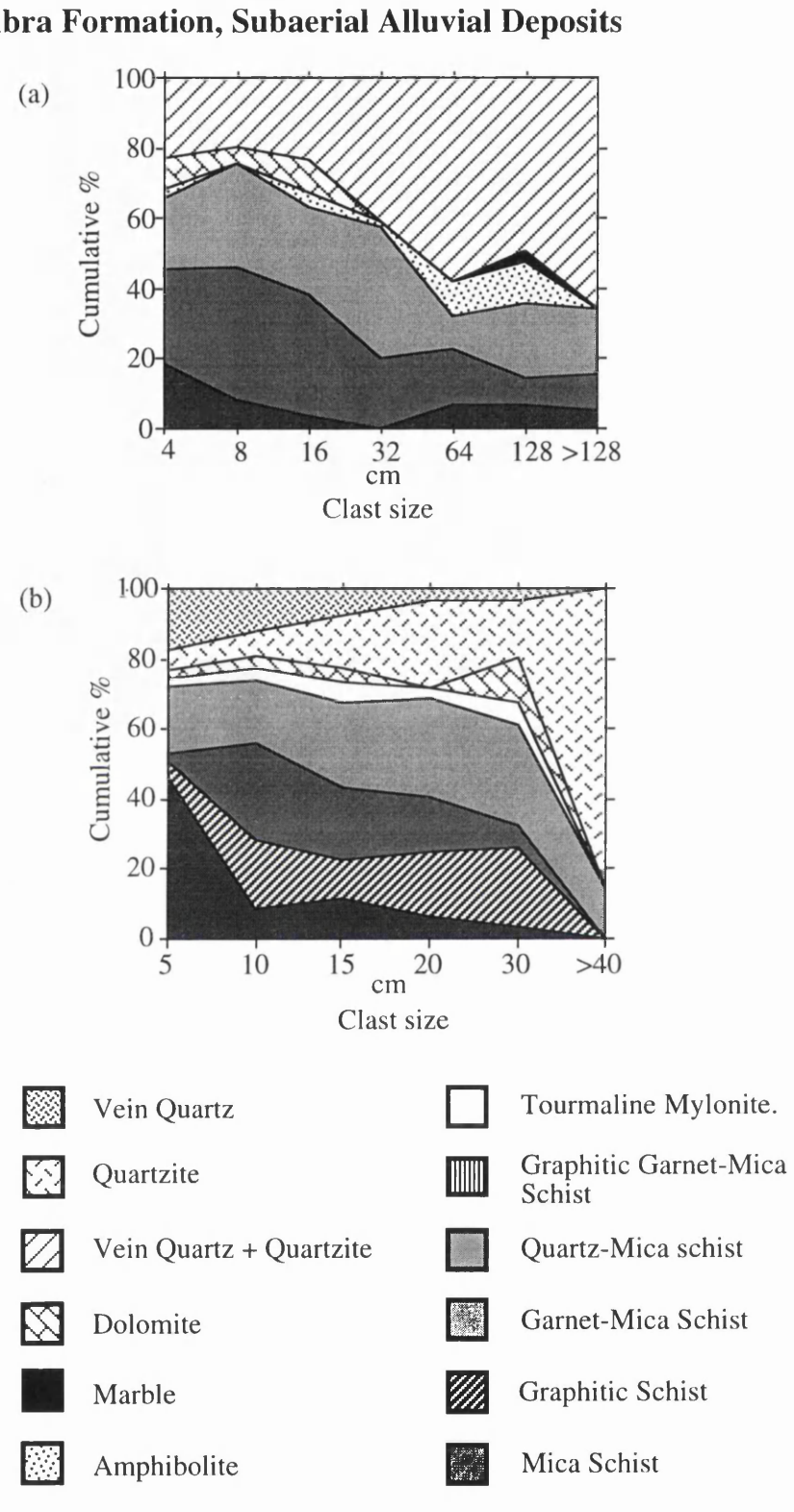

Fig. 3.5 Conglomerate composition v's clast size for two locations in the Alhambra Formation. Note the different size criteria used. In (a) a log scale with base 2 is used and in (b) a linear scale with 5cm intervals is used. More labile schistose clasts can be seen to decrease in quantity with size in both. Slightly different clast criteria were employed both times, due to local differences. Both these sampled horizons are hard to place stratigraphically but can be roughly attributed to the central portions of the formation.

size classes (C8, Dudar 6).

Vein quartz is rarely larger than 15-16cm in size. It can form up to 20% of the smallest size class, then rapidly decreases in quantity in the following interval (C1, C8, C12, C19, Dudar 5). However, in some examples it is found in quantities of 5-10% in sizes up to 32cm (Dudar 6).

Tourmaline gneiss and mylonite group lithologies are present in small amounts (2-3%) in the smallest clast sizes for some conglomerates (C8, C19, Dudar 7) but can be present in larger amounts (5-10%) and in larger clast sizes (Dudar 6). The trend for this group is for most clasts to be in smaller sizes.

Dolomite clasts sourced from the Alpujarride complex, are common in small clast sizes (up to 10cm) in conglomerates C1, C8 and C12 (Dudar 1 to 3), from the logged section at Pinos Genil Town. In C19 (Dudar 4) dolomite clasts are present in sizes up to 30cm across. In the remaining sampled conglomerates dolomite is present as coarse clasts, up 256cm in largest dimension. In Dudar 7, from the very top of the preserved exposure of the Dudar Formation at sample site No. 7 (Fig. 3.3d) it forms the largest number of clasts in a single class. It also increases in proportion with increasing clast size, forming the greatest number of clasts in the 128cm size class.

Pinos Genil Formation

In the Pinos Genil Formation the amount of schist is reduced overall, down to around 60% in the smallest clast size (**Fig. 3.4**). In PG1, from sample site No. 9, schist amount increases gradually to 70% at 10cm clast size, then to 100% at 15cm, finally decreasing to 40% at the largest clast size. In PG2, a near stratigraphic neighbour of PG1, schist abundance increases to 80% at 10cm clast size and then decreases through the remaining size intervals to just over 60% at the largest clast size. In the third example schist amounts do not increase but decrease slightly to around 55% before increasing to 90% of 64-128cm clasts. These differences reflect slight stratigraphical variations in composition, controlled by the availability of clasts types to the deposits, influenced perhaps by sediment transport processes. Alternatively there may be variations caused by sampling differences. However, the clast criteria used were specified strictly (see section 3.3), and two of the conglomerates were sampled one after another on the same morning.

Amphibolite increases in the larger grain sizes overall, as do serpentinite clasts in PG2. Tourmaline gneiss and mylonite group clasts are generally restricted to small clast sizes, except in PG3 were it occurs in 2-5% amounts across the median clast size range (8-64cm). Marble clasts occur in the larger clast size intervals, except in example PG3 where marble clasts compose a large proportion of all clasts across the entire clast size range, with the largest number in the median range. Quartzite can be missing altogether, or found in clasts of 15-20cm size. Dolomite too can be found in small amounts in this size range, and in the 5-10cm size class.

Alhambra Formation

The Alhambra formation shows a marked decrease in the amount of schist in the

formation (**Fig. 3.5**). The small size range quantity of schist still lies between 60-80%, but beyond this the quantity of schistose rocks generally decreases, to a low of 35% in ALH2 for 128cm size clasts, and 15% in ALH1 for 30-40cm clasts. Quartzite and vein quartz are the rocks that replace schists in the larger size intervals. Dolomite also increases toward the coarser end in ALH1. In ALH2 amphibolite increases with increasing clast size. In ALH1 tourmaline gneiss rocks compliment the pattern of the schists and decrease away to nothing at the <40cm size class. Marble is present as coarse 64-128cm clasts in ALH2 only. As has been said before, the possibility of detailed stratigraphic variation in clast abundance is high, so these selected conglomerates should be viewed as representative of the Alhambra Formation in a general sense only. However, the pattern of decreasing schist content with clast size is very clear.

In summary, the clast composition of the three late Miocene to Pleistocene fan formations at the eastern edge of the Granada Basin is dominated by schist. However, a systematic change in the proportion of schist clasts between formations is clear. In the Dudar formation schist clasts increase in proportion with increasing grain size. This gives way in younger sediments, to increasing proportions of quartz rich and amphibolite clasts in the coarsest clast sizes. All schists become finer grained in character, but the proportion of schist clasts in the small clast sizes *does not increase*, remaining fixed at around 60%.

3.8 Interpretation of clast composition data

Stratigraphic variations of clast abundance

Each rock type found in the conglomerates of the study area can be found exposed within the Sierra Nevada source region. Normally clasts which are earliest into the sedimentary pile within a basin come from the top of the uplifting source, and those that enter last are from the bottom of the source. In this way the composition of the source is inverted and an unroofing sequence formed.

However, in reality detailed stratigraphic variations in conglomerate composition are difficult to interpret, as the controls on sediment dispersal can be complex. Sediment may be held within the source area before final deposition in the basin, possibly for some time. This introduces the possibility of clast mixing, which would scramble a detailed unroofing trend. This could cause fluctuations in the composition of the sedimentary sequence produced. General trends in composition may be reliable though, and may indicate changes within the source region that relate specifically to important tectonic movements.

Sediment recycling may have taken place in the deposits of the eastern flank of the Granada Basin, a processes which should complicate and thoroughly mix any detailed unroofing signature from the Sierra Nevada. The detailed changes in clast proportions are difficult to interpret with any certainty, but some larger amplitude variations do indicate important changes in the Sierra Nevada source, during the late Miocene to Pleistocene.

In the La Peza formation, the earliest deposits of the Granada Basin, clasts are derived solely from the Alpujarride complex. Abundant rounded, and bored, dolomite clasts often showing veining and brecciation are common. The lower units of the internal zones may not

have been exposed at this time (late-mid Miocene approx. 14-11Ma), as there is no higher grade pelitic metamorphic rocks within the formation. Nevertheless, there is no evidence to suggest that the Nevado Filabride Complex was not exposed. Significantly no detritus is recognised as having originated in the Malaguide Complex, which lies tectonically above the Alpujarride Complex. The deposition of the La Peza Formation directly upon the Alpujarride Complex indicates the removal, and therefore the extension of the Betics prior to the early Miocene.

Beach deposits formed against an Alpujarride landmass, that had little erosional relief. Away from shore shallow marine conditions combined with little terrigenous input favoured the development of thick bioclastic carbonates, also present in the Quentar Formation. No conglomerate grade material sourced from the Nevado Filabride Complex is present in the calc-arenites, however as is presented in **Chapter 4**, numerous sand grains of siliceous metamorphic rock fragments are present, increasing in abundance towards the top of the formation.

The sediment in the Dudar formation was rapidly deposited in a subsiding basin with a moderate water depth (300m, M. Keen pers com.). Its textural and compositional immaturity (roundness, clast size and sorting) suggest that it is fresh material that has been derived direct from the Internal zones in one cycle of erosion and deposition during the Miocene. Its depositional style of laterally continuous sheets of poorly sorted, matrix supported conglomerates and its compositional immaturity suggests rapid deposition in mass flow deposits with little sediment mixing before deposition. Therefore the Dudar formation is the best candidate for the preservation of an unroofing signature from the Sierra Nevada. In the logged section at Pinos Genil the measured conglomerates (C1,8,12,19) show significant variations in the proportions of schists, dolomite, amphibolite, serpentinite and quartzite. These variations may be caused by:

1. Spatial variations in erosion due to faulting
2. Periodic tapping of sediment storage basins within the source area
3. Extension of drainage area into new source regions.
4. Localised uplift within the drainage basin.
5. Changes in river coarses.

The most important variation in clast abundance are the changes in amounts of dolomite sourced in the Alpujarride complex. The pattern is one of early dominance of the detrital record by the dolomite in the La Peza and Quentar formations, followed by an influx of Nevado Filabride rocks and a late resurgence of dolomite clasts in the final extant deposits of the Dudar formation. This pattern indicates the absence of the Nevado Filabride as a source in the late Serravalian/Tortonian. The sudden influx of coarse Nevado Filabride detritus is indicative of a considerable increase in relief in the Internal Zones of the Sierra Nevada in the early Tortonian, associated with the unroofing of the lower Nevado Filabride units, and the extension and rapid subsidence of the Granada basin. At this time the Alpujarride may have been overlapped and covered by the later deposits of the La Peza and Quentar Formations and

the earliest fan deposits of the Dudar Formation.

The late increase in the number of dolomite clasts from the Alpujarride document the re exposure of the Alpujarride at the Basin edge, and may relate to uplift of the basin flanks, rejuvenating this area as a sediment source. It is this basin edge uplift that is the crucial tectonic implication drawn from the variation in clast type abundance. It is supported by the angle of dip of the basin flank deposits, which increases in acuteness in older deposits (see **Chapter 2** and **section 3.1**). In the succeeding Pinos Genil and Alhambra formations the lack of clear provenance trends of this type suggest increased mixing and possible recycling of detritus. However, the Nevado Filabride complex continued to be the dominant provenance for detritus.

Clast abundance variation with clast size

The interpretation of **Figs. 3.3** to **3.5** is concerned mostly with the processes of sediment breakdown and maturing. Similar rock types are grouped together where possible on the diagrams, and given similar ornaments. This allows the size evolution of rock types to be seen more clearly.

There is a general decrease in the proportion of schistose clasts through each successive formation, with a corresponding increase in quartzose clasts, especially in the largest clast sizes. In the Dudar Formation, which is demonstrably first cycle (see above), schist clasts increase in quantity with size. Schists are prone to breakup at many points due to their prominent anisotropic fabric, with elongate and plate shaped minerals such as amphiboles and micas. They form blade and plate shaped clasts and are often angular (see **Plate 3.2**). The fact that they make up the majority of the coarse clasts in the Dudar formation suggests that they have not undergone a great deal of abrasion and reworking, and are indeed first cycle deposits. Quartzose clasts such as quartzite and vein quartz, and others such as amphibolite and marble, are more resistant to abrasion by virtue of their more massive crystalline nature and harder mineralogy, so consequently reduce in size less easily and tend to form more rounded clasts.

In the Pinos Genil formation a similar pattern is seen with an initial increase in schist amount then an overall decrease. The quantity of large clasts of schist (20-128cm) is noticeably down in two examples PG1 and PG2 (**Fig. 3.4a**), but up in PG 3 (**Fig. 3.4b**). Vein quartz also appears in larger clast sizes than before. The increase of schists in the largest clast size class in PG 3 is preceded by a decrease in the 32-64cm class.

This increase in coarse schist clasts may be controlled partly by the inability of the source to produce blocks of 64-128cm size in quartz rich rocks due to a combination of lithological thicknesses, faulting or joint patterns; factors that control the size of blocks that are produced at the point of erosion within the source (for example **Plates 3.1** and **3.2**). Another possibility is the continuation of a primary basement source for schists, combined with recycling of older sediments. Where the schist quantity falls off, a combination of harder rock types (amphibolite and marble mainly, but also vein quartz) take their place.

The pattern of decrease in the number of schists clasts in the Alhambra Formation, in the coarse clast sizes, is complimented by an increase in hard quartzose rock types. This indicates that schist clasts are being preferentially broken down into smaller sizes. The conglomerates of the Alhambra formation have the highest textural maturity of the formations

at the eastern flank of the Granada Basin (**Fig. 3.1**). **Figure 3.5** shows that they also have the highest compositional maturity, with the greatest proportion of quartz rich rocks types.

However, the 60-80% schist content of the finest clast size interval is no lower than that observed in the Dudar and Pinos Genil Formations, which are less mature. The continual breakdown of coarser clasts feeds schist clasts into the smaller size classes, so the overall level of small schist clasts would be expected to increase, but it does not. Schist material in the small clast sizes must also break down to remove material from the fine end of the conglomerate size range. This is balanced by the breakup of the larger clasts which feeds material into the small clast population, and simultaneously reduces the proportion of schist in the coarse grain sizes. Thus the proportion of small schist clasts remains the same. It is maintained by the breakdown of large clasts and the simultaneous breakdown of small clasts.

This break down of clasts occurs simultaneously across the grain size spectrum. Clast breakdown at the fine end of this spectrum will result in the production of sand grade material (<2cm). This process may be expected to have had a profound effect on the composition of sand in the three fan formations at the eastern edge of the Granada Basin. It will ensure a continuos input of coarse lithic grains to the sand, thus in principle preventing the development of increasing maturity in the sand fraction from deposit to deposit. The next chapter discusses sandstone petrography and tests the validity of this prediction.

The relative paucity of coarse schist clasts in the Alhambra formation also lessens the evidence for the persistence of a primary basement source in the Sierra Nevada, and strengthens the argument for the recycling of previously existing conglomerates. However, this assertion cannot be proven unequivocally as other variables have not been fully constrained. For instance, the depositional environment of the Alhambra formation is clearly different from the Dudar Formation, braided sub-aerial fan deposition compared with very rapid, sub-aqueous deposition by sheet and debris flows in the Dudar Formation. The effects of slower sedimentation, in a slightly more distal position, in an oxidising weathering environment, in the Alhambra Formation, may well have had the same effect on conglomerate composition as recycling would on the earlier deposits of the Dudar and Pinos Genil Formations. Reworking could easily have taken place upon the surface of the Alhambra Formation alluvial fan.

However, the Pinos Genil Formation was also deposited in a subaerial alluvial fan, but shows much less schist clast reduction than the Alhambra Formation. Considering the present outcrop pattern of a geological map of the area, the Alhambra Formation is only 2-4 km more distal from source than the Pinos Genil Formation. Transport distance is not a significant variable that can explain the difference in observed composition despite the similarities in depositional environment. It is possible that a primary source in the Nevado Filabride Complex was still dominant during deposition of the Pinos Genil Formation, that maintained a higher schist content. This further suggests that the Alhambra Formation is the likely result of recycling, of older previously deposited conglomerates in the Dudar and Pinos Genil Formations. Otherwise the compositional difference between the Pinos Genil and Alhambra Formations is difficult to generate, from the same source in the Sierra Nevada. The Alhambra formation is likely to have a provenance in a source more mature than the primary source in

the Nevado Filabride Complex. The Dudar and Pinos Genil Formations provide a conveniently located source of clasts with a strong Nevado Filabride signature.

The sampled conglomerates only detail a small portion of the fan deposits, though they appear in the field to be representative of the deposits encountered. The data presented here, however, do not exclude the possibility of intra-formation compositional changes, that have not been identified. Such variations would be an ideal target for future work, and may indicate important processes of intra-formation sedimentary dynamics and possible recycling.

Conglomerate composition-size evolution model and the Granada Basin

Figure 3.6a shows a theoretical model of size evolution in an imaginary conglomerate clast population, derived from a source region composed of equal amounts of quartzite and mica schist. The gravel produced goes through several cycles of deposition and erosion. The evolution of clast population takes place in a closed system where no new material enters and none is lost.

In the first cycle of erosion and deposition there is an even distribution of both lithologies across the clast size range. The source is presumed to produce gravel, *at the point of erosion*, in both lithologies, that has a complete and even size distribution.

The more labile schist clasts will break down at a faster rate than the quartzite. With another cycle of erosion and deposition an imbalance in the clast population is produced that changes the provenance signature in the conglomerate and decreases its accuracy as a provenance indicator. Mica schist breaks down to create smaller clasts, which increases the proportion of schist clasts at the fine end of the grain size distribution, and decreases the proportion of schist clasts at the coarse end. Quartzite therefore increases in proportion in the coarser fraction. In a closed system, even though there is not a net increase in coarse quartzite clasts there is an increase in the ratio of coarse quartzite to coarse schist. This is because one component of the system (schist) is reduced in size much quicker than the other (quartzite).

An open system is depicted in **Figure 3.6b**. However no new material enters the system, consistent with a pure recycling sedimentary evolution. Material can exit to the left of the size/composition diagram as it is reduced to sand size. As for the closed system, the finer conglomerate sizes are constantly fed from coarser material breaking down, but *do not show an increase* in the amount of schist clasts in the finer classes. This is because material constantly leaves the conglomerate size system as sand. Unless there is an input of fresh coarse material the amount of coarse schist will decrease, in the same way as the closed system discussed above. This constant production of sand sized material will have a pronounced effect on the composition of sandstones within recycling deposits. The possible effects upon the evolution of sandstones within the Granada Basin are discussed in the following chapter.

The composition of the conglomerates of the eastern edge of the Granada Basin and the differences between formations are consistent with this open system behaviour. It can not only explain the changes of texture but also the composition of the sediments in the eastern Granada Basin.

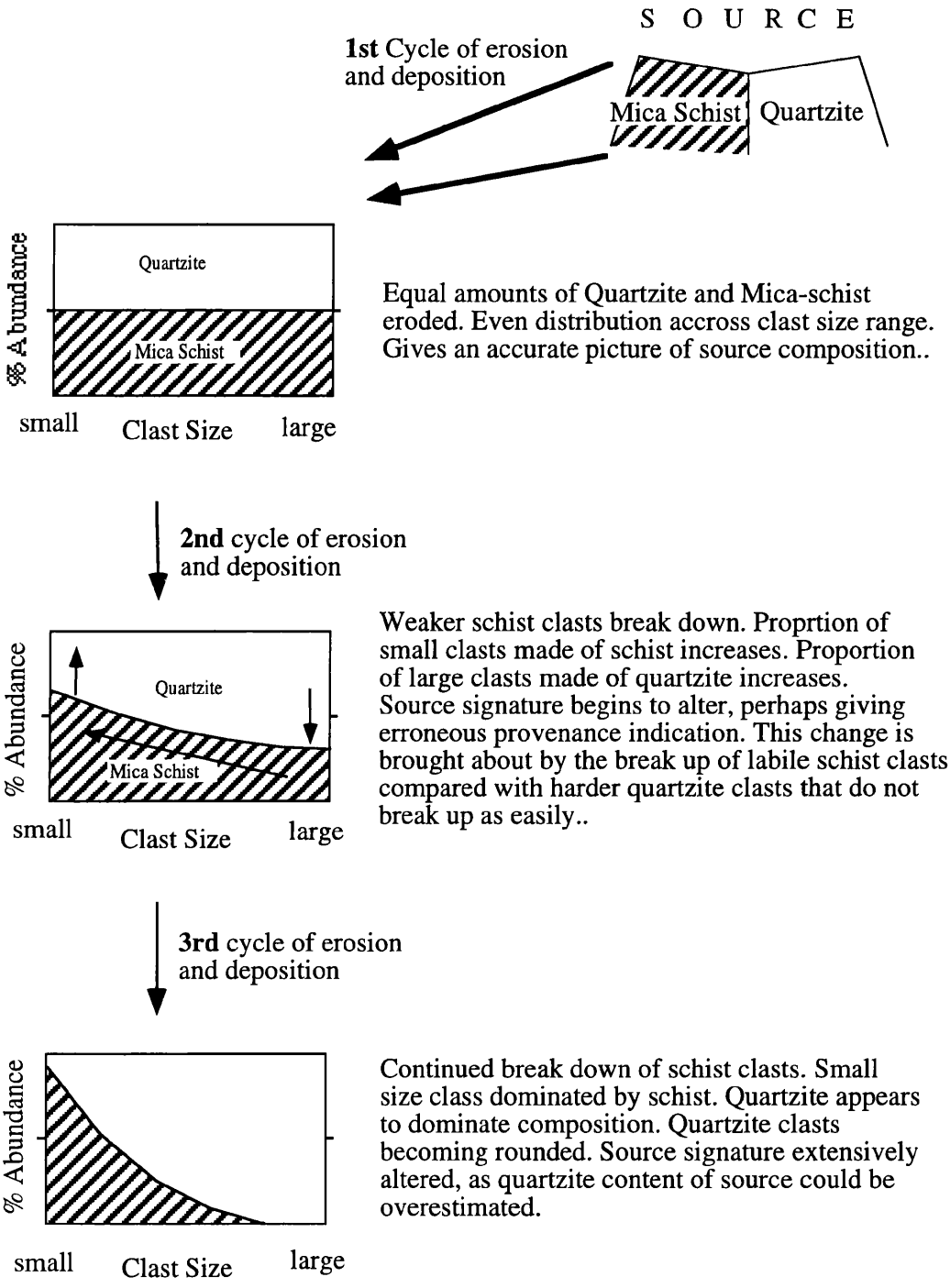

Fig. 3.6a Theoretical model of conglomerate clast size evolution through successive stages of sediment recycling in a closed system. In this model the grain size range represents the entire spectrum from the largest loose blocks, down to the point just prior to the generation of monomineralic sand grains. No fresh sediment is added in each recycling stage and no material is effectively removed. The different compositional patterns for each clast size are a function of the effects of clast breakdown forces on a mix of lithologies with differing hardnesses, and resistance to abrasion .

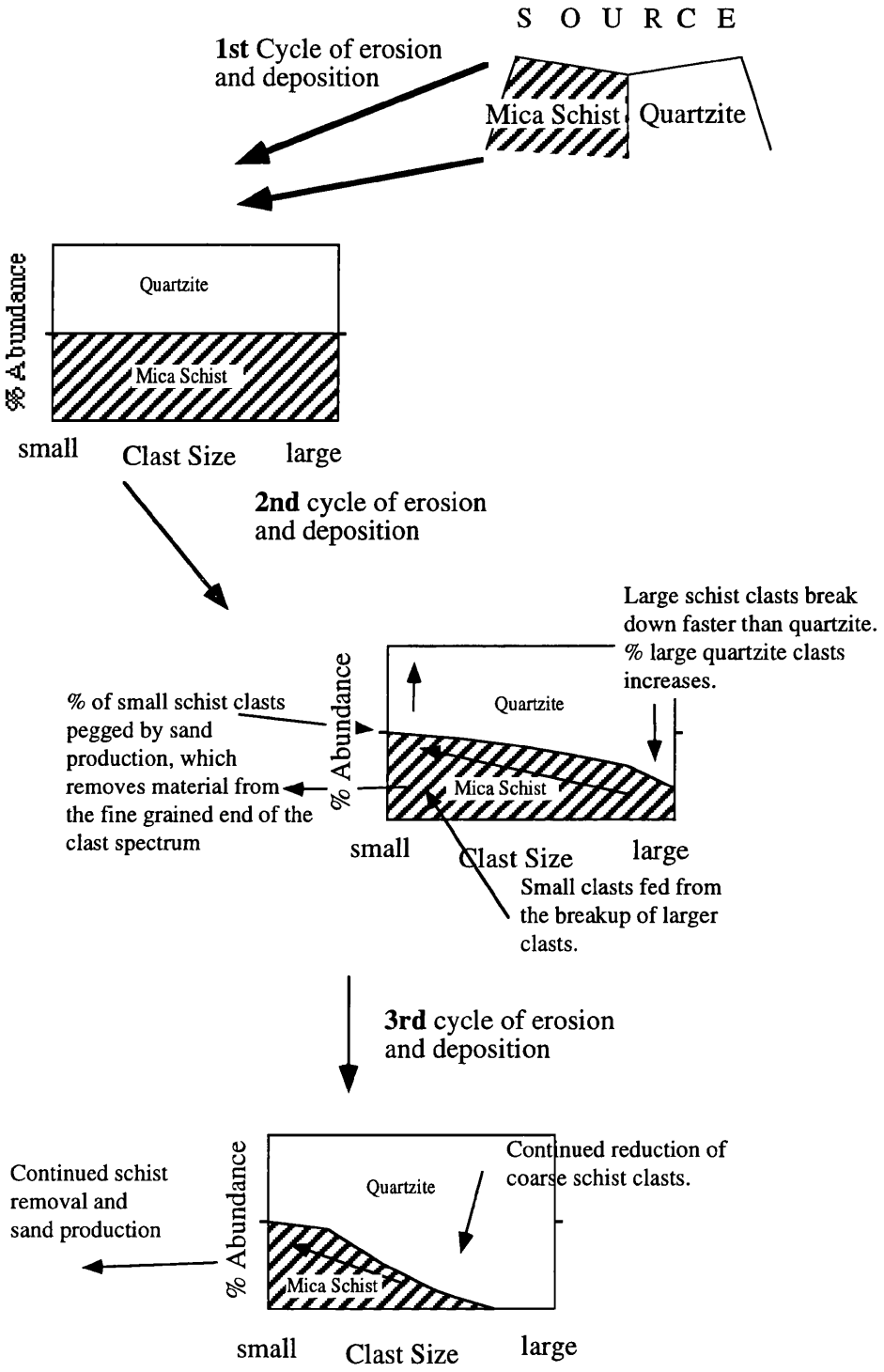

Fig. 3.6b Theoretical model of conglomerate clast evolution in an open system. In contrast to the closed system model, fresh material can enter the system at any grain size, and leaves the sytem continuously at the fine grained end thus allowing the quantity of small schist clasts to remain at the level set in the first cycle of deposition. This is what appears to happen in the fan sediments of the eastern Granada Basin.

3.9 Conclusions

1. The provenance of sediment within the late Miocene to Pleistocene deposits of the eastern Granada Basin rests in the Internal Zones of the Betic Cordillera, situated in the western Sierra Nevada (see **Fig. 2.1**).

2. The earliest provenance of detritus in the eastern deposits of the Granada Basin was in the grey, brecciated dolomite of the Alpujarride complex. Some of the earliest shallow marine carbonates of the La Peza and Quentar formations contain fragments of the graphitic staurolite schist that is inter-thrust with the dolomite formations in the Alpujarride near to the unconformity with the basin sediments (sample site No.4 **Fig. 3.1**).

3. The Dudar Formation contains abundant course, compositionally and texturally immature detritus sourced from the Nevado Filabride complex, in the Sierra Nevada. From this point onwards the detritus in the eastern edge of the Granada Basin is dominated by clasts sourced in the Nevado Filabride complex. Schists dominate the composition of conglomerates. The change from relatively quiescent shallow marine carbonate deposition during La Peza and Quentar Formation times, to intense fan sedimentation marks the sudden generation of erosional relief within the area of the Sierra Nevada in a significant tectonic event, during the late Tortonian. The presence of Nevado Filabride detritus indicates the unroofing of the core of the Internal Zones Metamorphic Core Complex at this time.

4. The Alpujarride complex was re-established as an important sediment source for the latest deposits of the Dudar Formation. This supports a model of basin flank uplift, allowing the uncovering of older sedimentary deposits and of the Alpujarride. The angles of dip of the La Peza, Quentar and early, proximal Dudar Formation increase towards the basin edge, and also with increasing age.

5. Phyllitic schist becomes more common in the Pinos Genil formation indicating the enlargement of provenance area, probably within the Alpujarride complex, or the Mulhacen Unit. Stratigraphic variations in clast type abundance within the conglomerates of the Dudar, Pinos Genil and Alhambra formations document variations in source configuration, and may relate to tectonic events, that shifted or enlarged drainage patterns, or allowed sediment storage areas within the source to be tapped.

6. In the Dudar formation schists dominate the conglomerate composition and form the majority of large clasts. The Dudar formation has the greatest compositional immaturity of any of the formations that make up the eastern flank of the Granada Basin.

7. In the Pinos Genil Formation schists form slightly less of the total number of large clasts. This is marked by a slight increase in the number of quartzose and mafic igneous lithologies forming large clasts. Schists continue to make up the same proportion of small clasts as seen in the Dudar Formation.

8. In the Alhambra formation there is a significant fall in the proportion of large clasts made of schist. Again as in the Pinos Genil formation this fall is balanced by an increase in the number of large clasts formed of hard quartz rich lithologies. In the small clasts sizes there is a slight increase in the proportion of schist (around 5%). The Alhambra Formation is the most compositionally mature formation in the eastern Granada Basin.

9. No new lithologies are introduced as conglomerate clasts throughout the sequence of the eastern Granada Basin. On a large scale there has therefore been no important change in the compositional character of the source region in the Sierra Nevada during the deposition of the conglomerate formations.

10. As each formation shares the same source region the compositional maturity differences between each formation must be explained by some sedimentary process, or combination of processes. There are two possibilities:

i Changes in sedimentary environment from marine to terrestrial in the late Tortonian, would have resulted in increased weathering rates. Combine this with a slightly more distal location for each younger formation and the conditions are set for increasing compositional maturity.

ii The second possibility involves sediment recycling of earlier deposits, starting with the Dudar Formation being incorporated into the Pinos Genil Formation, and then both of these into the Alhambra Formation. There is evidence for the uplift of the basin flanks from the dip angles of the La Peza, Quentar, and Dudar Formations, and the reappearance of the Alpujarride as a source. This could uplift earlier deposits into the realm of becoming sediment sources themselves, in a similar fashion to what is happening to the eastern flank of the basin today, as the Rio Genil erodes the study area and carries it off into the active Granada Basin.

As the Alhambra formation presents the greatest contrast in maturity, with a significant reduction in the amount of schist, it is possible that the Alhambra formation alone is derived from the recycling of earlier deposits. The relatively small differences in composition between the Dudar and Pinos Genil Formations could be due largely to the differences in depositional environment, and have involved little recycling of earlier sedimentary deposits.

It is not possible to unequivocally attribute the differences in compositional maturity observed to either process. However, the increased rounding and significant reduction of large schist clasts in the Alhambra formation, deposited in a similar environment to the Pinos Genil formation, combined with the evidence for uplift of earlier sedimentary deposits strongly suggest the possibility of reworking of earlier deposits.

12. A model of clast composition evolution in a recycling open system can explain the observed pattern of clast composition with size in the Granada Basin. Labile schist clasts break down quickly in comparison to harder quartz rich clasts, reducing the proportion of coarse schist clasts in succeeding cycles of erosion and deposition. Despite this the proportion of small schist clasts does not increase, but remains at the same level. This is predicted by the open system recycling model where sand production removes schist material constantly from the conglomerate size range.

4. Sandstone Petrography

4.1 Introduction

This section completes the conventional petrographic examination of the grain size spectrum of the sediment in the study area, from boulders to sand. It should complement and extend the data presented in Chapter 3 on conglomerate petrography, and not be seen as an entirely distinct topic. The rationale for studying the composition of the sediments as presented in section 3.1 applies here also. Source remains unchanged, apart from the possibility of the recycling of previous sedimentary deposits, so any quantitative changes in compositional and textural maturity can be related to sedimentary dynamics within the basin, and recycling in particular.

In this section details of the petrography of the sand component of the mid-Miocene-Pleistocene sediment of the eastern flank of the Granada Basin are presented. Sandstone petrography has been used in many cases as an indicator of sedimentary provenance, sediment maturity (for example Dickinson and Suckzec 1979, Dorsey 1988) and to constrain diagenetic processes (eg. Morton 1985). Here, however, sandstone composition is to be used, not only to indicate provenance but also to investigate the effects of sedimentary recycling and sedimentary processes on the provenance information carried by the sediment, in what is an almost closed system.

The data presented below consists of petrographic descriptions of texture and quantitative estimates of composition obtained by point counting. Each formation in the study area is described in turn, firstly in terms of general petrography (composition, fabric, diagenesis). Details of point counts are presented for each formation and the data used to place the sediments within the context of the sandstone provenance discrimination models of Dickinson and Suckzec (1979) and Dickinson et. al. (1983). The data is then critically assessed using with regard to source evolution and, more critically, in terms of sediment compositional evolution through possible stages of recycling.

4.2 Sample Locations

Figure 3.1 is a sketch map of the study area, in the eastern edge of the Granada Basin. It shows the disposition of metamorphic basement rocks and the overlying sediments of the Granada Basin. The locations of sampling sites within the Basin are numbered 1 to 13, along with descriptions of each, detailing stratigraphic level. They include the same sites where conglomerates were sampled.

4.3 Petrography of the Sediments

For each formation a generalised petrographic description is presented below. The range of composition of grain types is described first. Quantitative details of composition

derived from point counting are given below in **section 4.4**, but first a general description of the range of grain types is presented. Following this the textures of deposits in each formation are described, including details of any matrix, cements and grain alterations. These latter factors are critical in assessing the sediments suitability as a provenance indicator, and as an indicator of sedimentary processes. The composition of the sandstones is useful for studying processes of sediment breakdown, only if there has been no post depositional alteration by grain dissolution and cementation. If changes to sediment composition are to attributed to variations in sedimentary processes, including recycling, post-depositional changes need to be well constrained. This is particularly important for the sediments in the last deposit of the border of the basin, in the Alhambra Formation, because is the breakdown of these deposits that is most critical as an indicator of sedimentary processes. Further to this, an understanding of the framework components and cements is critical to the interpretation of the geochemistry of the sediments which is presented in Chapter 5. Particular correlations and signatures can be skewed by diagenetic alteration and the addition of cements, especially carbonate cements.

La Peza and Quentar Formations

Composition: These formations comprise various facies of calc-arenite (sensu. Pettijohn 1975). They are shallow marine carbonates, dominantly composed of bioclastic carbonate grains but with an important terrigenous detrital component derived from a metamorphic source. They are packstones and grainstones in the classification of Dunham (1962), and biomicrites in the classification of Folk (1962).

The bioclasts include broken fragments of bryozoans, foraminifera, molluscs, calcareous algae and echinoids (see **Plates 4.1, 4.2, 4.3**). The metamorphic terrigenous detritus is composed of fragments of low to high grade metamorphic rocks. These fragments include polycrystalline quartz, mica schists, garnet mica schists and phyllitic and graphitic schists. Muscovite is common, either as single crystalline grains or as coarse polycrystalline grains. Metamorphic heavy minerals are present in a small but significant quantity, most notably garnet and epidote, but also tourmaline, hornblende and rarely zircon. There is some evidence of sedimentary recycling, as in sample QR2 (**Plate 4.4**) there is a grain that is clearly a fragment of an earlier sedimentary deposit. It consists of angular quartz grains supported by a sparry calcite cement.

Texture: The calcarenites are mostly coarse grained and moderately well sorted. Carbonate grains are broken, probably syn-depositionally, and are subangular to angular, as are the terrigenous silicate grains. They are well compacted with little porosity, which is all primary. Indeed the calc-arenites form resistant orange-brown cliffs in their area of exposure due to their indurated nature. Occasionally grains of monocrystalline muscovite are kinked indicating some post depositional compaction. They are grain supported, though some micrite matrix is present (**Plate 4.2**). This matrix increases in abundance upwards in the formation, towards the base of the Dudar Formation. No cement is present between grains. However, the skeletal cavities of bioclasts such as bryozoans and foraminifera often contain sparry calcite. Some echinoid plates have a rim of syntaxial calcite cement (**Plate 4.2**). This all suggests a

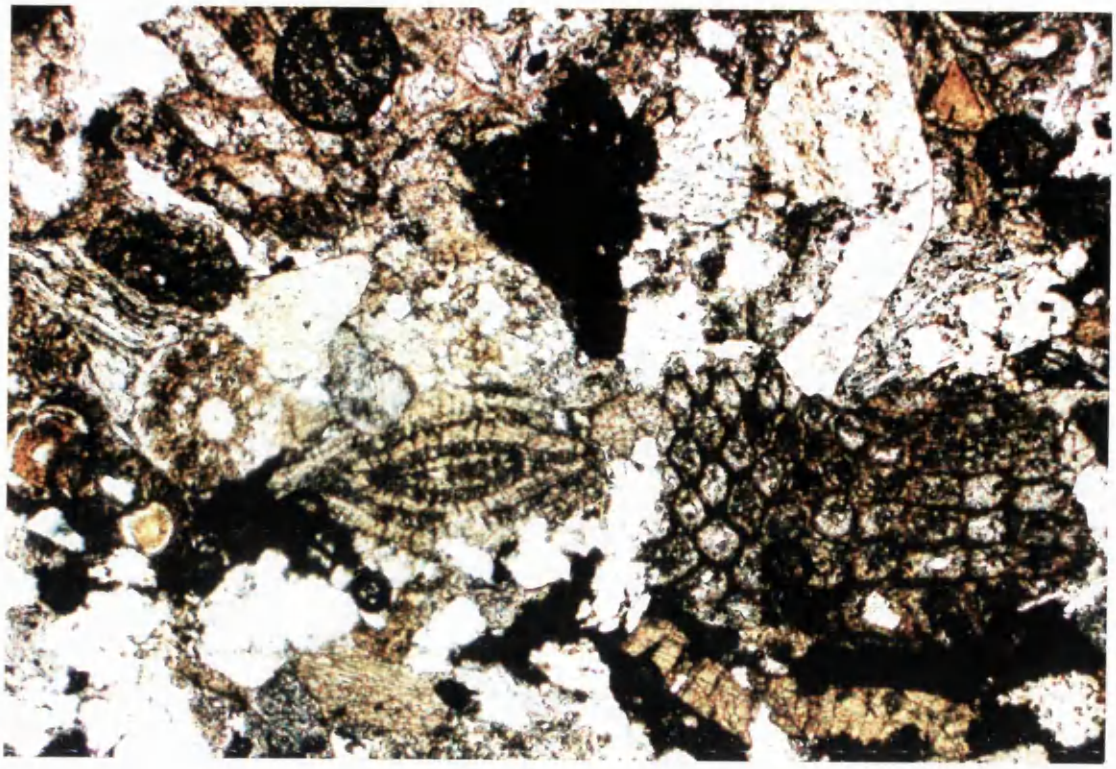

Plate 4.1 Quentar Formation, sample QR4 from sample site No.5 (Fig. 3.1). Plane Polarised Light, mag. X25. From centre left to right, fragments of echiniod spines, foraminifera and bryozoa (with calcite spar in body cavaties) A dark fragment of calcareous algae is visible above the centre of the view. In the bottom right below the bryozoan, micrite mud surrounds a broken mollusc fragment.

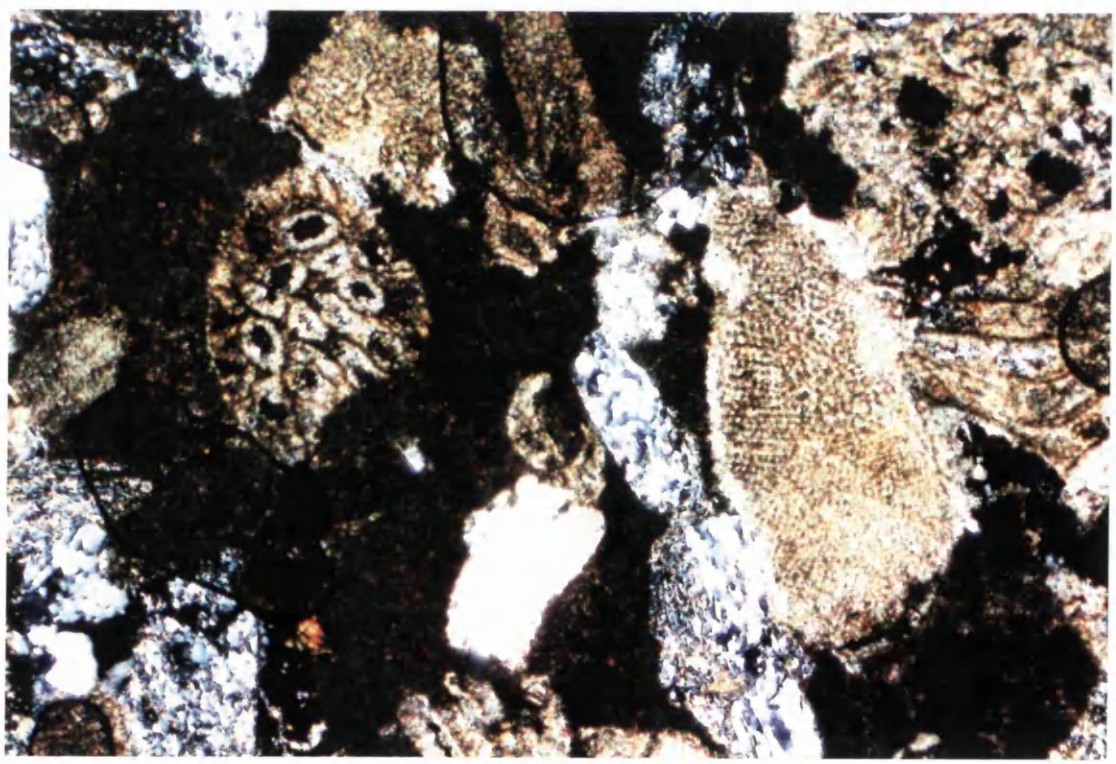

Plate 4.2 Sample QR4. Crossed polarised light, mag. X25. Echinoid and mollusc fragments, and low to medium grade metamorphic rock fragments in an extensive micrite mud. On the right is a section through an echinoid plate, with a syntaxial calcite spar rim.

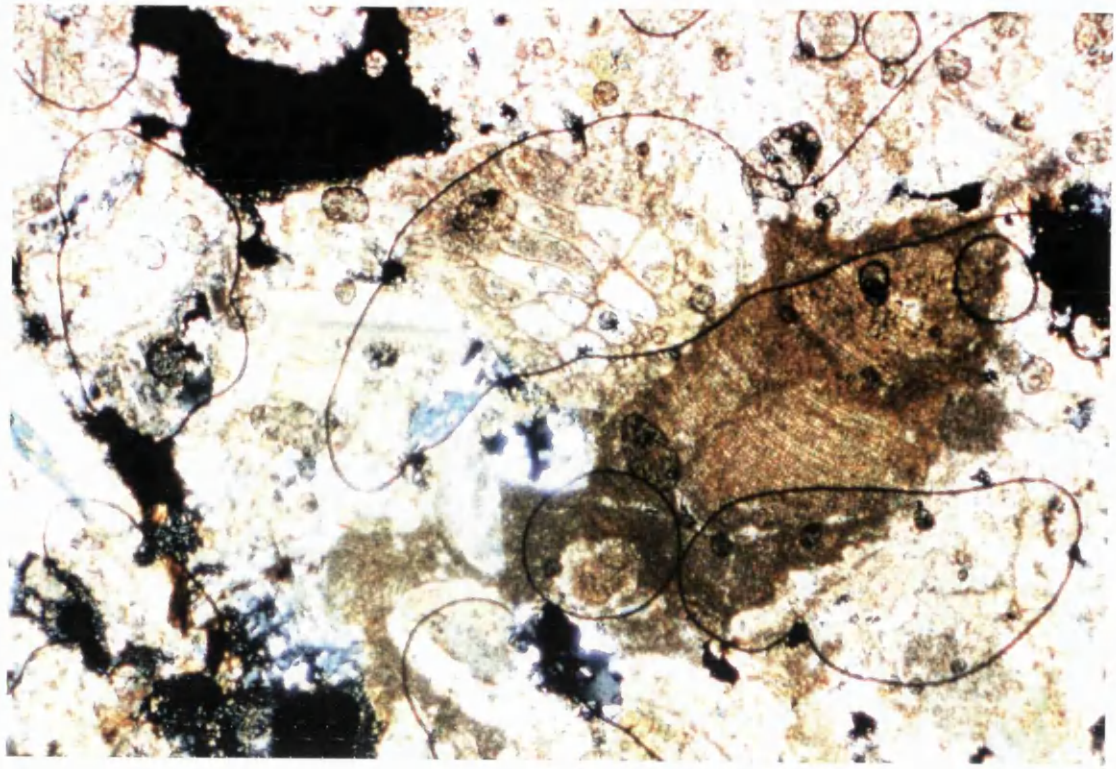

Plate 4.3 Quentar Formation, sample QR2, sample site No.4 (Fig. 3.1). Plane polarised light, mag. X25, This slide has many air bubbles in the fixing glue. In the lower right is a large fragment of calcareous algae, and below this a section of a bryozoan. Some mollusc fragments are in the centre left. Micrite mud matrix in lower middle of view.

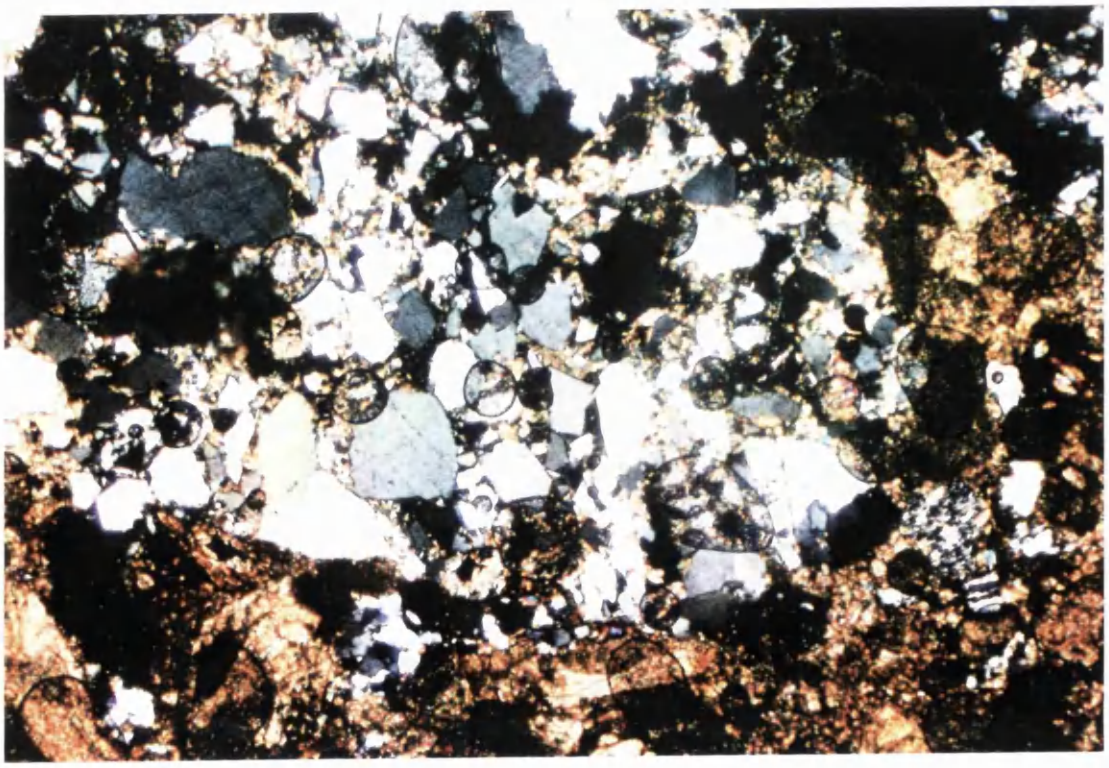

Plate 4.4 Sample QR2. Cross polarised light, mag. X25. View shows recycled sedimentary lithic grain (in top left quadrant) composed of angular quartz grains cemented by calcite spar.

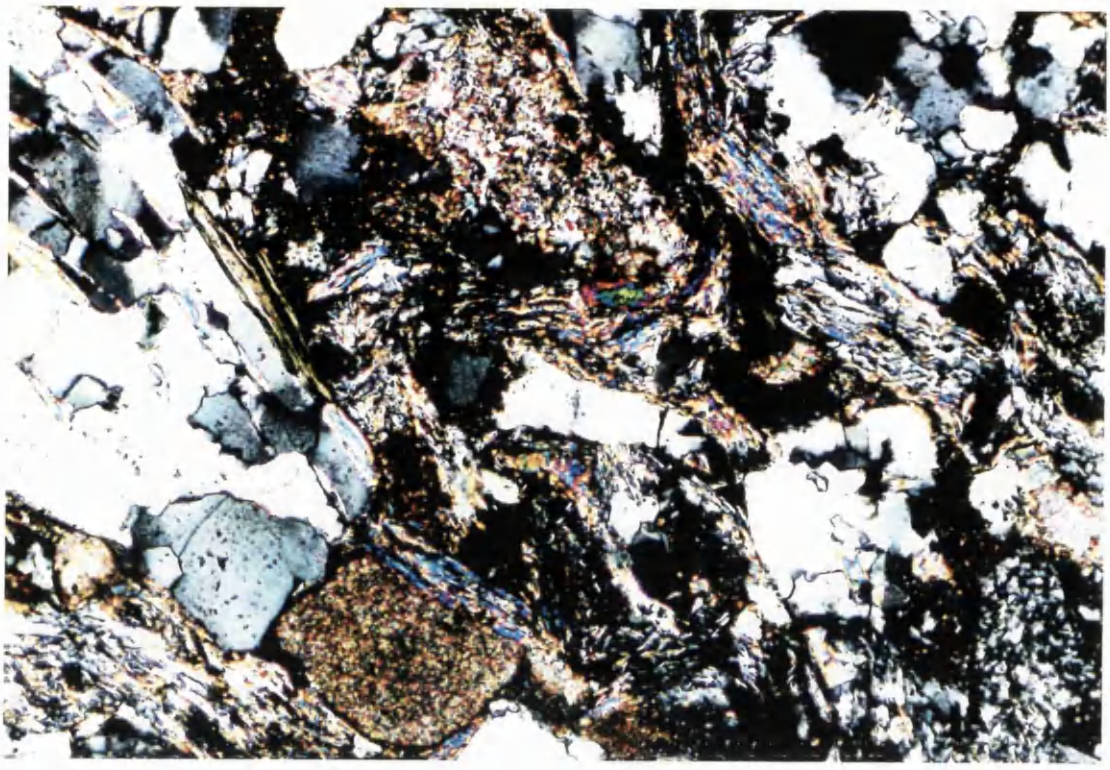

Plate 4.5 Sample D1. Cross polarised light, Dudar Formation, sample site No. 6. Mag. X25. Grains shown: high grade mica schist (left), fine grained carbonate (lower centre left), med-low grade mica rich schists (centre, top centre, right), coarse quartz-mica aggregates (top right), angular to subangular mono and polycrystalline quartz. Low grade schists and mica aggregates are squeezed between more rigid grains to form a pseudomatrix.

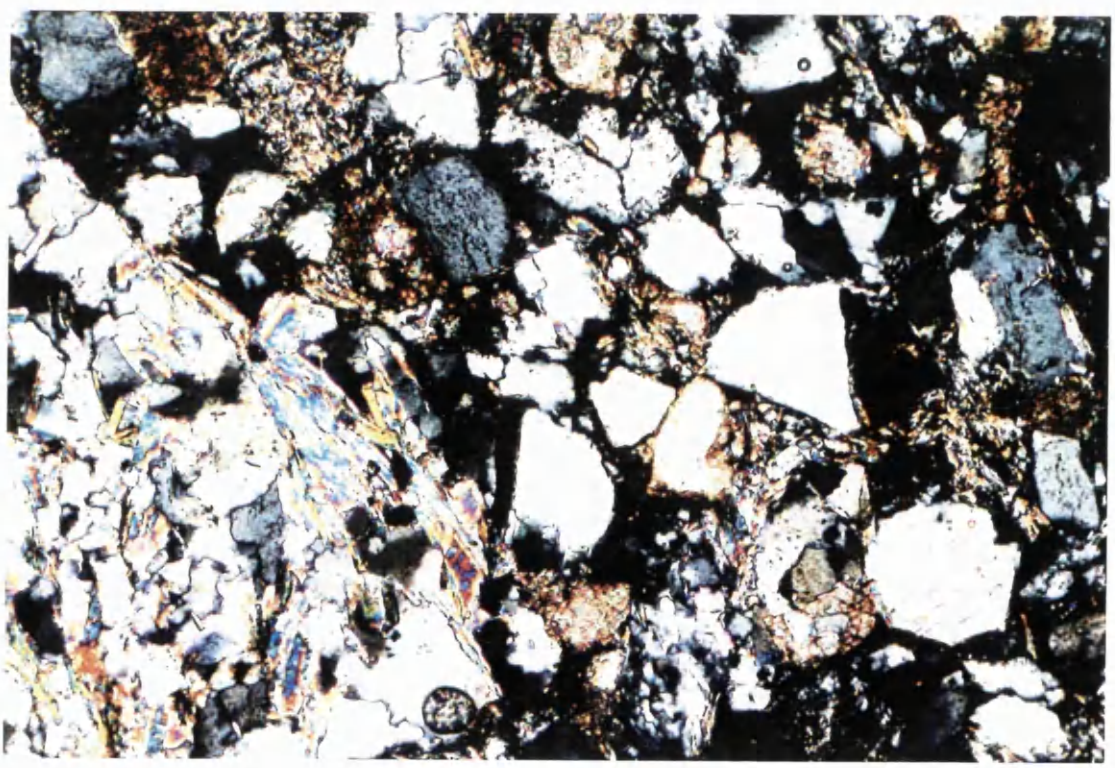

Plate 4.6 Sample D1. Cross polarised light, mag. X25. General view of petrography showing coarse high grade mica schist (lower left), angular and subangular mono and polycrystalline quartz. In the lower right is a grain showing some red staining, this is a grain of plagioclase feldspar. Note the low number of grain contacts, which are mostly single point and some planar.

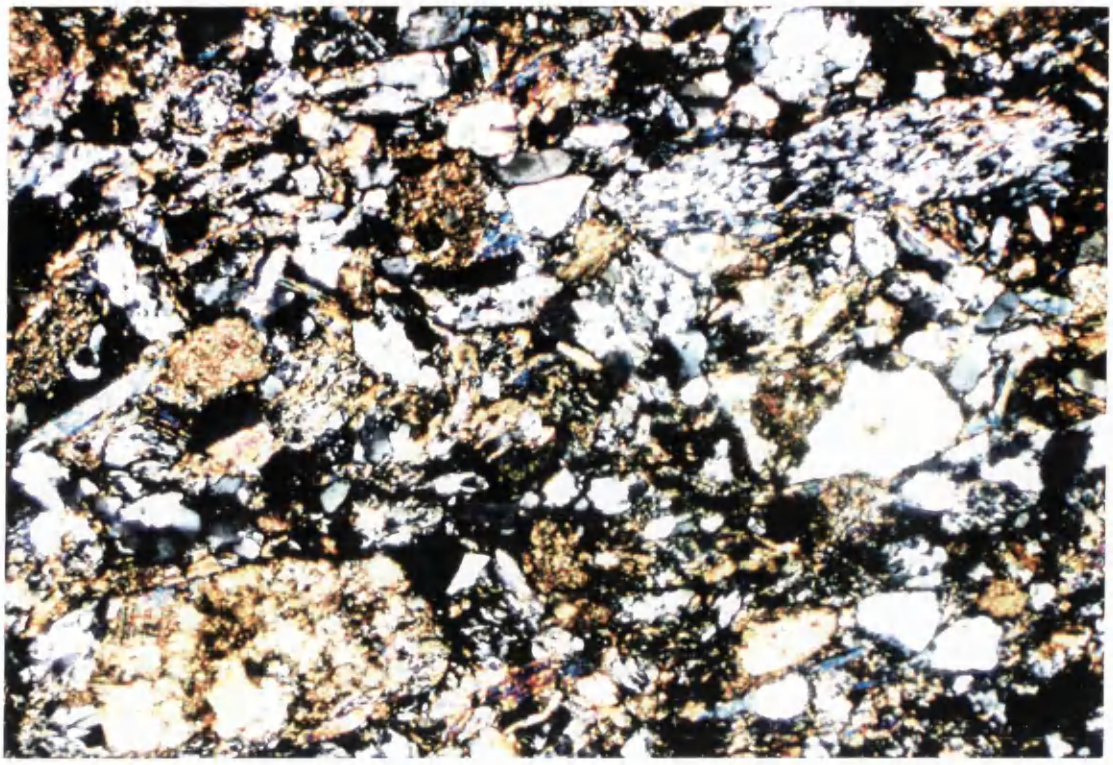

Plate 4.7 Sample D1. Cross polarised light, mag. X25. Lithic grains in Dudar Formation. Marble fragment in lower left, low grade phyllitic schist in upper right. Angular/subangular quartz, fresh monocrystalline muscovite in centre left. Muscovite often interstitial to quartz and lithic grains. Note the high carbonate grain content, and the small amount of micrite matrix , noticable around the large angular quartz grain on the right. Poorly sorted.

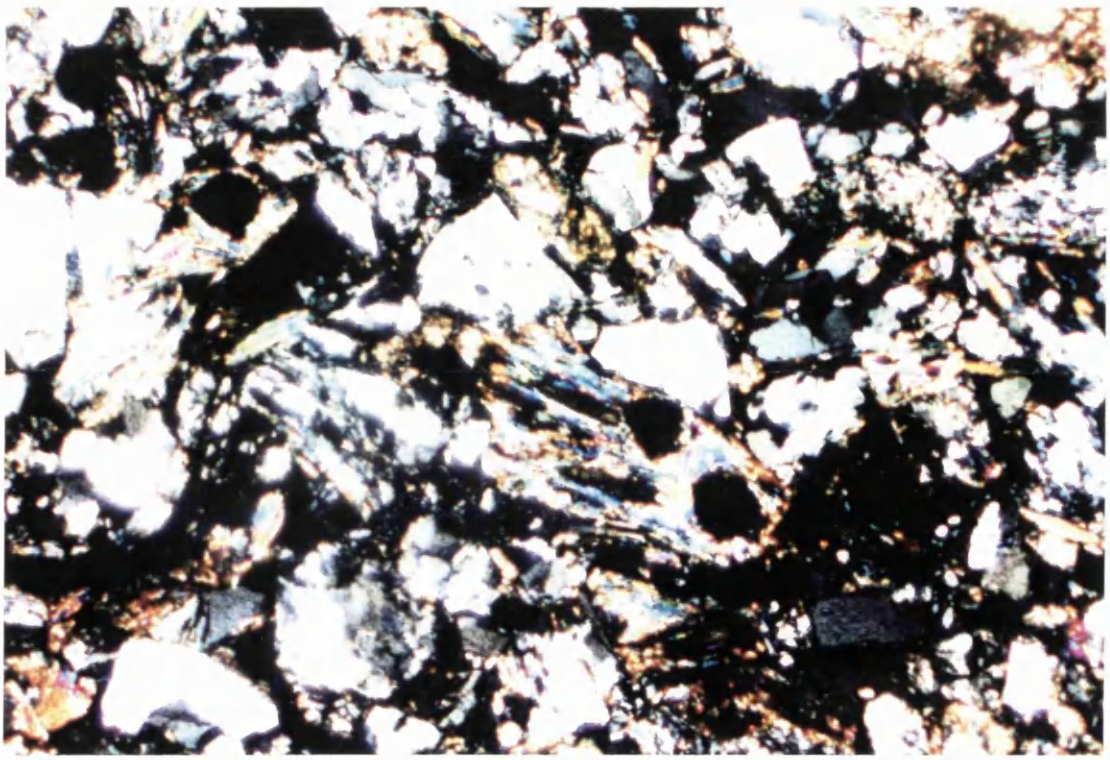

Plate 4.8 Sample S13. Crossed polarised light, sample site No.1. Mag. X25. Garnet-mica schist in centre of view. Angular quartz and subangular polyquartz are abundant. Numerous grains of fine grained monocrystalline muscovite.

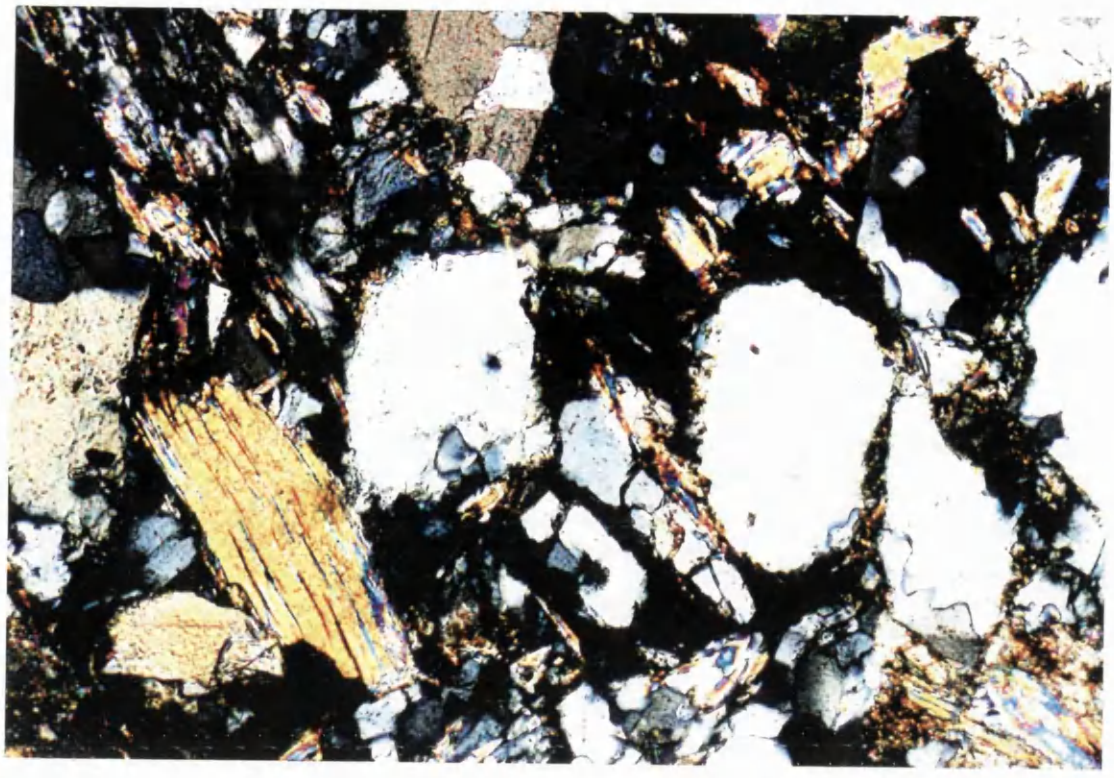

Plate 4.9 Dudar Formation, sample S13, location No.1 (Fig. 3.1) Cross polarised light. Grain of coarse monocrystalline muscovite, with top end kinked is the only clear evidence of compaction. Polycrystalline quartz is subangular. Feldspar-Quartz aggregate at left and other medium grained mica schist fragments. Numerous small laths of muscovite. Poorly sorted sediment with point/point grain contacts. Mag. x 25

Plate 4.10 Dudar Formation. Sample DU2, sample site No.1 (Fig. 3.1). Mag x 25. Heavy minerals. Largegrain is amphibole, sourced from the amphibolite outcrops in the Ophiolite unit of the Mulhacen complex. Under the amphibole to the right and also above to the left are several angular grains of garnet. All the heavy minerals in the Dudar Formation are quite fresh; dark rims around garnet is relief, not alteration. Some crystals to the lower right are in a garnet-mica schist fragment, picked out by a brown alteration product of muscovite in this area.

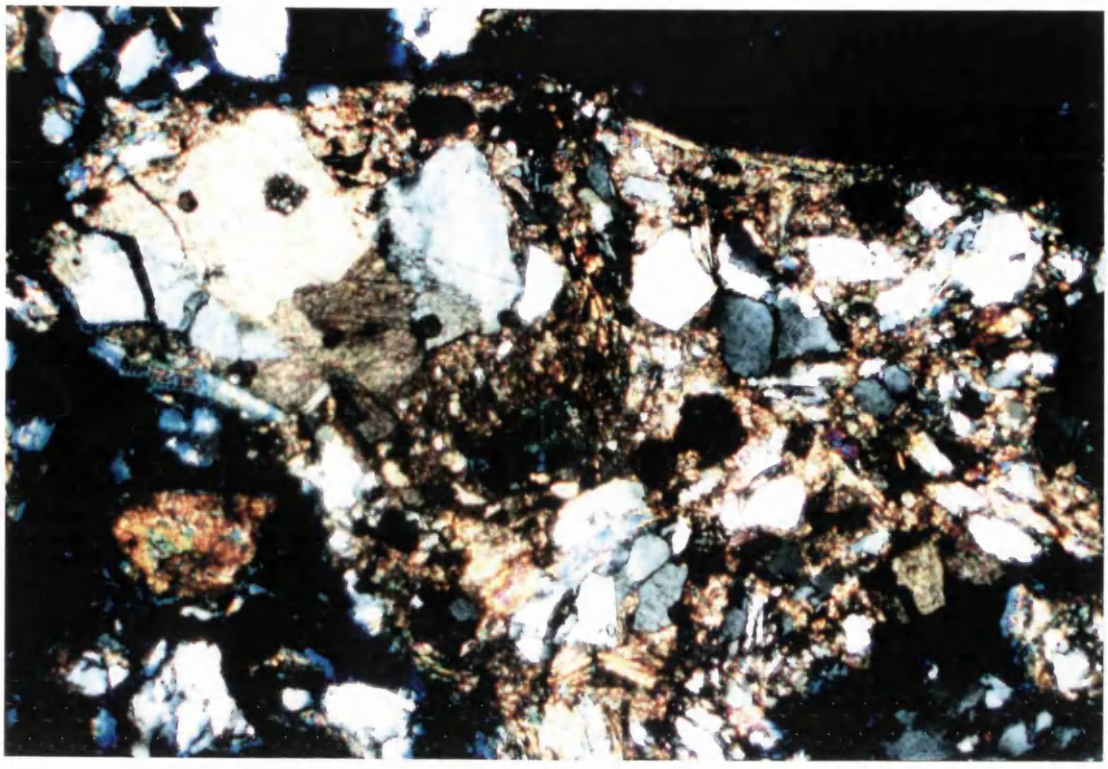

Plate 4.11 Dudar Formation, sample 5.8, sample site No.8 (Fig. 3.1). Grain mount in cross polarised light. Surviving fragment that shows sedimentary texture. Angular to subangular grains in micrite. Large grain of quartz-calcite aggregate, possibly a siliceous marble, is seen at the top left of the view. This is a poorly sorted sediment. Mag x25

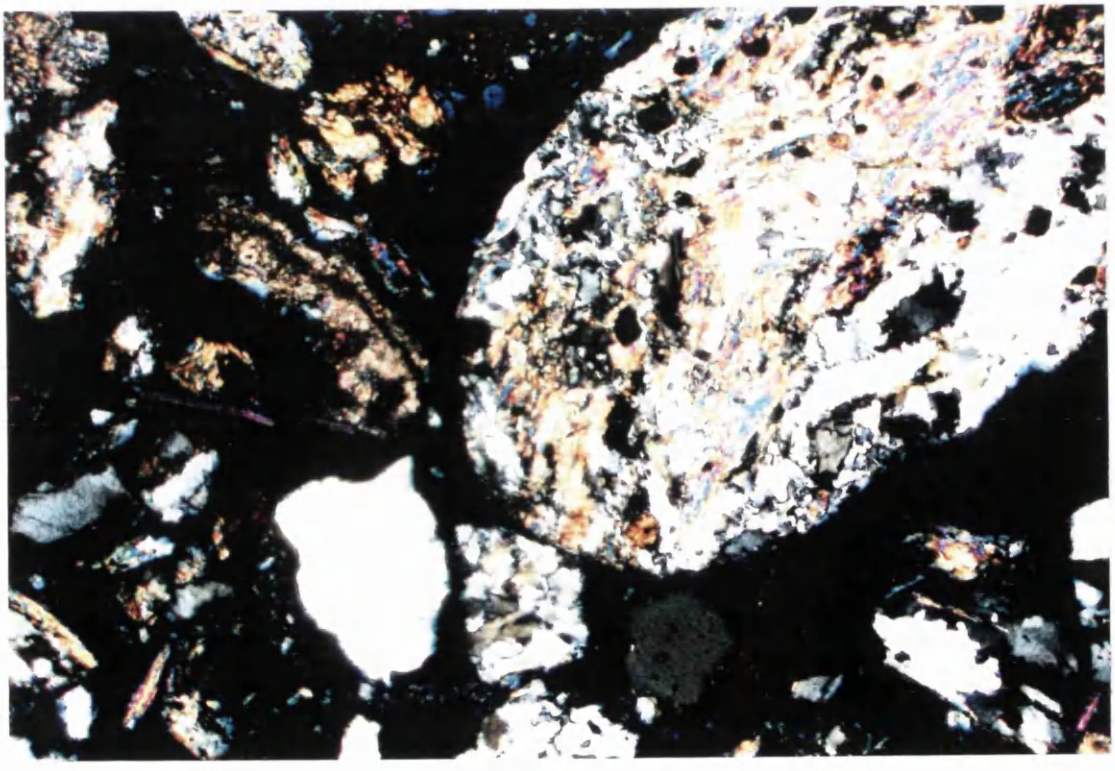

Plate 4.12 Pinos Genil Formation, sample 5.2 sample site No.9 (Fig. 3.1). Grain mount in cross polarised light. Coarse, well rounded garnet-mica schist grain. Note that smaller grains of polycrystalline and monocrystalline quartz remain angular and subangular. Other components include possible micrite matrix (liberated in the grain mount) and muscovite which occurs as single monocrystalline grains and in lithic fragments. Mag x2.5

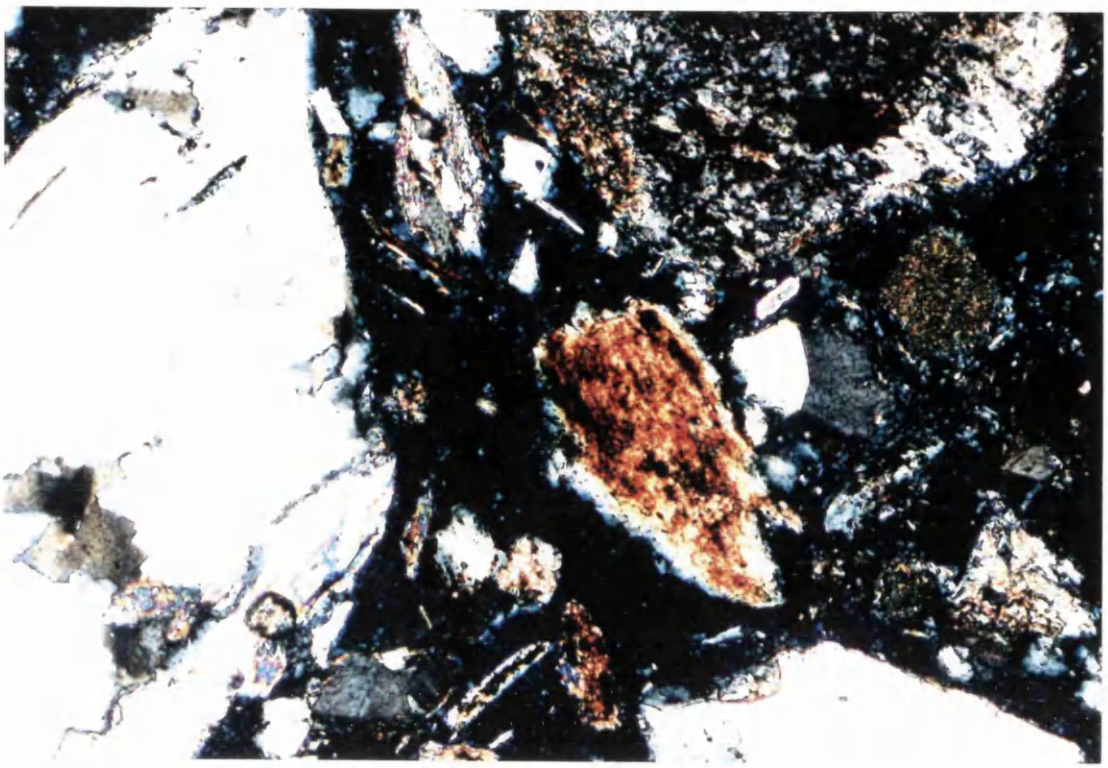

Plate 4.13 Pinos Genil Formation, sample site No. 9 (Fig. 3.1). Grain Mount in cross polarised light. Mag. x 25. Centre is an oxidised fragment of muscovite, demosnstrating the increase in weathering experienced by the terrestrially deposited Pinos Genil Formation compared to the Dudar Formation.

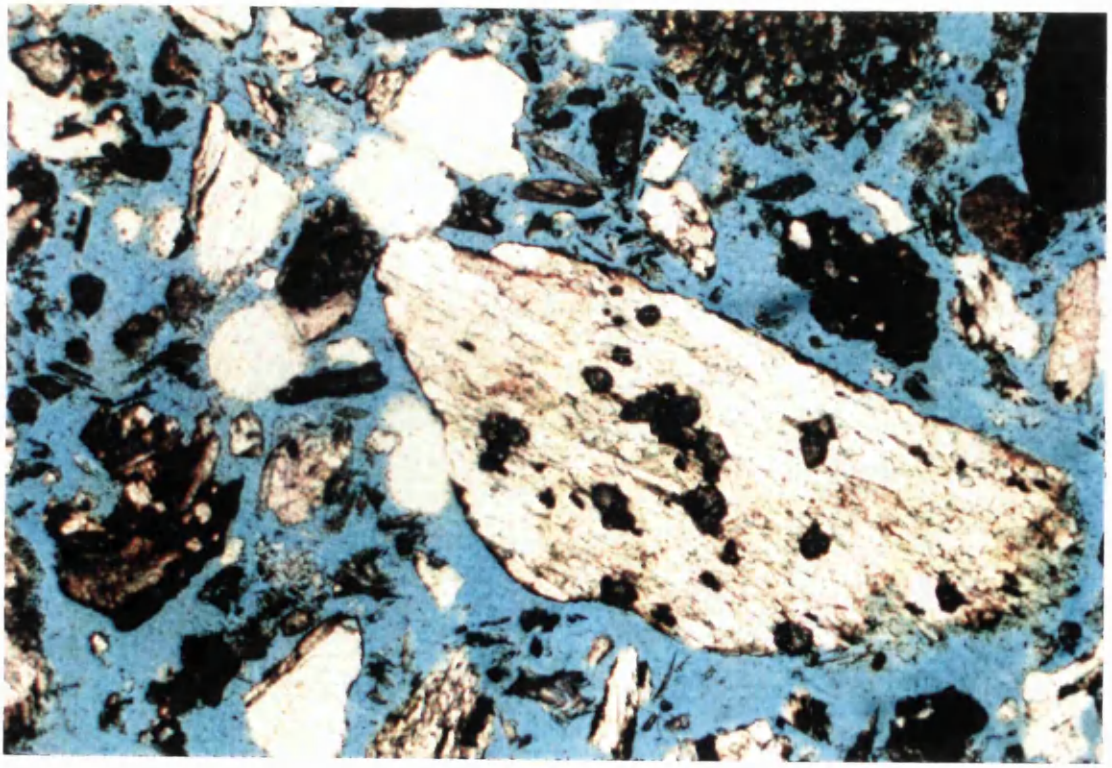

Plate 4.14 Pinos Genil Formation. Location No. 9 (Fig. 3.1). Mag. x 25. Plane polarised light. This sample shows oxide coatings of lithic grains. Note also rounding of large lithic grain to centre and right, but also more irregular possibly fractured end to the right

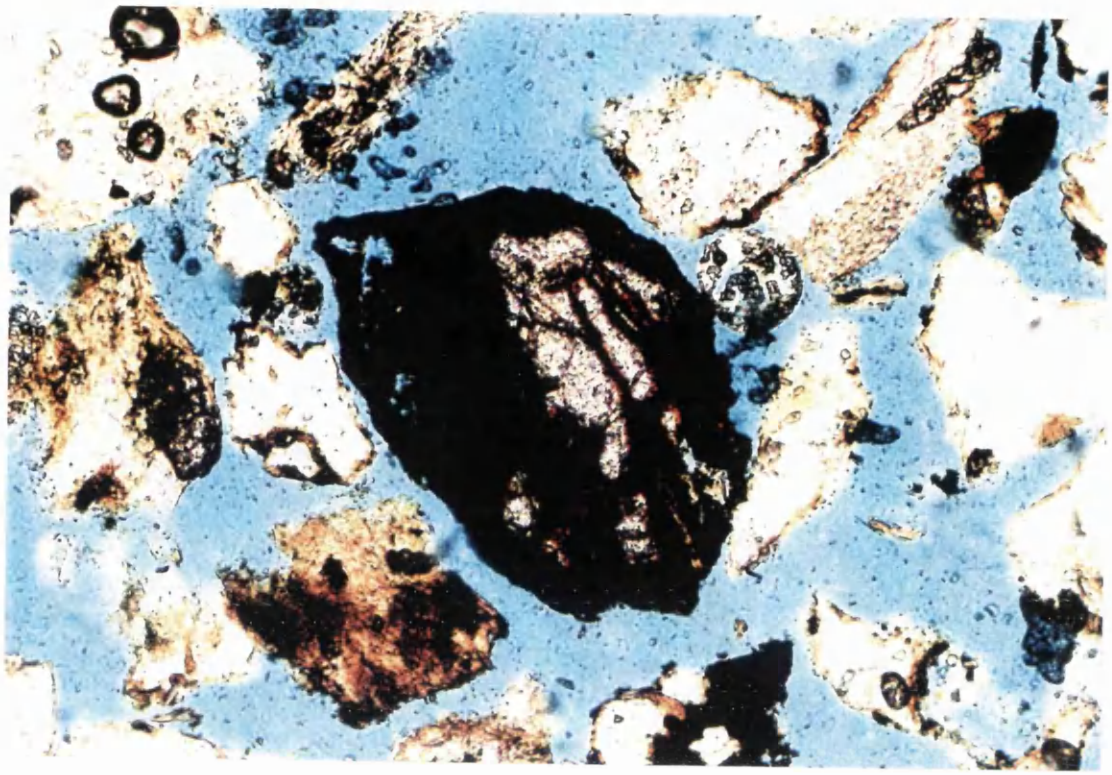

Plate 4.15 Alhambra Formation. Location No. 10 (**Fig 3.**1). Mag. x 25. This shows the alteration of a detrital garnet to opaque oxides. Compare this with the fresh garnets from the Dudar Formation in **Plate 4.10**.

possible earlier period of deposition and cementation prior to erosion and reworking of the carbonate detritus into the present clacarenite deposits.

Dudar Formation

Composition: Carbonate detritus, though not rare, is reduced in amount, and grain components are dominantly silicates derived from a terrigenous source of metamorphic character.

The sand component is dominated by metamorphic polycrystalline and monocrystalline quartz grains (**Plate 4.6**). Lithic grains are abundant, and are all fragments of metamorphic rocks. Included are mica-schists, garnet-mica schists, amphibolites, marbles, polycrystalline muscovite grains and phyllitic and graphitic micaceous low grade metamorphic rock types (see **Plates 4.5 to 4.6**). High grade metamorphic rock types are represented in great numbers in contrast to the generally lower grade rock types found in the Quentar formation. Muscovite is common occurring as fresh monocrystalline grains (**Plate 4.9**), and as polycrystalline aggregates derived from coarse grained, high grade, metamorphic rocks. The heavy minerals are all fresh (**Plate 4.10**), the most common being garnet and epidote, but tourmaline, hornblende, zircon and iron oxides are also present. Plagioclase and alkali feldspar are present in small amounts.

Texture: Grain size is variable from fine to coarse grained, but individual samples are moderately to well sorted. Grains are angular in samples from the proximal part of the Dudar Formation Fan-Delta deposit (Locations No. 1,2 & 3, **Fig. 3.1**), and angular to subangular in distal samples (Locations No. 6, 7 & 8, **Fig. 3.1**). These distal locations are also at a higher stratigraphic level than the samples in the proximal locations. Subangular grains are mainly metamorphic fragments. Grains are fresh and unweathered and there is no obvious post depositional alteration such as pressure solution or grain dissolution. Muscovite grains are often oriented parallel to each other sometimes in sufficient numbers to impart the appearance of schistosity to the sediment when viewed in thin section. Grain contacts are just touching or planar suggesting that there has been little post depositional compaction. Muscovite grains are sometimes kinked, indicating some compaction. However, some fine grained micaceous grains can be found squeezed into interstices between harder quartz and lithic grains forming a pseudomatrix (**Plates 4.5, 4.6**). Some conventional matrix is present, and in places extensive amounts of micrite mud (**Plate 4.11**), especially in distal samples and near the base of the fan (samples at Location 3, **Fig 3.1**). However, grain support is the norm for the proximal reaches of the fan-delta. In general the texture of the sediments of the Dudar Formation is immature, with a rather chaotic poorly sorted appearance and individual grains are often hard to distinguish in thin section. This immaturity is imparted by the angularity of grains, the presence of extensive pseudomatrix and some conventional matrix, and of large amounts of heavy minerals and mica.

Pinos Genil Formation

Composition: There is no qualitative difference between the sands of the Pinos Genil and Dudar Formations. The composition is dominated by quartz and low to high grade

metamorphic lithic grains. Muscovite is abundant. Carbonate mud matrix is present in some samples, and a calcite spar cement is important in some samples.

Texture: The Pinos Genil Formation sediments are moderately to poorly sorted with many samples matrix supported, while the remainder are grain supported, some of which are cemented by coarse calcite spar. Detrital matrix is present in most samples which consists of a brown stained mass of fine quartz and mica flakes. Pseudomatrix is present in some samples; fine grained, usually micaceous, low grade metamorphic lithic fragments are squeezed into the interstices between hard quartz and lithic grains. Quartz grains are angular to subangular. Some large schist fragments are rounded or well rounded (**Plate 4.12**), but lithic grains are mostly subangular to subrounded. There is no grain suturing and grain contacts are point to point or planar. Many muscovite grains are altered (**Plate 4.13**), appearing brown with a coating of iron oxide. These grains frequently exhibit diminished birefringence and some chloritisation. Micas within some schist fragments also show alteration. However, most muscovite grains are fresh. Some lithic grains are also coated with brown iron oxide similar to that which colours the matrix, giving the sediments their red colour (**Plate 4.14**). Large grains of polycrystalline chlorite are also present. It is unclear if these are detrital or if they are pseudomorphs generated by post depositional processes.

Alhambra Formation

Composition: The range of composition of sand grains in the Alhambra Formation is the same as the underlying Dudar and Pinos Genil Formations. Coarse grains of high grade metamorphic rocks are common, as is a large amount of fine grained muscovite detritus. Monocrystalline quartz is common and feldspar grains are present but in small amounts. Brown micrite is present in some samples, as is calcite spar cement.

Texture: The Alhambra Formation sediments are poorly sorted. Lithic grains are dominantly subangular to subrounded, but very large grains are rounded. Monocrystalline quartz grains are angular to subangular. Mica grains are small; there appear to be no large polycrystalline grains of muscovite, despite the presence of coarse grains of high grade metamorphic rocks. Some samples taken were matrix supported, while some again are grain supported. There is no evidence of grain dissolution, and compaction appears to have been minimal. Low grade, fine grained micaceous rock fragments, along with mica grains form a pseudomatrix in some samples, appearing squashed between harder lithic and quartz grains. Many grains are badly weathered and chloritisation of muscovite and biotite is common. Grains often have a coating of brown iron oxide. Garnet is often badly affected and oxidised to opaque material over much of each grain (**Plate 4.15**).

4.4 Suitability of Granada Basin sediments for provenance and sedimentary process analysis

To study provenance characteristics and the dynamics of sedimentation in the sediments of the Granada Basin it is necessary first to constrain the effects of depositional processes versus post depositional diagenetic alterations on the composition of the sediment.

The composition of the sediment must be controlled only by the provenance and the altering effects of erosion and transport.

The compositional immaturity of the sediments, and the Dudar Formation in particular, suggests that not only are these deposits first cycle orogenic, but also that little diagenetic alteration has occurred. The abundance of heavy minerals such as epidote and amphiboles is high. According to Morton (1985) these minerals are susceptible to intrastratal solution. The presence of these unstable grains throughout the Miocene to Pleistocene sediments of the eastern Granada Basin, and especially the Dudar Formation, indicates that extensive destruction of labile sand grains has not occurred. In the Dudar Formation this has resulted from initial rapid deposition, and no intra-formational diagenetic alteration. Any subsequent changes in the abundance of, or composition of heavy minerals and lithic fragments in the Pinos Genil and Alhambra Formations has been due to processes of erosion and deposition in a terrestrial environment, with a higher rate of weathering.

In each formation there is no evidence of intrastratal grain dissolution or replacement, save perhaps some chlorite grains in the Alhambra formation, which have an uncertain origin. No pressure solution effects or grain suturing are seen. Post depositional compaction has been small and porosity can be high. Some samples, deposited in terrestrial environments do have a calcite cement (interpreted as caliche), but no evidence of grain replacement.

Some grains from the Pinos Genil and Alhambra Formations are badly altered, showing extensive chloritisation and oxide staining (**Plate 4.14**). Iron oxide coats many grains, which must have been acquired before deposition in a terrestrial fluvial environment. The oxide coatings show no evidence of post depositional alteration.

It is reasonable then to assume that there has been no diagenetic alteration of the framework components of the sandstones that make up the eastern flank of the Granada Basin. Therefore these sediments are suitable for provenance studies but especially the assessment of the effects of sedimentary erosional and depositional processes on sand composition. Any grain alteration seen is due to pre-depositional weathering during erosion and transport. The Dudar Formation is the oldest deposit in the basin with a terrigenous source, and perhaps also once the deepest buried, but it contains the freshest, most immature sediment in the Granada Basin. It might be reasonable to expect this deposit to be the most diagenetically altered. As demonstrated in **Chapter 3**, the source for detritus remained constant in composition, save for the reworking of the earliest sedimentary deposits. Differences in composition between formations, and the increasing weathering and alteration in younger sediments is due to deposition in a subaerial environment, combined with possible reworking of older deposits into younger deposits. In sections to follow evidence is presented that allows conclusions to be drawn about the degree of sediment breakdown between formations.

4.5 Quantitative Sandstone Composition: Point Counting Results

In this section results of point counting are presented. These data quantitatively detail the composition of the framework grain components of the sediments of the eastern border of the Granada Basin. **Table 4.1** lists the grain parameters employed, for framework grains and

Table 4.1 Definition of point counting grain parameters

Conventional framework grain parameters:	
Qm	Monocrystalline quartz
Qp	Polycrystalline quartz of metamorphic origin. Monomineralic by definition. Presence of any amount of other minerals classifies grain as lithic.
F	Monocrystalline plagioclase and K-feldspar
L	All polymineralic metamorphic lithic grains. Subdivisions outlined in **Table 4.2.**
M	Monocrystalline muscovite and biotite.
Heavy Minerals	Monomineralic grains of garnet, epidote, tourmaline, zircon, amphibole.
Matrix	Fine grained interstitial material with grain size <0.0625mm, composed of mica, quartz, chlorite. Carbonate mud also common
Cement	All calcite sparite.
Recalculated Parameters	
Qt	Qm + Qp
Lt	L + Qp

also for the subdivision of lithic grains by type. Appendix 1, A1. describes the method used in detail. The actual counting results are included in Appendix 3.

The analyses of the sandstones from each formation are plotted on ternary diagrams to allow easy comparison and the assessment of any compositional trends. The diagrams also allow assessment of the inter-dependence of different grain types. The plots employed are the sandstone classification plot of Pettijohn (1954) in **Fig. 4.1**, and the similar QFL and QmFLt provenance discrimination plots derived by Dickinson and Suczek (1979) in **Fig. 4.2**. Using the first plot allows the sandstones from the Granada Basin to be classified quantitatively.

In **Chapter 1** the development of ternary provenance discrimination plots for sandstones is reviewed, and **Fig. 1.3** outlines the provenance types discriminated. The tectonic setting of the Granada Basin is well constrained, within an orogenic zone at a convergent plate margin. The uplift of the Betic Cordillera in such a setting should produce sand that would plot within the recycled orogenic provenance areas on the QFL and QmFLt plots. Therefore, using the Granada Basin sands acts as a test of the discriminating power of these plots. A conclusion is reached below on the plot that best discriminates the correct tectonic setting of the Granada Basin sedimentation.

The aim of this study is also to constrain the effects of sedimentary processes on the composition of sediment in orogenic settings. After provenance has been discussed this issue is addressed, using patterns of composition and especially details of the lithic grain populations in the sediments.

4.5.1 Sandstone classification

In **Fig. 4.1** analyses of the sandstones from the Eastern Granada Basin have been plotted on ternary diagrams with monocrystalline quartz, total lithic fragments and feldspar (QmFLt) as the end members. The sandstone classification areas as defined by Pettijohn (1954) are indicated. All samples can be classified as **lithic arenites**. This is due to their high content of metamorphic lithic grains and the paucity of feldspar.

This diagram was found later by Dickinson and Suczek (1979) to allow discrimination between different provenance types , and sandstones generated in different tectonic settings. This application of the QmFLt plot is discussed below with regard to the sandstones of the Granada Basin.

4.5.2 Q-F-L, Qm-F-Lt and Qp-Lvm-Lsm ternary plots

Q-F-L

Analyses of sands from each formation have been plotted on QFL ternary diagrams, shown in **Fig. 4.2**, with one plot for each formation. All samples plot around the junction between the recycled orogenic and the magmatic arc provenance fields. For the Pinos Genil and Alhambra formations most samples plot in the undissected and transitional arc provenance areas. Samples from the Dudar Formation mostly plot within the recycled orogen field. A slight inter-formational variation is evident. The proportion of lithic grains increases upwards

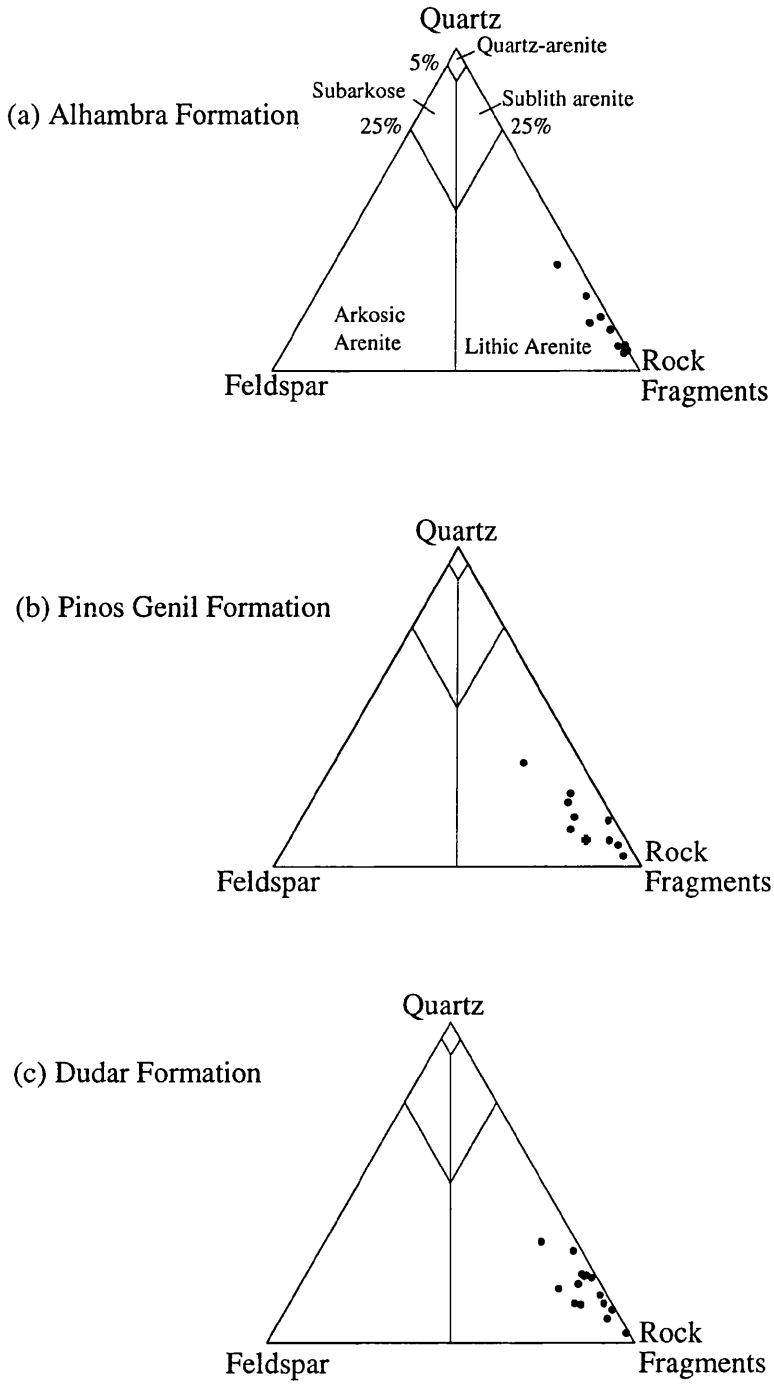

Fig. 4.1 Classification of sandstones from the Miocene to Pleistocene fan formations of the Eastern Edge of the Granada Basin. All samples lie within the Lithic Arenite area on the ternary plot proposed by Pettijohn (1954).

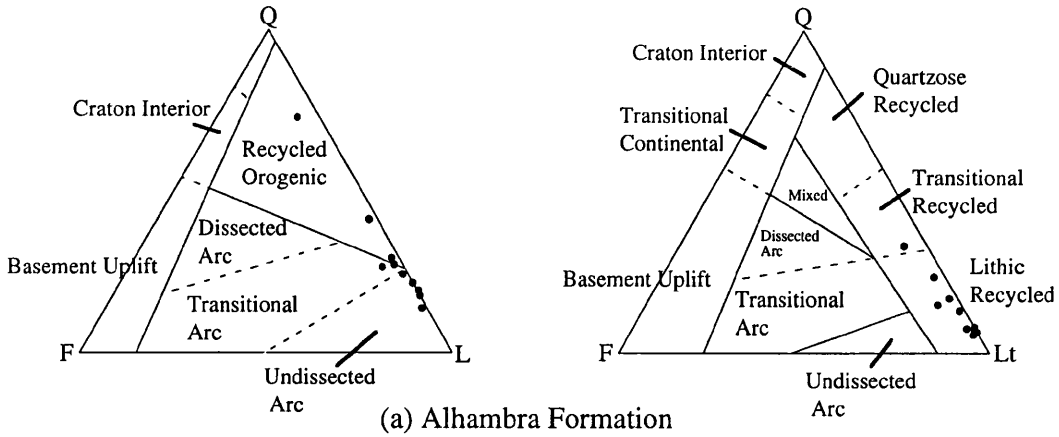

(a) Alhambra Formation

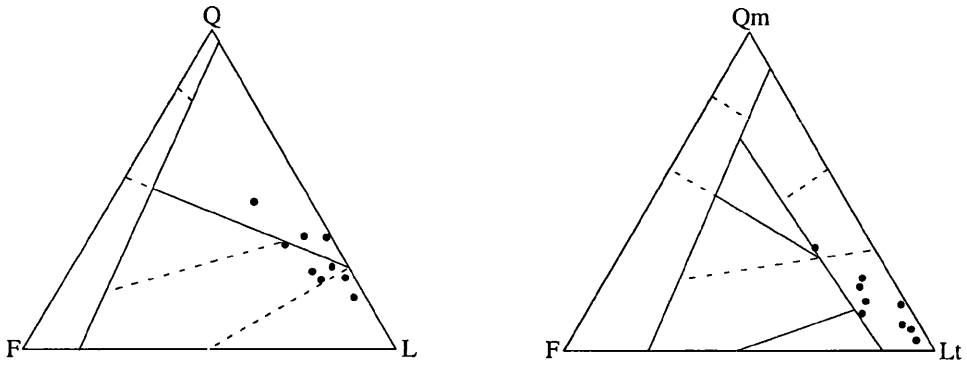

(b) Pinos Genil Formation

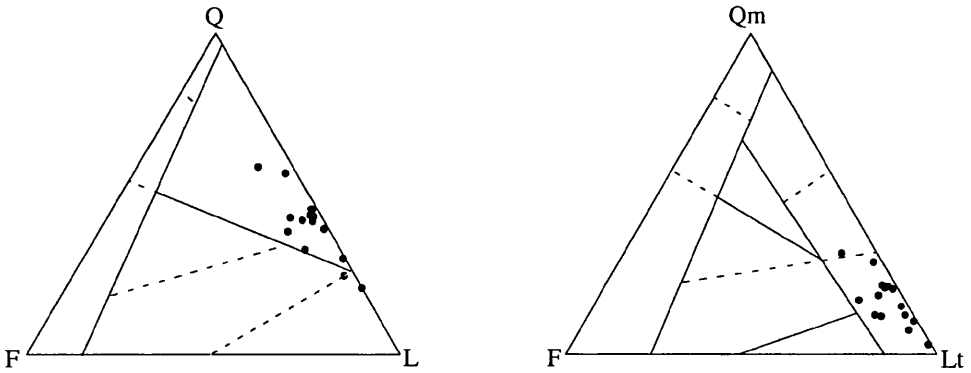

(a) Dudar Formation

Fig. 4.2 QFL and QmFLt plots for the (a) Alhambra formation, (b) Pinos Genil Formation and (c) Dudar Formation sands. Sands mainly record recycled orogen provenance areas, but also partly undissected arc provenance in (a) and (b) for QFL.

stratigraphically and total quartz decreases. The feldspar content of all formations is limited, most so in the Alhambra Formation.

Figure 4.3 shows a QFL diagram with averages plotted for each formation with the standard deviation for each around the average point. The separation of the fields is obvious, but each average value is within or close to the standard deviation field of other formations and the values are not truly distinct. However, Ingersoll and Suczek (1979) caution against placing great statistical meaning on standard deviation fields. The most that can be said is that the Dudar Formation contains the most quartz rich samples, the Pinos Genil Formation the most feldspar rich and the Alhambra Formation contains the most lithic rich samples.

Qm-F-Lt

The Granada Basin samples fall on this plot (see **Fig. 4.2**) almost entirely within the **lithic recycled provenance** area of the recycled orogenic provenance field. One sample in each formation is richer than the others in monocrystalline quartz, so plots in the transitional recycled area. These few outlying samples could be accounted for by the effects of grain size. Coarse quartz is polycrystalline, but breaks down to liberate fine grained mono-crystalline quartz grains. The effects of grain size on framework modes is discussed below. Between formations there is no discernible difference in the provenance type indicated by the QmFLt plot. The Alhambra Formation has less feldspar than samples from the other older formations. However, the Alhambra Formation sands have the same range of monocrystalline quartz and lithic grains as the other formations.

In **Figure 4.3** the average values plus standard deviation areas are plotted on the QmFLt diagram. The separation between formations is much smaller than that obvious on the QFL plot. The only variation that is significant is the difference in feldspar content between the formations. The Alhambra formation has the smallest amount of feldspar, and the Pinos Genil formation contains the samples with the largest amount. The feldspar content of the Dudar Formation stretches over the content of the Alhambra formation and the feldspar poor part of the Pinos Genil Formation. The Alhambra and Pinos Genil formations can be visually separated using the average plots, but the Dudar Formation overlaps them both.

The differences visible between the two plots, with the increased separation of the formations on the QFL diagram compared with the QmFLt diagram are due to variations in the polycrystalline quartz content of each formation. However, the total content of polycrystalline grains (i.e.. Qp+L), including lithic grains, is quite uniform between formations.

Using the QFL plot alone indicates that the *Dudar Formation has the highest level of compositional maturity of all the formations*, with the highest total quartz content. However, *it has the lowest textural maturity of all.* The Dudar Formation was rapidly deposited in a first cycle of sedimentation from a rapidly uplifting crystalline basement source, and was deposited and rapidly buried in a marine environment. The mismatch between composition and texture, especially when compared to the younger formations, is puzzling. These younger formations are more texturally mature, and have suffered greater weathering, but they are less compositionally mature. However, the extent to which grains have broken down to their

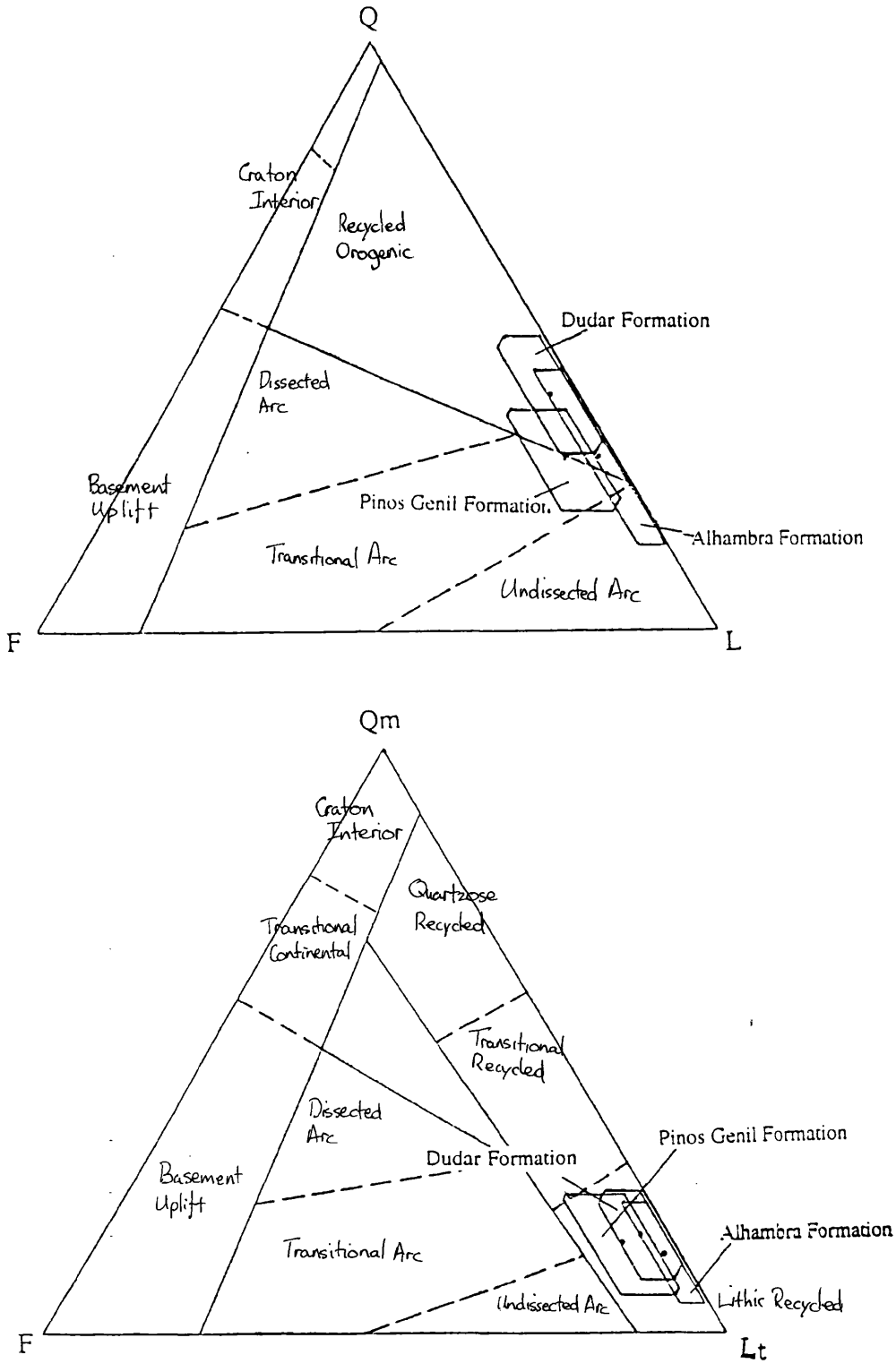

Fig. 4.3 QFL and QmFLt ternary plots (after Dikinson and Suczek, 1979) showing average values for the sands from each fan formation at the eastern edge of the Granada Basin. The areas plotted around the averages represent the standard deviation of values from the mean. Ther is a greater separation between the three fan formations on the QFL plot compared with the QmFLt plot. The Alhambra Formation in each case represents the most restricted range of values.

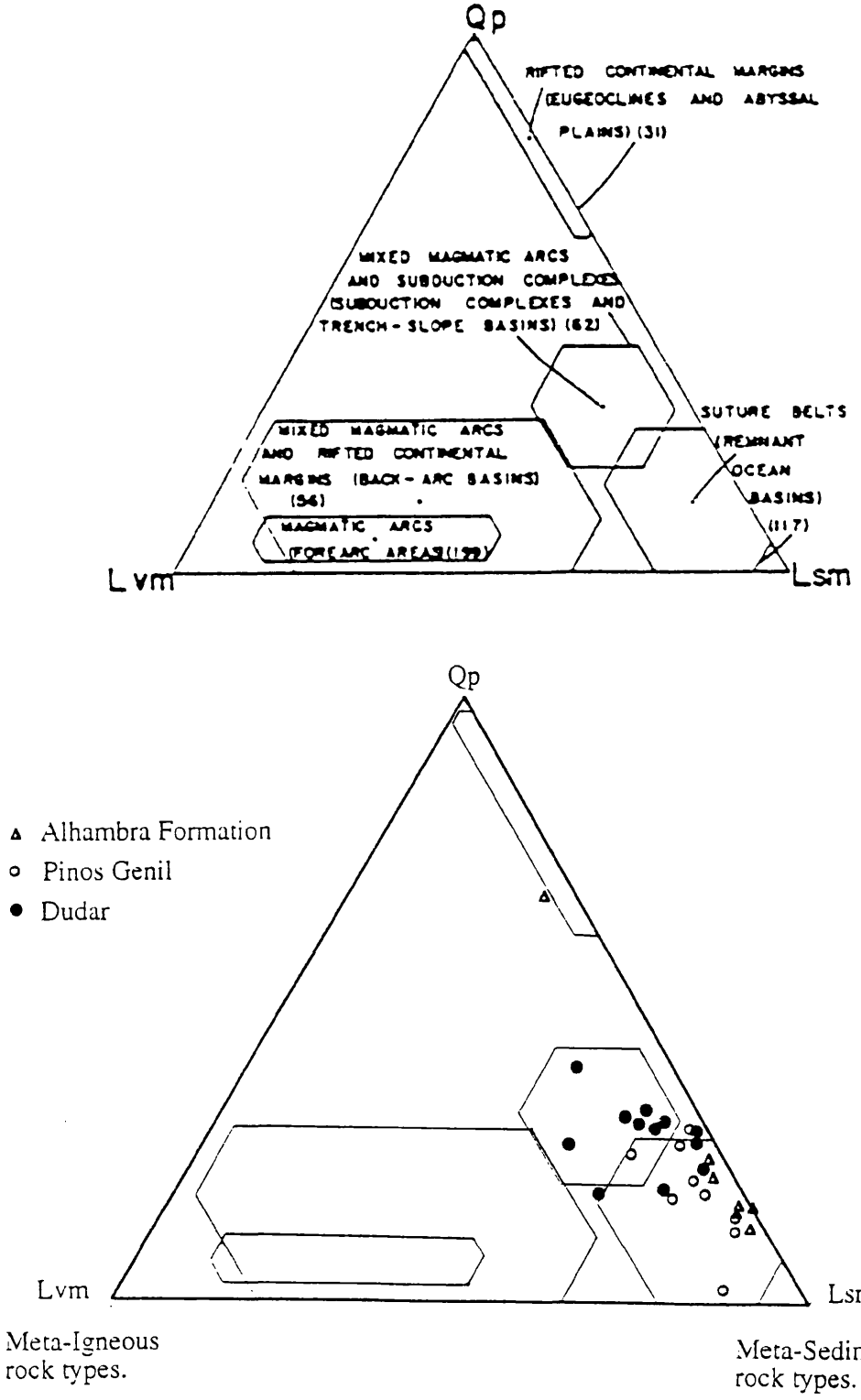

Fig. 4.4 Qp-Lv-Ls ternary plot (after Dickinson and Suczek 1979). Data from sands in the three fan formations from the eastern border of the Granada Basin. The Dudar Formation has the highest polycrystalline quartz content, and the highest content of meta-igneous lithic grains.

mineral constituents is the same as the other younger formations, as indicated by the QmFLt plot.

Qp-Lvm-Lsm

Figure 4.4 presents the details of the Qp-Lvm-Lsm ternary plot, with provenance fields as derived by Ingersoll and Suczek (1979). Plotted are the values for the Dudar, Pinos Genil and Alhambra Formations, recalculated to 100%. The Dudar Formation plots mostly within the area defined for mixed magmatic arcs and subduction complexes, with some samples within or at the edge of the field for suture belts. The Pinos Genil Formation shows a separation from the Dudar Formation, and plots within the suture belt field. The two formations overlap roughly in the area where the two provenance fields overlap on Ingersoll and Suczek (1979) diagram. The Alhambra Formation coincides mostly with the Pinos Genil Formation, plotting within the suture belt area. It is very poor in meta-igneous rock fragments, and represents the most restricted range of composition of all the formations with respect to this diagram. There is one sample from the Alhambra formation that plots far from the others near the rifted continental margin provenance area. This sample has the lowest lithic content of all the Alhambra formation samples, and somewhat paradoxically the highest Qp content. It is an exception to the general trend of the formation and does not represent a significant component of composition.

4.5.3 Discriminant function analysis of point counting results

Canonical discriminant analysis was performed using the results of point counting of the conventional framework components of the sandstones from the eastern Granada Basin. This was intended to assess the magnitude of compositional differences between formations, the ability of the groups so defined to classify their own samples and also to examine more closely the causes of the differences between sandstone compositions.

Table 4.2 presents the average framework grain contents of each of the three sandstone formations from the Granada Basin, recalculated to percent values. This allows a qualitative comparison of the differences in the content of grain components. The most important differences between formations appear to be the decrease in poly-crystalline quartz and carbonate and the increase in lithic grains and mica grains from the Dudar Formation through the Pinos Genil Formation to the Alhambra Formation. The change in maturity from the Dudar Formation up to the Alhambra Formation has been attributed to the decrease in the quantity of polycrystalline quartz, and the increase in lithic grains.

Discriminant function analysis was performed on the raw point counting data, not on data recalculated to percentage values. The analysis was carried out by Dr. K. Johnson, using the SAS statistical package. The results are presented in **Tables 4.3** and **4.4**, and in **Fig. 4.5**.

For each sample values along two discriminating axes were calculated, Can 1 and Can 2. **Table 4.3** shows that Can 1 is the most discriminating, with 72% of the discriminating power. The total canonical structure details the variables that account for the variation between groups along Can1 and Can 2. For Can 1 the most important variables are poly-crystalline quartz, lithic grains, carbonate grains and mica grains. The values quoted are a measure of the

	n=15 Dudar Formation		n=9 Pinos Genil Formation		n=10 Alhambra Formation	
	%	Stan. Dev.	%	Stan. Dev.	%	Stan. Dev.
Qm	10.59	6.05	11.29	6.42	10.15	5.67
Qp	15.00	5.53	10.12	4.42	11.93	4.98
F	2.49	2.15	5.62	3.42	1.62	1.65
L	35.23	13.24	47.04	11.4	53.35	17.93
Mica	7.38	3.64	10.59	5.62	11.74	6.89
Carbonate	23.57	20.91	9.25	10.72	3.96	9.73
Heavy minerals	2.89	1.68	4.01	1.61	3.21	1.43
Opaques	2.85	3.36	1.87	1.22	4.04	2.32

Table 4.2 Average values of framework grain components for each of the three Formations from the eastern Granada Basin. Errors are expressed as one standard deviation.

difference from group 1 (Dudar Formation) to groups two and three (Pinos Genil and Alhambra Formations). The larger the number the bigger the difference, positive numbers show an increase and negative numbers a relative decrease. These results agree with the more qualitative changes noted by comparing formational averages in **Table 4.2**.

Fig. 4.5 is a graph of Can 1 versus Can 2. Each sample from the three formations is plotted by its calculated values of Can 1 and Can 2. This shows that the Dudar Formation is distinguished from the other formations by values of Can 1, but that Can 1 does not distinguish the Pinos Genil and Alhambra Formations from each other. However, Can 2 is able to distinguish the Pinos Genil and Alhambra Formations. Looking at **Table 4.3** it can be seen that the most important variables for Can 2 are the feldspar and opaque mineral contents. The average percentage content of feldspar (see **Table 4.2**) is much higher in the Pinos Genil Formation than in any other deposit, and is one of the major variables operating in the control of the provenance characterisation of the sandstones (**Figs. 4.2** and **4.3**).

The Dudar Formation samples are better defined and can be separated well from the other formations. The Pinos Genil and Alhambra Formations are nearer to each other in composition than to the Dudar Formation, and are distinguished only on the basis of feldspar and opaque mineral content.

Table 4.4 presents a summary of the percentage classifications of samples into the groups defined by their parent population. This gives a clear estimation of how well defined each of the compositional groups from each formation are. The number of samples from each group that are classified into each group is given. Samples that do not classify into any of the three formational groups are put under 'other'. For group 1, the Dudar Formation sands, 86.67% of the samples are classified into the Dudar Formation group, but the remaining 13.33% of samples are not classified into any group. Group 2, the Pinos Genil Formation sands are not classified well and these samples do not define a very distinct group, though they appear not to dominantly belong to any of the other two formational groups either. Only 33% of the Pinos Genil sands are classified to the Pinos Genil group. Group 3 is better defined with 66.67% of the sands being defined as belonging to the Alhambra Formation. It is clear that the Dudar Formation is the best defined group, a conclusion which supports the conclusion of the canonical discriminant analysis as presented above and in **Fig. 4.5**.

These statistical parameters indicate that the Dudar Formation sands are compositionally distinct from the Pinos Genil and Alhambra Formation sands. The Dudar Formation has the fewest number of sandstones from other formations classified as part of it. As all the sandstones of the Eastern Granada Basin originate from the same source region, the distinct composition of the Dudar formation compared with the other formations must be explained by some fundamental sedimentary process, which has affected the compositional signature of the sediments.

4.5.4 Provenance characterisation; new provenance classification

In general the sediments of the Granada Basin fall in the provenance areas of recycled orogen or suture belt, according to the provenance discrimination plots of Dickinson and

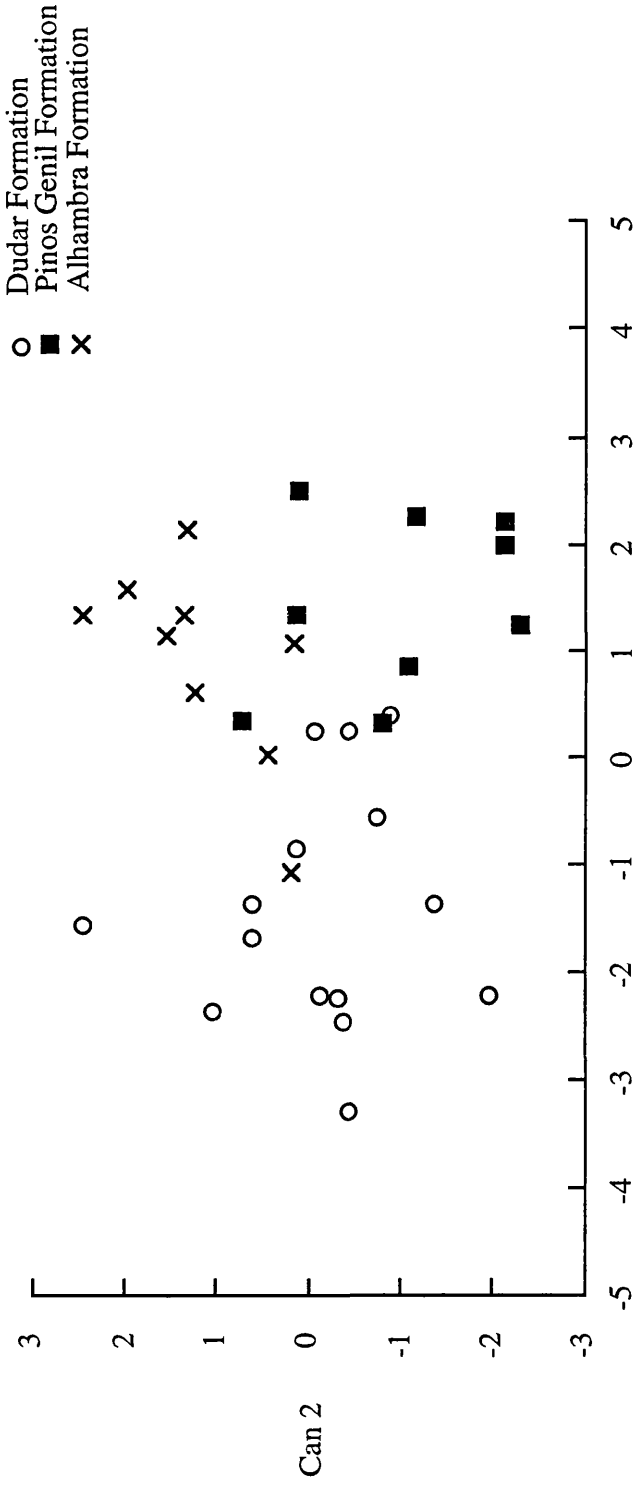

Fig. 4.5 Graph showing canonical discriminating functions for sandstones from the eastern Granada Basin. The Dudar Formation samples are successfully discriminated from the other formations by its values on Can 1. The Pinos Genil and Alhambra Formations cannot be discriminated along Can 1 but are discriminated by Can 2.

	Can 1	Can 2
Eigenvalue	1.8712	0.7082
Proportion	0.7254	0.2746
Cumulative	0.7254	1.0000

Total canonical structure

	Can 1	Can2
Qm	-0.017467	-0.128226
Qp	-0.572113	0.034792
F	0.283520	-0.727732
L	0.485686	0.300611
Carbonate	-0.550889	-0.254733
Heavy minerals	0.301224	-0.203527
Micas	0.434153	0.238376
Opaques	-0.018009	0.518383

Table 4.3 Results of canonical discriminants analysis of point counting data from Granada Basin Sandstones. The data used were the raw counts from the point counting analysis, not recalculated percentages.

Group	**1**	**2**	**3**	**Other**	**Total**
1	13	0	0	2	15
	86.67	0	0	13.33	100.00
2	1	3	2	3	9
	11.11	33.33	22.22	33.33	100.00
3	1	1	6	1	9
	11.11	11.11	66.67	11.11	100.00
Total	15	4	8	6	33
Percent	45.45	12.12	24.24	18.18	100.00

Error count estimates (this is a summary of the errors of classification associated with each group as presented in the above table);

Group	**1**	**2**	**3**
	0.1333	0.6667	0.3333

Table 4.4 Summary of percentage classification of Granada Basin samples into formational groups. This gives some measure of the amount of similarity between groups.
Group 1: Dudar Formation
Group 2: Pinos Genil Formation
Group 3: Alhambra Formation

Suczek (1979). However there are some exceptions that require explanation. It is also beneficial to compare the results presented here with the detailed provenance types used by Dickinson and Suczek (1979) to construct the provenance discrimination diagrams. Before this, it is best to heed Dickinson and Suczeks (op.cit) warning about plotting individual samples upon the ternary diagrams and drawing conclusions about provenance characteristics from them. The data used to construct the diagrams were averages of suites of sandstones, often containing many samples. This means that much data dispersion has been constrained, and restricted into a few points, thus perhaps eliminating overlap between provenance fields. So, in the present case the correct interpretation may only be derived from plotting the averages of each formation on the diagrams. However, below follows a discussion that interprets the full spread of samples and the provenance implications therein.

For the QFL diagrams, significant numbers of samples plot in the transitional and dissected arc provenance areas. The average values for each formation all fall in the recycled orogen area, though often right on the edge of the field. This may be the most important trend seen in the data. However, the standard deviation fields for the Pinos Genil and Alhambra Formations have significant portions in the transitional and undissected arc provenance areas. This is due to increased feldspar in the Pinos Genil Formation and increased lithic fragments in some samples of both the Pinos Genil and Alhambra Formations. The lithic fragments contained within the Granada Basin sediments are metasedimentary, with minor mafic and acidic metaigneous rocks, but no volcanic rocks are observed as grain components. It is volcanic rock fragments which are expected to drive sediment composition towards the lithic pole in the QFL plot according to Dickinson and Suczek (op.cit.). Within the range of variation of the Pinos Genil and Alhambra formations sands which contain no volcanic lithic grains plot in the transitional and undissected arc provenance fields. The conclusion from this is that some samples from the eastern Granada Basin are erroneously assigned provenance by the QFL plot of Dickinson and Suczek (1979).

However, in their paper there is one sandstone suite derived from a foreland uplift provenance type that plots well within the transitional arc field. This suggests that this provenance type may have a tendency to overlap into the arc fields. The samples Dickinson and Suczek (1979) use to define the lithic rich end of the recycled orogen field are mostly foreland uplift derived. Secondary in importance are samples with a subduction complex source, which plot nearer the lithic pole as chert content increases. Samples nearer to the lithic pole are taken to indicate an increasing ratio of oceanic to continental fragments. The Granada Basin samples do not have an oceanic component but plot towards the lithic pole. In the Qm-F-Lt plot, the Granada Basin samples all plot in the lithic recycled provenance area. Dickinson and Suczek (1979) have this area defined by a grouping of foreland uplift derived sandstone suites. For the Qm-F-Lt plot the provenance assignment of the Granada Basin samples is unequivocal, and more informative. The best provenance classification possible for the Granada Basin sediments using the Q-F-L and Qm-F-Lt plots is as sands derived from a foreland uplift provenance. However, this is a foreland uplift provenance that contains no chert and recycled sediment in the sense put forward by Dickinson and Suczek. The high lithic

content of the Granada Basin sands may be due to large grain size or to a preponderance of relatively fine grained lower grade metamorphic lithic fragments.

The apparent poorness of fit of the Granada Basin sediments into established provenance discrimination schemes leads to an important point. In **Chapter 1** in the discussion about provenance, the possibility of poorly recognised provenance types was raised. The discrimination diagrams produced so far (eg. Dickinson and Suczek, 1979), may not fully encompass sands generated in all possible tectonic settings. This is not to suggest that these diagrams are incorrect, but only that as they depend on actualistic data for their construction, their accuracy is limited to the classification of similar data. This is potentially serious, since if provenance is sought for ancient sandstones that are now out of their depositional tectonic setting, inaccuracies of interpretation could result from the erroneous classification of provenance type.

For the Granada Basin Sediments it is possible that they define an area on the Q-F-L and Qt-F-Lt plots that is characteristic, not of 'foreland uplift' or dissected orogen, but are characteristic of core-complex uplift. The Betic Orogen is somewhat unusual in the composition of sediment it has produced, because it has generated sediments sourced from high grade metamorphics early in the sedimentary history of the latest (and most significant) basement uplift. Normally these rocks are deeply buried beneath low grade metamorphic and sedimentary cover rocks at the time of the beginning of significant uplift in orogenic regions. Due to the superposition of the tectonic units of the Internal Zones, and the possible strike-slip dominated assembly of the area (see **Chapter 7**) the low grade cover to the region was removed prior to the late Oligocene-present evolution of the Internal Zones. The late Miocene extension and uplift of the Nevado Filabride Complex in the core of the Sierra Nevada, in core-complex style, revealed high grade metamorphic rocks to provide a source for sediment. The upper plate of the core-complex, the Alpujarride Complex, though dominantly at a lower metamorphic grade than the Nevado Filabride contains some very high grade metamorphic rocks also, making it unusual in the 'normal' view of core-complex models, where the upper plate is composed of low grade rocks or sediments. Core-complex evolution is one of the main methods of cover removal in extending terranes. However, the long history of evolution in the Betics has seen the prior removal of any sedimentary cover from the high grade metamorphic rocks below.

The Granada Basin then contains sediment made of high grade metamorphic fragments, deposited in a first cycle of rapid sedimentation in an orogenic region. This contrasts with the classifications of Dickinson and Suczek (1979) for recycled orogenic provenance types where the lithic recycled provenance area is largely defined by subduction complex sediment sources, dominated by sedimentary rock fragments. Core-complexes characteristically reveal high grade metamorphic rocks in their core areas, so perhaps the Granada Basin sediments outline a possible new provenance characterisation.

In the Qp-Lvm-Lsm plot (**Fig. 4.4**) the provenance areas indicated are the mixed magmatic arc, subduction complexes and suture belts. The suture belt provenance, dominated by metasedimentary rock fragments is the expected provenance type. The Dudar formation

however plots in the mixed magmatic arc and subduction complex area, due to its higher content of polycrystalline quartz, derived primarily from metamorphic sedimentary sources. The content of meta-igneous grains that defines this field is little greater than that for suture belt sources, and it is the increased amount of polycrystalline quartz derived from subduction complexes, in the form of chert that distinguishes the subduction complex from suture belt sources.

There is no difference in source between the formations in the eastern Granada Basin, but some variations in composition and therefore indicated provenance are observed, most critically on the Qp-Lvm-Lsm diagram. As the source is constrained and constant for all the formations, the differences in composition must be explained by some mechanism other than variation in source.

4.6 Lithic framework component

In the sediments of the eastern Granada Basin the proportion of framework grains that are lithic is as high as 76% (one sample from the Alhambra Formation). More typically, in the Dudar Formation the content ranges from around 20% to 55%, and in the Pinos Genil Formation up to 63%. Some samples in the Dudar formation are apparently poor in rock fragments, but this is due to the high carbonate content, often occurring as matrix, which has the effect of diluting the terrigenous component.

Lithic grains are an important component of the Miocene-Pleistocene sediments of the Granada Basin. As lithic grains break down to liberate monocrystalline mineral grains, this latter fraction of the sediments in this study not only share the same source region as the lithic fragments, and conglomerate clasts, but are *derived* from the break-down of these components. To study the lithic grain component of the sediments may shed some light upon the progress of the break-down of these grains, and the generation of the monocrystalline grain population. The patterns of total lithic content in the sediment may also be related to the patterns of change in the conglomerate clast populations presented in **Chapter 3**, especially the removal of schistose material from the conglomerate grain sizes. (See **Chapter 3**; the expected increase in small clasts of schist in the Alhambra formation, consistent with a closed system recoiling model, does not occur. This suggests that schist grains were reduced to sand sized material constantly, in the same way that the number of small schist clasts were fed by the break up of larger clasts, as is also discussed in that chapter.)

4.6.1 Grain types and provenance.

The grain categories used to count the lithic population are presented in **Table 4.5**, along with descriptions. All lithic grains encountered were metamorphic, of meta-sedimentary and meta-igneous character. Individual detailed lithologies are sometimes recognisable, but the categories that were arrived at after considering the full range of lithic fragments present provide the best generalisations of lithic type possible. They are aimed at grouping similar grain types based on the presence or absence of tectonic fabric, general composition and grade of metamorphism. In this way this scheme is similar to that proposed by Ingersoll and Suczek (1979) and Dorsey (1985).

Table 4.5 Definition of lithic grain parameters for point counting

b. Metamorphic lithic grain parameters:

Quartz-Mica Tectonite	Coarse to medium grained schist grains with clear foliation. Internal grain size <0.0625mm.
Garnet-Mica Schist	As above but with Garnet porphyroblasts.
Quartz-feldspar schists	Foliated aggregates of quartz and feldspar.
Quartz-Mica aggregates	With no foliation or schistocity visible.
Feldspar-quartz aggregates	Polycrystalline aggregate with no discernible foliation or schistocity.
Amphibolite	Coarse-medium grained aggregates and schists of amphibolite, muscovite, quartz and feldspar often with garnet and epidote. Clearly fragments of amphibolites that also form conglomerate clasts.
Marble	Coarse polycrystalline calcite.
Epidote rich rock	Coarse aggregate of epidote group minerals and quartz.
Mica	Polycrystalline aggregates of muscovite. Some derived clearly from coarse, high grade mica-schists. Others fine grained, lower grade mica schists often graphitic.
Mylonite	Highly strained polycrystalline quartz with minor muscovite and occasional tourmaline.
Low Grade Met	Fine grained (<0.0625mm) low grade phyllites and slates.

Recalculated Parameters

Lvm	Feldspar-Quartz Schists + Feldspar-Quartz Aggregates + Amphibolite + Serpentinite + Mylonite
Lsm	Quartz-Mica Schist + Quartz-Mica Aggregate + Garnet-Mica Schist + Marble + Epidote rich Rock + Low Grade Metamorphic
Q-M producers	Quartz-Mica Schist + Quartz-Mica Aggregate + Garnet-Mica Schist

The provenance of the schist fragments is most probably in the Nevado Filabride Complex and parts of the Alpujarride complex, but mostly the former. The grains that have no preferred fabric, at least on the scale of sand grains, perhaps originate from quartzites, or certainly from less sheared meta-sediments, but this point is somewhat ambiguous. Polycrystalline aggregates of muscovite are common, and can be attributed to schists, and sometimes are clearly from coarse grained, high grade schists. Polycrystalline carbonate fragments are derived from marble source rocks. The epidote rich fragments, can in some cases be attributed to derivation from mafic meta-igneous sources, such as amphibolites contained in the Ophiolite unit of the Mulhacen complex. However, epidote is sometimes common within schists that are found as clasts in the Basin, derived also from the Mulhacen complex. Fragments of tourmaline mylonite are infrequently seen, but are derived from exposures of these highly strained acid igneous intrusions, exposed at detachments within the Sierra Nevada source.

4.6.2 Variation of lithic grain content.

Qp-Lvm-Lsm

The Qp-Lvm-Lsm ternary plot is discussed above in terms of provenance discrimination. This is because it serves to group metamorphic lithic grains together and discriminate source types based on protolith characteristics. As proportions of igneous and sedimentary protoliths vary between tectonic setting some measure of provenance type may be derived from the proportions of each type of grain. As described earlier the source lithologies are well known in the Betics, and the Sierra Nevada in particular. Lvm is derived from the ophiolite unit of the Mulhacen Complex and some acid intrusives now exposed often as mylonites within detachment zones in the Internal Zones. In general there should be no dramatic stratigraphic changes in source for the sediments of the Eastern Granada Basin, but in the Qp-Lvm-Lsm plot we see a shift from mixed magmatic arc to suture belt provinces stratigraphically upwards. There is some overlap, but the change is still clear.

This can be interpreted in two ways. Firstly, there is a change in source configuration, an interpretation that implies uplift and tectonism. Secondly, the clear maturity increase into the Pinos Genil, and especially the Alhambra formations, caused by increased terrestrial weathering rates and the possibility of sedimentary recycling, may be responsible for the reduction in the observed proportions of meta-igneous rock fragments in the sandstones. This may be because meta-igneous mineralogy is less resistant to alteration by weathering and/or recycling than the quartz dominated mineralogy of the metasedimentary rocks in the Sierra Nevada.

Total grain population

Average values for each lithic grain type counted are presented in **Table 4.6** along with the standard deviation for each. Some samples have a large (larger that the % content) standard deviation, making the average content in some cases difficult to interpret. **Figure 4.6** shows the range of variation for each formation of four of the most volumetrically important grain types.

	n=12 Dudar Formation		n=10 Pinos Genil Formation		n=8 Alhambra Formation	
	%	Stan. Dev.	%	Stan. Dev.	%	Stan. Dev.
Quartz-Mica Tectonite	40.7	12.2	45.3	11.3	52.0	8.5
Quartz-Mica Aggregate	12.1	16.8	14.3	7.6	16.2	4.9
Garnet-Mica Tectonite	1.5	1.8	4.5	4.7	7.7	6.1
Feldspar Tectonite	0.4	0.9	0.3	0.5	0.5	0.5
Feldspar Aggregate	5.3	3.4	3.8	2.5	2.2	4.9
Amphibolite	1.6	3.2	1.2	1.6	0.4	0.5
Mica Aggregate	15.2	6.0	12.0	5.6	10.9	4.5
Epidote rich rock	5.7	6.2	3.7	4.7	1.2	1.0
Low Grade Metamorphic	7.7	11.0	7.3	6.0	11.1	6.0
Serpentinite	0.5	1.0	0.2	0.5	0.0	0.0
Mylonite	0.3	0.8	0.5	1.2	0.0	0.0

Table 4.6 Average values of lithic grains expressed as percentage contents of the total lithic population. The second number is the standard deviation of the values used to calculate the mean.

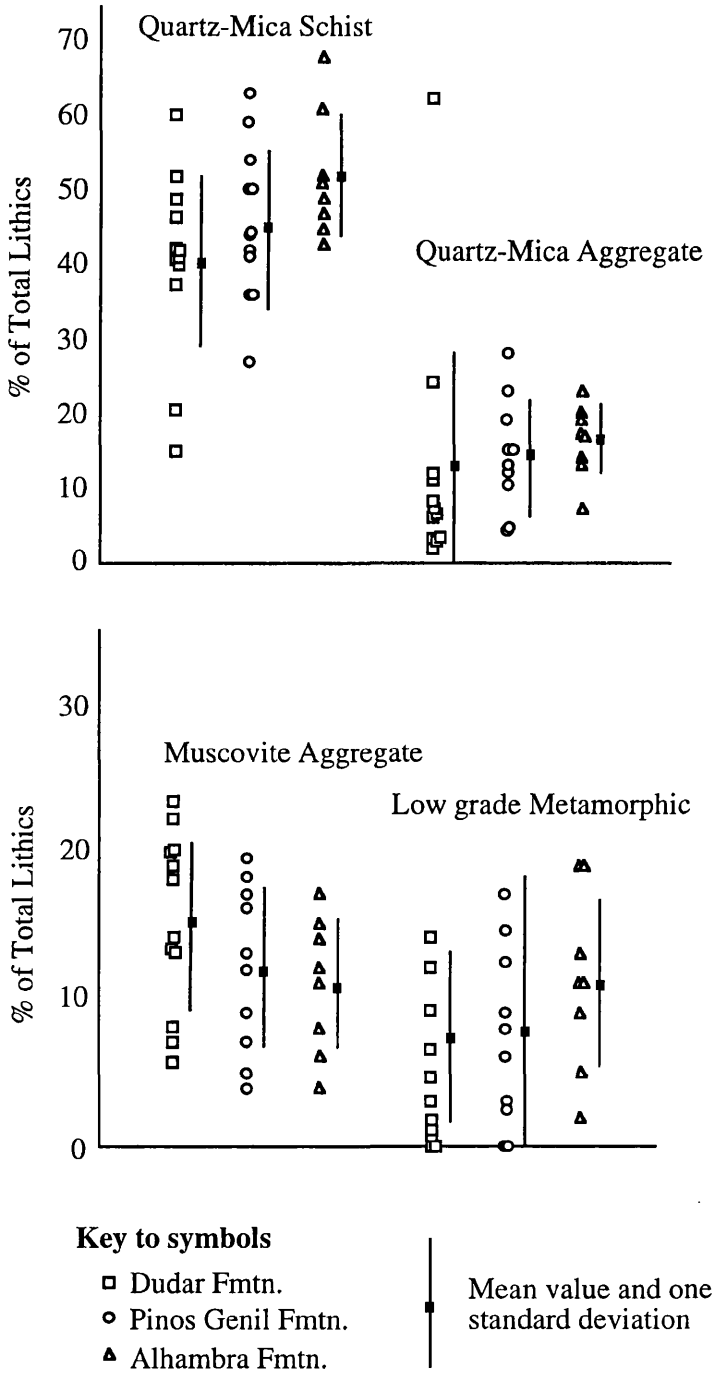

Fig. 4.6 Variations in percentage abundances of four lithic grain types for the three fan formations of the eastern Granada Basin. Note that variations between formations appear to be systematic.

The variations in the range of percentage contents of the lithic component of the sediment appear systematic. For quartz-mica schist fragments the range of contents becomes more restricted in younger sediments. Not only this the percentage content of the range increases. For quartz-mica aggregates the trend is similar, but the increase in percentage value is smaller. The range of values for muscovite aggregates decreases stratigraphically upwards along with a slight decrease in average content. For low grade metamorphic fragments the trend is to increased amount in younger sediments. All samples taken from the Alhambra formation contain some low grade fragments, where there are samples from the other, older formations that have no low grade metamorphic grains. The magnitude of the range of values between formations does not appear to change. These differences are clear, but the trends are slight in some cases, there is little significant difference between most samples. However, the interpretation of the general trends observed may be significant for the consideration of the progress of the breakdown of metamorphic lithic sand grains in the sediments of the Granada Basin, and similar intramontane basins.

Qm-M-Quartz mica schist and aggregates

Figure 4.7 shows values for monocrystalline quartz and muscovite against the lithic fragments that break down to liberate both these minerals. It should give some indication of the degree of grain break-down within these sandstones. A clear trend is visible across the centre of the plot. This is the expected trajectory for samples as lithic grains break-down. It is the position of each suite of sandstones on this trend that is important for assessing the maturity and the progress of the break-down of lithic fragments in the sedimentary environment during weathering and/or sedimentary recycling. The differences visible here are small. There is a progressive elongation of the field covered by each successive formation. The Pinos Genil and Alhambra Formations contain samples that show a greater degree of lithic grain breakdown of quartz and mica bearing lithic fragments, compared with the Dudar Formation. However, the number of these samples are small and most samples for each population plot in the same region of the plot. The sandstones from the formations cannot be said to be significantly distinct from each other.

4.7 Grain size dependant composition

Before an interpretation of the sand grain composition data, presented above, is given in terms of sediment maturity and break-down processes, the effect of grain size upon the apparent composition of the sediments must first be assessed.

Ingersoll et. al. (1984) discuss the merits of the Gazzi-Dickinson point counting method for alleviating the possible distorting effects of grain size upon the modal compositions of arenites. This method attributes sand sized crystals within lithic fragments to the class of mineral not the class of rock fragment. This allows the composition of unsorted sediment samples to be compared with unsorted samples with differing grain size biases without sorting out grain size fraction to be analysed. However, this method decreases the amount of specific provenance information that is available from detailed rock types. It is suitable for studying large sandstone suites to remove the effects of grain size and to look at

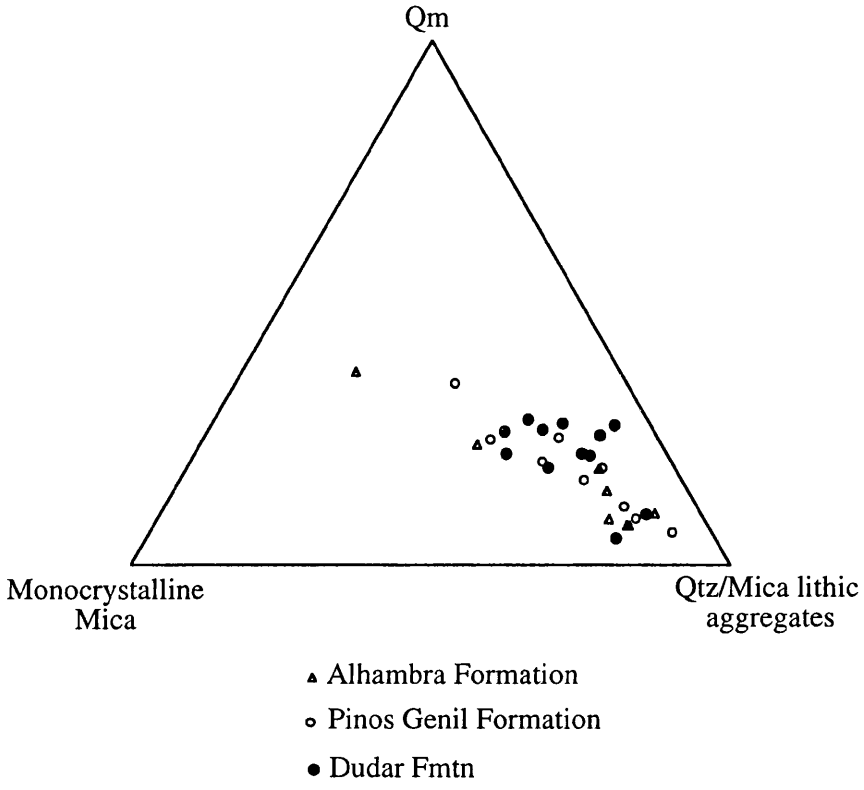

Fig. 4.7 Ternary diagram showing interdependance of monocrystalline Quartz, monocrystalline mica and lithic aggregates that can produce monocrystalline quartz and mica. This gives a clearer picture of the breakdown of lithic sand grains.

general composition, as plotted on Dickinson and Suczek (1979) plots. The lithic grain content will be reduced, but this may highlight contributions from low grade metamorphic or fine grained sources as opposed to coarser grained high grade metamorphic and plutonic provenances. The derivation of the plots though was not based upon data acquired by the Gazzi-Dickinson method. This method was not applied in this study, so a careful characterisation of the grain size effect on composition is needed.

The effect of grain size on observed composition can be great. Tortosa et. al. (1991) discuss the grain size varying composition of sands derived from a terrane composed of plutonic rocks intruding lower to upper grade metamorphic rocks in central Spain. Point counts of the five phi graded grain size intervals that comprise the sand sized interval were made for sands derived from granites, gneiss and slates/schists. The results when plotted on a Q-F-L ternary plot reveal significant compositional differences between grain size fractions. For the feldspar rich granites and gneisses compositions range from the Q-F tie line across the plot to the lithic pole. More relevant for this study, slate and schist compositions depended on the grain size of the sediment fraction. All were poor in feldspar and lie along the Q-L tie, but quartz content varies from 45% for the finest fraction to 3% in the coarsest fraction. Quartz types also vary in proportion with grain size. The proportion of polycrystalline quartz grains with more than 3 sub-crystals is high for sands that are derived from slates and schists, and greatest in the coarsest grain sizes. For the same grain size derived from granites and gneiss, the proportion of monocrystalline quartz is much greater, often twice as much. This all demonstrates how composition can depend strongly on the grain size of the sediment, and is also related to the grain size of the source rocks. Fine grained low grade metamorphic rocks are more likely to produce lithic fragments at any grain size than a coarse grained granite, as the latter is more likely to break-down along mono-mineralic grain boundaries.

Conventional Framework Components

Figure 4.8 shows the values of six conventional framework components plotted against the average grain size of selected samples from each of the Dudar, Pinos Genil and Alhambra Formations. The average grain sizes vary from around 0.1mm (very fine sand) to 0.7mm (coarse sand). The first important aspect to appreciate is the spread of samples with grain size. Each formation contains samples of *all grain sizes*, formations cannot be separated on the basis of their grain size. This suggests that the compositions of each formation will be affected in a similar manner by grain size, and that variations observed in population groupings on ternary and other plots are significant, and not due to grain size variations between the formations.

Table 4.7 presents the correlation coefficients for grain types against grain size for each formation. It is notable that the Dudar Formation has the lowest degree of correlation between grain size and composition. The Pinos Genil and Alhambra Formations have greater degrees of correlation, most notably for Qm, Lithic grains and monocrystalline mica grains. Lithic grains are positively correlated with grain size but all other grain type abundances in the Pinos Genil and Alhambra Formations are negatively correlated with grain size. The Dudar

	Dudar Formation	Pinos Genil Formation	Alhambra Formation
Qm%	0.005	-0.76	-0.86
Qp%	0.25	-0.14	-0.71
Feldspar%	0.26	-0.32	-0.60
Lithic Grains %	0.60	0.59	0.76
Heavy Minerals %	0.22	-0.44	-0.38
Mica Grains %	0.08	-0.83	-0.89

Table 4.7 Correlation Coefficients for framework grain types versus average grain size of sample.

	Dudar Formation	Pinos Genil Formation	Alhambra Formation
Quartz-Mica Tectonite	0.55	-0.43	0.72
Quartz-Mica Aggregate	-0.28	0.32	0.71
Garnet-Mica Tectonite	0.5	-0.53	0.15
Amphibolite	0.03	-0.64	-0.10
Mica Aggregate	-0.20	-0.11	0.77
Epidote rich rock	0.19	0.39	0.33
Low Grade Metamorphic	-0.25	0.59	0.55
Total Schist	0.43	-0.29	0.42

Table 4.8 Correlation Coefficients for Lithic grain types versus average grain size of sample.

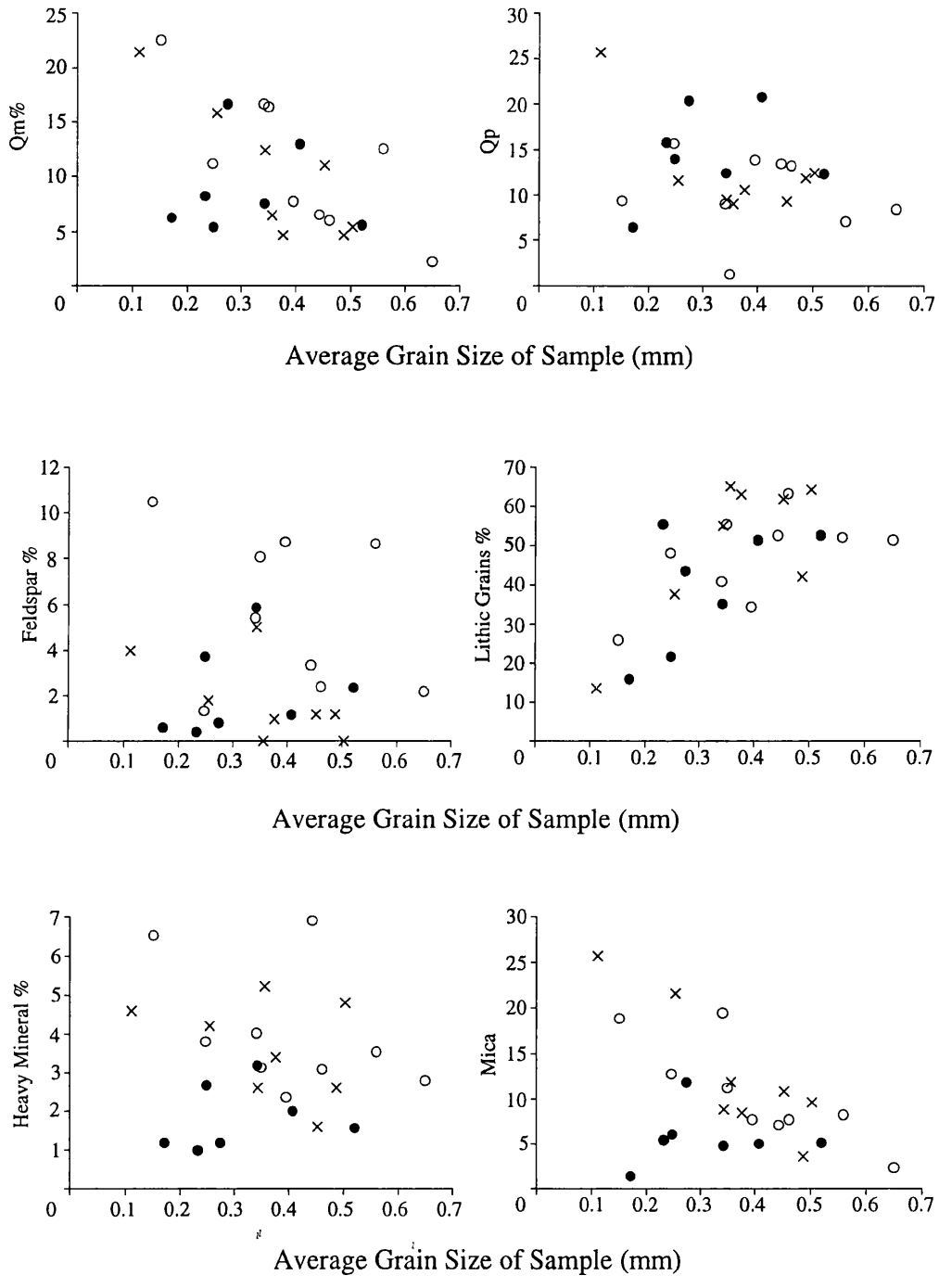

Fig. 4.8 Variations in percentage abundances of six grain types within the sandstones of the Miocene to Pliestocene of the eastern Granada Basin.

Formation follows an apparently distinct trend of poor positive correlation of composition and grain size.

Some correlations are evident between framework components and grain size. Monocrystalline quartz shows a general negative correlation, especially if the values from the Dudar Formation are removed. These latter values appear to form in part a flatter pattern across the graph, but some samples clearly follow the trend set by the other formations. Polycrystalline quartz exhibits a weak negative trend, again with the Dudar Formation samples cutting across this with a weak positive pattern. Feldspar is less clear and shows no distinct trend. It is interesting to note though that the Alhambra Formation samples have the highest content of feldspar as a percentage of the total framework components of the sand. This appears in contradiction to the conclusion reached from plotting recalculated Q-F-L parameters on ternary diagrams, where the Alhambra Formation appears to have the uniform lowest feldspar content.

Lithic grains show a very strong positive correlation with increasing grain size. This is as predicted in the considerations presented above. No Formation shows a distinct trend. Heavy minerals show a weak negative correlation with increasing average grain size. The Dudar Formation samples form a separate trend again, being slightly positive, and are generally poorer in heavy minerals than the other formations.

Finally, monocrystalline mica follows a negative trend, particularly when the Dudar Formation samples are removed. These latter appear again to in part follow a distinct flatter, and possibly weakly positive correlation with average grain size.

Lithic Grains

Figure 4.9 presents details of how proportions of individual rock types vary with changing grain size. Plotted are the percentage proportions of each rock type of the total lithic fragment population for each sample. As discussed above the total lithic grain population shows a strong positive correlation with increasing average grain size. If individual grain types are plotted in a similar fashion it is possible to identify the grain types which are mostly responsible for the trend in the whole population, and to see rock types which do not positively correlate with increasing grain size. It is important to identify these rock types as they can increase the lithic component of fine grained sediments and affect provenance indications significantly. In the present case this effect is not so critical, but it may be interesting to note negative correlations in unexpected rock types (i.e. normally coarse grained).

Table 4.8 contains the correlation coefficients for the relationships between lithic grain abundance and the average grain size of the sample. It can be seen that the Dudar Formation has the lowest degree of correlation between composition and grain size. However, the Alhambra Formation has a strong correlation between composition and grain size for some grain types, especially schistose types with a strong planar fabric.

Quartz-Mica schist fragments show a positive correlation with grain size, though it is a diffuse trend. The Dudar Formation contains samples with the lowest content of this grain type. For quartz-mica aggregates, the overall content is lower, and the correlation is positive. No

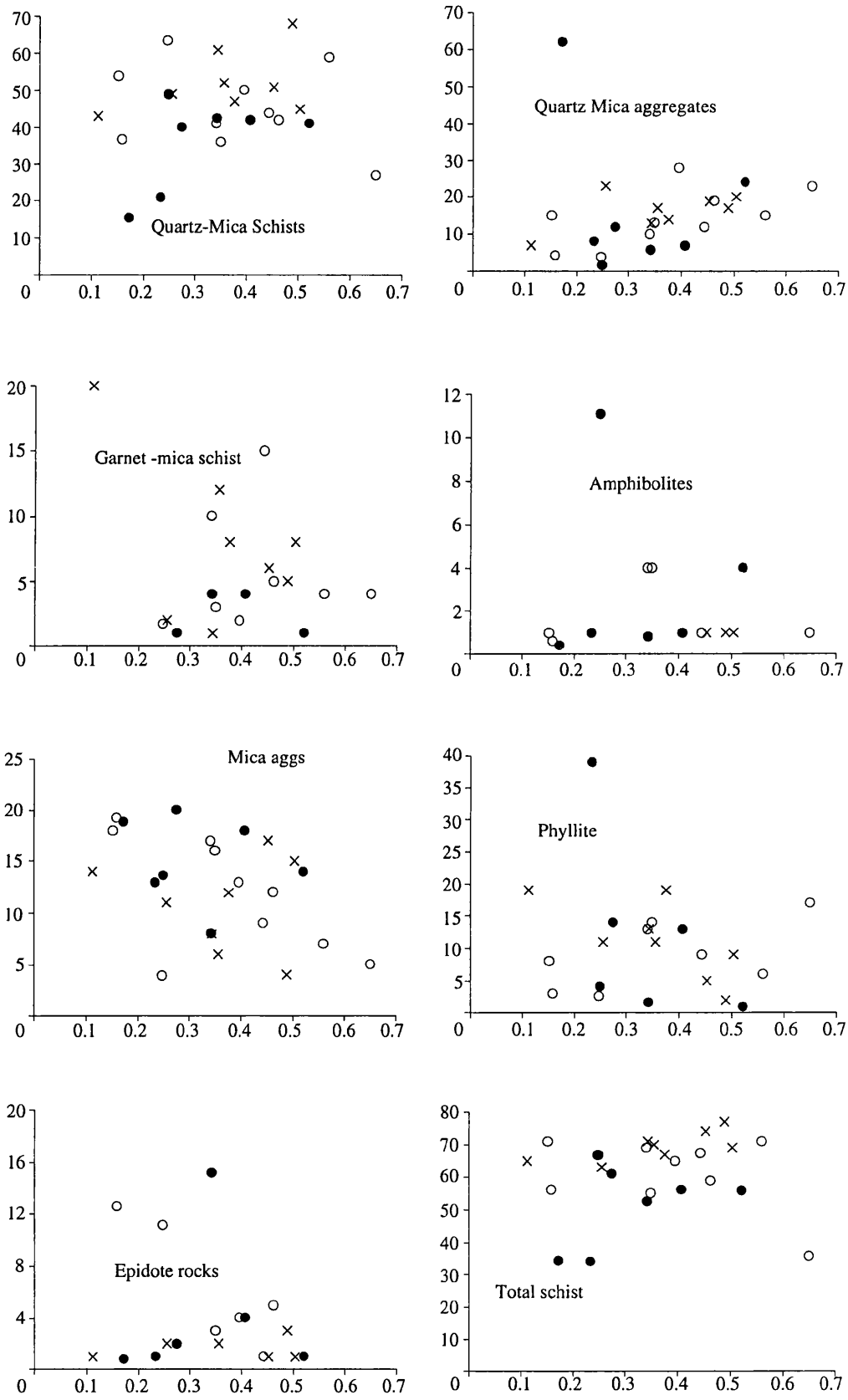

Fig. 4.9 Variations in the abundance of eight rock fragment types with changing average grain size of sediment. The percentage contents are of the total rock fragment population.

formation has a distinct range of content. One sample is abnormally rich in quartz-mica aggregate fragments.

For garnet-mica schist fragments there is the possibility of two trends, one weakly positive, and the other negative. The Dudar formation samples only participate in the positive trend in the lower value range. Both the Pinos Genil and Alhambra formations form the body of the positive and negative trends that meet in samples with the greatest grain size. It is interesting that the finest grained sample of all has the highest content of garnet-mica schist. This is unusual as such metamorphic rocks are usually coarse grained, which would preclude their inclusion intact in fine grained sandstones, as they would be expected to have broken down into their constituent minerals at such grain sizes. This also precludes the development of a negative correlation of content with increasing grain size; a positive correlation is expected. However, elements of a negative correlation are clearly seen here.

Total schists have also been plotted, and show a rather flat, but slightly positive trend. Samples from the Dudar Formation show a slight reduction compared with the other formations. Muscovite aggregates exhibit a weak negative correlation, but the field of variation is diffuse and a clear conclusion is not obvious. The Alhambra Formation samples do however show a much clearer negative correlation with grain size. Trends for phyllite and low grade metamorphic rock fragments are diffuse, but the Pinos Genil formation shows a negative correlation. This latter result is perhaps the expected one. The cause of a negative trend then may be the scarcity of low grade grains, as they are diluted in the coarse grain sizes by the coarser, higher grade lithologies, but would form a large proportion of the finer grained sand fraction where high grade grains are scarce. It is important to distinguish *absolute* amounts of material opposed to *proportions* or ratios in this discussion.

The two remaining rock types are related to meta-igneous sources. The amphibolites show no clear trend, as they are generally not common in the sediments and are even missing completely in many. The epidote rich rocks show some similarity to the garnet-mica schists. The main grouping is in low values and exhibits a weak positive trend, with no formation distinct. Some samples have high values, two from the Alhambra Formation and one sample from the Dudar Formation. The Alhambra formation samples taken alone lie on a negative correlation with increasing grain size.

Additionally to the considerations above, the plots in **Figs. 4.8** and **4.9** allow another way of viewing intra-formational variations in composition. This helps to highlight features which may elucidate grain break-down processes. As the three formations share the same source the effects on sand composition of weathering differences between formations and of recycling of sediment can be clarified.

4.8 t statistic analysis of point counting data

The previous sections raise some questions about the similarity of the ranges of grain composition between sandstones from the three fan formations that comprise the eastern border of the Granada Basin. The plots of grain size against composition (**Figs. 4.8** and **4.9**) indicate some different controls on composition between formations and also tentatively

suggest variations in grain contents. Discriminant function analysis of the main framework grain types distinguish the Dudar Formation from the other deposits on the basis of poly-crystalline quartz, lithic grain, carbonate grains and mica grain contents.

The calculation of a test statistic based on the sample parameters allows the comparison of sets of data to see if they could be derived from the one parent population with an increased degree of quantitative certainty than merely a visual interpretation would give. A t statistic analysis was performed on the point counting data from the Dudar, Pinos Genil and Alhambra Formations to test the degrees of similarity between the sandstones derived from these deposits. **Tables 4.9** and **4.10** present the results of these tests.

Table 4.9 presents the results of t statistic analysis for the comparison of the conventional framework grain contents of the sandstones taken from the Dudar, Pinos Genil and Alhambra Formations. When the calculated number for the grain type exceeds the critical value of the test statistic for the comparison in question then the hypothesis that the grains of that type in each formation were derived from the sample parent population is rejected. Put simply, the calculated values of the test statistic reveal the grain types which vary in amount most between formations. For the Dudar Formation compared to the Pinos Genil Formation the largest difference is in the content of Feldspar grains. All other grain types could be derived from the same parent population.

For the Pinos Genil-Alhambra Formation comparison the greatest differences are in the contents of feldspar and opaque mineral grains. Finally, for the comparison between the Dudar and Alhambra Formations the greatest difference is in the content of lithic, mica and carbonate grains. How does this compare with the result of the discriminant function analysis?

Agreement is seen in the differences in the lithic, carbonate, mica and feldspar grains but the polycrystalline quartz, which accounts for an important change in composition between formations, could (based on the t statistics presented here) be in all formations derived from the same population. The remaining grain types show non-significant differences between formations. However, the Dudar Formation is least similar to the Alhambra Formation.

Table 4.10 presents the results of t analysis of the lithic grain type abundance variations between formations. Comparing the Dudar and Pinos Genil Formations the only significant difference is contained in the content of Garnet-Mica Schist grains. This is seen on **Fig. 4.9**. Comparing the Dudar and Alhambra Formations reveals the greatest dissimilarities between any two formations, confirming the compositional contrast shown by the total framework grain contents. Significant differences are seen in the content of Quartz-Mica Tectonites, Garnet-Mica Schists and the Epidote bearing rock types. No significant differences are seen between the Pinos Genil and Alhambra Formations.

These patterns of test statistic values suggests that the Dudar Formation is the most compositionally distinct of the three formations examined, and that the grain compositions of the Pinos Genil and Alhambra Formations are more similar to each other than to the Dudar Formation. This is in agreement with the results of discriminant function analysis presented above.

	Dudar-Pinos Genil	Pinos Genil-Alhambra	Dudar-Alhambra
Critical test statistic t:	**1.717**	**1.74**	**1.714**
Qm	0.26	0.93	0.18
Qp	1.46	0.83	1.41
F	1.80	3.31	1.08
L	1.45	0.90	2.91
Mica	1.12	0.40	2.07
Carbonate	1.23	1.13	2.76
Heavies	1.05	1.15	0.49
Opaques	0.54	2.47	0.973

Table 4.9 Results of students t analysis comparing means and standard deviations of point counting results. The significance level was selected as 10% for this two tailed test, which gives the critical t values listed above. When the calculated t value for the comparisons of values between formations exceeds the critical value for the number of combined samples then the null hypthesis of similarity of parent populations must be rejected.
n for Dudar - Pinos Genil Formation comparison is 24, for Pinos Genil-Alhambra Formations is 19 and for the Dudar - Alhambra Formation comparison is 25.

	Dudar-Pinos Genil	Dudar-Alhambra	Pinos Genil-Alhambra
Critical test statistic t:	**1.725**	**1.734**	**1.746**
Quartz-Mica Tectonite	0.91	2.77	1.39
Quartz-Mica Aggregate	0.38	0.67	0.61
Garnet-Mica Schist	2.05	3.35	1.26
Feldspar Aggregates	1.15	1.68	0.90
Amphibolites	0.36	1.04	1.36
Mica Aggregates	1.28	1.72	0.45
Phyllite	0.10	0.79	1.14
Epidote Rich Rock Type	0.84	2.02	1.47

Table 4.10 Results of students t analysis of lithic grain point counting totals. Conditions are the same as for **Table 4.X** above.

4.9 Discussion and interpretation of sandstone composition

Variation in composition due to grain size has been shown to affect, in a predictable way, the *intra*-formational composition. However, it is not a significant factor on an *inter*-formational level (**section 4.6**). Therefore differences in composition between formations, for instance the increased proportion of Qp in the Dudar Formation, are real trends, and not a consequence of grain size variation. As discussed in **Chapter 3**, the ultimate primary source of the sediments remained unchanged throughout deposition. Differences in composition must therefore be due to the effects of differential weathering and possible recycling of sediments. This has predictable consequences for composition. Quartz content should increase as less stable minerals are selectively removed by reworking and more prolonged terrestrial weathering. Lithic grain content should decrease, as grains again break down to their mineral constituents.

The *conglomerates* of the eastern Granada Basin conform to this predicted trend. Quartz rich rocks become more common and labile schist lithologies become finer grained. Textural maturity increases also, as roundness increases and maximum clast size generally decreases. These changes have been attributed to increased abrasion due either to increased transport distance combined with terrestrial weathering rates and extended fan top residence times, reworking of earlier deposits into younger, or a combination of all these factors. The accompanying sands could reasonably be expected to have suffered the same fate, therefore they should mirror the same compositional trends.

Variations in 'conventional' framework components (Q-F-L, Qm-F-Lt) are discussed first , followed by the variations in lithic components (for example Qp-Lvm-Lsm). It is lithic grains that provide the best clues to the progress of sand grain break-down within these sediments. It is also important in connection with this to invoke the evidence for conglomerate breakdown processes presented in **Chapter 3**.

Conventional framework components

For the Q-F-L plot the Dudar formation has the greatest quartz content, thus it is the most compositionally mature formation. However, the increased maturity of the Dudar formation sands is due to high Qp/L. Even so, in the Qm-F-Lt plot there is no observed difference in the range of Qm/Lt between the formations. This latter evidence indicates that the extent of polycrystalline lithic grain break down is the same for all the Granada Basin sediments, and therefore the textural maturity of each formation is no different. However it must be emphasised that the mineralogical-compositional maturity of the Dudar Formation is the greatest of the three formations.

The higher mineralogical maturity of the Dudar formation may be due to higher quartz content in the source region in the early stages of sedimentation. Coarser grained and higher grade metamorphic rocks present in the Sierra Nevada source could produce greater quantities of Qp on breaking down. The reduction in Qp/L in the younger formations could be accounted for by an increased input of finer grained, lower grade metamorphics. These would be more likely to remain as lithic clasts. Proportions of finer grained low grade metamorphic

rocks do increase in abundance in younger deposits (**Fig. 4.6**) However, this poses a problem as finer grained, and presumably lower grade metamorphics would be expected to be the first rocks eroded from the higher levels of an orogen, and to be deposited in the oldest sediments derived from that orogen. The relative proportion of schistose lithic grains also increases in the younger Pinos Genil and Alhambra Formations, corresponding with an increase in lithic grains less Qp. This suggests that Qp is proportionally larger in the Dudar Formation due to a scarcity of relatively finer grained lithic source rocks.

It is clear that the Dudar Formation is compositionally distinct from the other formations. Discriminant function analysis reveals that the Dudar Formation shares the fewest characteristics with the Pinos Genil and Alhambra Formations, and that these two formations are significantly more similar to each other than either are to the Dudar Formation. What sets the Dudar Formation apart is its higher content of poly-crystalline quartz and carbonate and its lower content of lithic grains and mica grains. The Pinos Genil and Alhambra Formations are distinguished on the basis of Feldspar and opaque mineral contents. The conclusions of the statistical analysis of the point counting data support the qualitative assessments made on the basis of visual comparisons using ternary diagrams and the calculation of simple formational averages.

The pattern of decreasing compositional maturity within the sands is surprising as the Dudar formation retains the greatest apparent immaturity. It has suffered the least intense weathering environment of all the detrital formations in the Granada Basin, and was deposited rapidly in marine conditions. Grains are fresh, especially chemically less stable heavy minerals, and rock fragments are angular. The Pinos Genil and Alhambra formations, in contrast, have suffered terrestrial weathering, grains are often altered or coated in iron oxides, and lithic sand grains become increasingly rounded. The conglomerate composition data presented in **Chapter 3** indicates that the Dudar formation has the greatest content of the most labile schistose clast types, compared with the younger sediments. A clear conclusion is that the maturity of the sands decreases in younger formations, in contrast to the conglomerates.

How does the content of lithic grains increase to replace Qp in importance? Sediment source characteristics must be changing. This can happen in two ways. Firstly, the *primary* source of sediment may change in character, becoming probably finer grained, allowing more lithic grains to be produced for a given grain size. Secondly, more schist grains could be produced by the increased break down of lithic detritus, especially from conglomerate clasts, either due to reworking of earlier deposits, or increased weathering and abrasion in a terrestrial environment. In **Chapter 3** a model of conglomerate compositional evolution was presented, taking place in a system where material could be removed once it became too fine grained to be considered as conglomerate. This generation of sand from the break-down of conglomerate clasts has a profound effect on the compositional evolution of sands that accompany conglomerates. In a sense the sands have a *secondary* source within the conglomerates, that constantly break-down to produce what would appear as first cycle sand sized detritus, even if it is produced during reworking in a second cycle of sedimentation. In this way the

compositional immaturity of the sand fraction can be maintained while the immaturity of the conglomerate fraction decreases.

It is the most labile clasts that reduce in size, the schists with their cleavage weakness, and the finer grained quartz-poor phyllitic and graphitic lithologies. Quartz rich and coarser grained rocks that may produce Qp are less likely to break-down, due to their greater, quartz induced hardness. As schist grains break down, the numbers of grains increase in an exponential fashion, so the sandstone may see an increase in the amount of lithic grains. In this way maturity of proximal second or third cycle sands can decrease, rather than increase, until conglomerate grade material has finally disaggregated. In this way also the initial, least reworked or weathered and abraded deposits of the Dudar Formation have the highest Qp content, separating them compositionally from the younger deposits and imparting the greatest compositional maturity.

The patterns seen in the conglomerate composition in **Chapter 3** conform to the expected effects of the increase in maturity upon composition. For the Alhambra Formation the content of fine grained schist clasts is no greater than the older more mature, and less weathered formations. The sands in the Alhambra Formation must have been fed from the break-down of conglomerate clasts, because break-down has clearly taken place in the coarser clast sizes, as the amount of schist there is dramatically reduced.

Feldspar

The ratio of feldspar to quartz and lithic fragments is smallest in the Alhambra formation. The Dudar and Pinos Genil formations have a greater relative amount of feldspar. The Alhambra formation represents the most restricted range of composition of all the formations, due to its lower feldspar content. This reduction in feldspar content is consistent with the state of weathering in the Alhambra Formation, or as the product of the recycling of earlier deposited sediments. Of all the common rock forming minerals (quartz, feldspar, micas), plagioclase feldspar is the least stable in the weathering-depositional cycle (Nesbitt and Young 1989).

However, the feldspar content of the Pinos Genil Formation is greater than the Dudar formation. The Pinos Genil alluvial fan is a subaerial deposit, so should show the effects of greater weathering intensity compared with the Dudar Formation. Many grains are affected, but the feldspar ratio to quartz and lithic grains is high. This pattern is hard to explain as feldspar content would be expected to decrease. Available source rocks for feldspar may have increased in the source during Pinos Genil Formation deposition, compensating for selective removal by weathering and/or recycling. The proportion of feldspar rich lithic grains is largest in the Pinos Genil Formation (see **Table 4.6**), suggesting that this may be the case.

The comparison between the Q-F-L and Qm-F-Lt plots is valuable, as it allows some preliminary statements to be made about the state of break-down of the detrital grains in the formations in question. Based on the Q-F-L plot there is a trend in compositional maturity, that appears to decrease in younger sediments, contrary to expectations based on conglomerate petrography and weathering states. However, the Qm-F-Lt plot reveals trends in textural

maturity, because it groups together all polycrystalline grains (i.e.. Qp+L=Lt). (In any case the distinction of Qp in sedimentary petrography is somewhat arbitrary, as it is essentially a lithic grain type, often attributable to either an igneous, metamorphic or sedimentary provenance.) In the Qm-F-Lt plot there is no distinction between the three formations possible based on Qm/L. The conclusion from this is that all formations share the same level of lithic grain breakdown, though no comment is possible upon the types of lithic grains involved from these ternary plots alone. An interpretation of the lithic grain data is detailed below.

Lithic variations

Apparent trends are visible on the plots in **Fig. 4.6**, both in the range of values and absolute proportions of lithic grains.

Quartz-mica schist increases as a percentage of lithic fragments with decreasing age of formation. The average values increase also, with a slight dip in values for the Pinos Genil Formation. This trend can be accounted for by an increased input of schist grains from the source. Quartz-mica aggregates also increase in abundance slightly. Both these trends are consistent with increased break-down of schist clasts of all sizes, which would have the effect of increasing the number of schist grains. Through each cycle of break-down, the number of grains will at least double. The increased proportion of schist grains in the sand fraction of the sediments in the Pinos Genil, and especially the Alhambra formation is in contrast to the decreased number of schistose conglomerate clasts in these formations. However, it is consistent with the explanation given above.

Muscovite aggregate proportions decrease in younger sediments. These aggregates are derived primarily from relatively coarse grained, high grade metamorphic schist fragments. Their reduction in number indicates a reduction in the break-down of such coarse lithic fragments, and a reduction in amount of coarse grained schist. However, the proportion of schist clasts *increases* in the Alhambra formation. There is a trend to a negative correlation between quantities of quartz-mica schist/aggregates and muscovite aggregates (**Fig. 4.10**). However this pattern is consistent with the reduction in Qp in younger sediments, and supports the assertion that this is due to the reduction in the break-down of coarser, quartz rich schistose lithologies. The source rocks are becoming finer grained, as more labile lithologies break-down faster, they produce larger quantities of detritus thus swamping the coarser, harder material. There is no grain size determined inter-formational compositional bias for the sandstones themselves, as demonstrated in **section 4.7**. However, the 'internal' grain size of lithic fragments may become smaller, resulting in an apparent increase in lithic grains for any detrital grain size.

The reduced availability of high grade, coarse grained metamorphic rock, *and/or* the increased availability of lower grade, finer grained metamorphic rock, can explain the reduction in amount of muscovite aggregates. It also explains the simultaneous increase in proportions of quartz-mica schist, the decrease in Qp *and* the increase in lithic fragments when data is plotted on a Q-F-L diagram.

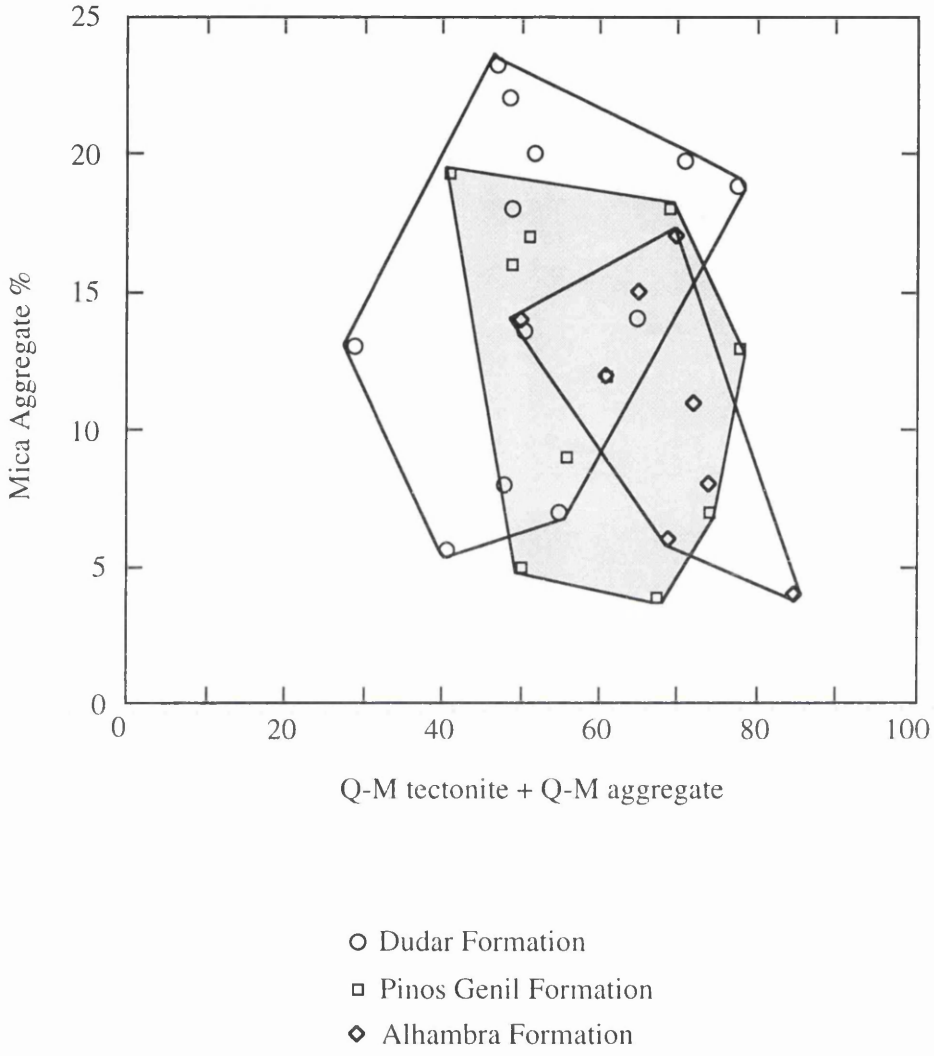

Fig. 4.10 Percentage values for mica aggregates plotted against Quartz-Mica tectonite (schists) plus Quartz-Mica aggregates. This is intended to depict any relationship, as suggested by the variations in percentages of these grain types pictured in **Fig. 4.5**.

Further evidence to support this comes from the increased proportion of low grade, phyllitic lithic fragments in the Alhambra formation. It shows that an abundance of finer grained rock correlates with increased lithic grain content in sandstones. Phyllite and similar low grade metamorphic rocks become more abundant in the conglomerates of the Pinos Genil formation, suggesting that the average grade of material sourced in the Sierra Nevada may be dropping through time. This could be due to the uncovering of phyllitic lithologies in the Alpujarride during basin flank uplift, as discussed in **Chapter 3**. However, dolomite is conspicuously absent from the Pinos Genil and Alhambra Formations in quantities that would suggest an important Alpujarride source.

The range, or spread, of percentage values for each formation presented in **Fig. 4.6** is more difficult to interpret. In general there is a reduction in range for samples in younger sediments, except for the low grade metamorphic rock fragments whose range remains the same between formations. The range of values may be partly grain size controlled, samples with smallest average grain size having the lowest schist grain content. As demonstrated, however, grain size range is the same for all the formations, making the significance of the differences seen here less clear. A possibility is that sands in later formations are the result of better mixing of detritus. This could take place as the deposition of the Pinos Genil and Alhambra formations was probably slower than that for the Dudar formation. This would allow mixing to take place on fan tops, analogous to, and supported by, the increased weathering which is evident, as discussed above. Recycling of older sedimentary deposits into younger deposits is another mechanism that would thoroughly mix sediment and reduce compositional variations.

The trend on **Fig. 4.7** (Q-M-QMschist) shows elongation in the direction of increased break-down, or disagregation of lithic grains. The separation between formations is not significant, so the conclusion reached here could be that there is little change in the state of lithic grain break-down between formations. However, there is a slight trend to a thinning of the fields into younger formations, and a slight elongation towards grain break-down in the Alhambra formation. This indicates that the Alhambra formation may represent the greatest extent of lithic grain reduction. This again is consistent with the general weathering state of the sediments, and the paucity of feldspar in the Alhambra Formation.

Grain size correlations

There are some differences evident upon the grain size correlation plots in **Figs. 4.8** and **4.9** that shed further light upon the break-down and general maturity of the sediment. For the conventional framework components there are some features in compositional range that set the Dudar Formation apart from the younger deposits. For instance the flatter trend followed by monocrystalline quartz, and the heavy mineral and monocrystalline mica contents.

For the heavy mineral content, the Dudar Formation shows the lowest percentage values of all the deposits. This is consistent with an increased degree of lithic grain break-down in the Pinos Genil and Alhambra Formations. The flat trend seen in the content of monocrystalline mica in the Dudar formation is harder to account for. Perhaps mica is still retained in lithic

fragments to a greater degree in the Dudar formation and has not been released to increase in quantity in finer grained sands.

4.10 Conclusions

The conglomerates of the Eastern Border of the Granada Basin indicate an increase in compositional maturity in younger formations that could be reasonably be expected to be reflected in coeval sandstones. However, there is no increase in compositional maturity in the sands of the eastern Granada Basin with decreasing age of deposit. Maturity decreases in the younger formations.

Feldspar content increases in the terrestrial Pinos Genil Formation which is not consistent with the observed increase in weathering of the younger formations. However, the content of heavy minerals also increases in these more weathered deposits. This points to the possibility of increased input to the sand fraction from the break-down of metamorphic lithic grains and a new feldspar source. This is supported by the trend towards increased lithic fragments in the Pinos Genil and Alhambra Formations, and especially the increased content of quart-mica schist. This trend may also be partly due to an increase in finer grained lithic fragments, consistent with the observed increase in the number of grains of phyllite and low grade metasedimentary rocks.

An increase in the quantity of schist fragments may be accounted for by the break-down of finer grained metamorphic rocks. This increase in schist fragments balances a decrease in the content of polycrystalline quartz in the Pinos Genil and Alhambra Formations. This has the effect of changing the indicated provenance areas on Q-F-L and Qp-Lvm-Lsm ternary discrimination diagrams, and seemingly decreasing the observed maturity of those formations. However, the Qt-F-L plot indicates that the total content of polycrystalline grains is no different between formations, and that the only significant compositional change that can be attributed to the more weathered state of the latter deposits, is the decrease in feldspar in the Alhambra Formation.

Discriminant function analysis confirms the compositional distinction between the Dudar Formation and the Pinos Genil and Alhambra Formations, which are more similar to each other than to the Dudar Formation. The Dudar Formation sands are compositionally distinct because of a higher content of poly-crystalline quartz and carbonate, and a lower content of lithic and mica grains. The Dudar Formation is well defined, being able to classify 82% of its own samples. The Pinos Genil and Alhambra Formations are less well defined. The Alhambra Formation sands classify 66% of the data. For the Pinos Genil Formation sands only 33% of the data is classified as belonging to the Pinos Genil Formation.

The cause of these compositional distinctions can be attributed to the increased abrasion of sediment during the deposition of the latter formations. Subaerial deposition and the possibility of extended fan-top residence may have been sufficient to generate the alteration of grains and the increased break-down of lithic grains. However, the composition of the Alhambra formation did not become any more mature as a result of this. The composition was, at least, being maintained. Signs of increased grain breakdown are indicated however, but

these processes have not progressed to such a degree that the maturity of the sediment has begun to significantly increase.

The break-down of lithic grains, and conglomerate clasts, as suggested in **Chapter 3**, may be more consistent with a model of sedimentary recycling. Conglomerate composition becomes more quartz rich. It may be this reduction in schist content in the conglomerates that feeds the observed increase in lithic clasts in the sandstones. In this way the composition of the sandstones is at least maintained, despite the evidence for increased weathering.

The composition of second and third cycle sediments in a proximal intramontane setting may then change in unexpected ways. The complications of breaking grains of the entire grain size spectrum (conglomerate to sand) in a setting where distance sorting has little effect, means that sand maturity lags behind that of coarser sediment. Conglomerates mature first, and in doing so, feed material into the sand fraction, maintaining or even increasing its immaturity. This could be interpreted as a change of source, or the persistence of a primary first cycle source region. This factor should be taken into account when making tectonic inferences from sandstone detrital modes, using provenance discrimination plots.

Finally the provenance classification of the sandstones from the eastern Granada Basin based on detrital modes, using the scheme of Dickinson and Suczek (1979) and Dickinson et.al. (1983) indicates the possibility of erroneous provenance assignment. This may be due to the un-recognised composition of sands derived from high grade metamorphic sources exposed in metamorphic core-complexes, such as the Sierra Nevada that borders the Granada Basin. Most of the Granada Basin sands fall in the correct field of recycled orogen provenance, but an important number of samples fall in the arc provenance area. Even in the recycled orogen areas the sands used to define the provenance areas by Dickinson and Suczek (1979) are mostly associated with subduction complexes and foreland uplift provenance types. The Granada Basin sediments suggest the possibility of a new provenance type for the Q-F-L and Qm-F-Lt diagrams representing core complex exhumation.

The Granada Basin sediments are unusual as they are high grade metamorphic detritus produced by a rapid orogenic uplift. Most rapidly generated sediments are low grade metamorphic or sedimentary as they represent the cover to an orogen which is the first crust to be eroded on uplift. Uplift rates wane before the exposure of initially deeply buried metamorphic rocks. High grade metamorphic rocks are often exposed in mature, now stabilised, immobile crust in the interiors of plates. The Caledonides in the Highlands of Scotland are an example. In these cases the sedimentary cover can build up and through time sediments become increasingly mature. The sediments in the Granada Basin are unusual because they represent a fresh, *first cycle* input from such a high grade source.

5. Sandstone Geochemistry

5.1 Introduction

The provenance of sandstone has for some time been recognised as being controlled primarily by tectonic setting (eg. Middleton 1960). In the same way as sedimentary basins are classified in type by tectonic setting (Dickinson 1974), plate tectonics determines the rock types common in particular settings. This in turn determines the composition of sandstones derived from source areas whose characteristics are controlled in this way. Other controls on composition include climate, relief, sorting and ultimately diagenesis (Pettijohn et. al. 1972, Bhatia 1983, Argast and Donnelly 1987).

Classical petrographic analysis has been applied in order to delineate the mineralogical characteristics of sediments derived in differing tectonic environments (eg. Schwab 1975, Dickinson and Suczek 1979). The characterisation of modern sediments, and ancient deposits with well constrained tectonic settings allows comparisons to be drawn with the compositions of sediments of uncertain tectonic origin. This application in provenance has been largely successful allowing the reconstruction of ancient tectonic scenarios when sediment source regions have been removed.

Petrographical methods are limited by the ability of an observer to recognise minerals and lithic fragments, in order that they may be related back to source. Postdepositional processes such as diagenesis and especially metamorphism can result in the destruction and replacement of original mineralogy whilst retaining original chemical composition, thus making petrographic analysis redundant for provenance characterisation. This has prompted many workers to look to geochemical studies in order to overcome these problems (eg. Van de Kamp and Leake 1985, Argast and Donnelly 1987). If neo-mineralisation occurs with little, or no net change in composition of the sediment during diagenesis or metamorphism, then the geochemistry will accurately reflect provenance. This could allow the depositional settings of metasedimentary (or indeed meta-igneous) protoliths to be established. However, postdepositional alterations that obfuscate original framework mineralogy, may also change the bulk chemical composition of the sandstone by the addition of cement material, for example. The application of geochemical classification techniques presumes that this has not happened. Some changes may be obvious, like large Ca contents due to carbonate cementation, but where metamorphism has altered the texture of the rock the causes of such changes may not be clear, and the provenance worker has to presume the composition of the sandstones is due only to original framework mineralogy. More work is required, to try to resolve such issues.

Several provenance discrimination schemes based on major and trace element abundances have been proposed. Bhatia (1983) proposed that the tectonic setting of sandstones can be distinguished using major element compositions. He found the following to

be the most discriminating; Fe2O3+MgO%, TiO2%, Al2O3/SiO2, K2O/Na2O and Al2O3/(CaO+Na2O). Using these parameters, sands from oceanic and continental island arcs, active continental margins and passive continental margins can be discriminated.

Following on from such work as Middleton (1960) and Maynard et.al. (1982), Roser and Korsch (1986) developed the discriminating power of SiO2 combined with K2O/Na2O. They assign distinct areas on the bi-variant plot for arc-related, active margin and passive margin provenances. Additionally to this they emphasise the importance of interpreting trends of individual samples rather than averages. Most importantly they plot sandstone-mudstone pairs and characterise distinct trends in composition that in themselves could serve to discriminate source.

Bhatia and Crook (1986) developed provenance discrimination based on the more immobile trace elements (eg. La, Ce, Nd, Th, Zr, Nb, Y, Sc, Co). Oceanic Island arc, Continental Island Arc, Active Continental margins and Passive Margins can be distinguished using ratios of trace elements in bi-variant discrimination plots.

Argast and Donnelly (op. cit.) show how the elemental distributions in deeply buried North American greywackes are similar to those seen in shallow buried recent sediments from the Black Sea. They conclude that burial alteration does not necessarily cause great elemental changes. However, other factors may still affect the composition of sediments, especially weathering during erosion and transport. These processes begin chemical differentiation, that bias the composition of the sediments away from the original, fresh source rock composition, towards the ultimate maturity of a quartz arenite. Such alteration will of coarse affect the ability of sediment to indicate provenance, and will thus place limits on its use in tectonic reconstruction.

The chemical changes observed during the production of sediment are dependant upon the mobility of the elements in the constituent minerals. Cullers et. al. (1988) compared the composition of fresh source rock to the composition of detritus in soils and stream sediments nearby, in order to elucidate the effect of chemical differentiation in the sedimentary cycle on provenance determination. Enrichments and depletion of REE elements is common, up to a factor of 50, but usually less than 15. Most patterns resemble source, and discrimination of source rock types is possible especially using the more immobile elements.

Nesbitt et. al. (1990) demonstrate that the enriched LREE content of muds from the Amazon fan is due to extreme weathering of source rocks, and not due to diagenetic or even source rock properties. They comment on results of Nesbitt (1979), that weathered products of the Tooronga granodiorite are preferentially leached of HREEs. The leached elements are released from primary source minerals on breakdown during chemical weathering. The clay fraction becomes enriched therefore in more immobile LREEs, and particle size sorting enriches distal deposits in LREE rich muds. However, the problem of recognising distinct REE patterns in ancient sediments, and especially of muds, and their use in discriminating provenance still remains.

Argast and Donnelly (1987) also comment upon the grain size control of chemical composition. Their samples were greywackes with grain sizes of coarse silt and fine sand (4-5

phi). Coarser samples were richer in SiO2 and Zr (related to sorting of zircon into coarser fractions) and poorer in Al2O3 and K2O than finer grained samples. This is explained by an increased amount of illite in finer grained samples. This demonstrates how size sorting is important in producing chemical variations, so must be constrained when tectonic reconstructions are attempted based on provenance indications derived from sediment composition.

Chemical weathering is the major control on composition and the changes wrought upon provenance signature. Nesbitt and Young (1989) demonstrate how bulk changes of composition from fresh source rocks are predictable from kinetic and thermodynamic mineral data. They compare their predictions with data from weathering profiles of mainly silicic igneous rocks. The main changes involve an initial reduction of CaO+Na2O followed, at more advanced stages of weathering, by removal of K2O and FeO tot + MgO. Al2O3 remains as a relatively immobile component in the analyses they present.

5.2 Aims of Chapter 5, and samples used.

The primary aim of this chapter is the *documentation* of the major and selected trace element geochemistry of sandstones from the eastern flank of the Granada Basin. This has been done by the XRF analysis (see **Appendix 1**) of samples from the Dudar and Alhambra Formations. These formations where chosen because, as demonstrated in **Chapter 3**, they share a constant source region, but exhibit quantitative differences in weathering state and textural maturity. Any *inter-formational* variations in chemistry can then be attributed, by analogy with the work quoted above, to weathering or other sedimentary processes, including recycling, and not to primary-source variation.

Further to this, *intra-formational* grain-size dependant compositional variations are also detailed. The data was gathered by separately analysing the fine, medium and coarse grained fractions of the sands, excluding silt and mud fractions. This was done in order to investigate trends of chemical fractionation due to sediment breakdown processes within a proximal intra-montane setting. It may also help to separate trends due to weathering from those caused by sediment break-down and size reduction.

The composition of the sediments is also placed in a provenance context using the scheme of Roser and Korsch (1986). This is interesting as it appears to indicate not the contemporary tectonic setting of the sediment, but may provide valuable information on the protoliths to the metamorphic Internal Zones of the Betic Cordillera. The scheme introduced by Bhatia (1983) could not be applied to the data collected for this study. Here Fe total was measured as equal to Fe2O3 + (FeO x 1.11112), as a convention of the XRF analysis method. Bhatia uses Fe expressed as Fe2O3, thus direct equivalence between his scheme and the data presented here is not possible without introducing perhaps unacceptable uncertainty.

The locations of sample sites are listed in **Fig. 3.1**. The methods used in analysis are detailed in **Appendix** 1, and the actual results are listed in **Appendix 3.** Detection limits are given for both major and trace elements. For some elements the uncertainties so expressed are

great enough to make the results meaningless. These elements have been eliminated from consideration (especially U, Th and Cu).

5.3. Major element geochemistry

5.3.1 Inter-formational variations

Figure 5.1 presents Wt.% of eight major elements plotted against Wt % SiO_2, for undifferentiated (bulk) sediment samples from the Dudar and Alhambra Formations. Between formation variations are evident. The SiO_2 content of the Alhambra Formation tends to higher values compared with the Dudar Formation. This may be expected to correlate with higher quartz content (Schwab 1975, Van de Kamp and Leake 1985), and greater maturity, but total framework quartz (Qm + Qp) *decreases* in the Alhambra formation to be replaced with lithic fragments (see Chapter 4).

Studies of weathering in source rocks by Cullers et.al. (1988), document an increase in quartz at the expense of feldspar and other accessory minerals, that is reflected in an increase of SiO_2. Nesbitt and Young (1989) conversely, describe changes in abundance of minerals in the weathering profile of the Stone Mountains in Georgia. As the Chemical Index of Alteration (C.I.A.) increases the level of quartz decreases, though only slightly. In the Granada basin an increase in SiO_2 correlates with a decrease in quartz and an increase in lithic fragments and mica grains. It has been argued in Chapter 4 that the increase in lithic fragments is perhaps due to a change to finer grained source rocks, that could be more micaceous, and graphitic (especially in the Sierra Nevada). However, this would not be inclined to push SiO_2 content up. Alternatively the increase in lithic fragments may be due more to an increase in the break down of conglomerate clasts, especially schist clasts, which are seen to decrease in size, and increase in roundness and quantity in the Alhambra Formation. Again though, this would not increase SiO_2 content, but only maintain it, and even work to alleviate the effects of chemical weathering for all elements, as the breaking clasts would act like a fresh primary source.

The increase in SiO_2 content in the Alhambra Formation is probably caused by increased weathering intensity in the prevalent subaerial depositional environment. This process acted on *all* sandstone grains. Two controls on composition could then have operated;

1. one determining the framework grain components through clast break-down and possible recycling;
2. the other determining changes in bulk chemistry through the action of chemical weathering on all these grains.

Thus SiO_2 is left as a structurally stable and relatively insoluble element on all grains, while other elements are lost from all grains. Meanwhile, the framework grain population

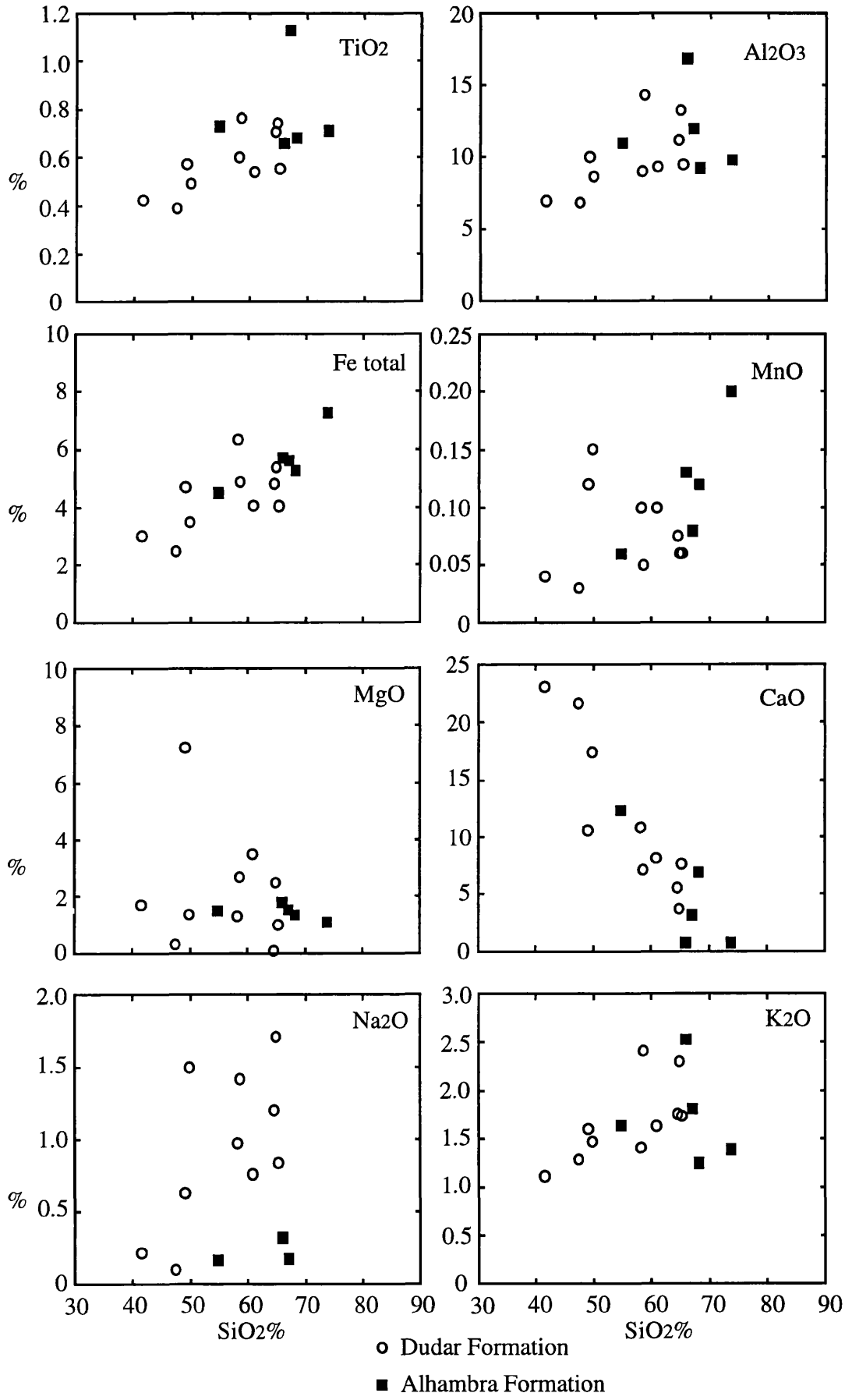

Fig. 5.1 Harker diagrams showing variation in eight major elements with increasing SiO2 content for bulk sands (64u to 1mm) from the Dudar and Alhambra Formations.

appears little changed, or as demonstrated in **Chapter 4**, it becomes less mature due to separate sediment dynamic processes connected to sediment source, and/or recycling.

TiO2 is consistently higher in the Alhambra Formation samples. This could be explained by a relative increase in Ti bearing minerals. Rutile is a stable heavy mineral phase during weathering, comparable to zircon and tourmaline. Heavy mineral abundance increases in the Pinos Genil and especially the Alhambra Formation. Rutile is present in greater quantities in the Alhambra Formation compared with the Dudar and Pinos Genil Formations (**Fig 6.1**).

Fe total increases also in the Alhambra Formation, and overall follows a positive correlation with SiO_2. The increase in Fe is consistent with a relative increase in Fe in residues during weathering (Goldich 1938, quoted in Pettijohn 1975). It is relatively immobile compared to most elements, save perhaps Al_2O_3. However, the overall intra-formational positive correlation with SiO_2, especially in the Dudar Formation samples is harder to account for. This correlation indicates that the bulk of iron is borne by a silicate phase, most probably in micas or heavy mineral species such as amphibole and garnet. However, biotite is not common, and is much less stable than muscovite (Nesbitt and Young 1989).

Electron microprobe analysis of detrital muscovite from the Dudar Formation was performed to asses the extent of weathering alteration and the suitability of the muscovite for isotopic dating (See **Chapter 7**). Typically they contain between 1 and 2% FeO wt %, but occasionally samples have up to 3-4% FeO. Mica is very common in the sediments of the eastern Granada Basin, making up between 7 - 12% of the volume of the sediment, suggesting that it is a contributor of only up to 3-4% of total Fe. Mica is also a common constituent of the lithic grain population which makes up to 50% of the sediment (**Table 4.4**). The increased amount of mica, lithic grains and heavy minerals in the Alhambra Formation *may in part* contribute to the increase of Fe total in the Alhambra Formation. However, Fe bearing silicate heavy minerals such as garnet and amphibole, that are the likely sources of the bulk of Fe, decrease in quantity in the Alhambra Formation. Epidote however, does increase and can make up to 2% of the *total framework components* of some Alhambra Formation sandstones. Intra-formational Fe v SiO_2 in the Dudar Formation may also be partly controlled by increased mica content.

Al_2O_3 content is slightly higher in the Alhambra Formation. This is consistent with its immobile nature during weathering (Pettijohn 1975, Nesbitt and Young 1989). It would be expected to increase relatively in the more weathered Alhambra Formation, similarly to SiO_2, being concentrated perhaps in stable muscovites. The increase in heavy minerals may also play an important part. Epidote amounts increase in the Alhambra formation as well as an increase in the total heavy mineral content. This works to increase Al_2O_3 in a way not related to weathering intensity, and perhaps contradictory to it. This effect could be significant, as the total heavy mineral population of the Alhambra Formation samples analysed, averages at 7%. Epidote is also a component of several lithic grain types, which together with all lithic grains make the largest single framework component.

Other major elements show patterns of decrease when plotted against SiO_2. CaO shows a marked decrease into the Alhambra Formation, that correlates with a decrease in framework carbonate. This is caused by a cessation in biogenic carbonate grain production with the establishment of terrestrial depositional conditions in the late Tortonian. Carbonate cements are not uncommon in the Alhambra Formation, but are less common than in the Dudar Formation.

Na_2O is reduced in amount quite considerably in the Alhambra Formation, even to below detection limits in some samples. This is consistent with the patterns predicted for weathering by Nesbitt and Young (1989) where Na_2O is lost in tandem with CaO due to its high mobility. This is accomplished usually by loss of plagioclase, but here the content of plagioclase in the least weathered samples is low initially, so the low Na_2O content is unlikely to be associated with changes in plagioclase. Other minerals that may contain Na are the amphiboles, and even micas. High pressure amphibolites, as have been recorded in the Internal Zones, are often Na rich. The content of amphibole is reduced markedly in the Alhambra formation, perhaps accounting for some Na loss, through weathering solution of certain mineral species.

MgO contents are lower in the more weathered Alhambra Formation. This is especially clear if all grain size fractions are included (**Figs. 5.2** and **5.3**). Values range from 0.3 to 7.5 wt% in the Dudar Formation, but are restricted to between 0.4 to 2.1 wt% in the Alhambra Formation. The correlation trend is slightly negative with increasing SiO_2, an expected trend of variation (Bhatia 1983). The decrease in MgO may be due to the observed decrease in Mg bearing minerals such as garnets and amphiboles in the Alhambra Formation. MgO may also be reasonably expected to increase with FeO which is greater in the Alhambra Formation, as Mg and Fe commonly occur together in similar phases. This does not appear to be the case, suggesting that Fe is not primarily carried in Mg bearing minerals, and strengthening the argument for Fe in muscovite or Epidote.

MnO shows a positive correlation with SiO_2 overall and the highest values in the Alhambra Formation (**Figs. 5.2** and **5.3**). Garnet is probably the most important Mn bearing mineral in the sediments, but it decreases in the Alhambra Formation, and there is no trend to Mn rich garnets in the Alhambra Formation. Mn may be relatively immobile, or share a chemical affinity with Fe, which also increases in the Alhambra Formation. However, the general range of content of the bulk of samples is the same for both formations.

K_2O values correlate positively with SiO_2. The Alhambra Formation samples plot in the SiO_2 rich end of this positive correlation, suggesting a tendency towards higher K_2O values in the more weathered formation. Nesbitt and Youngs (1989) weathering trend suggests a loss of K_2O only at advanced stages of decomposition. However, for the Morton Gneiss of Minnesota Goldrich (1938) found that K_2O was lost during weathering in amount second only to Na_2O. It is possible that values in the Alhambra Formation have been suppressed in this way preventing a significant increase in K_2O. However, in the absence of significant K-feldspar, potassium is carried in the Dudar and Alhambra Formations in muscovite. Muscovite is a relatively stable mineral (Pettijohn 1975) which resists weathering alteration well (Kelly and

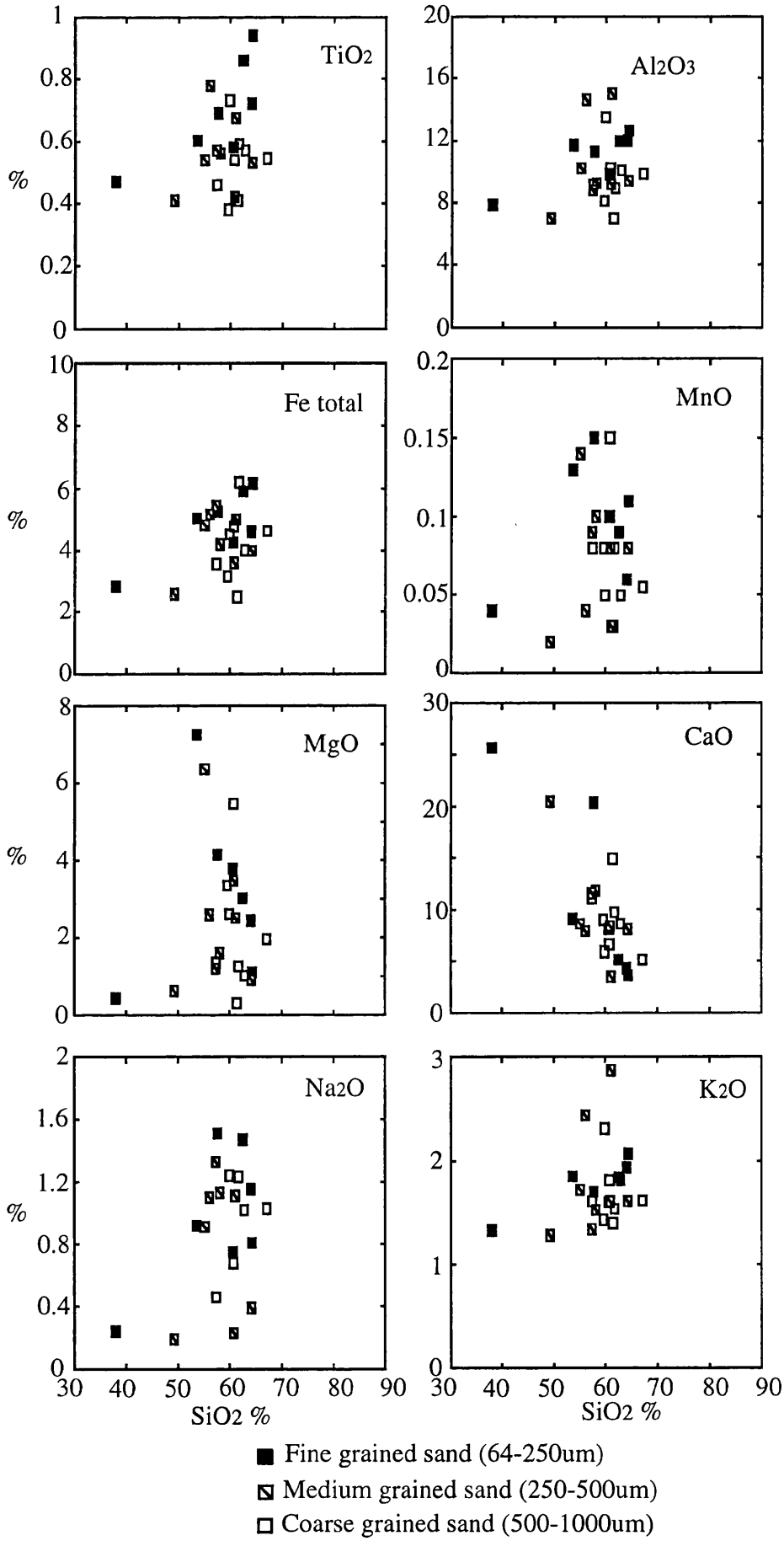

Fig. 5.2 Variation of eight major elements with grain size fraction for samples from the Dudar Formation.

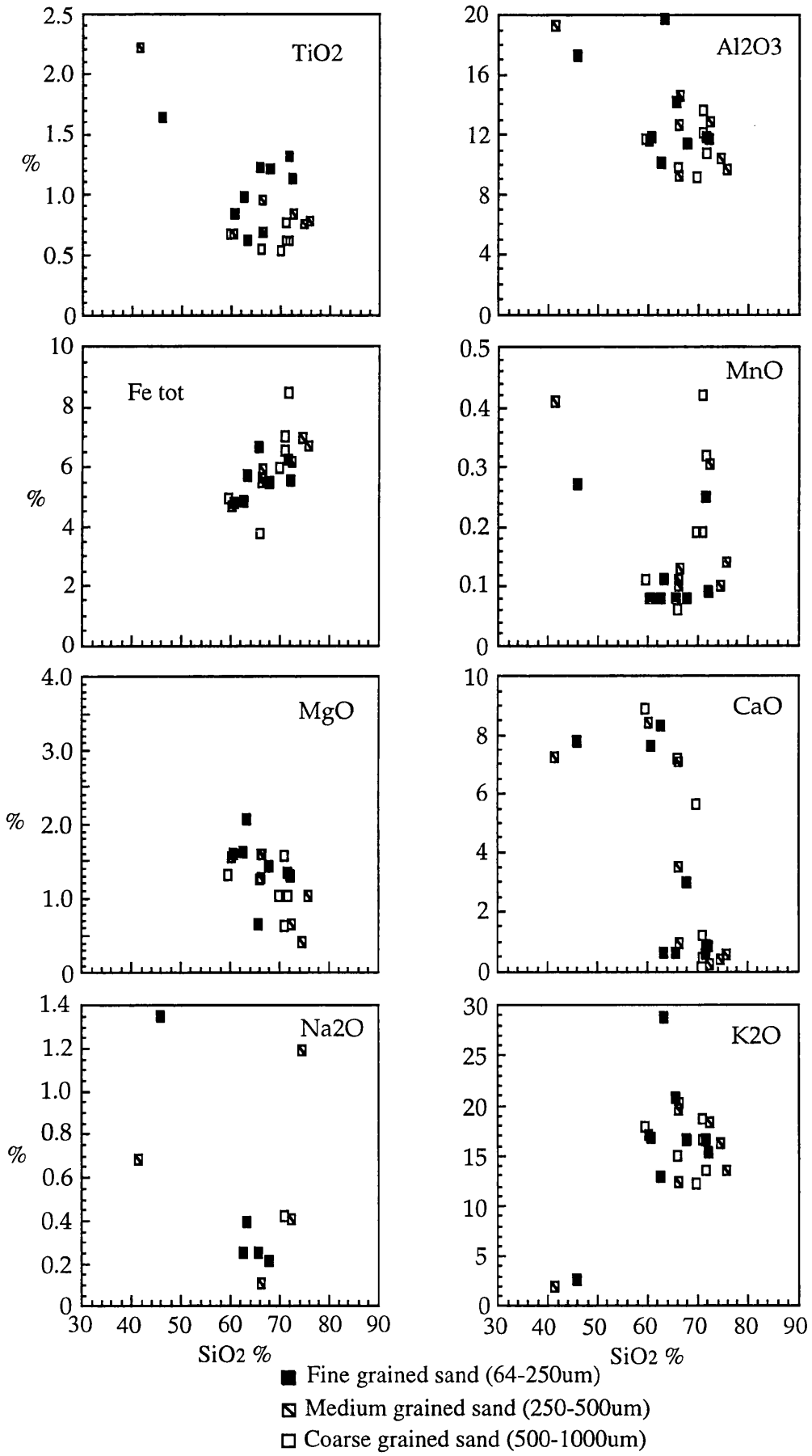

Fig. 5.3 Variation of eight major elements with grain size fraction for samples from the Alhambra Formation.

Bluck 1990, Clauer 1981). Chemical analysis of detrital micas from the Quentar formation and micas in conglomerate clasts from the Dudar Formation (see Chapter 7), show no obvious loss of K_2O, wt% values being around 7-9%. The increase in mica and metamorphic lithic fragments in the Alhambra formation, may account for the slight trend to increased K_2O in the Alhambra Formation. The lack of a large increase in K_2O because of increased muscovite may be due to the balancing effects of increased weathering.

K_2O correlates with Al_2O_3, suggesting that they are held in the same minerals, most probably muscovite. The trends for the Dudar formation samples for K_2O and Al_2O_3 are well defined in **Fig. 5.1,** suggesting a common source. In contrast the diffuse nature of the trends from the Alhambra Formation suggest a more ambiguous source. However, the data set is limited in **Fig. 5.1** and so some trends can be difficult to interpret.

Niggli al-alk

Figure 5.4 plots K_2O wt% against Niggli al-alk. The use of al-alk stems from its discriminating ability with regard to sheet silicates. Van de Kamp and Leake (1985) highlighted its ability to discriminate K incorporated in sheet silicates, including micas, but especially clays (illite and montmorillonite) from K incorporated into feldspars. Shale components of sandstone-shale pairs from their chosen localities had consistently higher values of al-alk compared to the sands, confirming the presence of clay minerals. Van de Kamp and Leake (1994) confirm that high values of al-alk in the Fountain Formation of Colorado compared with values from modern sands from the same source indicate clay alteration of the ancient sandstones. Thus increased al-alk indicates higher mica or, more probably, clay mineral content, that may relate to alteration caused by weathering, or diagenesis.

In **Fig. 5.4** the bulk samples for the Dudar and Alhambra Formations are plotted. Both data sets show a correlation between K_2O and al-alk, indicating that K is not sited in feldspars, but in sheet silicates. The correlations though are not the same, the Dudar formation being steeper than the Alhambra Formation. The separation of the fields for each formation are clear, the Alhambra Formation having higher values of al-alk. This may correlate with increasing alteration in the terrestrial depositional environment of the Alhambra Formation, that could have generated clays. It may also relate to the increased quantity of mica in the Alhambra Formation. Van de Kamp and Leake (1994) plot K_2O vs al-alk for the Colorado samples and include on the plot the area defined by the compositions of smectite and illite, and that also of muscovite. The edge of the clay area is indicated on **Fig. 5.4** and also the direction to where muscovite plots.

Fig. 5.5 shows all the grain size separates for the samples from the Dudar and Alhambra Formation. Again the results plot in distinct areas, with the Alhambra Formation plotting with increased al-alk. The distinct correlations are clear also. The influence of clay minerals appears to dominate the trend of the Alhambra Formation samples. There is a high content of muscovite in these samples as derived from petrographic analysis, but this does not dominate the K_2O - al-alk correlation. The Dudar formation samples in contrast clearly show

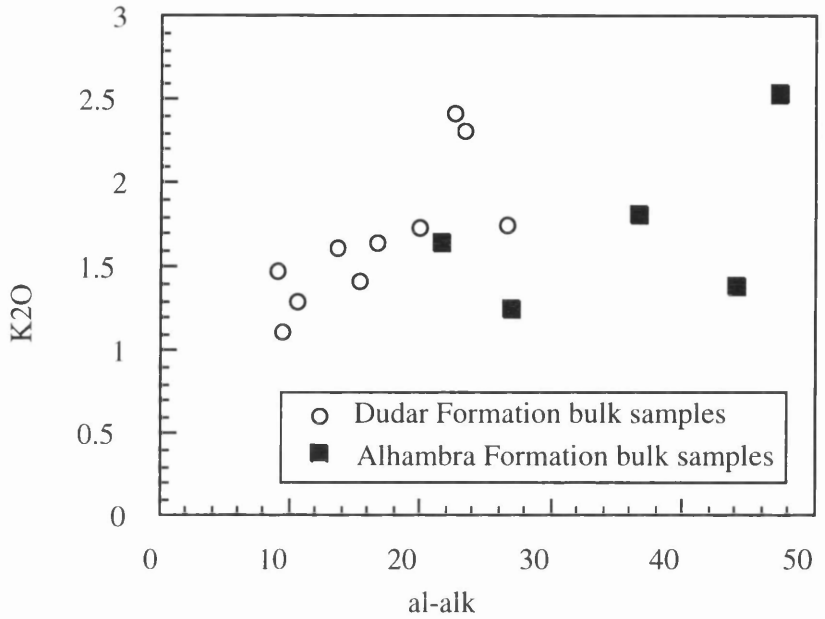

Fig. 5.4 Variation of K2O with niggli al-alk for bulk samples from the Dudar and Alhambra Formations. Note good correlation in Dudar Formation and higher values of al-alk in Alhambra Formation.

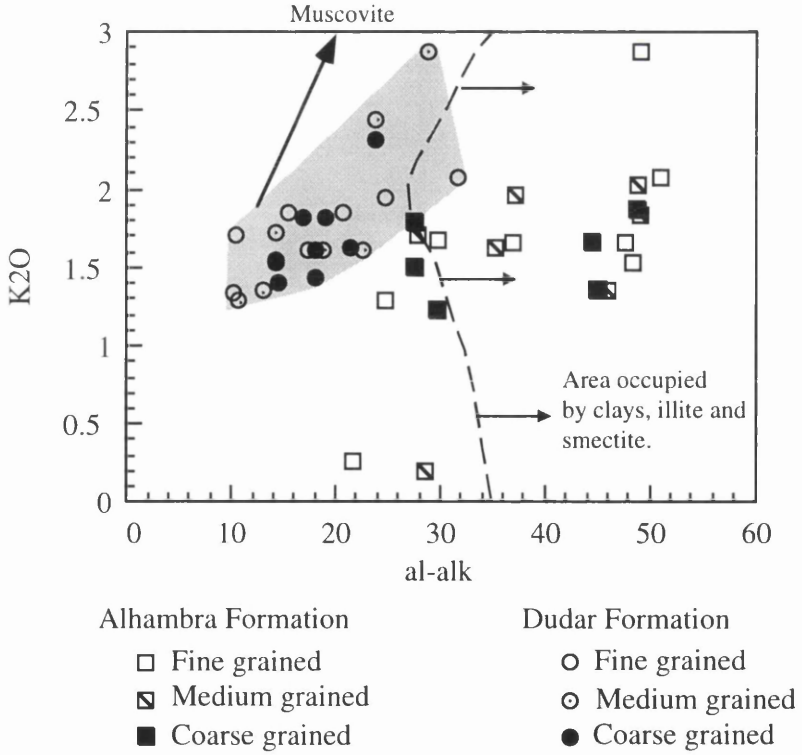

Fig. 5.5 Variation of K2O content with niggli al-alk for all grain size separates from the Dudar and Alhambra Formations. Both formations plot distinctly and appear to has different correlations between K2O an al-alk.

an increased influence of muscovite combined with an important clay component, as the trend does not head directly towards muscovite, but is deflected downwards.

In summary, the Alhambra Formation has higher Niggli al-alk values than the Dudar Formation, that when plotted against K_2O suggest a higher content of smectite and illite clay minerals. This is despite the documented increase in mica content (see **Table 4.4**) in the Alhambra Formation, which does not appear to affect the K_2O - al-alk correlation. The composition of the Dudar Formation sediments are more influenced by muscovite, which itself may be relatively unaltered. The Dudar Formation contains fewer clay alteration products. However, the trend for the Dudar Formation does lie off the tie line to muscovite, and shows the influence of clay minerals in the sediment.

Summary

Distinct patterns of variation between samples from the Dudar and Alhambra Formations can be seen for most major elements discussed above. These can be summarised;

- Increase in SiO_2 in the Alhambra Formation. Can be attributed to increased weathering that this formation has suffered. Increased quartz content is not responsible as this is reduced in the Alhambra Formation.

- Increase in TiO_2 in the Alhambra Formation. Rutile increases noticeably in the Alhambra Formation. Greater TiO_2 may be caused by such a concentration of stable minerals such as Rutile, that may be released from the break-down of conglomerate clasts.

- Increase in Fe total in Alhambra Formation. Fe is carried in silicate minerals as it correlates positively with SiO_2, most probably muscovite and epidote, both of which increase in abundance in the Alhambra Formation.

- Increase in Al_2O_3 in the Alhambra Formation. Consistent with its immobility, causing a concentration in more weathered samples.

- Decrease in CaO in the Alhambra Formation. Reduction in biogenic production in terrestrial environment, and reduction of cement formation. Also consistent with weathering model, as Ca is a soluble element.

- Decrease in Na_2O in the Alhambra Formation. Consistent with high Na mobility during chemical weathering. Perhaps lost through reduction in Na bearing minerals such as amphibole. Loss of Na through decreased feldspar content also possible.

- Decrease in MgO in the Alhambra Formation. Does not share same mineral sites as Fe, in general. Lost perhaps by destruction of garnets and amphiboles, which are reduced in the Alhambra Formation.

- MnO has highest value in the Alhambra Formation, but no great distinction is possible between formations. Garnet is the most likely host, but garnet quantities reduce in amount in the Alhambra Formation, and there is no trend towards Mn rich values for garnets in the Alhambra Formation.

- Increase in K2O in the Alhambra Formation. Consistent with relative immobility, but also with presence in detrital muscovites, that show no reduction in typical K2O contents in the

Dudar Formation. Increased mica content in the Alhambra Formation may contribute to higher K2O.

- The changes observed can often be attributed to a reduction in the range of values of particular elements, rather than a shift in the range of values. This suggests the operation of selective differentiation processes.

- Niggli al-alk values are greater in the Alhambra Formation. This indicates the greater amount of clay minerals in these sediments. These are possibly the products of alteration due to greater chemical weathering intensity. Dudar Formation samples show a greater influence of muscovite, despite containing less muscovite than the Alhambra Formation.

5.3.2 Intra-Formational Variations

Figures 5.2 and **5.3** show plots of eight major elements plotted against SiO_2 for the fine, medium and coarse grain sizes of the sediments from the Dudar and Alhambra Formations. The distribution of elements between the Formations from these plots agrees with those discussed above for the bulk sediments. The purpose of this section is to see if there are any grain size correlatable trends in composition that may parallel those interpreted as due to weathering differences between formations. In this way break-down of sediment may be separated from weathering effects. Some aspects of the grain size control of composition are discussed above in the introduction.

SiO_2 content in general shows little variation with grain size. When trends of individual samples are considered there is a move, very slightly, towards a concentration of SiO_2 in coarser grain sizes. For the Dudar Formation (**Fig. 5.2**) this trend is marginally reflected in the increase of samples with lower SiO_2 content. Despite this the main grouping of samples show no difference in SiO_2 content.

One sample is very poor in silica. This is due to the high content of CaO in this sample in carbonate mud. It is at the bottom of the Dudar Formation at the transition with the calc-arenite Quentar Formation. However, it shows a marked progressive intra-sample increase in SiO_2 content towards the coarse grain sizes. In the Alhambra Formation the fields of each grain size plot together indistinguishably, but intra-sample trends are to higher amounts of SiO_2.

TiO_2 is uniformly increased in finer grained fractions in both formations. This is consistent with the increase in the bulk samples of the Alhambra Formation compared with the Dudar Formation discussed in section 5.3.1. However, as suggested above the increase of TiO_2 is consistent with an increase of ultra-stable rutile in the more weathered and perhaps reworked deposits of the Alhambra Formation. This presents a problem as this would not be consistent with a decrease in size of rutile into the finer grain sizes. However, it is likely that the grain size of rutile and other TiO_2 bearing accessory minerals is small to begin with in the source rocks.

For both the Dudar and Alhambra Formations, Al_2O_3 values are again hard to separate for each grain size fraction. If individual sample trends are considered some pattern does emerge. Fine grained fractions tend to have a progressively higher content of Al_2O_3 compared with coarser grained fractions. This can be expected as Al_2O_3 is relatively immobile (Pettijohn

1975, Nesbitt and Young 1989) and may also be concentrated in clay minerals in the finer grained fraction. This is the pattern produced through increased weathering (Cullers 1988, Nesbitt and Young 1989) and seen in the more weathered Alhambra Formation. Enrichment may also be a product of sediment breakdown, thus indicating the possibility of an increased input of the products of grain break-down to the Alhambra Formation. This is consistent with increased weathering and abrasion during deposition or the incorporation of earlier deposits by re-working.

For Fe tot. there is little variation in content with grain size. In the Dudar Formation individual trends hint at an increase in finer grained samples, but the number of samples restricts the confidence of this statement. In the Alhambra formation overall there is no distinction possible between grain size fractions. The expected trend is that demonstrated by van de Kamp and Leake (1985) who show that Fe and Mg increase in shales, from sand-shale pairs that share the same source.

For MnO in the Alhambra Formation there is an individual sample trend to higher values in coarser fractions. However, this is reversed for the Dudar Formation. This could be interpreted as indicating the survival of MnO in garnet that is concentrated in the coarser grain sizes in the Alhambra Formation. This pattern would be expected to be the same in the Dudar Formation, or even stronger, as grain break-down has not proceeded to any length. Perhaps MnO is more easily removed from the finer grained sediment fraction, so became concentrated in coarse sands during weathering or reworking.

MgO contents for the Dudar Formation show little change or predictable variation with grain size. The Alhambra Formation does show an intra-sample trend to increased MgO in fine grained samples. This is perhaps contradictory to the trend seen for the bulk samples, where the more weathered Alhambra Formation samples have lower MgO. The range of values is much reduced in the Alhambra Formation, indicating that the real trend during weathering is to loss of MgO. If this is the case then the obvious mobility of Mg in sediments would preclude its concentration in fine grained sediment. However, the minerals that contain Mg may be prone to reduction in size, especially mafic minerals, for instance amphibole which is present in the sediments, sourced from the Ophiolite unit of the Mulhacen Unit. This issue is difficult to resolve.

No trend in CaO with grain size is seen, except for the negative correlation with SiO_2. As Na_2O is reduced in the more weathered Alhambra Formation due to high Na_2O mobility, it is perhaps surprising that in the Dudar Formation there is a trend to higher Na_2O in the finer grained fraction. For the Alhambra Formation the trend is reversed. This pattern in the Alhambra Formation is consistent with Na_2O loss due to weathering. In the Dudar Formation the samples are less weathered, so initial trends of compositional variation are more likely to be preserved unbiased by other processes such as weathering. The Alhambra Formation trend to less Na_2O in fine grained samples reflects chemical differentiation by weathering processes, which have reversed the trend imparted by the source rocks.

Finally, for K_2O in the Dudar formation there is an intra-sample trend to a decrease in content in fine grained fractions. This is enhanced slightly in the Alhambra Formation. Most

samples for both formations plot in a cluster. The increase in K_2O in finer grained samples is consistent with the findings of Roser and Korsch (1986) for sand-shale pairs, and by Argast and Donnelly (1987) for different sizes in fine grained sands and silts. K_2O concentration in the finer fractions of the Granada Basin samples is also consistent with weathering studies, that show that K_2O is lost only at advances stages of weathering (Nesbitt and Young 1989). K_2O would be expected as a 'refractory' element to be left, along with Al_2O_3, in fine residues and clays.

Niggli al-alk

As discussed above, the Dudar and Alhambra Formation sands plot in distinct areas on a graph of K_2O v Niggli al-alk, and with distinct correlations, showing different influences of muscovite and clay minerals. In **Fig. 5.5** all grain size separates are plotted, clearly indicating the separation of the two formations (shaded area for Dudar Formation). If individual sample trends are traced, there is a tendency for al-alk value in the Alhambra Formation to be larger in the fine grained fractions. This is consistent with data presented by van de Kamp and Leake (1985) for sand shale pairs, and relates to the expected increase in clay minerals and sheet silicates in fine grained fractions. However in the Dudar Formation such trends are not as clear, and that which does emerge appears to show an increase of al-alk in the coarse sand fraction. This may relate to the increased influence of muscovite in the less weathered and reworked Dudar Formation. Mica contents in the Dudar Formation have been noted to vary with increasing grain size in a slightly positive manner, in stark contrast to the Alhambra Formation (**Fig. 4.7**), thus perhaps elevating the al-alk content in the coarse grained fraction of the sands.

Summary

Grain size dependant trends of composition for major elements are seen in samples from the Dudar and Alhambra Formations. The *expected* trends are for mobile elements to be reduced in finer grained fractions and for immobile elements to be concentrated as a result of the action of chemical weathering. This trend should be more pronounced in the more weathered Alhambra Formation. Some distinct trends caused by weathering can be separated from source dependant, compositional variations. The variations can be summarised;

- SiO_2 increases in the coarser grained fractions of both formations. This is because fine fractions concentrate sheet silicates and clay minerals especially. Quartz is less likely to be abraded to smaller grain sizes than other minerals that are also more prone to weathering alteration.

- TiO_2 increases in the finer grained fractions. This appears consistent with the weathering trend outlined in section 5.3.X were TiO_2 is larger in the Alhambra Formation. It is probably related to the tendency for Rutile to be concentrated in finer grained fractions as it occurs as small grains in source rocks.

-Al_2O_3 is concentrated in the finer grained fractions of both formations. This is consistent with its immobility during chemical weathering and because other less stable elements are removed, increasing the apparent concentration.

- Fe total concentrations show a weak trend to an increase in finer grained fractions. This is consistent with established weathering trends (Goldich 1938, Nesbitt and Young 1989, and section 5.3.X above) were Fe is concentrated during weathering.

- MnO concentrations exhibit contradictory trends for the Dudar and Alhambra Formations. Concentrations are smallest in the coarse fraction of the Dudar formation, and greatest in the coarse fraction of the Alhambra Formation. The pattern for the Alhambra formation indicates the effect of weathering upon the initial grain size dependant compositional trend. The Dudar Formation represents the unweathered grain size trend.

- Na_2O shows a similar variation to MnO. It is increased in the fine fraction of the Dudar Formation but decreased in the fine fraction of the Alhambra Formation. The latter trend is consistent with the effects of weathering on the Na_2O abundance in the Alhambra formation as a whole, and also the expected loss of mobile elements from the more easily altered fine fraction. The weathering effect is very clear here, as it has reversed the compositional trend imparted by the sediment source.

- MgO shows no trend in the Dudar Formation, but does is increased in the fine fraction of Alhambra Formation sands. This contradicts the apparent weathering trend that indicates a reduction in MgO content in the Alhambra Formation.

- K_2O values in both formations show an increase in fine grained fractions. This is consistent with the grain size trends of Roser and Korsch (1986) and Argast and Donnelley (1987). It is perhaps a source determined trend, but it is also consistent with weathering effects, as K_2O increases in the Alhambra Formation, and is a relatively resistant element to weathering.

- Niggli al-alk values in the Alhambra Formation increase in the fine grained fraction, consistent with increased weathering and the tendency of clay minerals and other sheet silicates to concentrate in fine sediment fractions. For the Dudar Formation the trend is more diffuse but tends to an increase in al-alk in the coarse fraction, perhaps related to increased influence of unaltered muscovite.

Generally, compositional trends in the Alhambra Formation are better defined, and clearly show the influence of weathering. The relatively unaltered equivalents of the Alhambra Formation contained in the Dudar Formation show more equivocal trends, that in some cases clearly indicate source rock control of composition uncomplicated by weathering or grain break-down alteration.

5.4 Trace Element Geochemistry

5.4.1 Inter Formational Variations

Figures 5.6a,b,c present correlation plots for selected trace elements in bulk sand samples from the Dudar and Alhambra Formations. Analyses for both formations are plotted together in these plots to allow easy assessment of differences in trace element composition.

Zr is clearly more abundant in the Alhambra Formation, and correlates positively with SiO2, indicating its probable presence in Zircon. Y correlates positively with Zr, as they can

both occur together in zircon (Argast and Donnelly, 1987). The correlative relationship between the two supports this suggestion. The increase in Zr and Y in the Alhambra formation is consistent with an increased amount of zircon (**Fig. 6.1**), concentrated by weathering and abrasion processes that have selectively removed less stable mineral species.

Zn correlates well with Pb, indicating possible substitution in minerals such as sphalerite and galena. No mineralisation is documented in the Sierra Nevada source region, but ophiolitic rocks and serpentinites are common. Zn and Pb levels are generally higher in the Alhambra Formation, possibly related to increased input from more mafic sources. Heavy minerals increase in number in the Alhambra Formation, as do micas, providing possible sites for Zn and Pb, both as major elements and substituting for others. Zn shows a good correlation with Rb also, indicating its probable presence in K bearing phases such as mica. Pb also correlates positively with Rb, though less well.

Rb values are generally indistinguishable for each formation, except for a slight trend to lower values in the Alhambra Formation, defined only by a few samples at the extremes of the fields for either formation. The spread of values is wide; for this reason Rb is used on the x-axis for many plots, especially to see grain size trends and general compositional variations in other elements. It was used in preference to a major element, as the data set for trace elements is more complete.

Y values do not correlate with Rb indicating that it is present probably in non-K bearing minerals. The absence of a negative correlation also shows that Y has no relationship at all with Rb, supporting a probable presence in Zircon.

Ce correlates well with Rb, indicating that it does not occur in carbonates, but probably K bearing sheet silicates (van de Kamp and Leake 1985). Values are generally higher in the Alhambra Formation. La values are also elevated in the Alhambra Formation. The patterns of enrichment of these two LREEs in the more weathered Alhambra Formation is consistent with observed patterns of LREE content in the products of intense weathering (Nesbitt et.al. 1990) and in soil and stream profiles (Cullers et. al. 1988). La shows a positive correlation with Ba, but not with Rb, with which it shows no correlation. La may be expected to occur in K-feldspar and in micas. In the sediments of the Dudar and Alhambra Formation feldspar is uncommon, so the likely site for La, and Ce, is in the abundant muscovite that is observed. However, La does not correlate with Rb, which is the best indicator of affinity with K bearing minerals. Plots of all grain size separates (**Figs. 5.7** and **5.8**) do show a good correlation between La and Rb in the Alhambra Formation, but a diffuse spread for the Dudar Formation. The trend in the Alhambra formation suggests a home for La in muscovite, but the Dudar Formation data is more equivocal.

Ba shows no difference in values between the Dudar and Alhambra Formations. It correlates well with Rb, suggesting that it resides mainly in K bearing minerals.

Sr values are lower in the Alhambra Formation (**Fig. 5.6b,c**). It shows no correlation with CaO wt% indicating that it is not carried by carbonate minerals or cements. It does correlate with Rb however, suggesting its inclusion in K bearing minerals, most probably muscovite.

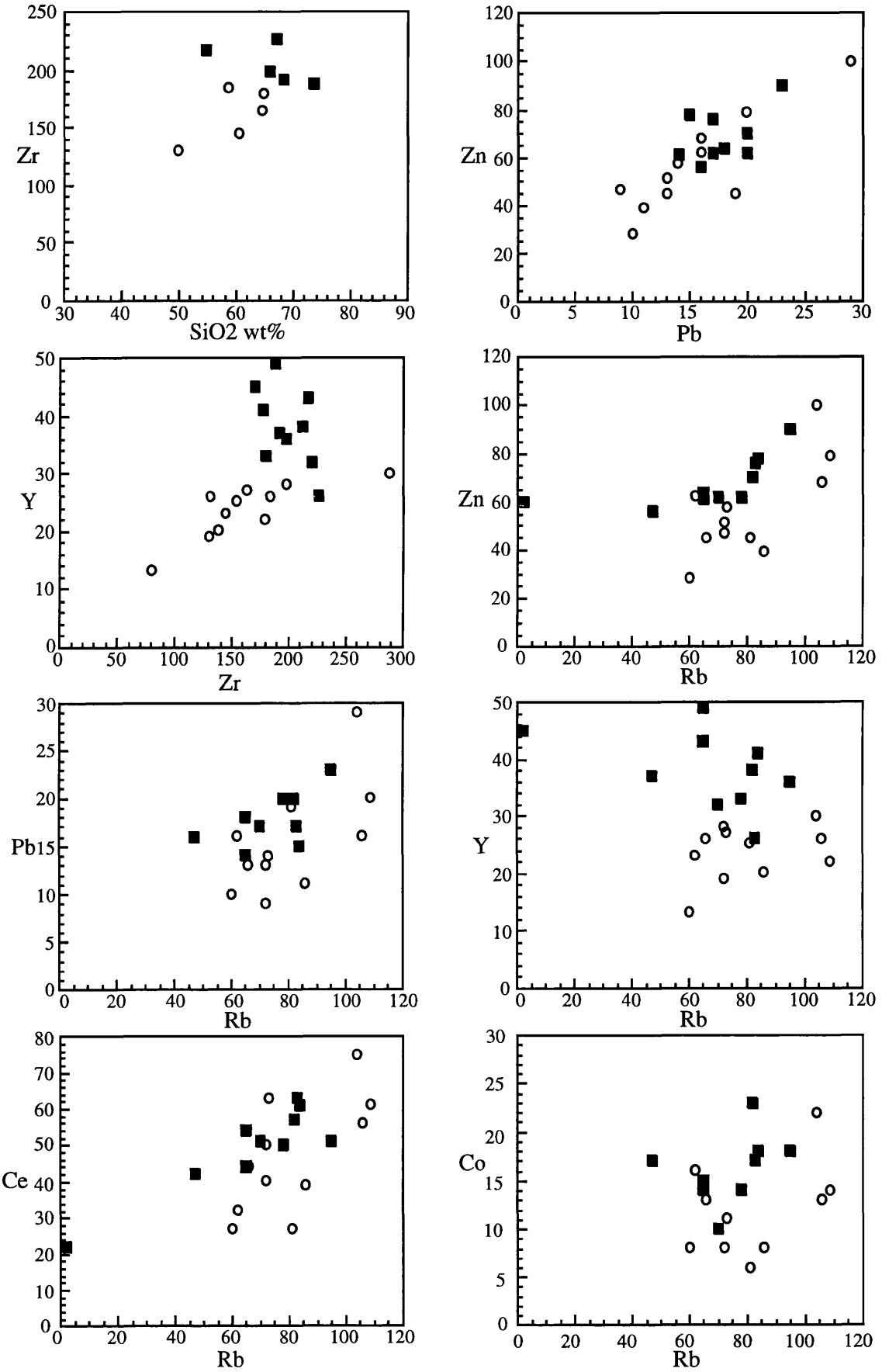

Fig. 5.6a Trace element correlation plots for bulk samples from the Dudar and Alhambra Formations.

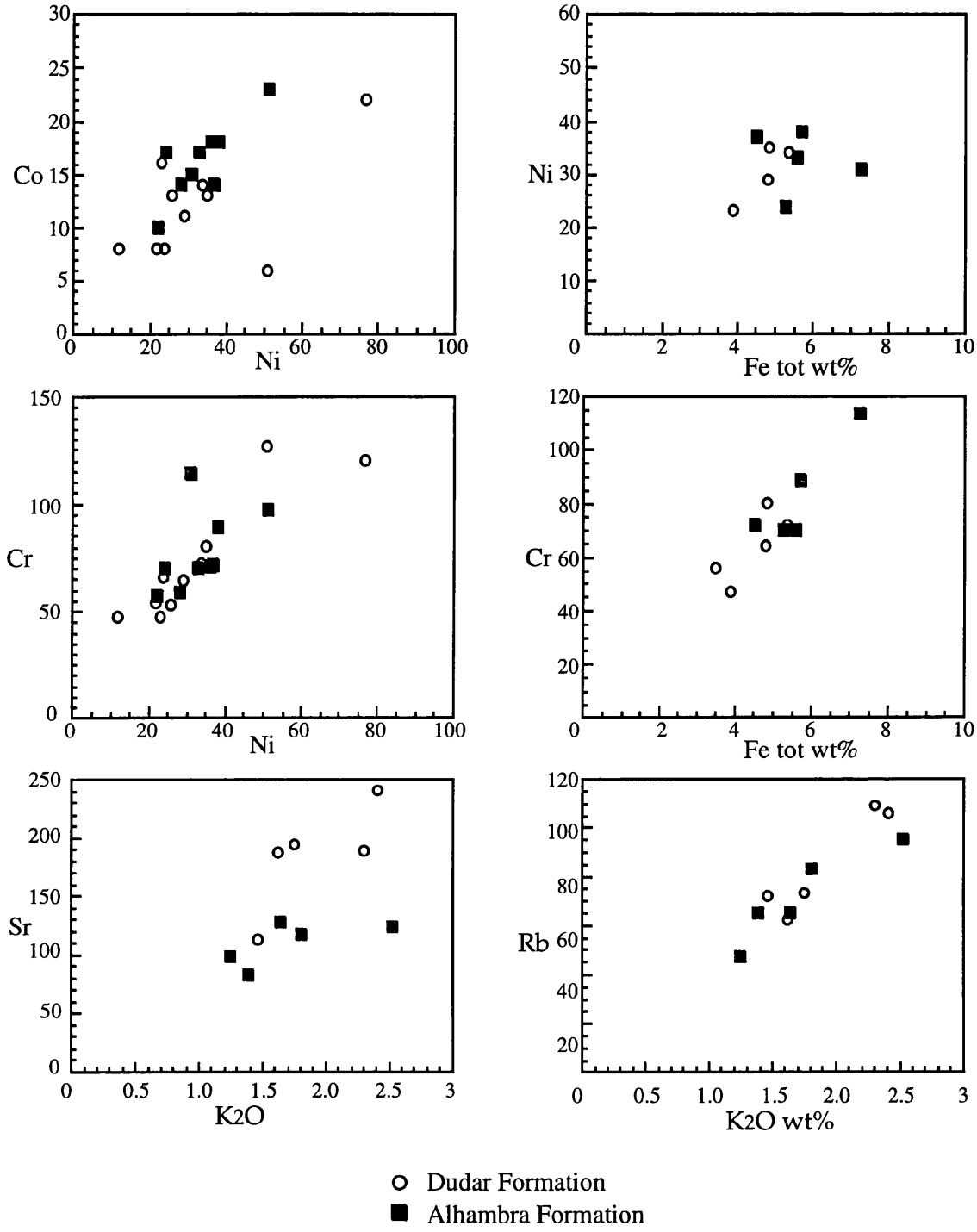

Fig. 5.6b Trace element corrleation plots for bulk sands from the Dudar and Alhambra Formations. All trace element values are in p.p.m.

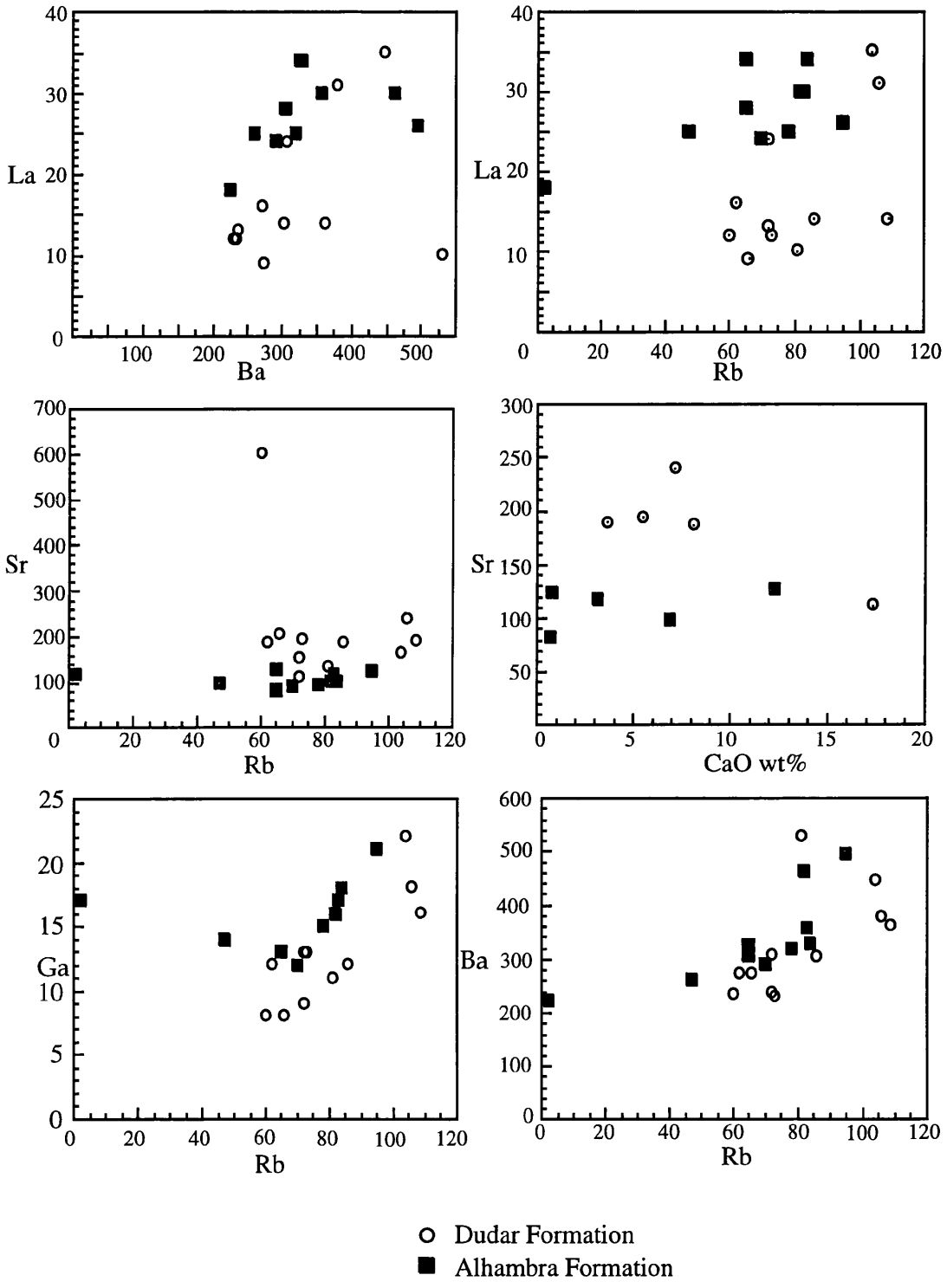

Fig. 5.6c Trace element correlation plots for La, Ga, Ba and Sr from bulk sands of the Dudar and Alhambra Formations.

Ga values correlate positively with Rb also, again indicating a common source, probably in sheet silicates. The Alhambra Formation has generally higher values of Ga, though this is not dramatic and noticeable only because the Alhambra Formation samples plot on the high Ga side of the correlation trend (**Fig. 5.6c**).

Trace elements present in mafic minerals, associated with basic igneous or meta-igneous rocks are present. Co is present in levels above 10ppm, and shows an increase in Alhambra Formation samples. Ni also shows slightly higher values in the Alhambra Formation, and correlates well with Co suggesting their occurrence together in mafic minerals. The most likely candidates are heavy minerals, such as amphibolite, garnet and epidote that are common in these sediments, but also more minor components such as chloritoid. Heavy mineral content increases in the Alhambra Formation, perhaps contributing to the increased contents of Co and Ni. Cr occurs in levels above 50ppm, suggesting the dilution of a mafic mineral source within the Sierra Nevada. Serpentinite is a common constituent of conglomerates, and has inclusions of chromite. The positive correlation between Cr and Ni identifies the source of these elements as being within mafic-ultramafic rocks, and not from clays generated during weathering and diagenesis (van de Kamp and Leake 1985). Amphibolites are also common, providing a source for ultra-mafic minerals.

Cr correlates with Fe-total, Alhambra formation samples having the higher Cr content. This correlation further emphasises the presence of Cr, and therefore Ni and Co in mafic minerals. However, when plotted against Ni there is little difference in content for bulk sediment samples. The grain size fraction plots (**Fig 5.7, 5.8**) also allow comparison of the range of Cr contents. They show that there is a trend to higher Cr in the Alhambra Formation.

In **Figs. 5.7** and **5.8** there is a suggestion that Ni, Co and Cr may correlate positively with Rb. This is especially true of Ni in the Alhambra Formation. This correlation suggests that such elements can occur in K bearing minerals. This is possible for hornblende, but also for certain white micas. The muscovites in the study area are also quite Fe rich (see Chapter 7) and some contain measurable quantities of Cr. This also suggests an alternative site for Rb and K in mafic minerals. However, the correlations with Rb are not very well defined for Co and Cr, especially in the Dudar formation, suggesting that contributions from K bearing phases are indeed small.

Summary

Patterns of variation for the trace elements discussed above are clear. The Alhambra Formation shares source with the older Dudar Formation but is demonstrably more intensively weathered. These changes can be related to progressive weathering which in turn can be attributed to changing environment, and longer fan top residence, or can be compounded by processes of sedimentary recycling. The changes can be summarised;

- Increase in Zr and Y in the Alhambra Formation. Related perhaps to increased concentration of zircon, due its resistance to weathering.

- Increase in Zn and Pb in the Alhambra Formation. Related to increases in heavy minerals/opaques and/or micas in Alhambra Formation.

- Increase in Ce and La in the Alhambra Formation. Consistent with weathering trends (Nesbitt et. al. 1990 and Cullers et. al. 1988) showing enrichment in LREE. Perhaps related to increased amount of mica and micaceous rock fragments in the Alhambra Formation.

- Decrease in Sr in the Alhambra Formation. Consistent with increased weathering and Sr mobility.

- Increase in Ga in the Alhambra Formation.

- Trends towards increases of Co, Ni and Cr in the Alhambra Formation. Correlations indicate a source in ultramafics in the Sierra Nevada. Increase caused perhaps by an increase in heavy minerals in the Alhambra Formation. However, mafic minerals decrease in abundance in the Alhambra Formation. Correlation with Rb indicates possible sources in K bearing minerals, especially Hornblende, but also some Fe rich white micas.

- Rb and Ba show little difference. Consistent with stability of K sites in muscovite. Rb tends to slightly lower values in the Alhambra Formation, in opposition to a slight increase in K2O. However, more samples are needed to substantiate these trends.

5.4.2 Intra-Sample Variations

Figures 5.7 and **5.8** show scatter diagrams for trace element concentrations in the fine, medium and coarse grain size fractions of sands from the Dudar and Alhambra Formations. Concentrations are plotted against Rb, as this element has a wide spread of values for all samples. Additionally the data set for major elements is not as complete as that for trace elements, so to maximise the presentation of data a trace element on the x-axis is most useful. The presence or absence of correlations with Rb is of less importance than the relative intra-sample variations in trace element concentration caused by grain size sorting. Emphasis is placed on recognising and interpreting trends for individual samples, and their consistent grain size fractions. Unfortunately, these are not easily seen on the scatter diagrams so trace element values are presented in **Appendix 3** for easier comparison.

In the Dudar Formation Zr is preferentially concentrated in the coarse fractions of samples. This contrasts with the Alhambra Formation were it is concentrated in the fine fraction. A concentration of Zr in more mature deposits, and in coarser grained sediment is the expected pattern. The higher Zr content of the coarse fraction of the Dudar sands may be due to preferential concentration of zircon. Concentration is greater overall in the Alhambra Formation, consistent with the prediction made above for the concentration of Zr in more mature sediment. The concentration in the fine fraction can be explained by the immobility of Zr and the stability of zircon. When grains are broken down the greater surface area so generated allows alteration and elemental fractionation, so the more immobile elements such as Zr will be concentrated, as other less stable elements are removed. However, zircon, as it is an ultra-stable mineral should be expected to concentrate in the coarse grain size fraction. As zircon is the main carrier of Zr, this element should also be concentrated in the coarse fractions. The pattern seen in the Dudar Formation must be nearer the initial pattern imparted by the source, which was changed by more intense weathering combined with possible

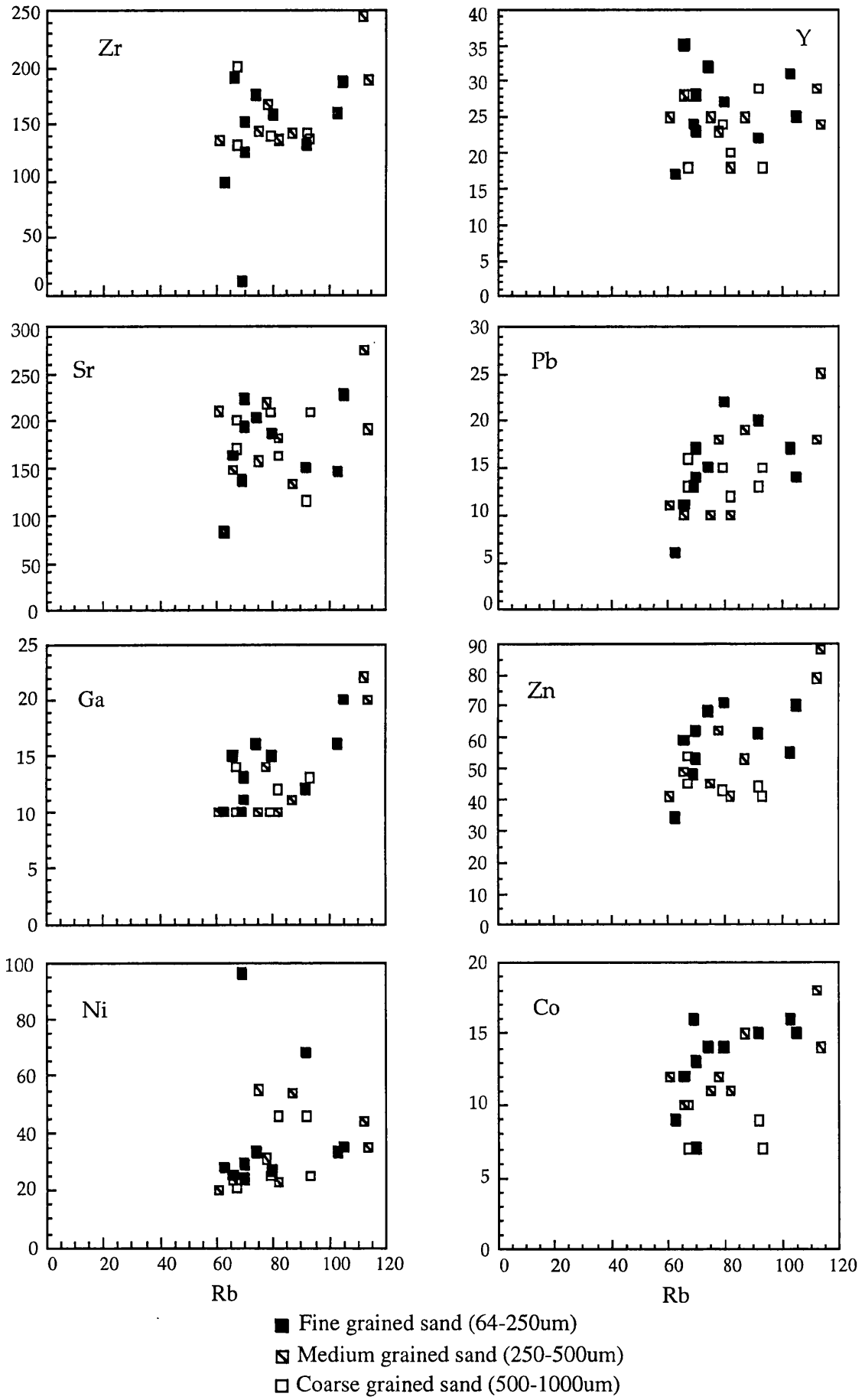

Fig. 5.7a Scatter plots for trace elements vs Rb from grain size fractions of samples from the Dudar Formation. All values are in parts per million (p.p.m.)

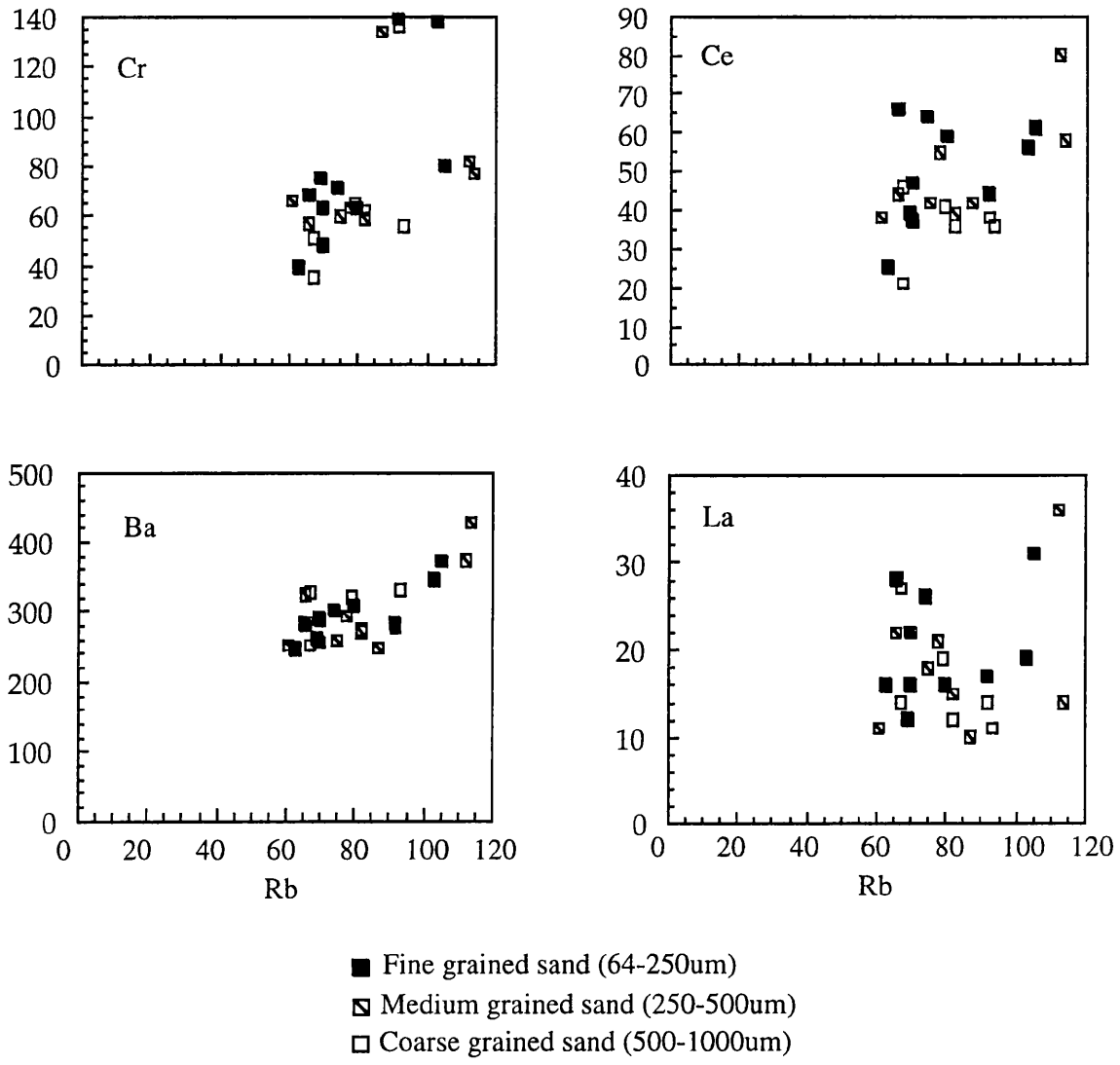

Fig. 5.7b Trace element scatter diagrams for samples from the Dudar Formation

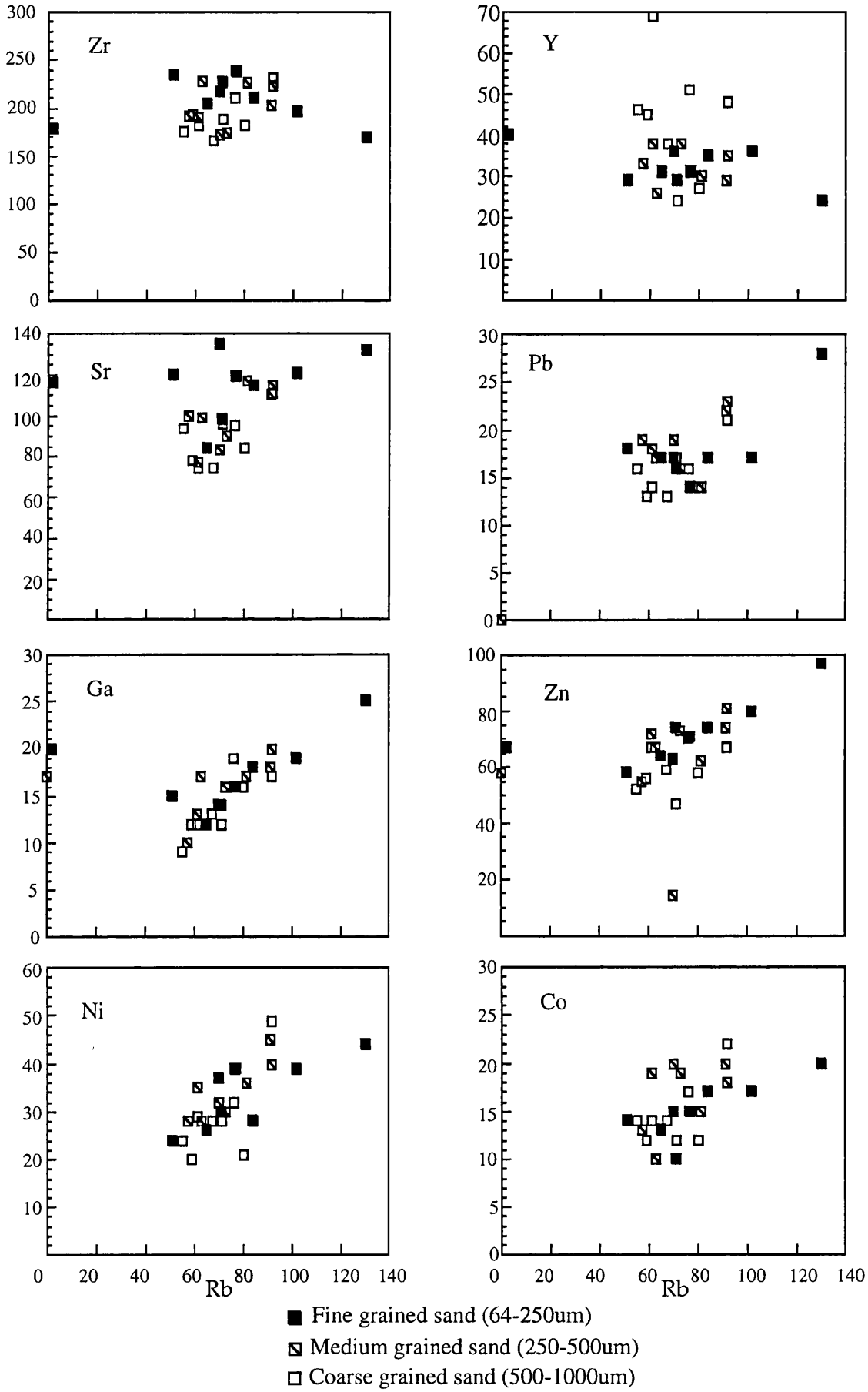

Fig. 5.8a Scatter plots of trace elements vs Rb for grain size separates from the Alhambra Formation sandstones. All values in p.p.m.

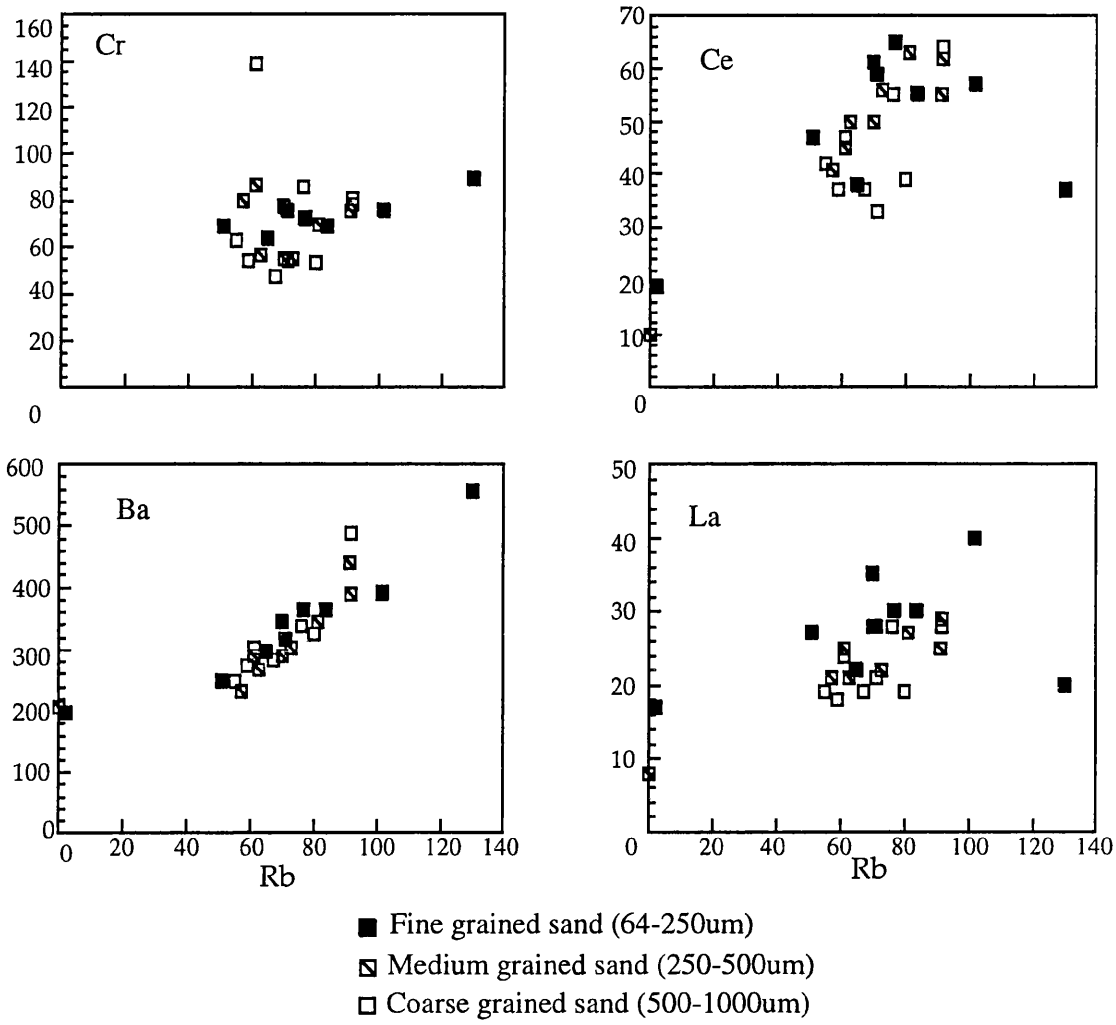

Fig. 5.8b Scatter plots of trace elements vs Rb for grain size separates from Alhambra Formation sandstones.

reworking of earlier sediment to produce that seen in the Alhambra Formation. Zircon may be breaking down to form smaller grains in the Alhambra Formation, or there is a predominance of fine grained zircons in the source, which in the fresh Dudar Formation sandstones in masked by other less stable elements in more labile sand grains.

Y values in both formations show an increase in the fine fraction. This is consistent with the increase in Y for the more weathered Alhambra Formation. It shows that Y is relatively immobile, thus being concentrated during grain break-down, and may occur in relatively resistant minerals such as zircon. However, this result is inconsistent with the data for Zr presented above, despite being easier to account for in terms of weathering and grain break-down. The correlation between Y and Zr (**Fig 5.6**) suggests that Y should follow a similar pattern of variation to Zr.

Sr shows a similar pattern to Zr. It is reduced in the fine fraction of the Dudar Formation, but increased in the fine fraction of the Alhambra Formation. The Dudar formation trend is explicable as weathering tends to remove Sr, an effect that is emphasised in fine grained sediment fractions. Weathering effects are seen as the reduced Sr level in the Alhambra formation as a whole. The intra-formational trend in the Alhambra Formation is harder to explain, unless other, even more mobile elements were lost during weathering and grain break-down, that could produce a relative increase in Sr. Van de Kamp and Leake (1985) present trace element data for sandstone-shale pairs from the north-east Pacific Margin, where Sr is generally decreased in the shales compared with the sands, for most samples, supporting the general loss of Sr in fine grained sediment fractions. However, samples from the Colorado river show the opposite trend (Van de Kamp and Leake, op.cit), suggesting that the fractionation of Sr is not uniform.

A possible explanation for the observed trend in Sr variation may be an increase in micaceous material in the fine fraction of the Alhambra Formation. Sr values for muscovite from conglomerate clasts, that represent probable source rocks for mica in the sands, are between 70 - 200 ppm (see **Chapter 7**). This is within the range of Sr content of the sediments as a whole, but considering dilution effects, Sr must be present in other minerals also. However, muscovite is resistant to alteration and the increased concentration in the fine fractions, and in matrix materials may contribute to an increase in Sr in these fractions. This would work contrary to the tendency to decrease in fine fractions due to Sr solubility and mobility.

Rb values also show contradictory trends in both formations. In the Dudar Formation Rb is greatest in the coarse fraction, but in the Alhambra Formation Rb is greatest in the fine fraction. Rb may be expected to follow the variations of K closely due to a strong affinity and similar ionic radius. K_2O is seen usually to increase in fine sediments, and also as a result of weathering (Roser and Korsch 1986, Argast and Donnelly 1987, van de Kamp and Leake 1985, Nesbitt and Young 1989). Variations of K_2O with grain size in the Granada Basin sediments follow this trend, but Rb follows this trend only in the Alhambra Formation.

Variation in Pb content in the Dudar Formation with grain size is a little unclear. In the Alhambra Formation Pb levels are consistently up in the finer grained fraction. This is consistent with the findings of van de Kamp and Leake (1985) where Pb levels are elevated in

shales, indicating a trend towards increased Pb in finer grained sediment, and also for the inter-formational trend to increased Pb in the more altered Alhambra Formation.

Ga values are consistently increased in fine grained fractions for both the Dudar and Alhambra Formations. Ga correlates well with Rb in the *bulk sand* analyses, and behaves in tandem with Rb for grain size fractions from the Dudar Formation, but not in the Alhambra Formation.

The content of Zn is smallest in the fine grained fraction of the Dudar Formation. This would indicate the relative mobility of Zn, or the resistance to abrasion of Zn bearing minerals that would become concentrated in the coarse grained fractions of sediment.. However, van de Kamp and Leake (1985) show that Zn values are larger in finer grained sediments, thus indicating the immobility of Zn during size reduction. In the Alhambra Formation Zn values conform to this model, and increase in the finer grained fraction.

Ni, Co and Cr increase in amount in the fine fractions of both the Dudar and Alhambra Formations. This pattern is consistent with the increase seen in the Alhambra Formation as a whole, as these elements are relatively immobile and resistant to liberation during weathering, and also as suggested here, are concentrated during grain break-down. This also indicates the utility of these elements in indicating ultramafic source for fine grained sediment.

Values of Ce and La also increase in the fine faction of the Dudar and Alhambra Formations. These elements are LREEs, that have been found to be resistant to loss, and thus to concentration in fine grained sediments (eg. Nesbitt et. al. 1990, Cullers et. al. 1989). They are important as they can be used in provenance discrimination (Bhatia and Crook 1986), and their immobility makes them suitable for application to more mature sediment and also to finer grained, distally derived sediment. However, van de Kamp and Leake show a general reduction in values of Ce and La in shales.

Ba values in the Dudar formation samples mostly increase in finer sediment, though this is not a uniform trend. In the Alhambra Formation values are larger in the fine grained sands in a more consistent way, suggesting behaviour as a relatively immobile element. Ba often correlates well with both K_2O and Rb (El Fegi 1989, and **Fig. 5.6c**). K_2O increases in the fine fractions of both the Dudar and Alhambra Formations, so Rb and Ba could be reasonably expected to do the same. However, Rb is seen to increase in the fine fraction of the Alhambra Formation only, and is lowest in the fine fraction of the Dudar Formation. The pattern of Ba content in the Dudar formation, where no absolutely clear trend emerges is probably related to the contradictory correlations of increasing K_2O and decreasing Rb in the fine fraction. The Alhambra Formation trend in Ba content conforms to expected element relationships.

Summary

For several elements contradictory patterns of variation with grain size are seen between the Dudar and Alhambra Formations. These can be summarised;

- Zr, Zn, Sr, Rb. These trace elements are most abundant in the coarse fraction of the Dudar Formation, but most abundant in the fine fraction of the Alhambra Formation. These

contradictory variation patterns clarify the effects of increased weathering, and possible grain break-down on the composition of the sands in the Alhambra Formation. The patterns preserved in the Dudar Formation sands will more closely resemble patterns in the source, as these sediments have suffered little weathering alteration. However, in the Alhambra Formation, the reversed patterns seen are a result not of grain size control of composition but more the effects of increased weathering alteration. Immobile elements are concentrated in fine grained fractions, as more mobile elements are more effectively removed from these fraction due to greater grain surface area. The Sr contents of the Alhambra Formation grain size fractions may relate more to *mineralogical* concentrations, especially of muscovite in the fine grained fraction.

The remaining elements show more consistent patterns of variation with grain size:

-Ba, Y, Pb, Ga and also Co, Ni and Cr. These elements increase in the fine grained sand fraction of both the Dudar and Alhambra Formations. These patterns are generally consistent with concentration during grain break-down, due to their relative immobility and compatibility. These elements also increase as a whole into the Alhambra Formation, which is considerably more weathered than the Dudar Formation. The preservation of Co, Ni and Cr contents in finer sediment emphasises the utility of these elements for discriminating ultramafic source rocks, even in fine grained sediments. However caution must be exercised in applying these criteria to the estimation relative contributions of source. Concentration by weathering alteration or/and sediment sorting could lead to the over-estimation of the contribution of a mafic source to sediment.

- Ce and La. These elements, part of the LREE group, show elevated concentrations in the fine fraction of the sands from both the Dudar and Alhambra Formations. This is consistent with studies carried out by Nesbitt et. al. (1990) of muds that are the product of intense tropical weathering that show elevated LREE contents. Values in the more weathered Alhambra Formation are greater than the Dudar Formation, showing how weathering across the grain size range works to concentrate immobile LREEs.

5.5 Provenance

Roser and Korsch (1986) developed the geosynclinal classification of sediment geochemistry proposed by Middleton (1960), and related plate tectonic settings to sandstone composition. The scheme is based on K_2O/Na_2O ratios and SiO_2 content. Other geochemical provenance discrimination schemes include that devised by Bhatia and Crook (1986) that utilises immobile trace elements and REEs.

A stated aim of those proposing tectonic discrimination schemes based on chemical composition, is to enable the provenance of mineralogically altered sediments to be identified. This would allow sediments that have been diagenetically changed, as well as the products of metamorphism, to have their original depositional setting deduced, as long as bulk chemistry has been isolated from gross changes, for instance by large scale fluid interaction. This could be of great use in tectonic reconstruction, especially of palaeo-destructive/collisional margins where sedimentary sequences are likely to be involved in burial and metamorphism. It could

also be of use in predictive ways, perhaps in the search for distinctive mineral deposits of economic importance.

In **Fig. 5.9** data from the sediments of the Dudar and Alhambra Formations is plotted on the discrimination diagram of Roser and Korsch (1986). The tectonic setting of the Betic Cordillera is a destructive-collisional plate margin, where Africa has been moving relative to the European Plate, most recently in a strike-slip manner, but also compressively. The "expected" indication of setting to emerge from any compositional analysis of the sediments of the Granada Basin would be in the Active Continental Margin (ACM) type. As presented in Chapter 4 the provenance indication derived from framework mineralogy of the sediments is not unequivocal. For the Dudar Formation in particular, indications include foreland uplift provenance type, and the Alhambra Formation is attributed in large part to Arc Provenance types. In **Fig. 5.9** the provenance indicated for the sediments of the Granada Basin is a Passive Margin tectonic setting. This is clearly not the case, so what has happened?

The provenance indicated by the geochemistry of the Dudar and Alhambra Formation sandstones has been inherited from the *source* of the sediment, in the Internal Zones in the Sierra Nevada. The provenance type indicates that the protoliths to the meta-sediments that constitute the bulk of the internal zones, were deposited in a passive margin setting. This is an important result in itself, and has implications for the geological history of the Betic Cordillera, and the tectonic provenance of the Internal Zones. Deposition must have taken place in a passive margin setting during the late Palaeozoic and early Mesozoic, for the Veleta Unit schist protoliths, and the carbonate dominated sequence in the Mulhacen Complex. The preservation of a passive margin signature is aided by the absence of any large scale igneous intrusions or volcanics. The paucity of, especially acidic, intrusives depresses the content of Na2O and elevates the K_2O/Na_2O ratio into the passive margin sequence. Other core-complex type terrains consist of much more extensive igneous intrusions, and thus sediment derived from them would possibly plot in more K_2O/Na_2O poor provenances. The Internal Zones may be exceptional in this respect. The petrographic signature of the sediment from the Internal Zones core-complex in the Sierra Nevada may be typical of core-complex provenance, but the geochemical signature may not be.

However, this signature of Passive Margin sediments requires further examination. Chemical changes are common in metamorphism, not least by the action of hydrothermal fluids and magmatic interactions. K and especially Na are prone to alteration and the loss of Na in particular could elevate K/Na and place samples in the passive margin field. Nevertheless, the lithology of the internal zones strongly suggests a passive margin setting for the deposition of the protoliths to the metamorphic rocks. The paucity of significant intrusive rocks, and granites in particular again suggest that the rocks of the internal zones have not been extensively chemically altered. However, this is an unconstrained statement and requires further work for clarification.

The evidence for the preservation of a passive margin geochemical signature, due perhaps to the absence of intrusives, suggests the metamorphism seen in the Internal Zones was not typical of orthogonal continental convergence and/or subduction. It is possible that the

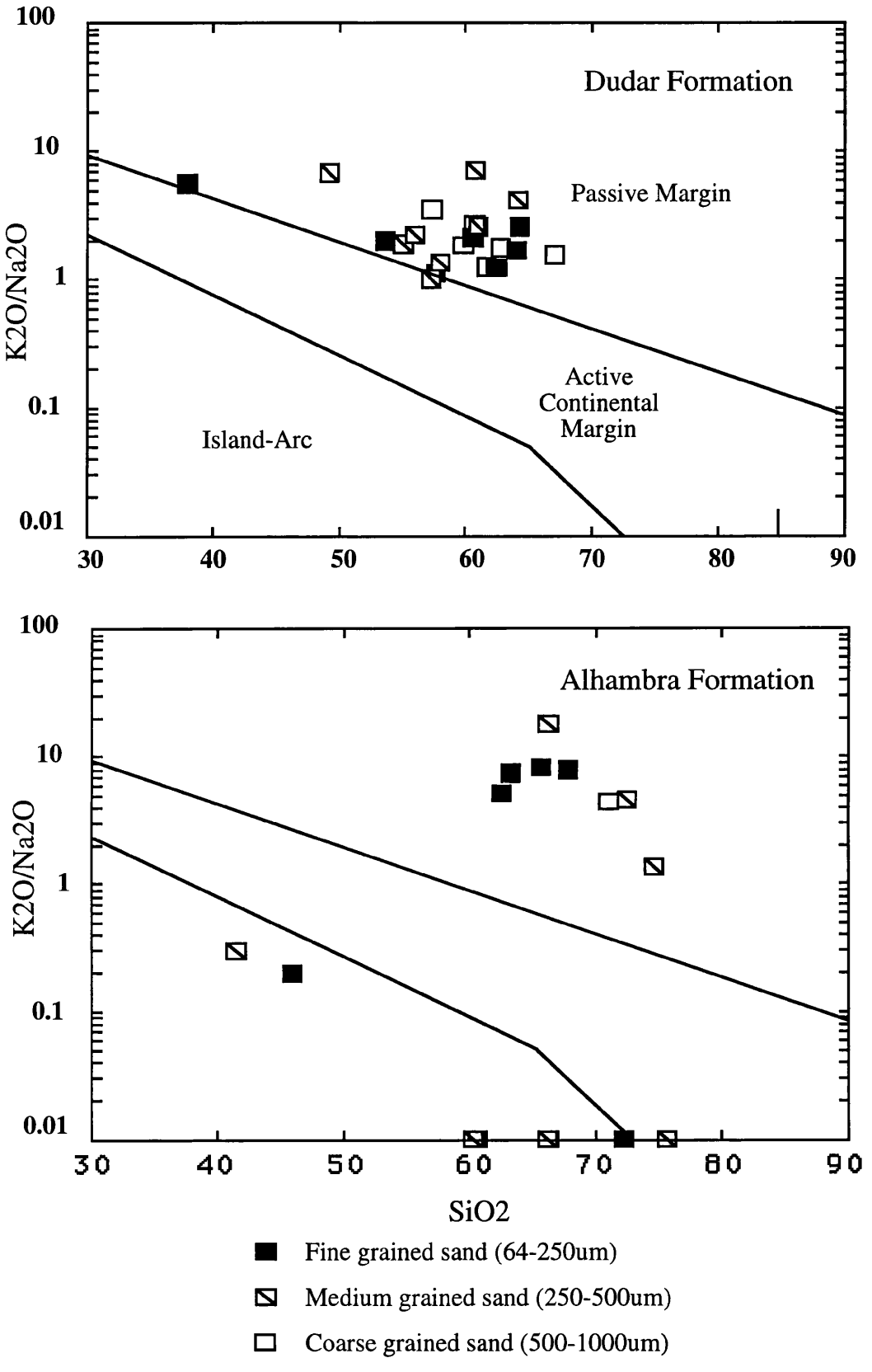

Fig. 5.9 K2O/Na2O vs SiO2 plots with provenance discrimination areas as indicated by Roser and Korsch (1986). Above are plotted the three component grain size fractions for the sands of the Dudar and Alhambra formations.

Internal Zones represent the metamorphosed end product of a passive margin setting, but metamorphosed in a strike-slip regime. This would be less likely to involve igneous activity, and can account for many features of the Betics. This suggestion of strike-slip involvement in the formation of the Betics is discussed fully in **Chapter 7**.

For the Alhambra formation, the bulk of sediments show an emphasised trend to passive margin provenance, with higher SiO_2 and K_2O/Na_2O. Many samples plot at the X-axis. This is because Na_2O has been removed during weathering and transport. One sample (A9.7) has the fine and medium grained fractions plotting in the Island-Arc provenance area. This is due to the suppression of SiO_2 because of high Fe-total; they should not be considered as typical of the Alhambra Formation. The indicated provenance is spurious.

Grain size fractions are plotted on **Fig. 5.9** and show trends compatible with grain size variations discussed above for individual elements. There is a tendency for finer grained fractions to have lower K_2O/Na_2O and lower SiO_2. On the other hand, Roser and Korsch (1986) present trends for individual sand mud trends for numerous samples that show muds in passive margin settings that have consistently lower SiO_2, but slightly higher K_2O/Na_2O. In the Dudar Formation fine grained fractions have elevated Na2O, which would depress the K_2O/Na_2O values despite increasing K_2O in the fine fractions. Overall, there is little real distinction possible between grain size fractions and the trends observed are not consistent for all samples in the Dudar and Alhambra Formations. Fine fractions do have slightly higher SiO_2 values that are consistent with Roser and Korsch's observations.

5.6 Chemical Classification and Maturity.

Pettijohn et. al. (1972) presented a classification scheme for sandstones based on Log Na_2O/K_2O vs Log SiO_2/Al_2O_3. Inherent in this scheme in the notion of compositional maturity. As maturity increases the Log SiO_2/Al_2O_3 ratio increases as SiO2 becomes concentrated with the reduction of other elements, and Log Na_2O/K_2O decreases as K_2O increases in concentration. On the plot, maturity increases to the lower right as SiO2 increases. Different classifications of sandstone type can be distinguished using this plot.

In **Fig. 5.10** analyses for bulk sandstones from the Dudar and Alhambra Formations have been plotted on the Log Na_2O/K_2O vs Log SiO_2/Al_2O_3 diagram. They plot across the boundary between Lithic Arenite and Arkose. The Alhambra Formation sands show lower Log Na_2O/K_2O, related to lower Na_2O content. All samples from the two formations, including all grain size separates, here undifferentiated, are plotted in **Fig. 5.11**. They show the same pattern, with the Alhambra Formation samples mostly having lower Log Na_2O/K_2O values, that plot in the Arkose field.

Maturity increases to the right, so there is no compositional maturity difference between the formations. However, Na_2O values clearly decrease. This is expected with a maturity increase on the plot, as subdivided by Pettijohn et. al. (1972). Na_2O is more likely to be lost before any change in SiO_2/Al_2O_3 ratio as Al_2O_3, in particular, is quite immobile during weathering. Movement to the right on this plot for the sediments of the Granada Basin would require further degrees of weathering, and reworking in order to change SiO_2/Al_2O_3. The

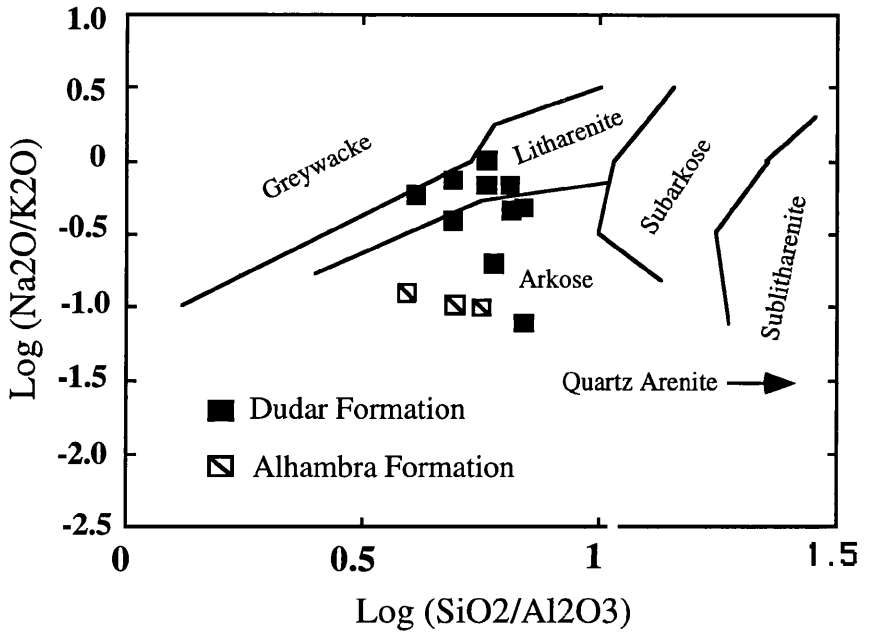

Fig. 5.10 Classification of bulk (64u-1mm grain size) Granada Basin sandstones using the Log (Na2O/K2O)vs Log (SiO2/Al2O3) plot of Pettijohn et. al. (1972). This plot also indicates relative compositional maturity, which increases to the right.

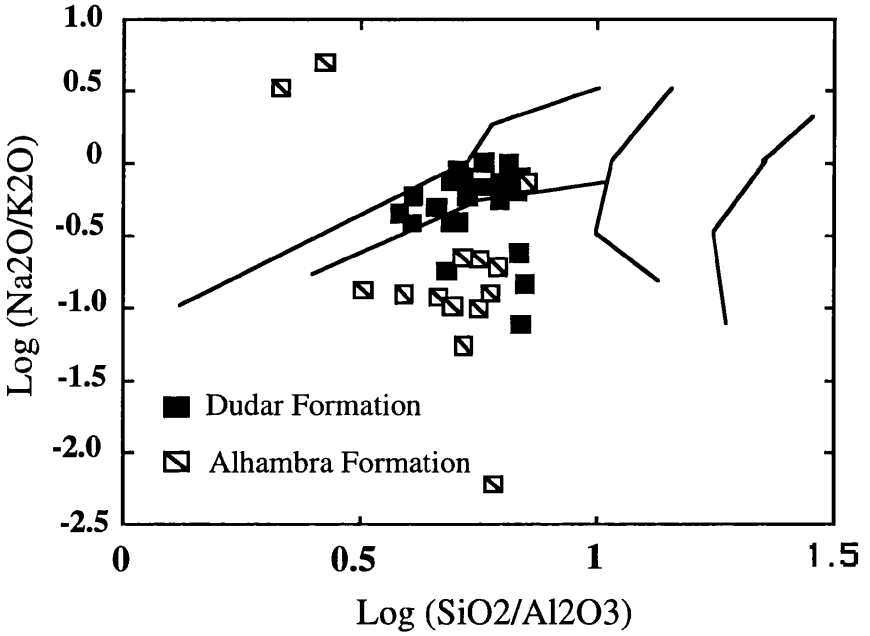

Fig. 5.11 All samples of Dudar and Alhambra Formation sands plotted regardless of grain size on the Log (Na2O/K2O) vs Log (SiO2/Al2O3) plot of Pettijohn et. al. (1972). The pattern seen is in aggreement with thebulk sand in Fig. 5.X above, where the Alhambra formation has generally lower values of Log (Na2O/K2O).

differentiation of the Dudar and Alhambra Formation sands is consistent with an initial increase in sediment compositional maturity.

The classification of the sandstones in the Arkose field is clearly incorrect, and at odds with the classification derived through framework mineral modes. All sands are classified as lithic arenites from framework modes. Many samples, especially from the Dudar Formation, correctly fall in the lithic arenite field on the Log Na_2O/K_2O vs Log SiO_2/Al_2O_3 plot. The problem may be in the presumed amount of feldspar available to carry Na_2O and K_2O. There is very little feldspar at all in the Granada Basin sediments, so they are patently not arkoses. However, mica contents are high, as is the content of often micaceous metamorphic rock fragments which must supply most of the K_2O content of the sediment. Na rich micas are also common in the Sierra Nevada. Mica increases in the Alhambra Formation, as does the lithic content. As already suggested this may account for increased K_2O and thus reduced Log Na_2O/K_2O on **Fig. 5.10**. This contrasts with the conventional arkose composition where the K_2O content is controlled by K-feldspar, resulting in lower Log Na_2O/K_2O. This indicates a problem with the general applicability of classification schemes, and emphasises the necessity to combine various approaches to the solution of any question. In this case it is the excess of muscovite, combined with weathering removal of Na which moves the sediment into the arkose field.

In conclusion, the use of the Log Na_2O/K_2O vs Log SiO_2/Al_2O_3 plot for sands from the Dudar and Alhambra Formations allows compositional maturity changes between formations to be assessed. No move to the right on the plot, indicating increased SiO2 and increased maturity, is seen for the Alhambra Formation. Reduced Na_2O is clear, indicating probable increased weathering, consistent with observations of grain alteration, clast roundness, oxide staining and clay content (al-alk). However, lithic grain content increases in the Alhambra Formation, indicating a decrease in maturity.

5.7 Conclusions

The sediments of the Dudar and Alhambra Formations of the eastern flank of the Granada Basin share the same source region, in the Nevado-Filabride and Alpujarride units of the Internal Zones. Bulk chemical composition could be reasonably expected to be near identical in both formations. However, differences are clear in the state of weathering alteration in the deposits; the Alhambra Formation shows evidence for greater weathering in a subaerial environment. Framework modes of grain composition show a difference between the two formations (Chapter 4), the Alhambra Formation is *less* mature than the Dudar Formation. This is surprising considering the greater alteration of the Alhambra Formation, and the increased maturity of coeval conglomerates. Therefore geochemistry of the Alhambra Formation should show patterns consistent with greater immaturity, mobile elements being preserved or even increased in abundance.

Major element variations

The greater weathering observed in the Alhambra Formation, compared with the Dudar Formation, is the dominant control on composition. Patterns of variation of major elements are seen;

- increases in SiO_2, TiO_2, Fe total, Al_2O_3 and K_2O in the Alhambra Formation.
- decreases in CaO, Na_2O, MgO in the Alhambra Formation.

These changes are consistent with increased weathering of the Alhambra Formation, and clearly suggest that the Alhambra Formation is geochemically more mature than the Dudar Formation. This is despite the framework mode decrease in maturity.

An important point about changing sediment provenance signatures can be made. Weathering due to deposition in a subaerial environment, fan-top reworking, and possible sediment recycling has not changed the range of grain components, and may in fact be the cause of decreasing maturity through grain break-down. However, it has made a big change in chemistry, resulting in a concentration of the more immobile elements in the more weathered formation.

Changes are also observed in the composition of various grain size fractions;

- increases in TiO_2, Fe total, Al_2O_3 and K_2O in fine grained sediment fractions.
- decrease in SiO_2 in fine grained sediment fractions.

Other changes *emphasised* by weathering combined with grain break-down are;

- decrease in CaO and Na_2O in fine fractions.

Due to greater particle surface area fine fractions are more prone to alteration, and show the greatest effects of chemical differentiation. These patterns are also consistent with observed changes of these elements into the Alhambra Formation due to weathering.

- However, for MnO, Na_2O and MgO the patterns of grain size fraction variation between formations are not consistent. In the Dudar Formation Na_2O and MnO are largest in fine sand fractions, but in the Alhambra Formation they are largest in the coarse sand fractions, being reduced, or eliminated in the fine fractions.

The pattern in the Alhambra Formation is expected as these elements are mobile and prone to loss. Coarse material will retain Na_2O in particular, in more extreme alteration conditions. MgO shows little preferred grain size controlled trend in the Dudar Formation, but is increased in the fine fraction of the Alhambra Formation. In these cases the Dudar formation preserves a source signature of variation in the grain size fractions controlled by the size of particular minerals in the source rocks. This has been altered by weathering during deposition of the Alhambra Formation. These latter effects are clearly separable as weathering effects. For the other elements mentioned just above, the weathering effect is clear also but grain size alone exerts a strong control, *in the same sense* as weathering and abrasion. In general trends of variation between formations, and for grain size fractions of individual samples, are better defined in the Alhambra Formation. Weathering has clearly ironed out fresh, source dependant variations.

Niggli al-alk

Sandstones from the Dudar and Alhambra Formations occupy distinct areas on a plot of K_2O vs Niggli al-alk. The Alhambra Formation samples have higher values of al-alk, indicating a higher content of clay minerals. This indicates greater alteration due to weathering state in the Alhambra Formation. The Dudar Formation shows the greater influence of unaltered muscovite on the K_2O - al-alk correlation.

For grain size fractions, the Dudar formation exhibits a trend to greater al-alk in coarse fractions, perhaps related to concentrations of muscovite. In the Alhambra Formation al-alk is greatest in fine fractions, conforming to a model of clay concentration in fine sediment. This is consistent with grain break-down and alteration during weathering, abrasion and possible sedimentary recycling.

The distinctions possible with these data illustrate the utility of al-alk in indicating clay alteration, and possibly size sorting of sheet silicates. It also indicates changes in provenance signature within proximal sediments derived from the same source in an intra-montane setting.

Trace element variations

For trace elements distinct patterns of variation are also seen;

- Increases in Zr, Zn, Y, Pb, Ga, Co, Ni, Cr, Ce and La in the Alhambra Formation.
- Sr values are decreased in the Alhambra Formation.
- Rb and Ba show no difference between the formations.

These patterns of variation are clearly related to increased weathering and grain break-down in the Alhambra Formation.

The signature of ultramafic rocks (from Co, Ni and Cr) is amplified in the Alhambra Formation, because of greater weathering and grain alteration. Care must then be exercised in estimating the importance of a mafic source directly from sediment composition, without constraining maturity, or weathering.

Intra-sample grain size trends show a range of variation;

- Ba, Y, Pb, Ga, Co, Ni, Cr, Ce and La increase in fine grained fractions in both formations

These elements are largely the same as those that show an increase due to weathering in the Alhambra Formation. However, as these elements show an increase in the Dudar Formation which is not related to weathering intensity alone, they must also have their fractionation pathways controlled partly by grain break-down.

- Zr, Zn, Sr and Rb values show contradictory variations in either Formation. They are concentrated in the coarse fraction of the Dudar Formation, but are concentrated in the fine fraction of the Alhambra Formation. Weathering is here the main control, as all these elements (except Sr) are concentrated in the Alhambra Formation. The patterns in the Dudar Formation samples indicate the primary element distribution determined by the source, in the same way as some major elements. For Sr, a mineralogical control may operate to increase levels in the fine grain size fraction of the Alhambra Formation, as muscovite in concentrated in finer grained samples, and in matrix materials.

The data presented for the Dudar and Alhambra Formations demonstrate the magnitude of change of element distributions that can occur in sediment through the actions of chemical weathering, grain break-down and possible sedimentary recycling. This has implications for provenance recognition using sediment geochemistry, especially when *quantities* of elements are used to indicate *absolute contributions* from distinct provenance types (eg. ultramafics), as opposed to the interpretation of the mere presence or absence of elements as an indicator of source type. These data are more significant yet because both sedimentary formations considered here are in a very proximal setting, only tens of kilometres from the source terrain. Prolonged transport would accentuate sorting effects and the grain size compositional biases documented above, and repeated cycles of erosion and deposition would remove some provenance information altogether.

Provenance indication

The samples of the Dudar and Alhambra Formations when plotted on a bivariate plot of SiO2 vs K2O/Na2O (Roser and Korsch 1986), indicate a Passive Margin setting as the environment of deposition. This is at odds with the actual tectonic setting of the Granada Basin, in an Active Margin setting.

This is interpreted as indicating the depositional tectonic setting of the protoliths of the meta-sedimentary rocks that constitute the Internal Zones, that are the source for the sediment in the Granada Basin. The effects of the difference in inter-formational weathering between the Dudar and Alhambra Formations is seen also, as the Alhambra Formation samples plot further to the right on the plot, with higher SiO2 values and higher K2O/Na2O. This indicates increased compositional maturity. Passive margin sandstones, that define this area on the plot are usually considered as mature deposits, often as the product of advanced sedimentary reworking. However, the sands of the eastern Granada Basin are clearly immature when normal petrographic methods are applied. Care must be taken when placing sediments in schemes of classification for provenance in isolation of other considerations. Otherwise errors are possible in assumptions crucial to tectonic interpretations. The preservation of a passive margin sequence in an orogenic setting suggests an evolution for the Betics which does not involve orthogonal continental collision or subduction. Large scale transpressional strike-slip may account for much of Betic evolution, and be responsible for metamorphism with reduced magmatic activity.

Sedimentary classification and maturity.

Samples from both the Dudar and Alhambra Formations are plotted on a graph of Log Na_2O/K_2O vs Log SiO_2/Al_2O_3 as suggested by Pettijohn et. al. (1972) for distinguishing different types of sandstone based on major element chemistry. All Granada Basin samples plot in the left of the plot, in the lithic arenite and arkose fields. Maturity increases to the right, to where quartz arenites plot. Thus the immaturity of the Dudar and Alhambra Formation samples is indicated correctly. However, the Alhambra Formation plots in the Arkose field, an incorrect classification, as there is little feldspar in deposits of the Granada Basin. The Alhambra Formation has lower values of Log Na_2O/K_2O, as Na_2O is decreased due to loss

during terrestrial weathering of the Alhambra Formation, but shows no change in Log SiO_2/Al_2O_3 indicating no great increase in compositional maturity. However, the decrease in Na2O does indicate a trend to increased maturity, which increases on the Log/Log plot to the lower right.

The incorrect assignment of the Alhambra Formation samples again emphasises the problem of applying classification schemes to samples in an unconstrained manner, and may cause erroneous conclusions to be reached if applied to meta-sedimentary equivalents that have little original texture or mineralogy preserved.

To conclude, patterns of major and trace element variation in the sediments of the eastern flank of the Granada Basin are consistent with increased weathering in younger deposits. This can be attributed mainly to a subaerial depositional environment, but also to possible sedimentary reworking of older into younger. Weathering also constrains and reinforces some trends of element variation caused by sediment size sorting.

The most important conclusion is the realisation of the difference in geochemical provenance signature obtained by weathering sediment from the same source in different ways. This can emphasise and diminish elements of source character, such that provenance implications could be compromised.

The data presented here also demonstrates how the application of geochemical classifications and discriminations, without the constraint of petrographic information could lead to erroneous conclusions about depositional environments and tectonics.

6. Heavy Minerals

6.1 Introduction

It has been known for some time that heavy minerals carry a great deal of information about their origins, and can relate quite specifically to sources and often to distinctive rock types within that source. It is often their relative instability combined with their chemical variability that makes them valuable in provenance studies.

The primary reason for studying heavy minerals in sediments is to establish provenance, to elucidate characteristics of areas lost by erosion and to infer palaeogeography. The total assemblage of heavy minerals in a sediment can be used to outline a *petrographic province*. Combine this with lithosome geometry and palaeocurrents and the character and position of the source region can be determined. *Correlation* between sequences is possible in theory, using heavy mineral assemblages when other petrological details are similar. This approach is obviously limited when source regions are many, correlation only being realistic within a single petrological province.

A further approach uses heavy minerals to look at *diagenetic processes*. Several schemes have been proposed that put heavy minerals in an order of stability during attack by intra-stratal solution. Bramlette (1941) was one of the first to demonstrate that intra-stratal dissolution does occur, noting that concretions in a shale that grew in-situ contained a greater diversity of heavy minerals than the surrounding rock. Pettijohn (1941) noted, after correlating much data on heavy minerals and the depositional age of sediments, that the diversity of assemblages decreases with increasing age. His conclusion was that intra-stratal solution was responsible. This view was challenged almost immediately by Krynine(1942) who attributed the variations recorded as being due to source rock petrology.

Several factors work to make the heavy mineral assemblage found in a sediment less than ideally representative of the source region. These are;

- The climate of the source area affecting the conditions of weathering and erosion.
- Abrasion and chemical dissolution during transport.
- Hydraulic effects that determine sorting,.
- Intra-stratal solution.

Below, the relative stabilities of heavy mineral species in response to environmental factors is discussed.

6.2 Objectives and layout of chapter 6

In this study heavy minerals are used as indicators of the effects of weathering, and possible sedimentary recycling, upon the provenance signature carried by the sediments of the eastern Granada Basin. Conglomerate composition and texture suggests a maturing trend with younging. If this is the case, heavy minerals should be removed from the sediment, the most

unstable going first. However, framework modes indicate decreased maturity, and an increase in heavy mineral abundance in the Alhambra Formation (Chapter 4). Geochemical trends on the other hand suggest increased maturity, patterns of element variation being consistent with the weathering state of the formations (Chapter 5).

The primary aim of this chapter is to document the characteristics of the heavy mineral population of the Miocene - Pleistocene sediments of the eastern flank of the Granada basin, in both the range of minerals present and detailed chemical variation within certain species. All samples share the same source, so as in previous chapters, differences between different sedimentary formations can be attributed to other factors, primarily weathering, but also the possibility of sedimentary recycling. These data are used to infer patterns of change in the composition of the heavy mineral population so that effects to the sedimentary provenance signature carried by the heavy mineral population in the sediments can be determined. This may be due to variations in weathering intensity that caused differences in alteration state between formations. A general statement on the evolution of sediment composition in proximal intra-montane settings can be attempted.

Firstly the results of a whole population study are presented. This documents the proportions of different heavy minerals in samples from the Dudar, Pinos Genil and Alhambra Formations. The sample set is the same as that discussed in **Chapter 4** for sandstone petrography: heavy minerals were separated from the same samples, by the method presented in **Appendix 1**.

Following this, features of the surface texture of the heavy minerals in the sediments are presented. These are discussed in terms of features such as etching, that indicate processes of mineral dissolution. Finally intra-species chemical variation of garnets, epidotes and tourmalines are presented. Electron microprobe data on individual detrital grains have been collected that may highlight any differences in the compositional range of these species between formations. Differences, if present can be attributed to differences in weathering between formations. This also provides a useful documentation of tourmaline compositions from a meta-sedimentary source terrane.

6.3 Heavy Mineral Stability in Sedimentary Rocks

Before making a study of heavy minerals in sediments an it is important to understand the influence of factors that can work to detract from the importance of heavy mineral to provenance studies. During its life in the sedimentary cycle a mineral undergoes weathering, erosion, transport, deposition and finally diagenesis. Several studies have examined the effects of each of these, and constructed schemes where minerals are put in an order of stability. **Table 6.1** contains a number of such stability series.

Physical properties of minerals are important in determining their stability. For example sillimanite is chemically stable but breaks up easily along prominent cleavage. Minerals that have good cleavage may be reduced in sediments by physical breakdown. Otherwise chemistry is the main control of stability, and particular compositions of a mineral can be less stable than others. For example Raeside (1959) notes that Fe rich garnets are the most unstable variety.

Order of Persistence (Pettijohn 1941)	Weathering (Dryden and Dryden 1946)	General Chemical Stability		
		(Pettijohn et.al. 1973)	Acid leaching (Morton 1985)	Deep burial, saline or alkaline pore fluids (Morton 1985)
olivine	zircon	olivine	olivine, pyroxene	olivine, pyroxene
silliminite	tourmaline	hornblende	amphibole	andalusite, silliminite
pyroxene	silliminite	actinolite	sphene	amphibole
sphene	monazite	augite	apatite	epidote
andalusite	chloritoid	diopside	epidote, garnet	sphene
Ca-amphiboles	kyanite	hypersthene	chloritoid, spinel	kyanite
glaucophane-riebeckite series	hornblenede	andalusite	staurolite	staurolite
epidote	staurolite	epidote	kyanite	garnet
kyanite	garnet	kyanite	andalusite, silliminite	apatite, chloritoid, spinel
staurolite	hypersthene	garnet (iron-rich)	tourmaline, rutile, zircon	rutile, tourmaline, zircon
monazite		silliminite		
xenotime		sphene		
apatite		zoisite		
garnet		apatite		
zircon		garnet (iron-poor)		
tourmaline		staurolite		
rutile		monazite		
		rutile		
		zircon		
		tourmaline		
		anatase		

Table 6.1 Schemes of heavy mineral stability in sediments, including those for weathering and intra-stratal solution.

For weathering Raeside *op. cit.* notes that an absolute scale is still wanting as there are differences in the nature of weathering environments, and also mineral properties are variable due to structural and chemical differences. Minerals with different chemical and physical properties react differently to different environments. Large scale studies of regional variations are probably required to lessen, and draw attention to, the effects of local differences in weathering or mineral chemistry that may affect the *local* order of mineral stability, and subsequently affect interpretations of provenance drawn from sandstone compositions.

Russell (1937) studied the heavy mineral composition of Mississippi river sand to test the predicted changes brought about by transport in rivers. Abrasion during transport over hundreds of miles has little effect on the bulk composition of the heavy mineral populations. The earlier scheme of Thoulet (1913) was, he suggested less to do with abrasion in transport and more to do with weathering and dissolution after deposition.

Much attention has focused on the role of intrastratal solution as a mechanism for the removal of heavy minerals during diagenesis. Pettijohn (1941) concluded that it was the major cause of the decreasing variety of heavy minerals with age in ancient sandstones, and Bramlette (1941) demonstrated its occurrence in sandstones. The action of fluids and their pH is important. Morton (1984) demonstrated that the relative stability of heavy minerals varies with the pH of the dissolving fluids. He constructed two stability orders, one for acid weathering and another for deep burial with alkaline fluids (**Table 6.1**).

Morton (1984, 1987) looked at the heavy minerals in north sea sandstones. From these he analysed detrital garnets using an electron microprobe. Sands buried to more than 3.5km are garnet free due to the percolation of high temperature pore fluids. As depth increases the stability of garnets decreases, although this depends on mineral chemistry of the garnets. Garnets low in Ca are more stable persisting to greater depths than high- Ca garnets. This contrasts with earlier studies were Fe- rich garnets are the least stable. This difference can probably be explained by the difference in the environment of dissolution, between weathering and erosion and intrastratal dissolution during diagenesis. Solution compositions are the main variables that result in differing mineral stabilities both within and between mineral species.

The main causes of heavy mineral dissolution are climate, which determines the intensity of chemical weathering, and intrastratal solution during diagenesis. The latter is well constrained and results in the bulk of changes to heavy mineral populations.

6.4 Whole Population Studies

Heavy Minerals were separated from sandstones of the Dudar, Pinos Genil and Alhambra Formations and mounted on glass slides to allow petrographic analysis of the range of minerals present in the sediments. The methods involved are detailed in Appendix A.1. The results of ribbon counting of the samples are presented in graphical form in **Fig. 6.1**, and average contents of heavy minerals for each formation are separately listed in **Table 6.2**.

The sediments of the Granada Basin are petrographically immature. They contain an abundance of heavy minerals, constituting 5.7% of the Dudar Formation sands and 7.2% of the Alhambra Formation (see **Table 4.4**). This suggests that they represent a component of a very fresh source signature. However, the Alhambra Formation shows greater weathering and

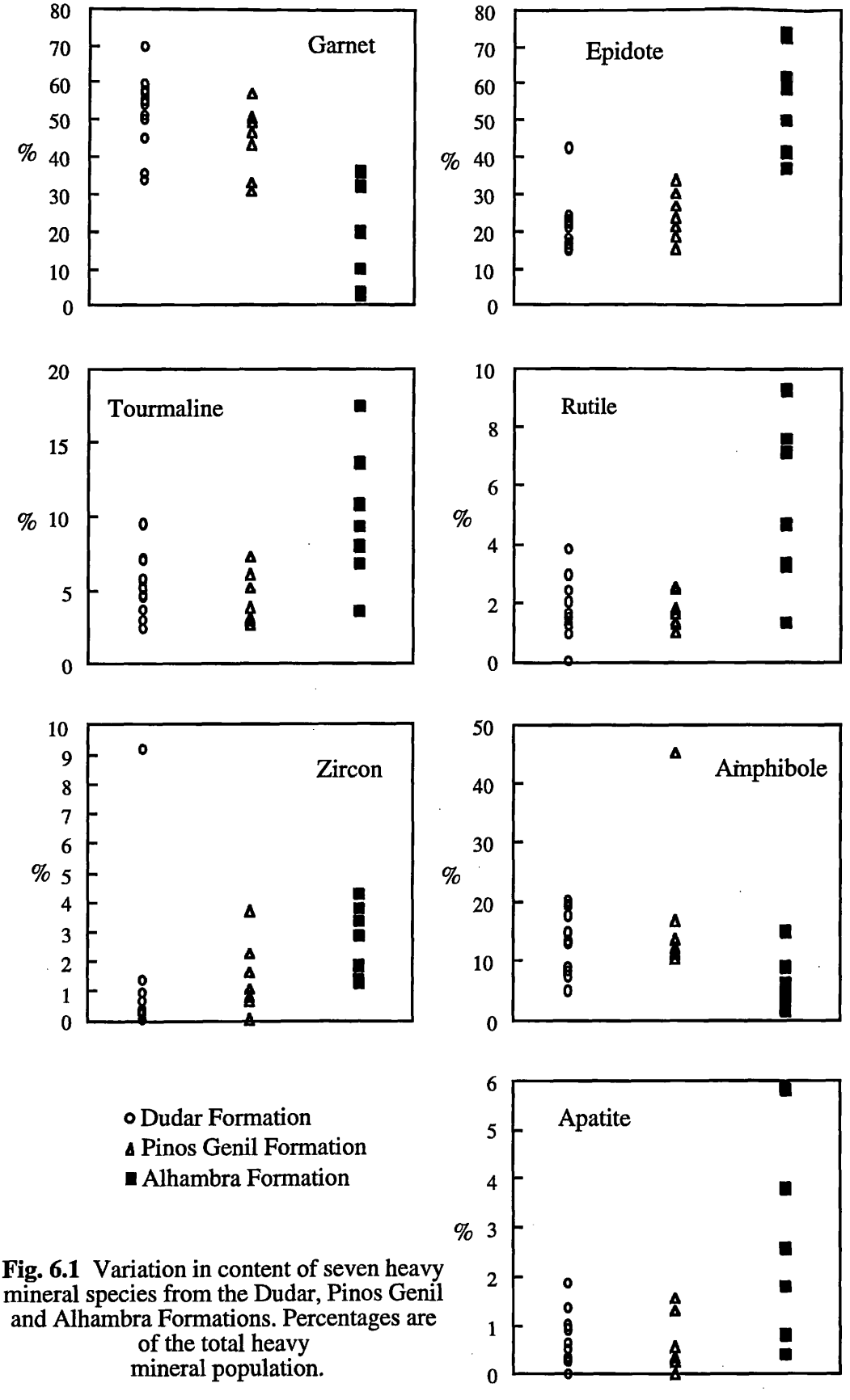

Fig. 6.1 Variation in content of seven heavy mineral species from the Dudar, Pinos Genil and Alhambra Formations. Percentages are of the total heavy mineral population.

	Dudar Formation		Pinos Genil Formation		Alhambra Formation	
	Av.	St. Dev.	Av.	St. Dev.	Av.	St. Dev.
Garnet	53.8	9.6	44.5	9.5	17.9	12.1
Epidote group	18.7	3.3	24.1	6.5	53.6	15.0
Tourmaline	5.2	2.1	4.4	1.8	10.4	4.4
Rutile	1.7	1.1	1.7	0.6	5.5	2.7
Zircon	1.3	2.8	1.4	1.2	2.8	1.2
Apatite	000	000	0.7	0.6	2.6	1.8
Amphibole	13.5	5.2	17.0	12.5	7.2	5.2

Table 6.2 Average percentage contents of heavy minerals for the Dudar, Pinos Genil and Alhambra Formations. Percentages are of the total heavy mineral population.

textural maturity, suggesting a greater compositional maturity also, but as seen (Chapter 4) lithic fragments and heavy minerals increase indicating a *decrease* in compositional maturity. Clearly this decrease in compositional maturity is determined partly by source, but possibly by reworking and clast and grain break-down, as argued in **Chapter 4**. The weathering of the Alhambra Formation does not work to reduce this effect significantly, as grains are weathered, but not destroyed.

However, it might be reasonable to expect changes in the quantities of heavy minerals, or in the character of the population of each heavy mineral species. The range of stable heavy minerals (tourmaline, rutile, zircon) may increase in proportion in the Alhambra Formation. If so, then weathering has worked to increase immaturity, in a predictable way, but only on a fraction of the total framework grains. This could allow the influence of source and weathering control to be clarified.

The following section outlines details of the variations in heavy mineral content between the three formations. After this an order of stability of heavy minerals for this study is suggested.

6.4.1 Variations in Inter-Formational heavy mineral content

Figure 6.1 depicts the variation in content of seven heavy minerals between the Dudar, Pinos Genil and Alhambra Formations. **Table 6.2** contains the average values for each formation plus standard deviations from the averages. Trends of variation with age of formation can be seen, that can be attributed to the extent of weathering alteration in each, because the source of detritus for each formation is the same throughout.

Garnet decreases quite markedly in abundance in younger deposits, especially in the Alhambra Formation where, in some samples, it forms less than 10% of the heavy mineral population, compared with a high of 70% in the Dudar Formation. Garnets are common in many schists in the Internal Zones, most prominently in the Nevado-Filabride complex, where they are best developed in the graphitic schists of the Veleta unit and the coarse non graphitic schists of the Mulhacen complex. The Alpujarride also contains some garnet bearing rocks. They can be large and euhedral, usually brown or red in colour, or small with some retrogression. They often occur as broken fragments and are badly altered in the Alhambra Formation, but fresh in the Dudar Formation (see **Plate 4.10**). The decrease in garnet content is balanced mainly by the increase in epidote group minerals, and may be due to source input changes. The reduction in garnet proportions could also be attributed to the action of weathering. However, garnet is most often attributed with greater stability than epidote (**Table. 6.1**, stability schemes) in intrastratal solution. For terrestrial weathering and resistance to abrasion, garnet is further down the list of stability, and often near epidote. Loss of garnet is therefore more likely than loss of epidote when considering weathering and abrasion as garnet is more labile than epidote.

Epidote group minerals follow an opposite pattern and increase quite distinctly in the Alhambra Formation. Epidote here is defined as including a wide range of composition, spanning epidote, zoisite, clinozoisite and rare allanite. This range of epidote group minerals occur as equant yellow epidotes, but most often as colourless, equant grains. Epidote group

minerals are common in many schists from the internal zones, mainly in the Mulhacen complex units, from amphibolites sourced from the Ophiolite unit.

Epidote group minerals form the largest percentage of heavy minerals in the Alhambra Formation, and their increase in the Alhambra Formation is be the major cause of the decrease in garnet percentage content. If the increase in epidote proportion was due to an addition of epidote from a new source, then the total heavy mineral content could be expected to increase to more than 7% in the Alhambra Formation. The change in epidote proportion is therefore probably due to a change in the dynamics of heavy mineral production. The increase in epidote can be explained in two ways. Firstly it increases in proportion as it is more stable than garnet, and other minerals, so survived the more intense weathering environment in the Alhambra Formation, being concentrated due to selective removal of *other* minerals. The second possibility is an increase in epidote minerals in the source rocks, indicating a change in provenance character. However, on the basis of other considerations (see **Chapter 3**) source is little changed, and all lithologies present in the oldest Dudar formation can be recognised in the Sierra Nevada, indicating no source change from then to the present day. If recycling was important, source would be even less likely to change. The first case is more likely. Epidote is also no more stable in proposed weathering and abrasion stability schemes than garnet.

Amphibole decreases in abundance in younger deposits. Green hornblende is characteristic of the amphibolites common as clasts in associated conglomerates. This decrease in amount is consistent with amphibole being a relatively unstable mineral in stability schemes. It would be expected to decrease in abundance in more weathered deposits. However, it has been identified as a source of the distinctive ultramafic trace elements Co, Ni and Cr which increase in the Alhambra Formation (**Chapter 5**). These elements are often concentrated in sediments due to weathering, but as amphibole is less abundant in the more weathered formations that show enrichment in these elements, they must be retained in minerals other than amphiboles, or have been transferred to alteration products of amphibole.

The three so called 'ultra-stable' minerals, tourmaline, rutile and zircon all show a marked increase in the Alhambra Formation. Tourmalines are dominantly blue-black varieties, and show pleochroism to brown and pale brown. They are common in many schist lithologies, but also as augen in mylonitised granitic gneiss, that are common in detachment zones in the Sierra Nevada. Their source is exclusively from the Nevado-Filabride complex, most probably the Mulhacen unit rocks. Rutile is small and rare, and occurs in amphibolites sourced in the Ophiolite unit of the Mulhacen complex in the Internal Zones. Zircons are small, rare and rounded. Their source is prominently from the Nevado-Filabride complex. The Alpujarride Complex is not a likely source as it is dominantly composed of carbonate rocks in the Sierra Nevada source region.

The Pinos Genil Formation shows decreased proportions of tourmaline and rutile compared to the Dudar Formation. For both of these the lower value range in each formation is similar. However, the Alhambra Formation has many more samples that have higher values of tourmaline and rutile than the highest content in the Dudar or Pinos Genil Formations.

For zircon, quantities show a clearer shift to higher values in the Alhambra Formation

sands. One sample in the Dudar formation is very rich in zircon. This does not affect the general trend, or average values greatly, and may be due to unusual circumstances or analytical error. For the stable minerals the trend observed is consistent with concentration in more weathered deposits, due to the removal of less stable minerals, and is an expected trend.

Apatite contents are similar in the Dudar Formation and the Pinos Genil Formation The spread of values contracts in the Pinos Genil Formation compared to the Dudar Formation. The range increases to much higher values in the Alhambra Formation. Apatite is a stable mineral, and can be expected to increase in amount in more weathered deposits.

In summary, stable mineral species, such as zircon, increase in concentration in the more weathered Alhambra Formation. The terrestrial Pinos Genil Formation shows a decrease in these species compared with the relatively unweathered marine Dudar Formation. Less stable garnet and amphibole show a decrease in the more weathered formations, supporting the control of composition by weathering in a predictable way. However, epidote, which has a similar stability in weathering and intrastratal solution to garnet, exhibits a dramatic increase in quantity in the Pinos Genil and especially in the Alhambra Formation. This is difficult to explain by relative weathering stability alone. The range of composition of epidote is wide and includes such minerals as zoisite and clinozoisite, which are often not included on stability schemes due to greater rarity in sediments. It is possible that this range of composition is more stable than epidote *sensu stricto*.

The other possibility is an increased input of epidote from source. In Chapter 3 it is demonstrated that the present day source region rocks can all be found in the oldest deposits in the Granada Basin. Therefore primary source for these sediments in the Sierra Nevada remains unchanged throughout deposition, until the present, except for a few detailed variations and the covering and unroofing of the Alpujarride rocks. Increased input of epidote from primary sources is therefore unlikely. Continued break-down of conglomerate clasts has been argued as a cause of the observed decrease in compositional maturity of the Alhambra Formation sandstones. This is the only other possible source of minerals. However, it would also act in the same way for other minerals such as garnet, which decreases in abundance. Because the grains and clasts that break-down act like a continued primary source, it should maintain the immaturity, or increase the immaturity of the heavy mineral population of the Alhambra Formation, in the same sense as lithic fragments. But weathering exerts a clear influence on the heavy mineral assemblage, as the stable minerals increase at the expense of less stable types despite the overall decrease in maturity of the Alhambra Formation.

The conclusions reached are therefore

- Weathering is the main control of inter-formational variations in heavy mineral content.

- weathering does work to predictably increase concentrations of chemically and physically stable heavy minerals.

- some species of epidote group minerals are relatively stable in the weathering environment.

6.4.2 Proposed weathering stability order

The following is a proposed order of stability of the seven heavy minerals discussed above for the weathering and depositional environments of the Pinos Genil and Alhambra Formations. The composition of the Dudar Formation is considered to be a near base-line for the abundance of heavy minerals in a fresh derivative from the Internal Zones of the Sierra Nevada. The order of stability is based on the percentage fractional change from the Dudar formation base-line. The minerals are listed with the percentage value they represent of the Dudar Formation contents;

Pinos Genil Formation	
Apatite	135%
Epidote	129%
Amphibole	126%
Zircon	108%
Rutile	100%
Tourmaline	85%
Garnet	82%

Alhambra Formation	
Apatite	500%
Rutile	323%
Epidote	286%
Zircon	215%
Tourmaline	200%
Amphibole	53%
Garnet	33%

The pattern in the Alhambra Formation is more pronounced and clearly conforms to general expectations of mineral stability (see **Table 6.1**). The Pinos Genil Formation samples are clearly slightly anomalous, and may preserve the greater influence of source. This suggests that the Pinos Genil Formation is a nearer equivalent of the Dudar Formation, differing only in terrestrial depositional environment. The Alhambra Formation, on the other hand, shows increased differentiation, due certainly to terrestrial deposition and weathering. However, if the Alhambra Formation is the product of the erosion of the same source as for the Dudar and Pinos Genil Formations, then changes in heavy mineral abundance should be similar to those seen in the Pinos Genil Formation, which was deposited in a similar environment. But changes are much more pronounced in the Alhambra Formation.

The possible explanation for this is recycling of older deposits into younger. This would effect a greater differentiation of composition due to weathering and abrasion. Maturity indicators from conglomerate composition indicate that only in the Alhambra Formation is the range of clast composition changed significantly in the direction of increasing maturity. Sandstone framework modes show the opposite trend, again only significantly in the Alhambra Formation. This has been explained as the result of input to sands from the break-down of conglomerate clasts, in a way that increases clast maturity but feeds a decrease in sand maturity in the early stages of detritus break-down. The Alhambra Formation alone may have a significant proportion of recycled detritus.

6.5 Surface features of detrital heavy minerals.

This section discusses observed surface features for selected heavy mineral grains from the eastern Granada Basin sandstones. These features may indicate processes of grain degradation and break-down. Surface characteristics were studied using a scanning electron

microscope (see **Appendix 1**).

Morton (1979) studies surface features of heavy minerals from Palaeocene sands of the North Sea, using a scanning electron microscope. He attributes the features observed to post burial intra-stratal alteration (*chemical* origin), or to abrasion damage acquired during erosion and transport (*mechanical* origin). Chemically produced features develop in a progressive way, increasing in intensity with depth of burial, and are controlled by mineral structure. Mamilliations form first, often appearing irregular, or etch pits can develop. These develop with further alteration to form regular faceted surfaces, which can cause the formation of highly 'skeletal' deeply faceted grains. Mechanical features are irregularly arranged, except were cleavage is important. Indentations, grooves and broken blocks are common. Conchoidal fractures impart angular smoothness to grains, while these other processes generate rough surfaces. Grains can retain evidence of physical abrasion damage, and also features related to diagenesis, when they are reworked into younger deposits

The chemical alteration features of Morton (1979) are generated by intra-stratal solution. However, the degree of diagenetic alteration of grains in the Granada Basin has been argued to be small, if present at all. The Dudar formation is the oldest detrital sediment body and will have been the deepest buried, though this is entirely unconstrained, and burial need not have been at all deep. Even so, mineral assemblages in the Dudar Formation are the most immature of all formations, stable heavy minerals are not concentrated and relatively unstable garnets are more abundant. Grains show no alterations or replacements, compared with the more weathered and altered Pinos Genil and Alhambra Formations. Therefore diagenesis can be expected to play no major role in alteration of heavy minerals or the formation of distinct surface features. Abrasion may be expected to be the major cause of any alterations.

Below, observed features in garnets, epidotes and tourmalines from the Dudar, Pinos Genil and Alhambra Formations are detailed. These shed light on the processes responsible for grain alteration that cause changes in provenance signature. The hypothesis that abrasion should be the dominant control on grain alteration is tested.

6.5.1 Observed surface features

Plates 6.1 to **6.18** are selected electron microscope photographs of detrital heavy minerals from the Granada Basin. Surface features related to alteration processes are clearly visible on the grains.

Plates 6.1-6.5 show garnet grains from the Dudar Formation with a variety of surface features. In **Plate 6.1** a sub-hedral garnet shows only some abrasion damage, but is otherwise very fresh. This indicates a short residence time in transport before deposition, and no activity of post depositional solution. **Plates 6.2** and **6.4** show initial stages of etching, mamilliations and etch pits. These advance to form regular facets (**Plates 6.3** and **6.5**). Conchoidal fractures are often seen. It is possible that these are a product of the disagregation procedure, (by gentle hand crushing) and not due to transport abrasion. These should therefore be interpreted with caution. The garnets in the Dudar formation show a range of alteration states, from very fresh to advanced faceting. Abrasion damage is not a major alteration factor in the samples seen.

Plates 6.6 - 6.10 show garnet grains from the Alhambra Formation for comparison. In

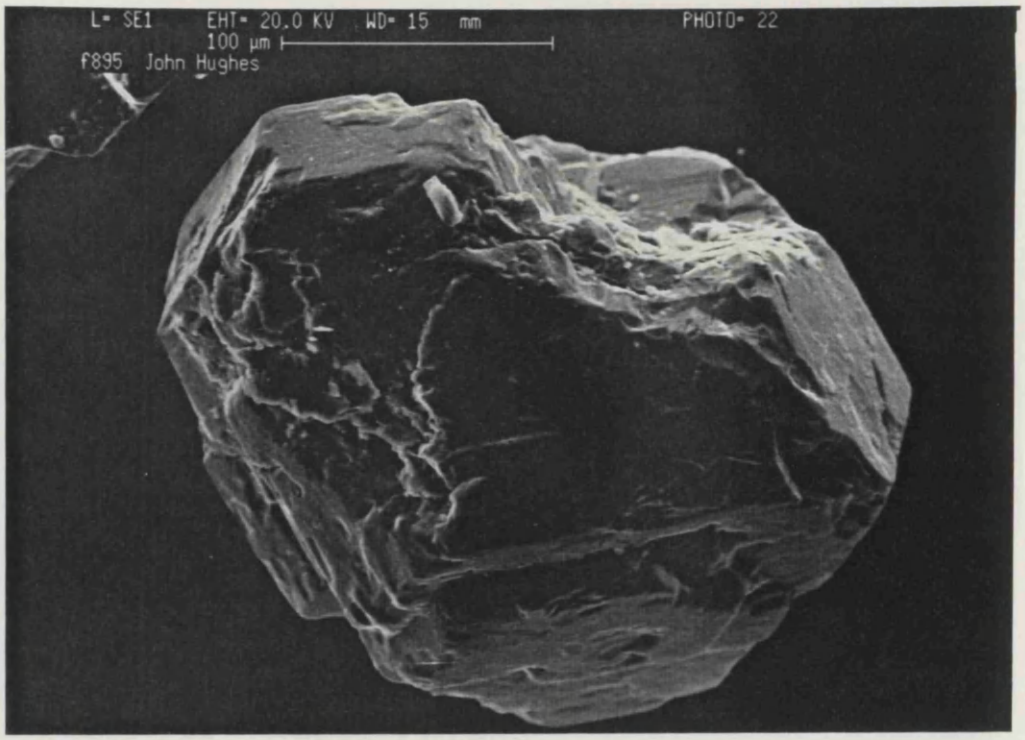

Plate 6.1 Dudar Formation. Sample 2.3 Sub-hedral garnet with smooth faces and no evidence of chemical alteration. Some rough edges and gouged pits record possible abrasion damage accumulated during transit and deposition.

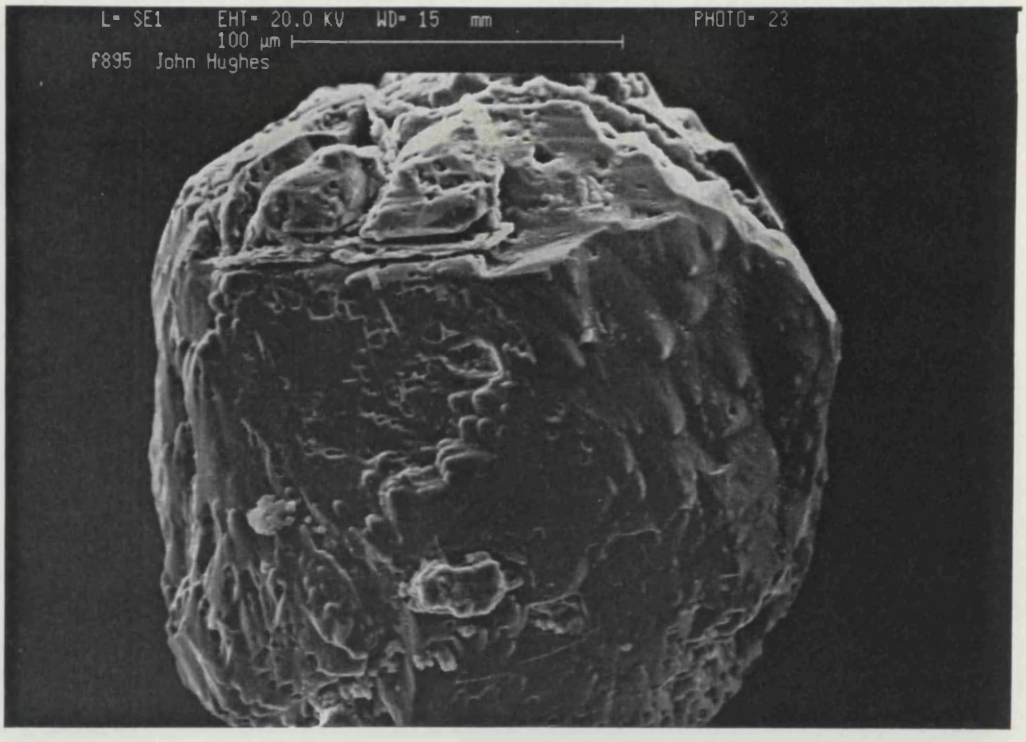

Plate 6.2 Dudar Formation. Sample 2.3 again. This garnet from the same sample as plate 6.1 shows mamiliated outer surface, but also a more affected surface with nunerous etch pits. These are crystolographically controlled and suggest the developement of faceting that results in more skeletal grains. The relationship between the mamiliae and the etch pits is not clear except that they appear to represent different stages in alteration of the grain.

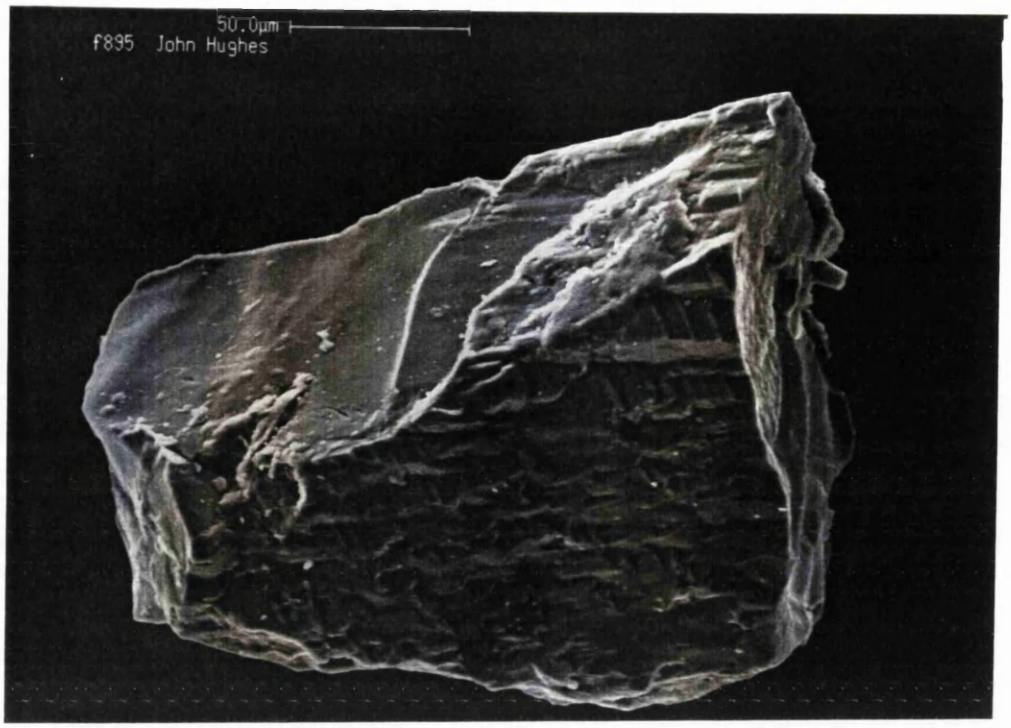

Plate 6.3 Dudar Formation. Sample 2.3. Garnet grain showing conchiodal fracture surface but also etched and faceted surface. This represents a further stage in alteration from the developement of etch pits. The regular arrangement of features clearly indicates the crystallographic control of form during etching.

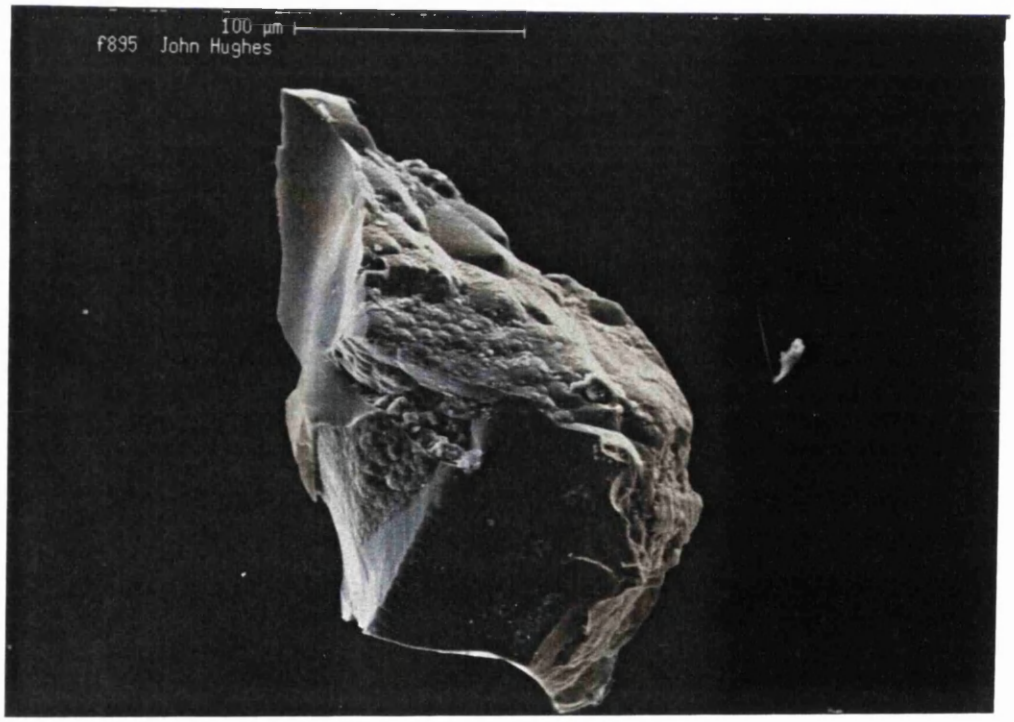

Plate 6.4 Dudar Formation. Sample 2.3. Broken fragment of garnet grain, showing smooth conchoidal fracture surfaces. Remaining external surfaces show mamilliations, and the 'micro-scaly' texture of Morton (1979), indicating the earlier stages of alteration.

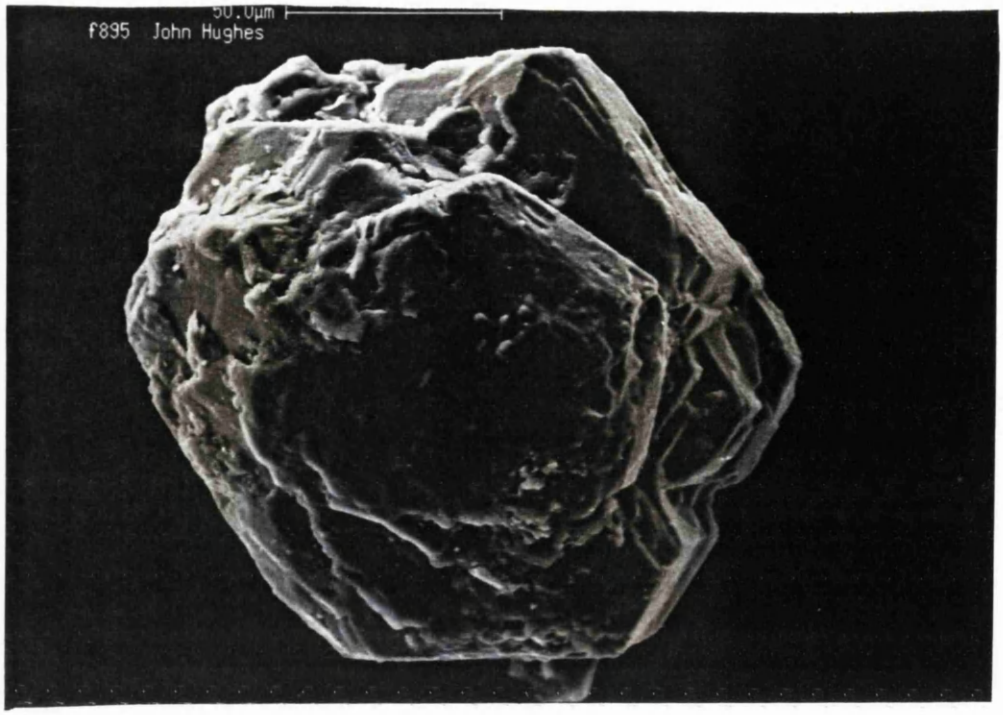

Plate 6.5 Dudar Formation, sample DU2. Garnet grain showing rough exterior surface (left) and etched and faceted features (right) with well developed faces.

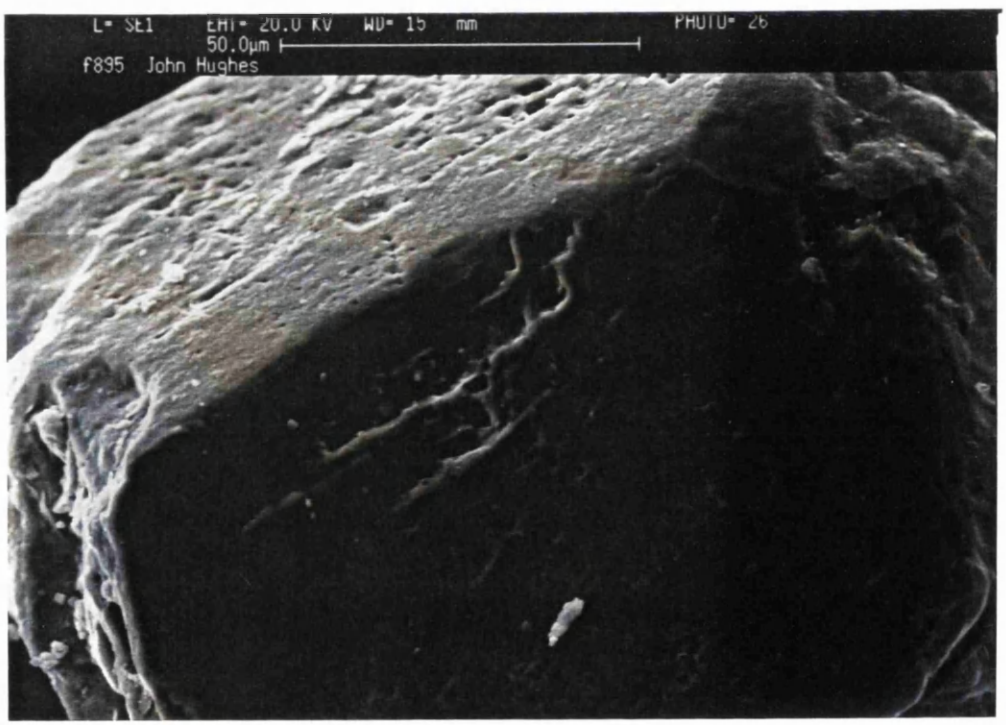

Plate 6.6 Alhambra Formation, sample A.8.3. Sub-hedral faces of garnet crystal, with regularly arranged etch pits. Rough broken or abraded surfaces visible to right and left.

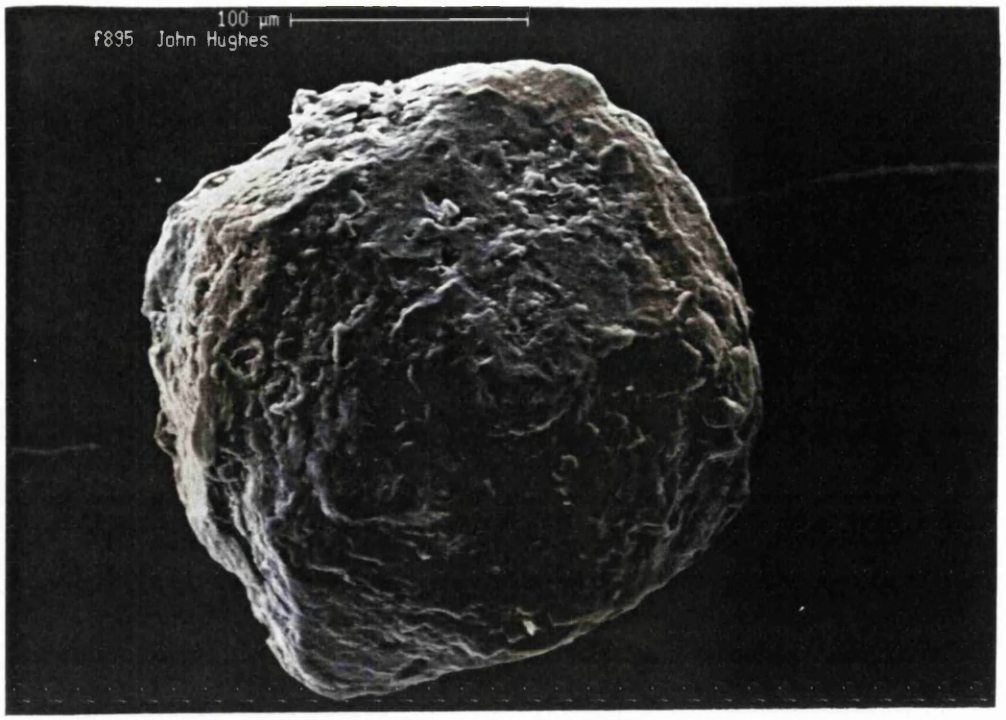

Plate 6.7 Alhambra Formation sample A8.3. Sub-rounded garnet , rough irregular pitted surface indicates abrasion rather than chemical alteration.

Plate 6.8 Alhambra Formation, sample A8.3. Broken fragment of garnet, with conchiodal fractures and rough pitted surfaces, related presumably to abrasion in transport. No chemical etching or even mamilliations.

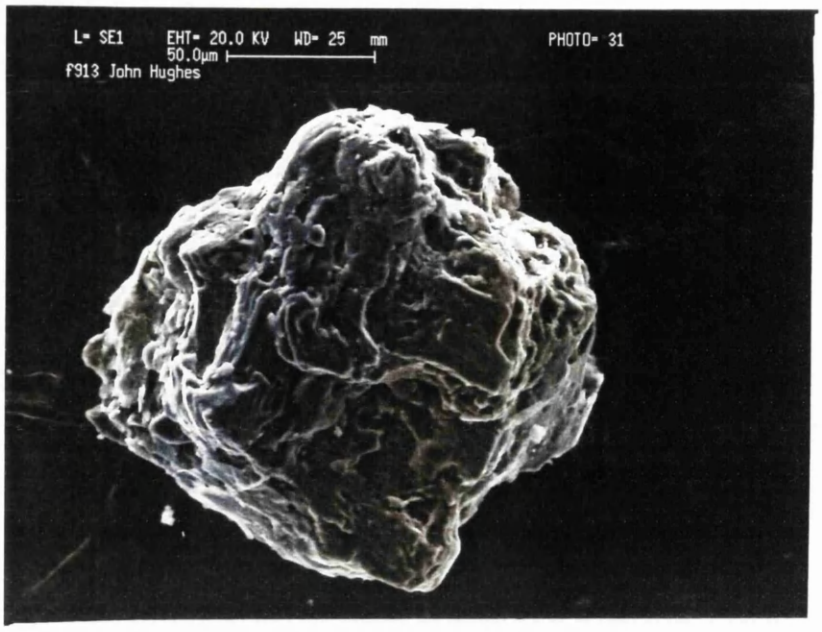

Plate 6.9 Alhambra Formation, sample A9.4. Rough garnet grain, showing poor faceting, but the beginnings of a regularity of form associated with skeletal grains. More advanced physical alteration than grains in the Dudar Formation.

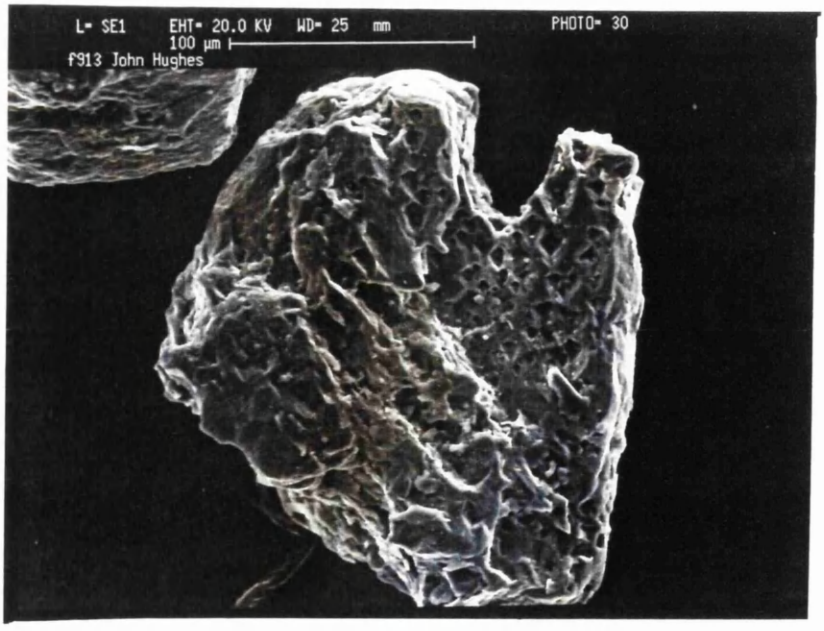

Plate 6.10 Alhambra Formation, sample A9.4. Garnet grain showing advanced alteration of form, but lacking amalgamation of etch pits to form distinct facet features.

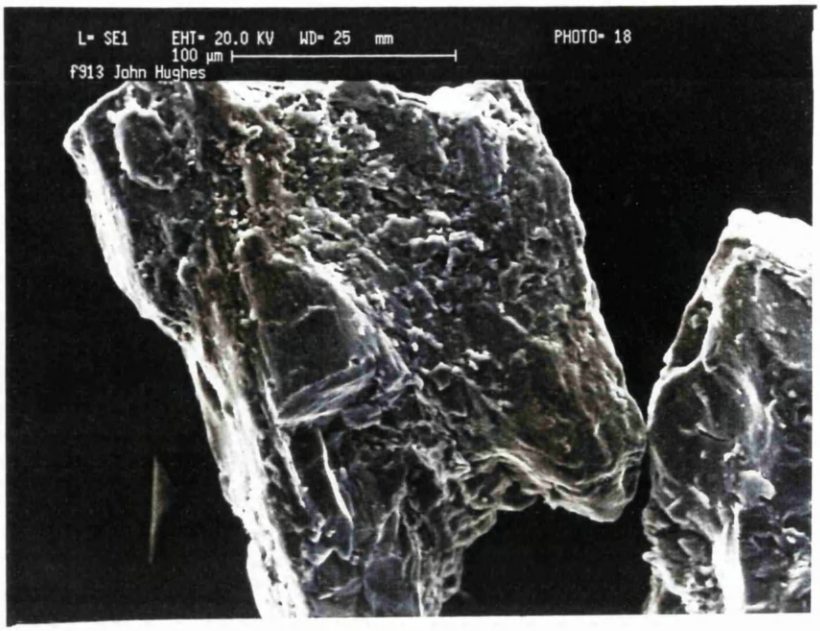

Plate 6.11 Pinos Genil Formation, sample 5.7. Epidote grain. Shows typical rectilinear form and rough abraded surface.

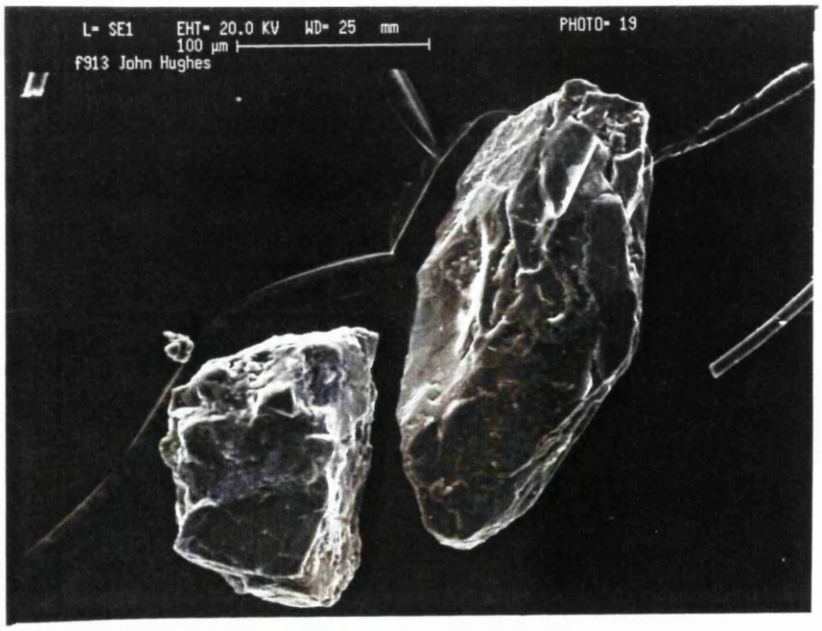

Plate 6.12 Pinos Genil Formation, sample 5.7. Sphene (left) and Epidote (right) grains. Epidote is smooth, with no evidence of abrasion damage, and no indication of chemical alteration. Many grains are seen like this suggesting that epidote may be a relatively stable mineral in these sediments.

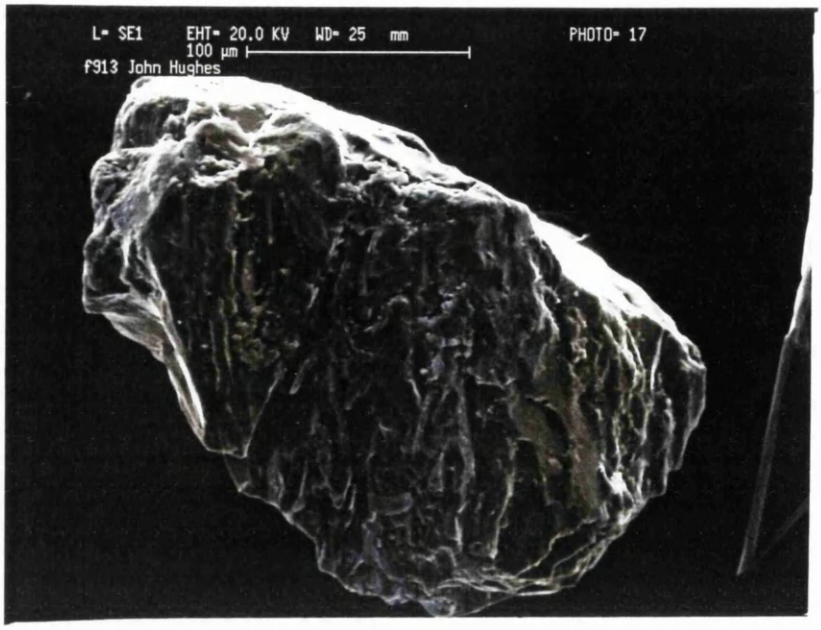

Plate 6.13 Pinos Genil Formation, sample 5.7. Apatite, rough suface suggests abrasion damage. There is also a suggestion of regularily arranged features running vertically in the photograph that may relate to crystallographic control. This may indicate chemical alteration.

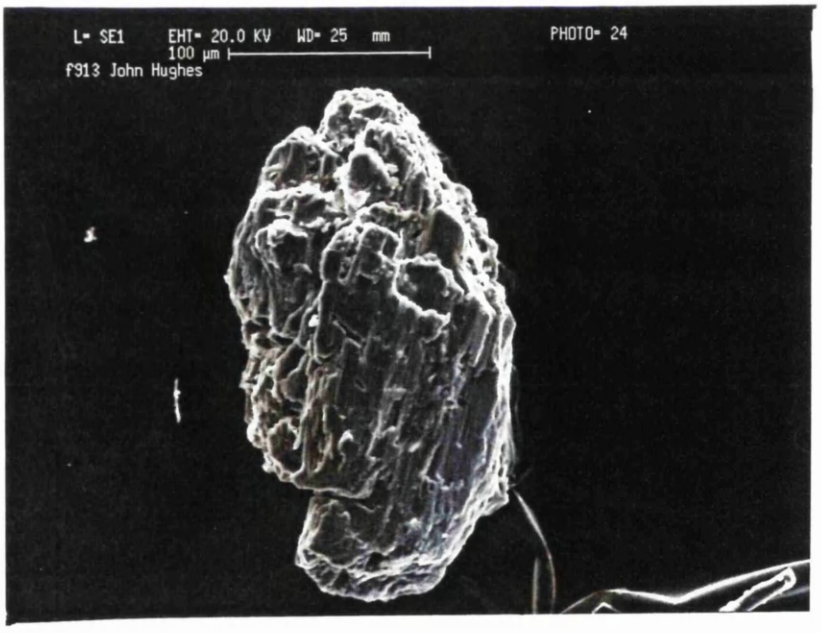

Plate 6.14 Pinos Genil Formation, sample 5.7. Amphibole grain. Clear control of grain morphology by cleavage, accentuated by chemical alteration, generating a slightly faceted grain.

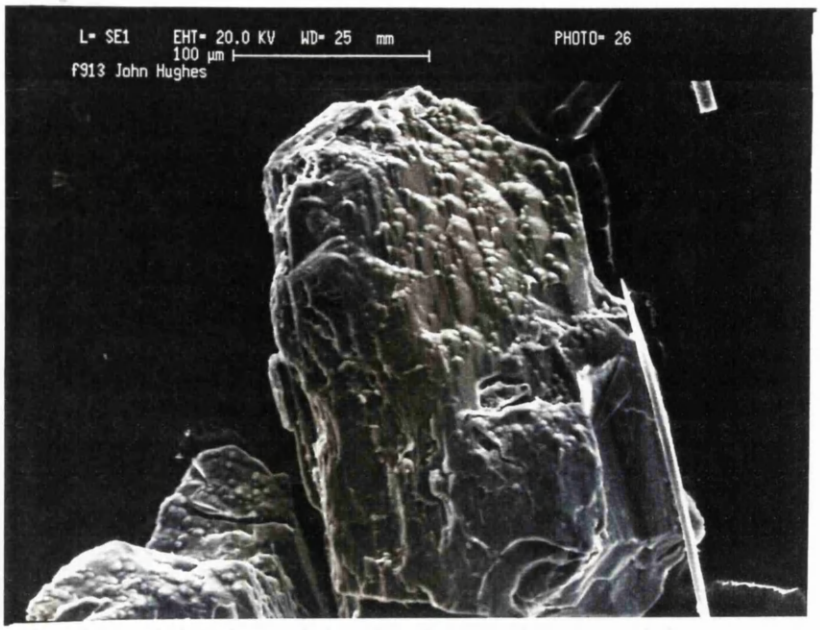

Plate 6.15 Pinos Genil Formation, sample 5.7. Amphibole grain. Mamilliations on prism termination highlight 'rods' defined by cleavage. Mamilliations here clearly controlled by crystal structure. Remainder of grain has some rough areas indicating some abrasion damage.

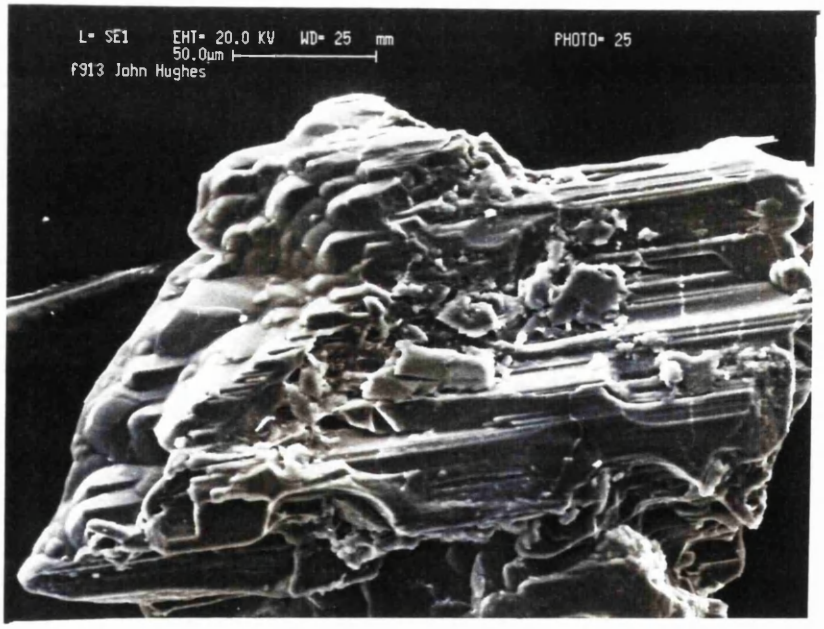

Plate 6.16 Pinos Genil Formation, sample 5.7. Well formed mamilliations on cleavage controlled prism terminations, again determined by crystallographic preference.
- Amphibole grain.

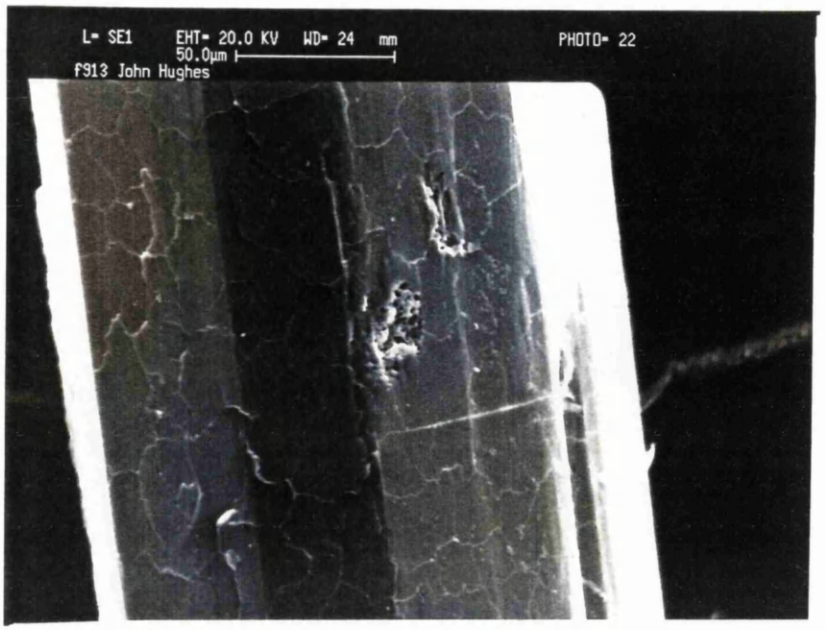

Plate 6.17 Pinos Genil Formation, sample 5.7. Close up of tourmaline grain. Euhedral crystal faces. A network of surface cracks is visible, that could become be the locus for abrasion damage. A few small fragments are broken off that appear to correspond with these cracks. Otherwise this grain show virtually no evidence of abrasion, and no evidence of chemical degredation.

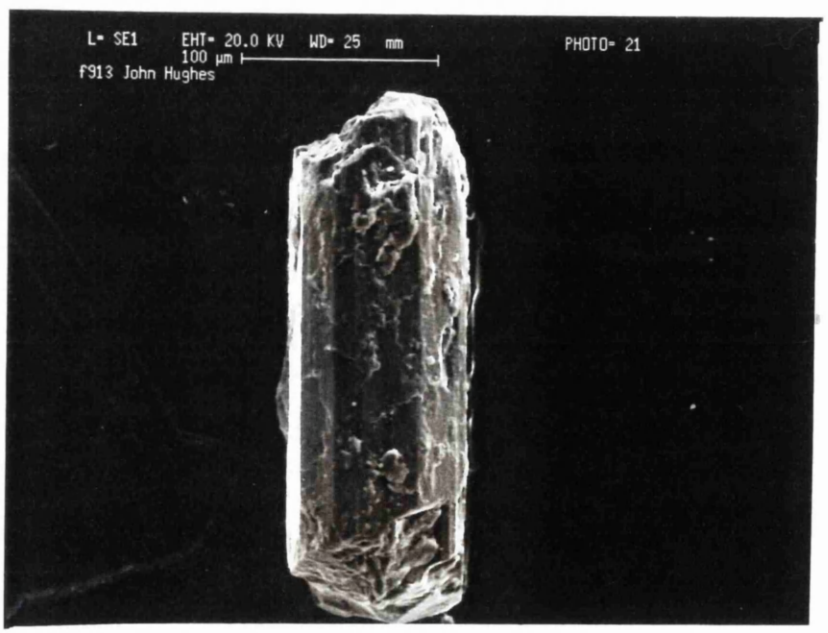

Plate 6.18 Pinos Genil Formation, sample 5.7. Tormaline grain. Other than the prism ends, which are rough and broken in appearance, the grain is euhedral, and shows little other evidence for abrasion damage, and no chemical alteration at all. This is especially obvious when comapred to garnet grains from the Dudar and Alhambra Formations.

Plate 6.6 a garnet shows euhedral faces with developing etch pits. Rough edges are also seen, related to abrasion damage. **Plate 6.7** shows a garnet with no chemical alteration features, but only a rough surface indicating abrasion during transport. Discounting the Conchoidal fractures in the garnet of **Plate 6.8** the remaining surfaces show irregular pits and broken edges characteristic of abrasion damage. **Plates 6.9** and **6.10** show garnets at advanced stages of physical degradation, having lost any recognisable original exterior surfaces or form. They show developed facets, the garnet in **Plate 6.10** shows a more intermediate stage of change with abundant etch pits. The garnets of the Alhambra Formation indicate the greater influence of physical alteration, with irregular rough surfaces, but also advanced chemical degradation.

Plate 6.11 and **6.12** show epidote grains from the Pinos Genil Formation. No etching or chemical alteration is clear on these grains. **Plate 6.11** suggests abrasion during transport to generate the rough surface. For the epidote in **Plate 6.12** the surface of the grain is very smooth and shows no major indentations or breakages. Epidote may therefore be a relatively stable mineral in the environment of deposition of these Granada Basin sediments.

Plate 6.13 shows an apatite grain from the Pinos Genil Formation. It has a rough surface that indicates abrasion damage, but there is a slight regularity of form that may indicate a small amount of crystallographic control of chemical alteration. However, apatite is the most stable mineral in the sediments, as argued above, so the effects of chemical weathering are likely to be small. Thus the features observed in **Plate 6.13** are most likely to be caused by abrasion.

Amphiboles are a common constituent of the heavy mineral population, and are the most unstable species present in these sediments (see **Table 6.1 and Section 6.4.2**). **Plates 6.14 - 6.16** show amphibole grains from the Pinos Genil Formation. The good prismatic cleavage is clearly a major control not only on the general morphology of the mineral but also on the manner of alteration. **Plate 6.14** shows a grain that exhibits the early stages of developing facets. **Plates 6.15 - 6.16** show grains that have developed mamilliations at prism terminations, suggesting a crystallographic control of altered morphology.

Finally **Plates 6.17** and **6.18** show tourmaline grains from the Pinos Genil Formation. They are both very fresh in appearance and show no evidence of chemical alteration. Grains are often euhedral, and have only some rough areas produced by abrasion. In **Plate 6.17** a network of small cracks can be seen on the surface of the grain. The crystal faces are otherwise smooth and euhedral. Some small chips are broken from the surface that may be controlled by the crack network. Along some of these cracks material appears to be lifting from the surface of the grain, suggesting a likely site for the localisation of any abrasion damage by catching these lifted segments.

6.5.2 Discussion of surface features

The heavy minerals of the Miocene to Pleistocene sediments of the eastern Granada Basin show evidence for chemical and physical causes of alteration. Mamilliations, etch pits and faceted surfaces suggest chemical alteration. So far this type of change has been attributed solely to post-depositional diagenetic processes. However, it has been demonstrated that the sediments of the present study have apparently suffered little compaction, alteration or

neomineralisation. Thus the existence of alteration surface features attributable to chemical processes can be interpreted in two ways;

- pore waters have had a diagenetic effect on the heavy minerals, and garnet especially, in the Dudar through to the Alhambra Formation, despite the lack of other obvious diagenetic signals.
- **or** chemical weathering during transportation can have the same effect as intra-stratal solution effects by pore waters.

The second possibility implies the loss of heavy minerals much more rapidly than if abrasion were the only transport related degradation effect. The time needed to form such features is critical in this interpretation. The origin of etched and faceted features is more likely to occur in the time scale provided by intra-stratal residence of the grains. Therefore intra-stratal alteration of the heavy mineral grains has occurred but it has not proceeded to the extremes seen in deeply buried sandstones (e.g.. Morton 1985), because the sediments of the eastern edge of the Granada Basin have not been buried deeply and have not suffered great compaction.

Grains in the Alhambra formation show much more intense abrasion effects compared with the Dudar Formation, indicating a more destructive transport environment and the possibility of slower deposition. Reworking of earlier deposits is also a possibility consistent with increased abrasion. The Alhambra Formation also shows the most profound chemical alteration with etched and faceted grains, even though the Alhambra Formation is the least deeply buried deposit, and was deposited in a terrestrial fan environment, which could preclude the entrapment of significant pore fluids. However, the maturity of the deposit is increased overall indicating the effects of, mainly, weathering . The inclusion of grains with abraded faceted surface features is possible evidence of recycling of detritus from earlier deposited and intra-stratally altered formations.

The range of alteration in all formations is wide, each contain very altered grains alongside fresh grains. This indicates that heavy minerals are liberated from host rocks at many points in the sedimentary cycle, and that they spend different times in the environment where alterations can occur. Weathering can take place on alluvial bars during dispersal of sediment. This alone supports the model of continuous break-down of lithic clasts and grains throughout sedimentation, which inputs material to the sandstones from what is effectively a very fresh, extremely proximal source. Thus a mixture of grains with different alteration states is possible. This is seen in the Dudar Formation, but also in the Alhambra Formation, where more extreme alteration of grains is seen.

Epidote appears not to suffer great alteration in the Pinos Genil Formation. This suggests that it may be a relatively stable mineral in these sediments. However, epidote is often considered to be less stable than garnet (see Table 1). The increase in the effects of pre and syn-depositional weathering seen in the Pinos Genil and Alhambra Formations compared with the Dudar Formation would suggest that epidote should decrease in abundance and show greater evidence of alteration than garnet. Here the opposite is true; epidote increases

considerably in the Alhambra Formation. This is consistent with the unaltered appearance seen in **Plates 6.11** and **6.12**.

These observed surface features are clues to the processes of grain alteration and possible destruction. These processes may be responsible for the changes in the heavy mineral population seen between the three basin flank formations. The effects of abrasion appear to be greater in the younger deposits, which show the greatest modification from the initial composition of the sediments (taken to be the most immature Dudar Formation). Chemical alteration processes may also have operated, aiding physical alteration processes to change the heavy mineral population.

The next section considers if the changes seen in bulk population abundances are reflected in the compositional range of individual mineral species. Thus it is hoped to establish if certain compositions of selected minerals are more or less stable than others. It is important to constrain this, as the effects upon provenance signature could be significant. This is especially so as certain compositions of minerals can be diagnostic of the presence of certain rock types with a source region. The implications of noticeable changes to provenance signature carried by heavy minerals, within a proximal system such as the eastern Granada Basin deposits, that have only suffered a few cycles of sedimentation, are significant.

6.6 Intra-species chemical variation

Garnet, epidote and tourmaline grains were analysed for major elements using an electron microprobe (see **Appendix 1**). This section presents selected results from this study. The primary objective is to document the compositional range of these heavy minerals, but also to relate differences in the compositional range of these minerals to sedimentary processes. Again the sediments of the eastern flank of the Granada Basin are an ideal place to constrain these effects, they act like a natural laboratory, as all deposits share the same ultimate source area, but have different depositional environments and states of alteration, that are related above to weathering and/or reworking. Differences in composition are due primarily to sedimentary processes and not source controlled.

Morton (1985, 1987) found patterns of variation of intra-species chemical composition in garnets from sediments of the North Sea. These changes he related to burial depth and intensity of intra-stratal solution effects. Low Ca garnets are more stable than high Ca garnets, the former are therefore concentrated in the sandstones. In this way the effects of diagenesis has a greater effect upon provenance signature. Morton cautions that diagenetic history should be constrained before making provenance assessments.

Weathering during transportation appears to be the dominant control upon compositional differences between the sediments of the eastern Granada Basin. Bulk sediment geochemical indicators are generally consistent with this (see **Chapter 5**). However, as shown above, heavy mineral grains not only exhibit physical abrasion surface features, but also features normally associated with chemical alteration through the action of intra-stratal solution. Therefore patterns of compositional change within individual mineral species may exist also. This section presents evidence to constrain these variations, if present, and to establish changes to provenance signature.

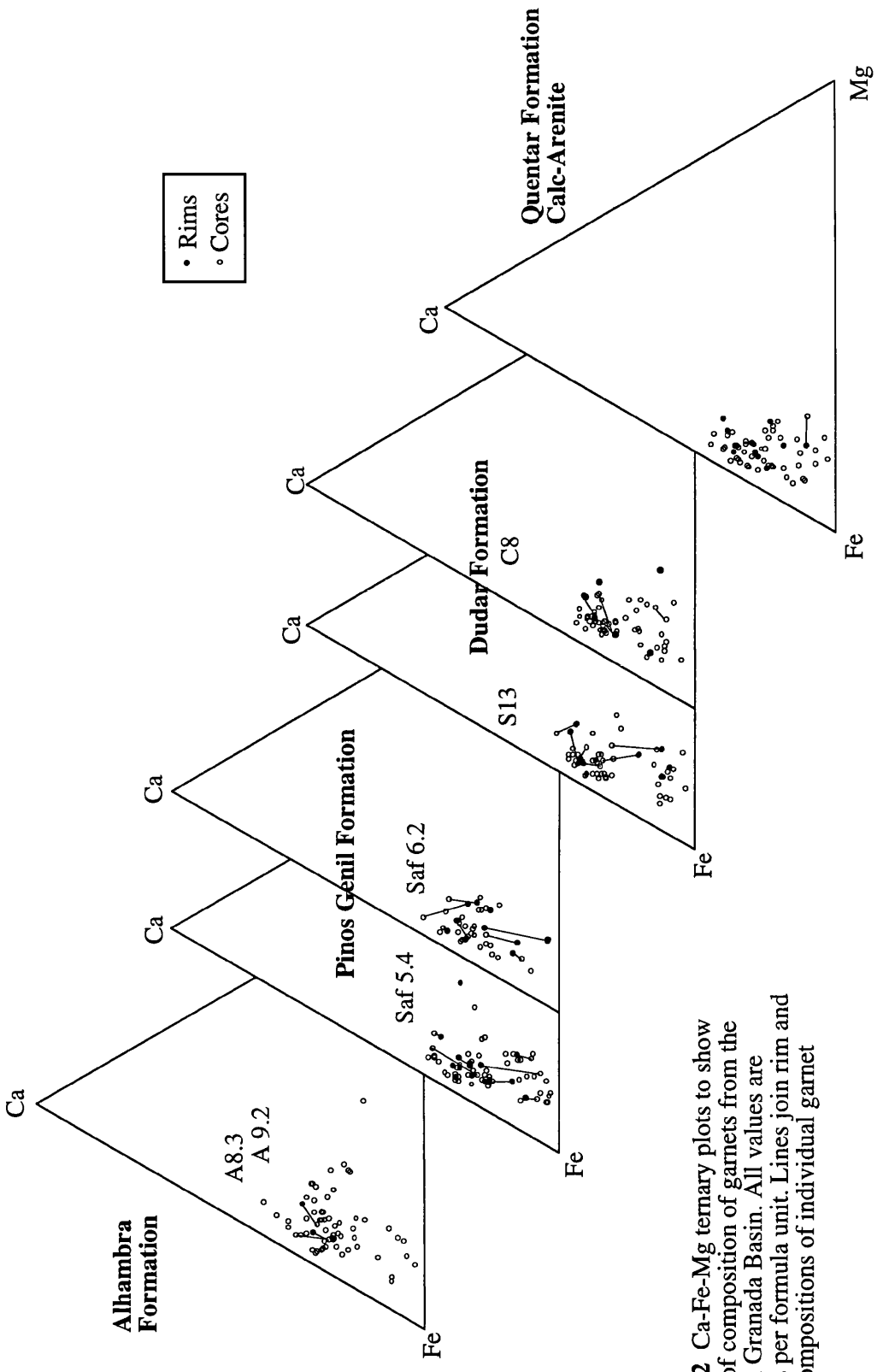

Fig. 6.2 Ca-Fe-Mg ternary plots to show range of composition of garnets from the eastern Granada Basin. All values are cations per formula unit. Lines join rim and core compositions of individual garnet grains.

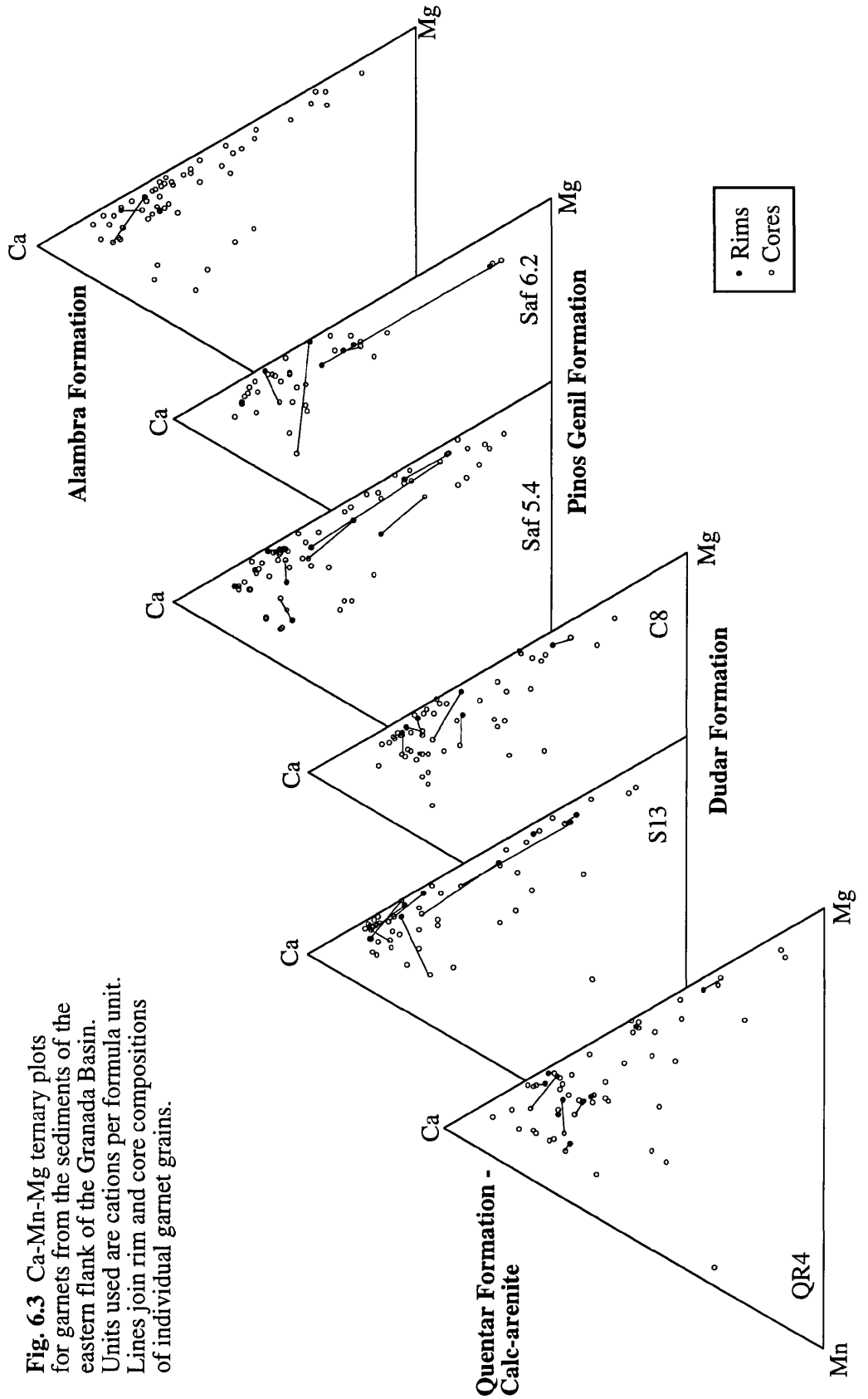

Fig. 6.3 Ca-Mn-Mg ternary plots for garnets from the sediments of the eastern flank of the Granada Basin. Units used are cations per formula unit. Lines join rim and core compositions of individual garnet grains.

6.6.1 Garnet

Garnet was chosen for detailed study because it is common in the sediments (**Fig 6.1**), and is chemically variable. Previous studies of garnet stability also exist allowing comparisons. Garnet abundance also shows a marked decrease into the more weathered and altered Alhambra Formation, suggesting that selective removal of certain compositions of garnet (like Mortons (1985) Ca-rich garnets) has taken place, and may be the mechanism through which garnet abundance decreases.

Several hundred grains were analysed and the results are listed in **Appendix 4** Ternary diagrams are employed to present the compositions, using combinations of the common garnet type end member elements; Ca, Mg, Mn and Fe. **Fig. 6.2** presents Ca-Fe-Mg ternary plots for 6 selected samples, one from the Quentar Formation, two each from the Dudar and Pinos Genil Formations and two combined from the Alhambra Formation. The units used throughout are cations per formula unit. All garnets are iron rich almandines.

There is little apparent difference in composition indicated between garnets from different formations. There is a common grouping that becomes clearer in younger formations, around 25% Ca content, but the general range of composition remains very similar. However, the grouping evident in the Alhambra Formation Garnets appears slightly more Ca rich.

In **Fig. 6.3** the dominating influence of Fe is removed and the garnets are plotted with Ca-Mn-Mg end members on the ternary plot. Ca dominates the composition, and the lack of solid solution between Mn and Mg is clear by the curved plotting area and the rim-core tie lines on the plot. Again no apparent shift or reduction in range of composition of these detrital garnets is seen between Formations.

It is clear that the observed reduction in garnet numbers in the Alhambra Formation due to weathering or abrasion has not been achieved by the selective removal of a particular composition of garnet, but rather has removed garnets of all compositions. Also the chemical alteration processes that produced the observed surface features, detailed above, has not selectively removed garnets either. However, the following section presents a discriminant function analysis of the Cation-per-formula -unit data used to construct the ternary plots presented here. This was conducted in order to clarify any compositional trends that may be too subtle to be revealed by the visual interpretation of the plots alone.

6.6.2 Discriminant function analysis of garnet compositional data

Discriminants analysis distinguishes the presence of only three groups caused by the compositional variation of the detrital garnets from the Granada Basin. Three discriminant axes were determined. **Table 6.3** presents the results of the discriminant analysis. Axis Can 1 is the most discriminating with 67% of the discriminating power over the data. The total canonical structure reveals that the crucial variables in discriminating groups along Can 1 are mainly Fe, and to a lesser extent Mg. **Figure 6.4** plots the calculated values of Can 1, 2 and 3 for each sample. It can be seen that there is no clear separation of any formation possible based on garnet composition. Most samples cluster around similar values of discriminant function. For values of Can 1 the Alhambra Formation samples appear be the most distinct, having the widest

	Can 1	Can 2	Can 3
Eigenvalue	0.1692	0.0793	0.0035
Proportion	0.6714	0.3146	0.0140
Cumulative	0.6714	0.9860	1.0000

Total canonical structure

	Can 1	Can2	Can 3
Ca	-0.373603	0.707966	-0.054814
Fe	0.832568	-0.127877	-0.130440
Mg	-0.524428	-0.004429	-0.094253
Mn	0.133250	0.373752	0.914542

Table 6.3 Results of canonical discriminants analysis of electron microprobe analysis of detrital garnets from the Granada Basin Sandstones. The data used was cations per formula unit for the four elemnts listed above.

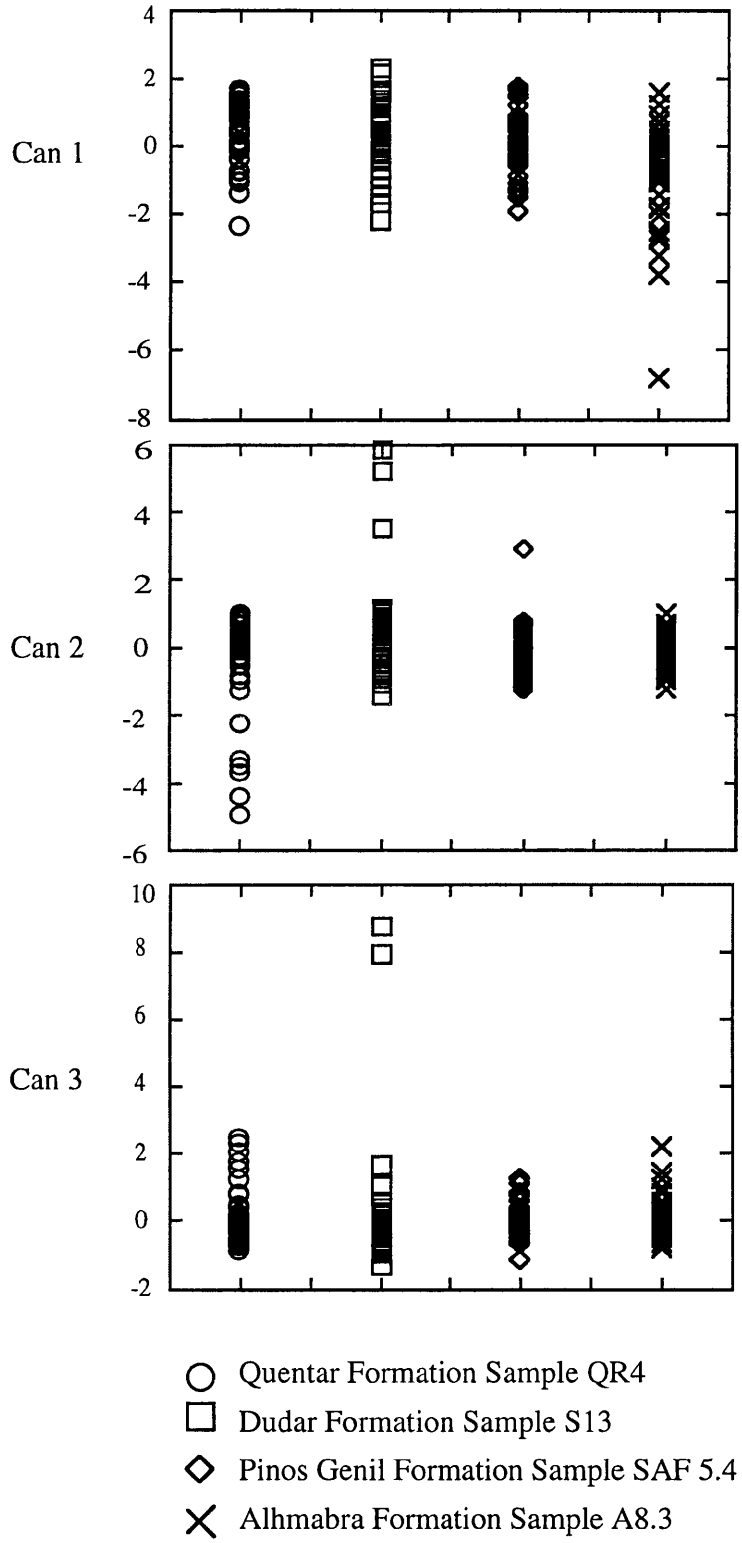

Fig. 6.4 Graphs to show the variation in calculated discriminant values Can1, 2 and 3 for detrital garnet compositions from the Granada Basin.

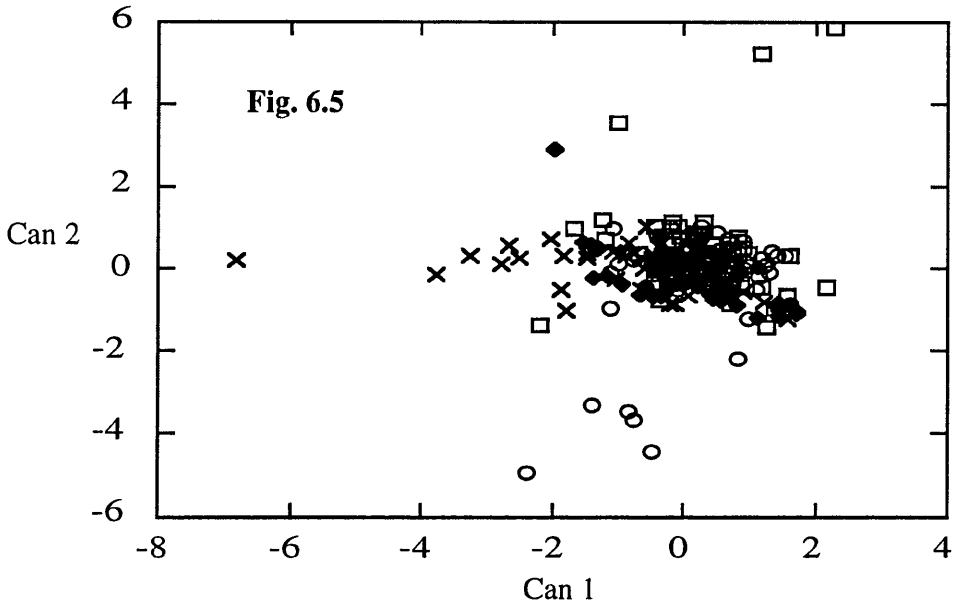

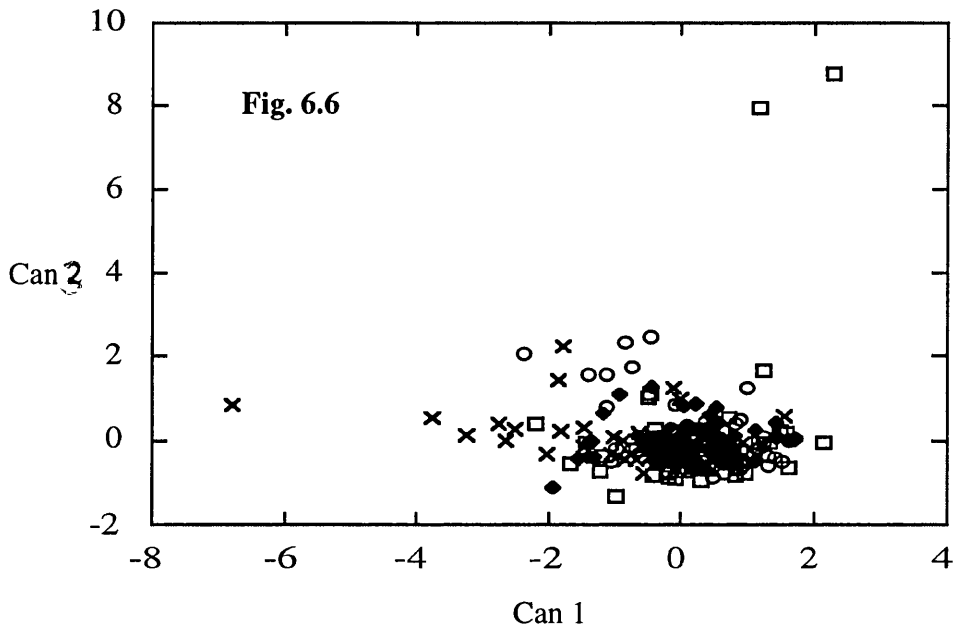

- Quentar Formation, sample QR4
- Dudar Formation, sample S13
- Pinos Genil Formation, sample SAF 5.4
- Alhambra Formation, sample A8.3

Figs. 6.5 and **6.6** showing respectively values of Can1 versus Can 2, and Can 1 versus Can 3. Most samples plot in the same general areas on the graphs but some samples show trends that are distinct for certain formations.

range of values and extending well into the negative value range. Values of Can 2, the second most discriminating axis, distinguish the Quentar and Dudar Formation samples well. According to the total canonical structure this is mainly due to variations in Ca content.

Figure 6.5 shows Can 1 plotted against Can 2, and the separate areas defined by the Quentar and Alhambra Formations in particular. The Dudar and Pinos Genil Formations cannot be separated visually at all on this plot, as even though the Dudar Formation occupies a much larger area the Pinos Genil Formation samples plot within this. Most samples however plot in the same general area. Differences exist but they are relatively small and do not result in clear separation of the formations. **Figure 6.6** shows a similar plot of Can 1 against Can 3. The main distinctions visible are between the combined Dudar and Pinos Genil Formations group and the Alhambra Formation. These differences seen on these plots suggest the presence of three groups; the Quentar Formation, the Dudar and Pinos Genil Formations and the Alhambra Formations.

Despite the indicated discriminating power of Can 1 being the greatest the clearest indicated distinction possible when values of discriminating functions are plotted for individual samples is observed along Can 2. This distinction between formations is due to variations in Ca content of the garnets, and is perhaps just visible on **Fig. 6.3**. However, these variations are not great and must be interpreted with some caution.

6.6.3 Epidote

Epidotes were analysed for compositional variation because they increase significantly in younger sediments to become the most important heavy mineral in the Alhambra Formation. They are also chemically variable, and normally expected to be less stable than even garnet, so should show more pronounced changes in compositional range when subjected to weathering or diagenesis. However, the increase in abundance is contrary to this model of epidote stability, and surface features record only abrasion damage, with no chemical alteration being obvious. Compositional patterns in epidotes may show an increasing abundance of relatively unstable grains.

The main variation in epidote composition is in Fe and Ca contents. **Figure 6.7** shows such a Ca vs. Fe bi-variant plot with compositional fields defined for epidote group minerals (data used from Deer et. al. 1986). The samples from the Granada Basin do not plot within these fields, but generally between the epidote and clinozoisite fields. The samples in **Fig. 6.7** are from the Quentar Formation calc-arenite deposit. Compared with the Dudar, Pinos Genil and Alhambra Formation samples plotted on **Fig. 6.8**, they are more Ca rich. In **Fig.6.8** the three formations are largely inseparable, so why should the Quentar Formation, with silicate detritus derived from the same source, be any different? Perhaps source characteristics changed, but this is unlikely. However, the populations are distinct, thus indicating the change is not merely a reduction in the range of composition, precluding selective removal. The composition of epidotes has changed quite distinctly, suggesting source control.

Between the three siliciclastic formations epidote compositions do not show a significant change, and the formations all overlap. The range of Fe content increases however, extending in to Fe poor compositional ranges in the younger formations. Ca content shows no

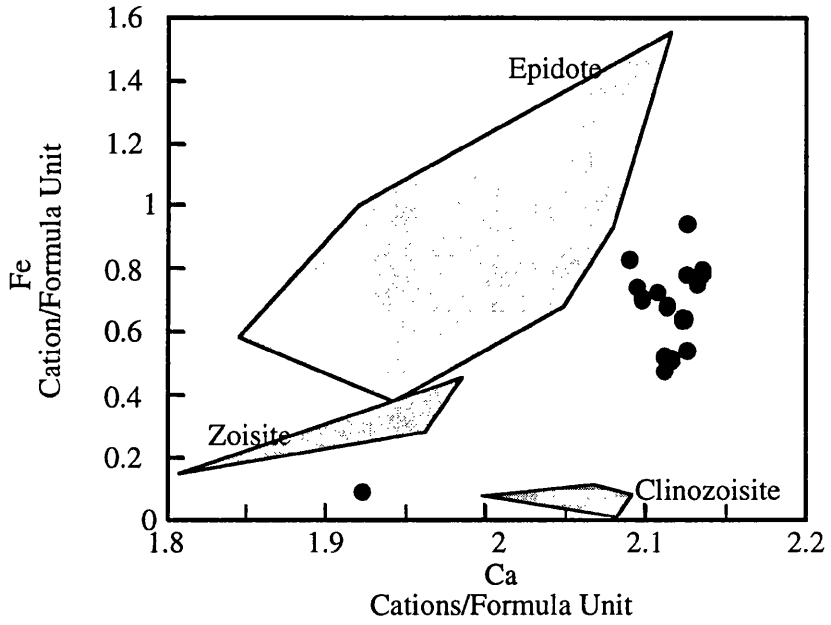

Fig. 6.7 Compositional fields of epidote group minerals, data from Deer et.al. (1986). Data for detrital epidotes from the Quentar Formation plotted also.

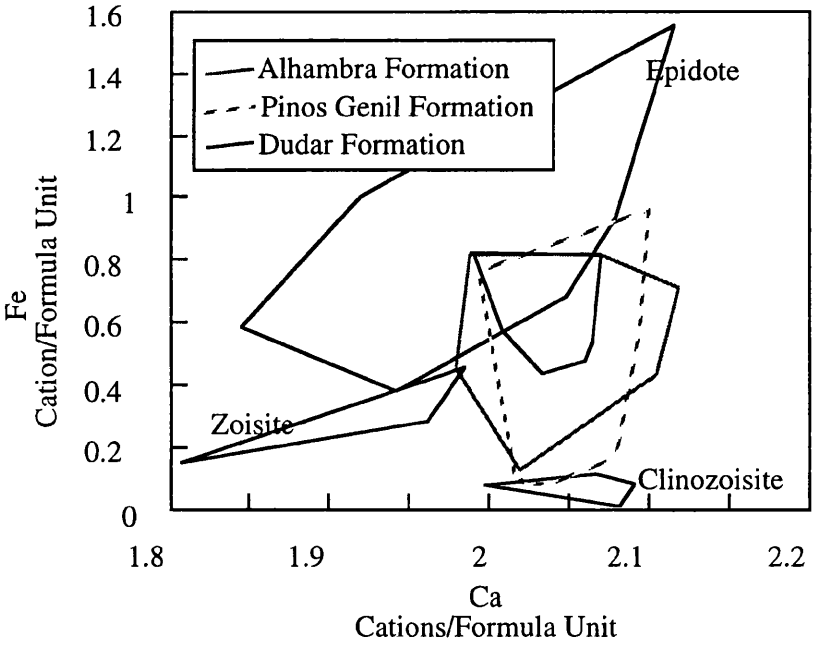

Fig. 6.8 Composition fields for epidote group minerals and compositional fields for detrital epidotes from the eastern flank of the Granada Basin. Other than an expansion in the range of Fe content, little difference can be discerned between formations. The younger formations have more Fe poor epidotes, suggesting the possible removal of Fe epidotes during weathering and reworking abrasion.

change of this sort. The increase in epidote abundance accompanies an increase in compositional range, and not an increase in abundance of all compositions. It also indicates that source characteristics for epidotes in the three youngest formations change.

6.6.4 Tourmaline

There are few exceptions to the dearth of compositional data available for tourmalines (e.g.. Power 1968, Morton 1991, Deer et.al. 1986 and refs. therein). This paucity stems from the complex chemistry of tourmaline and the difficulty in measuring boron. Only recently have boron measurements been possible using an electron microprobe. The potential use of tourmaline in provenance studies is great, due to its chemical variability, combined with its great chemical and physical stability.

The purpose of analysing detrital tourmalines from the Granada Basin sediments was not only to see if weathering may have had an affect on compositional range, but to document the composition of tourmaline from the Internal Zones of the Betic Cordillera. The sediments of the Granada Basin provide a convenient way of obtaining a diverse and well mixed sample from the Internal Zones. Sediments provide a useful compositional probe into source terranes at convenient sampling scales.

The major compositional variation in tourmaline is in Mg and Fe contents. **Fig. 6.9** presents a FeO-MgO bi-variant plot with areas defined for different tourmaline varieties using data from Deer et. al. (1986). Superimposed on these fields are data for tourmalines from the Dudar, Pinos Genil and Alhambra Formations. They plot in a linear trend mostly within the dravite field. A few samples plot in the area near the schorl field, defining the trend passing at higher FeO values than the schorl field. Dravites are associated with metamorphic rocks, but also metosomatic assemblages (Deer et. al. 1986). The source of tourmaline is discussed above in **Section 6.3.1.**

The Dudar Formation samples appear to have slightly lower contents of FeO and slightly higher MgO. **Fig. 6.10** shows data for samples from the Quentar Formation calc-arenite. They show generally higher FeO and lower MgO values compared with younger deposits, and the extended trend above 10 wt% FeO is well defined. The Quentar Formation samples correspond more closely to the composition of the Pinos Genil and Alhambra Formations than to the Dudar Formation. Despite these differences the general range of composition of tourmalines in each formation is very similar.

The differences seen are difficult to explain by weathering, or indeed source changes. The range of grain sizes analysed was the same throughout. The tourmalines deposited in the Quentar Formation should be the same as those in the Dudar Formation. However, slower deposition, even in shallow marine conditions, from a more subdued topography in Quentar Formation times may have resulted in weathering loss through the greater time spent in transit and deposition. The Pinos Genil and Alhambra Formations share a similar range of composition to the Quentar Formation, and are more weathered than the Dudar Formation. It is only the Dudar Formation, rapidly deposited, immature first cycle detritus related to sudden uplift and erosion of the Internal Zones in the Sierra Nevada, that has a slightly different range of tourmaline composition. This range overlaps with the other formations. Therefore the range

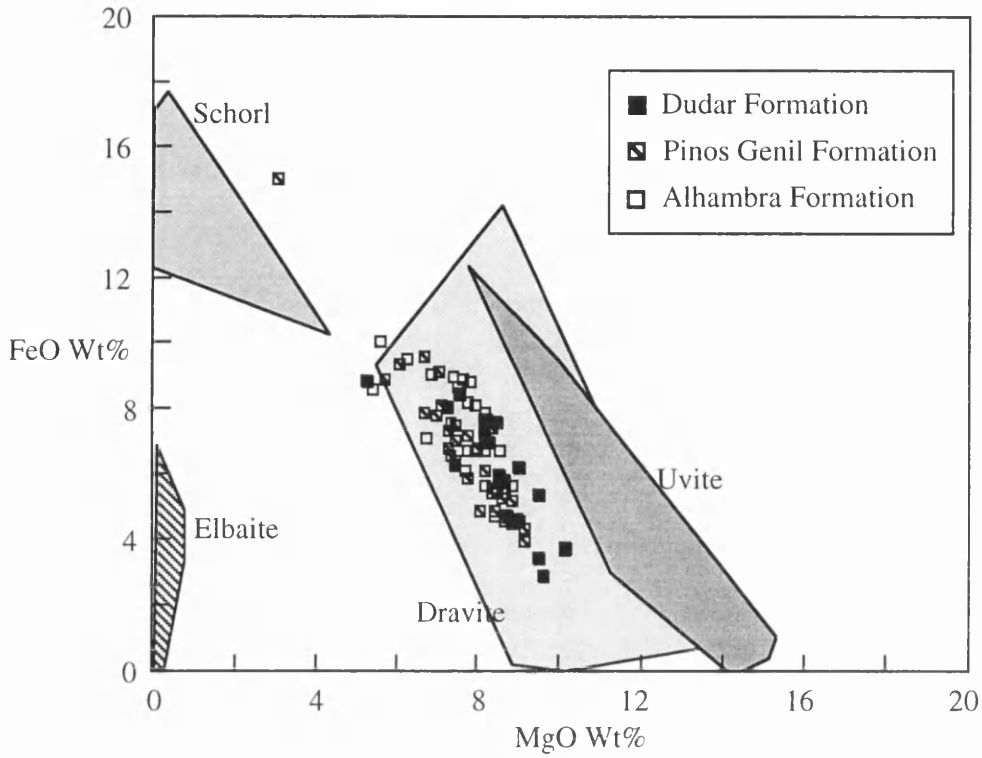

Fig. 6.9 Plot of Wt% FeO vs MgO, using data of Deer et. al. (1986) to define compositional fields for tourmaline varieties. Also plotted are all the analyses of detrital tourmalines from the deposits of the eastern flank of the Granada Basin. No significant separation can be seen between samples from different formations.

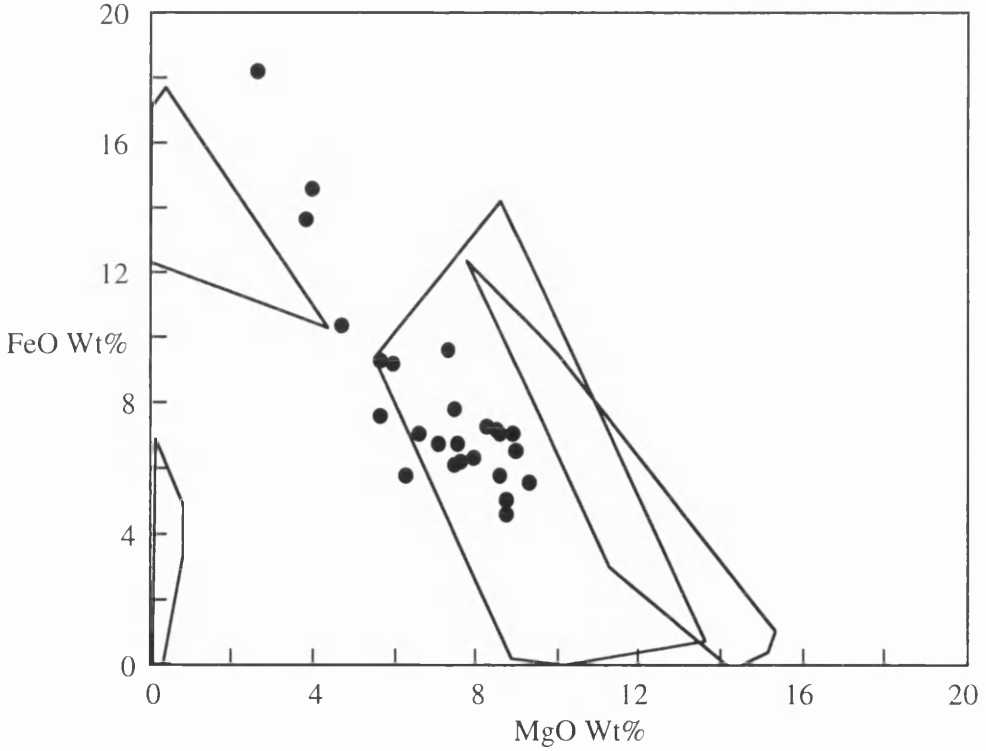

Fig. 6.10 Wt% FeO vs MgO for detrital tourmalines from the Quentar Formation. Compared with the younger deposits in **Fig. 6.6** above, tourmalines are more FeO rich.

seen in the other formations could be a differentiated product of more intense weathering of the same source. This implies that MgO rich tourmaline are marginally less stable than FeO rich -MgO poor tourmalines. However, the Dudar Formation sample analysed here does not contain any grains with the high FeO content seen in the Quentar and other Formations. This suggests less differentiation of a distinct compositional range and more the possibility of a different source composition. However, the distinctions possible here are very tentative and the differences seen are very small. Further work is needed before use as a provenance tool in the Granada Basin.

The quantity of tourmaline increases rather than decreases into the younger formations. Paradoxically *this is because of weathering*, as other less stable minerals decrease in quantity the proportion of tourmaline and other stable heavy minerals increases. Weathering does affect stable minerals, albeit more slowly than for other minerals. This means that compositional changes are conceivable, and that certain compositions of stable minerals are possibly more resistant to destruction than others. So it is perhaps possible that FeO poor MgO rich tourmalines are marginally less stable than FeO rich MgO poor varieties, as suggested above.

Similarly to epidote the increased proportions are not due to an input of new Compositionally different tourmalines, but to an increase across the range of composition. This further emphasises the lack of a change in source during deposition.

6.7 Summary and Conclusions

This study of the heavy minerals from part of the Granada Basin highlights complex controls on mineral occurrence and composition. Apparently contradictory patterns are common in these sediments.

Patterns of enrichment and depletion of heavy mineral species are generally consistent with established schemes of mineral stability. Garnet and amphibole decrease in proportion, while tourmaline, zircon, rutile and apatite increase significantly in proportion in the Alhambra Formation compared with the Dudar Formation. Epidote increases significantly in the Alhambra Formation, suggesting that it may be a relatively stable mineral in the prevailing depositional environments in the Granada Basin, contrary to established stability schemes.

This increase in mineralogical maturity is consistent with the increased pre and syn-depositional weathering and alteration that the Alhambra Formation exhibits. However, heavy mineral proportions of total framework composition (see Chapter 4) increase in the Alhambra Formation, indicating a decrease in maturity. Other indicators show that lithic grain proportions also increase in the Alhambra Formation indicating a decrease in framework mode maturity. However, weathering and alteration, perhaps accentuated by sediment reworking, acts on all grains still, and clearly had a predictable effect upon the heavy mineral population. The continued break-down of grains, suggested as a mechanism for decreasing maturity in the Alhambra Formation has not maintained a fresh heavy mineral population. Even so, this evidence of increased maturity and abundance of stable heavy minerals is the clearest yet to support a recycling model for the source of the Alhambra Formation. Despite the break-down of lithic clasts the stable heavy minerals are likely to survive recycling thus increasing their

concentration in younger sediment.

Surface features on heavy mineral grains indicate the action of chemical and physical alteration processes. Samples from the Dudar Formation show the least physical abrasion, but do show mamilliations, etch pits and developing facets associated with chemical attack. These features are normally associated with intra-stratal solution effects. Diagenesis is not considered to be an important factor in the alteration of the Granada Basin sediments, so these features may have formed in the transport environment, or at the outcrop in the source region before erosion. However, the time scale involved for their formation is important, and residence in buried sediment has the most likely time scale for alteration like this. Etching has probably taken place in an intra-stratal location, but has not proceeded to extremes.

Etched grains are also seen in the Alhambra Formation, but the physical abrasion of these sediments has been the greatest. Physical abrasion increased through time as the depositional environment changed from marine to terrestrial, alluvial deposition. The etching seen is in some grains more extreme than in the Dudar Formation. Some grains may have been etched in a previous deposit and subsequently re-eroded to be incorporated in the Alhambra Formation, as they have a battered abraded appearance, but with etch features also.

The presence of grains with a range of alteration features, including unaffected grains is problematic. If intra-stratal solution were the main control of chemical alteration features, then all grains may be expected to have similar degrees of alteration. The best explanation for this is a variation in pore fluid composition and presence.

Epidote shows little or no chemical alteration features, only smooth surfaces or irregular abrasion damage. This supports the assertion, derived from the increase in proportion of epidote in the Alhambra formation, that epidote is a relatively stable mineral, in the prevailing erosional and depositional environment.

The chemical and physical alteration features observed provide a mechanism for the changes in population composition seen in the younger Pinos Genil and Alhambra formations. Intra-mineral species composition may also be expected to show a maturing trend to increased concentrations of mineral compositions that are more resistant to alteration by weathering, abrasion or intra-stratal solution processes. Electron-microprobe studies document the compositional range of garnet, epidote group minerals and tourmaline. For each mineral, little difference of compositional range can be seen except in detailed circumstances.

No significant difference in the compositional range of garnet is seen between samples from the different formations at this edge of the Granada Basin. Weathering and intra-stratal chemical alteration have not singled out a particular composition of garnet for preferred destruction. Epidote minerals show a shift from Ca rich types in the Quentar Formation calc-arenite, to more Ca poor types in the younger siliciclastic formations. A change in source characteristics is the likely mechanism for this, not sedimentary dynamics, perhaps related to the unroofing of the Nevado-Filabride complex. More Fe poor epidotes are seen in the Pinos Genil and Alhambra Formation, an expansion of compositional range, which must be related to source. Tourmaline compositions also show no overall differences between the formations. However, the Dudar Formation contains samples with the highest MgO contents. As this

formation is the least weathered, most rapidly deposited formation, this range of composition may represent the initial source compositional range. The conclusion, (very tentative) is that MgO rich tourmalines are less stable than MgO poor-FeO rich varieties in the weathering environment prevalent during deposition of the Pinos Genil and Alhambra Formations.

For the garnets, weathering and abrasion have not affected the compositional range, though they probably have resulted in the observed decrease in garnet content. Mechanical breakage, where grains split, is the likely cause of reduced garnet content, and would not necessarily favour the removal of a particular composition of garnet.. For the epidote group and tourmalines, proportions increase, despite increased weathering and chemical alteration. This is due to their greater relative stability against mechanical degradation compared with garnet. This is also due to weathering, but with the opposite result compared to the garnets. But for epidote, the increase in proportion has been achieved with an expansion of the compositional range indicating a probable change in source. For tourmaline the expansion in numbers is achieved with no increase in compositional range. However, weathering has not biased the internal compositional ranges of individual minerals, despite being the likely determinant of changes in relative heavy mineral abundances.

A complex interplay of sediment dynamic processes, dependant upon mineral stability, and detailed small scale changing source characteristics has generated the observed heavy mineral population. This illustrates the variation in provenance signature that can be generated, even in a very proximal setting, where provenance should be clearest and most unambiguous. Perhaps the proximity of the source imparts some of its own variability on the sediments, in a very detailed fashion. Mixing has taken place, but has not proceeded to the point where each sample becomes an average, the type of which characterises most provenance studies, involving sediment composition.

7. Isotopic Age Dating

7.1 Introduction

In this chapter the results of dating experiments carried out on detritus from the Granada Basin sediments and source region rocks in the Sierra Nevada are presented. This introduction discusses ideas concerning isotopic dating and its use in provenance and in constructing tectonic synthesis.

Dodson (1973) developed the concept of the closure temperature, the temperature in a mineral below which isotopic diffusion stops. Temperature evolution within a sample, or terrain, can be related to depth of burial estimates using assumptions for geothermal gradient. This can then be used to describe the uplift history of the region, and tectonic syntheses can be developed (e.g.. Dempster 1985, Copeland et. al. 1987, Wagner 1977, Holm 1993, Zeitler et. al. 1989, Dallmeyer 1989).

Sedimentary basins are important in developing tectonic models because each layer of sediment has a particular age of deposition, a time correlated record of the changing composition of the source area. A record of source uplift is potentially preserved in a basin that lies adjacent to an uplifting region.

The conglomerate clasts and mineral grains in a sedimentary basin not only contain a record of rock types in the source. They also carry pressure, temperature and age date information, related to uplift. Using the depositional age of the sediment and combining it with age dates of detritus is a powerful way of detailing source cooling and uplift history, and linking it with sedimentary deposition.

The use of isotopic dating in provenance work has been largely restricted in application to conglomerate clasts, for the obvious reasons that lithology is easily recognised and tied back to source (for example Cuthbert, 1991, Haughton, 1988). However, conglomerate clasts are limited to relatively proximal locations, and until recently particle size limited the dating of detritus to conglomerates, leaving the potential use of sandstones for such provenance work untouched.

However, some previous studies have used sand-sized detritus as the focus for age dating work. Fitch et.al (1966) applied the K-Ar technique to detrital micas from the Triassic in Cheshire, and Mitchell and Taka (1984) developed the theme, looking at micas from more widespread Triassic sandstones.

Muscovite is the ideal candidate for age dating of sedimentary detritus, as it is resistant to break-down and alteration of K-Ar systematics, is common in sedimentary rocks (even those distally deposited, and recycled), but most of all carries a strong source age signature. Even so, the studies of Fitch et. al. (1966) and Mitchell and Taka (1984) suffered because of bulk sample analysis. The techniques available did not allow detailed clarification of different

contributions from sources with differing ages, because they could not analyse individual grains. Their age dates are averages, that certainly have meaning, but tectonic inferences, and palaeogeographic reconstructions are necessarily more general and 'average' than they might be if individual age contributions from all possible sources could be distinguished.

7.2 ^{40}Ar-^{39}Ar Laser Analysis

The development of the laser ablation technique for 40Ar-39Ar age dating has allowed very small samples to be analysed, overcoming the problems with bulk analysis outlined above. Fortunately for the provenance worker individual sand grains can now be analysed, and even parts of sand grains (e.g.. De Jong et. al. 1992). The potential for provenance discrimination and tectonic and palaeogeographic reconstruction is enormous. Muscovite is the preferred mineral for analysis but biotite, feldspar, amphibole and even tourmaline are or could be employed. Kelly and Bluck (1989 and 1992) employed 40Ar-39Ar dating on muscovites from turbidites of the Southern Uplands of Scotland. From the data they implied variations in sedimentary environment controlling sediment dispersal and a source with ages between 458 to 502 Ma. Copeland and Harrison (1990) analysed detrital K-Feldspar and muscovite grains from the distal Bengal fan. Ages range from 0-18Ma, and each sediment sample contains grains with ages equal to the depositional age of the sample. They infer episodic uplift of the Himalayas throughout the Neogene.

The application of the technique has only begun but shows great promise in adding greatly to provenance investigations, especially of recycled and distally deposited sediments, especially in laterally displaced orogens, such as the Caledonides.

7.3 Objectives and Layout of Chapter 7

The original intention was to apply the ^{40}Ar-^{39}Ar laser ablation technique to detrital minerals, mainly muscovites, taken from Neogene sediments from the Eastern Granada Basin, in order to fingerprint the cooling and uplift of the sediment source in the Internal Zones of the Sierra Nevada. The uplift and extension of the source could be constrained in relation to basin formation. This is not only significant for the history of the Betic Cordillera, but also for the timing of Sierra Nevada core complex extension, unroofing and sedimentation.

The sedimentary record provides an additional constraint upon tectonic movements and uplifts, especially marine sediments as deposited around the Sierra Nevada, that facilitate very precise palaeontological dating. Syn-tectonic sedimentary rocks are often unavailable in the core complexes so far examined in North America, and where present are usually terrestrial, so of limited stratigraphical use.

The Internal Zones are blessed with being surrounded by syn-tectonic sedimentary basins that contain significant thicknesses of marine sediment, that can offer tight biostratigraphical constraints. These sediments can limit the time of extension and basin formation and also the rate of uplift, depending upon the coincidence of detritus cooling ages and depositional age of the sediment. The range of ages is crucial in this respect, but may be affected by sedimentary processes: recycling of sediment may broaden the distribution of ages in the sediment. Sediments in the Granada Basin offer the chance to evaluate the effects of

weathering and/or recycling upon the signature of uplift generated by the Sierra Nevada and stored in the ages of detritus in the sediments, as well as constraining the tectonic style and timing of core complex unroofing of the Internal Zones. The foregoing chapters detail compositional trends in the sediments in the eastern Granada Basin, and the effects of weathering/recycling upon composition. This provides a context for the understanding of detrital dating especially the possible loss of provenance information through reworking.

Unfortunately, technical problems prevented the extensive application of the ^{40}Ar-^{39}Ar laser ablation technique to detrital materials from the Granada Basin. The study was extended to include the use of the K-Ar dating technique on muscovites from conglomerate clasts and basement source rocks. Rb-Sr dating was also applied to obtain whole rock-muscovite ages for many of the conglomerate clasts and in-situ Internal Zone lithologies. The intention was to combine Rb-Sr ages with K-Ar and ^{40}Ar-^{39}Ar ages to establish a time-temperature (t-T) path for the Internal Zones in the Sierra Nevada. The t-T paths for the conglomerate clasts are further constrained by the depositional ages of the sediment they reside in. Thus the utility of dating sedimentary detritus is highlighted by extending the t-T pathways to surface temperatures.

The next section reviews isotopic dating efforts in the Betic Cordillera, as related to models of palaeogeographical and palaeotectonic evolution. This is to provide some context for the discussion of the data produced for this thesis. Some of the interpretation and conclusions reached would be unclear without this context. After this the age data is presented, ^{40}Ar-^{39}Ar first, then K-Ar and finally Rb-Sr. The Rb-Sr age dating is presented in conjunction with the previously presented data, because the conclusions reached from the analyses are dependant upon the combinations of dates on individual samples. Following this a synthesis of data is attempted with regard to cooling and uplift within the source region of the Granada Basin in the western Sierra Nevada, discussing fully the implications for models of Betic evolution. Finally conclusions are presented.

7.4 Isotopic Age Dating in the Betic Cordillera.

Considering the interest in the Betic Cordillera, and advances in understanding of the area in the past thirty years, there appears to be a paucity of isotopic age dates that place tectono-metamorphic and sedimentary evolution in a quantitative time framework. Only relatively recently have important beginnings been made in establishing an isotopic chronology for the orogen.

Something of the early history of the Betics is preserved in whole-rock ages of igneous intrusions. In the eastern Betics, in the Sierra de Los Filabres, tourmaline granite gneiss and meta-granite from the Mulhacen Complex of the Nevado Filabride, have Rb-Sr whole rock isochrons with ages of 269±6 Ma, and 240±10 Ma (Priem et. al. 1966), interpreted as the time of intrusion. This places a maximum age on the subsequent metamorphic evolution of the Nevado Filabride, and indicates a long history of tectonism stretching from the lower Permian, and confirming *at least* a Carboniferous age for the deposition of the sedimentary protoliths to the meta-sedimentary rocks that are intruded. Priem et. al. (1966) also obtained Rb-Sr and K-

Ar ages from muscovites from their granite-gneiss that cluster around 13-14 Ma. This indicates a much more recent isotopic and, by inference, thermal evolution. Most recent cooling has taken place a considerable time after the beginning of the tectono-magmatic evolution of the Mulhacen complex. This suggests the superimposition of Oligo-Miocene metamorphism or thermal resetting on older metamorphic evolution.

Hebeda et. al. (1980) dated unmetamorphosed relicts of basic intrusives, again from the eastern Betics. They obtained a whole-rock Rb-Sr age of 146±3 Ma, again interpreted as the date of intrusion. This places a constraint upon the timing of the thrusting that superimposed the Alpujarride and Nevado-Filabride complexes, suggesting it took place no earlier than the late Jurassic.

Dating of the main metamorphic evolution has concentrated on distinguishing distinct tectonic phases, as recognised in P-T paths exemplified by Bakker (1989) and Puga et. al. (1989) for the Mulhacen complex. Early high pressure metamorphism is recognised. Monie et. al. (1991) obtained an ^{40}Ar-^{39}Ar age from distinctive high pressure amphibole of the Mulhacen Complex of 48 Ma, that they interpret as dating the end of the high pressure evolution. Puga et. al.(1989) report K-Ar ages from muscovite of 60 Ma, and from chloritoid of 85 Ma in rocks of the Mulhacen Complex of the Sierra Nevada, and De Jong et. al. (1990) present dates from Mulhacen Complex 'main phase' deformation micas of 40.6 and 66.1 Ma. All these dates indicate cooling post the first, high pressure, metamorphic peak in the Nevado Filabride, which has been related to subduction during the latest Cretaceous - earliest Paleocene. De Jong et. al. (op. cit.) also present tourmaline K-Ar ages of 116Ma and 80-85Ma, though the meaning of these is not clear, other than to suggest that metamorphism extended over a long time period, or just a possible time of formation of tourmaline.

Later resetting of ages is clear in many areas. As already mentioned the granite-gneiss of Priem et. al. (1966) produced K-Ar and Rb-Sr ages of 12-13 Ma, despite an intrusion age of 269 Ma. Also from the Mulhacen complex of the Nevado Filabride Monie et. al. (1991) analysed hornblende and muscovite. They obtained ages of 24.6 Ma and 16 Ma respectively. De Jong et al. (1990) report K-Ar and Rb-Sr ages from the Mulhacen complex of around 13-15 Ma, suggesting a very young history, despite P-T paths suggesting decompression from 37Km depth since the early Cenozoic. They infer significant reheating related to extensional tectonics that introduced a transient mantle heat source to the base of the crust. The 13-15 Ma ages date cooling post this event. Slow cooling is inferred by De Jong et. al. as the emplacement of mantle material is dated at 22 Ma (Loomis 1979 and Priem et. al. 1979), from the aureoles of the Ronda peridotite masses. Puga et. al. (1989) also identify a late heating event from mineral paragenesis in the Mulhacen Complex of the Sierra Nevada, but it accompanies an increase in pressure, perhaps related to thrusting. With this event they associate an age of around 20 Ma from K-Ar on muscovite.

De Jong et. al. (1992) identify periods of reheating leading to age resetting from ^{40}Ar-^{39}Ar age spectra and laser spot ages of muscovites, from the Mulhacen Complex of the Sierra de los Filabres in the eastern Betics. Laser spots in the centre of a single main phase muscovite record ages of 30Ma interpreted as placing a minimum age on the cooling post the main

metamorphism. The edge of the same grain produced ages around 25 Ma, indicating resetting by volume diffusion of Ar, caused by reheating at this time due to extensional tectonics. They also obtained ^{40}Ar-^{39}Ar age spectra with plateaus of 14 and 17 Ma, and low temperature release ages below this, at between 10 and 15 Ma. De Jong et al. (1992) suggest resetting of older Oligocene cooling ages of around 20 Ma at three times; 17-19 Ma, 13-15 Ma and 8-10 Ma.

These ages tie in with the preferred model for Betic tectonic evolution of de Jong et. al. (1992) and van Wees et. al. (1992). The main cooling and resetting seen at around 25 Ma corresponds to extensional tectonism that resulted in the emplacement of the peridotite masses in the Alpujarride nappes of the western Betics. Cooling in these rocks is recorded at 22 Ma (Loomis 1979). These masses are allochthonous thrust sheets within the Alpujarride, possibly overthrusting the External Zones. This implies compression, that may have resulted in the rapid cooling of the rocks in the Alpujarride complex and also in the Nevado Filabride, by the introduction of cool rocks beneath the thrust sheets. The earlier established extensional pattern was inverted and cooled simultaneously. Nappe sealing sediments constrain this to have finished by at least 18-15.5 Ma (Zeck et. al. 1989 and Zeck et. al. 1992). This corresponds to the main cooling age estimated to be around 20 Ma in the Mulhacen Complex. The remaining reset ages correspond to phases of magmatism in basins surrounding the Sierra de Los Filabres (Bellon et. al. 1983) beginning from 15 Ma, but concentrated at 10-12 Ma. Hot fluids may have been circulating that could have partially reset muscovite. This magmatism is related to crustal extension, that occurred during the Serravallian and Tortonian, resulting in the formation of the intramontane sedimentary basins such as the Granada Basin. However, it is limited in extent to the eastern Betics near Almeria.

Fission track constraints suggest a Tortonian cooling for the Nevado Filabride in the Sierra Nevada (Johnson, 1994, pers. comm., and an unspecified conference abstract). Ages from apatites and zircons are concordant, indicating rapid (>100°C) cooling at low temperature ranges (250°-100°C). These ages are near those for the deposition of the coarse clastic sediments in the Granada Basin, in the Dudar Formation, and similar episodes in other basins such as the Guadix and Alpujarre basins. Considering the syn-sedimentary uplift of the eastern margin of the Granada Basin (see Chapter 3), that corresponds also with the sudden influx of coarse sediment sourced in the Nevado Filabride, it seems that these fission track ages are recording the uplift of the Nevado Filabride core of the Sierra Nevada 'core complex'. The unroofing of this core is recorded in the sediments of the Granada Basin. The hanging wall consisted of the Alpujarride Complex with the Granada Basin atop, which slid away, uplifting and extending as the Nevado Filabride rose. However, this late event associated with the unroofing of the Nevado Filabride Complex, is not recorded in the cooling ages of detritus in the Granada Basin, as the source for the sediment in the internal zones had already cooled by the time of unroofing and erosion into the basin.

Cooling patterns in the Alpujarride Complex are alluded to above, and in general indicate very rapid cooling of the complex during the late Oligocene to early Miocene. Monie et. al. (1991) present several ^{40}Ar-^{39}Ar ages. One sample gives an age of 25 Ma that is taken to indicate a minimum age of the end of the high pressure evolution recognised in the middle

Alpujarride nappes. Other ages are around 19 Ma, dating cooling post this main metamorphic climax. Rocks at the detachment between the Alpujarride and the underlying Nevado Filabride were dated too, and gave ages of 16 and 17 Ma, interpreted as dating the end of ductile extension in the Internal Zones. This corresponds with the resetting times in the Mulhacen Complex of De Jong et. al. (1992) around 17-19 Ma with the resetting due to extensional heating.

In the western Betics the thrust units containing the Ronda Peridotite masses have K-Ar cooling ages of around 22 Ma (Loomis 1979, Priem et. al. 1979). Further east Zeck et. al. (1989) obtained WR-Muscovite ages of around 21 Ma from schists and gneisses from the Alpujarride complex. As the closure temperature of muscovite for Rb-Sr is estimated to be approximately 500°C, this indicates a time soon after the metamorphic climax in the area, and further brackets the cooling episode that involved the thrusting of the peridotite masses in the west. Further work by Zeck et. al. (1992) on these rocks combining various geochronometers revealed high rates of cooling, and inferred uplift, in the order of 150-350°C/my and 5-10 km/Ma The data are further constrained by nappe sealing sediments containing an 18-15.5 Ma marine fauna. The Rb-Sr ages obtained are between 18.8 and 22.4 Ma, and ^{40}Ar-^{39}Ar and K-Ar ages of muscovite and biotite are between 18.4 and 20.3 Ma. The close correspondence of these ages indicates very rapid cooling, not only through the closure temperature envelope, but to surface temperatures also, requiring rapid exhumation and removal of up to 10 km of crust in a period of as little as 1 Ma.

Zeck et. al. (1992) attribute this rapid cooling to lithospheric slab detachment, that removed a significant load from the base of the orogenic welt. Isostatic readjustment drove uplift which contributed to high rates of cooling and encouraged tectonic (not erosional) unroofing. There is evidence from seismic tomographic studies for the presence of a low velocity presumably detached lithospheric slab beneath the Betics (Blanco and Spakman 1991) to support this hypothesis. This model of Betic evolution contrasts with the hypothesis of van Wees et. al (1992) of compression-cooling that explains the structural context of the Ronda peridotites. The slab detachment mechanism may however, explain the more recent Tortonian uplift and extensional evolution of the Internal Zones, but not the late Oligocene and early Miocene cooling pathways. Zeck and Andriessen (1992) expand the data set to include fission track ages from zircons from the Alpujarride rocks. They obtained an age of 15-16Ma, which appears to contradict their associated nappe sealing sediment age of 18 Ma. The late cooling rate may also be in question.

Johnson (op. cit.) also presents fission track data from the Alpujarride rocks on either side of the Sierra Nevada in the central Betics. The ages are 12-15 Ma for apatite and 16-20 Ma for zircon. This contrasts with the much younger 7-9 Ma ages for the Nevado Filabride footwall to the core complex beneath the main detachment. This indicates the Alpujarride had cooled earlier than the Nevado Filabride; consistent with their relative structural positions.

The relative cooling pathways of the Alpujarride are important as they constrain the timing of superposition of both complexes. In the Sierra Nevada and central and western Betics the Alpujarride cooled rapidly from around 22Ma to 12Ma depending on location. The

Nevado Filabride in the Sierra Nevada Appears to share the higher temperature cooling ages, but lower temperature cooling ages appear to be younger on the whole. Younger cooling and resetting in the western Nevado Filabride is suggested, indicating a possible diachronaity of tectonism. The P-T paths for the two complexes only appear to converge significantly post the earliest Miocene resetting and cooling event, that involved the emplacement of the Ronda Peridotites (Bakker et. al. 1989). The more detailed evolutionary model of Van Wees et. al. (1992) does not really resolve the detailed differences due to position of rocks. Also, the model for rapid uplift, put forward by Zeck et. al. (1992), is constrained by rapid uplift to the surface, as the nappes dated are unconformably overlain by marine sediments. The model of Van Wees op. cit. does not place the rocks at the surface, and does not account for the final removal of at least 10km of crust post the cooling of muscovite for Ar retention, as they invoke a compressionally driven cooling episode

Summary

In summary, isotopic dating of rocks in the Internal Zones of the Betic Cordillera has highlighted a history of magmatic and metamorphic evolution beginning in the Permian, and reaching a high pressure climax in the late Cretaceous and early Tertiary, perhaps consistent with north-westwards subduction of African crust. The subsequent history has been one of decompression and cooling of rocks now at the surface. A maximum of around 40km of crust has been removed since, presumably by tectonic rather than erosional means, inferred from a lack of sufficient sediment derived from the orogen.

The metamorphic evolution of the various tectonic units has been complex, and plurifacial, suggesting significant differences in metamorphic evolution for separate units within the Alpujarride and Nevado Filabride Complexes, which may indicate that these units were metamorphosed in widely separated locations. The Alpujarride unit exhibits the highest grade of metamorphism in the Betics, up to ecolgitic grade, that contrasts strongly with the low temperature/high pressure metamorphism in the Nevado Filabride. The metamorphic pile is now inverted in the Alpujarride, with the highest grade rocks now structurally above the lowest grade rocks.

P-T paths relate a major reheating event in the Oligocene that is dated at around 25 Ma, caused potentially by extension that introduced hot mantle material to higher levels at the base of the crust. Cooling after this has been related to inversion of the extended crustal section, resulting in the underthrusting of cold rock under hot, and the emplacement of mantle lithosphere bodies in thrust sheets in the Alpujarride Complex. Alternatively uplift has been caused by the removal of a subcrustal root, evidence for a detached subducting slab beneath the orogen is clear (Blanco and Spakman 1991). The removal of such a subcrustal load would allow rapid isostatic uplift , that could have cooled rocks rapidly. Removal of crustal material in this model is achieved by tectonic denudation driven by gravity.

Age data is plotted against closure temperature in **Fig.7.1** for the Alpujarride Complex, and in **Fig. 7.2** for the Nevado Filabride complex. Trends and times of cooling can be

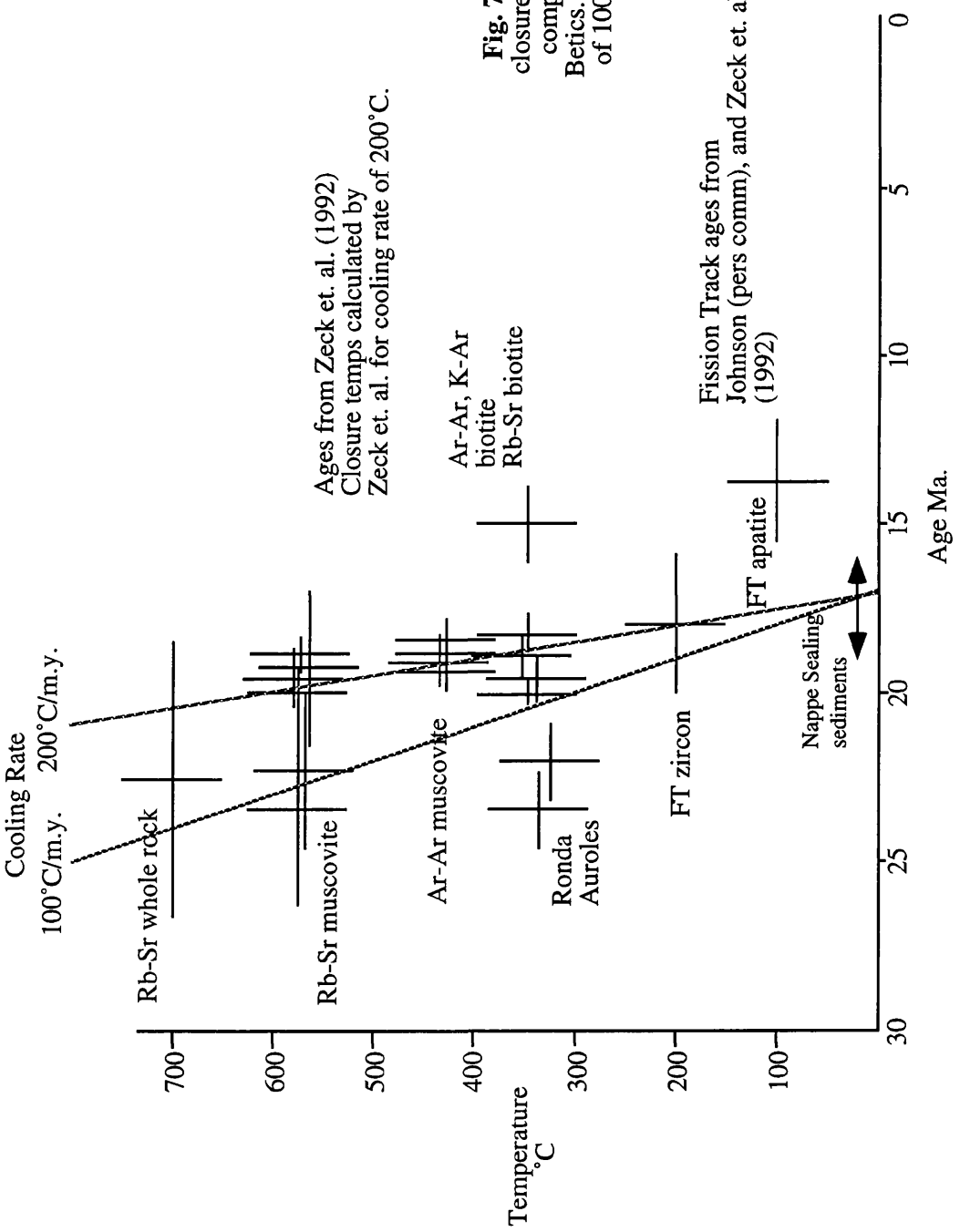

Fig. 7.1 Isotopic age plotted against closure temperature for the Alpujarride complex, in the central and western Betics. This plot suggests a cooling rate of 100-200°C between 25 and 15 Ma.

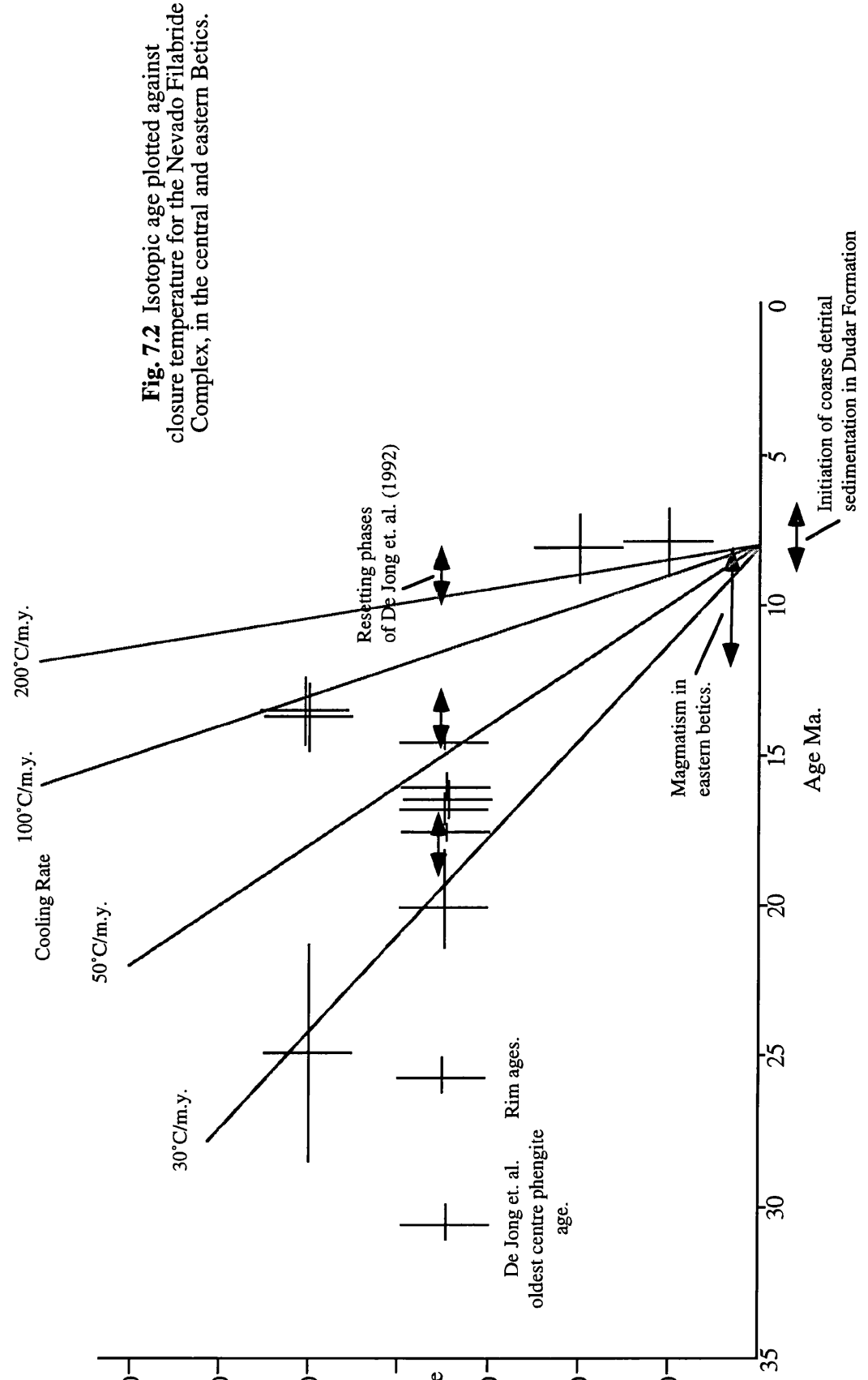

Fig. 7.2 Isotopic age plotted against closure temperature for the Nevado Filabride Complex, in the central and eastern Betics.

highlighted. Lines representing rates of cooling are superimposed on the plots to aid interpretation.

Cooling in the Alpujarride complex is dated at 20-15Ma, and is extremely rapid following the superposition of the two metamorphic Complexes during the last reheating event in the Oligocene. Nappe sealing sediments of 18Ma are marine and testify to limited erosional relief in the Internal Zones. Continued heating events reset Ar isotopic systems in the Nevado Filabride at 17-19, 13-15 and 8-10Ma, the last two events of which marginally postdate magmatism around the Sierra de los Filabres as recorded by Bellon et. al. (1983), and may record the influence of magmatic fluids. Ages from the Alpujarride/Nevado Filabride detachment zone indicate the end of ductile movement at 16-17Ma. Fission track ages constrain the low temperature evolution of the Nevado Filabride in the Central Betics to 7-9Ma, up to 10Ma after the cooling of the overlying Alpujarride Complex. This last event corresponds to coarse clastic sedimentation in surrounding basins linked to the generation of substantial relief in the Internal Zones, as uplift and core complex extension ensued, unroofing the Nevado Filabride rocks in the Sierra Nevada.

7.5 ^{40}Ar-^{39}Ar Laser Probe Dates.

Detrital muscovite separates from the Quentar Formation calc-arenite, and the Dudar Formation fan-delta sandstones were irradiated alongside muscovite separates taken from conglomerate clasts in the Dudar Formation, in preparation for analysis by laser probe. Unfortunately individual detrital grains could not be isolated for analysis, so bulk detrital samples were analysed to obtain an average age. This results in the loss of detailed age information as each muscovite grain could be from a diverse number of sedimentary sources, each with a different cooling history. For the separates from the conglomerate clasts, the ages of all muscovites are presumed to be uniform as the rock will have suffered a consistent thermal evolution, therefore the analysis of several grains together results in little loss of age information.

7.5.1 Suitability of muscovites for age dating

Before muscovites from the sedimentary environment of the Granada Basin were dated, their state of alteration was assessed. This was done by electron microprobe analysis. Traverses were recorded across muscovite grains to check for any unusual compositions, and especially for loss of potassium. **Fig. 7.3** shows values of the ratio K_2O/Al_2O_3 across several grains from a dated conglomerate clast D2, and from a detrital grain from the Quentar Formation calc-arenite. This is similar to the sample characterisation carried out by Kelly and Bluck (1992), except that they use ratios of elemental weight %. Al is a framework element in micas and is not likely to change its absolute concentration by very much, so low K will be revealed as a low ratio. The ratios are quite consistent and show relatively smooth variations. This indicates that the muscovite grains are unaffected by alteration, and most importantly do not seem to have suffered K loss. This is very important as loss of K will affect K-Ar and also ^{40}Ar-^{39}Ar ages. K_2O contents are consistently around 9 to 9.5 wt % in the points analysed.

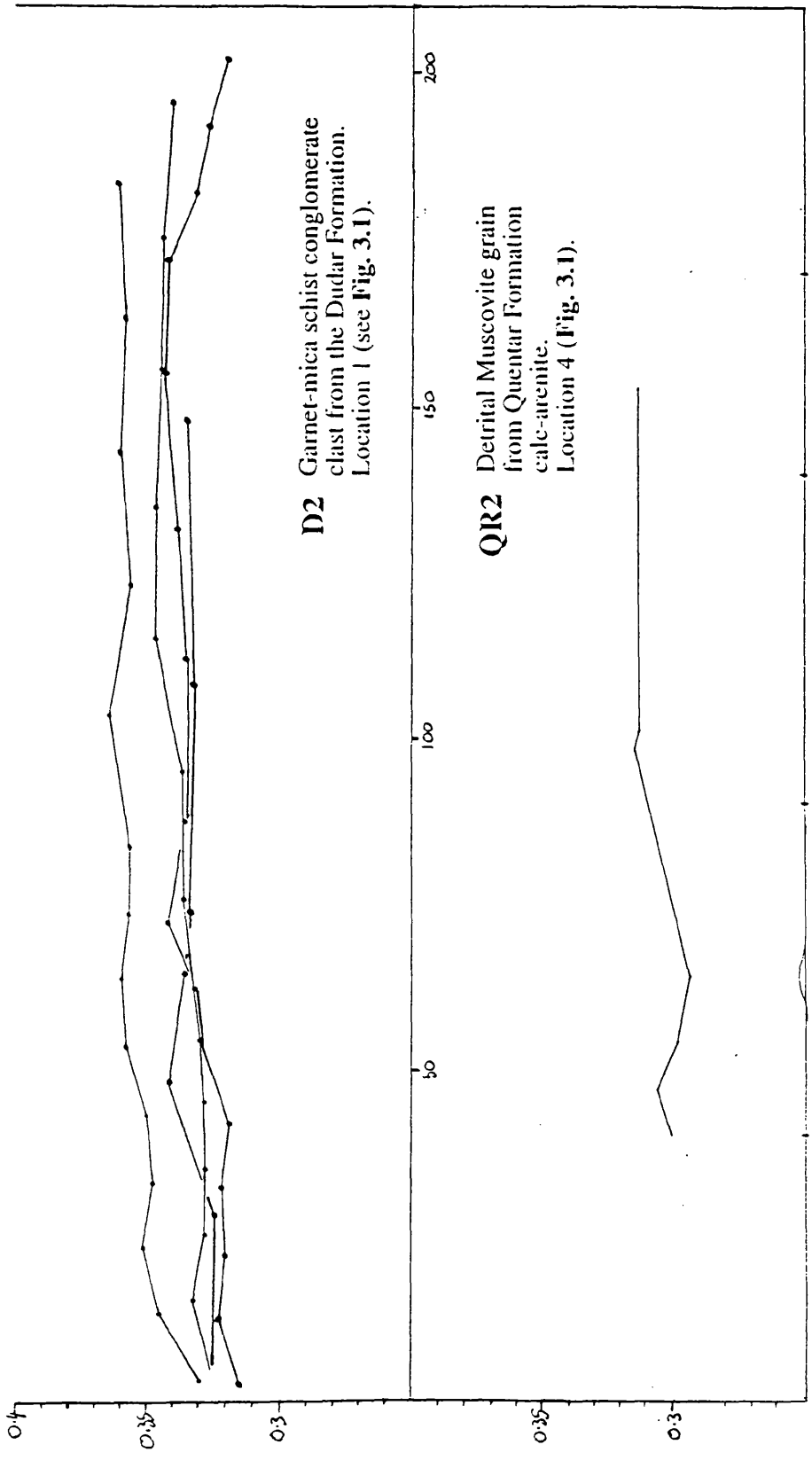

Fig. 7.3 K2O/Al2O electron microprobe transects accross muscovite grains, taken from a conglomerate clast (D2) from the Dudar Formation and a detrital muscovite (QR2) from the Quentar Formation. These data were collected to asses the degree of weathering alteration of the grains, in advance of isotopic dating. Variations are smooth, and values are relatively consistent suggesting no significant alteration of muscovite in these marine deposits.

Some studies have been made of the effect of alteration and patterns of loss of K and Ar upon age estimates. Mitchell and Taka (1984) established patterns of loss for K and Ar from biotites and muscovites, from published data of tropical weathering profiles and detrital muscovite dating. Both elements are lost in tandem until around 20% loss of K, and no effect on age is seen until this point. Therefore small amounts of alteration are of little worry in isotopic dating of micas. However, biotite degrades much faster than muscovite, which should be taken into account. Muscovite will always be of more use, especially in recycled sediments. Muscovites in the Quentar and Dudar Formations appear fresh and unaltered (**Plates 4.6 and 4.9**), so dates derived from them are reliable, and contain information about the source only.

Step heating was performed on all samples, save the Alpujarride in-situ basement sample. The results are listed in **Table 7.1** and age spectra are presented in **Fig. 7.4.**

7.5.2. Bulk detrital muscovites

Age spectra for the bulk detrital muscovite samples from the Quentar and Dudar Formations (**Fig. 7.4**) are surprisingly flat, and consistent in age between samples. This is especially surprising because the ages that contribute to make up the spectra are unconstrained. However, this uniformity is informative. Ages in all micas may be very similar. Grain size is unconstrained, but the overall flatness of the spectra suggest no differentiation of 39Ar% and therefore age between different grain sizes of muscovite, that may come from distinct sources. The effective diffusion diameter within the muscovites is probably always less than the grain size, in any case. The similarity of ages of the four detrital samples suggest not only a uniformity of source but also uniformity of cooling age in the source.

In sample DU2 there is an excess of radiogenic Ar in the last heating step, causing an old age compared to the plateau age. This indicates an older age component in the source of around 25Ma, which has largely been reset at around 18Ma.

In QR4 the earliest gas fraction has an age of 37Ma. Excess radiogenic Ar has been absorbed by some component of the detrital muscovite population during its earlier residence in the source area. DU1 and QR2 also have early released gas fractions with slightly older ages, again indicating absorption of an older gas component, not fully released from the source during the later reheating that generated the plateau ages of around 17-18 Ma.

An initial picture of the recent thermal evolution of the source in the Internal Zones of the Sierra Nevada emerges from these data. Flat spectra indicate a main heating and re-equilibration event around 17-18 Ma, proceeded by an earlier thermal event with a minimum age of 25 Ma, as suggested by the late gas fraction age in sample DU2. An even older gas fraction is indicated in the early released gas fractions of some samples. However, without detailed analysis of individual grains that contribute to the average analysis the exact contributions of sources, and the presumed uniformity of age within the source, suggested here, remains conjectural. The interpretation of these detrital ages depends strongly upon the data obtained by analysing conglomerate clasts of Internal Zone lithologies found in the same deposits as the sand samples.

Bulk Detrital Muscovite Separates Samples	Sample	Cumulative % 39Ar	Apparant age Ma ± 1 Ó
Quentar Formation Calc-Arenite (Locations **4** and **5 Fig. 3.1**)	QR2	15	18 ± 1
		34	17 ± 1
		47	15 ± 1
		86	16 ± 1
		100	17 ± 1
	QR4	0.9	34 ± 7
		17	17 ±1
		39	18 ± 1
		52	16 ± 1
		87	18 ± 1
		100	19 ± 1
Dudar Formation Fan Delta (Location 1 **Fig. 3.1**)	DU1	36	17 ± 1
		89	15 ± 1
		100	12 ± 1
	DU2	21	18 ± 1
		45	17 ± 1
		88	18 ± 1
		100	25 ± 1
Conglomerate Clast Muscovites	D2	3	10 ± 3
		15	15 ± 1
		59	14 ± 1
		89	14 ± 1
		95	20 ± 2
		100	16 ± 2
Dudar Formation (Location 1 **Fig. 3.1**)	D3	4	23 ± 3
		11	28 ± 1
		19	18 ± 1
		54	17 ± 1
		66	19 ± 1
		76	18 ± 1
		89	19 ± 1
		100	22 ± 1
	D4	21	14 ± 1
		55	16 ± 1
		100	15 ± 1
Samples D3 and DU3 are the same lithology.	DU3	4	17 ± 4
		17	18 ± 1
		43	16 ± 1
		64	17 ± 1
		95	17 ± 1
		100	12 ± 3
Basement			
	QR1 Muscovite	Two heating steps Unconstrained 39Ar amount	25.3 ± 1.6
Alpujarride (Location 4 **Fig. 3.1**)			28 ± 2.2
	QR1 Biotite		23.9 ± 2.7

Table 7.1 Results of 40Ar-39Ar laser probe step heating of detritus (bulk detrital muscovite separates, conglomerate clast muscovites) and source (Alpujarride Basement, 10m below basal unconformity with Quentar Formation).

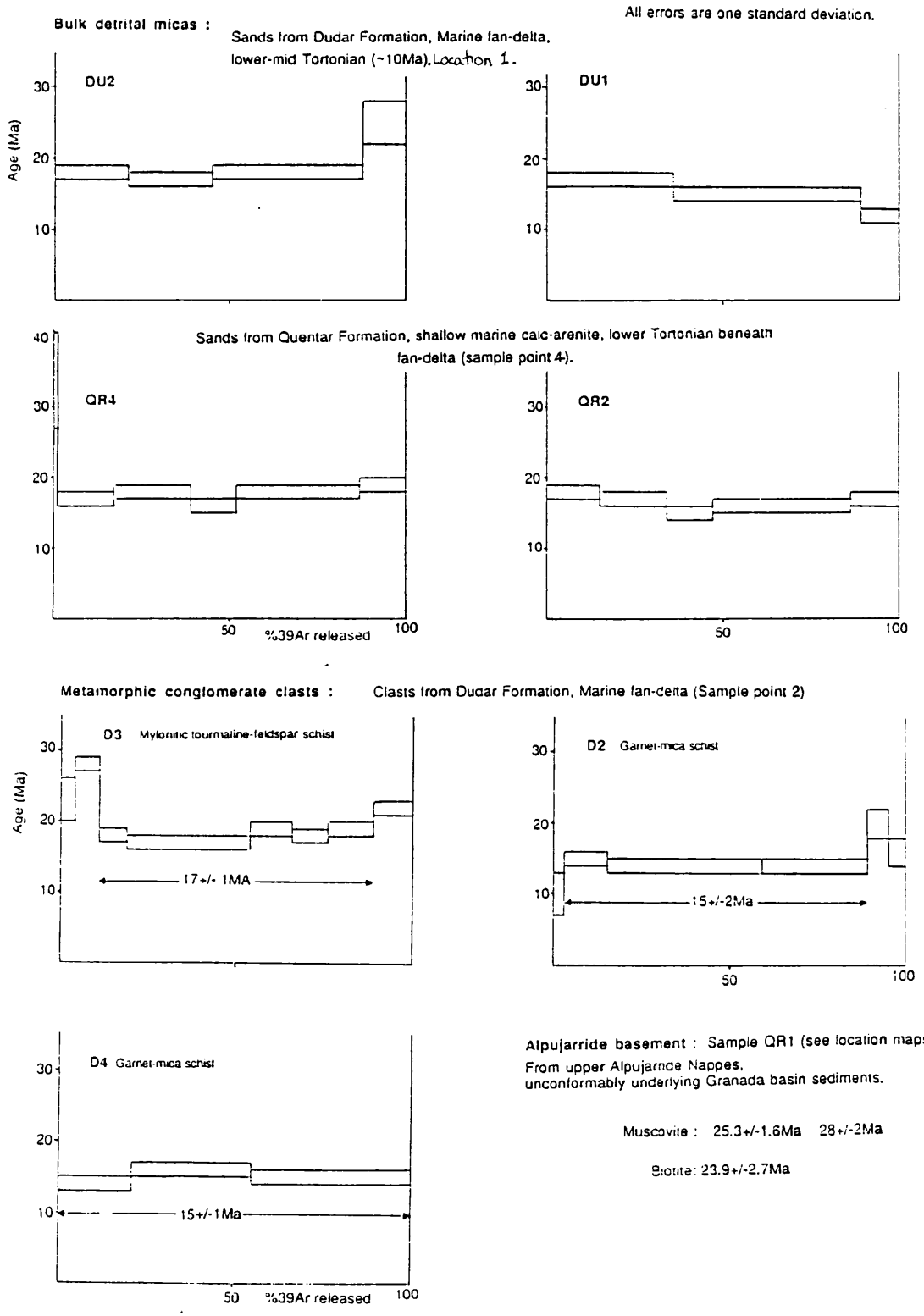

Fig. 7.4 40Ar-39Ar age spectra derived from laser step heating of bulk detrital muscovites and conglomerate clast muscovites from the Quentar and Dudar Formations. See also **Table 7.1** for details of individual heating steps and cumulative 39Ar quanntites.

7.5.3. Conglomerate Clast Muscovites

Three lithologies were analysed, and of these one was analysed twice. Step heating was also performed on muscovite separates. These conglomerate clasts are typical of rocks found within the Sierra Nevada, and are representative, in a restricted way, of the source of detrital muscovites in coeval sandstones and conglomerate sand matrix. Therefore these results are crucial in the interpretation of bulk detrital analyses.

Descriptions of the clasts are presented in **Appendix 2**. The rock types are outlined on **Fig. 7.1**. A detailed discussion of conglomerate clast variety in these Miocene deposits of the Eastern Granada Basin is presented in **Chapter 3** along with a discussion of source locations. The four clasts analysed here are from the Nevado Filabride unit within the Sierra Nevada, specifically the Mulhacen complex. The tourmaline mylonitic gneiss is very distinctive, and is located in detachment zones within the Mulhacen complex. Its presence in the conglomerates of the Dudar Formation is important for the unroofing history of the Sierra Nevada.

Sample D3, the tourmaline-mylonite gneiss, gives a saddle shaped spectrum that has a plateau age of 17±1 Ma. This lithology was analysed twice, from different conglomerate clasts from different horizons, and the ages were found to be identical. The early gas fractions have a component of excess radiogenic Ar indicating possible absorption of an older component of Ar representing a relict of an earlier thermal history, that may even be exotic to the samples analysed here. Argon may have been imported from another source with an older age. However, this cannot be resolved. The earliest apparent age is 23±3 Ma, similar to the suggestion in detrital sample DU2 of an earlier 25 Ma event.

Garnet-mica schist clast D2 has a low temperature Ar fraction age of 10±3 Ma, suggesting a mild resetting at this time. This nearly coincides with fission track ages of 7-9 Ma for the Nevado Filabride obtained by Johnson (pers. com.) Ages rise to a well developed plateau age of 15±2 Ma. The last released gas fractions have an old age of 20 Ma, again suggesting a minimum age for an earlier thermal event in the Mulhacen complex.

Garnet-mica schist conglomerate clast D4 also has a well developed plateau age of 15±1 Ma, but much detail is obscured because only three heating steps were carried out.

All three plateau ages obtained by ^{40}Ar-^{39}Ar analysis of conglomerate clasts are indistinguishable within error. They indicate a major thermal-cooling event around 16Ma (on average) during the late Burdigalian (Harland et. al. 1989), within the Mulhacen complex of the Internal Zones in the Sierra Nevada. This is a little younger than the age obtained from the bulk detrital samples of nearer 18 Ma. An older Ar component is also indicated in the analysis of the clasts, supporting the conclusion that the source of detritus underwent more than one thermal phase in the late Oligocene early Miocene. Further to this, the spectra obtained from the garnet-mica schist clast D2 has a low temperature gas component with an age of 10Ma, suggesting a mild resetting, or thermal pulse at this time in the early Tortonian. This latter age is close to the age of deposition of the sediments of the Quentar and Dudar Formations in the late Serravalian to early Tortonian (Rodriguez et. al. 1989, Boccalleti et. al. 1987).

7.5.4. Alpujarride Basement

The basement to the Granada Basin is in the Alpujarride nappe complex of the Internal Zones in the Zujerio Unit (Minesterio de Industria y Energia, 1972; La Peza 1:50000 map sheet). In the Sierra Nevada region the rock type is dominantly grey dolomite, but some micaceous lithologies suitable for isotopic dating work can be found. A notable example, that lies immediately beneath the first deposits of the basin at many places (Location 4, Fig. 3.1 and at the Balcon de Canales on the Sierra Nevada road) is a black graphitic staurolite schist. It is an important source of siliceous detritus within the Quentar Formation near the basal unconformity. Important detachments are present within the basement in this zone, accommodating extension of the whole zone during Internal Zone core-complex style extension and uplift. The staurolite schist is in tectonic contact with the brecciated dolomite above slickenside covered fault planes that may extend to the base of the sediments, accommodating basin detachment and movement away from the uplifting core of the Sierra-Nevada.

The cooling time, and by inference uplift time of this basement rock is already partly constrained by the age of the sediments that lie directly upon it, at a best estimate of late Serravallian - early Tortonian (12-8 Ma). The age of the Alpujarride evolution beneath the Granada Basin is important as it constrains the time of origin of the Basin and whether or not the cooling of the Alpujarride was directly connected with it.

Muscovite and biotite were dated, the former in two laser fusion steps, with unconstrained ^{39}Ar, that do not constitute step heating as performed on the previously discussed samples. For muscovite the ages obtained are 25.3±1.6 Ma and 28±2.2 Ma, ages that overlap within error. For biotite the single fusion age obtained is 23.9±2.7 Ma. These ages confirm cooling of this portion of the Alpujarride complex went through the closure temperature for biotite (see **Table 7.2**) during the late Oligocene or very earliest Miocene, a minimum of 8Ma before the deposition of the shallow marine calc-arenites of the Quentar Formation. The implications for cooling history and tectono-sedimentary evolution of the Betic Orogen are discussed below.

7.6 K-Ar Dating

Muscovites were separated from an additional 13 conglomerate clasts from both the Dudar and Pinos Genil Formations, and 6 basement rocks, representing the source region, taken from the Internal Zones of the Sierra Nevada. These muscovite separates were dated using the K-Ar method, which produces ages comparable to the ^{40}Ar-^{39}Ar method. It is the dynamics of K decay that determine both, and the temperature of closure to isotopic diffusion is the same for both methods because it is the same isotopic system that is being utilised (Faure, 1986). However, the incremental heating method that allows aspects of the thermal history of a sample to be clarified using the ^{40}Ar-^{39}Ar dating method, is not available. K-Ar dates are total fusion dates, leaving them open to some interpretation, especially if the presence of excess Ar is suspected.

Method	Closure Temperature
K-Ar, Ar-Ar Hornblende	550°C ± 100° (Cliff 1985)
Rb-Sr Muscovite	500°C ± 50° (Wagner et. al. 1977)
Rb-Sr K-Feldspar	400-500°C (Geletti 1990)
K-Ar, Ar-Ar Muscovite	350°C ± 50° (Purdy and Jager 1976, Wagner et. al. 1977)
Rb-Sr Biotite	300°C ± 100° (Cliff 1985, Wagner et. al. 1977) estimates vary considerably eg. 300-345°C (Dallmeyer 1978) 225°C (Turner and Forbes 1976) >400°C (Vershure et. al.1980)
Fission Track Zircon	200-250°C (Hurford 1991)
Fission Track Apatite	50-120°C (Hurford 1991)

Table 7.2 Closure temperatures for several commonly used geochronometers.

Here the dating of conglomerate clasts by K-Ar compliments and extends the data set obtained from ^{40}Ar-^{39}Ar analysis, and helps to clarify possible contributions to the bulk detrital muscovite age spectra. However, the presence of an older ^{40}Ar component is indicated by the step heating spectra discussed above for the detrital and conglomerate clast separates. This suggests that the K-Ar dates presented here may be prone to be slightly older as a result, and should be interpreted with a reasonable degree of caution. ^{40}Ar-^{39}Ar ages have plateau ages that indicate age without the influence of excess argon which can be discerned by older age steps at either side of the plateau. This places a constraint upon the most reliable range of K-Ar ages.

Table 7.3 presents the K-Ar analyses in full, and **Fig. 7.5** graphically combines these with selected ^{40}Ar-^{39}Ar results, to allow age patterns in different elements of the deposits and source to be inspected. The conglomerate clasts and basement rocks analysed are described in **Appendix 2.**

7.6.1. Conglomerate clasts

For conglomerate clasts from the Dudar Formation most ages lie between 12 and 16 Ma, indicating a major phase of source cooling at this time. The clasts analysed are dominantly from the Mulhacen Units of the Nevado-Filabride complex, with the others clearly from the Veleta unit or the graphitic portions of the Mulhacen. Two clasts from conglomerate C8 (see also **Fig 2.6**) have significantly older ages within uncertainty, recording cooling through closure at 20-23 Ma. The K contents of the samples are mostly normal, except for C8C and S1, both with under 6 wt% K. Radiogenic $\%^{40}Ar$ contents are however, not unusual compared with other samples, and the age of S1 is similar to sample C1E which has a normal K content.

The four clasts dated from the Pinos-Genil Formation contain the youngest dated detritus in this study (sample SAF-1A), and the oldest (SAF-B). The spread from 9 to 30 Ma indicates at least 20my of post metamorphic cooling and possible reheating history in the Internal Zones. The remaining two ages correspond with the 12-16 Ma cooling period outlined by the Dudar Formation clasts. K contents and radiogenic $\%^{40}Ar$ are within reasonable limits.

7.6.2. Basement Rocks

For the dated in-situ Mulhacen Unit rocks there is a group of ages at 11-13 Ma, a little younger than the main grouping outlined by the Dudar Formation conglomerate clasts. These groupings cannot really be separated on the basis of uncertainty limits, but they overlap. Sample UTH1 has an age of 20Ma, corresponding to the cooling time of the C8 conglomerate clasts from the Dudar Formation. However, UTH1 has a low K content of only 4.42% suggesting that the age estimate could be too old. The one dated sample from the Veleta Unit has a similar age of 21 Ma, and normal K content, suggesting that ages of 20Ma are reliable. The repetition of the age in some conglomerate clasts, and the suggestion of an older ^{40}Ar component in detrital muscovite derived from ^{40}Ar-^{39}Ar step heating (see above) also confirms the reality of this age component in the Internal Zones of the Sierra Nevada.

One rock from the Alpujarride Complex was dated using K-Ar. This produced an age of 72.6±2 Ma. This is much older than anything else determined in this study, and suggests a

Conglomerate clasts	Sample	Radiogenic 40Ar/10-10mol/g	Radiogenic %40Ar	K (wt%)	Age Ma ± 1 σ
Dudar Formation	C19C	1.904	23.65	8.27	13.2 ± 0.7
	C11D	1.696	23.41	7.41	13.15 ± 0.7
	C11B	2.144	48.37	7.95	15.5 ± 0.4
	C8C	1.885	35.90	5.38	20.1 ± 0.7
	C8A	2.993	33.33	7.48	22.9 ± 0.9
	C1E	1.728	49.41	7.90	12.6 ± 0.4
	C1B	2.203	30.54	8.10	15.61 ± 0.6
	C1C	2.018	26.15	8.03	14.4 ± 0.7
	S1	1.217	26.36	5.67	12.3 ± 0.6
Pinos Genil Formation	SAF-2E	2.01	10.36	7.75	14.9 ± 1.8
	SAF-1A	1.409	32.24	8.17	9.9 ± 0.4
	SAF-B	4.331	20.52	8.22	30.1 ± 1.8
	P2	1.759	25.45	7.53	13.4 ± 0.7
Basement Rocks					
Nevado-Filabride					
Mulhacen Unit	C2	1.136	42.05	6.90	11.0 ± 0.4
	UTH3	1.377	27.98	6.97	11.4 ± 0.5
	UTH1	1.593	47.11	4.42	20.7 ± 0.6
	UTH4	1.739	23.65	8.27	13.2 ± 0.7
Veleta Unit	VE	2.485	54.13	6.62	21.5 ± 0.6
Alpujarride					
	ALP4	10.7	52.2	8.32	72.6 ± 2.0

Table 7.3 K-Ar age dates formuscovites from conglomerate clasts from the Dudar and Pinos Genil Formations and Basement samples of source lithologies from the Internal Zones in the Sierra Nevada.

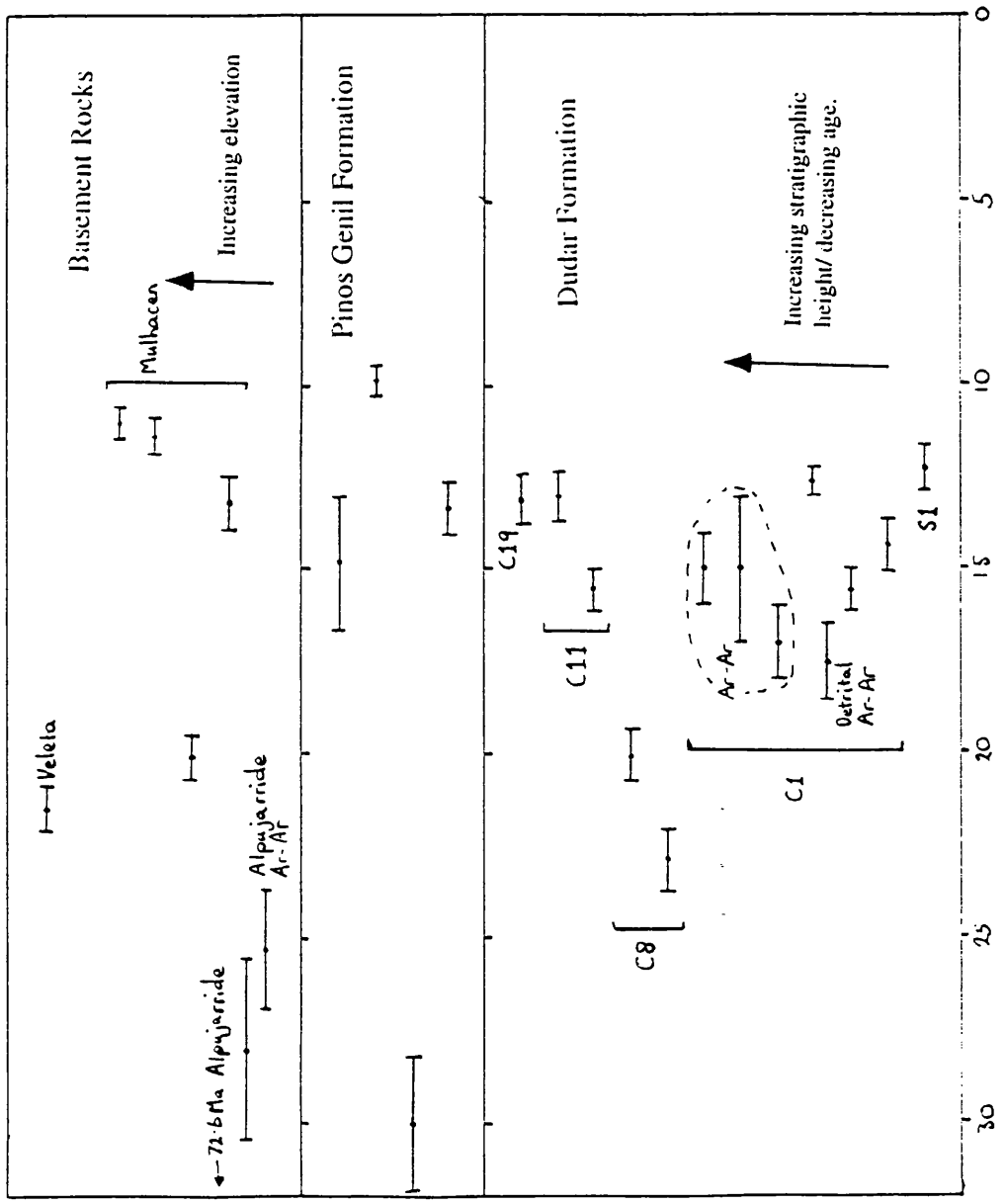

Fig. 7.5 Graph depicting the distribution of K-Ar and 40Ar-39Ar isotopic ages from detritus and source rocks of the Granada Basin. See also **Tables 7.1** and **7.2** for details of ages and errors. The error bars here are 1σ.

long history of evolution and cooling of nappe sequences in the Internal Zones. Excess radiogenic ^{40}Ar is possible as a contaminant, but a source of old ^{40}Ar is still required, with a most likely home within the Internal Zone rocks. This lithology is a low grade quartz-mica phyllite. It has suffered little metamorphism, and could possibly contain some relict detrital micas, that would result in an older age, but one that has largely been reset and replaced by new growth of muscovite in low grade metamorphism. ^{40}Ar-^{39}Ar determinations upon the staurolite schist that forms the basement to the Granada Basin at many points reveals an age of approximately 26-27Ma for cooling of muscovite. The metamorphism of this rock is more severe, so the age will represent the minimum age of cooling post the metamorphic climax. The ages in the Alpujarride appear to be significantly older than the underlying Nevado-Filabride rocks. The age pattern in the Nevado-Filabride is also confirmed by the analysis of conglomerate clasts sourced from the unit.

7.7. Summary of ^{40}Ar-^{39}Ar and K-Ar ages

40Ar-39Ar and K-Ar dating of conglomerate clast muscovites highlights trends of ages. They form a main group concentrated around 12 -16 Ma, with ages at 10 Ma and 17Ma. Another less well defined group indicates a cooling time of around 20-23 Ma. This age component is confirms the older age steps seen in 40Ar-39Ar age spectra, indicated at 25Ma and older. Detrital separates produce bulk average 40Ar-39Ar ages that are slightly older than the main 12-16 Ma grouping derived from conglomerate clasts. As the conglomerate clast lithologies are the likely source for sand sized detrital material, they represent the range of ages that go to make up the bulk detrital muscovite age spectra. It is reasonable to suggest a mix of a dominantly 12-16Ma (early Langhian to late Serravalian) with a minor relict component of a 20-25 Ma (mid Chattian to late Aquitanian), that may be partly source from the Alpujarride Complex.

Basement source rocks in the Nevado-Filabride confirm the above assertion of a Serravalian cooling of source through the closure temperature of muscovite for ^{40}Ar-^{39}Ar and K-Ar. Two samples also produce dates of 20-22Ma coincident with the older cooling phase indicated by the conglomerate clasts. Rocks from the Alpujarride indicate older cooling still, before 25Ma for muscovite, and possibly as early as the late Cretaceous. The Alpujarride may be a minor source of detritus for the sediments. The older Alpujarride age component within the source region does not appear to have been very significant in the age patterns of detritus. However, it may be a source of the older ages seen in some parts of ^{40}Ar-^{39}Ar age spectra (samples DU2 and QR4). The older ages attributed to the Alpujarride must be interpreted with reasonable caution, as only two sample were analysed.

The next section presents the results of Rb-Sr dating on the same samples discussed above. Combining all geochronometers allows the cooling rates of these rocks to be estimated, from which exhumation rates can be inferred and tectonic models formulated.

7.8 Rb-Sr Dating

The samples chosen for Rb-Sr dating were the same as those dated by ^{40}Ar-^{39}Ar and K-Ar methods. As the closure temperatures for these systems are different the t-T path of each

sample can be obtained by dating. This extends the known cooling history of the Internal Zone rocks in the Sierra Nevada. From this, and the ages and facies of sedimentary deposits preserved in the Neogene Intramontane basins, something of the Oligo-Miocene tectonic evolution and palaeogeography of the Betic Orogen can be constructed.

Muscovites from eleven conglomerate clasts from the Dudar Formation, and six basement rocks, that have been previously dated by ^{40}Ar-^{39}Ar and K-Ar means were analysed for Rb-Sr isotopes. The results were combined with analyses of whole rock powders to define isochrons and to regress, using the method of York (1969), to initial compositions of $^{87}Sr/^{86}Sr$. The analytical results are given in **Table 7.4** along with the muscovite-whole rock ages. The full method followed is given in **Appendix 1.**

For a full interpretation it is necessary to view all the ages derived from one rock together. **Table 7.5** presents all data combined for each sample plus the cooling rate, where appropriate. This is to allow any anomalous patterns to be highlighted, that may need explanation using the full range of analytical data. As the Rb-Sr system has a higher closure temperature than the K-Ar and ^{40}Ar-^{39}Ar systems (see **Table 7.2**), any cooling trajectory (a *heating* path resets all ages) will result in Rb-Sr age being older as the higher temperature is passed through earlier. This is the expected pattern. However, this is not the case for many of the lithologies analysed in this study. Many have Rb-Sr ages that are younger than the ^{40}Ar-^{39}Ar and K-Ar determinations on the same rock.

These results have not been discarded, even though their age information appears erroneous in the geological context, because they may indicate something important about Rb-Sr systematics in the source, which may have wider geochemical consequences. In light of the age determinations that *are* in context, there is no reason to believe that the majority of erroneous dates are due to analytical problems, so therefore must indicate some feature of the chemistry of the source.

The following sections discuss the ages, highlighting the main groupings and discusses those that are reliable and those that appear to be anomalous, giving reasons.

7.8.1 Main Rb-Sr Age Groups

Most results, however, appear reasonable in the light of the Cenozoic evolution of the Betic Orogen. Four dominant age groups emerge. The first is 64.13 Ma, from a conglomerate clast, a lithology attributed to the Veleta Unit of the Internal Zones. This age is near the oldest age recorded in this study of 72 Ma in the Alpujarride Complex. Cooling had taken place in some rocks after the early HP metamorphism during the early Tertiary, that was not subsequently reset by later thermal events. The second age is 27.47 Ma coincident with the older ^{40}Ar-^{39}Ar and K-Ar dates derived from the Alpujarride Complex.

The third, and main, group is concentrated around 22-18 Ma, just preceding the main group of clast and basement ^{40}Ar-^{39}Ar and K-Ar dates. This is reasonable, because Rb-Sr dates a higher temperature point in the t-T path of a rock. This supports a major cooling event in the Nevado-Filabride complex at this time in the early Miocene.

Conglomerate Clasts

Sample		Rb ppm	Sr ppm	$^{87}Rb/^{86}Sr$	$^{87}Sr/^{86}Sr$	$^{87}Sr/^{86}Sr$ initial	Age +/- 1 theta
C1B	WR	-	-	1.6086	0.7226	0.7221	**22.06**±1.11
	M	-	-	3.6899	0.7233		
C1E	WR	87.3	104.7	2.4153	0.7127	0.7118	**27.47**±0.62
	M	322.9	93.6	9.9880	0.7157		
C8A	WR	81.2	105.7	2.2254	0.7279	0.7280	**-0.59**±0.79
	M	351.9	109.1	9.3492	0.7279		
C11B	WR	80.3	393.8	0.5901	0.7116	0.7111	**64.13**±0.19
	M	417.4	73.8	16.3865	0.7260		
C11D	WR	71.8	201.0	1.0354	0.7202	0.7047	**1045.3**±14.86
	M	12.4	776.6	0.0462	0.7054		
C19C	WR	42.9	84.5	1.4701	0.7234	0.7229	**28.01**±4.56
	M	267.4	167.4	4.6282	0.7247		
D2	WR	35.2	284.5	0.3584	0.7093	0.7092	**8.35**±0.25
	M	269.9	112.7	6.9328	0.7100		
D3	WR	324.7	61.8	15.2575	0.7642	0.7602	**18.41**±0.06
	M	1788.9	10.5	503.0420	0.8917		
D4	WR	127.4	167.5	2.2020	0.7184	0.7178	**18.33**±0.45
	M	434.5	199.2	6.3163	0.7195		
P2	WR	315.6	98.4	9.3616	0.7434	0.7480	**-34.88**±1.36
	M	377.7	161.9	6.7745	0.7447		
S1	WR	129.9	500.5	0.7520	0.7224	0.7224	**8.41**±2.31
	M	402.9	167.2	6.9838	0.7232		

Table 7.4 Details of Rb-Sr muscovite dating of conglomerate clasts from the Dudar Formation, at sample Location 1 (see **Fig. 3.1**) next to Pinos Genil town. WR- whole rock, M-muscovite

In-Situ Internal Zone Source Rocks

Sample		Rb ppm	Sr ppm	$^{87}Rb/^{86}Sr$	$^{87}Sr/^{86}Sr$	$^{87}Sr/^{86}Sr$ initial	Age +/- 1 theta
ALP4	WR	132.9	41.01	9.3770	0.7260	0.5906	**1009.08**±37.41
	M	221.9	59.7	10.7912	0.7464		
C2	WR	71.4	66.9	3.0928	0.7132	0.7128	**8.14**±0.86
	M	364.4	188.6	5.5932	0.7135		
UTH1	WR	401.2	56.6	20.5501	0.7272	0.7261	**10.8**±0.13
	M	1342.5	98.7	39.4388	0.7326		
	F	786.5	317.2	7.1883	0.7283		
UTH3	WR	12.0	99.4	0.3831	0.7168	0.7168	**10.61**±1.29
	M	391.9	90.8	11.4139	0.7185		
VE	WR	79.1	197.1	1.1622	0.7200	0.7199	**12.22**±1.65
	M	360.9	106.1	9.8603	0.7216		
QR1	WR	259.4	3.9	193.2155	0.7288	0.7299	**-0.8**±0.16 (!)
	M	197.3	157.3	3.6369	0.7299		

Table 7.4 (Continued). Details of Rb-Sr age determinations of in-situ basement source rocks of the Internal Zones of the Sierra Nevada.
F - Alkali Feldspar

	Sample	Biotite 300±50° Muscovite 350±50° 40Ar-39Ar	K-Ar	Muscovite 500±50° Rb-Sr	Cooling Rate °C/m.y.
Conglomerate clasts					
Dudar Formation	C19C		13.2 ± 0.7	28.01 ± 4.56	10.1
	C11D		13.15 ± 0.7		
	C11B		15.5 ± 0.4	64.13 ± 0.19	3.1
	C8C		20.1 ± 0.7		
	C8A		22.9 ± 0.9		
	C1E		12.6 ± 0.4	27.47 ± 0.62	10.1
	C1B		15.61 ± 0.6	22.06 ± 0.1	23.2
	C1C		14.4 ± 0.7		
	S1		12.3 ± 0.6	8.41 ± 2.31	
	D2	15 ± 1		8.35 ± 0.25	
	D3	17 ± 1		18.41 ± 0.06	106.4
	D4	15 ± 1		18.33 ± 0.45	45.04
Pinos Genil Formation	SAF-2E		14.9 ± 1.8		
	SAF-1A		9.9 ± 0.4		
	SAF-B		30.1 ± 1.8		
	P2		13.4 ± 0.7		
Basement Rocks					
Nevado-Filabride	C2		11.0 ± 0.4	8.14 ± 0.86	
Mulhacen Unit	UTH3		11.4 ± 0.5	10.61 ± 1.29	
	UTH1		20.7 ± 0.6	10.8 ± 0.13	
	UTH4		13.2 ± 0.7		
Veleta Unit	VE		21.5 ± 0.6	12.22 ± 0.16	
Alpujarride					
	ALP4		72.6 ± 2.0		
	QR1 M	25.3 ± 1.6			35.7
		28 ± 2.2			mus.-biot.
	Biotite	23.9 ± 2.7			

Table 7.5 All ages from conglomerate clasts and basement rocks, with calculated cooling rate where appropriate. Cooling rate derived from closure temperatures listed in **Table 7.2** Negative Rb-Sr ages of samples C8A, P2 and QR1, and the 1Ga ages of samples C11D and ALP4 are omitted.

The final group is concentrated at around 10-8 Ma. This is younger than the youngest ^{40}Ar-^{39}Ar or K-Ar ages derived on conglomerate clasts and basement rocks. The argument for closure temperature coincidence used above applies here too, and highlights an anomaly. Rb-Sr ages are usually older than ^{40}Ar-^{39}Ar or K-Ar ages from the same sample. Seemingly reliable ages are seen to be anomalous because of this age mismatch. Without the combination of dating methods to highlight the problem, these ages may have been accepted as indicating cooling in the source. This clearly requires some explanation on a *sample to sample* basis.

Other ages are very clearly erroneous. For samples C8A, P2 and QR1 a negative isochron slope is formed. Additionally for samples C11D and ALP4, their ages are in the region of 1 Ga. These dates are clearly at odds with the Cenozoic evolution of the Betic Orogen and the mobile nature of the Alpine Orogenic Belt. The explanation of these ages lies in the distribution of Rb and Sr between muscovite and the whole rock. Consideration of these may shed light on processes of alteration that may be important for age dating as a whole and also for the detailed geochemical nature of the Internal Zones in the Sierra Nevada, as it affects provenance signature.

7.8.2 Non-anomalous ages

Several samples yield Rb-Sr age determinations that have relationships with K-Ar determinations on the same sample which are reasonable in the geological context, and have the expected pattern of K-Ar ages that are younger than Rb-Sr ages (see **Table 7.5**). These samples are all conglomerate clasts from the Dudar Formation ; C19C, C11B, C1E, C1B, D3 and D4. No basement samples give a conventional age relationship when dated by Rb-Sr and K-Ar, except sample ALP4 which gives an anomalously old Rb-Sr age indication. In this section the results which are taken to be reasonable (just listed), and that indicate something significant about the Internal Zones are discussed. Other Rb-Sr ages appear too young, but otherwise these samples have normal whole-rock and slightly low muscovite K compositions, which may be a significant factor. These samples need to be understood and their reliability with reference to the K-Ar determinations assessed. This may be best done by considering the character of the so called 'normal' ages, and comparing them with the samples that have anomalous ages, to see if there is any controlling factor.

For sample C19C, between 10-15% of the rock is muscovite. Considering this, the Rb value of the whole rock (WR) is derived mostly from the muscovite content (see **Table 7.4**). This also applies to Sr, though Sr must reside in significant sites other than muscovite, as the WR value is more than 15% of the muscovite value. No unusual mineralogy is noted in C19C, and muscovite is unaltered. K-Ar analysis of muscovite from C19C reveals a normal K content of 8.27 wt%. The Rb-Sr age determination on C19C is considered to be trustworthy.

Sample C11B has a relatively high Sr content in the WR, for which muscovite only accounts for a small portion. Petrography indicates the presence of important carbonate in C11B, which may be a late addition to the rock, perhaps replacing earlier phases. This higher Sr content in the WR will have the effect of pushing the WR $^{87}Rb/^{86}Sr$ down, reducing age. (See **Figure 7.6** for a summary of the possible changes to isochron systematics that can affect

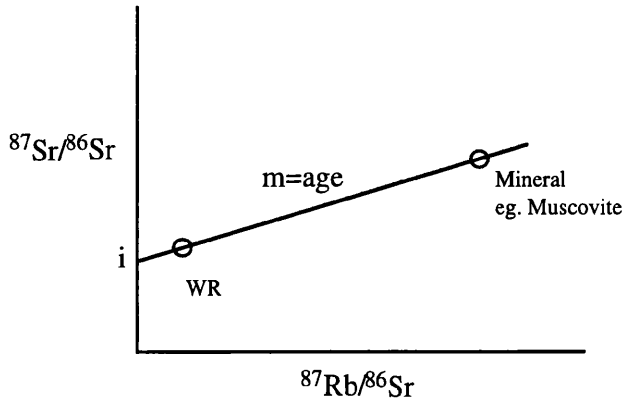

Measured isotopic ratios define points on plot. The gradient of the isochron so formed defines age since closure of system to diffusion, and initial 87Sr/86Sr.

Possible trajectories of data points to achieve age reduction. Whole rock alteration is most likely. The addition of Sr by carbonate precipitation and replacement from fluids is easily achieved and would lower 87Rb/86Sr. For 87Sr/86Sr to increase requires a Sr composition with an old isotopic signature. Changes to muscovite are less likely due to its chemical stability. Changes to WR SR content by precipitation of carbonate is the likely cause of low Rb-Sr ages in samples S1 and D2.

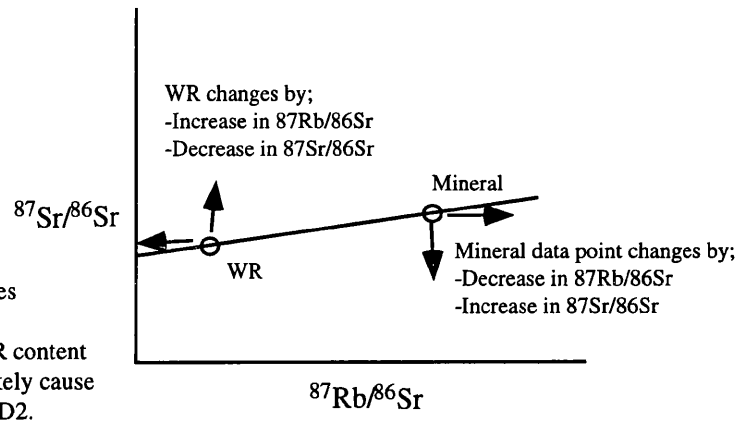

Whole Rock values can have 87Rb/86Sr values larger than the mineral, giving a negative age estimate. This pattern is also likely in Muscovite-WR isochrons of biotite rich rocks, as occurred with sample QR1.

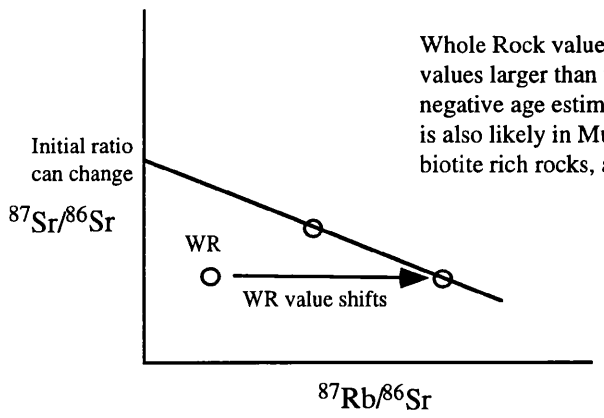

Age estimates can increase also by the importation of an young component of 87Sr/86Sr into the whole rock, which moves the point down on the plot, increasing the gradient of the isochron.

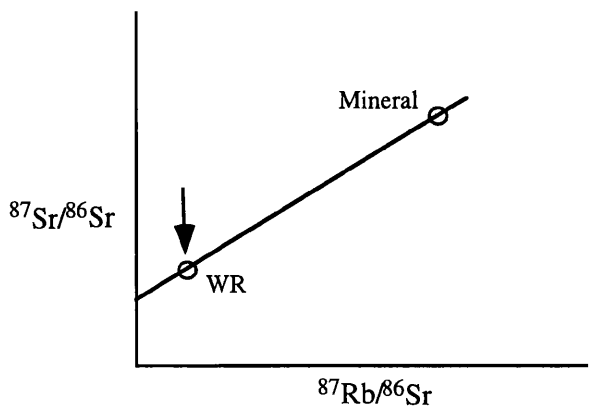

Fig. 7.6 Possible ways of changing age indications on Rb-Sr isochron diagrams

measured age). The 64 Ma age indicated for C11B may therefore be a minimum estimate. However, the points on the isochron are not close, due to high $^{87}Rb/^{86}Sr$ for the muscovite. This will lessen the effect on age of a shift in WR values. The K content of muscovite from C11B is 7.95 wt%, a normal muscovite value, confirming that muscovite compositions are not suspect. This further suggests that the Rb-Sr age determination on C11B is trustworthy.

Sample C1E has a similar high Sr WR value as C11B, possibly resulting in a lower age than might be accurate. Carbonate is again present, the probable cause of elevated Sr values in the WR. Rb values in the WR are controlled primarily by muscovite, which constitutes around 25% of the rock. Muscovite from C1E has a K content of 7.9 wt%, a normal value, suggesting that muscovite determinations of Rb and Sr are reliable. For sample C1B the data on Rb and Sr contents is unavailable. However, the WR and muscovite $^{87}Rb/^{86}Sr$ values are close, generating a larger uncertainty on the age. Carbonate is present in the rock, and WR Sr/Sr values are near those for the muscovite. The age should be interpreted as a minimum.

For sample D3 the muscovite Rb/Sr is very high, reducing the chances of the age being affected by whole rock composition. The Sr content of the WR is high compared with muscovite, suggesting a significant site for Sr other than muscovite. Around half of the Rb content of the WR is accounted for by the 10% content of muscovite in sample D3. The rest possibly resides in plagioclase and alkali feldspar. Sample D4 has WR and muscovite $^{87}Rb/^{86}Sr$ values that are much closer than for sample D3. This decreases the level of confidence in this age determination. However, WR Rb levels are set by the approximately 40% content of muscovite in the rock. Sr levels in the WR are a little high to be explained by muscovite content alone, the result perhaps of some carbonate in the rock. As argued above, this may work to decrease $^{87}Rb/^{86}Sr$ in the WR thus making the indicated age an underestimate. These ages appear to be in context with each other, and as one is apparently quite reliable due to large muscovite $^{87}Rb/^{86}Sr$, they are probably significant and therefore require interpretation.

These ages discussed above represent a set that are considered to be mostly reliable. It is suggested, from high Sr contents in WR analyses and from the presence of carbonate, as calcite in the rock, that ages may be a slight underestimate in same samples. For some other samples the Rb-Sr age is younger than the accompanying K-Ar on the same sample. However these 'young' Rb-Sr ages are reasonable in the geological context of the Internal Zones, and are only recognised as being possibly anomalous by the relationship with the K-Ar ages. The method of age reduction discussed above may be applicable to these samples. The next section discusses these data.

7.8.3 Anomalous ages

Young ages

Some Rb-Sr ages appear anomalous because they are younger than the K-Ar and ^{40}Ar-^{39}Ar ages derived from the same samples. Samples D2, S1, C2, UTH3 and VE all show this pattern, but have Rb-Sr ages that are geologically reasonable in the evolutionary context of the Betics. These need to be considered on a sample to sample basis to evaluate the reliability of the Rb-Sr versus the K-Ar age determinations.

Sample D2 produced an ^{40}Ar-^{39}Ar plateau age of 15Ma, but a Rb-Sr age of 8.35 Ma. This is clearly at odds with accepted isotopic intra-sample age distributions that depend on, and define, cooling pathways for rocks. The ^{40}Ar-^{39}Ar muscovite age was obtained by step heating, and the plateau defined represents the most reliable age, as contributions from excess argon sources are identifiable. The muscovite composition may be quite reliable in this case. This points to the whole-rock for a cause of the young age. However, there is no data on the K content of the muscovite analysed from D2. The Rb content of the whole rock can be attributed to the content of muscovite in the rock. Sr content is quite high in the WR which makes the $^{87}Rb/^{86}Sr$ value low, which places the WR point near the $^{87}Sr/^{86}Sr$ axis on the isochron, lowering the derived age. Similar to samples C1E and C11B petrographic evidence confirms the presence of significant carbonate in sample D2, which often appears to be invasive in character. This is possibly the source of the high whole-rock Sr content. Sr with an older age signature was perhaps introduced into the rock, by fluid interaction, but did not affect the muscovite composition. This addition of Sr must have taken place at temperatures below the closure temperature of muscovite to Sr diffusion, at 500°C. This presumes that the muscovite is not in equilibrium with the WR composition. If it were, the Rb-Sr age would be correct, and date the time of closure of the muscovite to diffusion of Rb and Sr. This is not absolutely resolvable with the data presented here. However, the relationship between the K-Ar and Rb-Sr ages on D2 suggest the possibility of late low temperature addition of Sr by addition of carbonate, as calcite, that reset the age without opening muscovite to diffusion of Rb-Sr. However, as already stated the K content of the muscovite is unconstrained. Other samples with similar anomalous age relationships have low K contents in the muscovites analysed. This may adversely affect the reliability of the K-Ar ages.

In C1E and C11B, discussed above, the Rb-Sr ages indicated are not less than the accompanying K-Ar ages, but could be at least minimum cooling age estimates. As argued their ages may have been lowered by the presence of Sr bearing carbonate in the WR, as Sr contents are higher than the muscovite. In all these cases, and including D2 the favoured age lowering mechanism is increased Sr content in the WR, probably with an older $^{87}Sr/^{86}Sr$ value. However, for sample D2 calcite is present, but there is no other important difference in mineralogy, compared with samples C1E and C11B, that may account for the Rb-Sr being lowered below the K-Ar age.

Conglomerate clast S1 gives an age of 8.41 Ma, but a K-Ar age of 12.3 Ma. Again muscovite Rb and Sr compositions are not unusual. K content is a little low however at 5.67%, which may tend to force K-Ar age up. For the whole-rock, Rb levels are determined by the 30% content of muscovite in the rock, but Sr levels are high, at 500 ppm, and WR $^{87}Sr/^{86}Sr$ values are near those of the muscovite. However, carbonate is not present in sample S1, so high Sr levels must derive from some other component of the mineralogy. This suggests that for this sample Sr levels were not reset by addition of Sr, but represent the correct, original WR value that muscovite equilibrated with above 500°C. This is where the possibility of the K-Ar age being erroneous becomes increasingly likely. The low K content of the muscovite from S1, as derived in the K-Ar dating process, may lower the age determined. Mitchell and Taka (1984)

demonstrate that K and Ar loss due to weathering are usually achieved in fixed relative amounts and that the relationship is linear and predictable up to 10% K loss. However, it is not possible to say if the chemistry of the muscovite in sample S1 has been affected by weathering to any extent. Another possibility for sample S1 and other samples from the Granada Basin is the presence of paragonite mica, or another low K mica. If this is the case then Rb-Sr determinations are likely to be relatively reliable.

In three basement rock samples dated (C2, UTH3 and VE) Rb-Sr ages are younger than the K-Ar determinations on the same samples. Sample C2 gives an Rb-Sr age of 8.14±0.86 Ma and a K-Ar age of 11 ± 0.4 Ma. Rb contents in the WR of C2 can be attributed to muscovite, as can the Sr content. The K content of the muscovite, derived from K-Ar dating is low, at 6.9 wt%, which would tend to increase K-Ar age. (Microprobe studies on muscovites from conglomerate clast D2, Alpujarride basement sample QR1 and some detrital grains from the Quentar Formation indicate that the K content of muscovites is typically 9%.) Unlike sample D2 there is no carbonate in the grain framework of the rock that could result in altered Sr values that could lower Rb-Sr age. The possibility that low K content in the muscovite analysed from sample C2 has affected the K-Ar age is the only explanation of the anomalous age relationship that presents itself.

For sample UTH3 the K-Ar and Rb-Sr ages overlap within error, so no significant difference between them can be identified. It is possible therefore, that the variation within error can accommodate the K-Ar age of 11.4 Ma being older than the Rb-Sr age of 10.61 Ma. This result indicates the possibility of extremely fast cooling within the Mulhacen Unit at this time which could lead to such a close coincidence of ages. However, the Sr content of the WR is as large as the muscovite value. Also, at 12ppm the Rb content of the WR is lower than might be expected in a rock with 30% coarse muscovite that has a Rb content of 391ppm. The data points on the isochron for UTH3 are not close, so the Rb-Sr age may be reasonably reliable. The best interpretation possible, without further detail, is to accept the ages with their errors as probably representing rapid cooling around 11Ma.

Sample VE gives a Rb-Sr age 9 My younger than the associated K-Ar determination. Muscovite K content in sample VE is again low at 6.62 wt%, that may make the K-Ar age too old. Whole-rock Rb content can be attributed to muscovite content, but Sr WR content is not explained by muscovite and must reside elsewhere in the rock. The $^{87}Sr/^{86}Sr$ value for the whole rock is high compared to the muscovite, and suggests that an older component of $^{87}Sr/^{86}Sr$ may have been introduced to the rock, that has not equilibrated with the muscovite compositions.

For UTH1, feldspar was added to the isochron, to improve the regression to initial $^{87}Sr/^{86}Sr$. Using feldspar generates an age of 10.8 Ma. Utilising just muscovite and feldspar in a partial mineral isochron, produces an even younger age of 9.41 ± 0.15. The closure of potassium feldspar to Rb-Sr diffusion takes place at between 400 and 500°C (Gilletti et. al. 1990) a similar temperature to muscovite. However, the K content of the muscovite in UTH1 is low at only 4.42%, putting the K-Ar age in some doubt. In this case the Rb-Sr age is taken as reliable.

In these samples that exhibit Rb-Sr ages that are younger than accompanying K-Ar ages the rock may not have acted as a closed system. Rb-Sr isotope characteristics may have changed by the import of material, possibly by fluid interaction at temperatures sub-500°C. At higher temperatures equilibration with mica would have taken place and the Rb-Sr ages would be more likely to be older than K-Ar ages. However, these changes are subtle, and have only been recognised because of the anomalous relationship between ages derived from dating methods that record different isotopic closure temperatures. The presence of carbonate in some samples that may be invasive to the rock appears to correlate with increased Sr contents

It is interesting to note the close coincidence of ages around 8-12 Ma. This is a time of important basin formation, and cooling as recorded in fission track ages in the Sierra Nevada (Johnson, pers. comm.). Coarse clastic sedimentation also took place at the end of this time in the intramontane basins of the Betics. Rapid uplift is inferred within the Sierra Nevada from the abundant coarse clastics in the Granada Basin, in sediments of Tortonian age (8-11 Ma). It is tempting to attribute some significance in terms of source cooling and uplift, to the Rb-Sr ages obtained, based on this coincidence.

However, the possibility of age reduction in Rb-Sr systematics suggest that no significance should lightly be given to any demonstrably young age determination. Indeed, the interpretation of the Rb-Sr ages that appear to be geologically feasible must be tempered by the possibility of some age changes due to fluid interaction and isotopic mobility.

However, K-Ar ages of these anomalous K-Ar/Rb-Sr pairs could have suffered through the low K content evident in muscovites. Even though these muscovites are fresh and unaltered, the possibility of these samples being low K micas, such as the Na mica paragonite, has not been excluded. Indeed X-ray diffraction testing of many mica separates for purity prior to dating revealed a sample trace that was distinctive of paragonite in many cases. Further detailed electron microprobe analysis would be required to clarify this issue.

The chances of excess argon being important in affecting K-Ar ages is constrained by step heating experiments. Excess argon is present but plateau ages suggest the important cooling to have taken place between 15 and 20 Ma. Generally the K-Ar ages conform to this or are slightly younger at around 10-13 Ma, which discounts any chance of older ages being produced by inclusion of excess argon. The K-Ar determinations appear to be consistent in their age indication which further suggests a reliable age indication from them, so it is these that are utilised in tectonic interpretation. Only the Rb-Sr ages that are not too old (see next section), or are not younger than associated K-Ar ages from the same sample, are used for making tectonic inferences from calculated cooling rates.

7.8.4 Disturbed Rb-Sr systematics

Samples C8A and P2 have negative isochron slopes, compared with K-Ar ages of 22.9 Ma and 13.4 Ma. Looking at C8A, the Rb content of the WR is largely explainable by the 20% muscovite content of the rock. Sr content in the WR is, however, high, and must reside in other phases of the rock. K content of the muscovites in C8A is also a little low, at 7.48 wt% K (see **Table 7.3**). But muscovite is unaltered, and is probably not the cause of the anomalous age,

making the K-Ar age believable over the Rb-Sr age. If the muscovite appears to be normal and capable of producing reliable data, then the negative age must lie in some property of the whole rock, which includes muscovite. The $^{87}Sr/^{86}Sr$ values of the whole rock are equal to those for the muscovite. This suggests the import of Sr with a composition the same, or older than the muscovite in sample C8A. However, there are no apparent late developed Sr carrying minerals in the rock. This requires clarification by further careful work aimed at detailing the Sr contents of different minerals in the rock.

For sample P2 the muscovite contents of Rb, Sr and K are not unusual, and the K-Ar age of 13.4 Ma can be accepted as significant. However, the whole rock composition is unusual, and has resulted in a reversal of the points on the isochron plot. The Rb content of the WR is very large however, and cannot be accounted for even by the 50% total content of muscovite in sample P2. Rb may be stored in another phase of the rock, most probably feldspar, which is common. The Sr content of the WR is explainable by the muscovite content. $^{87}Rb/^{86}Sr$ values are therefore higher in the WR than in muscovite.

Two age determinations produced results that are clearly too old for the geological context of the Tertiary Betic Orogen. Conglomerate clast C11D produced a Rb-Sr age of 1045.3 Ma but a K-Ar age of 13.15 Ma. Muscovite Rb and Sr contents are anomalous. Rb content is very low (12ppm) and Sr content very high for muscovite (776ppm). This suggests isotopic resetting of muscovite, or even analytical error. The $^{87}Sr/^{86}Sr$ value for the whole-rock is higher than for muscovite, as is $^{87}Rb/^{86}Sr$. This places the whole-rock and muscovite points in conventionally opposite locations, with the muscovite down-slope on the isochron from the whole-rock. There is a great deal of calcite in this sample, the probable source for reset whole rock compositions and high Sr content. The critical difference in this case is the low Rb content of muscovite, that rather than indicating an old age has placed muscovite on the low $^{87}Rb/^{86}Sr$ side of the whole-rock value. However, muscovite K content is reasonably within the expected range at 7.41 wt%.

Alpujarride basement sample ALP4 produced an age of 1009.08 Ma, compared with a K-Ar age of 72.6 Ma. Initial $^{87}Sr/^{86}Sr$ is an impossible 0.5906. Whole-rock Rb contents can be explained by the contribution from muscovite, but Sr is large in the WR so must be held by another mineral. There is little to suggest that this lithology would produce an anomalous age as no unusual petrographic characteristics are seen. However, the data points are quite close together with similar $^{87}Rb/^{86}Sr$, but the $^{87}Sr/^{86}Sr$ of the WR is low (though not very low at 0.726). It is this that has generated the impossible initial ratio.

Generally these highly anomalous ages suggest the possibility of significant reworking of Rb-Sr systematics, below the temperature where re-equilibration through the whole rock would take place. This demonstrates that these rocks were perhaps not closed systems during Oligo-Miocene cooling episodes. Veining is present in some of these lithologies, and carbonate is important in some. The Alpujarride complex in the Sierra Nevada is quite extensively veined throughout its exposure, with quartz, indicating hydrothermal activity in the structural level above the dominant sedimentary source in the Mulhacen unit of the Nevado Filabride. Additionally, the muscovite K contents of some samples are low, suggesting that some K-Ar

determinations give misleading ages. These white mica compositions are not the result of weathering or any other neo-chemical change, such as hydrothermal alteration, but are the primary composition of the micas. However, more detailed work to characterise composition is required to identify the nature and the source of disturbed isotopic systems in these whole rocks.

7.9 Cooling, uplift and sedimentation

Table 7.5 presents all the ages derived from conglomerate clasts and basement lithologies within the Internal Zones in the Sierra Nevada. Cooling rates have been calculated for those samples with apparently reasonable age relationships between different dating methods. The samples discussed above that have geologically unreasonable Rb-Sr ages are not discussed. Cooling rates have been calculated using the difference in closure temperature divided by the difference in age obtained using the different methods on each sample. **Fig. 7.7** presents age versus closure temperature for the samples from the Granada basin in a graphical form with different cooling rates superimposed to aid interpretation.

High temperature cooling: 500°-350°C

The temperature difference between the closure temperatures of the K-Ar/^{40}Ar-^{39}Ar and Rb-Sr dating methods is 150°, between 500°C and 350°C. Cooling rates for this higher temperature evolution from the dated conglomerate clasts from the Dudar Formation vary between 3.08 and 106.4 °C/Ma Two samples show a consistent cooling from 27-28 Ma to 12-13 Ma at 10°C/Ma Although basement rocks did not provide cooling rates, sample UTH3 could, within error have cooled at a very high rate of 200°C/Ma

Using an assumed geothermal gradient of 30°/km, (which is a conservative estimate, especially considering the high heat flow in the Betics at present) uplift rates for the 500-350°C cooling interval vary between 0.34 Km/Ma and 3.47 km/Ma. For a geothermal gradient of 35°C/km these exhumation estimates change to between 0.28-3.04 km/Ma This of coarse assumes that cooling is related to uplift, but in reality the complications involved in the tectonics of orogenic zones suffering compression and extension mean that this need not be the case. Van Wees et. al. (1992) suggest cooling in the Betics is driven by 'cold slab' underthrusting, cooling from below. This need not result in uplift, as in their model a previously extended crustal section is inverted. The uplift rates implied therefore must be interpreted as a maximum possible rate, and not as established fact.

For the staurolite schist, sample QR1, at the base of the Granada Basin infill, within the Alpujarride Complex, the cooling rate between the closure temperatures for ^{40}Ar-^{39}Ar muscovite, at 350° and biotite at 300°C, lies between 12.1 and 35.7°C/Ma This sample cooled much earlier and more slowly than the underlying Nevado Filabride rocks. This translates to an exhumation rate for this period of between 0.41 and 1.19 km/Ma

Low temperature cooling: 350°C to surface temperatures (20°C)

The lower temperature cooling (from 350°C to surface temperatures) and exhumation of the dated conglomerate clasts is constrained by the depositional age of the Dudar Formation

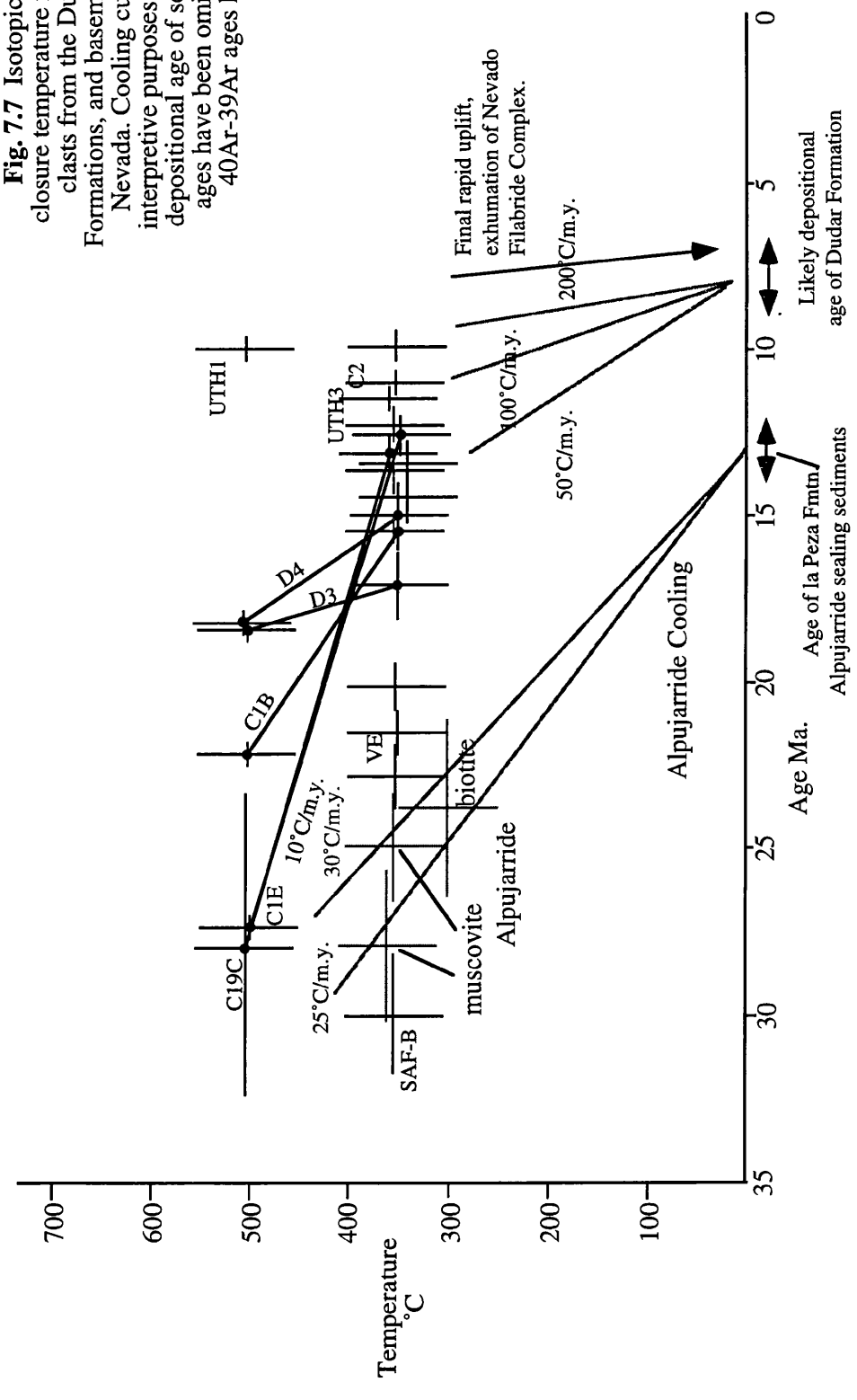

Fig. 7.7 Isotopic age plotted against closure temperature for dated conglomerate clasts from the Dudar and Pinos Genil Formations, and basement rocks from the Sierra Nevada. Cooling curves superimposed for interpretive purposes, and constrained by the depositional age of sediments. Young Rb-Sr ages have been omitted, but all K-Ar and 40Ar-39Ar ages have been included.

(**Figure 7.7**) during the late Tortonian (Rodriguez-Fernandez and Fernandez 1989, see also **Chapter 2**). This requires a very rapid cooling rate for most lithologies of between 50 and 200°C/my, which translates to 0.67-6.67km/Ma Some conglomerate clasts have cooled more slowly, at <20°C/Ma, having cooled to closure of ^{40}Ar-^{39}Ar earlier, at 30-20Ma.

The exhumation rate of the Alpujarride schist (QR1) is dependant on the late Serravalian age of the La Peza Formation which lies directly upon it in the eastern margin of the Granada Basin. Using this depositional age as the time of exposure of the Alpujarride schist at ambient surface temperatures produces a cooling rate of between 25°C and 30°C/my and an uplift rate of 0.83 and 1 km/Ma (see **Fig. 7.7**) between 28 Ma and 14 Ma. At this time when the Alpujarride rocks were cooling at this rate from 350°C to approx. 20°C (surface temperature), some Nevado Filabride rocks were also cooling from 500 to 350°C, during the same period (see **Fig. 7.7**). The Nevado Filabride rocks cooled more slowly, at 10°C/Ma This suggests a common history of cooling and possibly uplift between the late Oligocene and the Serravalian for the Alpujarride and Nevado Filabride. Some lithologies in the Nevado Filabride cooled to 350°C at a similar time to the Staurolite schist, sample QR1 in the Alpujarride Complex also cooled to 350°C, but exhumation occurred earlier in the structurally higher Alpujarride Complex.

However, cooling in the Alpujarride could be even slower. Sample ALP4 gives a K-Ar age, again recording cooling through 350°C, at 72 Ma, indicating the possibility of very slow cooling in the Alpujarride Complex of at most 6°C/Ma

The variations in cooling rates in the clasts and basement rocks of the Granada Basin suggest a complex pattern of cooling and inferred uplift of the basement crust in this area, as a result of non-homogenous behaviour of the Internal Zones block. Additionally the closure temperatures used above will be affected by the cooling rate. The faster cooling rates calculated will be minimum estimates, because as the cooling rate increases the closure temperature for the system in question will increase.

7.9.1 Cooling patterns and Sedimentation

The final rapid cooling in the Nevado Filabride Complex, from 350°C to surface temperature (20°C) occurs between 15-8 Ma. This coincides with the appearance of coarse Nevado Filabride detritus in the Dudar Formation, but only in the later stages of cooling. It is assumed that this cooling, expressed as uplift, was the source for the Dudar Formation sediments, including the >2m size blocks. However, the higher temperature evolution, from 500°-350°C, seen in samples D3 and D4 precedes unroofing and deposition in the Dudar Formation by some 7-8 Ma This cooling even occurs some 2-3 Ma before the earliest sedimentation in the Granada Basin. There is clearly no simple relationship between sedimentation and the cooling of source rocks. Cooling events identified by the dating of detritus may not be related to the uplift events that lead to sedimentation.

Very rapid cooling was taking place in the Nevado Filabride during 18-15 Ma, that appears to have produced no sedimentary record. Even when the sedimentary record begins, it starts with marine carbonate sediments and shallow marine conglomerates. These sediments

contain no detritus consistent with the development of substantial subaerial relief generated by rapid uplift related to cooling in the Internal Zones, despite rapid cooling being recorded in the isotopic ages of detritus. The cooling of the Alpujarride Complex situated next to the Granada Basin was slower than the Nevado Filabride, but occurred earlier than the last cooling in the Nevado Filabride. The cooling of the Alpujarride rocks was also complete by the time of la Peza Formation sedimentation, around 14Ma, just after the phase of rapid cooling in the Nevado Filabride from 500°-350°C.

The conclusion that must be reached is that the cooling of the Nevado Filabride and Alpujarride complexes was accomplished without the generation of subaerial relief, and therefore without significant (or no) uplift. More than this, the orogen cooled in sub-marine conditions. This begs comparisons, the most likely one being with the extensional evolution of the Aegean Sea, where crustal extension reveals high grade metamorphic rocks in core complex type structural settings, but at low elevations (Gautier and Brun, 1993). However, the crustal thickness in the Betics is still large, around 40km, and was possibly thicker in the past, making high topographic expression more likely. However, metamorphic conditions that record burial could have been encountered at the base of the crustal pile, meaning that the crust was only ever 40 km thick *at most*. The suggestion of 40 km thick crust may be the maximum thickness obtained. In such a mobile orogen that has undergone periods of alternating extension and compression, rocks can be brought to the surface from the base of the pile, without the need for conventional layer by layer exhumation related to thinning. The Ronda Peridotites are good examples, as are high pressure rocks in subduction zones (Platt 1988).

The earliest sedimentation across the orogen is shallow marine of late Oligocene-early Miocene age. Individual basins were not distinct at that time and deposition was continuous across the whole orogen. Distinct basins began to form in the late Serravalian to early Tortonian. Sea level rose in the Langhian, with the deposition of marls on the Alpujarride, and the beginnings of calc-arenite deposition. Marine conditions persisted past the beginnings of the intramontane sequences, until the Pliocene, when uplift of the whole region culminated in emergence from the sea, and the onset of terrestrial and lacustrine sedimentation.

The rapid cooling recorded in the Nevado Filabride combined with the Langhian rise in sea level suggests an extensional cause for cooling, not uplift related exhumation. Extension is least likely to result in the generation of subaerial relief, but paradoxically it also leads to crustal heating as isotherms rise. It is hard to reconcile cooling with possible extension, even when required in order to form the Neogene Intramontane basins.

The initiation of the Neogene Intramontane basins in the Betics began properly during the late Serravalian and early Tortonian, at a time when cooling in the Nevado Filabride was advancing. Extension clearly took place at this time, as indicated by basin formation, which may also account for cooling and some exhumation of rock. Basin formation in the Betics is often attributed to dominant strike slip tectonics (Monenat et. al., 1987, Stromberg, 1994). Cooling may also be related to strike-slip. However, extension must not have been so extensive

before the late Tortonian stage in the Granada Basin, as basin sequences are still dominated by marine carbonates, so local relief caused by extensional high angle faulting was not important.

Later extension resulted in a better defined basin edge with locally significant relief, where fans built out, depositing large quantities of coarse detrital sediment. Water depth also increased, emphasising the occurrence of increased basin subsidence related to source uplift and increased extension. Nevado Filabride sourced detritus appears for the first time. This sudden input of coarse (>2m) clastic detritus sourced in the Nevado Filabride Complex corresponds with the late cooling in the Nevado Filabride, that is very rapid and constrained by fission track ages of 9-7Ma (Johnson, pers. comm.).

The exposure of the Nevado Filabride is achieved by very rapid uplift. Across the expanding surface of the uplift, higher structural units in the Alpujarride Complex, and the Granada Basin sediments, became detached. These units slid off in core-complex fashion along multiple detachments, found throughout the hanging wall. An important detachment is located at the base of the Granada Basin sequence, that has allowed the basin to slide away from the uplifting Nevado Filabride core of the Sierra Nevada. This has important implications for sediment dynamics within intramontane basins and the preservation potential and recycling of such basins. The detachment has clearly evolved since sedimentation in the Dudar Formation, as bedding dips at 35°, *parallel to the detachment*, and away from the Sierra Nevada, and younger sediments have less, or horizontal dips (Introduction and Chapter 3).

The next section proposes an evolutionary model for the eastern Granada Basin that is consistent with the data collected for this thesis. Data on the cooling of the Internal Zones and the sedimentary and macroscopic structural evolution of the study area are integrated. This model, though specific to the study area can aid the formulation of a more general picture of Betic evolution.

7.10 Evolution of the eastern Granada Basin and Internal Zones.

Figs. 7.8 and **7.9** bring together the main isotopic cooling, sedimentary and structural events evident in the evolution of the eastern Granada Basin.

The Alpujarride complex of the Internal Zones rests on the Nevado Filabride in thrust contact in the Sierra Nevada. Cooling ages from the structurally highest unit of the Alpujarride beneath the basin sediments record cooling during the period 28-23Ma, that continued at a minimum of 25-30°C/my until the unit was exposed to allow deposition of the la Peza Formation upon it at around 14Ma in shallow marine conditions. The staurolite schist records high grade metamorphism, and the 28Ma cooling age puts a minimum age on the end of this event. This cooling, though related to uplift has no clear sedimentary record. There was no subaerial relief in the Internal Zones at the initiation of shallow marine carbonate sedimentation, and detrital sources are only in the local Alpujarride.

During the period 18-15 Ma, just before the beginning of sedimentation in the la Peza Formation in the late Serravalian, rapid cooling took place in the Nevado Filabride rocks. These rocks are now present as conglomerate clasts in the late Tortonian age Dudar Formation, deposited at least 7 my after the rapid cooling they record. This cooling appears not to have

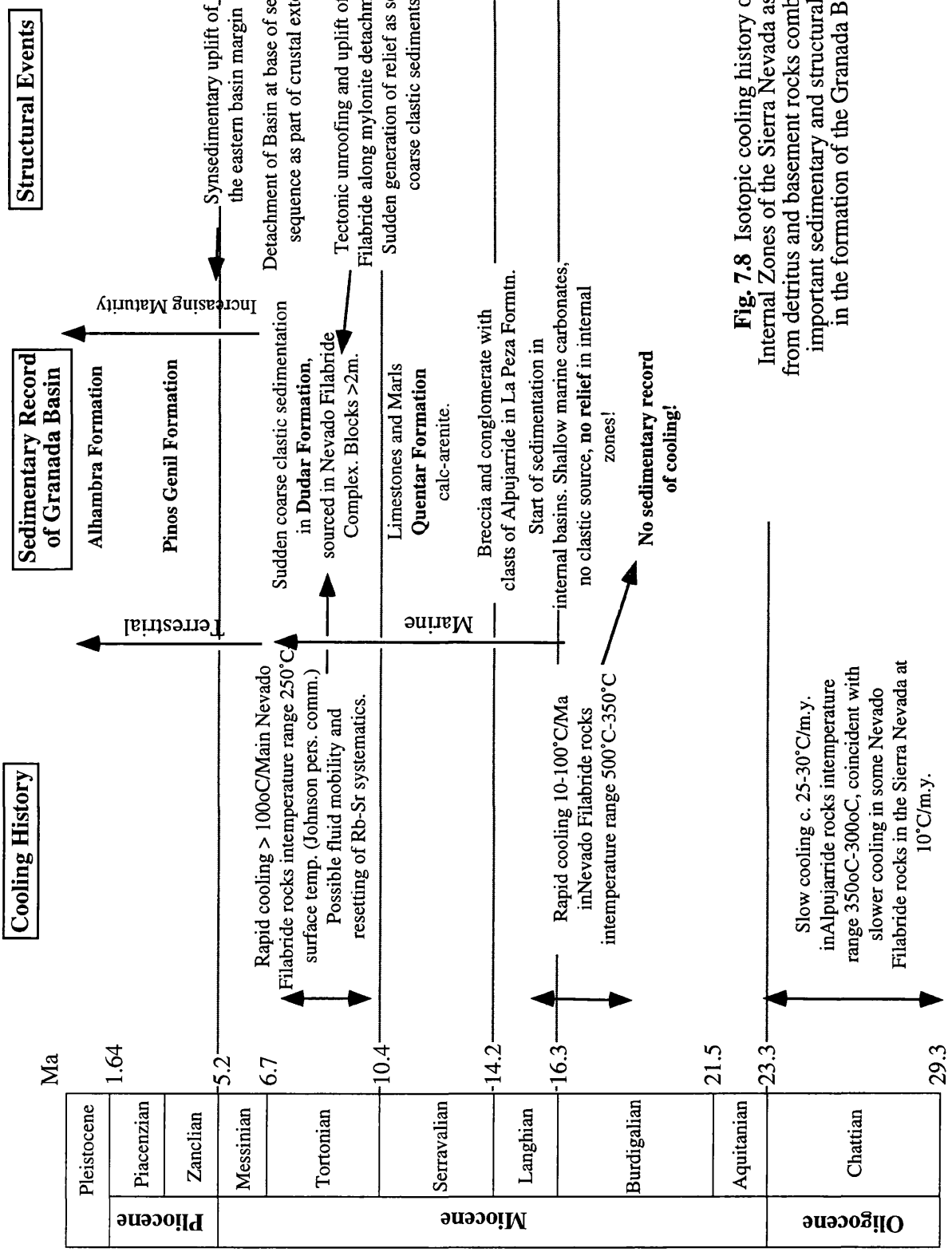

Fig. 7.8 Isotopic cooling history of the Internal Zones of the Sierra Nevada as derived from detritus and basement rocks combined with important sedimentary and structural events in the formation of the Granada Basin.

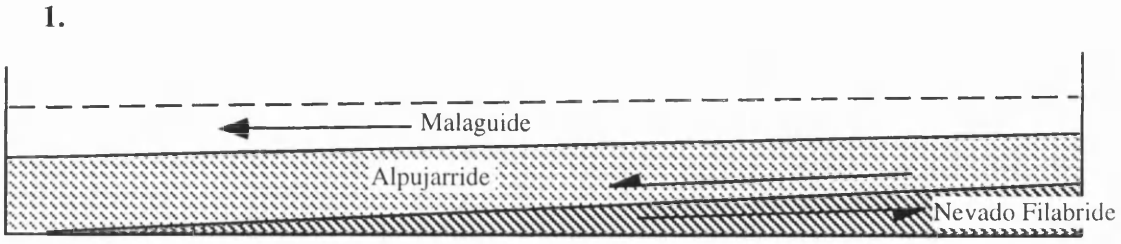

Late Oligocene. Cooling of Alpujarride, possible removal of Malaguides

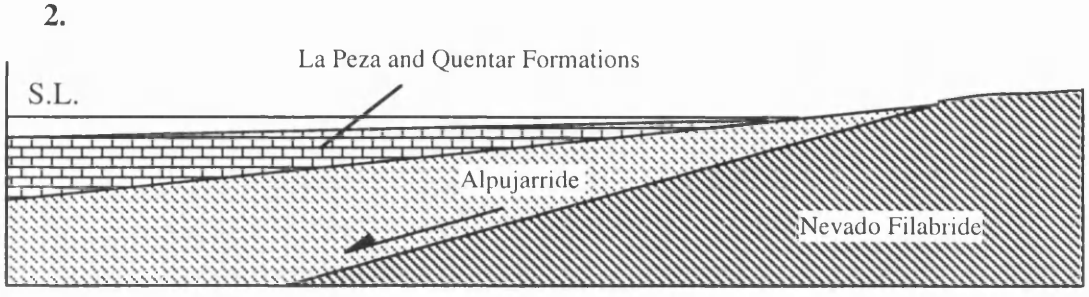

Early-Mid Miocene. Rapid cooling in Nevado Filabride prior to start of carbonate sedimentation in the early Granada Basin. Basin formation may have been related to extension that may have caused cooling.

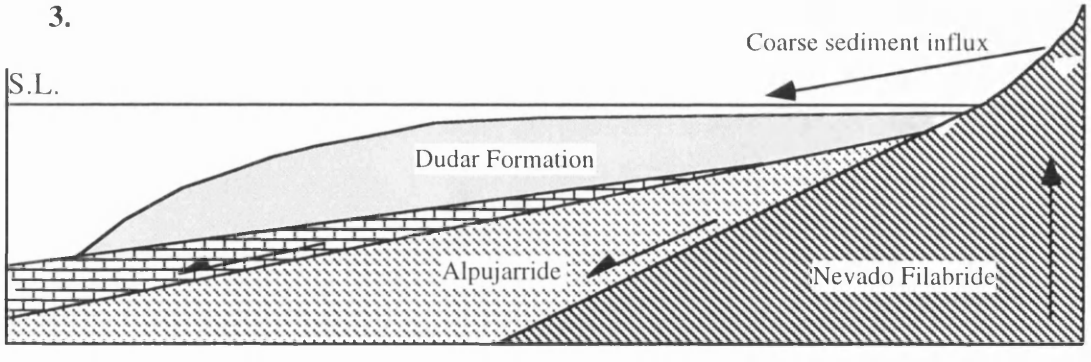

Tortonian. Increase in relief and uplift of Internal Zones souce area, influx of coarse detritus to form Dudar Formation Fan Delta.

Fig. 7.9 Cartoon evolution of the Eastern Granada Basin from the Late Oligocene to the Tortonian.

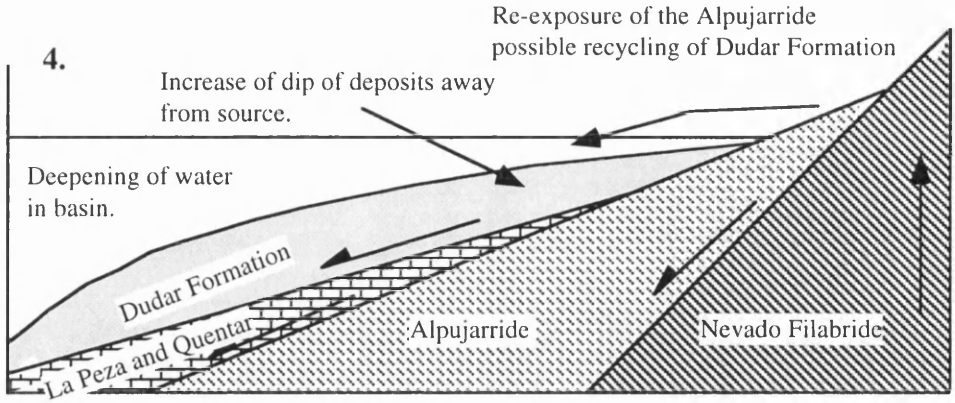

Late Tortonian. Continued uplift in the Nevado Filabride leads to detachment of basin sediments and the re-expusure of the Alpujarride Complex to supply clasts to the late Dudar Formation.

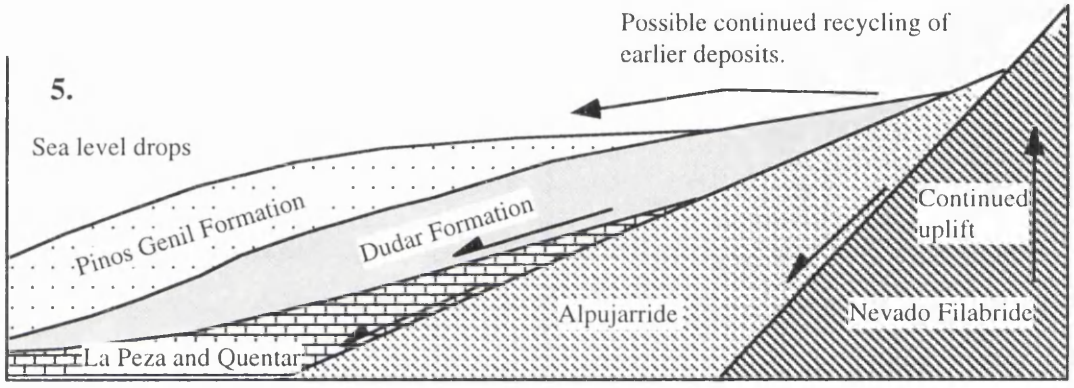

Pliocene. Marine regression, deposition of terrestrial Pinos Genil Formation.

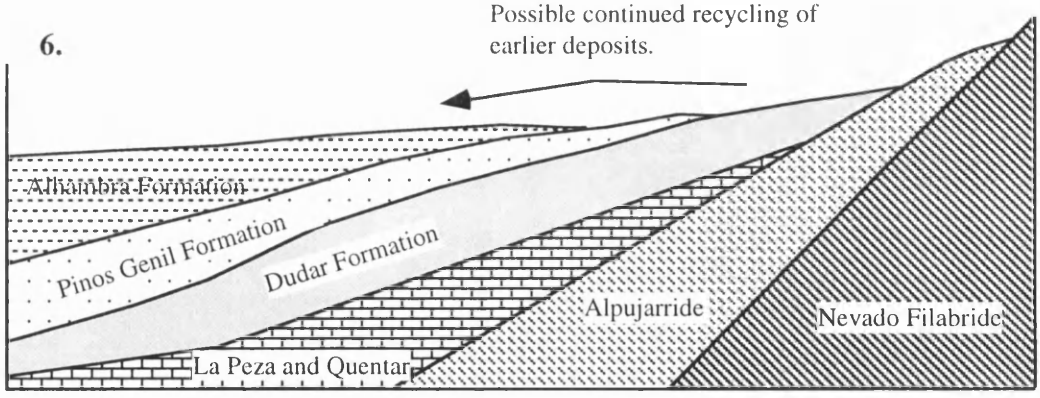

Pleistocene. Deposition of Alhambra Formation in more distal location and with more subdued source region.

Fig. 7.9 (Contd.) Cartoon evolution of the Eastern Granada Basin from the Late Tortonian to the Pleistocene.

been associated with the generation of orogenic relief, to establish a sedimentary source. Shallow marine carbonate deposition continued until the base of the Dudar Formation in the late Tortonian.

The presence of the dated conglomerate clasts in the Dudar Formation constrain the late cooling rate to >100°C. The sudden overwhelming of the shallow marine carbonate sequence by coarse clastic sediment, dominantly sourced from within the Nevado-Filabride Complex indicates the unroofing of the deeper Internal Zone rocks. Fission track ages of 7-9Ma (Johnson, pers. comm.) indicate rapid cooling coincident with sedimentation. Mylonite conglomerate clasts indicate the exposure of detachment zones in the Sierra Nevada, and suggest progressive extension across the region in a core complex style structural evolution. The Granada Basin persisted in marine conditions, with fan deltas fed from the uplifting basin margins.

In this model the Alpujarride, as befits its structural position on top of the Nevado Filabride, cooled earlier, and was exposed to allow unconformable sedimentation upon it, at least by 14Ma, in the early Serravalian. This is up to 6-7my before the unroofing of the Nevado Filabride, that occurred rapidly to feed detritus to the Dudar Formation in the late Tortonian. This unroofing of the Nevado Filabride was achieved by great uplift where the Alpujarride Complex cover was removed by core-complex extension. Significant local topographic relief was generated , that before that time was not present in the Internal Zones.

Continued uplift resulted in the emergence of the basin, and the transition from marine to terrestrial environments in the Pliocene. Uplift of the Nevado Filabride continued, dragging the basin flank upwards and imparting a regional dip to the Alpujarride and the overlying Granada Basin sequences, directed away from the uplifting core of the Sierra Nevada. This is postulated to have possibly resulted in recycling of uplifted basin deposits into younger sequences, thus accounting for the observed increase, with decreasing age, of maturity in the Pliocene and Pleistocene fan formations. Presently, due to this uplift, the active subsiding depocentre has contracted, and the basin flanks are eroding, being recycled into the centre of the basin. Drainage is no loner internal, but extends to the sea, via the Rio Genil and Rio Guadilquivir. The preservation potential of such first cycle deposits derived from high grade metamorphic rocks in a rapid orogenic uplift is low, because the deposits, being so very proximal, become involved in the uplift themselves and become available for erosion and recycling. Their initial deposition in the basin is a result of internal drainage within the mountain belt. This distinguishes these deposits from similar coarse deposits in other orogens.

It now remains to see how this evolution fits in to the overall history of the Betic Cordillera. Some aspects of the Granada Basin geology imply wider conditions and settings.

7.11 Implications for the evolution of the Betic Orogen

In this section the specific evolution of the rocks of the eastern Granada Basin, as derived from the data presented in this thesis, is related to more general schemes addressing the Betic Orogen as a whole. The nature of the Betic Orogen raises questions about its evolution, and especially the role of continental collision and subduction.

Cooling, sedimentation and orogenic features

Cooling in the Internal Zones in the Sierra Nevada took place without the generation of significant relief, in the aftermath of very high grade metamorphism. Of course cooling could have taken place as a result of extension, which would work against creating relief. Despite this, crustal thickness must have been up to 40km or more before cooling, to account for the observed metamorphism. This thickness of crust would normally have a surface expression. This is consistent with the Betics being within a compressional zone at the convergence of Africa with Iberia during the post Triassic closure of Tethys, as many models of Betic evolution suggest, but there is no evidence of orogenic scale relief being generated, just the deposition of shallow and deep marine carbonate sediments. Extension is therefore the probable mechanism of cooling. Critical to an understanding of the Betics is how extension can occur in a zone of plate convergence.

Many features normally associated with continental collision and subduction are not present in the Betic Cordillera, for example arc volcanism, plutonism, and during cooling in the Oligo-Miocene post metamorphic phase, topographic relief. Also, the sediment derived from the Internal Zones has a geochemical signature indicating provenance in a passive margin setting (see **Chapter 5**) due to a lack of igneous intrusions that would change the chemical signature of the original protolith material. This does not sit easily with suggestions of orthogonal compression, subduction zone tectonics or continental collision as a cause of the observed metamorphism. It is worth considering alternative explanations for the observed geological evolution.

The cooling evidence presented by Zeck et. al. (1992) suggests rapid uplift ending in exhumation in the early Miocene, which they suggest is achieved by extensional tectonism caused by rapid uplift forced by the loss of a subcrustal root. This extension is consistent with the deposition of nappe sealing marine sediments at this time, indicating subsidence, or at least low relief across the orogen at the time. De Jong et. al. (1992) and Van Wees et. al. (1992) propose an alternative view of inverted extensional tectonics to cause rapid cooling by cold underthrusting during compression, that would have inverted a period of subsidence and earlier basin formation. The amount of thrusting required to emplace the Ronda and Beni Bousera mantle peridotite bodies, from a great depth, must have been large. It is difficult to reconcile the large amount of thrusting that is clearly required with the fact of little topographic relief that is suggested by a lack of contemporaneous sedimentary inputs.

The rapid cooling in the Nevado Filabride Complex of the Sierra Nevada predates the earliest sedimentation in the Granada Basin, but postdates the rapid cooling in the Alpujarride rocks to the south. This rapid cooling in the Nevado Filabride is synchronous with marine deposition upon the Alpujarride. It is also synchronous with deposition and extension in the Alboran Sea (Campillo et. al., 1992). The sedimentary evidence is not consistent with thrusting and compression across the orogen as a cause for cooling, as proposed by De Jong et. al. (1992), and Van Wees et. al (1992). Thrusting can certainly explain the cooling in both complexes, but not the development of the basinal areas that were still submerged and did not receive much detrital sediment. Also, if the Alpujarride was on top of the Nevado Filabride, and

cooling proceeded from below, then the Nevado Filabride would have cooled earlier and more rapidly. This is not the case.

Extension driven cooling that proceeds from the top down is more consistent with all the evidence, than the cold slab underthrusting proposed by Van Wees et. al. (1992). Evidence for extension, not only exists in the mid Miocene formation of the Internal intramontane basins in the Betics, but also in the External basins that opened up along the north margin of the External Zones during the late Oligocene and early Miocene (Stromberg 1994). However, the emplacement of the Ronda Peridotite masses is crucial in constraining these models. They are allochthonous thrust sheets, that are most probably emplaced by compression, which ended at 22 Ma (Hebeda et. al., 1980). Sedimentation began in marine conditions not long after, so conditions may have rapidly changed to dominantly extensional by the early Miocene. Changes between extensional and compressional tectonism appear to be a feature of the Betics and occur on a short time scale.

Additionally, extensional collapse has been invoked to explain the evolution of the Betics. In the models of Platt and Vissers (1989) and Doblas and Oyarzun (1989), compression, expressed as thrusting in the Internal Zones of the Betics and the Rif of Morocco is suggested to be an expression of extensional collapse centred around the Alboran Sea . These models, and especially Platt and Visser's model, require a thickened crustal welt to have existed in the Oligocene from which gravitational spreading ensued. Metamorphic rocks certainly indicate burial to up to 40 km depth, but again, there is no sedimentary record of such a thickened crust at this time. The flysch units of the Gibraltar arc, though they are the right age, are too mature to have been derived from an uplifted orogenic zone (Stromberg, 1994), unless they represent the recycled cover to the region. It is clear that at the beginning of the sedimentation in the intra-montane basins of the orogen, relatively quiescent marine conditions prevailed over a submerged Betic orogenic zone. The removal of a thickened crustal root as proposed by Platt and Vissers (1989) suggests rapid uplift at around 19 Ma. This time is also coincident with the rapid cooling in the Alpujarride complex as recorded by Zeck et. al. (1992), who suggest the detachment of a sub-crustal mass. The removal of such a layer of thickened lithospheric mantle from beneath the Betics would encourage upper crustal uplift. This in turn would encourage extension to begin across the surface of an expanding uplifted region. However, these rapidly cooled rocks are unconformably overlain by marine carbonates containing a planktonic fauna. Extension appears to be taking place without substantial uplift. This suggests that the root zone to the orogen was perhaps still in place at the time suggested by Platt and Vissers for gravitationally driven extension to have taken place from their suggested thickened crust.

Rapid Late Miocene Core-Complex exhumation

However, geophysical evidence does indicate that there is a detached mass beneath the Betics, that has been attributed to a detached subducted slab (Blanco and Spakman, 1991). Rapid uplift *has* occurred in the Betics, that does have a conspicuous sedimentary record derived from rapidly generated topographic relief. However, this uplift occurred *later* than the

cooling episode of the early Miocene, which appears to have produced no sediment. This uplift is recorded in the coarse sedimentation in the Dudar Formation of the Granada Basin, and also in other basins surrounding the Sierra Nevada. This late Tortonian (approx. 9-8Ma) uplift may be associated with the detachment of the subcrustal mass imaged by Blanco and Spakman (1991), and be the cause of extension across the region and the core-complex evolution of the Sierra Nevada. The timing of this is later than the timing suggested by Platt and Vissers, and is not related to the main cooling event seen in isotopic ages of latest Oligocene to early Miocene.

Diachronous cooling

The cooling ages of the Alpujarride complex in the basement to the Granada Basin show that the Alpujarride Complex cooled before the Nevado Filabride, and at a slower rate. Cooling rates in the south-central Alpujarride, south of the Granada Basin and east of Malaga, are much more rapid than those recorded in the Granada Basin and occur at a later time (Zeck et. al. 1992). This suggests a non uniform cooling evolution for the Alpujarride rocks. A similar case can be made for the Nevado Filabride rocks. De Jong et. al. (1992) discuss ages ranging from 30 Ma to 14 Ma for the Mulhacen complex in the eastern Betics. This places a minimum age on the most recent metamorphism of the Unit, but also indicates, when combined with the ages presented here for the Sierra Nevada in the central Betics, a variety of cooling times and rates. This may suggest a diachronaity of cooling in the Betics, that is closely spaced, relative to the scale of orogenic processes. This may represent possible differences of metamorphic conditions and therefore geothermal gradients even within a single tectonic unit. Future studies must be careful in generalising from one area to the whole orogen, and must instead aim to present a meaningful scheme, that can explain these variations in conditions.

Plurifacial metamorphism

The lithostratigraphic sequence in the Internal Zones is complex, and involves the superposition of varying grades of plurifacial metamorphic rocks. The highest grade rocks are in the Alpujarride complex, of granulite facies, at the highest structural position, not at the base of the pile as might be expected. Their presence in the upper plate, hanging wall of the internal zones 'core-complex' detachment also suggests a more complex evolution for the Betics than just a cover-basement detachment, as is common in the metamorphic-core-complexes of North America. High grade rocks are superimposed against high grade rocks by the extensional development in the Internal Zones. The distinctive high grade metamorphic detrital signature produced by the unroofing of the Nevado-Filabride complex in the Sierra Nevada in a significant orogenic uplift (though on a small scale) indicates that the lower grade and sedimentary cover rocks of the Internal Zones had been removed at an earlier stage. The different units in the Internal Zones have been interthrust sometime after they had obtained their metamorphic signatures. Additionally, the metamorphism in the Internal Zones is plurifacial, and different elements of the Alpujarride and Nevado Filabride Complexes evolved through very distinct P-T paths, suggesting evolution in different places (Bakker et. al. 1989). The problem remains of how they came together into a single structural succession in the

Internal Zones. The Betic orogen may not be the product of simple orthogonal continental collision, but the result of multiple stages of metamorphism, extension and compression. The extensional collapse model of Platt and Vissers (1989) and Doblas and Oyarzun (1989) is perhaps too simplistic in assuming a single collisional metamorphism followed by post metamorphic cooling and extension.

Summary

In summary, several salient features of the Betic Cordillera are clear;

1 Rapid cooling of Internal zone rocks in the late Oligocene and early Miocene that was not related to uplift and the generation of subaerial relief.

2. Rapid changes between extension and compressional tectonism.

3. A tentative suggestion of diachronous cooling across the orogen.

4. Plurifacial metamorphic evolution of the Internal Zones, with the later superposition of nappes with differing metamorphic histories. This suggests a prolonged history of evolution, confirmed by early Permian intrusion ages for plutonic rocks.

5. Exposure of high grade metamorphic rocks superimposed against high grade metamorphic rocks in extensional detachments. This is indicative of early loss of low grade cover rocks, perhaps contained in the Malaguides.

6 Late Miocene core-complex style extensional evolution and uplift of the Internal Zones. This is related to exposure of high grade metamorphic rocks and the generation of course sediment deposited in surrounding sedimentary basins.

These important features may best be explained by an evolutionary model that does not involve subduction and orthogonal continental collision as the main driving force. The following section puts forward an alternative viewpoint.

7.11.1 Strike Slip and the Evolution of the Betic Cordillera

The purpose of this section is to detail evidence to indicate that the evolution of the Betic Cordillera has been due in large part, or *entirely* due, to transpressional transform tectonics, rather than to orthogonal continental collision. The history of interaction of the African and European plates is one of oblique convergence since the late Jurassic. Africa has moved eastwards with reference to Europe, and the Tethys ocean has contracted to form the Mediterranean Sea (See **Fig 7.10**, Dewey, 1989, motion derived from Atlantic Ocean magnetic lineations). This has generated, through compression, the Alpine orogenic belt stretching from the Straits of Gibraltar to the Middle East.

The dominant motion from the Jurassic to the beginning of the Tertiary at the Straits of Gibraltar has been left lateral strike-slip, according to Dewey (1989). At 65 Ma, until 9 Ma NNE directed compression took over, and from 9 Ma to the present, motion has been right lateral strike-slip. The amount of compression across the straits of Gibraltar has been small compared to that experienced further east. On the diagrams of Dewey et. al. (1989), in **Fig. 7.10**, the compressional movement suggested at the Africa-Iberia plate boundary is around 200 km. This compares with 600-800km in the central and eastern Mediterranean areas. These

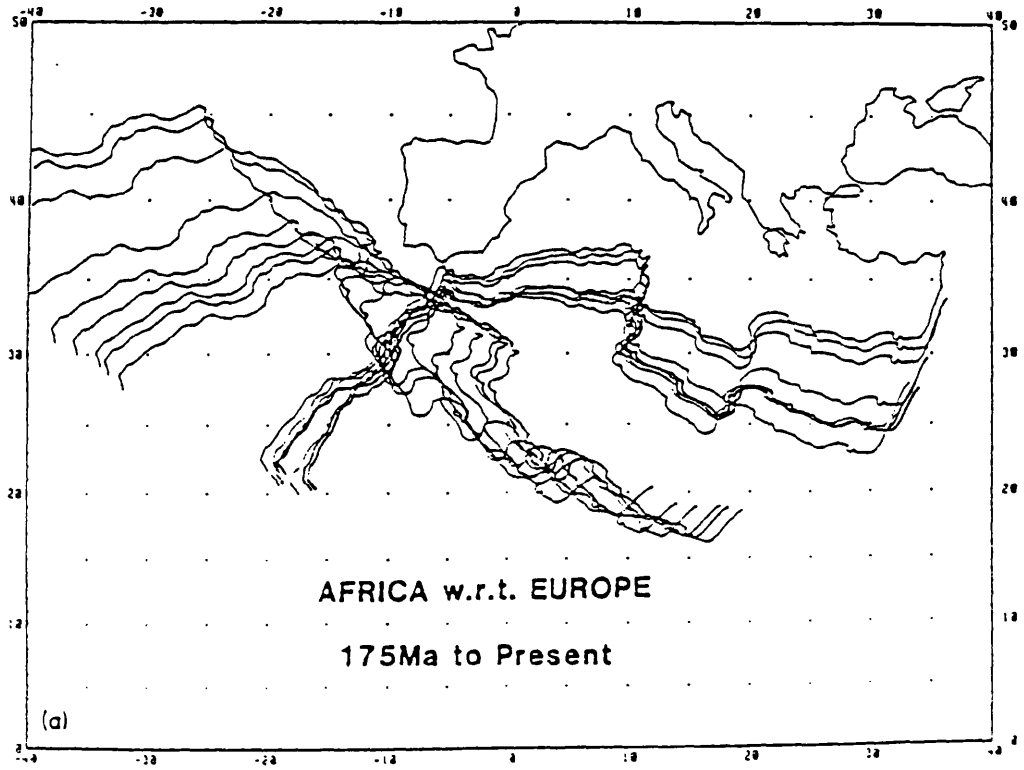

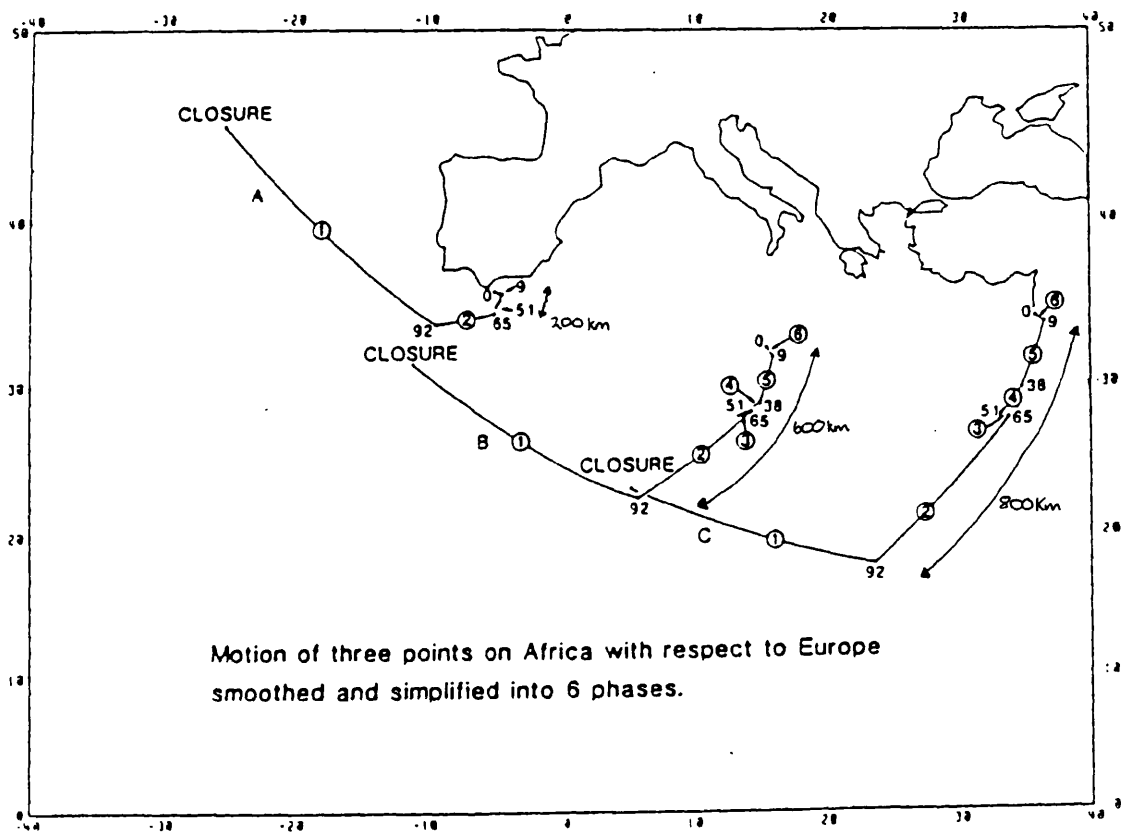

Fig 7.10Diagrams from Dewey et.al. (1989), that illustrate the relative motion of Africa with to respect to Europe. Note how the amount of closure of Tethys to form the Meditteranean is much greater in the east compared to the amount of compression across the Straits of Gibraltar.

compressional motions were not orthogonal, but involved a large component of left lateral transpression. This left-lateral motion is particularly acute at the Straits of Gibraltar. This evidence for plate movements, derived from magnetic lineations in the Atlantic, suggests a long (200Ma?) history of interaction at the boundary between the African and Iberian plates, within a transform boundary setting.

Srivastava et. al. (1990) present a more detailed reconstruction of plate motions (**Fig. 7.11**). Transform boundaries existed to the north and south of Iberia from the late Jurassic to the mid Cretaceous. By the mid Cretaceous movement ceased on the Iberia-Africa boundary, and all motion was taken up by the Bay of Biscay/Pyrenees fault. From 110 Ma till 37 Ma (late Eocene) Iberia moved as part of the African plate, with no relative movement between the two. This precludes any significant tectonism in the crust between Africa and Iberia for a significant period. The crust there must have been sufficiently mobile, however, to allow movement between Africa and Iberia to restart in the late Eocene. Again, as suggested by Dewey et. al. (1989), the dominant movement between Iberia and Africa was strike-slip, though the figure of Srivastava et.al (1990) (**Fig. 7.11**) suggests right-lateral movement. However, compression was minor, and severely curtailed during the period when Iberia moved as part of Africa. This inferred period of quiescence, when Iberia moved as part of Africa, does not sit easily with suggestions of tectonism and metamorphism as has been dated to have taken place in the late Cretaceous and early Tertiary (Puga et. al., 1989, Moine et. al., 1991).

Roest and Srivastava (1991) also show the relative motion of Iberia and Africa across the Azores plate boundary since the Eocene (42 Ma, see **Fig. 7.12**). Strike slip motion is dominant and right lateral in nature. Compression between Iberia and Africa amounts to around 100 km, and is oblique. It is clear from these studies and reconstructions that transpression may have been the dominant tectonic driving force in the Betic-Rif domain.

Campillo et. al. (1992) discuss the evolution of the Alboran basin, and suggest the importance of a transform regime developed in response to oblique convergence of Africa and Iberia. Their evolutionary model shows how structures form as the stress regime across the Alboran basin varies (**Fig 7.13**). Transtention encouraged the formation of pull-apart depressions that filled with pelagic sediments. Transtention gave way to transpression in the Miocene when the stress regime become orientated more north-south. Angular unconformities record this transition to compressional tectonics. However, strike-slip motions continued in an east-west direction, concentrated through the Strait of Gibraltar. This continued transtentional motion resulted in small pull apart basins in this area. Campillo et. al. (1992) invoke the possibility of tectonic transport of terranes along this dominantly strike-slip plate boundary, and the separation of the sedimentary and basement Alboran components from the continental lithosphere below, thus allowing some freedom of movement.

The role of strike-slip tectonics has long been recognised in the formation of the Neogene age intramontane basins in the Betics (e.g.. Montenat et. al., 1987). The Granada Basin is located on the boundary between the Internal and External Zones, a boundary which is considered to be an important strike-slip fault, representing the contact between the Iberian

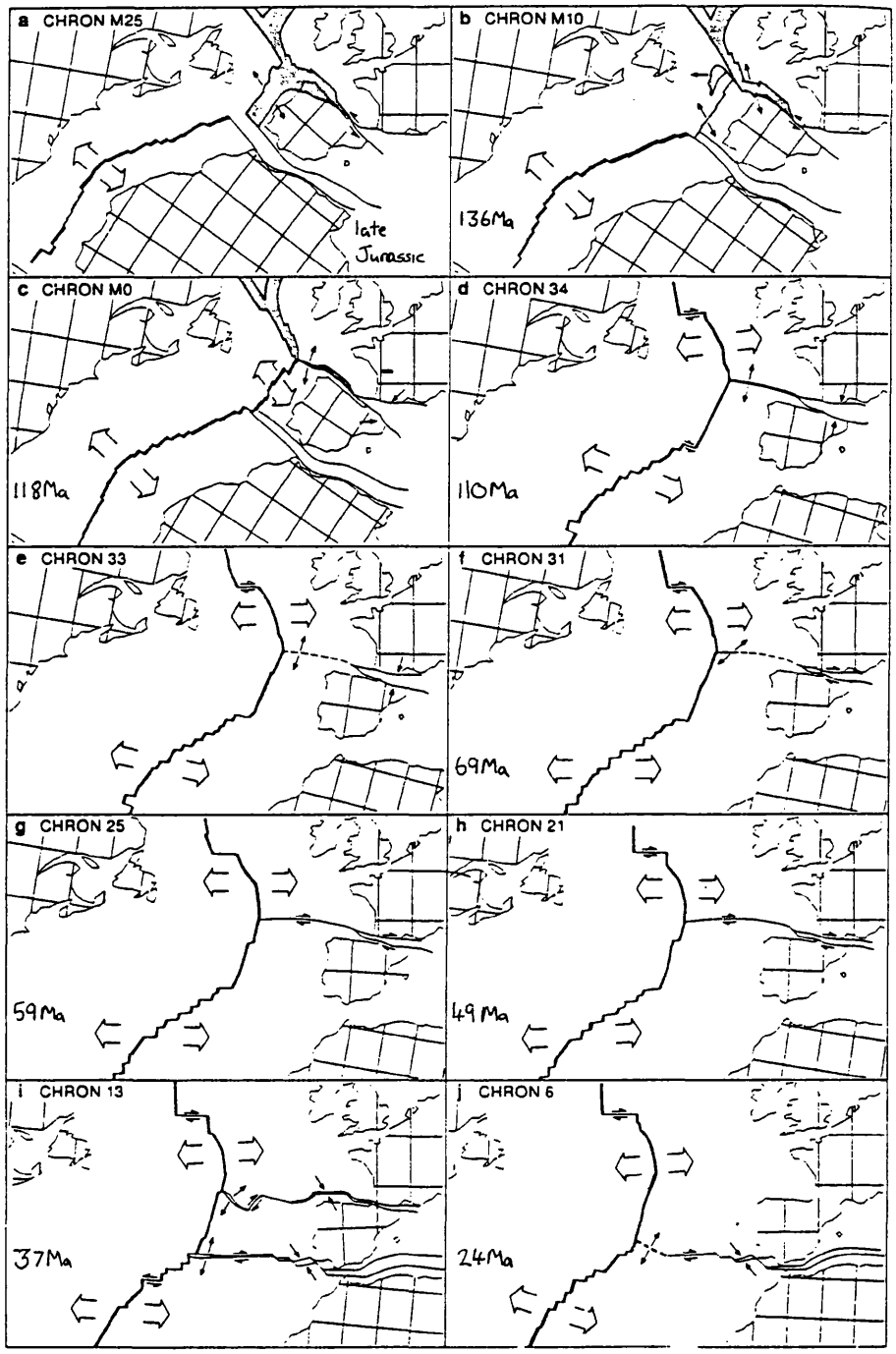

Fig. 7.11 Taken from Srivastava et.al. (1990). This diagram reconstructs the motions of the African, European, Iberian and North American plates since the late Jurassic, as derived from Atlantic ocean magnetic lineations. Note that from 110 Ma (frame d) to 37 Ma (i) Africa and Iberia move together as the same plate and that movement is instead taken up at the Pyrenees. Again, as in the models of Campillo (1992) and Roest and Srivastava (1991) (see Figs. 7.X and 7.X) relative motion between the European and African plates is dominantly right-lateral strike-slip from about 69 Ma (f), in contrast the reconstruction of Dewey et.al. (1989) (Fig. 7.X) However, before this time Iberia and Africa rotated considerably anti-clockwise south of Europe, which would have have been accomplished with left-lateral motion.

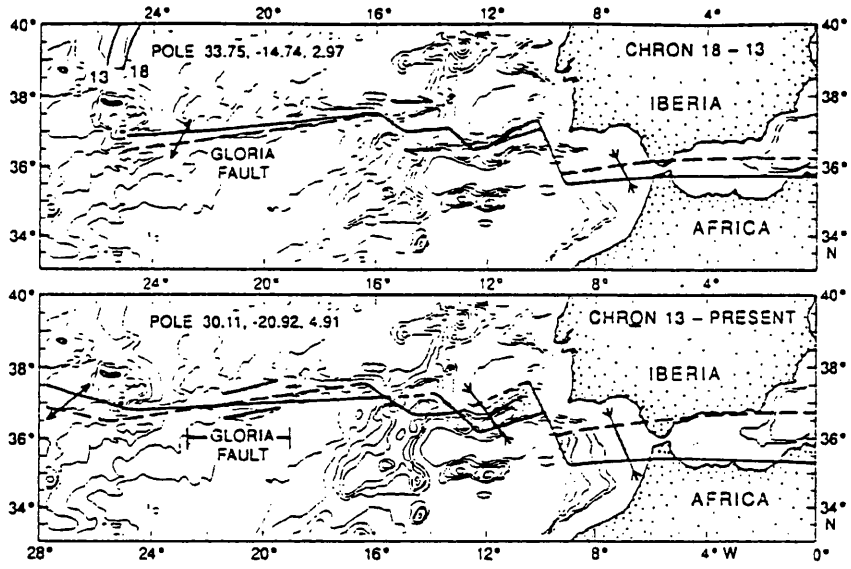

Fig. 7.12 From Roest and Srivastava (1991). This shows the relative motions of Iberia and Africa along the Azores-Gibraltar Fracture Zone since 42 Ma. Movement is dominantly righ-lateral strike slip, with around 100 km of compression between Iberia and Africa being accommodated by transpressive motion. (Chron 18: 42 Ma, Chron 13: 36 Ma)

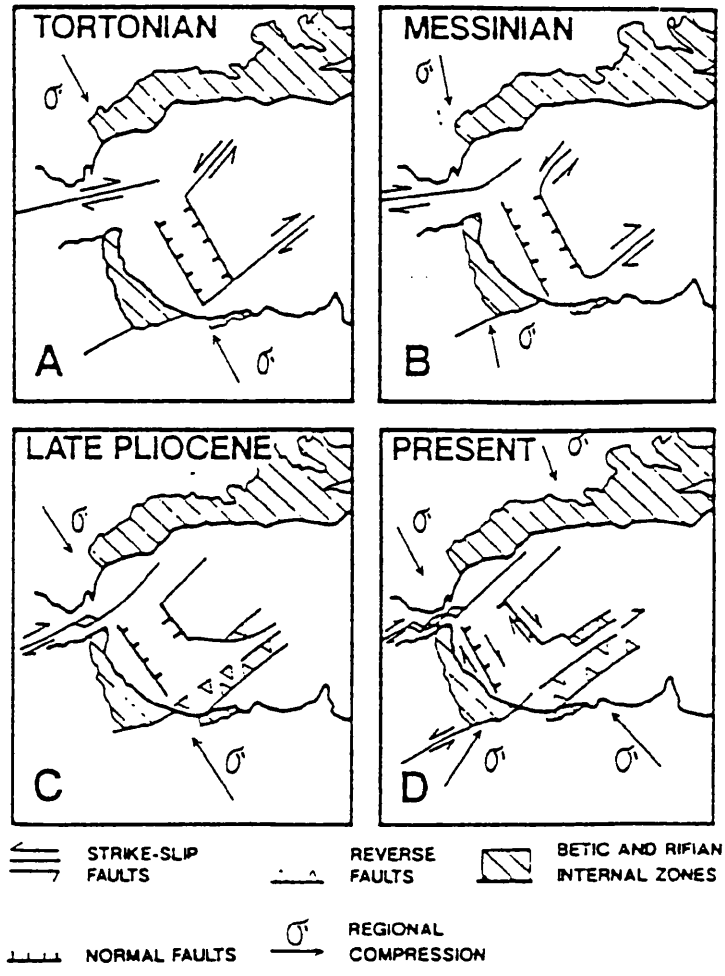

Fig. 7.13 Late Miocene to recent evolution of the Alboran Sea, from Campillo et.al. (1992). Movement is a complex mix of transtention and transpression, that varies in response to changes in the stress regime. Right-lateral strike slip dominates, and compression across the Alboran Sea is small.

passive margin sequence impinged upon by the westward moving Alboran Microplate during the Miocene (Sanz de Galdeano, 1992 and Leblanc and Oliver, 1984).

The palaeomagnetic work of Platzman (1992) and Allerton et. al. (1993) has highlighted important rotations of crustal blocks in the External Zones of the orogen and in the Rif of Morocco. The rotations are about vertical axes, which suggests that they are dominantly the result of strike-slip fault movements. The evidence presented by Platzman (1992) supports the model of evolution involving a westwards moving Alboran microplate, even though Platzman rejects this hypothesis. The model is consistent with rotations in the Rif of Morocco that are anti-clockwise and rotations in the Betics that are clockwise.

A crustal scale shear zone is proposed by Larouziere et. al. (1988) that runs NE-SW through the eastern Betics to Morocco (**Fig. 7.14**). This is also spatially associated with volcanism, that includes calc-alkaline extrusives. Left-lateral strike-slip is the clear control of this volcanism, along a zone of shear that penetrates deep into the crust.

In summary, there is a lot of direct evidence for the influence of strike-slip tectonics on the evolution of the Betic orogen. The formation of the intramontane basins is associated with extensive strike slip faulting, especially in the eastern Betics. The most compelling line of evidence is however, the plate tectonic scenario, as derived from magnetic lineations in the Atlantic. This highlights a prolonged (200Ma) history of dominantly transform tectonics at the contact between Iberia and Africa. Additionally, the lack of a collisional ridge apparently post the main metamorphic climax, as inferred from a lack of contemporaneous sediment deposition, and the lack of subduction related features such as magmatism and volcanism, suggests that orthogonal continental collision is not responsible for the metamorphism and structural evolution of the Betics. Strike-slip tectonics, operating in a transpressional manner, offers a possible mechanism for the evolution of the region.

Transpression could explain the variations in cooling, and reheating episodes, that are closely spaced both spatially and temporally. Strike slip may also account for the metamorphism in the Internal Zones, as well as the variations in thermal history. This possibility has also been proposed for the metamorphism in the Dalradian block (Dempster and Bluck, *in preparation*). Variations in fault geometry impose local compression and extension that can be closely spaced (Ingersoll, 1988). Movements along strike-slip faults could superimpose tectonic units with varying metamorphic evolutions, and even emplace the entire Internal zones into the region. This is significant as the Internal zones are somewhat anomalous in the region. They consist of metamorphic rocks derived from a passive margin sequence, emplaced by thrusting and strike-slip against an unmetamorphosed passive margin. The small degree of convergence observed to have taken place at the straits of Gibraltar could not have generated such a metamorphic sequence, that contains very high grade metamorphic rocks, in a position so close to a passive margin that shows no signs of metamorphism itself, or the detritus that may have been derived from such an active metamorphic tectonic unit. The external zones show no evidence for the nearby presence of the Internal Zones until the late Oligocene when the Internal Zones began to impinge. The metamorphism in the Internal Zones is older than the deformation of the external zones caused by the overthrusting of the

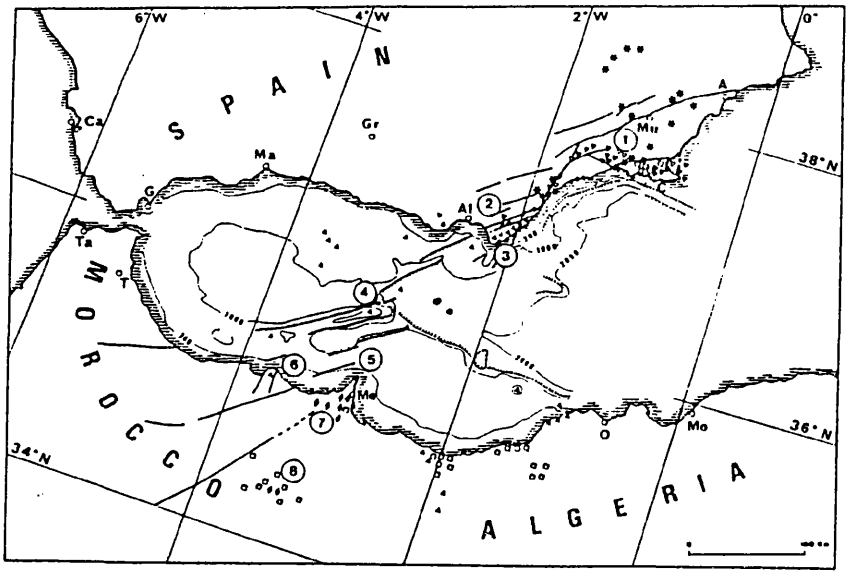

Structural sketch map of the Betic Rif area. *A*—Alicante; *Mu*—Murcia; *Al*—Almeria; *Gr*—Granada; *Ma*—Malaga; *Ca*—Cadiz; *Ta*—Tanger; *T*—Tetouan; *Me*—Melilla; *O*—Oran; *Mo*—Mostaganem. Symbols: asterisks—lamproite; open triangles—anatectic; squares-alkali-basalt; solid triangles—calc alkalic; diamonds—shoshonitic magmatism.

Fig. 7.14 From Larouziere et.al. (1988), showing trans-Alboran shear zone, with location of transcurrent faults, attributed to left-lateral movement. Magmatic activity is spatially associated with faulting and crustal mobility in the SE Betics.

Internal Zones. Strike-slip tectonics offers a mechanism to emplace such a 'terrane' along strike, either from the east, or as is generally favoured (Sanz de Galdeono, 1992) from the west. This may be analogous to the assembly of the Caledonides by strike slip means.

7.12 Conclusions

1. Conglomerate clasts and bulk detrital muscovite separates from the late Tortonian Dudar Formation and Pliocene Pinos Genil Formation of the eastern deposits of the Granada Basin record ^{40}Ar-^{39}Ar and K-Ar cooling ages of between 10 and 30 Ma. Most samples have ages between 12-17 Ma, and there is a second minor group around 20-23 Ma and one sample at 30 Ma.

2. Basement lithologies from the Nevado Filabride complex in the Sierra Nevada have K-Ar cooling ages of between 10-13 Ma and 20-22 Ma. In the overlying Alpujarride Complex one sample gives ^{40}Ar-^{39}Ar ages of 25 Ma and 28 Ma for muscovite and 23 Ma for biotite. Another Alpujarride Complex sample gives a K-Ar age of 72±2 Ma, indicating a possible history of metamorphism and cooling lasting since the Cretaceous.

3. Rb-Sr ages for conglomerate clasts are concentrated around 22-18 Ma, with two samples with ages of 28-27 Ma, and one sample with an age of 64.13 ± 0.19 Ma. Rb-Sr ages for basement lithologies are uniformly younger than K-Ar ages from the same samples, suggesting the probable resetting of isotope systematics. However, mylonitic tourmaline-feldspar rock from a detachment zone in the Mulhacen complex in the Sierra Nevada gives a reliable 10±1.29 Ma Rb-Sr age.

4. The combination of age determinations using methods that have different closure temperatures allow minimum cooling rates to be calculated. From these, and an assumption of geothermal gradient, uplift rates can be inferred. For the conglomerate clasts dated in the Dudar Formation the cooling rate varies between 3.08 and 106.4 °C/Ma, between 500°C and 350°C. This translates into uplift rates, using a 30°C/km geothermal gradient, of between 0.34 and 3.47 km/Ma for this temperature interval.

The depositional age of the sediments of the Dudar Formation further constrain cooling from the closure of the K-Ar system at 350°C to surface temperatures. Cooling from 350°C to surface temperatures was rapid, at a minimum of 50°C to a maximum 200°C/Ma between 15-8 Ma. This translates to possible uplift rates of between 0.67-6.67 km/Ma The basement rocks dated from the Sierra Nevada share this cooling rate, though they have cooled a little later than the conglomerate clasts.

The Alpujarride rocks beneath the unconformity at the base of the Granada Basin, where deposition is dated as Serravalian (14-11Ma approximately), cooled at a slower 25°C-30°C/Ma, between 25-14Ma, preceding the cooling in the Nevado Filabride Complex. This can be related to uplift at rates of 0.83 to 1 km/Ma

5. The main times of cooling indicated by isotopic dating predate clastic sedimentation in the Dudar formation by 7-8 Ma, and 3-4 Ma before the earliest sedimentation in the Granada Basin. These earliest sediments are shallow marine carbonates and contain no detritus consistent with rapid cooling in the underlying Internal Zone rocks only 3 Ma before. Cooling

took place without uplift in the Internal Zones during the approximate period 20-15 Ma. There was no relief in the area at the beginning of Granada Basin sedimentation that could have been a significant source of siliciclastic detritus.

There is no simple relationship between sedimentation in the Dudar and Pinos Genil Formations and the isotopic ages recorded by these sediments. The cooling event recorded in the isotopic ages of sediment is not connected to the event in the source that generated the sediment.

6. Late rapid cooling, that began at 15Ma onwards, immediately predates the sudden unroofing of the Nevado Filabride Complex that shed very coarse detritus into the Dudar Formation Fan-delta sequence during the late Tortonian. This change in sedimentary environment, brought on by the emergence of a significant detrital source, is also coincident with cooling recorded by fission track ages in the Sierra Nevada (Johnson, 1994).

7. Anomalous Rb-Sr ages indicate possible resetting of isotope systematics. Carbonate present in several samples (but not all affected samples) may be the cause of altered Sr contents in whole-rock analyses. It is possible that this carbonate was introduced by fluid interaction at temperatures below 500°C, otherwise isotopic ratios in muscovite would have been reset, and age dating would date cooling after this event. Veining is abundant in the Sierra Nevada, especially in the Alpujarride Complex, indicating much fluid activity. Further dating work must use carefully characterised samples to avoid the effects of late alteration of isotopic systems.

8. Late (Tortonian) cooling is related to uplift of the eastern flank of the Granada Basin, and exhumation of the Internal Zones in core complex style extension. Earlier deposits were included into the source region, making them available for reworking into younger sediments. This links source cooling, recorded by isotopic dating, to the increased maturity of coarse sediment seen in younger deposits of the Basin. This late uplift is also linked to the development of extensional detachments at the base of the sequence and within the sediments, and the development of angular unconformities at the base of the Pinos Genil Formation due to the uplift of the Dudar Formation. Thus isotopic dating, basin extension, source uplift and exhumation, sediment maturity and provenance can be interrelated.

More general conclusions about the nature of the Betic Cordillera are also reached:

8. Several features of the Betics may be best explained by strike-slip tectonics. The formation of the intramontane basins, including the Granada Basin, has been often attributed to right-lateral strike-slip faulting during the Neogene. Large scale plate tectonic considerations suggest that transpressional strike-slip has been the dominant setting for the Betics since the late Jurassic. Compression across the region has been around 100-200 km since this time, and always oblique. Features such as diachronous cooling of tectonic units, plurifacial metamorphism, and the juxtaposition of these units after they had acquired their metamorphic characteristics may be best explained by strike-slip. Along strike variations in geometry of faults can generate local variations in compression and extension, with consequences for metamorphism, thrust nappe movements and basin formation.

9. Strike slip may also be responsible for the emplacement of the Betic-Rif domain at the boundary between Iberia and Africa in a similar fashion to the terrane assembly of the western U.S.A. The Betics are anomalous compared to the Spanish Hercynian basement, and impinge upon the passive margin sequence in the External Zones. They have clearly not been metamorphosed in-situ, otherwise the External Zones would be more affected, and would also show sedimentary evidence for the adjacent presence of a thickened crust undergoing metamorphism, but the external zones do not exhibit such evidence. The Internal Zones may be an exotic terrane that has been emplaced into the region, most probably by strike-slip tectonics.

8. Conclusions

1. *Relationship between source cooling and sedimentation.*

The isotopic dating work on detritus from the Granada Basin and the basement source lithologies for these rocks in the Sierra Nevada region, indicates a *complex relationship between source cooling and sedimentation in the adjacent receiving basin.*

^{40}Ar-^{39}Ar, K-Ar and Rb-Sr geochronometers record significant cooling in the source terrain in the Sierra Nevada that began at 30 Ma and continued to around 10Ma. Within this time period the most intense period of cooling was from 18Ma to 13Ma (approx.), with cooling rates at a maximum of 100°C per million years. There is no record of any sedimentation at the start of this period in the Granada Basin. When deposition did begin, during the Langhian, it was shallow marine carbonate deposition, with a basal deposit of well rounded marine conglomerates sourced from the Alpujarride Complex dolomites. This suggests rather quiescent conditions across the orogen simultaneous with cooling, or the possibility of the orogen starting to uplift below sea-level. This poses problems, particularly for the accommodation of rapid cooling in the basement rocks that took place coevally with shallow marine carbonate deposition in the early Granada Basin. Also on a more general scale, it suggests possible difficulties in the reading of the record of cooling and uplift in sediments derived from active orogenic areas. The coeval sedimentary record of cooling of the Internal Zones in the Sierra Nevada is in sediments that preserve no signature whatsoever of the cooling, and if interpreted in isolation would lead to the conclusion that there was no significant tectonic activity in the Internal Zones at that time.

Coarse fan sedimentation in the succeeding Dudar Formation clearly indicates tectonic activity and rapid source uplift within the Sierra Nevada at the time of sedimentation. But the *uplift recorded by the coarse sediments of the Dudar Formation is not directly related to the isotopic cooling ages recorded by this detritus.* The cooling ages preserved in the detritus pre-date uplift and sedimentation by up to 10Ma. There is, in this case, a significant lag between source cooling, which was not directly associated with the production of sediment, and the uplift and erosion of the rocks in the Internal Zones of the Sierra Nevada.

This lag between the time of cooling recorded in detritus and the time of deposition of the detritus can be explained if we consider that during cooling (if it involves uplift) the level that is exposed and producing sediment is potentially 10Km above the level where cooling is being recorded. However, structural detachments can account for considerable crustal thinning that need not involve uplift and associated sedimentation. The Internal Zones in the Sierra Nevada have evolved as a metamorphic core-complex, with several intra-basement detachments, and, at a higher level, with detachments within the sediments of the overlying Granada Basin. In such cases cooling need not be associated with uplift and a

contemporaneous record of sedimentary deposition in adjacent areas.

The important anomaly in the Granada Basin, is that the sediment deposited during cooling of the Internal Zones in the Sierra Nevada, belies any tectonic activity related to the cooling as recorded in the source by ^{40}Ar-^{39}Ar, K-Ar and Rb-Sr dating methods. Conversely the later tectonic event related to the uplift of the Internal Zones core complex, that produced copious amounts of coarse sediment has no record in the isotopic ages preserved in the detritus produced. Clearly, provenance studies that use isotopic dating of sedimentary detritus to reach conclusions about source evolution, need to accommodate the possibility of complex relationships between source cooling and sedimentation.

2. *Provenance characterisation of orogenic sourced sediments*

Sandstone composition data from the sediments of the Granada Basin suggests that sediments that are derived from high grade metamorphic source uplifts in core-complexes may represent a previously unrecognised or poorly constrained provenance type.

Petrographic analysis of sandstones from the Dudar Formation and younger sediments of the Granada Basin reveal that they are composed of high grade metamorphic rock fragments, sourced in the high grade metamorphic core of the Internal Zones core complex. They are early cycle deposits and faithfully reflect their ultimate basement source. On provenance classification diagrams, such as the QFL and QmFLt ternary plots of Dickinson and Suczek (1979), Granada Basin sandstones mostly fall in the recycled orogen field, a generally correct provenance assignment, but some samples fall in the arc provenance fields. The fact that some samples fall in the arc field, that is a plainly incorrect provenance assignment hints at possible problems of applying such a method to all sandstones.

In detail, the samples used by Dickinson and Suczek (1979) to construct the recycled orogen fields, where the Granada Basin samples cluster, are not the same type of sample as taken from the Granada Basin. The particular recycled orogen areas where the Granada Basin samples group on the plots by Dickinson and Suczek, are *defined* by sandstones with a high content of oceanic derived lithic grains, that are mainly low grade and include chert. As the plots of Dickinson and Suczek (1979) are created from real sandstone analyses, they define an actualistic subdivision, which from the evidence presented here may include significant overlap between detailed provenance types. Despite indicating a generally correct setting of recycled orogen provenance, the Granada Basin samples record a high lithic component composed of high grade metasedimentary detritus.

The Granada Basin contains sediment sourced from a high grade metamorphic block that had no low-grade metamorphic and sedimentary cover at the time of formation of the Granada Basin. The high grade metamorphic rocks exposed in the Internal Zone core testify to the removal of up to 40Km of crustal thickness in order to expose these rocks for erosion. However, the large quantities of sediment that could account for this removed crust are not present in the Betics, and there is no evolved, mature sedimentary cover consistent with the erosional level in the Internal Zones. The Granada Basin sediments are unusual as they are the immature beginnings of the evolution of a sedimentary cover layer, that have their first source

in very high grade metamorphic rocks, exposed from a great depth, whose exhumation appears not to have involved significant sedimentation. This contrasts with the expectation that the first sedimentary input to orogenic cover development would be from low grade metamorphic and sedimentary rocks in the highest levels of crust involved in orogenesis.

Chemical provenance classification of the sandstones from the Dudar and Alhambra Formations indicates a passive margin provenance for deposition. This is erroneous classification for the Granada Basin sandstones occurs because of the immaturity of the sandstones, which reflect the source area in the Sierra Nevada so well that the provenance indicated is likely to indicate the depositional setting of the protoliths to the metasediments of the Internal Zones in the Sierra Nevada. This again emphasises the care which should be exercised in applying provenance discrimination schemes. The role of high grade metasedimentary source terrains as a provenance type is poorly constrained, but should be considered for inclusion in future discrimination schemes. However, this case in the Betic Orogen may indicate the utility of using the geochemistry of metasedimentary rocks to indicate protolith depositional setting, in the way that such workers as van de Kamp and Leake (1985) hoped for.

The best way to interpret sandstone composition data in order to determine provenance and accurately make tectonic inferences is by an integrated basin model approach involving basin type and formation mechanisms combined with tectonic setting. Tectonic regime unifies basin attributes, including basin forming mechanisms and crustal type, so therefore determines sediment composition. However, there are exceptions to this, as Cox and Lowe (1995) demonstrate. Evolving sedimentary cover matures with time by recycling due to re-sedimentation in new basin environments that can originate by any basin forming mechanism and tectonic regime that affects source terrains. Inherited crustal type can be involved with basin formation by a mechanism normally associated with a different crustal composition and therefore sediment composition. In this way any provenance approach that involves the construction of definitive models associating sediment composition with tectonic environment in a deterministic way will not succeed every time.

Provenance constantly changes, as sediment becomes source itself and is recycled and mixed with fresh basement inputs. Even through a single basin evolution cycle provenance will change, expanding or contracting due to tectonic influences, and sediment previously deposited will be recycled. Each example is unique, and must be explored using a wide a range of analytical approaches. This demands the careful application of sandstone provenance modes in making tectonic or palaeogeographical inferences.

The exposure of high grade rocks in the cores of metamorphic core complexes such as in the Internal Zones of the Sierra Nevada is a common feature. Perhaps this particular source signature is characteristic of core complex evolution, and should be recognised as a distinct provenance type. However, the absence of significant igneous intrusives and thick (<1km) mylonites, that are common features of the North American Core Complexes, from the Sierra Nevada may mean this Betic example is rather unique, and that other core complex signatures may have a higher content of feldspar, and lower lithic grain content.

3. *Patterns of conglomerate and sandstone compositional change*

Petrographic analysis of the conglomerates and sandstones from the Eastern Granada Basin indicate unexpected patterns of sediment composition evolution.

Conglomerates in succeeding formations become increasingly mature. Estimation of clast roundness shows a decrease in angular clasts and an increase in abundance of rounded and well rounded conglomerate clasts in the younger Pinos Genil and Alhambra Formations compared to the Dudar formation. Quantitative measurements of clast composition versus size of clast reveal that compositional maturity increases in the younger formations. Labile schistose lithologies become less common as clasts in younger formations, and quartzites and other quartz rich clasts become more common, especially in the coarser grain sizes. This is interpreted as indicating the break-down of the labile schist clasts. However, schist clasts do not increase by more than 5% as a proportion of the smallest clast sizes, despite increasing their number by break-down. This is resolved if the smallest schist clasts are also breaking down to fragments smaller than 2cm across, the limit for recording conglomerate. Therefore the sand-size fraction may be fed by the break-down of conglomerate material.

The break-down of conglomerate material is interpreted as having taken place by one of two methods. Firstly, the environment of deposition changes at the end of Dudar Formation times, from very rapid marine to subaerial alluvial fan deposition. It is possible that slower depositional rates, in a more intense weathering environment combined with extended fan-top residence and reworking could have resulted in a more mature conglomerate clast population derived from the same source. Secondly, however, the depositional geometry and basin edge structural evolution suggest that sedimentary recycling from earlier deposits may have also played an important part in increasing maturity. The basin edge was uplifted dramatically by the rise of the Internal Zones Core-Complex during active sedimentation, resulting in complex structural instabilities in the sedimentary deposits, angular unconformities between formations and the inclusion of the earliest sediments into the source area.

The sandstones deposited with the conglomerates share the same depositional conditions and sources so may be expected to show a parallel maturing trend. However, and *despite evidence of increased grain alteration through subaerial weathering, the sandstones do not increase in maturity*, but show an increase in the lithic grain content at the expense of quartzose grains. This is interpreted as indicating an increased input of lithic sand-sized grains derived from the break-down of schistose conglomerate clasts, that results in the increased maturity of the conglomerates. Sand maturity in this case lags behind the development of conglomerate maturity because the break-down processes that increase conglomerate maturity act like a primary sediment source feeding the sands. This is likely to be a short lived phenomena, confined to proximal settings and early stages of recycling. Conglomerate evolution has advanced in the Granada Basin significantly in only three possible recycling stages, and the preservation potential of such intramontane deposits is low due to their proximity to and involvement in tectonic activity. However, this pattern of composition evolution could have an influence on the interpretation of provenance information where such processes could be identified.

Major and trace element geochemistry of sandstones from the Dudar and Alhambra Formations of the eastern Granada Basin show patterns of systematic change that are related to the different textural maturaties and state of alteration of the sediments in response to weathering environment. The Alhambra formation is the most chemically mature of the formations, having higher overall SiO2. This is despite the decrease in the maturity of modal grain composition. Mobile elements such as Na and Ca decrease significantly in the Alhambra Formation, and more immobile elements such as Al and K increase. These latter element abundances are probably associated with sheet silicate abundance, and the relative stability of muscovite, which increases in abundance in the Alhambra Formation. Chemical weathering during transport and deposition works to increase chemical maturity in all sand grains, despite the decrease in maturity of the overall grain framework mode. In this case whole-rock geochemistry appears to mask the complexities of the processes that affect the detrital framework compositional modes. Increasing maturity is recorded in the increase of silica, despite the decreasing, or at least not increasing, maturity of the detrital framework composition. If viewed alone then a potentially incorrect understanding may be reached of the evolution of sediment composition within proximal settings, and especially in the detailed dynamics of the early stages of sedimentary recycling. Without the petrographic data to constrain interpretation, the evolution of sediment composition could be viewed incorrectly as a smooth path of increasing silica related to increasing petrographic framework maturity.

The heavy mineral population of the sediments show an increase in the proportion of stable mineral species such as zircon and tourmaline, in the younger Pinos Genil and Alhambra Formations. This can be attributed to the increased intensity of weathering alteration experienced during transport and deposition, which selectively removed less stable mineral species, especially garnet. Epidote increases in abundance quite significantly in the Alhambra Formation, suggesting that it is relatively stable, or that some source control was operating. Again, this increase in maturity is in the opposite sense to the maintained or increased lithic content of the sediment as a whole. Electron microprobe studies of the compositional range of garnet indicate no preferential removal of any particular composition by weathering or reworking in the Granada Basin. Epidote compositions become less Ca rich and Fe poor varieties become more common in the Alhambra Formation. Tourmaline compositions show no change at all in the more mature sediment of the Alhambra Formation. Weathering experienced during transport and deposition has not biased the internal compositional ranges of individual minerals, despite being the likely determinant of changes in relative heavy mineral abundances. This contrasts with the Studies of Morton (for example, 1985, 1991), where it is seen that deep burial and diagenetic processes have had systematic effects on mineral composition. Such evidence of a lack of compositional selection within heavy mineral species populations in sediments, as seen in the Granada Basin sediments may indicate the absence of significant post-depositional alteration.

4. *Implications for models of Betic Evolution.*

The isotopic dating of sedimentary detritus from the Granada Basin and metamorphic source rocks of the Internal Zones suggest a long history of evolution. Dates of 64 and 72Ma where obtained indicating prolonged post tectonic cooling. The most recent cooling episodes occurred in the late Oligocene and Miocene. The Alpujarride Complex cooled before the Nevado Filabride Complex, consistent with the Alpujarride Complexes higher structural position. Rapid cooling took place in the Sierra Nevada during the mid to late Miocene, consistent with very rapid cooling recorded in other parts of the Internal Zones (Monie, 1991, Zeck et. al. 1992).

Isotopic dating combined with the sedimentary evidence from the Granada Basin can partially constrain the palaeogeography and tectonics of the Betics during the Miocene. Cooling must have taken place in a crustal section submerged below sea-level. This suggests extension driven cooling, or the presence of a dense crustal root that acted against crustal buoyancy and prevented subaerial exposure, and the generation of significant amounts of sediment.

Other considerations on a Betic orogen-scale, though not constrained by the data presented in this work, suggest the possibility of strike-slip tectonics as the primary driving force in the evolution of the Betics. The dominant motion at the plate boundary between the African and Iberian plates since the Jurassic has been oblique left-lateral. This best accounts for the late Miocene evolution of the intra-montane basins, such as the Granada Basin, as transform basins, but it can also provide a possible mechanism to explain metamorphic patterns, and the juxtaposition of tectonic units with different tectono-metamorphic histories, and not least the emplacement of the Internal Zones against the External Zone passive margin during the Oligocene.

Appendix 1 Methods

A1. Petrographic methods

A1.1 Sample selection and thin section preparation

Thin sections were prepared of Spanish samples, which were selected to be as unaltered and as representative as possible of their locality. Many of these late Cenozoic age samples are poorly consolidated, and were impregnated with epoxy resin to protect their integrity during cutting, and to preserve textural relationships. Other samples did not survive sampling or transport intact, and were gently disaggregated by hand using the fingers or with a mortar and pestle. They were then sieved to select the sand size particles (0.0625mm to 2mm). The sample could then be set in resin and sectioned normally. Most sections were left without cover slips to allow staining to reveal feldspars. Cover slips were added later.

A1.2 Feldspar Staining

The method used was a modified from the Houghton (1980) and El Fegi (1989). The following procedure was followed:

1) Sections were placed face down over 45% Hydrofluoric Acid in a plastic beaker just smaller than the size of the slide that allowed the sample to be exposed to HF fumes and to be etched. Over this a larger plastic beaker was placed enclosing both thin section and HF containing beaker, allowing the concentration of HF fumes over the sample. Each slide was exposed to fumes initially for 45 seconds (as Houghton) but better results were obtained when this time was lengthened to 60 - 70 seconds.

2) After etching the slide was immersed in saturated Na - cobaltinitrite solution for 45 seconds. The concentration of the Na - cobaltinitrite was 4g per 6mls water.

3) Then the slide was rinsed twice in tap water to remove surplus Na - cobaltinitrite. The water used for this was replaced every 5 slides, or when discoloured.

4) Next the slide was dipped into 5% BaCl solution for 1-2 seconds and agitated gently.

5) A second rinse in tap water followed by a rinse in distilled water was then applied.

6) Leaving the slide slightly wet, K-rhodizonate solution was dripped on to cover the slide. A few seconds of application was sufficient and the solution was quickly washed off using distilled water. The concentration of K -rhodizonate used was 0.05g to 50mls water. This was a little stronger than that suggested by Houghton (1980). This must be

made up fresh each time as it fades quickly with time.

7) Each slide was finally let to dry on some paper towels.

The best results were achieved with fresh solutions, even BaCl, which is a stable solution.

Potassium feldspars stain yellow and plagioclase stains red. The K-feldspar staining was on the whole more pronounced than the red plagioclase stain but the stronger twinning in the latter helped compensate. It was also found that carbonate grains and cements, fine grained rock fragments and micas often became stained with the red K - rhodizonate solution. This was easily observed and posed little problem to correct identification of grains.

A1.3 Point counting

Sections were analysed using a swift automatic point counter and mechanical stage. Stage intervals could be adjusted to always be larger than the largest grain in the sample. In very poorly sorted samples where some grains are very large it was impractical to set the stage in this way, so care was taken to move the stage on, only counting large grains once.

Grain size was measured using an eyepiece graticule, calibrated against a subdivided millimetre marked on a special slide, made for this purpose. The precision of this method could not be exact but is around 0.005mm when using the X10 objective lens. On critical grain sizes uncertainties can be expressed as follows;

0.0625mm ± 0.005 = 8%	
	Fine sand
0.25mm ± 0.005 = 2%	
	Medium sand
0.5mm ± 0.005 =1%	
	Coarse sand
2mm ± 0.005 = 0.25 %	

This is considered to be an acceptable uncertainty, especially as the most important grain size determinations were carried out on the medium grain size.

Rock fragments were counted as such not as the mineral species encountered under the crosshair, as in the Gazzi-Dickinson point counting method. Though this method has its merits, it will in certain circumstances obscure provenance information, and may even confuse interpretations, especially in sediments from compositionally heterogeneous source regions. Categories of rock types were based upon the types actually present, but an attempt at fitting these into more general classes was made. The Spanish samples contain no primary igneous fragments, only metamorphosed rock types are present. The scheme was tailored to extract as much petrographic source information as possible. The ideas and classification of lower and mid rank metamorphic clasts (Lm1 and Lm2) by Dorsey (1988) were used as a starting point.

Sedimentary petrography and provenance

The character of a sedimentary source area can be determined from sediment from studying grains and recognising lithological types. Conglomerates are ideal for this, as they preserve source rocks intact. If the objective of a provenance study is to document source characteristics then the recognition of rock types is critical. However, rock fragments break down, and as this happens they eventually disassociate into their mineral constituents, which are not directly recognisable as rock types. The initial grain size of source rocks is important as it determines the point in the grain size reduction process that intact fragments of source rocks 'disappear'. This is not a compositional change but merely an artefact of the way sand grains are classified. A more sophisticated approach is then needed, that will average the mineralogy observed in an attempt to suggest possible source rock types; the composition is still there but textural and mineralogical associations are lost or at best confused.

Point counting

Point counting is the most commonly applied quantitative method of recording the framework mode composition of sandstones. A predetermined number of grains are examined and assigned to different genetic classes. The final results can be expresses as % of the total number of grains counted with associated uncertainties (Van der Plas and Tobi, 1965). Subjectivity is a major source of uncertainty, especially were lithic grains are concerned, but can be reduced by increased operator experience, and by strict but easily applied selection criteria.

There are two point counting methods in general use. The simplest assigns minerals, lithic fragments, matrix and cement to their own categories, subject to further subdivision of type, *regardless of size*. The grain edge is the limit for classification. The second method is the Gazzi-Dickinson method (Ingersoll et.al., 1984). Subgrains of a single mineral in larger poly-mineral grains are assigned to the mineral class of the subgrain, not the class of the whole grain, when the subgrain is bigger than 0.0625mm (official downward limit of sand sized material). When the subgrain is smaller than 0.0625mm then it is assigned to the class of the whole grain that it partly makes up, usually a lithic grain or polycrystalline quartz. This method is designed to reduce the differences in modal composition caused by grain size. However lithologic information is suppressed, and provenance description lost.

Another problem occurs when the intra-grain size of a lithic fragment is not consistent. Sometimes the grain can be counted as a rock fragment, when a small sub-grain is encountered. At other times when a large sub-grain comes under the cross hairs, the lithic fragment is broken down into its mineral constituents. Depending on what part of a grain is encountered it can be classified in two different ways, which is not a consistent or rigorous method of classification. Despite this, the Gazzi-Dickinson method is useful in large scale studies as it evens out differences due to grain size, and allows rocks to be compared from region to region without the complication of detailed local rock types.

A1.3 Conglomerate petrography

Petrographic studies of sediment were extended to the conglomerate grade material in each basin. Clast types were measured against size. Size classes used are either in phi or decimal intervals of 5cm. The cut off point was set in phi at 2cm, the smallest clast possible in a formal definition of a conglomerate. The aim was not so much to produce a modal record of conglomerate composition, as in point counting, this would involve counting every clast in a defined area. Rather the aim was to see how composition changes with clast size to understand the breakdown of sediment, and the effects on source signature. Larger clasts are necessarily scarce and so uncertainties on count totals for modal compositions from a defined area or fixed number of sampling points would be high. So a significant number of clasts ($\geq$ 50) were counted in each size class, where possible, thus producing essentially modal compositions for each size interval, but for the total conglomerate size range. In each case a starting point was chosen and clasts marked off using a black marker pen as they were measured with a steel tape measure. The largest dimension was always measured, a common practise. This causes problems in the comparability of size information from conglomerates with that of finer grained sediments derived from methods sieving, which is selective not upon the largest dimension of clasts but on the intermediate or smallest dimension. This problem will be particularly acute when blade or disc shaped clasts are being measured, something which is dependant upon lithology and especially the presence of planar anisotropic fabrics, as in slates and schists.

A2 Sedimentary geochemistry

A2.1 Sample preparation

Each sample was sieved using disposable nylon mesh, separating the fine, medium and coarse grain size intervals. Most sands had been previously disaggregated for normal thin section/grain mounts (**section A1.1**.) and the complete sand size range isolated. In all four grain size fractions were generated for each sample; the total sand, and 3 component grain size ranges.

Each separate was then crushed using a jaw crusher followed by an agate TEMA mill and ball crusher. This reduced each sample to at least 100 mesh powder ready for pressing into a pressed pellet or fusing into a glass disc.

A2.2 XRF conditions

Samples were analysed using a Philips PW1450/20 Sequential X-Ray Analysis Spectrometer. 60 samples including standards can be done in each run, analysing 3 unknowns and one standard at a single time. Five crystals are employed (LiF 200, Ge, Pe, TLap and LiF 220) and two detectors, one Scintillation and a Flow detector using a 90% Argon - 10% Methane mixture. Twenty-six elements were measured. Major elements were measured on fused glass discs in duplicate, using a Cr X-Ray tube and Trace elements were determined on pressed powder pellets using a Mo X-Ray tube

The major elements measured were (expressed as wt% oxides);

SiO_2, TiO_2, Al_2O_3, Fe (Total), MnO, MgO, CaO, Na_2O, K_2O, P_2O_5

Trace elements measured were (expressed in ppm);

Ba, Ce, Co, Cr, Cu, Ga, La, Ni, Pb, Rb, Sr, Th, U, Y, Zn, Zr

A3 Heavy Minerals

A3.1 Separation

Sediment samples were gently disaggregated by hand with a mortar and pestle. Some samples needed little crushing but the harder ones were first reduced in size by passing them through a mechanical jaw crusher. Point counting of some whole sediment samples indicates a heavy mineral content of up to 10%, so the amount of material required to obtain a sufficient heavy mineral yield was often relatively small at about 10-20 grammes. Precise weighing of the sample was not carried out. The resulting disaggregated sample was then washed in tap water to remove fine dust particles. This involves washing the sample repeatedly until the water running off the sample is clear, indicating that all dust has been removed. The sample was then dried prior to being sieved through disposable nylon mesh to facilitate easy separation, as the method used works best on a limited grain size, and to allow later analysis of a specific and consistent grain size interval. Grain size fractions removed were between 64 and 250um (very fine and fine sand). Heavy minerals were separated from the light fraction using tetrabromoethane, a liquid with a specific gravity of 2.96g/cc.

A3.2 Grain Mounting

After separation the heavy mineral fraction was mounted in Canada balsam on glass slides for optical examination. The slides were hardened by heating, thus not permitting the rolling of grains for more comprehensive identification. Hardened Canada balsam slides are also much easier to store. Some of the separate was retained, mounted in resin and polished for analysis by electron microprobe.

A3.3 Whole population studies, counting method

Each separate had its mineral content examined using the ribbon counting method. This involved taking spaced bands of constant width, oriented across the slide, within which each mineral encountered is assigned to a mineral class. Counting was performed on a Swift automatic point counter set as not to move the stage as normal when the grain was counted. The bands across each slide were defined by the extremes of an eyepiece graticule set vertically. The slide was moved from left to right using the manual slider on the mechanical stage. The results obtained can then be presented as percentage frequencies. This method of identifying minerals by their optical characteristics is at times subjective, relying on the observers experience. Fortunately heavy minerals often have distinctive characteristics which allow identification easier than for some colourless light species. Garnet, tourmaline, epidote, amphiboles, zircon and rutile for example are quite distinctive, so the percentage abundances of these presented here should be quite reliable. As a consequence further analysis uses only those minerals which are reliably identified. Five-hundred counts were made per sample,

including opaque minerals, giving errors in accordance with Van de Plas and Tobi (1965).

A3.4 Mineral species studies

A3.4.1 Electron Microprobe conditions

Electron microprobe analysis was applied to the study of intraspecies chemical variation. of garnet, epidote and tourmaline. Analyses were performed using three machines:

Glasgow Cambridge Instruments Microscan 5

This was equipped with a Link systems 1000 Electron Dispersive Spectrometer with a count time of 100s and an accelerating voltage of 20 Kv.

Edinburgh Cambridge Instruments Microscan 5

This machine is identical to the machine that used to exist in Glasgow. However it operates using wavelength dispersive spectrometers, with a count time of 10s per element, and an accelerating voltage of 20 Kv.

Cameca SX-50

This new machine at Glasgow University uses four wavelength spectrometers. It can measure x-rays emitted from elements with as low an atomic weight as boron, thus allowing the analysis of Tourmaline. An acceleration voltage of 15 Kv at 20nA is used. It is equipped with secondary and back scattered electron imaging, and can allow photographs of samples to be taken and used interactively whilst doing analysis. The most useful feature for multi point analysis schemes, for a varietal study of a single species of mineral, is the ability to preset analysis points for the machine to carry out automatically. Before this however points of interest on the sample must be defined, and some qualitative or semi-quantitative measure of mineralogy is needed. To do this a photographic map of the sample was made using reflected light (as the near surface of the slide is what is analysed in EMPA). The slide was then mapped out using a SEM, using an EDS analyser to quickly locate grains of the minerals of interest, which were then marked on the photographic maps.

A3.5 Scanning electron microscope

The machine used was a Cambridge Instruments Stereoscan 360 equipped with a Link EDX AN10000 detector. The surface morphologies of heavy mineral grains were studied using the SEM in secondary electron imaging mode, Some of the heavy mineral separates for some representative samples were mounted on sticky carbon pads on small metal stubs and carbon coated. For some, grains were picked out by hand from separates and grains of the same mineral mounted together for easier study and comparison.

One important aspect of this work was also to unambiguously establish the total mineralogical range within the heavy mineral fraction, and especially to confirm the presence of epidote group minerals, that often present a non typical appearance in grain mounts. This complemented identifications made in ribbon counting of the heavy mineral population.

A4 Isotopic Dating

A4.1 Mineral separation

Mica was the main target for extraction from conglomerate clasts, sandstones and basement source rocks from the Granada Basin.

Detrital Micas

For $^{40}Ar/^{39}Ar$ dating detrital micas were picked by hand from disaggregated sediments. A range of grain sizes was picked to even out any operator bias, and clean, unaltered, chlorite free grains were chosen.

Conglomerate clast and Basement rocks

Clasts and basement rocks from Spain and Scotland were first crushed by jaw crusher, and particularly hard samples using a roller crusher. Once reduced to at least 1cm size chips, the sample was split and some material then placed in an agate TEMA crusher to generate a whole rock powder. To separate micas, water was added to the crushing of the remaining sample split. The water prevents the destruction of the flat shaped micas (T. Dempster, pers. comm., see also Kelly and Bluck 1989). Presumably they have more time to orientate to the edges of the crushing vessel during the slowed, water inhibited movement of the TEMA. The wet crushed material was then sieved through disposable nylon mesh to remove the relatively uncrushed micas from the associated fine fraction. XRD analysis of this fine residue and the whole rock powder shows that the wet crushing method preserves up to 50% of mica content. The mica fraction produced thus was not pure and still required some further purification. For $^{40}Ar/^{39}Ar$ laser probe dating this was done by hand as the samples required were small. For Rb-Sr and K-Ar dating larger pure mica samples were needed A Frantz Isodynamic magnetic separator was employed for this.

Feldspar was separated from only two rocks. This was done by careful use of heavy liquids, changing the specific gravity of tetrabromoethane with acetone, and using natural mineral standards to fix the desired gravity of liquid. The non-magnetic fraction left after mica separation was the starting point for separation. The most magnetically susceptible minerals also have the greatest density so were already removed from the sample before heavy liquid separation was attempted.

Sample purity checks

XRD analysis was used to check sample purity, especially for the presence of chlorite. Ridding mica, and especially biotite of chlorite is notoriously difficult. Fortunately few biotite samples were analysed, and Muscovite responds much better to chlorite purification. Often a sample needed to have its grain size dramatically reduced by wet mortar and pestle crushing in order to reach the point where monomineralic grains of mica were liberated from chlorite, quartz and feldspar. The effects of this grain size reduction on final results are not constrained but are likely to be negligible.

A4.2 $^{40}Ar/^{39}Ar$ Dating

The theory of this method of dating is well established and will not be reiterated here. MacDougall and Harris (1989) provide a thorough documentation from first principles to details of interpretation.

Sample preparation

Three sample irradiations were done, the first using the Petten reactor in the Netherlands, and the other two at the Ford reactor, Michigan in the U.S.A..

For the first irradiation mica was wrapped in high purity aluminium foil and placed in glass tubes along with some flux monitor, MMhb-1 (Samson and Alexander 1987), also wrapped in foil. In the remaining irradiations samples were placed within a specially made aluminium sample holder, manufactured by the Dept. of Geology and Geophysics at the University of Edinburgh, for Dr. J.Harris. Samples rested within holes of two dimensions (2mm deep by 1.5 and 2mm diameter) that were drilled into aluminium discs. These discs had a larger hole through the centre to enable several of them to be held together by a central rod with a screw top for securing the whole assembly. This design was intended to minimise post irradiation handling, the discs could be slid off the central rod and placed directly into the laser port.

The initial samples were removed from their aluminium foil and placed in small wells (2-3mm deep and 2mm diameter) drilled into aluminium rod (10mm long and 3mm diameter). The Al containers could then be loaded into the laser port connected to the argon extraction system.

The original intention was to date single detrital micas from sediments. Unfortunately in the first group of samples individual micas were not placed within sample holes on their own, but in bulk for a specific sediment sample. It was found to be difficult to pick out a single grain using the laser, so it was decided to analyse the bulk population of each sediment sample by step heating. In the second and third batches individual grains were isolated in separated containment. For micas from conglomerate clasts and basement rocks ages of grains should at least be nearly identical so analysis of many grains is permissible without the loss of much information.

The second and third group of samples were not step heated, the volume of material was not considered to be sufficient to generate enough gas for a reliable analysis. Individual detrital micas were fused in one step. This produces a result analogous to a conventional K-Ar dating, though the advantage of the laser ablation technique is that it allows very small samples to be analysed, even on a an intra-grain scale.

Sample Analysis Problems

Serious problems were encountered with the second batch of samples analysed. In consequence none of the results obtained are reliable and they have been discarded for the purposes of interpretation and analysis.

The problems originated during irradiation of the sample holder at the reactor in

Michigan. The integrity of the canister which contained the holder was tested by immersing the whole assembly in liquid, and then looking for escaping air bubbles. Unfortunately water entered the canister and during irradiation the sample holder became badly corroded. Sample recovery was compromised by the radioactive nature of the material and by the corrosion of the holder which had fused together many of the discs that contained samples (see above for details of the holder design). Force was used to cut the samples free, after some length of time had elapsed to let radiation levels decrease to a safe level to allow staff at the reactor centre near the samples. Sellotape was used to close the openings of the holes containing samples, during the extraction procedure (using a hacksaw blade to cut between discs). Material was lost in this operation, probably by sticking to the sellotape.

Most of the samples were analysed, but many of the ages determined were not geologically meaningful in the context of the Betic Cordillera. This put into question the reliability of the remaining ages that could be considered reasonable, and as a result the entire data set was rejected. Questions about the effect of the irradiation and the associated corrosion of the sample holder on the chemistry of the samples and the age dates determined on them were addressed by analysing the chemistry of several samples that were not selected for age dating. They were mounted onto SEM stubs and their qualitative major element chemistry analysed by EDS. None of these samples had unusual or clearly affected chemical compositions. So what went wrong?

Blank levels in the ^{40}Ar-^{39}Ar mass spectrometer were high during the analyses, and error levels were also high. This suggests a poorly maintained or dirty mass spectrometer system. The samples analysed in the system before these samples were detrital illites from oil bearing sandstones from North Sea reservoirs. Hydrocarbons increase the level of ^{41}Ar in the system and also the correction required for their presence. As a result error levels increase and the reliability of age determinations decreases.

These problems represent a lost opportunity to characterise the age characteristics of sedimentary detritus derived from a well constrained orogenic source that was deposited in a proximal setting. Much time (4-5 months) was wasted, as well as a great deal of money.

Analysis Procedure

All analyses were performed at the S.U.R.R.C. at East Kilbride. The first set of samples were analysed by Dr. R Burgess and the remainder under the direction of Dr. P. McConville, by himself and later by Dr. D. Philips of Anglo-American Research Laboratories Pty. Ltd. The bulk of the following description is based on details supplied by R. Burgess and relates specifically to the first set of samples, and generally to the rest.

Before analysis the laser port and extraction system were evacuated to ultra high vacuum ($>10^{-8}$ mbar). During this the samples were heated using a heat lamp for 24 hours at about 100°C to remove any adsorbed atmospheric argon. The pumpdown process took about 4-7 days.

A laser was used to ablate the samples in order to extract argon. The laser used was a Nd:YAG continuous wave laser with a wavelength of 1064nm, used in TEM_{00} mode. The

beam diameter was varied between ≤3mm and 20um. For stepped heating the beam was set at about 2mm, to cover the entire sample. Power output was adjusted manually during step heating. No temperature measurements were made during the experiments. Each heating step lasted 1 minute, followed by 4 minutes of gettering, using a SAES NP10 getter at 400°C. At the end of this time the gas was equilibrated into the mass spectrometer for 1 minute. Isotopic measurements were performed using a MAP 215 mass spectrometer using an electron multiplier detector. Seven masses were measured (35, 36, 37, 38, 39, 40, 41) in 11 cycles lasting about 20 minutes. At the end of this time peaks were regressed to the inlet time. Mass 41 gives an indication of hydrocarbon levels and 35 the background level of Cl in the mass spectrometer. Blanks were determined using the same procedure as sample analysis but without firing the laser. Blanks were taken after every second analysis. Typical values for the first set of samples analysed were;

$32\pm6 \times 10^{-13}$ cm^3 STP ^{40}Ar

$4\pm0.7 \times 10^{-13}$ cm^3 STP ^{39}Ar

$3\pm0.3 \times 10^{-13}$ cm^3 STP ^{38}Ar

$3\pm0.5 \times 10^{-13}$ cm^3 STP ^{37}Ar

$1\pm0.4 \times 10^{-13}$ cm^3 STP ^{36}Ar

Data were corrected for nuclear interference corrections, mass discrimination, ^{37}Ar decay (Roddick 1983) and background amounts. Small air corrections were applied based upon the amount of ^{36}Ar released from the samples (i.e., ^{40}Ar* = ^{40}Ar - [^{36}Ar x 296]). Uncertainties were calculated by the propagation of errors.

A4.3 K-Ar Dating

Following acid digestion, samples were analysed for potassium by flame photometry, using a Corning 410C instrument. Argon was extracted by heating the sample in vacuo using an induction coil. The isotope dilution method was applied using a ^{38}Ar spike. Isotopic abundances were measured using a MS10 mass spectrometer in static mode.

A4.4 Rb-Sr Dating

A4.4.1 Rb-Sr Chemistry:

Sample Dissolution:

Weighed samples are dissolved in PFA teflon screw-top beakers (Savillex), using 10mls 40% HF and 1ml 14M HNO_3 on a hotplate overnight. The beakers were removed, cooled, and then the solution was dried down under lamps. The residue was then dissolved in 3 mls 14M HNO_3 overnight on a hotplate, and dried down as before. The residue was then dissolved in 8 mls 6M HCl on a hotplate. Weighed amounts of ^{87}Rb and ^{84}Sr spikes were then added to this solution in order to determine the Rb and Sr concentrations using isotope dilution analysis. The spiked solution was dried down and the final residue taken up in 2 mls 2.5M HCl. For some samples the spikes were added earlier at the initial sample weighing time, just before the

addition of HF.

Column chemistry:

Rb and Sr were separated using standard cation exchange chromatography techniques. The sample was transferred to a centrifuge tube and any residue centrifuged off. The solution was then loaded onto a preconditioned cation exchange column containing 10 mls Bio-Rad AG50W x 8, 200-400 mesh resin. The sample was washed in with 2 x 1 ml 2.5M HCl and eluted with 21 mls 2.5M HCl. The Rb fraction was then collected with a further 5 mls 2.5M HCl and evaporated to dryness under heat lamps. 20 mls 2.5M HCl was then eluted. The Sr fraction was collected with a further 10 mls 2.5M HCl and evaporated to dryness. Sr blanks were less than 5ng.

A4.4.2 Mass Spectrometry

All Sr samples were run on a VG 54E thermal ionisation mass spectrometer. Rb was run on a VG MM30 thermal ionisation mass spectrometer.

Sr

Sr samples were dissolved in 1ml 1M H_3PO_4 and were loaded onto a single outgassed Ta filament. A small current was passed through the filament to dry the sample. The current was then increased slowly until the H_3PO_4 fumed off and the filament glowed dull red. Sr beams were managed to give an intensity of 1.5 pA ^{86}Sr. Peak intensities were corrected for zero, dynamic memory and Rb interference (if necessary). The $^{87}Sr/^{86}Sr$ ratio was corrected for mass fractionation using $^{86}Sr/^{88}Sr = 0.1194$. Repeat analysis of NBS 987 Sr standard gave $^{87}Sr/^{86}Sr = 0.71028 \pm 2$ (2s).

Rb

Rb samples were dissolved in 1ml high purity H_2O and loaded onto one side filament of an outgassed triple Ta filament assembly. The sample was dried carefully, taking care not to let the load bubble up on the filament. Rb beams were run with a current of 3 A through the centre filament and up to 1 A on the side filaments.

Age Calculation

The regression procedure of York (1969) was used with a decay constant for ^{87}Rb of 1.42×10^{-11} yr^{-1}, to calculate isochron ages. Blanket errors of 0.01% and 0.35% (1σ) were applied to $^{87}Sr/^{86}Sr$ and $^{87}Rb/^{86}Sr$ respectively, for isochron regression.

A4.5 Mica Chemistry

Electron microprobe analysis was carried out on detrital and conglomerate clast muscovites to ascertain their state of chemical alteration (see section A3.4 for electron microprobe conditions) and to clarify implications for the isotopic dating. This was done in a similar manner to Kelly and Bluck (1991) and for the same reasons. The potassium content was of particular interest as any alteration here would signal the greatest effect on Ar-Ar and K-Ar ages. Rb-Sr ages may also be affected by loss of Rb, as it has a similar ionic radius and

chemical affinity as K. Traverses across grains were performed, mainly perpendicular to cleavage, but also at angles across cleavage plains were possible.

Back scattered electron images were utilised on the Cameca SX-50 electron microprobe. These images show relative mean atomic weight by brightness contrasts. The heavier the substance, the brighter the image. This was very helpful in highlighting areas of possible alteration, and helped greatly to target analysis points.

Appendix 2 Point Counting Results

In the following pages the results of point counting of sandstones from the Quentar, Dudar, Pinos Genil and Alhambra Formations are presented in table form. Listed are the conventional framework components, expressed as percentage contents of the sediment. Below this, the lithic grain population components are listed, expressed as percentages of the total lithic grain content, *not* as percentages of the total grain content. The locations of all the samples listed is given in **Fig. 3.1**

The grain parameters are decribed in **Tables 4.1** and **4.5**, but the abbreviations used in the tables presented below are here described, in case any confusion may arise:

H.M. - Heavy Minerals
Q-M tect. - Quartz-Mica tectonite
Q-M agg. - Quartz-Mica aggregate
Ga-M sch. - Garnet-Mica schist
Q-Fsp sch. - Quartz-Feldspar schist
Fsp-Qtz agg - Feldspar-Quartz aggregate

	Quentar Formation		Dudar Formation										
Sample	**1.1**	**1.2**	**2.1**	**2.2**	**3**	**4.1**	**4.2**	**5.8**	**6.2**	**6.3**	**D1**	**DU2**	**S13**
Qm	6.2	6.6	5.3	5.5	1.7	7.5	7.4	15.5	15.2	13.5	8.2	16.6	13.0
Qp	6.4	6.2	13.9	12.2	10.3	12.3	9.2	15.3	16.6	17.2	15.8	20.4	20.8
F	0.6	1.0	3.7	2.4	0.3	5.8	5.0	1.2	2.2	4.2	0.4	0.8	1.2
L	16.0	17.0	21.7	52.6	46.1	35.0	21.6	21.9	39.1	38.4	55.4	43.4	51.2
M	1.4	8.4	6.0	5.1	5.4	4.8	4.0	9.8	11.0	13.2	5.4	11.8	5.0
H. M.	1.2	2.0	2.7	1.6	2.9	3.2	5.8	4.1	3.2	6.0	1.0	1.2	2.0
Opaques	-	1.8	3.2	0.2	0.6	5.3	4.0	6.9	11.8	1.2	-	1.2	1.4
Carbonate	67.8	57.0	43.5	20.3	32.7	26.0	43	6.8	1.0	5.7	13.8	4.6	5.4
Matrix	-	-	-	-	-	-	-	55.7	-	-	-	-	-
Cement	-	-	-	-	-	-	-	-	-	-	-	-	-
Lithics													
Q-M tect.	15.6	49.2	49.0	41.0	37.5	42.4	41.2	36.7	46.4	53.0	21.1	40.0	42.0
Q-M agg.	62	7.6	4.1	1.0	3.1	5.6	6.0	4.2	2.4	8.0	8.0	12.0	7.0
Ga-M sch.	-	6.0	11.9	8.0	3.7	4.0	1.2	-	-	2.0	-	1.0	4.0
Q-Fsp sch.	-	0.4	-	-	5.6	10.8	2.8	1.2	2.4	7.0	-	-	-
Fsp-Qtz Ags	1.2	1.6	11.1	4.0	-	-	-	-	-	-	3.0	9.0	7.0
Amphibolite	0.4	6.4	-	2.0	0.6	0.8	0.4	0.6	-	-	1.0	-	1.0
Marble	-	2.4	4.1	14	18.7	5.2	9.6	20.5	6.8	12.0	14.0	2.0	4.0
Epidote rock	-	5.6	-	1.0	15.0	2.4	0.7	12.6	10.8	3.0	1.0	2.0	4.0
Mica Aggs.	18.8	10.4	12.7	24.0	5.6	8.0	23.2	19.3	22.0	9.0	13.0	20.0	18.0
Mylonite	-	1.6	1.65	-	1.0	2.8	0.4	1.2	-	2.0	-	-	-
Low Grade	0.8	1.6.	4.9		0.6	1.6	6.4	3.0	9.2	4.0	39.0	14.0	-

Pinos Genil Formation

Sample	**5.1**	**5.2**	**5.3**	**5.4**	**5.5**	**5.6**	**5.7**	**6.2**
Qm	11.2	5.9	7.7	6.5	22.5	16.7	12.5	2.2
Qp	15.6	13.2	13.8	13.4	9.3	9.0	7.0	8.4
F	1.3	2.4	8.7	3.3	10.5	5.4	8.6	2.2
L	48.0	63.2	34.4	52.4	26.1	40.8	52.0	51.2
M	12.7	7.7	7.7	7.1	18.8	9.5	8.2	2.4
H. M.	3.8	3.1	2.4	6.9	6.5	4.0	3.5	2.8
Opaques	2.9	2.4	1.2	1.2	3.2	2.2	2.1	-
Carbonate	4.5	-	-	-	3.2	2.4	5.9	30.8
Matrix	-	-	-	-	-	-	-	-
Cement	-	1.9	24.1	9.2	-	-	-	-
Lithics								
Q-M tect.	63.6	42.0	50.0	44.0	54.0	41.0	59.0	26.0
Q-M agg.	3.9	8.0	-	-	15.0	10.0	15.0	-
Ga-M sch.	1.7	-	-	15.0	-	10.0	4.0	4.0
Q-Fsp sch.	1.7	5.0	2.0	-	-	1.0	1.0	-
Fsp-Qtz Ags	-	-	-	6.0	3.0	3.0	5.0	3.0
Amphibolite	-	-	-	-	1.0	4.0	-	1.0
Marble	9.9	9.0	16.0	4.0	-	1.0	3.0	21.0
Epidote rock	11.2	-	-	-	-	-	-	-
Mica Aggs.	3.9	19.0	28.0	9.0	18.0	17.0	7.0	5.0
Mylonite	1.7	-	-	-		-	-	-
Low Grade	2.6	-	-	9.0	8.0	13.0	6.0	17.0

Alhambra Formation

Sample	**8.1**	**8.2**	**8.3**	**9.1**	**9.2**	**9.3**	**9.4**	**9.5**	**9.6**
Qm	12.9	12.0	4.6	12.4	4.6	15.8	6.4	11.0	5.4
Qp	15.5	9.0	11.8	9.4	10.6	11.6	9	9.2	12.4
F	2.4	1.4	1.2	5.0	1.0	1.8	-	1.2	-
L	8.3	28.2	42.0	55.0	63.0	37.6	65	62.0	64.2
M	15.5	10.6	3.6	8.8	8.4	21.6	11.8	10.8	9.6
H. M.	2.8	1.0	2.6	2.6	3.4	4.2	5.2	1.6	4.8
Carbonate	0.3	2.8	31.4	1.0	-	3.4	-	-	-
Opaques	2.6	3.8	2.8	5.8	9.0	4.0	2.6	4.2	3.6
Matrix	39.4	31.2	-	-	-	-	-	-	-
Cement	-	-	-	-	-	-	-	-	-
Lithics									
Q-M tect.	45	-	68	61	47	49	52	51	45
Q-M agg.	7.4	-	17	14	14	23	17	19	20
Ga-M sch.	10.5	-	5	1	8	2	12	6	8
Q-Fsp sch.	1	-	-	1		1	-	-	1
Fsp-Qtz Aggs	14.8	-	-	3	-	1	-	-	-
Amphibolite	-	-	1	-	-	-	-	1	1
Marble	1	-	-	-	-	-	-	-	-
Epidote rock	1	-	3	-	-	2	2	1	1
Mica Aggs.	14.7	-	4	8	12	11	6	17	15
Mylonite	-	-	-	-	-	-	-	-	-
Low Grade	20	-	2	13	19	11	11	5	9

Appendix 3 Sandstone Geochemical Data

Below are listed the major and trace element data obtained from samples taken from the Dudar and Alhambra Formations. Samples were split into three grain size fractions which were analysed along with a bulk grain size sample. The letters appended to each sample represent a particular grain size fraction:

A - bulk sediment, including all sand grain sizes, 0.0625-2mm

B - fine sand grain size, 0.0625-0.25mm

C - medium sand grain size, 0.25-0.5mm

D - coarse grain size, 0.5-2mm

Some samples do not have all fractions represented, due to lack of sufficient material of the correct grain size to permit X-ray fluorescence analysis.

Major Elements

Dudar Formation

Samples	1.3A	2.2A	2.2B	2.2C	2.2D	2.3A	2.3B	2.3C	2.3D
SiO2	41.57	49.85	57.64	58.07	57.35	47.45	37.92	49.2	61.35
TiO2	0.42	0.49	0.69	0.56	0.46	0.39	0.47	0.41	0.41
Al2O3	6.93	8.62	11.26	9.26	9.18	6.85	7.86	6.98	6.98
Fe tot.	3.02	3.5	5.25	4.2	3.56	2.48	2.82	2.58	2.48
MnO	0.04	0.15	0.15	0.1	0.08	0.03	0.04	0.02	0.03
MgO	1.71	1.36	4.16	1.61	1.36	0.32	0.44	0.64	0.33
CaO	23.05	17.35	20.41	11.78	11.1	21.57	25.72	20.48	14.98
Na2O	0.22	1.5	1.51	1.13	0.46	0.1	0.24	0.19	0.00
K2O	1.11	1.47	1.7	1.53	1.61	1.29	1.33	1.28	1.4
P2O5	0.14	0.09	0.13	0.07	0.7	0.05	0.07	0.05	0.06

Samples	2.4A	2.4B	2.4C	2.4D	3A	3B	3C	3D
SiO2	65.38	64.29	64.18	62.8	49.13	53.6	55.1	60.7
TiO2	0.55	0.94	0.53	0.57	0.57	0.6	0.54	0.54
Al2O3	9.45	12.62	9.37	10.07	9.98	11.7	10.2	10.16
Fe tot.	4.04	6.16	3.98	4.0	4.69	5.03	4.83	4.76
MnO	0.06	0.11	0.08	0.05	0.12	0.13	0.14	0.15
MgO	1.0	1.11	0.92	1.03	7.21	7.26	6.37	5.48
CaO	7.65	3.65	8.07	8.61	10.54	9.04	8.59	6.62
Na2O	0.84	0.81	0.39	1.02	0.63	0.92	0.91	0.68
K2O	1.73	2.07	1.61	1.81	1.6	1.85	1.72	1.81
P2O5	0.07	0.2	0.09	0.09	0.09	0.11	0.09	0.08

Samples	4.1A	4.1C	4.1D	5.8A	5.8C	5.8D	6.1A	6.1B	6.1C
SiO2	58.25	57.24	61.65	58.64	56.05	59.86	64.96	64.09	61.03
TiO2	0.6	0.57	0.59	0.76	0.78	0.73	0.74	0.72	0.67
Al2O3	9.01	8.77	8.93	14.29	14.62	13.49	13.24	11.99	15.01
Fe tot.	6.3	5.13	6.2	4.87	5.16	4.52	5.38	4.61	4.99
MnO	0.1	0.09	0.08	0.05	0.04	0.05	0.06	0.06	0.03
MgO	1.3	1.22	1.27	2.67	2.6	2.61	2.48	2.45	2.51
CaO	10.79	11.59	9.71	7.14	7.9	5.93	3.67	4.3	3.5
Na2O	0.97	1.33	1.23	1.42	1.1	1.24	1.71	1.15	1.11
K2O	1.41	1.34	1.54	2.41	2.44	2.31	2.3	1.94	2.87
P2O5	0.1	0.1	0.1	0.11	0.11	0.12	0.09	0.08	0.065

Samples	6.3A	6.3B	6.3D	D1A	D1B	D1C	D1D
SiO2	64.63	62.50	67.11	60.87	60.62	60.77	59.54
TiO2	0.705	0.86	0.545	0.54	0.58	0.42	0.38
Al2O3	11.17	11.93	9.865	9.34	9.84	9.17	8.09
Fe tot.	4.8	5.9	4.62	4.06	4.26	3.59	3.16
MnO	0.075	0.09	0.055	0.1	0.1	0.08	0.08
MgO	0.075	3.025	1.97	3.5	3.79	3.48	3.35
CaO	4.58	5.15	5.17	8.1	8.13	8.39	8.97
Na2O	1.205	1.475	1.03	0.76	0.75	0.23	0.00
K2O	1.75	1.84	1.62	1.63	1.6	1.61	1.43
P2O5	0.095	0.125	0.07	0.09	0.11	0.06	0.07

Alhambra Formation

Samples	8.1A	8.1B	8.1C	8.1D	8.2A	8.2B	8.2C	8.2D	8.3A	8.3B
SiO2	54.74	60.7	60.31	65.96	67.11	67.87	66.29	59.64	68.26	62.57
TiO2	0.73	0.84	0.67	0.55	1.13	1.21	0.95	0.67	0.68	0.98
Al2O3	11.01	11.82	11.55	9.73	11.93	11.36	12.65	11.67	9.22	10.08
Fe tot.	4.51	4.78	4.67	3.76	5.61	5.45	5.5	4.96	5.27	4.85
MnO	0.06	0.08	0.08	0.06	0.08	0.08	0.1	0.11	0.12	0.08
MgO	1.49	1.6	1.54	1.24	1.52	1.43	1.58	1.31	1.36	1.62
CaO	12.32	7.6	8.39	7.2	3.17	2.99	3.48	8.89	6.93	8.33
Na2O	0.17	0.00	0.00	0.00	0.18	0.21	0.11	0.00	0.00	0.25
K2O	1.64	1.68	1.71	1.5	1.81	1.65	1.97	1.78	1.25	1.29
P2O5	0.08	0.09	0.08	0.06	0.09	0.09	0.08	0.7	0.05	0.05

Samples	**8.3C**	**8.3D**	**9.2B**	**9.2C**	**9.2D**	**9.3A**	**9.3B**	**9.3C**	**9.3D**
SiO2	66.19	69.9	71.64	72.5	71.04	66.01	63.31	66.36	70.99
TiO2	0.68	0.53	1.31	0.84	0.77	0.66	0.62	0.69	0.61
Al2O3	9.29	9.13	11.8	12.82	13.61	16.84	19.72	14.56	12.14
Fe tot.	5.62	5.97	6.23	6.15	7.01	5.71	5.7	5.89	6.54
MnO	0.11	0.19	0.25	0.305	0.42	0.13	0.11	0.13	0.19
MgO	1.28	1.04	1.33	0.655	0.62	1.79	2.07	1.6	1.57
CaO	7.08	5.63	0.55	0.27	0.46	0.74	0.61	0.93	1.22
Na2O	0.00	0.00	0.01	0.405	0.42	0.32	0.39	00.0	0.00
K2O	1.24	1.23	1.65	1.84	1.87	2.53	2.88	2.03	1.66
P2O5	0.04	0.05	0.05	0.06	0.06	0.08	0.07	0.09	0.09

Samples	**9.4A**	**9.4B**	**9.4C**	**9.4D**	**9.6B**	**9.6C**	**9.7B**	**9.7C**
SiO2	73.74	72.23	75.69	71.75	65.72	74.63	45.96	41.47
TiO2	0.71	1.13	0.78	0.61	1.22	0.76	1.64	2.21
Al2O3	9.77	11.67	9.68	10.73	14.18	10.4	17.24	19.285
Fe tot.	7.26	5.55	6.71	8.46	6.67	6.95	15.12	18.41
MnO	0.2	0.09	0.14	0.32	0.08	0.1	0.27	0.41
MgO	1.09	1.29	1.03	1.03	0.66	0.42	10.6	8.02
CaO	0.72	0.84	0.55	0.9	0.63	0.38	7.76	7.25
Na2O	0.00	0.00	0.00	0.00	0.25	1.19	1.35	0.69
K2O	1.39	1.53	1.35	1.35	2.07	1.62	0.27	0.205
P2O5	0.11	0.11	0.09	0.13	0.13	0.12	0.37	0.15

Trace Elements

Values are expressed as parts per million (p.p.m.)

Dudar Formation

Sample	1.3A	2.2A	2.2B	2.2C	2.2D	2.3B	2.4A	2.4B	2.4C	2.4D
Zr	154	130	11	143	137	98	138	160	135	137
Y	25	19	24	25	20	17	20	31	18	18
Sr	133	112	137	158	163	82	188	146	182	209
U	-	-	3	-	-	2	-	3	-	1
Rb	81	72	69	75	82	63	86	103	82	93
Th	4	2	4	-	1	1	2	4	5	8
Pb	19	9	13	10	12	6	11	17	10	15
Ga	11	9	10	10	12	10	12	16	10	13
Zn	45	47	48	45	41	34	39	55	41	41
Cu	49	1	5	1	1	6	-	-	-	-
Ni	51	386	96	55	46	28	24	33	23	25
Co	6	62	16	11	11	9	8	16	11	7
Cr	127	56	75	60	62	39	66	138	59	56
Ce	27	40	39	42	36	25	39	56	39	36
Ba	530	237	261	259	275	246	303	346	272	331
La	10	13	12	18	12	16	14	19	15	11

Sample	3A	3B	3C	3D	4.1A	4.1B	4.1C	4.1D	6.1A	6.1B
Zr	80	131	142	142	132	125	136	140	179	158
Y	13	22	25	29	26	28	25	24	22	27
Sr	603	150	133	115	206	223	210	209	189	186
U	1	1	-	-	-	3	-	3	3	2
Rb	60	92	87	92	66	70	61	79	109	80
Th	1	7	4	4	3	-	2	3	6	8
Pb	10	20	19	13	13	14	11	15	20	22
Ga	8	12	11	12	8	11	10	10	16	15
Zn	28	61	53	44	45	53	41	43	79	71
Cu	-	66	25	11	-	-	-	-	16	8
Ni	12	68	54	46	26	29	20	15	34	27
Co	8	15	15	9	13	13	12	14	14	14
Cr	47	139	134	136	53	63	66	65	72	63
Ce	27	44	42	38	44	47	38	41	61	59
Ba	235	282	249	278	274	290	252	320	361	308
La	12	17	10	14	9	16	11	19	14	16

Sample	6.1C	6.3A	6.3B	6.3C	5.8A	5.8B	5.8C	S13A	S13B	S13C
Zr	189	164	175	167	184	187	245	198	191	192
Y	24	27	32	23	26	25	29	28	35	28
Sr	191	194	203	219	240	227	247	154	163	148
U	-	-	1	2	3	3	3	2	2	3
Rb	114	73	74	78	106	105	112	72	66	66
Th	6	4	6	-	1	2	4	1	-	-
Pb	25	14	15	18	16	14	18	13	11	10
Ga	20	13	16	14	18	20	22	13	15	15
Zn	88	58	68	62	68	70	79	51	59	49
Cu	13	3	5	-	1	1	10	-	1	-
Ni	35	29	33	31	35	35	44	22	25	24
Co	14	11	14	12	13	15	18	8	12	10
Cr	77	64	71	63	80	80	82	54	68	577
Ce	58	63	64	55	56	61	80	50	66	44
Ba	428	231	301	295	379	372	374	308	282	324
La	14	12	26	21	31	31	36	24	28	22

Sample	S13D	D1A	D1B	D1D	SLT
Zr	201	144	151	132	289
Y	28	23	23	18	30
Sr	170	187	193	201	166
U	2	2	2	3	3
Rb	67	62	70	67	104
Th	1	-	-	-	1
Pb	13	16	17	16	29
Ga	14	12	13	10	22
Zn	45	62	62	54	100
Cu	-	-	-	1	17
Ni	21	23	24	21	77
Co	7	16	7	10	22
Cr	51	47	48	35	120
Ce	46	32	37	21	75
Ba	324	272	256	252	447
La	22	16	22	14	35

Alhambra Formation

Sample	8.1A	8.1B	8.1C	8.1D	8.2A	8.3A	8.3B	8.3C	8.3D	9.1A
Zr	217	217	227	188	226	192	234	191	175	220
Y	43	36	30	24	26	37	29	33	46	32
Sr	128	135	117	96	117	98	120	100	94	90
U	1	2	2	-	3	2	4	2	2	2
Rb	65	70	81	71	83	47	51	57	55	70
Th	-	-	12	13	7	-	-	-	-	-
Pb	14	17	14	17	17	16	18	19	16	17
Ga	13	14	17	12	17	14	15	10	9	12
Zn	61	63	62	47	76	56	58	55	52	62
Cu	4	4	4	-	13	-	3	2	1	2
Ni	37	37	36	28	33	24	24	28	24	22
Co	14	15	15	12	17	17	14	13	14	10
Cr	72	77	70	54	70	70	69	80	63	57
Ce	54	61	63	33	63	42	47	41	42	51
Ba	325	345	344	315	357	261	247	233	249	291
La	34	35	27	21	30	25	27	21	19	24

Sample	9.1B	9.1C	9.1D	9.2A	9.2B	9.2C	9.2D	9.3A	9.3B	9.3C
Zr	205	229	193	212	238	203	231	198	169	224
Y	31	26	45	38	31	29	75	36	24	35
Sr	84	99	78	102	119	110	111	124	132	115
U	2	2	1	2	3	2	2	2	2	3
Rb	65	63	59	82	77	91	92	95	130	92
Th	-	-	-	-	-	-		-	-	-
Pb	17	17	13	20	14	22	21	23	28	23
Ga	12	17	12	16	16	18	17	21	25	20
Zn	64	67	56	70	71	74	67	90	97	81
Cu	9	9	7	12	14	13	14	5	2	3
Ni	26	28	20	51	39	45	49	38	44	40
Co	13	10	12	23	15	20	22	18	20	18
Cr	64	57	54	97	72	76	81	89	89	78
Ce	38	50	37	57	65	55	64	51	37	62
Ba	297	269	275	462	364	440	490	495	556	390
La	22	21	18	30	30	25	28	26	20	29

Sample	9.3D	9.4A	9.4B	9.4C	9.4D	9.5A	9.5B	9.5C	9.5D	9.6A
Zr	210	188	227	190	182	180	210	174	182	177
Y	51	49	29	38	69	33	35	38	27	41
Sr	95	82	98	77	74	94	115	90	84	103
U	3	3	1	3	3	2	2	2	2	3
Rb	76	65	71	61	61	78	84	73	80	84
Th	-	-	-	-	-	-	6	1	1	1
Pb	16	18	16	18	14	20	17	16	14	15
Ga	19	13	14	13	12	15	18	16	16	18
Zn	70	64	74	72	67	62	74	73	58	78
Cu	1	4	5	7	5	13	7	5	-	6
Ni	32	31	30	35	29	28	28	30	21	36
Co	17	15	10	19	14	14	17	19	12	18
Cr	86	114	76	87	139	59	69	55	53	71
Ce	55	44	59	45	47	50	55	56	39	61
Ba	338	305	316	290	304	320	365	302	324	329
La	28	28	28	25	24	25	30	22	19	34

Sample	9.6A	9.6B	9.6C	9.6D	9.7A	9.7B	9.7C
Zr	177	196	172	165	170	178	142
Y	41	36	36	38	45	40	45
Sr	103	121	83	75	118	116	92
U	3	3	4	1	3	2	2
Rb	84	102	70	67	2	2	-
Th	1	5	1	-	-	-	-
Pb	15	17	19	13	-	-	-
Ga	18	19	14	13	17	20	17
Zn	78	80	14	59	60	67	58
Cu	6	4	13	8	-	7	-
Ni	36	39	32	28	178	228	153
Co	18	17	20	14	73	70	64
Cr	71	76	55	47	741	707	783
Ce	61	57	50	37	22	19	10
Ba	329	391	289	284	224	197	206
La	34	40	28	19	18	17	8

Appendix 4 Heavy Mineral Chemistry

Below are listed the chemical compositions of garnets, epidotes and tourmalines from the Tortonian to Pliestocene sandstones of the eastern Granada Basin. These data were obtained by electron microprobe analysis of polished grain mounts of mineral separates (see **Appendix 1** for further details).

Each grain analysed is identified by a number suffixed by a letter to identify the particular analysis used. Grain core and rim compositions are distinguished by the prefix's R (rim) and C (core).

Detrital Garnets Cations calculated on the basis of 24 oxygens

Quentar Formation

	C 15	R 15	16A	17A	18A	C19A	R19B	20A	1G	3D
SiO_2	37.816	37.659	37.538	43.81	37.093	37.106	37.989	37.572	37.754	37.749
TiO_2	0.150	0.183	0.035	0.074	0.00	0.084	0.039	0.059	0.162	0.149
Al_2O_2	21.413	21.689	21.696	18.669	21.561	21.395	21.607	21.278	21.264	21.599
FeO	30.008	29.887	33.462	27.13	37.056	33.87	33.386	31.632	32.241	30.303
MnO	1.700	1.886	0.371	3.994	0.813	0.223	0.15	0.52	0.467	0.073
MgO	1.730	1.638	3.278	0.733	1.914	1.767	1.828	0.723	3.823	1.153
CaO	8.674.	8.661	4.658	6.188	2.702	6.379	6.95	9.347	5.658	9.983
Na_2O	0.365	0.000	0.00	0.00	0.201	0.94	0.00	0.079	0.195	0.00
K_2O	0.015	0.031	0.044	0.001	0.00	0.049	0.00	0.013	0.008	0.015
P_2O_5	0.114	0.00	0.028	0.00	0.059	0.00	0.074	0.00	0.00	0.026
SO	0.005	0.00	0.00	0.00	0.035	0.00	0.061	0.001	0.013	0.00
Cr_2O_3	0.00	0.00	0.00	0.065	0.00	0.00	0.00	0.112	0.037	0.049
CoO	0.00	0.002	0.00	0.013	0.003	0.02	0.00	0.056	0.00	0.00
NiO	0.177	0.119	0.171	0.031	0.00	0.057	0.056	0.00	0.013	0.032
Total	102.2	101.7	101.3	100.7	101.4	101.04	102.1	101.4	101.6	101.8
Si	4.452	5.932	5.93	6.799	5.931	5.924	5.969	5.968	5.932	5.943
Ti	0.013	0.022	0.004	0.009	0.00	0.01	0.005	0.007	0.019	0.018
Al	2.972	4.027	4.042	3.415	4.064	4.026	4.002	3.984	3.938	4.008
Fe	2.955	3.937	4.423	3.522	4.955	4.522	4.387	4.202	4.237	3.99
Mn	0.17	0.252	0.05	0.525	0.11	0.03	0.02	0.07	0.062	0.097
Mg	0.304	0.385	0.772	0.169	0.456	0.42	0.428	0.171	0.895	0.271
Ca	1.094	1.462	0.789	1.029	0.463	1.091	1.17	1.591	0.953	1.684
Na	0.083	0.00	0.00	0.00	0.062	0.029	0.00	0.024	0.059	0.00
K	0.002	0.006	0.009	0.001	0.00	0.01	0.00	0.003	0.002	0.003
P	0.011	0.00	0.004	0.00	0.008	0.00	0.01	0.00	0.00	0.003
S	0.001	0.00	0.00	0.00	0.007	0.00	0.012	0.00	0.003	0.00
Cr	0.00	0.00	0.00	0.065	0.00	0.00	0.00	0.014	0.005	0.006
Co	0.00	0.00	0.00	0.013	0.00	0.003	0.00	0.007	0.00	0.00
Ni	0.017	0.015	0.022	0.031	0.00	0.007	0.007	0.00	0.002	0.004
Total	12.074	16.03	16.04	15.48	16.06	16.07	16.01	16.04	16.12	16.03

	4F	R 5A	C 5D	R 6A	R 6C	C 7A	R 7B	8A	9A	R 10A
SiO_2	37.333	36.86	37.487	37.971	38.006	38.153	38.1	37.221	37.3	37.634
TiO_2	0.055	0.085	0.067	0.01	0.107	0.093	0.01	0.142	0.092	0.168
Al_2O_2	21.246	21.227	21.671	20.772	21.263	21.832	21.414	21.359	21.217	21.146
FeO	34.855	28.646	29.157	30.555	31.23	31.931	30.839	33.775	34.836	31.98
MnO	0.191	3.161	3.308	1.799	1.824	0.438	0.308	3.707	0.645	1.957
MgO	1.929	1.195	1.105	2.29	3.372	4.178	4.219	1.454	3.301	1.634
CaO	4.57	8.267	8.81	7.234	7.222	5.785	5.915	4.038	3.042	7.285
Na_2O	0.077	0.167	0.015	0.11	0.242	0.173	0.09	0.2	0.00	0.088
K_2O	0.00	0.053	0.015	0.00	0.00	0.00	0.058	0.032	0.00	0.042
P_2O_5	0.00	0.00	0.053	0.00	0.013	0.00	0.00	0.00	0.00	0.009
SO	0.32	0.00	0.004	0.022	0.00	0.011	0.00	0.017	0.00	0.00
Cr_2O_3	0.00	0.00	0.00	0.022	0.00	0.002	0.003	0.00	0.00	0.00
CoO	0.011	0.00	0.00	0.021	0.009	0.026	0.002	0.00	0.00	0.00
NiO	0.113	0.163	0.00	0.00	0.00	0.004	0.039	0.00	0.00	0.00
Total	100.4	99.8	101.7	100.8	102.3	102.6	101.0	101.9	100.4	102.0
Si	5.989	5.938	5.927	6.031	5.963	5.917	5.98	5.934	5.964	5.952
Ti	0.007	0.01	0.008	0.001	0.013	0.011	0.002	0.017	0.011	0.02
Al	4.017	4.031	4.038	3.889	3.932	3.991	3.961	4.014	3.998	3.942
Fe	4.676	3.859	3.855	4.059	4.098	4.141	4.048	4.503	4.658	4.23
Mn	0.026	0.431	0.433	0.242	0.242	0.058	0.041	0.501	0.087	0.262
Mg	0.461	0.287	0.26	0.542	0.555	0.966	0.987	0.346	0.787	0.385
Ca	0.785	1.427	1.492	1.231	1.214	0.961	0.995	0.69	4.658	1.235
Na	0.024	0.052	0.005	0.034	0.073	0.052	0.027	0.062	0.087	0.027
K	0.00	0.011	0.003	0.00	0.00	0.00	0.012	0.007	0.00	0.008
P	0.00	0.00	0.007	0.00	0.002	0.00	0.00	0.00	0.00	0.001
S	0.006	0.00	0.001	0.004	0.00	0.002	0.00	0.003	0.00	0.00
Cr	0.00	0.00	0.00	0.003	0.00	0.00	0.00	0.00	0.00	0.00
Co	0.001	0.00	0.00	0.003	0.001	0.003	0.00	0.00	0.00	0.00
Ni	0.015	0.021	0.00	0.00	000	0.00	0.005	0.00	0.00	0.01
Total	16.01	16.07	16.04	16.04	16.09	16.1	16.06	16.08	16.03	16.07

Quentar Formation Sample QR4

	R10B	11A	13A	14A	R22A	C22A	23B	24A	25A	26C
SiO_2	37.411	37.762	37.884	37.003	35.256	36.702	36.413	36.406	37.149	36.76
TiO_2	0.252	0.356	0.104	0.126	0.081	0.124	0.074	0.124	0.053	0.122
Al_2O_2	20.917	21.459	21.276	21.593	20.474	21.00	21.242	21.077	21.508	20.706
FeO	31.801	28.773	28.123	31.007	33.589	33.578	31.042	37.448	36.101	32.27
MnO	1.705	4.011	2.169	1.334	0.96	2.081	2.405	0.56	0.334	2.24
MgO	1.907	3.23	1.179	2.052	1.382	1.059	0.953	2.683	4.378	2.315
CaO	7.02	5.838	10.81	7.862	5.86	6.705	8.345	3.309	1.522	6.52
Na_2O	0.065	0.153	0.008	0.00	0.00	0.264	0.147	0.182	0.27	0.106
K_2O	0.0	0.017	0.00	0.041	0.00	0.015	0.036	0.00	0.00	0.00
P_2O_5	0.111	0.00	0.00	0.00	0.00	0.00	0.102	0.00	0.08	0.003
SO	0.066	0.003	0.072	0.021	0.00	0.00	0.037	0.00	0.00	0.006
Cr_2O_3	0.07	0.017	0.095	0.00	0.00	0.00	0.012	0.095	0.00	0.00
CoO	0.022	0.029	0.014	0.02	0.00	0.015	0.043	0.00	0.00	0.00
NiO	0.00	0.116	0.054	0.164	0.034	0.092	0.156	0.00	0.00	0.00
Total	101.3	101.8	101.8	101.2	97.64	101.6	101.0	101.9	101.4	101.05
Si	5.943	5.93	5.962	5.877	5.872	5.885	5.847	5.829	5.886	5.891
Ti	0.03	0.042	0.012	0.015	0.01	0.015	0.009	0.015	0.006	0.015
Al	3.917	3.972	3.947	4.042	4.019	3.969	4.021	3.978	4.017	3.911
Fe	4.225	3.779	3.701	4.118	4.678	4.503	4.169	5.015	4.784	4.325
Mn	0.229	0.533	0.289	0.179	0.135	0.283	0.327	0.076	0.045	0.304
Mg	0.452	0.756	0.276	0.486	0.343	0.253	0.228	0.64	1.034	0.553
Ca	1.195	0.982	1.823	1.338	1.046	1.152	1.436	0.568	0.258	1.12
Na	0.02	0.046	0.003	0.00	0.00	0.082	0.046	0.056	0.083	0.033
K	0.00	0.003	0.00	0.008	0.00	0.003	0.007	0.00	0.00	0.00
P	0.015	0.00	0.00	0.00	0.00	0.00	0.014	0.00	0.011	0.00
S	0.013	0.001	0.014	0.004	0.00	0.00	0.007	0.00	0.00	0.001
Cr	0.009	0.002	0.012	0.00	0.00	0.00	0.002	0.012	0.00	0.00
Co	0.003	0.004	0.002	0.003	0.001	0.002	0.005	0.00	0.00	0.00
Ni	0.00	0.015	0.007	0.021	0.005	0.012	0.02	0.00	0.00	0.00
Total	16.05	16.07	16.05	16.09	16.12	16.16	16.14	16.19	16.12	16.15

	27C	R28C	C28I	29B	30B	31B	32A	33A	34A	35A
SiO_2	37.024	36.285	36.927	35.002	37.169	37.119	37.265	36.644	37.175	36.998
TiO_2	0.182	0.069	0.065	0.021	0.129	0.085	0.108	0.088	0.14	0.139
Al_2O_2	21.344	20.783	21.206	19.691	21.273	21.422	21.207	21.342	21.123	21.478
FeO	32.344	26.891	27.947	32.564	36.273	31.882	30.259	32.082	28.942	33.615
MnO	0.649	0.559	1.189	1.378	0.393	0.169	2.62	2.986	1.682	0.16
MgO	1.041	2.767	1.629	1.599	5.119	1.724	4.368	0.906	0.986	3.722
CaO	8.82	9.982	10.752	5.67	0.948	8.84	5.142	7.560	10.985	5.019
Na_2O	0.04	0.00	0.035	0.284	0.00	0.00	0.106	0.114	0.003	0.143
K_2O	0.00	0.036	0.015	0.03	0.00	0.001	0.00	0.00	0.013	0.035
P_2O_5	0.043	0.00	0.00	0.00	0.099	0.00	0.006	0.10	0.014	0.00
SO	0.00	0.00	0.00	0.007	0.00	0.027	0.054	0.056	0.00	0.00
Cr_2O_3	0.00	0.08	0.022	0.00	0.028	0.00	0.121	0.033	0.007	0.099
CoO	0.03	0.014	0.017	0.002	0.036	0.024	0.00	0.015	0.00	0.003
NiO	0.00	0.00	0.035	0.022	0.106	0.00	0.00	0.00	0.158	0.083
Total	101.5	97.5	99.8	96.3	102.11	101.3	101.3	101.9	101.2	101.5
Si	5.892	5.911	5.913	5.914	5.839	5.894	5.882	5.847	5.91	5.853
Ti	0.022	0.008	0.008	0.003	0.015	0.01	0.013	0.011	0.017	0.017
Al	4.003	3.99	4.002	3.922	4.039	4.009	3.945	4.014	3.958	4.005
Fe	4.305	3.664	3.743	4.602	4.766	4.234	0.35	4.281	3.848	4.448
Mn	0.087	0.077	0.161	0.197	0.052	0.023	1.028	0.404	0.227	0.021
Mg	0.247	0.672	0.389	0.403	1.199	0.408	0.087	0.215	0.234	0.878
Ca	1.504	1.742	1.845	1.027	0.16	1.504	0.87	1.293	1.871	0.851
Na	0.012	0.00	0.011	0.093	0.00	0.00	0.032	0.035	0.001	0.044
K	0.00	0.008	0.003	0.006	0.00	0.00	0.00	0.00	0.003	0.007
P	0.006	0.00	0.00	0.00	0.013	0.00	0.001	0.014	0.002	0.00
S	0.00	0.00	0.00	0.02	0.00	0.005	0.011	0.011	0.00	0.00
Cr	0.00	0.01	0.003	0.00	0.003	0.00	0.015	0.004	0.001	0.012
Co	0.004	0.002	0.002	0.00	0.004	0.003	0.00	0.002	0.01	0.00
Ni	0.00	0.00	0.004	0.003	0.013	0.00	0.00	0.00	0.02	0.011
Total	16.08	16.08	16.08	16.17	16.1	16.09	16.14	16.13	16.09	16.15

Quentar Formation Sample QR4

	36C	37A	R38A	C38B	39A	40B	41A	42A	43A	44A
SiO_2	37.207	36.964	35.895	37.442	37.004	36.684	36.381	37.441	37.621	37.092
TiO_2	0.076	0.193	0.115	0.105	0.157	0.017	0.098	0.157	0.00	0.038
Al_2O_2	21.642	21.333	20.823	21.503	21.018	21.258	21.093	20.701	21.686	21.522
FeO	32.665	29.41	28.212	30.007	32.169	38.413	34.423	32.449	35.253	35.715
MnO	0.283	2.928	0.542	0.397	1.425	0.486	1.531	1.279	0.284	1.637
MgO	1.686	1.205	2.206	2.11	2.456	3.986	1.664	3.196	4.937	3.984
CaO	8.293	9.659	9.473	9.993	6.138	0.683	5.469	6.012	2.617	1.774
Na_2O	0.00	0.067	0.086	0.059	0.074	0.247	0.233	0.094	0.168	0.123
K_2O	0.024	0.00	0.00	0.00	0.084	0.00	0.046	0.00	0.00	0.00
P_2O_5	0.00	0.064	0.047	0.029	0.00	0.064	0.004	0.00	0.08	0.067
SO	0.00	0.00	0.038	0.04	0.027	0.00	0.00	0.011	0.00	0.026
Cr_2O_3	0.042	0.00	0.078	0.00	0.00	0.004	0.073	0.022	0.056	0.00
CoO	0.00	0.006	0.01	0.00	0.035	0.041	0.00	0.016	0.00	0.024
NiO	0.063	0.003	0.007	0.123	0.091	0.089	0.00	0.066	0.04	0.062
Total	101.98	101.8	97.53	101.8	100.7	101.9	101.01	101.4	102.7	102.06
Si	5.88	5.861	5.876	5.888	5.92	5.843	5.861	5.937	5.867	5.866
Ti	0.009	0.023	0.014	0.012	0.019	0.002	0.012	0.019	0.00	0.005
Al	4.031	3.987	4.018	3.986	3.963	3.991	4.005	3.869	3.986	4.012
Fe	4.317	3.90	3.862	3.946	4.304	5.117	4.638	4.304	4.598	4.724
Mn	0.038	0.393	0.075	0.053	0.193	0.066	0.209	0.172	0.038	0.219
Mg	0.397	0.285	0.538	0.495	0.586	0.947	0.40	0.755	1.148	0.939
Ca	1.404	1.641	1.662	1.684	1.052	0.116	0.944	1.022	0.437	0.301
Na	0.00	0.021	0.027	0.018	0.023	0.076	0.073	0.029	0.051	0.038
K	0.005	0.00	0.00	0.00	0.017	0.00	0.009	0.00	0.00	0.00
P	0.00	0.009	0.007	0.004	0.00	0.009	0.001	0.00	0.011	0.009
S	0.00	0.00	0.008	0.008	0.005	0.00	0.00	0.002	0.00	0.005
Cr	0.005	0.00	0.01	000	0.00	0.001	0.009	0.003	0.007	0.00
Co	0.00	0.001	0.001	0.00	0.005	0.005	0.00	0.002	0.00	0.003
Ni	0.008	0.00	0.001	0.016	0.012	0.011	0.00	0.008	0.005	0.008
Total	16.09	16.12	16.1	16.11	16.1	16.18	16.16	16.12	16.15	16.13

	45A	46B	47B	48A	49B	50A
SiO_2	36.78	36.837	37.161	37.162	36.55	36.32
TiO_2	0.013	0.089	0.143	0.261	0.037	0.125
Al_2O_2	21.149	21.16	21.431	21.44	21.195	20.548
FeO	31.803	37.896	35.61	29.646	36.399	37.799
MnO	0.584	0.295	0.513	1.045	1.131	0.578
MgO	2.305	3.324	1.838	2.368	2.472	3.401
CaO	8.218	1.871	5.809	9.352	3.174	1.136
Na_2O	0.105	0.043	0.00	0.023	0.00	0.207
K_2O	0.01	0.00	0.008	0.017	0.00	0.017
P_2O_5	0.006	0.00	0.007	0.013	0.009	0.032
SO	0.012	0.035	0.012	0.062	0.032	0.00
Cr_2O_3	0.031	0.055	0.00	0.089	0.00	0.00
CoO	0.00	0.00	0.00	0.00	0.011	0.00
NiO	0.00	0.047	0.00	0.019	0.00	0.00
Total	101.02	101.65	102.53	101.49	101.01	100.16
Si	5.866	5.882	5.881	5.863	5.88	5.897
Ti	0.002	0.011	0.017	0.031	0.004	0.015
Al	3.976	3.982	3.998	3.987	4.019	3.932
Fe	2.242	5.06	4.713	3.912	4.897	5.132
Mn	0.079	0.04	0.069	0.14	0.154	0.079
Mg	0.548	0.791	0.434	0.557	0.593	0.823
Ca	1.404	0.32	0.985	1.581	0.547	0.198
Na	0.032	0.013	0.00	0.007	0.00	0.065
K	0.002	0.00	0.002	0.003	0.00	0.003
P	0.001	0.00	0.001	0.002	0.001	0.004
S	0.002	0.007	0.002	0.012	0.007	0.00
Cr	0.004	0.007	0.00	0.011	0.00	0.00
Co	0.00	0.00	0.00	0.00	0.001	0.00
Ni	0.00	0.006	0.00	0.002	0.00	0.00
Total	16.16	16.12	16.10	16.11	16.1	16.15

Dudar Formation Garnets Sample S13

	C - R							C - R		
SiO_2	37.42	36.96	36.38	36.25	36.76	36.40	37.12	37.38	37.26	36.64
TiO_2	0.09	0.00	0.12	0.09	0.01	0.03	0.08	0.07	0.08	0.17
Al_2O_2	21.18	21.42	20.6	20.39	20.99	20.83	20.8	20.76	20.11	20.69
Cr_2O_3	0.00	0.01	0.01	0.01	0.00	0.07	0.03	0.00	0.00	0.01
FeO	3.98	33.38	30.68	37.22	30.25	34.92	28.68	35.94	35.44	0.60
MgO	3.25	4.67	1.59	1.44	1.34	1.88	1.57	3.14	2.98	1.22
CaO	7.47	3.07	8.48	2.94	8.02	2.03	10.63	2.86	2.90	10.29
MnO	0.76	0.50	0.38	1.38	1.88	4.47	0.33	0.23	0.22	1.61
NiO	0.00	0.08	0.00	0.04	0.00	0.00	0.00	0.00	0.06	28.67
Na_2O	0.05	0.02	0.02	0.03	0.01	0.00	0.01	0.05	0.05	0.00
K_2O	0.00	0.00	0.00	0.00	0.00	0.00	0.00	0.02	0.00	0.03
Total	100.16	16.09	98.26	99.81	99.35	100.64	99.26	100.44	99.09	0.01
Si	5.94	5.89	5.94	5.94	5.95	5.91	5.97	5.99	6.04	5.90
Ti	0.01	0.00	0.01	0.01	0.01	0.00	0.01	0.01	0.01	0.02
Al	3.97	4.03	3.97	3.94	4.00	3.99	3.94	3.92	3.85	3.93
Cr	0.00	0.00	0.00	0.00	0.00	0.01	0.00	0.00	0.00	0.00
Fe	3.98	4.45	4.19	5.09	4.09	0.02	3.85	4.81	4.79	3.93
Mg	0.77	1.11	0.39	0.35	0.32	0.46	0.38	0.75	0.72	0.29
Ca	1.27	0.52	1.48	0.52	1.39	0.35	1.83	0.49	0.50	1.78
Mn	0.1	0.07	0.05	0.19	0.26	0.62	0.05	0.03	0.03	0.22
Ni	0.00	0.01	0.00	0.01	0.00	4.72	0.00	0.00	0.01	0.00
Na	0.01	0.01	0.01	0.01	0.00	0.00	0.00	0.02	0.01	0.01
K	0.00	0.00	0.00	0.00	0.00	0.00	0.00	0.00	0.00	0.00
Total	16.05	16.09	16.04	16.05	16.04	16.08	16.03	16.01	15.96	16.09
						C - R				
SiO_2	37.13	37.38	37.20	37.13	37.31	36.68	36.31	36.89	37.51	37.23
TiO_2	0.08	0.05	0.16	0.16	0.09	0.17	0.10	0.06	0.00	0.13
Al_2O_2	20.86	21.02	20.91	20.87	20.99	20.88	20.99	20.48	20.89	20.65
Cr_2O_3	0.06	0.01	0.00	0.00	0.00	0.04	0.01	0.06	0.02	0.08
FeO	28.00	33.29	29.81	29.01	28.35	35.48	35.51	35.52	34.36	29.27
MgO	1.64	4.45	2.31	2.22	1.34	3.49	3.80	2.45	5.04	1.34
CaO	8.50	3.37	8.33	8.41	11.48	2.43	2.25	3.25	1.12	10.19
MnO	3.89	0.15	1.51	1.67	0.26	0.38	0.33	0.84	0.58	0.37
NiO	0.00	0.00	0.00	0.00	0.00	0.00	0.05	0.08	0.00	0.00
Na_2O	0.02	0.02	0.01	0.00	0.00	0.04	0.02	0.02	0.01	0.02
K_2O	0.00	0.00	0.00	0.01	0.02	0.01	0.00	0.02	0.00	0.03
Total	100.18	99.73	100.23	99.48	99.85	99.60	99.37	99.67	99.53	99.31
Si	5.95	5.97	5.94	5.96	5.96	5.93	5.89	5.98	6.00	5.99
Ti	0.01	0.01	0.02	0.02	0.01	0.02	0.01	0.01	0.00	0.01
Al	3.94	3.95	3.93	3.95	3.95	3.98	4.01	3.92	3.94	3.92
Cr	0.01	0.00	0.00	0.00	0.00	0.00	0.00	0.01	0.00	0.01
Fe	3.74	4.45	3.97	3.89	3.79	4.80	4.82	4.81	4.59	3.93
Mg	0.39	1.06	0.55	0.53	0.32	0.84	0.92	0.59	1.20	0.32
Ca	1.46	0.58	1.42	1.45	1.97	0.42	0.39	0.56	0.19	1.76
Mn	0.53	0.02	0.20	0.23	0.04	0.05	0.05	0.12	0.08	0.05
Ni	0.00	0.00	0.00	0.00	0.00	0.00	0.01	0.01	0.00	0.00
Na	0.01	0.00	0.00	0.00	0.01	0.01	0.01	0.01	0.00	0.01
K	0.00	0.00	0.00	0.00	0.00	0.00	0.00	0.00	0.00	0.01
Total	16.04	16.03	16.05	16.03	16.03	16.06	16.10	16.02	16.00	16.01

Dudar Formation Garnets Sample S13

	C - R				C - R				C - R	
SiO_2	37.63	37.36	36.90	37.87	37.42	37.42	36.62	37.52	36.79	37.38
TiO_2	0.17	0.13	0.09	0.12	0.11	0.04	0.05	0.12	0.11	0.16
Al_2O_2	20.43	20.34	20.67	21.11	20.53	21.10	20.41	20.79	21.20	20.67
Cr_2O_3	0.03	0.03	0.04	0.06	0.00	0.00	0.00	0.02	0.06	0.02
FeO	27.07	29.82	31.80	28.12	28.99	26.56	35.96	27.99	28.98	29.74
MgO	1.15	1.74	1.18	3.28	1.25	2.65	1.87	1.77	2.35	1.11
CaO	9.32	8.62	8.85	9.38	10.29	11.40	3.02	11.12	9.87	10.50
MnO	3.71	0.61	0.29	0.66	0.41	0.31	1.54	0.12	0.09	0.74
NiO	0.00	0.01	0.02	0.03	0.04	0.02	0.00	0.00	0.05	0.00
Na_2O	0.01	0.03	0.02	0.02	0.02	0.03	0.02	0.00	0.00	0.02
K_2O	0.00	0.00	0.00	0.01	0.00	0.00	0.00	0.00	0.00	0.01
Total	99.52	98.70	99.87	100.64	99.06	99.54	99.50	99.44	99.50	100.36
Si	6.05	6.04	5.95	5.96	6.03	5.95	5.98	5.99	5.90	5.97
Ti	0.02	0.02	0.01	0.01	0.01	0.00	0.01	0.01	0.01	0.02
Al	3.87	3.88	3.93	3.91	3.90	3.95	3.93	3.91	4.01	3.89
Cr	0.00	0.00	0.00	0.01	0.00	0.0	0.00	0.00	0.01	0.00
Fe	3.63	4.02	4.29	3.69	3.89	3.53	4.90	3.74	3.88	3.96
Mg	0.28	0.42	0.28	0.77	0.30	0.63	0.45	0.42	0.56	0.26
Ca	1.61	1.49	1.53	1.58	1.77	1.94	0.53	1.90	1.70	1.80
Mn	0.50	0.08	0.04	0.09	0.06	0.04	0.21	0.02	0.01	0.10
Ni	0.00	0.00	0.00	0.00	0.00	0.00	0.00	0.00	0.01	0.00
Na	0.00	0.01	0.01	0.01	0.00	0.01	0.01	0.00	0.00	0.01
K	0.00	0.00	0.00	0.00	0.00	0.00	0.00	0.00	0.00	0.00
Total	15.95	15.96	16.04	16.03	15.97	16.05	16.02	16.00	16.08	16.02
		C - R								
SiO_2	36.68	37.01	37.31	36.71	36.54	36.72	36.74	37.28	37.00	36.92
TiO_2	0.07	0.10	0.02	0.15	0.08	0.06	0.05	0.11	0.09	0.12
Al_2O_2	20.63	20.55	20.56	20.83	20.76	20.05	20.92	20.84	20.89	20.58
Cr_2O_3	0.01	0.01	0.02	0.00	0.00	0.00	0.01	0.04	0.03	0.03
FeO	29.58	30.98	32.22	29.25	37.15	35.75	36.32	31.75	31.52	36.75
MgO	1.17	2.07	3.37	0.86	3.03	1.91	3.87	2.57	2.10	2.59
CaO	10.50	8.23	5.00	10.68	0.82	2.44	1.88	7.45	8.13	3.39
MnO	1.03	0.92	0.58	1.55	0.36	1.15	0.15	0.15	0.56	0.25
NiO	0.07	0.00	0.00	0.03	0.03	0.09	0.08	0.00	0.01	0.00
Na_2O	0.03	0.02	0.00	0.03	0.01	0.03	0.03	0.04	0.00	0.02
K_2O	0.00	0.01	0.01	0.00	0.00	0.00	0.00	0.00	0.00	0.00
Total	99.90	99.90	99.09	100.09	98.78	98.66	100.06	100.24	100.33	100.64
Si	5.91	5.95	6.01	5.91	5.98	6.03	5.92	5.95	5.92	5.94
Ti	0.01	0.01	0.00	0.02	0.01	0.01	0.01	0.01	0.01	0.01
Al	3.92	3.89	3.90	3.95	4.00	3.96	3.97	3.92	3.94	3.90
Cr	0.00	0.00	0.00	0.00	0.00	0.00	0.00	0.00	0.00	0.00
Fe	4.08	4.15	4.33	3.93	5.08	4.90	4.89	4.23	4.21	5.04
Mg	0.28	0.50	0.81	0.21	0.74	0.47	0.93	0.61	0.50	0.62
Ca	1.81	1.42	0.86	1.84	0.14	0.43	0.32	1.27	1.39	0.58
Mn	0.14	0.12	0.08	0.21	0.05	0.16	0.02	0.02	0.08	0.03
Ni	0.01	0.00	0.00	0.00	0.00	0.01	0.01	0.00	0.00	0.00
Na	0.01	0.01	0.00	0.01	0.00	0.01	0.01	0.01	0.00	0.01
K	0.00	0.00	0.00	0.00	0.00	0.00	0.00	0.00	0.00	0.00
Total	16.08	16.05	15.99	16.08	16.01	15.98	16.08	16.04	16.07	16.05

Dudar Formation Garnets Sample S13

SiO_2	37.35	37.10	37.31	36.76	36.68	36.49	37.03	36.78	37.27	36.76
TiO_2	0.07	0.14	0.08	0.15	0.08	0.06	0.10	0.13	0.14	0.15
Al_2O_2	20.98	20.96	20.99	20.81	20.72	20.73	20.95	20.53	20.75	20.58
Cr_2O_3	0.03	0.00	0.02	0.00	0.00	0.00	0.03	0.07	0.03	0.01
FeO	29.22	29.08	32.72	32.50	32.29	31.20	34.23	31.72	28.67	30.52
MgO	1.44	1.45	1.19	1.52	1.29	1.28	3.47	0.70	1.09	0.88
CaO	10.39	10.31	7.91	7.39	7.89	8.23	3.74	9.96	11.37	8.19
MnO	0.39	0.39	0.09	1.19	1.04	0.83	0.33	0.50	0.54	2.17
NiO	0.00	0.03	0.00	0.02	0.00	0.00	0.00	0.02	0.00	0.00
Na_2O	0.03	0.01	0.04	0.01	0.01	0.03	0.00	0.01	0.00	0.07
K_2O	0.00	0.00	0.02	0.00	0.01	0.01	0.00	0.00	0.03	0.01
Total	99.90	99.48	100.38	100.35	100.00	98.85	99.9	100.42	99.88	99.34
Si	5.97	5.96	5.98	5.92	5.93	5.94	5.95	5.92	5.97	5.97
Ti	0.01	0.02	0.01	0.02	0.01	0.01	0.01	0.02	0.02	0.02
Al	3.95	3.97	3.97	3.95	3.95	3.98	3.97	3.90	3.91	3.94
Cr	0.00	0.00	0.00	0.00	0.00	0.00	0.00	0.01	0.00	0.00
Fe	3.90	3.90	4.39	4.37	4.36	4.25	4.60	4.26	3.83	4.14
Mg	0.34	0.35	0.28	0.37	0.31	0.31	0.83	0.17	0.26	0.21
Ca	1.78	1.77	1.36	1.27	1.37	1.44	0.64	1.72	1.95	1.42
Mn	0.05	0.05	0.01	0.16	0.14	0.11	0.05	0.07	0.07	0.30
Ni	0.00	0.00	0.00	0.00	0.00	0.00	0.00	0.00	0.00	0.00
Na	0.01	0.00	0.01	0.00	0.00	0.01	0.00	0.00	0.00	0.02
K	0.00	0.00	0.00	0.00	0.00	0.00	0.00	0.00	0.00	0.00
Total	16.03	16.03	16.02	16.07	16.06	16.05	16.04	16.06	16.02	16.03

					C -	R	C -	R	
SiO_2	36.92	36.82	36.21	37.05	42.85	37.88	37.25	36.75	37.33
TiO_2	0.01	0.12	0.10	0.09	0.13	0.14	0.11	0.10	0.09
Al_2O_2	20.70	20.64	20.71	20.83	18.83	21.38	20.88	21.29	20.83
Cr_2O_3	0.00	0.01	0.00	0.00	0.00	0.08	0.02	0.00	0.07
FeO	35.09	30.60	31.03	28.72	23.49	26.34	29.29	30.18	29.08
MgO	3.12	0.77	0.95	1.43	1.91	3.34	1.31	1.34	4.52
CaO	2.12	9.61	8.96	10.96	11.31	11.01	9.81	10.37	6.69
MnO	1.83	1.16	0.63	0.14	0.51	0.33	1.20	0.23	0.87
NiO	0.00	0.00	0.01	0.06	0.09	0.01	0.00	0.00	0.06
Na_2O	0.05	0.01	0.03	0.00	0.02	0.01	0.02	0.04	0.01
K_2O	0.03	0.00	0.00	0.02	0.03	0.01	0.00	0.00	0.00
Total	99.86	99.76	98.64	99.31	99.18	100.53	99.90	100.30	99.55
Si	5.97	59.95	5.95	5.96	6.62	5.94	5.97	5.89	5.93
Ti	0.00	0.01	0.01	0.01	0.01	0.02	0.01	0.01	0.01
Al	3.94	3.93	3.99	3.95	3.43	3.95	3.94	4.02	3.90
Cr	0.00	0.00	0.00	0.00	0.00	0.01	0.00	0.00	0.01
Fe	4.73	4.13	4.24	3.86	2.99	3.44	0.05	4.04	3.86
Mg	0.75	0.19	0.23	0.34	0.44	0.78	0.31	0.32	1.07
Ca	0.37	1.66	1.57	1.89	1.87	1.85	1.68	1.78	1.14
Mn	0.25	0.16	0.09	0.02	0.07	0.04	0.16	0.03	0.12
Ni	0.00	0.00	0.00	0.01	0.01	0.00	3.88	0.00	0.01
Na	0.02	0.00	0.01	0.00	0.01	0.00	0.01	0.01	0.00
K	0.00	0.00	0.00	0.00	0.01	0.00	0.00	0.00	0.00
Total	16.03	16.04	16.07	16.03	15.43	16.05	16.02	16.10	16.05

Dudar Formation Garnets Sample C8

SiO_2	37.11	36.56	36.340	36.444	36.686	36.520	37.308	36.498	36.935	37.070
TiO_2	0.11	0.144	0.120	0.103	0.165	0.139	0.064	0.121	0.121	0.046
Al_2O_2	20.73	20.89	20.892	20.479	21.040	20.969	21.129	20.830	20.839	21.122
FeO	31.92	37.21	31.875	37.761	37.014	31.735	32.456	30.458	30.275	30.489
MnO	0.36	0.39	1.626	0.000	0.691	1.498	0.484	1.167	1.296	0.443
MgO	1.92	2.54	1.386	2.581	2.293	1.572	4.489	0.962	1.531	1.911
CaO	8.44	0.07	7.925	2.807	3.370	8.030	4.477	0.962	9.533	9.132
Na_2O	0.10	0.075	0.212	0.159	0.088	0.333	0.314	9.762	0.068	0.000
K_2O	0.01	0.004	0.028	0.000	0.003	0.000	0.014	0.188	0.006	0.022
P_2O_5	0.023	0.00	0.00	0.000	0.056	0.000	0.030	0.000	0.003	0.012
SO	0.047	0.068	0.00	0.000	0.00	0.005	0.012	0.000	0.026	0.038
Cr_2O_3	0.043	0.032	0.008	0.076	0.104	0.000	0.009	0.005	0.00	0.016
CoO	0.095	0.077	0.052	0.111	0.00	0.153	0.021	0.104	0.094	0.000
NiO	0.00	0.076	0.013	0.032	0.012	0.000	0.014	0.020	0.000	0.044
Total	100.91	100.94	100.48	100.55	101.52	100.94	100.82	100.11	100.72	100.343
Si	5.92	5.887	5.866	5.908	5.880	5.861	5.908	5.893	5.910	5.923
Ti	0.013	0.017	0.015	0.013	0.020	0.017	0.008	0.015	0.015	0.006
Al	3.90	3.964	3.975	3.913	3.975	3.967	3.944	3.964	3.930	3.978
Fe	4.26	5.011	4.303	5.120	4.962	4.260	4.299	4.113	4.051	4.074
Mn	0.05	0.053	0.222	0.000	0.094	0.204	0.065	0.160	0.176	0.060
Mg	0.46	0.691	0.334	0.624	0.548	0.376	1.060	0.231	0.365	0.455
Ca	1.44	0.438	1.371	0.488	0.579	1.381	0.760	1.689	1.634	1.563
Na	0.032	0.023	0.066	0.050	0.027	0.104	0.096	0.059	0.021	0.000
K	0.001	0.001	0.006	0.000	0.001	0.000	0.003	0.000	0.001	0.005
P	0.003	0.00	0.000	0.000	0.008	0.000	0.004	0.000	0.000	0.002
S	0.009	0.014	0.000	0.000	0.000	0.001	0.002	0.000	0.005	0.008
Cr	0.005	0.004	0.000	0.010	0.013	0.000	0.001	0.001	0.000	0.002
Co	0.012	0.010	0.001	0.014	0.000	0.020	0.003	0.013	0.012	0.00
Ni	0.00	0.010	0.002	0.004	0.001	0.000	0.002	0.003	0.000	0.006
Total	16.11	16.123	16.167	16.143	16.108	16.19	16.155	16.14	16.121	16.081
								C -	R	
SiO_2	37.61	37.070	37.101	37.294	37.884	36.693	36.576	37.284	35.651	
TiO_2	0.024	0.191	0.155	0.033	0.144	0.165	0.237	0.090	0.058	
Al_2O_2	21.206	21.074	20.930	21.170	20.771	20.772	20.572	20.84	20.366	
FeO	29.243	32.093	30.203	30.758	27.551	30.485	30.265	29.319	27.031	
MnO	0.207	0.448	0.261	0.432	3.371	1.743	1.410	1.046	0.319	
MgO	3.341	2.402	2.665	1.935	1.376	1.725	1.462	2.192	2.682	
CaO	9.216	7.326	8.841	9.622	9.831	8.632	9.122	8.974	9.630	
Na_2O	0.159	0.215	0.230	0.103	0.151	0.121	0.077	0.179	0.168	
K_2O	0.003	0.006	0.000	0.00	0.012	0.000	0.000	0.000	0.051	
P_2O_5	0.076	0.000	0.000	0.066	0.043	0.036	0.000	0.043	0.042	
SO	0.000	0.000	0.014	0.014	0.000	0.094	0.012	0.000	0.003	
Cr_2O_3	0.019	0.102	0.046	0.025	0.047	0.000	0.000	0.026	0.027	
CoO	0.152	0.007	0.044	0.089	0.005	0.005	0.267	0.046	0.000	
NiO	0.000	0.000	0.000	0.000	0.000	0.055	0.011	0.000	0.000	
Total	101.26	100.93	100.49	101.54	101.19	100.53	100.01	100.04	96.03	
Si	5.911	5.905	5.909	5.900	6.002	5.890	5.905	5.959	5.904	
Ti	0.003	0.023	0.019	0.004	0.017	0.020	0.029	0.011	0.007	
Al	3.929	3.957	3.929	3.947	3.879	3.93	3.915	3.926	3.976	
Fe	3.844	4.275	4.023	4.069	3.650	4.093	4.087	3.919	3.744	
Mn	0.028	0.060	0.035	0.058	0.452	0.237	0.193	0.142	0.045	
Mg	0.783	0.570	0.633	0.456	0.325	0.413	0.352	0.522	0.662	
Ca	1.552	1.250	1.509	1.631	1.669	1.485	1.578	1.537	1.709	
Na	0.048	0.066	0.071	0.032	0.046	0.038	0.024	0.055	0.054	
K	0.001	0.001	0.000	0.000	0.002	0.000	0.000	0.000	0.011	
P	0.010	0.000	0.000	0.009	0.006	0.005	0.000	0.006	0.006	
S	0.000	0.00	0.003	0.003	0.00	0.019	0.002	0.000	0.001	
Cr	0.002	0.013	0.006	0.003	0.006	0.000	0.000	0.003	0.004	
Co	0.019	0.001	0.006	0.011	0.001	0.001	0.035	0.006	0.000	
Ni	0.000	0.000	0.000	0.000	0.000	0.007	0.001	0.000	0.000	
Total	16.13	16.122	16.141	16.123	16.055	16.136	16.121	16.085	16.122	

Dudar Formation Garnets Sample C8

SiO_2	37.326	37.408	36.889	37.223	36.468	36.898	36.555	37.011	37.202	37.707
TiO_2	0.000	0.038	0.300	0.137	0.013	0.161	0.112	0.167	0.075	0.075
Al_2O_2	21.061	21.186	21.037	21.329	20.553	21.054	20.979	21.142	20.829	21.069
FeO	28.149	30.595	35.419	33.604	29.525	30.322	35.158	28.697	28.983	30.512
MnO	0.186	0.608	0.426	0.393	0.552	0.676	0.772	0.563	0.533	0.058
MgO	2.872	1.795	4.243	4.607	1.841	2.083	1.854	1.604	1.951	3.283
CaO	10.353	8.895	2.717	3.642	9.174	9.223	4.892	10.885	10.720	8.820
Na_2O	0.000	0.008	0.000	0.136	0.000	0.000	0.093	0.000	0.155	0.007
K_2O	0.000	0.018	0.000	0.000	0.059	0.004	0.012	0.000	0.000	0.000
P_2O_5	0.088	0.000	0.210	0.000	0.113	0.056	0.103	0.061	0.000	0.100
SO	0.001	0.078	0.000	0.051	0.023	0.064	0.074	0.034	0.022	0.000
Cr_2O_3	0.000	0.000	0.000	0.017	0.060	0.032	0.000	0.050	0.000	0.005
CoO	0.126	0.089	0.002	0.233	0.000	0.079	0.072	0.103	0.000	0.100
NiO	0.108	0.009	0.020	0.039	0.005	0.000	0.048	0.065	0.000	0.000
Total	100.27	100.73	101.26	101.41	98.39	100.65	100.72	100.38	100.47	101.74
Si	5.919	5.952	5.859	5.877	5.937	5.885	5.891	5.900	5.928	5.915
Ti	0.000	0.005	0.036	0.016	0.002	0.019	0.014	0.020	0.009	0.009
Al	3.937	3.973	3.938	3.969	3.944	3.958	3.985	3.973	3.912	3.896
Fe	3.733	4.071	4.705	4.437	4.020	4.044	4.738	3.826	3.863	4.003
Mn	0.025	0.082	0.057	0.052	0.076	0.091	0.105	0.076	0.072	0.008
Mg	0.679	0.426	1.005	1.084	0.447	0.495	0.445	0.381	0.463	0.768
Ca	1.759	1.517	0.462	0.616	1.600	1.576	0.845	1.859	1.830	1.482
Na	0.000	0.002	0.000	0.042	0.000	0.000	0.029	0.000	0.048	0.002
K	0.000	0.004	0.000	0.000	0.012	0.001	0.002	0.000	0.000	0.000
P	0.012	0.000	0.028	0.000	0.016	0.008	0.014	0.008	0.000	0.013
S	0.000	0.016	0.000	0.010	0.005	0.013	0.014	0.007	0.004	0.000
Cr	0.000	0.000	0.000	0.002	0.008	0.004	0.000	0.006	0.000	0.001
Co	0.016	0.011	0.000	0.030	0.000	0.010	0.009	0.013	0.000	0.013
Ni	0.014	0.001	0.003	0.005	0.001	0.000	0.006	0.008	0.000	0.000
Total	16.095	16.060	16.093	16.142	16.068	16.104	16.098	16.078	16.13	16.109
SiO_2	37.127	37.533	37.385	37.394	37.035	36.841	37.653	37.374	36.645	37.196
TiO_2	0.143	0.096	0.066	0.208	0.000	0.105	0.004	0.092	0.181	0.200
Al_2O_2	21.008	21.222	20.799	20.936	20.914	21.133	21.697	20.93	20.829	21.073
FeO	31.812	31.480	30.609	32.660	40.224	36.393	34.630	30.556	37.825	32.376
MnO	0.139	0.816	3.676	0.486	0.561	0.532	0.644	4.565	1.064	0.564
MgO	2.365	2.104	2.824	1.541	2.422	3.191	5.562	3.537	1.657	1.411
CaO	7.390	8.254	5.947	8.420	1.183	2.973	1.932	5.043	2.877	8.76
Na_2O	0.084	0.050	0.000	0.000	0.141	0.058	0.000	0.12	0.110	0.089
K_2O	0.002	0.039	0.009	0.017	0.079	0.003	0.000	0.000	0.023	0.000
P_2O_5	0.000	0.077	0.049	0.093	0.084	0.000	0.104	0.000	0.000	0.019
SO	0.000	0.044	0.035	0.034	0.000	0.000	0.015	0.000	0.000	0.000
Cr_2O_3	0.025	0.031	0.056	0.037	0.033	0.000	0.000	0.000	0.045	0.000
CoO	0.165	0.081	0.134	0.000	0.000	0.000	0.000	0.130	0.326	0.027
NiO	0.021	0.002	0.158	0.000	0.069	0.000	0.038	0.000	0.000	0.000
Total	101.28	101.83	101.75	101.82	102.74	101.23	102.28	102.35	101.58	101.72
Si	5.906	5.921	5.927	5.926	5.906	5.891	5.875	5.893	5.906	5.906
Ti	0.017	0.011	0.008	0.025	0.000	0.013	0.000	0.011	0.022	0.024
Al	3.939	3.946	3.886	3.910	3.931	3.983	3.990	3.89	3.957	3.944
Fe	4.365	4.154	4.058	4.328	5.365	4.867	4.519	4.029	5.098	4.300
Mn	0.019	0.109	0.494	0.065	0.076	0.072	0.085	0.610	0.145	0.076
Mg	0.561	0.495	0.667	0.364	0.576	0.761	1.294	0.831	0.3989	0.334
Ca	1.260	1.395	1.010	1.430	0.202	0.509	0.323	0.852	0.497	1.490
Na	0.026	0.015	0.000	0.000	0.044	0.018	0.000	0.037	0.035	0.027
K	0.000	0.008	0.002	0.003	0.016	0.001	0.000	0.000	0.005	0.000
P	0.000	0.010	0.007	0.013	0.011	0.000	0.014	0.000	0.000	0.003
S	0.000	0.009	0.007	0.007	0.000	0.000	0.003	0.000	0.000	0.000
Cr	0.003	0.004	0.007	0.005	0.004	0.000	0.000	0.000	0.006	0.000
Co	0.021	0.010	0.017	0.000	0.000	0.000	0.000	0.016	0.042	0.003
Ni	0.003	0.000	0.020	0.000	0.009	0.000	0.005	0.000	0.000	0.000
Total	16.119	16.088	16.11	16.075	16.139	16.114	16.109	16.17	16.11	16.108

Dudar Formation Garnets Sample C8

SiO_2	37.873	37.294	37.809	36.998	36.986	36.845	37.559	36.949	36.843	37.038
TiO_2	0.107	0.007	0.072	0.139	0.099	0.111	0.132	0.176	0.128	0.275
Al_2O_2	21.544	21.388	21.218	20.869	21.426	20.887	20.736	21.004	21.077	20.998
FeO	32.473	32.981	28.938	34.039	32.026	31.291	34.552	28.089	30.866	27.246
MnO	0.134	1.196	0.430	1.723	1.101	2.360	1.894	2.759	1.938	4.561
MgO	4.636	1.868	3.548	2.532	1.466	1.199	2.633	1.576	1.979	0.953
CaO	5.042	7.152	9.068	5.543	8.155	8.172	5.105	9.283	7.598	9.920
Na_2O	0.015	0.030	0.245	0.219	0.190	0.000	0.000	0.000	0.000	0.000
K_2O	0.002	0.000	0.000	0.000	0.037	0.000	0.031	0.021	0.020	0.049
P_2O_5	0.001	0.017	0.059	0.000	0.000	0.000	0.077	0.039	0.000	0.044
SO	0.019	0.010	0.007	0.000	0.030	0.000	0.008	0.000	0.000	0.000
Cr_2O_3	0.047	0.125	0.030	0.000	0.083	0.000	0.021	0.059	0.002	0.000
CoO	0.048	0.023	0.000	0.000	0.218	0.012	0.219	0.231	0.066	0.156
NiO	0.000	0.000	0.001	0.024	0.000	0.035	0.009	0.000	0.020	0.008
Total	101.94	102.09	101.42	102.09	101.82	100.91	102.98	100.19	100.54	101.25
Si	5.913	5.900	5.922	5.881	5.872	5.914	5.920	5.921	5.904	5.904
Ti	0.013	0.001	0.008	0.017	0.012	0.013	0.016	0.021	0.015	0.033
Al	3.965	3.968	3.917	3.910	4.010	3.951	3.852	3.967	3.981	3.945
Fe	4.240	3.636	3.791	4.525	4.253	4.200	4.554	3.764	4.136	3.632
Mn	0.018	0.043	0.057	0.232	0.148	0.321	0.253	0.375	0.263	0.616
Mg	1.079	0.989	0.828	0.600	0.347	0.287	0.619	0.377	0.473	0.226
Ca	0.844	1.501	1.522	0.944	1.387	1.405	0.862	1.594	1.305	1.694
Na	0.005	0.005	0.074	0.068	0.058	0.000	0.000	0.000	0.000	0.000
K	0.000	0.001	0.000	0.000	0.007	0.000	0.006	0.004	0.004	0.010
P	0.000	0.000	0.008	0.000	0.000	0.000	0.010	0.005	0.000	0.006
S	0.004	0.000	0.001	0.000	0.006	0.000	0.002	0.000	0.000	0.000
Cr	0.006	0.008	0.004	0.000	0.010	0.000	0.003	0.007	0.000	0.000
Co	0.006	0.001	0.000	0.000	0.028	0.002	0.028	0.030	0.009	0.020
Ni	0.000	0.000	0.000	0.003	0.000	0.005	0.001	0.000	0.003	0.001
Total	16.091	16.083	16.134	16.18	16.139	16.097	16.125	16.065	16.092	16.087
SiO_2	37.696	37.521	37.265	37.536	36.373	36.577	36.624			
TiO_2	0.035	0.062	0.148	0.181	0.11	0.130	0.145			
Al_2O_2	21.138	21.122	20.862	20.900	20.983	20.932	20.403			
FeO	31.453	34.340	29.762	31.410	38.386	36.932	37.071			
MnO	0.649	0.751	1.451	1.758	0.866	1.261	0.621			
MgO	4.128	2.709	1.786	1.765	2.371	1.383	1.723			
CaO	6.160	5.170	9.633	8.247	2.763	4.307	4.154			
Na_2O	0.148	0.286	0.000	0.157	0.000	0.152	0.228			
K_2O	0.010	0.000	0.000	0.038	0.000	0.075	0.020			
P_2O_5	0.114	0.104	0.153	0.070	0.003	0.049	0.035			
SO	0.034	0.076	0.000	0.000	0.044	0.027	0.008			
Cr_2O_3	0.055	0.003	0.138	0.005	0.011	0.086	0.085			
CoO	0.078	0.052	0.010	0.229	0.206	0.000	0.273			
NiO	0.018	0.041	0.000	0.029	0.000	0.000	0.108			
Total	101.72	102.24	101.21	102.33	102.12	101.87	101.5			
Si	5.913	5.921	5.914	5.924	5.836	5.878	5.907			
Ti	0.004	0.007	0.018	0.022	0.013	0.016	0.018			
Al	3.908	3.929	3.902	3.888	3.968	3.957	3.878			
Fe	4.126	4.532	3.950	4.146	5.151	4.963	5.000			
Mn	0.086	0.100	0.195	0.235	0.118	0.172	0.085			
Mg	0.965	0.637	0.422	0.415	0.567	0.331	0.414			
Ca	1.035	0.874	1.638	1.395	0.475	0.742	0.718			
Na	0.045	0.088	0.000	0.048	0.000	0.047	0.071			
K	0.002	0.00	0.000	0.008	0.000	0.015	0.004			
P	0.015	0.014	0.021	0.009	0.000	0.007	0.005			
S	0.007	0.015	0.000	0.000	0.009	0.005	0.002			
Cr	0.007	0.000	0.017	0.001	0.001	0.011	0.011			
Co	0.010	0.007	0.001	0.029	0.027	0.000	0.035			
Ni	0.002	0.005	0.000	0.004	0.000	0.000	0.014			
Total	16.126	16.130	16.078	16.124	16.165	16.144	16.162			

Pinos Genil Formation Garnets Sample SAF 5-4

								C - R		
SiO_2	36.883	37.133	37.011	37.417	36.722	37.468	37.229	37.154	36.845	37.076
TiO_2	0.094	0.131	0.057	0.120	0.059	0.083	0.078	0.087	0.047	0.053
Al_2O_2	21.362	21.263	21.583	21.729	20.924	21.749	21.801	21.424	21.427	21.256
Cr_2O_3	0.025	0.008	0.007	0.041	0.045	0.000	0.022	0.015	0.074	0.000
FeO	37.519	27.917	35.109	32.902	30.881	30.710	33.143	33.444	33.759	32.185
MgO	3.068	1.228	3.277	3.383	1.866	2.287	4.16	1.869	2.42	1.961
CaO	0.663	10.430	2.859	4.593	6.232	7.787	4.053	5.872	4.085	5.979
MnO	0.365	1.214	0.355	0.095	3.201	1.032	0.054	0.877	0.489	1.211
Na_2O	0.055	0.005	0.043	0.002	0.013	0.058	0.023	0.024	0.000	0.030
Total	100.04	99.32	100.30	100.28	99.94	101.17	100.56	100.76	99.14	99.75
Si	5.952	5.963	5.925	5.946	5.939	5.921	5.899	5.939	5.961	5.968
Ti	0.011	0.016	0.007	0.014	0.007	0.009	0.009	0.011	0.006	0.006
Al	4.063	4.024	4.072	4.069	3.982	4.051	4.071	4.036	4.085	4.032
Cr	0.003	0.001	0.001	0.005	0.006	0.000	0.003	0.002	0.009	0.000
Fe	5.063	3.749	4.700	4.372	4.168	4.059	4.392	4.471	4.567	4.332
Mg	0.738	0.294	0.782	0.801	0.449	0.537	0.982	0.445	0.583	0.470
Ca	0.115	1.795	0.490	0.782	1.078	1.318	0.688	1.006	0.708	1.031
Mn	0.050	0.165	0.048	0.013	0.438	0.138	0.007	0.119	0.067	0.165
Na	0.017	0.002	0.013	0.007	0.004	0.018	0.007	0.007	0.000	0.009
Total	16.012	16.009	16.038	16.003	16.061	16.052	16.058	16.035	15.986	16.015
				C - R				C - R		C -
SiO_2	36.969	37.03	37.322	37.812	37.81	36.881	36.974	37.582	37.519	36.918
TiO_2	0.122	0.111	0.106	0.058	0.071	0.104	0.070	0.033	0.011	0.129
Al_2O_2	21.139	20.927	20.88	21.906	21.997	21.349	21.261	21.713	21.819	21.056
Cr_2O_3	0.000	0.000	0.000	0.046	0.049	0.000	0.000	0.026	0.037	0.000
FeO	32.381	31.515	28.629	25.883	26.550	30.028	30.545	33.92	32.107	31.809
MgO	1.799	2.187	1.943	2.690	2.759	0.771	1.084	4.453	4.158	1.788
CaO	5.958	6.211	7.266	11.261	10.695	8.576	9.107	2.405	3.822	7.176
MnO	1.185	1.719	3.941	0.387	0.403	3.010	1.001	0.311	0.338	0.714
Na_2O	0.028	0.000	0.0324	0.027	0.011	0.000	0.000	0.0034	0.000	0.037
Total	99.582	99.70	100.12	100.07	100.35	100.72	100.04	100.44	99.81	99.62
Si	5.968	5.965	5.978	5.948	5.938	5.914	5.939	5.954	5.959	5.952
Ti	0.015	0.013	0.023	0.007	0.008	0.012	0.008	0.004	0.001	0.016
Al	4.022	3.973	3.9442	4.061	4.072	4.035	4.025	4.054	4.084	4.001
Cr	0.000	0.000	0.000	0.006	0.006	0.000	0.000	0.003	0.005	0.000
Fe	4.803	4.243	3.830	4.035	3.487	4.027	4.103	4.494	4.265	4.289
Mg	0.433	0.525	0.464	0.631	0.646	0.184	0.259	1.052	0.984	0.429
Ca	1.031	1.072	1.247	1.898	1.799	1.473	1.567	0.408	0.650	1.239
Mn	0.162	0.234	0.535	0.052	0.054	0.409	0.136	0.042	0.455	0.098
Na	0.009	0.000	0.010	0.008	0.003	0.000	0.000	0.001	0.000	0.012
Total	16.011	16.025	16.018	16.016	16.015	16.055	16.039	16.013	15.995	16.037
	R									
SiO_2	36.952	36.566	37.546	37.533	36.745	37.486	37.133	36.531	37.756	37.958
TiO_2	0.194	0.091	0.074	0.045	0.084	0.078	0.025	0.034	0.0322	0.067
Al_2O_2	20.912	21.098	21.553	21.567	21.109	21.554	21.436	21.189	21.636	21.805
Cr_2O_3	0.004	0.014	0.026	0.000	0.037	0.000	0.039	0.029	0.000	0.015
FeO	31.462	37.624	29.750	33.307	30.731	28.957	36.421	35.723	28.835	29.126
MgO	1.533	2.368	2.649	4.022	1.004	3.023	3.573	1.627	3.916	4.056
CaO	7.660	1.119	8.174	3.403	7.334	8.669	1.14	3.242	6.814	6.619
MnO	1.416	0.683	0.629	0.191	2.197	0.163	0.429	1.768	0.327	0.333
Na_2O	0.047	0.021	0.025	0.004	0.000	0.014	0.034	0.007	0.059	0.072
Total	100.18	99.58	100.43	100.07	99.242	99.94	100.23	100.15	99.376	100.05
Si	5.941	5.955	5.949	5.968	5.963	5.944	5.955	5.929	5.985	5.976
Ti	0.0234	0.011	0.008	0.005	0.010	0.009	0.003	0.004	0.004	0.008
Al	3.962	4.049	4.024	4.042	4.037	4.028	4.052	4.053	4.042	4.046
Cr	0.001	0.002	0.003	0.000	4.171	0.000	0.005	0.038	0.000	0.002
Fe	4.220	5.124	3.942	4.429	4.171	3.839	4.885	4.848	3.823	3.835
Mg	0.367	0.575	0.626	0.953	0.243	0.714	0.854	0.394	0.925	0.952
Ca	1.319	0.195	1.387	0.579	1.275	1.473	0.196	0.564	1.157	1.117
Mn	0.193	0.094	0.084	0.026	0.302	0.022	0.058	0.243	0.044	0.044
Na	0.015	0.006	0.008	0.001	0.000	0.004	0.011	0.002	0.018	3.835
Total	16.048	16.012	16.033	16.006	16.006	16.035	16.019	16.04	15.998	16.002

Pinos Genil Formation Garnets sample saf 5.4

						C -	R			
SiO_2	36.961	36.705	36.757	37.384	37.849	37.113	37.207	37.155	37.067	37.090
TiO_2	0.105	0.085	0.165	0.106	0.056	0.031	0.000	0.059	0.070	0.102
Al_2O_2	21.354	21.259	21.355	21.323	21.543	21.411	21.621	21.318	21.408	21.513
Cr_2O_3	0.026	0.014	0.018	0.000	0.000	0.000	0.027	0.000	0.000	0.045
FeO	33.984	38.067	29.900	27.892	26.476	36.464	25.553	25.525	29.866	30.379
MgO	1.455	2.539	0.714	1.398	2.569	2.726	1.704	1.265	1.700	1.567
CaO	6.293	0.928	8.846	11.187	10.612	1.499	11.029	10.224	8.854	8.800
MnO	0.448	0.566	2.369	0.799	0.412	0.811	2.604	3.765	0.387	0.569
Na_2O	0.024	0.047	0.039	0.018	0.005	0.034	0.000	0.019	0.017	0.012
Total	100.64	100.21	100.16	100.11	99.524	100.09	99.74	99.329	99.368	100.08
Si	5.930	5.941	5.915	5.953	5.993	5.977	5.929	5.966	5.953	5.931
Ti	0.013	0.010	0.020	0.013	0.007	0.004	0.000	0.007	0.008	0.012
Al	4.038	4.055	4.050	4.002	4.020	4.064	4.061	4.034	4.052	4.054
Cr	0.003	0.002	0.002	0.000	0.000	0.000	0.003	0.000	0.000	0.006
Fe	4.559	5.123	4.024	3.714	3.506	4.911	3.405	3.427	4.012	4.063
Mg	0.348	0.612	0.171	0.332	0.606	0.654	0.105	0.303	0.407	0.374
Ca	1.082	0.161	1.525	1.909	1.800	0.259	1.883	1.759	1.524	1.508
Mn	0.061	0.078	0.323	0.108	0.055	0.111	0.352	0.512	0.053	0.077
Na	0.007	0.015	0.012	0.005	0.002	0.011	0.000	0.006	0.005	0.004
Total	16.041	16.027	16.044	16.036	15.99	15.99	16.038	16.013	16.014	16.028
						C -	R	C -	R	C -
SiO_2	37.090	37.214	36.999	37.122	37.191	37.062	37.443	36.547	36.953	36.860
TiO_2	0.102	0.134	0.117	0.130	0.125	0.095	0.147	0.072	0.051	0.138
Al_2O_2	21.513	21.580	21.418	21.251	21.482	21.435	21.306	21.476	21.110	21.138
Cr_2O_3	0.045	0.000	0.049	0.011	0.000	0.037	0.000	0.044	0.000	0.000
FeO	30.379	30.747	28.797	28.441	30.719	31.712	29.436	35.991	37.445	32.993
MgO	1.567	2.018	0.858	0.739	1.584	2.189	2.106	1.977	2.314	1.646
CaO	8.800	7.910	9.765	9.167	8.906	8.075	9.056	2.900	1.831	6.482
MnO	0.569	0.435	2.492	3.327	0.166	0.281	0.186	0.970	0.634	0.353
Na_2O	0.012	0.041	0.003	0.014	0.040	0.000	0.000	0.042	0.009	0.061
Total	100.08	100.08	100.49	100.20	100.21	100.89	99.68	100.02	100.65	99.67
Si	5.931	5.939	5.918	5.957	5.938	5.895	5.975	5.917	5.948	5.951
Ti	0.012	0.016	0.014	0.016	0.015	0.011	0.018	0.009	0.006	0.017
Al	4.054	4.059	4.038	4.019	4.042	4.018	4.007	4.098	4.061	4.022
Cr	0.006	0.000	0.006	0.001	0.000	0.005	0.000	0.006	0.000	0.000
Fe	4.063	4.104	3.852	3.817	4.102	4.219	3.928	4.873	5.040	4.455
Mg	0.374	0.480	0.205	0.177	0.377	0.519	0.501	0.477	0.555	0.396
Ca	1.508	1.352	1.674	1.576	1.523	1.376	1.548	0.503	0.316	1.121
Mn	0.077	0.059	0.338	0.452	0.022	0.038	0.025	0.133	0.086	0.048
Na	0.004	0.013	0.001	0.004	0.012	0.000	0.000	0.013	0.003	0.019
Total	16.028	16.022	16.046	16.019	16.032	16.082	16.003	16.029	16.016	16.030
	R	C -	R	C -	R	C -	R			
SiO_2	36.930	37.181	36.710	36.959	37.036	36.827	37.440	37.238	37.271	37.663
TiO_2	0.120	0.107	0.118	0.032	0.034	0.095	0.105	0.030	0.102	0.057
Al_2O_2	21.277	21.307	21.236	21.536	21.345	21.424	21.709	21.745	21.616	21.643
Cr_2O_3	0.044	0.041	0.019	0.022	0.015	0.000	0.000	0.033	0.000	0.019
FeO	33.227	31.208	30.702	35.630	31.072	30.272	29.193	33.306	27.685	30.645
MgO	1.698	0.985	0.935	3.833	2.412	1.476	1.499	3.883	1.181	2.938
CaO	6.119	8.993	9.067	1.576	6.908	9.059	9.280	3.627	11.633	7.126
MnO	0.353	0.690	0.627	0.036	0.750	0.669	0.507	0.439	0.939	0.460
Na_2O	0.029	0.006	0.000	0.012	0.045	0.062	0.041	0.000	0.018	0.064
Total	99.79	100.52	99.41	99.96	99.617	99.88	99.775	100.28	100.44	100.61
Si	5.952	5.948	5.934	5.929	5.944	5.911	5.971	5.924	5.920	5.955
Ti	0.015	0.013	0.014	0.004	0.004	0.011	0.013	0.004	0.0122	0.007
Al	4.042	4.017	4.046	4.072	4.038	4.053	4.081	4.073	4.046	4.033
Cr	0.006	0.005	0.002	0.003	0.002	0.000	0.000	0.004	0.000	0.002
Fe	4.478	4.175	4.150	4.781	4.170	4.064	3.894	4.431	3.677	4.052
Mg	0.408	0.235	0.225	0.917	0.577	0.353	0.357	0.921	0.279	0.692
Ca	1.057	1.541	1.570	0.271	1.188	1.558	1.586	0.618	1.980	1.207
Mn	0.048	0.093	0.086	0.049	0.102	0.091	0.068	0.059	0.126	0.062
Na	0.009	0.002	0.000	0.004	0.014	0.019	0.013	0.000	0.005	0.019
Total	16.014	16.03	16.028	16.031	16.039	16.061	15.982	16.034	16.047	16.030

Pinos Genil Formation Garnets Sample saf 5.4

SiO_2	37.237	37.302	36.828	37.478	37.514
TiO_2	0.023	0.084	0.061	0.057	0.000
Al_2O_2	21.648	21.404	21.426	21.916	21.736
Cr_2O_3	0.000	0.007	0.000	0.000	0.000
FeO	35.592	31.215	0.000	33.899	31.652
MgO	3.478	1.435	2.821	4.768	3.788
CaO	2.128	7.950	3.493	2.223	4.672
MnO	0.323	0.884	0.397	0.114	0.303
Na_2O	0.002	0.026	0.011	0.022	0.014
Total	100.43	100.30	99.36	100.48	99.67
Si	5.947	5.964	5.947	5.928	5.969
Ti	0.003	0.010	0.007	0.007	0.000
Al	4.074	4.033	4.078	4.085	4.076
Cr	0.000	0.001	0.000	0.000	0.000
Fe	4.753	4.174	4.636	4.484	4.211
Mg	0.828	0.342	0.679	1.124	0.898
Ca	0.364	1.362	0.604	0.377	0.796
Mn	0.044	0.120	0.054	0.015	0.041
Na	0.001	0.008	0.003	0.007	0.004
Total	16.014	16.013	16.009	16.026	15.996

Sample saf 6.2 Garnets

			C - R			C - R				
SiO_2	37.237	36.663	37.012	36.868	36.890	36.565	36.625	38.602	36.658	36.806
TiO_2	0.035	0.065	0.137	0.179	0.071	0.101	0.078	0.103	0.040	0.108
Al_2O_2	21.562	21.251	21.299	21.261	21.151	21.331	21.396	21.098	21.472	21.288
Cr_2O_3	0.000	0.000	0.041	0.000	0.000	0.073	0.000	0.034	0.041	0.000
FeO	29.846	28.843	29.594	28.875	30.760	35.750	34.910	28.478	33.280	29.747
MgO	4.193	2.319	1.128	1.175	0.986	1.897	2.002	0.767	1.248	1.056
CaO	5.306	8.545	10.086	10.283	8.608	3.211	4.009	10.262	7.055	8.161
MnO	1.305	0.722	0.859	0.828	1.335	0.655	0.618	1.104	0.261	2.716
Na_2O	0.007	0.050	0.008	0.044	0.021	0.019	0.012	0.025	0.000	0.000
Total	99.52	98.46	100.16	99.514	99.82	99.60	99.65	100.47	100.06	99.88
Si	5.931	5.929	5.926	5.928	5.948	5.937	5.931	6.108	5.910	5.932
Ti	0.004	0.008	0.016	0.022	0.009	0.012	0.009	0.012	0.005	0.013
Al	4.047	4.051	4.019	4.029	4.019	4.082	4.084	3.935	4.080	4.044
Cr	0.003	0.000	0.005	0.000	0.000	0.009	0.000	0.004	0.005	0.000
Fe	3.975	3.901	3.962	3.883	4.148	4.854	4.728	3.765	4.487	4.010
Mg	0.995	0.559	0.269	0.281	0.237	0.459	0.483	0.181	0.299	0.254
Ca	0.905	1.481	1.730	1.772	1.487	0.558	0.696	1.739	1.219	1.409
Mn	0.176	0.099	0.116	0.113	0.182	0.090	0.085	0.148	0.036	0.371
Na	0.002	0.016	0.002	0.014	0.007	0.006	0.004	0.008	0.000	0.000
Total	16.04	16.04	16.047	16.042	16.037	16.01	16.019	15.902	16.042	16.033

Pinos Genil Formation Garnets Sample saf 6.2

						C - R		C - R		
SiO_2	37.583	36.784	37.122	36.815	36.940	37.056	36.661	36.777	37.088	37.027
TiO_2	0.045	0.115	0.141	0.189	0.121	0.036	0.046	0.062	0.084	0.037
Al_2O_2	21.699	21.113	21.513	21.584	21.828	21.426	21.482	21.667	21.513	21.594
Cr_2O_3	0.000	0.041	0.000	0.015	0.075	0.000	0.036	0.054	0.000	0.000
FeO	29.247	33.499	26.518	29.761	31.199	35.992	35.527	36.229	30.829	32.317
MgO	3.273	1.202	1.551	1.948	1.752	3.722	3.774	3.872	2.457	1.670
CaO	7.112	5.795	11.893	8.954	7.596	1.024	1.110	0.889	6.499	5.932
MnO	0.882	1.274	0.735	0.378	0.435	0.582	0.643	0.638	0.991	1.099
Na_2O	0.022	0.000	0.000	0.010	0.048	0.010	0.034	0.033	0.058	0.076
Total	99.863	99.82	99.47	99.655	99.99	99.84	9.313	100.22	99.52	99.75
Si	5.961	5.967	5.926	5.898	5.911	5.957	5.924	5.899	5.948	5.958
Ti	0.005	0.014	0.017	0.023	0.014	0.004	0.006	0.007	0.010	0.004
Al	4.056	4.029	4.048	4.075	4.116	4.059	4.091	4.096	4.066	4.095
Cr	0.000	0.005	0.000	0.002	0.009	0.000	0.005	0.007	0.000	0.000
Fe	3.879	4.537	3.540	3.987	4.175	4.839	4.801	4.860	4.135	4.349
Mg	0.774	0.290	0.369	0.465	0.418	0.892	0.909	0.926	0.587	0.400
Ca	1.208	1.005	2.034	1.537	1.302	0.176	0.192	0.153	1.117	1.023
Mn	0.118	0.175	0.099	0.051	0.059	0.079	0.088	0.087	0.135	0.150
Na	0.007	0.000	0.000	0.003	0.015	0.003	0.011	0.010	0.018	0.024
Total	16.09	16.012	16.033	16.042	16.019	16.01	16.027	16.046	16.017	16.002

		C - R						C - R		
SiO_2	36.865	36.764	17.312	37.007	36.999	36.429	36.534	37.146	37.080	36.215
TiO_2	0.061	0.063	0.040	0.046	0.092	0.057	0.100	0.129	0.062	0.103
Al_2O_2	21.697	21.375	21.648	21.858	21.479	21.195	21.544	21.447	21.621	21.179
Cr_2O_3	0.000	0.000	0.000	0.019	0.030	0.000	0.082	0.000	0.049	0.000
FeO	31.125	30.183	29.526	29.567	26.470	33.532	32.375	29.609	30.113	37.370
MgO	2.274	1.421	2.046	3.432	2.116	1.218	1.624	3.631	3.699	1.533
CaO	7.756	7.890	9.418	6.994	9.703	5.286	6.456	6.505	6.111	2.440
MnO	0.137	1.408	0.160	0.295	3.006	1.449	1.093	1.086	1.049	0.804
Na_2O	0.000	0.077	0.033	0.022	0.014	0.049	0.028	0.012	0.033	0.007
Total	99.915	99.22	99.90	99.24	99.91	99.21	99.84	99.56	99.82	99.65
Si	5.897	5.940	5.909	5.907	5.904	5.939	5.894	5.925	5.905	5.918
Ti	0.007	0.008	0.008	0.005	0.011	0.007	0.012	0.015	0.007	0.013
Al	4.091	4.070	4.071	4.112	4.039	4.073	4.096	4.031	4.058	4.078
Cr	0.000	0.005	0.000	0.002	0.004	0.000	0.010	0.000	0.006	0.000
Fe	4.164	4.078	3.940	3.947	3.533	4.572	4.368	3.949	4.011	5.107
Mg	0.542	0.342	0.487	0.816	0.503	0.296	0.391	0.863	0.878	0.373
Ca	1.319	1.366	1.610	1.196	1.659	0.923	1.116	1.112	1.043	0.428
Mn	0.019	0.193	0.022	0.040	0.406	0.200	0.149	0.147	0.141	0.111
Na	0.000	0.024	0.001	0.007	0.004	0.015	0.009	0.004	0.010	0.002
Total	16.050	16.027	16.048	16.034	16.065	16.025	16.045	16.045	16.060	16.031

Pinos Genil Formation Garnets Sample saf 6.2

			C - R							
SiO_2	37.121	37.311	36.972	37.777	37.026	36.779	37.030	37.312	36.759	37.168
TiO_2	0.096	0.082	0.178	0.060	0.101	0.084	0.107	0.126	0.057	0.073
Al_2O_2	21.641	21.713	21.400	21.667	21.577	21.523	21.630	21.726	21.329	21.570
Cr_2O_3	0.000	0.000	0.053	0.000	0.000	0.022	0.000	0.004	0.038	0.041
FeO	30.778	29.468	24.051	28.679	31.502	31.077	30.295	28.125	30.094	30.354
MgO	2.045	2.091	1.009	3.331	1.184	1.305	1.426	3.996	1.920	1.665
CaO	7.688	9.197	10.915	8.295	8.456	8.103	9.166	6.988	8.421	7.605
MnO	0.684	0.459	4.908	0.109	0.511	0.610	0.355	0.765	0.791	1.409
Na_2O	0.021	0.041	0.005	0.026	0.022	0.023	0.023	0.015	0.067	0.035
Total	100.07	100.36	99.49	99.946	100.38	99.53	100.03	99.06	99.47	99.92
Si	5.929	5.923	5.932	5.968	5.925	5.927	5.223	5.936	5.915	5.952
Ti	0.012	0.009	0.021	0.007	0.012	0.010	0.013	0.015	0.007	0.009
Al	4.073	4.063	4.047	4.035	4.069	4.088	4.077	4.074	4.045	4.071
Cr	0.000	0.000	0.007	0.000	0.000	0.003	0.000	0.001	0.005	0.005
Fe	4.111	3.912	3.227	3.789	4.216	4.188	4.052	3.742	4.050	4.065
Mg	0.487	0.495	0.241	0.784	0.282	0.313	0.340	0.948	0.460	0.397
Ca	1.315	1.564	1.876	1.404	1.450	1.399	1.571	1.191	1.452	1.305
Mn	0.927	0.062	0.667	0.015	0.069	0.0833	0.048	0.103	0.108	0.191
Na	0.006	0.013	0.002	0.008	0.007	0.007	0.007	0.005	0.021	0.011
Total	16.026	16.042	16.021	16.01	16.031	16.02	16.03	16.014	16.063	16.006

Alhambra Formation Garnets Sample A 8.3

		C - R		C - R		C - R				
SiO_2	39.338	38.789	38.259	38.286	38.052	37.896	38.062	38.036	38.603	38.619
TiO_2	0.043	0.078	0.040	0.061	0.085	0.073	0.034	0.052	0.120	0.129
Al_2O_2	22.324	21.520	21.514	21.552	21.404	21.412	21.276	21.418	21.353	21.569
Cr_2O_3	0.000	0.004	0.012	0.004	0.043	0.000	0.013	0.000	0.000	0.016
FeO	24.257	27.244	30.511	29.798	28.597	29.108	24.305	28.233	22.687	27.487
MnO	0.889	1.532	0.389	0.862	0.468	1.037	1.635	0.454	4.428	0.664
MgO	6.727	1.1.9	2.087	1.897	1.784	2.295	2.741	2.756	1.477	3.318
CaO	7.514	11.252	8.093	8.448	9.969	8.777	10.674	9.269	12.091	9.295
Total	101.09	101.53	100.91	100.91	100.40	100.60	98.74	100.22	100.76	101.10
Si	6.001	6.063	6.030	6.033	6.017	5.991	6.047	6.003	6.054	6.017
Ti	0.005	0.009	0.005	0.007	0.010	0.009	0.004	0.006	0.014	0.015
Al	4.015	3.965	3.998	4.004	3.990	3.991	3.985	3.985	3.948	3.962
Cr	0.000	0.000	0.002	0.001	0.005	0.000	0.002	0.000	0.000	0.002
Fe	3.094	3.561	4.022	3.927	3.782	3.848	3.230	3.727	2.976	3.581
Mn	0.115	0.203	0.052	0.115	0.063	0.139	0.220	0.061	0.588	0.088
Mg	1.529	0.258	0.490	0.445	0.420	0.541	0.649	0.648	0.345	0.770
Ca	1.228	1.884	1.367	1.426	1.689	1.487	1.817	1.568	2.032	1.552
Total	15.987	15.945	15.965	15.958	15.975	16.005	15.955	15.998	15.957	15.986

Alhambra Formation Garnets **Sample A8.3**

SiO_2	38.377	38.486	36.529	37.553	36.869	37.101	36.828	36.557	36.764	37.967
TiO_2	0.073	0.023	0.794	0.056	0.072	0.090	0.120	0.118	0.063	0.131
Al_2O_2	21.386	21.613	20.869	21.412	20.766	21.119	20.847	21.031	21.006	21.503
Cr_2O_3	0.011	0.009	0.000	0.001	0.021	0.006	0.000	0.002	0.007	0.002
FeO	30.254	34.340	33.909	26.282	30.139	26.669	27.445	27.256	35.525	28.108
MnO	1.259	0.399	0.915	2.079	3.681	0.444	1.624	1.632	2.025	1.202
MgO	1.078	4.232	2.438	2.912	2.220	1.303	1.241	1.184	1.510	1.539
CaO	8.986	2.412	3.965	9.879	5.573	12.271	10.824	11.049	2.805	10.578
Total	101.42	101.51	99.42	100.17	99.34	99.00	98.93	98.83	99.71	101.03
Si	6.048	6.030	5.917	5.94	5.971	5.957	5.953	5.917	5.983	5.982
Ti	0.009	0.003	0.097	0.007	0.009	0.011	0.015	0.014	0.008	0.016
Al	3.973	3.992	3.985	3.993	3.965	3.998	3.973	4.013	4.030	3.994
Cr	0.001	0.001	0.000	0.000	0.003	0.001	0.000	0.000	0.001	0.000
Fe	3.987	4.499	4.593	3.477	4.082	3.581	3.710	3.690	4.835	3.704
Mn	0.168	0.053	0.125	0.279	0.505	0.060	0.222	0.224	0.279	0.160
Mg	0.253	0.988	0.589	0.687	0.536	0.312	0.299	0.286	0.366	0.361
Ca	1.517	0.405	0.688	1.674	0.967	2.111	1.875	1.917	0.489	1.786
Total	15.956	15.971	15.994	16.056	16.036	16.032	16.046	16.061	15.993	16.004
SiO_2	38.106	37.349	39.890	37.061	37.613	38.069	37.946	37.296	38.282	37.053
TiO_2	0.035	0.154	0.043	0.060	0.168	0.077	0.080	0.085	0.043	0.084
Al_2O_2	21.275	21.093	22.274	21.347	21.558	21.663	21.582	21.377	21.596	21.175
Cr_2O_3	0.005	0.000	0.000	0.034	0.000	0.003	0.000	0.000	0.000	0.014
FeO	23.862	30.093	19.880	31.017	32.673	29.868	25.315	31.178	25.628	30.710
MnO	5.923	0.989	0.482	0.370	0.629	0.159	0.532	1.064	0.432	0.479
MgO	2.092	00.935	11.573	3.023	4.500	2.919	3.586	2.089	6.521	1.388
CaO	9.490	9.466	5.927	6.585	3.335	8.197	10.758	7.161	6.961	8.905
Total	100.79	100.12	100.07	99.90	100.48	100.96	99.79	100.25	99.46	99.71
Si	6.011	5.986	5.988	5.937	5.949	5.979	5.965	5.956	5.974	5.960
Ti	0.004	0.019	0.005	0.007	0.020	0.009	0.009	0.010	0.005	0.010
Al	3.956	3.985	3.942	4.031	4.020	4.011	4.000	4.025	3.973	3.996
Cr	0.001	0.000	0.000	0.004	0.000	0.000	0.000	0.000	0.000	0.002
Fe	3.148	4.053	2.496	4.155	4.322	3.923	3.328	4.164	3.345	4.131
Mn	0.791	0.134	0.061	0.050	0.084	0.021	0.071	0.144	0.057	0.065
Mg	0.492	0.199	2.589	0.722	1.061	0.683	0.840	0.497	1.517	0.333
Ca	1.604	1.626	0.953	1.130	0.565	1.379	1.812	1.225	1.164	1.535
Total	16.006	16.002	16.035	16.038	16.021	16.006	16.025	16.021	16.034	16.031
SiO_2	37.315	37.016	38.864	36.889	37.639	36.955	38.096	38.117	37.982	37.854
TiO_2	0.042	0.037	0.045	0.038	0.082	0.070	0.109	0.061	0.016	0.033
Al_2O_2	21.338	21.176	21.693	20.721	21.217	20.841	21.213	21.276	21.471	21.749
Cr_2O_3	0.000	0.000	0.000	0.015	0.005	0.000	0.001	0.000	0.000	0.003
FeO	34.726	37.616	24.205	36.298	30.314	31.876	25.716	28.519	30.487	30.594
MnO	0.273	0.244	1.473	0.515	0.409	1.111	1.197	0.517	0.714	0.265
MgO	4.266	3.347	4.447	3.470	2.386	1.528	4.907	3.175	4.171	2.576
CaO	1.919	0.081	9.826	1.591	8.257	7.273	8.243	8.788	5.464	7.803
Total	99.88	100.25	100.55	99.54	100.31	99.65	99.48	100.45	100.30	100.88
Si	5.966	5.960	6.025	5.975	5.981	5.971	5.994	6.003	5.992	5.968
Ti	0.005	0.004	0.005	0.005	0.010	0.008	0.013	0.007	0.002	0.004
Al	4.022	4.020	3.965	3.957	3.975	3.970	3.935	3.950	3.993	4.042
Cr	0.000	0.000	0.000	0.002	0.001	0.000	0.000	0.000	0.000	0.000
Fe	4.643	5.065	3.138	4.917	4.029	4.307	3.384	3.756	4.022	4.034
Mn	0.037	0.033	0.193	0.071	0.055	0.152	0.160	0.069	0.095	0.035
Mg	1.016	0.803	1.027	0.838	0.565	0.368	1.151	0.745	0.981	0.605
Ca	0.329	0.139	1.632	0.276	1.406	1.259	1.390	1.483	0.924	1.318
Total	16.018	16.025	15.987	16.04	16.021	16.035	16.025	16.014	16.009	16.007

Alhambra Formation Garnets **Sample A8.3**

SiO_2	38.135	37.464	37.489	42.258	37.391	37.554	37.479	37.027	37.552	38.812
TiO_2	0.129	0.121	0.049	0.079	0.081	0.009	0.069	0.131	0.062	0.024
Al_2O_2	21.542	21.301	21.361	20.396	21.066	21.347	21.223	20.699	20.974	21.642
Cr_2O_3	0.000	0.000	0.000	0.000	0.000	0.000	0.004	0.000	0.000	0.000
FeO	24.427	30.697	28.667	26.512	29.385	27.429	29.916	27.948	30.928	25.491
MnO	0.865	0.297	0.426	0.779	0.446	1.452	0.576	3.869	0.265	0.437
MgO	4.519	1.281	2.916	2.623	3.212	2.282	2.037	0.747	3.385	6.649
CaO	10.084	9.169	9.097	9.076	7.733	98.747	8.292	9.259	6.556	7.035
Total	99.70	100.33	100.00	101.72	99.31	99.82	99.59	99.68	99.72	100.09
Si	5.972	5.977	5.948	6.453	5.975	5.973	5.996	5.982	5.990	6.007
Ti	0.015	0.015	0.006	0.009	0.010	0.001	0.008	0.016	0.007	0.003
Al	3.977	4.006	3.996	3.672	3.969	4.003	4.003	3.943	3.944	3.949
Cr	0.000	0.000	0.000	0.000	0.000	0.000	0.000	0.000	0.000	0.000
Fe	3.199	4.095	3.804	3.386	3.9237	3.649	4.002	3.776	4.126	3.299
Mn	0.115	0.040	0.057	0.101	0.060	0.196	0.078	0.530	0.036	0.057
Mg	1.055	0.305	0.689	0.597	0.765	0.541	0.486	0.180	0.805	1.534
Ca	1.692	1.567	1.547	1.485	1.324	1.661	1.421	1.603	1.121	1.167
Total	16.024	16.005	16.047	15.702	16.03	16.024	15.994	16.030	16.030	16.016

SiO_2	37.652	37.303	37.031	37.616	38.022
TiO_2	0.064	0.048	0.115	0.066	0.054
Al_2O_2	21.576	21.161	21.116	21.271	21.565
Cr_2O_3	0.000	0.008	0.000	0.000	0.000
FeO	19.015	30.299	26.309	31.172	23.725
MnO	8.068	0.307	0.841	0.335	0.997
MgO	1.574	1.683	1.609	1.738	5.971
CaO	12.035	8.988	12.318	7.904	8.653
Total	99.98	99.79	100.01	100.10	98.99
Si	5.963	5.974	5.983	6.004	5.96.
Ti	0.008	0.006	0.014	0.008	0.006
Al	4.029	3.996	3.950	4.003	3.985
Cr	0.000	0.001	0.000	0.000	0.000
Fe	2.519	4.058	3.492	4.161	3.110
Mn	1.082	0.042	0.113	0.045	0.132
Mg	0.0372	0.402	0.381	0.413	1.395
Ca	2.042	1.542	2.094	1.352	1.453
Total	16.014	16.021	16.027	15.986	16.041

Detrital Epidotes Calculated on the basis of 13 oxygens

Quentar Formation Epidotes **Sample CA 1.1**

SiO_2	37.614	37.799	37.682	38.474	37.890	37.777	37.196	37.814	37.996	37.613
TiO_2	0.056	0.093	0.046	0.104	0.163	0.093	0.089	0.038	0.068	0.093
Al_2O_2	23.863	24.792	24.280	27.455	27.176	25.122	24.428	31.912	25.665	25.935
FeO	11.085	10.141	11.602	6.819	7.253	9.852	10.839	1.263	9.039	9.029
MnO	0.146	0.114	0.285	0.026	0.065	0.072	0.110	0.000	0.090	0.170
MgO	0.031	0.092	0.068	0.041	0.076	0.067	0.045	0.855	0.056	0.069
CaO	23.302	23.173	22.967	23.815	23.679	23.099	23.179	21.811	23.557	23.531
NaO	0.002	0.003	0.005	0.000	0.005	0.019	0.015	0.142	0.012	0.008
Total	96.09	96.21	96.93	96.734	96.31	96.10	95.90	93.83	96.48	96.45
Si	3.219	3.209	3.201	3.187	3.164	3.204	3.185	3.112	3.198	3.170
Ti	0.004	0.006	0.003	0.006	0.010	0.006	0.006	0.002	0.004	0.006
Al	2.407	2.481	2.432	2.681	2.675	2.512	2.466	3.096	2.547	2.577
Fe	0.793	0.720	0.824	0.472	0.507	0.699	0.776	0.087	0.636	0.636
Mn	0.011	0.008	0.020	0.002	0.005	0.005	0.008	0.000	0.006	0.012
Mg	0.004	0.012	0.009	0.005	0.009	0.008	0.006	0.105	0.007	0.009
Ca	2.137	2.108	2.091	2.113	2.118	2.099	2.127	1.923	2.124	2.125
NaO	0.000	0.000	0.001	0.000	0.001	0.003	0.002	0.023	0.002	0.001
Total	8.574	8.544	8.580	8.466	8.489	8.536	8.577	8.349	8.525	8.536
SiO_2	37.949	37.388	37.055	37.205	37.431	36.696	37.120	39.216	36.958	
TiO_2	0.033	0.083	0.095	0.257	0.136	0.115	0.017	0.026	0.014	
Al_2O_2	27.418	27.138	24.659	26.978	25.691	22.817	24.905	33.443	24.973	
FeO	7.342	7.635	10.932	7.282	9.563	12.886	10.477	0.727	10.227	
MnO	0.208	0.033	0.090	0.148	0.161	0.493	0.132	0.000	0.449	
MgO	0.047	0.039	0.013	0.196	0.058	0.031	0.023	0.015	0.044	
CaO	23.733	23.615	23.335	23.374	23.340	22.862	23.305	24.417	22.798	
NaO	0.004	0.001	0.009	0.026	0.012	0.013	0.018	0.012	0.000	
Total	96.73	95.93	96.19	95.46	96.39	95.91	95.99	97.86	95.46	
Si	3.157	3.142	3.167	3.139	3.165	3.187	3.170	3.101	3.171	
Ti	0.002	0.005	0.006	0.016	0.009	0.008	0.001	0.002	0.001	
Al	2.689	2.689	2.485	2.6833	2.561	2.336	2.508	3.117	2.526	
Fe	0.511	0.537	0.781	0.514	0.676	0.936	0.748	0.048	0.734	
Mn	0.015	0.002	0.007	0.011	0.012	0.036	0.010	0.000	0.033	
Mg	0.006	0.005	0.002	0.025	0.007	0.004	0.003	0.002	0.006	
Ca	2.116	2.127	2.137	2.113	2.115	2.128	2.133	2.069	2.096	
NaO	0.001	0.000	0.001	0.004	0.002	0.002	0.003	0.002	0.000	
Total	8.496	8.508	8.585	8.505	8.547	8.638	8.576	8.340	8.565	

Dudar Formation Epidotes **Sample S13**

SiO_2	37.875	37.752	37.849	37.854	37.829	37.411	37.365	37.089	37.203	37.636
TiO_2	0.116	0.100	0.077	0.117	0.088	0.043	0.052	0.048	0.139	0.118
Al_2O_2	26.508	23.882	26.051	24.808	26.175	24.772	25.158	23.428	23.788	26.021
Cr_2O_3	0.081	0.116	0.227	0.028	0.032	0.0722	0.020	0.000	0.000	0.020
MgO	0.000	0.000	0.000	0.000	0.000	0.000	0.000	0.0000	0.000	0.0000
CaO	23.628	23.430	23.997	23.805	24.102	23.357	23.303	23.103	23.326	24.247
MnO	0.073	0.141	0.191	0.024	0.173	0.028	0.253	0.338	0.142	0.125
FeO	8.792	11.420	8.148	10.407	8.556	11.082	10.249	12.202	11.549	8.483
NiO	0.088	0.000	0.029	0.000	0.000	0.000	0.040	0.007	0.051	0.000
Na_2O	0.023	0.014	0.021	0.023	0.015	0.006	0.000	0.000	0.024	0.000
K_2O	0.018	0.000	0.006	0.000	0.000	0.003	1.836	0.013	0.000	0.000
Total	97.202	96.857	96.600	97.067	96.972	96.774	96.449	96.229	96.225	96.652
Si	6.081	6.177	6.109	6.144	6.092	6.109	6.101	6.144	6.139	6.084
Ti	0.014	0.012	0.009	0.014	0.011	0.005	0.006	0.006	0.0173	0.014
Al	5.016	4.605	4.956	4.746	4.968	4.768	0.842	4.574	4.626	4.957
Cr	0.010	0.015	0.029	0.004	0.004	0.009	0.003	0.000	0.000	0.003
Mg	0.000	0.000	0.000	0.000	0.000	0.000	0.000	0.000	0.000	0.000
Ca	4.064	4.107	4.150	4.139	4.159	4.087	4.077	4.100	4.124	4.199
Mn	0.009	0.019	0.026	0.003	0.0237	0.004	0.035	0.047	0.019	0.017
Fe	1.180	1.563	1.100	1.413	1.152	1.513	1.399	1.690	1.594	1.147
Ni	0.011	0.000	0.004	0.000	0.000	0.000	0.005	0.001	0.007	0.000
Na	0.007	0.004	0.006	0.007	0.005	0.002	0.000	0.000	0.008	0.000
K	0.004	0.000	0.001	0.000	0.000	0.001	0.002	0.003	0.000	0.000
Total	16.397	16.503	16.392	16.471	16.414	16.498	16.471	16.565	16.535	16.422
SiO_2	39.038	37.143	38.933	37.934	37.663	38.830	38.896	37.486	37.690	37.818
TiO_2	0.102	0.071	0.192	0.197	0.121	0.069	0.049	0.133	0.071	0.248
Al_2O_2	31.902	23.965	32.161	26.586	25.545	31.419	32.175	25.449	25.339	25.429
Cr_2O_3	0.000	0.000	0.016	0.000	0.008	0.037	0.000	0.065	0.004	0.032
MgO	0.000	0.000	0.000	0.000	0.000	0.000	0.000	0.000	0.000	0.000
CaO	24.466	22.826	24.572	23.787	23.417	24.405	24.755	23.359	23.081	23.243
MnO	0.000	0.228	0.028	0.014	0.201	0.053	0.000	0.253	0.762	0.253
FeO	1.635	11.479	1.403	8.162	9.442	2.242	1.299	9.359	10.273	9.871
NiO	0.029	0.000	0.048	0.000	0.022	0.067	0.056	0.000	0.000	0.000
Na_2O	0.005	0.008	0.006	0.006	0.007	0.020	0.045	0.000	0.000	0.012
K_2O	0.000	0.000	0.010	0.000	0.003	0.000	1.948	0.019	0.000	0.010
Total	97.177	95.721	97.369	96.700	96.429	97.142	97.274	96.124	96.534	96.915
Si	6.016	6.149	5.986	6.099	6.119	6.011	5.986	6.112	6.132	6.124
Ti	0.012	0.009	0.022	0.024	0.015	0.008	0.006	0.016	0.009	0.030
Al	5.794	4.676	5.828	5.038	4.892	5.732	5.836	4.891	4.858	4.853
Cr	0.000	0.000	0.002	0.000	0.001	0.004	0.000	0.008	0.000	0.004
Mg	0.000	0.000	0.000	0.000	0.000	0.000	0.000	0.000	0.000	0.000
Ca	4.039	4.049	4.048	4.098	4.077	4.048	4.082	4.081	4.023	4.032
Mn	0.000	0.032	0.004	0.002	0.027	0.007	0.000	0.035	0.010	0.035
Fe	0.211	1.589	0.180	1.097	1.283	0.290	0.167	1.276	1.398	1.337
Ni	0.004	0.000	0.006	0.000	0.003	0.008	0.007	0.000	0.000	0.000
Na	0.001	0.003	0.002	0.002	0.002	0.006	0.013	0.000	0.000	0.004
K	0.000	0.000	0.002	0.000	0.001	0.000	0.000	0.004	0.000	0.002
Total	16.076	16.506	16.079	16.359	16.420	16.115	16.097	16.424	16.430	16.420

Dudar Formation Detrital Epidotes Sample S13

SiO_2	37.635	37.272	37.770	37.609	37.751	37.387	38.281	37.572	38.528	38.115
TiO_2	0.070	0.038	0.164	0.138	0.081	0.096	0.121	0.105	0.196	0.020
Al_2O_2	25.308	21.973	25.313	24.713	26.253	24.146	27.562	25.346	29.594	30.971
Cr_2O_3	0.000	0.000	0.044	0.056	0.004	0.000	0.049	0.000	0.008	0.000
MgO	0.000	0.000	0.000	0.000	0.000	0.000	0.006	0.000	0.047	0.000
CaO	23.781	23.604	22.911	22.843	23.251	23.599	23.872	23.543	24.234	24.851
MnO	0.000	0.354	0.000	0.225	0.076	0.121	0.073	0.166	0.066	0.010
FeO	10.114	13.727	10.476	11.024	8.912	11.109	6.890	10.051	4.240	2.607
NiO	0.000	0.000	0.000	0.000	0.000	0.033	0.000	0.055	0.000	0.000
Na_2O	0.000	0.002	0.000	0.010	0.033	0.000	0.008	0.014	0.008	0.013
K_2O	0.000	0.009	0.000	0.026	0.000	0.009	0.003	0.000	0.027	0.000
Total	96.909	96.980	96.68	96.64	96.36	96.50	96.86	96.85	96.95	96.59
Si	6.107	6.190	6.136	6.142	6.108	6.136	6.098	6.102	6.045	5.961
Ti	0.008	0.005	0.020	0.017	0.009	0.012	0.014	0.013	0.023	0.002
Al	4.840	4.301	4.846	4.756	5.007	4.671	5.174	4.851	5.472	5.709
Cr	0.000	0.000	0.006	0.007	0.000	0.000	0.006	0.000	0.001	0.000
Mg	0.000	0.000	0.000	0.000	0.000	0.000	0.001	0.000	0.011	0.000
Ca	4.135	4.200	3.988	3.997	4.031	4.150	4.074	4.096	4.074	4.164
Mn	0.000	0.050	0.000	0.031	0.010	0.017	0.010	0.023	0.009	0.001
Fe	1.373	1.907	1.423	1.505	1.206	1.525	0.918	1.365	0.556	0.341
Ni	0.000	0.000	0.000	0.000	0.000	0.004	0.000	0.007	0.000	0.000
Na	0.000	0.001	0.000	0.003	0.010	0.000	0.002	0.004	0.002	0.040
K	0.000	0.002	0.000	0.005	0.000	0.002	0.001	0.000	0.005	0.000
Total	16.464	16.656	16.418	16.464	16.383	16.517	16.299	16.462	16.199	16.184

SiO_2	37.707	37.986	37.753	37.686	37.704	37.239	37.672	37.664
TiO_2	0.055	0.062	0.063	0.077	0.176	0.111	0.081	0.062
Al_2O_2	25.945	28.881	25.562	26.339	26.613	24.576	25.825	23.975
Cr_2O_3	0.081	0.012	0.036	0.032	0.008	0.012	0.069	0.040
MgO	0.000	0.000	0.000	0.000	0.000	0.001	0.000	0.000
CaO	23.719	24.151	23.279	23.574	23.619	22.710	23.711	23.198
MnO	0.159	0.146	0.062	0.121	0.098	0.189	0.069	0.446
FeO	8.920	5.665	9.528	8.829	8.839	11.657	9.350	11.193
NiO	0.000	0.000	0.018	0.066	0.099	0.000	0.022	0.000
Na_2O	0.021	0.001	0.000	0.000	0.026	0.013	0.004	0.002
K_2O	0.008	0.000	0.003	0.000	0.021	0.022	0.000	0.000
Total	96.61	96.90	96.30	96.73	99.05	96.53	96.80	96.58
Si	6.102	6.015	6.136	6.083	6.057	6.109	6.096	6.177
Ti	0.007	0.007	0.008	0.009	0.021	0.014	0.010	0.008
Al	4.948	5.390	4.897	5.010	5.039	4.752	4.925	4.634
Cr	0.010	0.001	0.005	0.004	0.001	0.002	0.009	0.005
Mg	0.000	0.000	0.000	0.000	0.000	0.000	0.000	0.000
Ca	4.112	4.098	4.054	4.077	4.065	3.992	4.111	4.076
Mn	0.022	0.019	0.009	0.017	0.011	0.026	0.009	0.062
Fe	1.207	0.750	1.295	1.192	1.187	1.599	1.265	1.535
Ni	0.000	0.000	0.002	0.009	0.013	0.000	0.003	0.000
Na	0.007	0.003	0.000	0.000	0.008	0.004	0.013	0.006
K	0.002	0.000	0.007	0.000	0.004	0.005	0.000	0.000
Total	16.416	16.282	16.406	16.400	16.408	16.504	16.428	16.497

Pinos Genil Formation Detrital Epidotes Sample saf 5.4

SiO_2	37.733	37.362	37.953	37.852	37.498	37.935	37.661	38.026	37.843	38.070
TiO_2	0.151	0.060	0.111	0.079	0.125	0.114	0.163	0.141	0.119	0.176
Al_2O_2	26.145	24.380	26.468	26.604	25.100	26.362	25.990	26.001	25.834	26.239
Cr_2O_3	0.061	0.000	0.008	0.085	0.040	0.000	0.012	0.044	0.000	0.000
MgO	0.000	0.000	0.000	0.000	0.000	0.000	0.000	0.000	0.000	0.006
CaO	23.353	23.618	23.782	23.791	23.523	23.907	23.610	23.380	23.364	23.274
MnO	0.174	0.173	0.129	0.205	0.097	0.104	0.696	0.201	0.136	0.146
FeO	8.905	11.150	8.332	8.173	10.118	8.146	8.873	9.168	8.929	8.596
NiO	0.000	0.000	0.000	0.000	0.000	0.018	0.000	0.037	0.000	0.044
Na_2O	0.007	0.001	0.000	0.009	0.016	0.004	0.000	0.000	0.090	0.001
K_2O	0.006	0.000	0.026	0.000	0.000	0.006	0.010	0.000	0.021	0.000
Total	96.54	96.74	96.81	96.79	96.52	96.60	96.39	96.99	96.25	96.55
Si	6.101	6.117	6.104	6.087	6.112	6.111	6.101	6.125	6.136	6.137
Ti	0.018	0.007	0.013	0.009	0.015	0.014	0.020	0.017	0.014	0.021
Al	4.982	4.704	5.017	5.042	4.822	5.005	4.963	4.936	4.937	4.985
Cr	0.008	0.000	0.001	0.011	0.005	0.000	0.002	0.006	0.000	0.000
Mg	0.000	0.000	0.000	0.000	0.000	0.000	0.000	0.000	0.000	0.001
Ca	4.046	4.143	4.098	4.099	4.108	4.126	4.098	4.035	4.059	4.020
Mn	0.024	0.024	0.017	0.028	0.013	0.014	0.009	0.027	0.019	0.020
Fe	1.204	1.527	1.121	1.099	1.379	1.097	1.202	1.235	1.211	1.159
Ni	0.000	0.000	0.000	0.000	0.000	0.002	0.000	0.005	0.000	0.006
Na	0.002	0.000	0.000	0.003	0.005	0.001	0.000	0.000	0.003	0.000
K	0.001	0.000	0.005	0.000	0.000	0.001	0.020	0.000	0.004	0.000
Total	16.387	16.523	16.376	16.378	16.461	16.373	16.398	16.387	16.384	16.349
SiO_2	38.097	37.738	37.797	37.069	37.611	38.155	37.765	37.486	37.655	37.195
TiO_2	0.116	0.116	0.095	0.078	0.064	0.152	0.070	0.122	0.239	0.080
Al_2O_2	27.555	26.735	25.642	23.700	25.027	26.719	24.910	25.193	25.229	23.478
Cr_2O_3	0.183	0.126	0.000	0.008	0.000	0.036	0.004	0.040	0.101	0.000
MgO	0.000	0.000	0.000	0.000	0.000	0.000	0.000	0.000	0.000	0.000
CaO	23.760	23.772	23.434	22.548	23.641	23.582	23.365	23.336	23.574	23.362
MnO	0.056	0.150	0.066	0.219	0.191	0.000	0.052	0.083	0.240	0.187
FeO	6.661	7.904	9.758	10.931	10.514	8.332	10.431	10.611	9.473	11.659
NiO	0.000	0.000	0.048	0.000	0.048	0.018	0.000	0.041	0.026	0.055
Na_2O	0.000	0.004	0.000	0.000	0.005	0.005	0.006	0.021	0.006	0.009
K_2O	0.011	0.016	0.003	0.000	0.004	0.015	0.000	0.006	0.000	0.004
Total	96.44	96.53	96.84	96.55	97.10	97.02	96.64	96.941	96.54	96.03
Si	6.090	6.076	6.119	6.193	6.110	6.111	6.149	6.095	6.121	6.158
Ti	0.014	0.014	0.011	0.009	0.008	0.018	0.009	0.015	0.029	0.010
Al	5.192	5.073	4.892	4.666	4.792	5.044	4.781	4.828	4.833	4.581
Cr	0.023	0.016	0.000	0.001	0.000	0.005	0.006	0.005	0.013	0.000
Mg	0.000	0.000	0.000	0.000	0.000	0.000	0.000	0.000	0.000	0.000
Ca	4.070	4.100	4.064	4.036	4.115	4.047	4.076	4.066	4.106	4.144
Mn	0.008	0.020	0.009	0.031	0.026	0.000	0.007	0.011	0.033	0.026
Fe	0.890	1.064	1.321	1.527	1.428	1.116	1.420	1.443	1.288	1.614
Ni	0.000	0.000	0.006	0.000	0.006	0.002	0.000	0.005	0.003	0.007
Na	0.000	0.001	0.000	0.000	0.002	0.001	0.002	0.007	0.002	0.003
K	0.002	0.003	0.001	0.000	0.001	0.003	0.000	0.001	0.000	0.001
Total	16.289	16.368	16.424	16.464	16.488	16.348	16.450	16.477	16.428	16.544

Pinos Genil Formation Detrital Epidotes **Sample saf 5.4**

SiO_2	37.356	37.518	38.072	37.392	37.621
TiO_2	0.044	0.066	0.158	0.151	0.165
Al_2O_2	23.875	26.390	27.445	24.857	24.090
Cr_2O_3	0.722	0.053	0.037	0.093	0.000
MgO	0.000	0.000	0.000	0.000	0.000
CaO	22.508	23.764	24.156	23.316	23.181
MnO	0.439	0.108	0.017	0.101	0.228
FeO	11.848	8.840	7.097	9.957	11.532
NiO	0.099	0.000	0.037	0.140	0.011
Na_2O	0.020	0.021	0.000	0.001	0.000
K_2O	0.001	0.000	0.008	0.003	0.006
Total	96.26	96.76	97.02	96.01	96.83
Si	6.162	6.058	6.070	6.137	6.157
Ti	0.005	0.008	0.019	0.019	0.020
Al	4.641	5.022	5.157	4.800	4.646
Cr	0.009	0.007	0.005	0.012	0.000
Mg	0.000	0.000	0.000	0.000	0.000
Ca	3.978	4.111	4.125	4.093	4.065
Mn	0.061	0.015	0.002	0.014	0.032
Fe	1.634	1.194	0.946	1.364	1.578
Ni	0.013	0.000	0.005	0.018	0.001
Na	0.006	0.006	0.000	0.000	0.000
K	0.000	0.000	0.002	0.001	0.001
Total	16.511	16.422	16.331	16.449	16.500

Alhambra Formation Detrital Epidotes **Sample A8.3**

SiO_2	37.488	37.535	37.277	37.988	37.413	37.782	37.147	37.819	37.022	37.180
TiO_2	0.101	0.126	0.115	0.125	0.073	0.122	0.101	0.126	0.072	0.180
Al_2O_2	24.855	23.578	23.378	27.489	24.199	26.073	27.223	26.392	23.261	26.999
Cr_2O_3	0.000	0.064	0.000	0.176	0.016	0.109	0.132	0.0936	0.105	0.074
MgO	0.000	0.000	0.000	0.000	0.000	0.000	0.000	0.000	0.000	0.000
CaO	23.050	23.458	23.510	24.244	23.654	23.661	22.936	24.009	23.145	23.195
MnO	0.186	0.114	0.073	0.157	0.101	0.049	0.165	0.139	0.177	0.067
FeO	11.012	10.942	10.972	5.715	10.077	8.075	5.039	7.218	10.886	4.929
NiO	0.018	0.052	0.000	0.004	0.000	0.044	0.060	0.029	0.000	0.000
Na_2O	0.010	0.008	0.000	0.017	0.018	0.025	0.009	0.012	0.009	0.015
K_2O	0.000	0.007	0.000	0.003	0.009	0.002	0.005	0.003	0.000	0.001
Total	96.72	95.88	95.32	95.92	95.56	95.94	92.82	95.84	94.68	92.64
Si	6.119	6.196	6.193	6.093	6.169	6.126	6.121	6.119	6.193	6.135
Ti	0.012	0.016	0.014	0.015	0.009	0.015	0.012	0.015	0.009	0.022
Al	4.782	4.587	4.577	5.196	4.703	4.983	5.287	5.033	4.586	5.251
Cr	0.000	0.008	0.000	0.022	0.002	0.014	0.017	0.012	0.014	0.097
Mg	0.000	0.000	0.000	0.000	0.000	0.000	0.000	0.000	0.000	0.000
Ca	4.031	4.149	4.185	4.166	4.179	4.111	4.049	4.162	4.148	4.101
Mn	0.026	0.016	0.010	0.021	0.014	0.007	0.023	0.019	0.025	0.009
Fe	1.503	1.510	1.524	0.767	1.390	1.095	0.694	0.977	1.523	0.680
Ni	0.002	0.007	0.000	0.000	0.000	0.006	0.008	0.004	0.000	0.000
Na	0.003	0.003	0.000	0.005	0.006	0.008	0.003	0.004	0.003	0.005
K	0.000	0.001	0.000	0.000	0.002	0.000	0.001	0.001	0.000	0.000
Total	16.479	16.493	16.504	16.286	16.473	16.364	16.216	16.345	16.500	16.214

Alhambra Formation Detrital Epidotes Sample A8.3

SiO_2	37.131	37.331	38.030	37.343	36.662	37.086	37.855	37.673	37.044	36.464
TiO_2	0.249	0.074	0.121	0.107	0.058	0.036	0.109	0.120	0.114	0.107
Al_2O_2	22.010	25.756	27.714	23.453	23.974	23.554	27.048	25.753	23.365	20.773
Cr_2O_3	0.024	0.000	0.000	0.000	0.069	0.044	0.020	0.008	0.000	0.000
MgO	0.000	0.000	0.000	0.000	0.001	0.000	0.000	0.000	0.000	0.874
CaO	23.314	23.259	23.834	23.086	22.542	23.298	23.528	23.684	22.520	5.342
MnO	0.407	0.243	0.146	0.305	0.035	0.262	0.247	0.079	0.094	3.943
FeO	13.359	9.920	7.164	11.66	10.815	12.495	7.751	9.274	11.910	31.734
NiO	0.059	0.026	0.000	0.011	0.056	0.000	0.007	0.000	0.000	0.000
Na_2O	0.000	0.009	0.022	0.000	0.000	0.000	0.017	0.000	0.031	0.049
K_2O	0.000	0.008	0.018	0.020	0.002	0.014	0.011	0.000	0.007	0.017
Total	96.55	96.62	97.05	95.98	94.21	96.79	96.59	96.59	95.06	99.30
Si	6.184	6.070	6.059	6.179	6.145	6.117	6.080	6.105	6.185	6.211
Ti	0.031	0.009	0.014	0.013	0.007	0.004	0.013	0.015	0.014	0.014
Al	4.320	4.934	5.204	4.574	4.736	4.579	5.120	4.919	4.597	4.170
Cr	0.003	0.000	0.000	0.000	0.009	0.006	0.003	0.001	0.000	0.000
Mg	0.000	0.000	0.000	0.000	0.000	0.000	0.000	0.000	0.000	0.222
Ca	4.159	4.052	4.068	4.093	4.048	4.117	4.049	4.112	4.028	0.975
Mn	0.057	0.033	0.020	0.043	0.005	0.037	0.034	0.011	0.013	0.569
Fe	1.860	1.349	0.955	1.614	1.516	1.724	1.041	1.257	1.663	4.520
Ni	0.008	0.003	0.000	0.001	0.007	0.000	0.001	0.000	0.000	0.000
Na	0.000	0.003	0.007	0.000	0.000	0.000	0.005	0.000	0.001	0.016
K	0.000	0.002	0.004	0.004	0.000	0.000	0.002	0.000	0.001	0.004
Total	16.624	16.456	16.330	16.522	16.475	16.587	16.349	16.42	16.503	16.700
SiO_2	38.660	43.148	37.123	37.516	37.336	37.769	37.369	37.744	37.686	38.889
TiO_2	0.035	0.328	0.077	0.063	0.069	0.099	0.071	0.193	0.160	0.039
Al_2O_2	31.644	13.531	24.387	24.200	25.052	26.374	25.225	26.577	26.917	31.720
Cr_2O_3	0.008	0.035	0.008	0.000	0.028	0.073	0.024	0.057	0.000	0.082
MgO	0.000	8.933	0.000	0.000	0.000	0.000	0.000	0.000	0.000	0.000
CaO	24.722	7.828	23.043	23.375	23.552	24.133	23.379	23.618	23.696	24.452
MnO	0.035	0.124	0.024	0.211	0.125	0.205	0.049	0.219	0.209	0.000
FeO	2.169	17.280	10.663	11.552	9.761	8.279	9.604	8.629	8.377	2.209
NiO	0.000	0.089	0.000	0.000	0.085	0.000	0.000	0.118	0.000	0.048
Na_2O	0.021	3.597	0.000	0.013	0.021	0.000	0.003	0.010	0.008	0.031
K_2O	0.000	0.534	0.005	0.029	0.004	0.000	0.019	0.000	0.004	0.008
Total	97.29	95.43	95.33	96.96	97.87	96.93	95.74	97.16	97.06	97.48
Si	5.978	7.148	6.142	6.137	6.113	6.078	6.122	6.063	6.048	5.997
Ti	0.004	0.041	0.009	0.008	0.008	0.012	0.009	0.023	0.019	0.004
Al	5.767	2.642	4.755	4.666	4.834	5.002	4.870	5.031	5.091	5.764
Cr	0.001	0.005	0.001	0.000	0.004	0.009	0.003	0.007	0.000	0.010
Mg	0.000	2.206	0.000	0.000	0.000	0.000	0.000	0.000	0.000	0.000
Ca	4.096	1.389	4.084	4.097	4.131	4.161	4.103	4.065	4.074	4.040
Mn	0.005	0.017	0.003	0.029	0.017	0.028	0.007	0.029	0.028	0.000
Fe	0.281	2.394	1.475	1.580	1.337	1.114	1.316	1.159	1.124	0.285
Ni	0.000	0.012	0.000	0.000	0.011	0.000	0.000	0.015	0.000	0.006
Na	0.006	1.155	0.000	0.004	0.007	0.000	0.001	0.003	0.002	0.009
K	0.000	0.113	0.001	0.006	0.001	0.000	0.004	0.000	0.001	0.002
Total	16.137	17.122	16.471	16.527	16.463	16.404	16.435	16.396	16.389	16.117

Alhambra Formation Detrital Epidotes **Sample A8.3**

SiO_2	37.598	37.425	37.670	37.514	38.066	37.693	37.514	37.200	38.372	38.029
TiO_2	0.098	0.081	0.095	0.154	0.116	0.103	0.067	0.005	0.122	0.076
Al_2O_2	24.417	24.281	24.948	26.377	28.081	25.402	25.342	23.914	28.355	26.036
Cr_2O_3	0.000	0.060	0.153	0.020	0.000	0.000	0.000	0.000	0.028	0.020
MgO	0.000	0.000	0.000	0.000	0.000	0.000	0.000	0.000	0.000	0.000
CaO	23.287	23.284	23.581	23.765	24.194	23.537	23.248	22.823	23.897	23.695
MnO	0.163	0.215	0.159	0.014	0.122	0.069	0.163	0.083	0.112	0.125
FeO	11.465	11.092	10.352	8.183	6.256	10.257	10.235	10.999	6.312	8.656
NiO	0.000	0.000	0.040	0.022	0.015	0.063	0.000	0.000	0.000	0.018
Na_2O	0.000	0.000	0.000	0.000	0.020	0.008	0.020	0.001	0.016	0.003
K_2O	0.007	0.022	0.002	0.000	0.000	0.000	0.002	0.000	0.008	0.000
Total	97.03	98.29	97.00	96.05	96.87	97.09	96.59	95.03	97.22	96.66
Si	6.136	6.139	6.121	6.080	6.052	6.105	6.107	6.183	6.068	6.135
Ti	0.012	0.010	0.012	0.019	0.014	0.012	0.008	0.001	0.014	0.009
Al	4.696	4.695	4.778	5.038	5.262	4.849	4.862	4.685	5.285	4.95
Cr	0.000	0.008	0.020	0.003	0.000	0.000	0.000	0.000	0.004	0.003
Mg	0.000	0.000	0.000	0.000	0.000	0.000	0.000	0.000	0.000	0.000
Ca	4.072	4.093	4.105	4.127	4.121	4.084	4.055	4.064	4.049	4.095
Mn	0.022	0.029	0.022	0.002	0.016	0.009	0.022	0.012	0.015	0.017
Fe	1.565	1.522	1.407	1.109	0.832	1.389	1.394	1.529	0.835	1.168
Ni	0.000	0.000	0.005	0.003	0.002	0.008	0.000	0.000	0.000	0.002
Na	0.000	0.000	0.000	0.000	0.006	0.002	0.006	0.000	0.005	0.001
K	0.001	0.005	0.000	0.000	0.000	0.000	0.000	0.000	0.002	0.000
Total	16.505	16.501	16.469	16.381	16.306	16.459	16.456	16.474	16.277	16.380

SiO_2	37.851	37.161	37.694	37.717	37.705	37.353
TiO_2	0.146	0.083	0.127	0.119	0.103	0.057
Al_2O_2	27.173	23.825	25.262	24.295	25.777	23.960
Cr_2O_3	0.000	0.000	0.000	0.004	0.008	0.000
MgO	0.000	0.000	0.000	0.000	0.000	0.000
CaO	23.792	23.438	23.260	23.193	23.313	23.032
MnO	0.017	0.169	0.197	0.048	0.069	0.263
FeO	7.777	11.745	10.475	11.520	9.585	11.349
NiO	0.000	0.000	0.018	0.103	0.078	0.000
Na_2O	0.031	0.012	0.005	0.003	0.002	0.008
K_2O	0.000	0.000	0.007	0.008	0.001	0.013
Total	96.79	96.43	97.05	97.011	96.64	96.04
Si	6.066	6.126	6.115	6.156	6.111	6.161
Ti	0.018	0.010	0.015	0.015	0.013	0.007
Al	5.132	4.629	4.829	4.673	4.923	4.658
Cr	0.000	0.000	0.000	0.000	0.001	0.000
Mg	0.000	0.000	0.000	0.000	0.000	0.000
Ca	4.085	4.140	4.043	4.055	4.048	4.071
Mn	0.002	0.024	0.027	0.007	0.009	0.037
Fe	1.042	1.619	1.421	1.572	1.299	1.566
Ni	0.000	0.000	0.002	0.013	0.010	0.000
Na	0.009	0.004	0.002	0.001	0.001	0.003
K	0.000	0.000	0.001	0.002	0.000	0.003
Total	16.355	16.551	16.456	16.494	16.415	16.505

Detrital Tourmalines Cations calculated on the basis of 31 oxygens

Quentar Formation Sample CA 1.1

SiO2	34.747	35.689	33.277	35.323	35.352	33.184	35.228	34.969	35.519	36.018	35.178
TiO2	0.695	0.549	0.377	0.275	0.416	1.454	0.349	0.572	0.281	0.362	0.88
Al_2O_3	31.721	31.261	27.099	29.417	29.423	30.382	29.753	34.585	29.729	30.257	31.327
FeO	6.594	4.938	18.177	9.562	7.067	13.536	8.143	5.663	6.424	6.93	6.147
MnO	0	0.018	0.17	0.016	0.001	0.008	0.007	0.005	0.015	0.018	0.112
MgO	7.113	8.753	2.617	7.305	8.533	3.831	8.032	6.274	8.982	8.932	7.615
CaO	1.201	0.622	0.975	0.38	0.66	1.603	0.454	0.706	0.513	0.51	0.958
Na2O	1.775	2.448	2.186	2.652	2.55	1.389	2.529	1.902	2.618	2.291	2.066
K2O	0.022	0.015	0.063	0.02	0.006	0.043	0.027	0.03	0.013	0.008	0.026
B2O3	9.295	8.918	7.633	8.489	9.447	9.033	8.357	9.507	8.686	9.683	9.533
Total	93.163	93.211	92.574	93.439	93.455	94.463	92.879	94.213	92.78	95.009	93.842
Si	6.492	6.678	6.608	6.732	6.656	6.267	6.731	6.387	6.752	6.657	6.529
Ti	0.098	0.077	0.056	0.039	0.059	0.207	0.050	0.079	0.040	0.050	0.123
Al	6.984	6.894	6.341	6.607	6.528	6.763	6.700	7.445	6.660	6.591	6.852
Fe	1.030	0.773	3.018	1.524	1.113	2.138	1.301	0.865	1.021	1.071	0.954
Mn	0.000	0.001	0.013	0.001	0.000	0.001	0.001	0.000	0.001	0.001	0.008
Mg	1.125	1.387	0.440	1.179	1.361	0.613	1.300	0.971	1.446	1.398	1.197
Ca	0.335	0.174	0.289	0.108	0.185	0.451	0.129	0.192	0.145	0.141	0.265
Na	0.711	0.981	0.930	1.083	1.029	0.562	1.035	0.744	1.066	0.907	0.822
K	0.008	0.005	0.024	0.007	0.002	0.016	0.010	0.011	0.005	0.003	0.009
B	0.024	0.023	0.018	0.021	0.024	0.023	0.021	0.025	0.022	0.025	0.025
Total	16.807	16.994	17.737	17.303	16.956	17.040	17.278	16.719	17.160	16.844	16.782

SiO2	35.663	34.35	34.649	35.821	35.976	35.442	35.857	34.034	35.217	34.883	35.526
TiO2	0.415	0.624	1.195	0.207	0.234	0.268	0.659	0.915	0.554	0.294	0.214
Al_2O_3	32.171	32.416	31.162	30.567	32.238	30.961	31.313	33.758	31.489	31.73	30.031
FeO	4.549	9.217	6.956	5.491	6.259	7.666	5.637	7.477	6.663	9.045	6.998
MnO	0	0	0.025	0.008	0.019	0.001	0.012	0	0	0.088	0.005
MgO	8.736	5.641	6.595	9.283	7.989	7.503	8.593	5.692	7.543	5.959	8.568
CaO	0.565	0.706	1.342	0.467	0.453	0.216	0.458	0.939	0.446	0.752	0.383
Na2O	2.22	1.763	1.71	2.407	2.081	2.655	2.635	1.869	2.426	1.786	2.675
K2O	0.009	0.032	0.043	0.022	0.021	0.009	0.007	0.081	0.021	0.044	0.015
B2O3	8.775	9.327	8.208	9.307	9.017	8.544	8.842	8.2	8.833	8.988	8.495
Total	93.103	94.076	91.885	93.58	94.287	93.265	94.013	92.965	93.192	93.569	92.91
Si	6.661	6.394	6.601	6.696	6.656	6.696	6.678	6.398	6.615	6.542	6.756
Ti	0.058	0.087	0.171	0.029	0.033	0.038	0.092	0.129	0.078	0.041	0.031
Al	7.082	7.111	6.997	6.734	7.029	6.894	6.872	7.479	6.970	7.013	6.730
Fe	0.710	1.435	1.108	0.858	0.968	1.211	0.878	1.175	1.046	1.419	1.113
Mn	0.000	0.000	0.002	0.001	0.001	0.000	0.001	0.000	0.000	0.006	0.000
Mg	1.382	0.889	1.064	1.470	1.252	1.201	1.355	0.906	1.200	0.947	1.380
Ca	0.157	0.196	0.381	0.130	0.125	0.061	0.127	0.263	0.125	0.210	0.109
Na	0.888	0.703	0.698	0.964	0.825	1.075	1.051	0.753	0.976	0.718	1.090
K	0.003	0.012	0.016	0.008	0.008	0.003	0.003	0.030	0.008	0.016	0.006
B	0.022	0.024	0.021	0.024	0.023	0.022	0.023	0.021	0.022	0.023	0.021
Total	16.965	16.850	17.059	16.914	16.919	17.200	17.080	17.154	17.041	16.935	17.235

Quentar Formation Detrital Tourmalines — Sample CA1.1

SiO2	36.139	35.734	34.022	35.618	33.876
TiO2	0.178	0.031	0.778	0.218	0.801
Al_2O_3	31.473	32.796	32.611	30.336	28.489
FeO	3.55	6.041	10.223	7.142	14.577
MnO	0	0.021	0.041	0.003	0
MgO	9.921	7.492	4.687	8.287	4.003
CaO	0.302	0.041	0.469	0.263	0.677
Na2O	2.725	3.033	1.985	2.638	2.421
K2O	0	0.005	0.034	0.007	0.101
B2O3	8.556	9.702	9.235	8.507	8.353
Total	92.844	94.896	94.085	93.019	93.298
Si	6.787	6.542	6.347	6.756	6.554
Ti	0.025	0.004	0.109	0.031	0.117
Al	6.966	7.076	7.170	6.781	6.496
Fe	0.557	0.925	1.595	1.133	2.358
Mn	0.000	0.001	0.003	0.000	0.000
Mg	1.578	1.162	0.741	1.331	0.656
Ca	0.085	0.011	0.130	0.074	0.195
Na	1.096	1.190	0.793	1.072	1.004
K	0.000	0.002	0.012	0.003	0.038
B	0.022	0.025	0.024	0.021	0.021
Total	17.116	16.938	16.925	17.203	17.439

Dudar Formation Detrital Tourmalines — Sample SLT

SiO2	35.333	36.134	35.477	35.614	35.95	35.117	35.536	35.212	35.427	35.588
TiO2	0.221	0.221	0.41	0.273	0.395	0.376	0.773	0.39	0.092	0.505
Al_2O_3	32.72	30.401	31.934	29.93	32.646	29.97	31.73	29.72	29.493	30.931
FeO	8.776	3.673	4.678	6.205	2.869	7.612	6.233	8.399	7.676	5.805
MnO	0	0.856	0	0	0.008	0.003	0.009	0.008	0.021	0
MgO	5.267	10.133	8.68	9.013	9.638	8.151	7.458	7.585	8.229	8.642
CaO	0.176	0.856	0.97	0.667	0.445	0.003	0.121	0.23	0.282	0.51
Na2O	1.77	2.385	2.202	2.44	2.612	2.55	2.627	2.743	2.816	2.56
K2O	0.021	0.019	0.033	0.02	0.02	0.028	0.03	0.014	0.019	0.012
B2O3	9.388	8.393	9.137	9.303	8.818	9.139	9.017	8.064	8.513	8.789
Total	93.672	93.071	93.521	93.465	93.401	92.949	93.534	92.365	92.568	93.342
Si	6.554	6.835	6.594	6.688	6.670	6.659	6.627	6.773	6.778	6.684
Ti	0.031	0.031	0.057	0.039	0.055	0.054	0.108	0.056	0.013	0.071
Al	7.153	6.777	6.995	6.624	7.138	6.698	6.974	6.737	6.650	6.846
Fe	1.361	0.581	0.727	0.974	0.445	1.207	0.972	1.351	1.228	0.912
Mn	0.000	0.061	0.000	0.000	0.001	0.000	0.001	0.001	0.002	0.000
Mg	0.827	1.623	1.366	1.433	1.514	1.309	1.178	1.236	1.333	1.375
Ca	0.049	0.241	0.269	0.187	0.123	0.001	0.034	0.066	0.080	0.143
Na	0.703	0.967	0.877	0.982	1.038	1.036	1.050	1.130	1.154	1.030
K	0.008	0.007	0.012	0.007	0.007	0.010	0.011	0.005	0.007	0.004
B	0.024	0.021	0.024	0.024	0.023	0.023	0.023	0.020	0.021	0.022
Total	16.710	17.144	16.922	16.957	17.015	16.998	16.977	17.375	17.268	17.088

Dudar Formation Detrital Tourmalines **Sample SLT**

SiO2	35.619	36.29	34.723	35.853	35.816	35.393
TiO2	0.208	0.082	0.361	0.456	0.497	0.512
Al_2O_3	30.099	32.594	30.308	30.354	31.351	29.973
FeO	7.165	3.392	8.056	5.354	5.915	6.984
MnO	0	0.016	0	0	0.012	0
MgO	8.161	9.482	7.236	9.469	8.513	8.283
CaO	0.378	0.309	0.727	0.537	0.251	0.399
Na2O	2.597	2.484	2.431	2.579	2.701	2.69
K2O	0.03	0.012	0.026	0.026	0.008	0.022
B2O3	8.803	9.453	9.288	8.54	9.541	9.867
Total	93.06	94.114	93.156	93.168	94.605	94.123
Si	6.740	6.665	6.556	6.767	6.611	6.592
Ti	0.030	0.011	0.051	0.065	0.069	0.072
Al	6.712	7.054	6.744	6.752	6.820	6.579
Fe	1.134	0.521	1.272	0.845	0.913	1.088
Mn	0.000	0.001	0.000	0.000	0.001	0.000
Mg	1.308	1.475	1.157	1.514	1.331	1.307
Ca	0.107	0.085	0.205	0.151	0.069	0.111
Na	1.053	0.977	0.983	1.043	1.068	1.074
K	0.011	0.004	0.010	0.010	0.003	0.008
B	0.022	0.025	0.024	0.022	0.025	0.025
Total	17.116	16.818	17.001	17.167	16.910	16.855

Pinos Genil Formation Detrital Tourmalines **Sample SAF 6.2**

SiO2	35.723	35.84	36.389	35.936	35.564	35.768	34.92	35.112	35.391	35.415	35.399
TiO2	0.404	0.31	0.447	0.309	0.564	0.506	0.708	0.454	0.414	0.595	0.834
Al_2O_3	31.654	31.273	32.167	32.259	31.434	31.294	30.691	29.112	30.078	31.222	30.838
FeO	5.2	7.369	4.564	4.906	4.501	4.556	7.848	9.114	7.429	6.417	7.763
MnO	0.028	0	0	0.014	0	0.01	0.031	0	0.004	0	0.013
MgO	8.44	7.257	8.905	8.435	8.812	9.023	6.644	7.025	8.368	7.434	6.986
CaO	0.387	0.464	0.408	0.094	0.666	0.682	0.226	0.425	0.545	0.334	0.09
Na2O	2.452	2.411	2.35	2.589	2.289	2.356	2.572	2.598	2.488	2.561	2.835
K2O	0.017	0.002	0.026	0.02	0.013	0.021	0.012	0.016	0.009	0.022	0.024
B2O3	7.455	7.53	9.93	9.797	9.002	10.329	9.678	9.382	9.687	9.871	9.546
Total	91.76	92.456	95.186	94.359	92.845	94.545	93.33	93.238	94.413	93.871	94.328
Si	6.834	6.837	6.615	6.595	6.660	6.546	6.540	6.651	6.592	6.558	6.575
Ti	0.058	0.044	0.061	0.043	0.079	0.070	0.100	0.065	0.058	0.083	0.117
Al	7.137	7.030	6.891	6.977	6.938	6.750	6.774	6.499	6.602	6.814	6.751
Fe	0.832	1.175	0.694	0.753	0.705	0.697	1.229	1.444	1.157	0.994	1.206
Mn	0.002	0.000	0.000	0.001	0.000	0.001	0.002	0.000	0.000	0.000	0.001
Mg	1.368	1.172	1.371	1.311	1.398	1.399	1.054	1.127	1.320	1.166	1.099
Ca	0.110	0.132	0.111	0.026	0.186	0.186	0.063	0.120	0.151	0.092	0.025
Na	1.005	0.985	0.915	1.018	0.918	0.924	1.032	1.054	0.993	1.016	1.128
K	0.006	0.001	0.009	0.007	0.005	0.007	0.004	0.006	0.003	0.008	0.009
B	0.019	0.019	0.026	0.026	0.023	0.027	0.025	0.024	0.025	0.025	0.025
Total	17.371	17.397	16.693	16.757	16.912	16.607	16.823	16.988	16.901	16.757	16.935

Pinos Genil Formation Detrital Tourmalines **Sample SAF 6.2**

SiO2	37.004	35.5	35.592	35.118	35.733	35.829	35.271	35.806	35.055	35.461	35.414
TiO2	0.683	0.261	0.324	0.73	0.203	0.635	0.322	0.66	0.463	0.724	0.139
Al_2O_3	29.827	30.434	31.838	30.113	32.112	31.659	31.436	30.723	29.625	30.599	31.155
FeO	7.152	6.67	5.217	8.146	6.795	5.836	6.577	5.197	9.61	7.503	3.967
MnO	0	0.007	0.012	0	0	0	0.023	0.001	0.009	0.042	0
MgO	7.744	7.992	8.587	7.077	7.239	7.714	6.577	8.846	6.663	4.434	9.137
CaO	0.305	0.498	0.04	0.288	0.29	0.271	0.077	0.375	0.162	0.317	0.153
Na2O	2.751	2.465	2.715	2.732	2.369	2.486	2.667	2.745	2.606	2.663	2.565
K2O	0.009	0.024	0.013	0.025	0.015	0.021	0.008	0.012	0.02	0.009	0.006
B2O3	9.047	11.143	8.91	9.13	8.772	9.024	9.535	9.987	9.194	10.535	9.469
Total	94.522	94.994	93.248	93.359	93.528	93.475	92.493	94.352	93.407	92.287	92.005
Si	6.864	6.481	6.661	6.622	6.671	6.673	6.613	6.602	35.055	6.592	6.667
Ti	0.095	0.036	0.046	0.104	0.029	0.089	0.045	0.092	0.463	0.101	0.020
Al	6.520	6.548	7.022	6.692	7.065	6.949	6.946	6.676	29.625	6.704	6.912
Fe	1.109	1.018	0.816	1.285	1.061	0.909	1.031	0.801	9.610	1.166	0.624
Mn	0.000	0.000	0.001	0.000	0.000	0.000	0.002	0.000	0.009	0.003	0.000
Mg	1.216	1.236	1.361	1.130	1.145	1.217	1.044	1.381	6.663	0.698	1.457
Ca	0.084	0.136	0.011	0.081	0.081	0.075	0.022	0.103	0.162	0.088	0.043
Na	1.093	0.964	1.089	1.104	0.948	0.992	1.071	1.085	2.606	1.061	1.035
K	0.003	0.008	0.005	0.009	0.005	0.008	0.003	0.004	0.020	0.003	0.002
B	0.023	0.029	0.023	0.023	0.022	0.023	0.024	0.026	9.194	0.027	0.024
Total	17.009	16.457	17.035	17.050	17.027	16.935	16.802	16.771	93.407	16.443	16.784

SiO2	35.711	33.744	34.947	35.877	34.764	35.146	35.691	36.112
TiO2	0.463	1.402	0.924	0.672	0.445	0.84	0.5	0.336
Al_2O_3	31.641	28.266	32.627	30.883	30.793	30.668	31.094	32.258
FeO	4.857	15.014	8.873	4.341	9.346	7.057	6.112	4.541
MnO	0	0.216	0.016	0	0.023	0.001	0.019	0
MgO	8.049	3.04	5.722	9.121	6.067	7.471	8.153	8.675
CaO	0.379	1.372	0.607	0.587	1.106	0.317	0.274	0.097
Na2O	2.665	1.734	1.995	2.602	1.995	2.685	2.622	2.6
K2O	0.014	0.114	0.039	0.027	0.031	0.022	0.021	0.008
B2O3	10.37	9.603	9.483	10.076	9.954	9.155	9.02	10.047
Total	94.149	94.505	95.233	94.186	94.524	93.362	93.506	94.674
Si	6.542	6.392	6.416	6.601	6.446	6.600	6.677	6.591
Ti	0.064	0.200	0.128	0.093	0.062	0.119	0.070	0.046
Al	6.831	6.310	7.059	6.696	6.729	6.788	6.855	6.939
Fe	0.744	2.378	1.362	0.668	1.449	1.108	0.956	0.693
Mn	0.000	0.015	0.001	0.000	0.002	0.000	0.001	0.000
Mg	1.249	0.488	0.890	1.421	0.953	1.188	1.292	1.341
Ca	0.104	0.387	0.166	0.161	0.306	0.089	0.076	0.026
Na	1.046	0.704	0.785	1.026	0.793	1.080	1.051	1.017
K	0.005	0.042	0.014	0.010	0.011	0.008	0.008	0.003
B	0.027	0.024	0.025	0.026	0.026	0.023	0.023	0.026
Total	16.612	16.941	16.844	16.702	16.776	17.004	17.009	16.682

Alhambra Formation Detrital Tourmalines **Sample A8.3**

SiO2	35.349	35.572	35.808	35.316	34.989	35.285	35.602	35.59	35.339	35.814	35.429
TiO2	0.516	0.582	0.247	0.333	0.745	0.594	0.563	0.5	0.899	0.545	0.876
Al_2O_3	29.244	31.487	31.996	29.526	32.076	31.128	31.376	29.065	30.672	31.464	30.665
FeO*	8.218	5.385	5.672	7.861	8.562	5.373	5.462	8.984	6.738	4.649	6.726
MnO	0.022	0.01	0.016	0	0	0	0.019	0.033	0.003	0	0
MgO	7.769	8.566	8.194	8.159	5.401	8.648	8.491	7.41	7.947	8.929	7.721
CaO	0.429	0.631	0.416	0.4	0.294	0.805	0.774	0.285	0.379	0.531	0.489
Na2O	2.699	2.379	2.496	2.597	2.157	2.516	2.103	2.59	2.694	2.461	2.624
K2O	0.03	0.029	0.012	0.038	0.016	0.022	0.014	0.025	0.026	0.025	0.025
B2O3	10.09	9.888	9.877	9.869	9.783	9.404	10.146	9.564	10.135	9.646	9.125
Total	94.366	94.529	94.734	94.099	94.023	93.775	94.55	94.046	94.832	94.064	93.68
Si	6.589	6.542	6.564	6.604	6.471	6.567	6.532	6.683	6.508	6.611	6.627
Ti	0.072	0.081	0.034	0.047	0.104	0.083	0.078	0.071	0.125	0.076	0.123
Al	6.424	6.825	6.912	6.507	6.991	6.827	6.784	6.432	6.657	6.845	6.760
Fe	1.281	0.828	0.869	1.229	1.324	0.836	0.838	1.411	1.038	0.718	1.052
Mn	0.002	0.001	0.001	0.000	0.000	0.000	0.001	0.002	0.000	0.000	0.000
Mg	1.226	1.334	1.272	1.292	0.846	1.363	1.319	1.178	1.239	1.396	1.223
Ca	0.119	0.173	0.114	0.112	0.081	0.223	0.212	0.080	0.104	0.146	0.136
Na	1.078	0.937	0.980	1.041	0.855	1.003	0.827	1.042	1.063	0.973	1.052
K	0.011	0.010	0.004	0.014	0.006	0.008	0.005	0.009	0.009	0.009	0.009
B	0.026	0.026	0.026	0.025	0.025	0.024	0.026	0.024	0.026	0.025	0.023
Total	16.828	16.757	16.777	16.870	16.702	16.935	16.622	16.932	16.769	16.798	17.005
SiO2	34.634	38.183	36.27	35.482	35.218	35.216	35.427	35.15	35.385	35.539	35.487
TiO2	0.629	0.743	0.116	0.669	0.794	0.401	1.177	0.371	0.523	0.629	0.414
Al_2O_3	30.412	30.065	32.644	30.533	31.179	29.301	29.754	29.365	30.343	31.281	29.376
FeO*	10.059	6.107	4.722	6.739	5.563	8.894	7.574	9.015	6.722	5.417	8.085
MnO	0.019	0.008	0	0	0	0.03	0.006	0.006	0.001	0.007	0.008
MgO	5.58	7.703	8.418	8.185	8.335	7.644	7.304	6.866	7.902	8.366	7.936
CaO	0.457	0.563	0.073	0.503	0.727	0.457	0.391	0.315	0.45	0.707	0.424
Na2O	2.47	2.215	2.364	2.562	2.345	2.693	2.605	2.699	2.685	2.529	2.7
K2O	0.032	0.025	0.002	0.037	0.019	0.015	0.001	0.04	0.021	0.013	0.024
B2O3	10.651	6.711	10.129	9.572	9.375	9.443	8.697	10.159	9.137	10.338	10.067
Total	94.943	92.323	94.738	94.282	93.555	94.094	92.936	93.986	93.169	94.826	94.521
Si	6.389	7.267	6.600	6.593	6.563	6.625	6.712	6.571	6.659	6.501	6.602
Ti	0.087	0.106	0.016	0.094	0.111	0.057	0.168	0.052	0.074	0.087	0.058
Al	6.611	6.744	7.000	6.687	6.848	6.496	6.643	6.470	6.729	6.743	6.441
Fe	1.552	0.972	0.718	1.047	0.867	1.399	1.200	1.409	1.058	0.829	1.258
Mn	0.001	0.001	0.000	0.000	0.000	0.002	0.000	0.000	0.000	0.000	0.001
Mg	0.872	1.242	1.297	1.288	1.316	1.218	1.172	1.087	1.259	1.296	1.250
Ca	0.126	0.160	0.020	0.139	0.202	0.128	0.110	0.088	0.126	0.193	0.118
Na	0.976	0.903	0.922	1.020	0.936	1.086	1.057	1.081	1.083	0.991	1.076
K	0.011	0.009	0.001	0.013	0.007	0.005	0.000	0.014	0.008	0.005	0.009
B	0.028	0.017	0.027	0.025	0.024	0.024	0.022	0.026	0.023	0.027	0.026
Total	16.653	17.421	16.600	16.906	16.874	17.040	17.085	16.799	17.019	16.671	16.839

Alhambra Formation Detrital Tourmalines Sample A8.3

SiO2	35.006	34.838	35.162	35.882	35.021	34.915	35.399
TiO2	0.284	0.839	0.751	0.162	0.555	0.519	0.326
Al_2O_3	30.348	30.365	31.896	30.609	29.354	29.63	29.751
FeO*	6.697	9.505	7.123	5.609	8.815	8.674	6.74
MnO	0.003	0	0	0.001	0.006	0	0
MgO	7.977	6.221	6.69	8.853	7.82	7.481	8.553
CaO	0.619	0.756	0.346	0.304	0.541	0.468	0.469
Na2O	2.39	2.347	2.482	2.593	2.584	2.547	2.509
K2O	0.024	0.03	0.023	0.034	0.033	0.011	0.014
B2O3	10.461	10.007	8.701	9.167	9.66	8.769	9.276
Total	93.809	94.908	93.174	93.214	94.389	93.014	93.037
Si	6.497	6.451	6.599	6.729	6.565	6.652	6.684
Ti	0.040	0.117	0.106	0.023	0.078	0.074	0.046
Al	6.638	6.626	7.054	6.765	6.485	6.653	6.620
Fe	1.039	1.472	1.118	0.880	1.382	1.382	1.064
Mn	0.000	0.000	0.000	0.000	0.000	0.000	0.000
Mg	1.254	0.976	1.063	1.406	1.241	1.207	1.368
Ca	0.171	0.209	0.097	0.085	0.151	0.133	0.132
Na	0.950	0.931	0.998	1.042	1.038	1.040	1.015
K	0.009	0.011	0.008	0.012	0.012	0.004	0.005
B	0.027	0.026	0.022	0.023	0.025	0.022	0.023
Total	16.625	16.818	17.066	16.965	16.977	17.166	16.958

Appendix 5 Detrital Muscovite Compositions

Below is listed the major element concentrations for detrital and conglomerate clast muscovites taken from the Quentar and Dudar Formations. These are presented graphically in **Fig. 7.3**, as transects across individual grains, in order to asses the possibility of chemical alteration that might affect isotopic dating. Ratios of K_2O/Al_2O_3 are presented in **Fig. 7.3.**

Quentar Formation Sample QR4									**Dudar Formation Sample D2 M1**							
Transect:		**Left (on Fig. 7.3)**						**Right**	**Left**							
SiO2	47.401	46.588	42.944	46.537	46.718	46.727	46.354	47.262	45.755	45.810	48.764	48.306	48.360	46.371	48.720	49.660
TiO2	0.484	0.575	0.272	0.353	0.256	0.364	0.282	0.301	0.653	0.517	0.588	0.530	0.484	0.505	0.490	0.394
Al2O3	29.458	29.077	27.505	29.999	30.897	31.197	29.550	30.248	29.247	30.202	31.971	31.308	31.907	30.056	31.147	30.485
FeO	4.151	4.144	2.914	3.288	3.332	3.155	3.155	3.223	3.519	1.671	1.582	1.481	1.623	1.484	1.449	1.619
MnO	0.000	0.000	0.000	0.055	0.023	0.000	0.002	0.000	0.022	0.038	0.006	0.000	0.056	0.000	0.013	0.000
MgO	2.147	2.042	1.866	2.039	1.864	1.872	1.981	2.059	4.209	2.116	2.233	1.964	2.064	2.034	2.377	2.654
CaO	0.000	0.039	0.051	0.126	0.027	0.037	0.051	0.050	0.201	0.000	0.042	0.109	0.000	0.045	0.098	0.000
Na2O	1.159	1.109	1.221	1.382	1.258	1.245	1.115	1.268	0.766	0.765	0.954	1.055	0.864	0.804	0.942	0.694
K2O	9.486	9.244	8.297	9.271	9.205	9.131	9.317	9.657	8.811	9.332	9.742	9.506	9.715	9.170	9.680	9.787
P2O5	0.000	0.015	0.018	0.004	0.000	0.000	0.000	0.000	0.000	0.000	0.002	0.000	0.000	0.000	0.036	0.000
SO	0.000	0.000	0.000	0.033	0.022	0.057	0.000	0.000	0.063	0.000	0.000	0.000	0.040	0.000	0.000	0.015
CrO2	0.005	0.082	0.030	0.009	0.037	0.051	0.015	0.000	0.085	0.135	0.009	0.018	0.000	0.134	0.001	0.004
CoO	0.000	0.000	0.000	0.000	0.000	0.000	0.000	0.000	0.000	0.000	0.000	0.000	0.000	0.019	0.000	0.000
NiO	0.000	0.021	0.000	0.049	0.000	0.102	0.067	0.082	0.072	0.000	0.121	0.029	0.013	0.000	0.011	0.074
Total	94.297	92.935	85.118	93.145	93.64	93.939	91.889	94.150	93.403	90.586	96.013	94.306	95.124	90.622	94.964	95.385
Si	6.459	6.441	6.438	6.400	6.375	6.351	6.449	6.427	6.281	6.410	6.428	6.473	6.431	6.466	6.484	6.577
Ti	0.05	0.06	0.031	0.036	0.026	0.037	0.029	0.027	0.067	0.054	0.058	0.053	0.048	0.053	0.049	0.039
Al	4.731	4.739	4.860	4.863	4.969	4.998	4.846	4.889	4.733	4.981	4.968	4.945	5.001	4.940	4.886	4.759
Fe	0.473	0.479	0.365	0.378	0.380	0.359	0.367	0.389	0.404	0.195	0.174	0.166	0.181	0.173	0.161	0.179
Mn	0.000	0.000	0.000	0.006	0.003	0.000	0.000	0.000	0.003	0.004	0.001	0.000	0.006	0.000	0.001	0.000
Mg	0.436	0.421	0.417	0.418	0.379	0.379	0.411	0.412	0.861	0.441	0.439	0.392	0.409	0.423	0.472	0.524
Ca	0.000	0.006	0.008	0.019	0.004	0.005	0.008	0.000	0.030	0.000	0.006	0.016	0.000	0.007	0.014	0.000
Na	0.306	0.297	0.35	0.369	0.333	0.328	0.301	0.233	0.204	0.208	0.244	0.274	0.223	0.217	0.243	0.178
K	1.649	1.631	1.587	1.627	1.602	1.583	1.654	1.664	1.543	1.666	1.638	1.625	1.648	1.631	1.644	1.654
P	0.000	0.002	0.002	0.000	0.000	0.000	0.000	0.000	0.000	0.000	0.000	0.000	0.000	0.000	0.004	0.000
S	0.000	0.000	0.000	0.006	0.004	0.010	0.000	0.002	0.011	0.000	0.000	0.000	0.007	0.000	0.000	0.003
Cr	0.001	0.009	0.004	0.001	0.004	0.005	0.002	0.003	0.009	0.015	0.001	0.002	0.000	0.015	0.000	0.000
Co	0.000	0.000	0.000	0.000	0.000	0.000	0.000	0.001	0.000	0.000	0.000	0.000	0.000	0.002	0.000	0.000
Ni	0.000	0.002	0.000	0.005	0.000	0.011	0.008	0.001	0.008	0.000	0.013	0.003	0.001	0.000	0.001	0.008
Total	14.104	16.086	14.067	14.128	14.080	14.066	14.075	14.048	14.154	13.975	13.970	13.950	13.955	13.928	13.960	13.920

Dudar Formation Detrital Muscovites

Sample D2 M1						**Sample D2 M2**									
	----------Right														
SiO2	49.892	49.343	49.108	49.765	49.260	48.868	49.660	49.714	49.352	49.825	50.213	50.560	48.772	50.092	42.849
TiO2	0.487	0.368	0.415	0.473	0.456	0.437	0.456	0.450	0.320	0.350	0.338	0.389	0.348	0.480	0.534
Al2O3	30.889	30.626	31.061	30.984	30.287	30.960	30.830	30.832	30.696	30.563	30.672	30.993	29.585	30.721	27.602
FeO	1.728	1.670	1.574	1.913	1.832	1.914	2.169	1.622	1.789	1.680	1.755	1.817	1.817	1.847	2.586
MnO	0.013	0.000	0.057	0.045	0.024	0.000	0.000	0.041	0.000	0.000	0.076	0.102	0.000	0.000	0.000
MgO	2.674	2.677	2.699	2.648	2.847	2.631	2.835	2.489	2.733	2.816	2.768	2.827	2.649	2.773	3.184
CaO	0.071	0.000	0.043	0.021	0.015	0.035	0.092	0.048	0.033	0.018	0.004	0.020	0.050	0.034	0.128
Na2O	0.773	0.843	0.956	0.975	0.918	0.735	0.825	0.824	0.971	0.949	0.834	1.129	0.780	0.685	0.666
K2O	9.705	9.766	9.870	9.743	9.637	9.517	9.522	9.682	9.634	9.749	9.678	9.946	9.758	9.942	8.626
P2O5	0.000	0.000	0.034	0.000	0.000	0.000	0.000	0.000	0.059	0.000	0.151	0.000	0.000	0.000	0.000
SO	0.042	0.000	0.000	0.018	0.000	0.028	0.000	0.028	0.000	0.035	0.009	0.038	0.047	0.021	0.049
CrO2	0.050	0.047	0.000	0.024	0.070	0.535	0.216	0.263	0.154	0.119	0.202	0.083	0.112	0.136	0.093
CoO	0.000	0.011	0.000	0.000	0.006	0.003	0.000	0.000	0.000	0.014	0.000	0.000	0.000	0.000	0.007
NiO	0.000	0.000	0.025	0.000	0.091	0.000	0.000	0.000	0.000	0.038	0.036	0.034	0.029	0.000	0.000
Total	96.324	95.351	95.841	96.608	95.442	95.682	96.606	95.993	95.742	96.157	96.736	97.938	93.947	96.731	86.323
Si	6.545	6.544	6.489	6.523	6.538	6.470	6.511	6.546	6.523	6.556	6.560	6.545	6.579	6.555	6.341
Ti	0.048	0.037	0.041	0.047	0.046	0.044	0.045	0.045	0.032	0.035	0.033	0.038	0.035	0.047	0.059
Al	4.776	4.787	4.837	4.787	4.738	4.831	4.765	4.785	4.782	4.740	4.723	4.729	4.704	4.738	4.814
Fe	0.190	0.185	0.174	0.210	0.203	0.212	0.238	0.179	0.198	0.185	0.192	0.197	0.205	0.202	0.320
Mn	0.001	0.000	0.006	0.005	0.003	0.000	0.000	0.005	0.000	0.000	0.008	0.011	0.000	0.000	0.000
Mg	0.523	0.529	0.532	0.517	0.563	0.519	0.554	0.488	0.538	0.552	0.539	0.545	0.533	0.541	0.702
Ca	0.010	0.000	0.006	0.003	0.002	0.005	0.013	0.007	0.005	0.002	0.001	0.003	0.007	0.005	0.020
Na	0.197	0.217	0.245	0.248	0.236	0.193	0.210	0.210	0.249	0.242	0.211	0.283	0.204	0.174	0.191
K	1.624	1.652	1.664	1.629	1.632	1.608	1.593	1.626	1.624	1.637	1.613	1.642	1.679	1.660	1.629
P	0.000	0.000	0.004	0.000	0.000	0.000	0.000	0.000	0.007	0.000	0.017	0.000	0.000	0.000	0.000
S	0.007	0.000	0.000	0.003	0.000	0.005	0.000	0.005	0.000	0.006	0.001	0.006	0.008	0.003	0.009
Cr	0.005	0.005	0.000	0.002	0.007	0.056	0.022	0.027	0.016	0.012	0.021	0.008	0.012	0.014	0.011
Co	0.000	0.001	0.000	0.000	0.001	0.000	0.000	0.000	0.000	0.002	0.000	0.000	0.000	0.000	0.001
Ni	0.000	0.000	0.003	0.000	0.010	0.000	0.000	0.000	0.000	0.004	0.004	0.004	0.003	0.000	0.000
Total	13.926	13.958	14.000	13.974	13.978	13.943	13.951	13.922	13.973	13.973	13.922	14.012	13.969	13.939	14.097

Dudar Formation Detrital Muscovites

Sample D2	**M3**																
SiO2	49.953	47.838	49.736	49.526	50.141	50.394	49.909	50.161	50.575	50.845	50.396	50.913	50.634	49.688	51.019	48.481	49.249
TiO2	0.446	0.464	0.408	0.541	0.479	0.443	0.490	0.446	0.323	0.396	0.356	0.401	0.330	0.315	0.282	0.612	0.353
Al2O3	30.402	31.102	30.345	29.941	30.449	30.487	30.035	29.811	30.211	29.077	29.104	29.331	28.808	28.289	28.991	31.065	27.976
FeO	1.721	1.950	1.737	1.846	1.554	1.650	1.793	1.739	1.687	1.867	1.789	2.027	1.896	1.910	1.917	1.820	1.880
MnO	0.000	0.000	0.046	0.022	0.001	0.000	0.000	0.000	0.023	0.079	0.000	0.010	0.000	0.000	0.085	0.021	0.003
MgO	2.837	2.694	2.843	2.855	2.971	2.853	2.801	3.249	3.035	3.094	3.034	3.143	3.210	3.425	3.182	2.302	3.085
CaO	0.063	0.000	0.018	0.000	0.034	0.008	0.091	0.070	0.054	0.000	0.069	0.049	0.043	0.002	0.042	0.062	0.010
Na2O	0.822	0.875	0.858	0.958	0.824	0.860	0.669	0.830	0.561	0.709	0.494	0.367	0.544	0.569	0.414	0.919	0.517
K2O	9.754	9.221	9.601	9.509	9.585	9.799	9.673	9.762	9.939	9.807	10.022	10.032	9.893	9.698	10.066	9.785	9.477
P2O5	0.093	0.000	0.000	0.000	0.000	0.000	0.000	0.000	0.038	0.000	0.000	0.000	0.000	0.000	0.003	0.102	0.011
SO	0.043	0.000	0.014	0.000	0.063	0.028	0.043	0.003	0.000	0.000	0.000	0.044	0.000	0.000	0.000	0.052	0.000
CrO2	0.216	0.020	0.076	0.132	0.206	0.101	0.079	0.076	0.019	0.000	0.000	0.096	0.000	0.053	0.000	0.000	0.020
CoO	0.000	0.020	0.000	0.000	0.000	0.008	0.004	0.012	0.003	0.015	0.000	0.004	0.011	0.000	0.010	0.002	0.004
NiO	0.032	0.000	0.076	0.084	0.000	0.000	0.021	0.000	0.000	0.019	0.014	0.000	0.061	0.014	0.093	0.000	0.093
Total	96.382	94.185	95.759	95.415	96.305	96.632	95.608	96.160	96.467	95.908	95.277	96.416	95.431	93.963	96.274	95.225	92.679
Si	6.556	6.426	6.567	6.570	5.572	6.590	6.598	6.600	6.621	6.702	6.689	6.681	6.710	6.691	6.726	6.454	6.715
Ti	0.044	0.047	0.041	0.054	0.047	0.044	0.049	0.044	0.032	0.039	0.036	0.040	0.033	0.032	0.028	0.061	0.036
Al	4.703	4.924	4.723	4.682	4.704	4.699	4.680	4.623	4.662	4.517	4.553	4.537	4.500	4.490	4.490	4.875	4.496
Fe	0.189	0.219	0.192	0.205	0.170	0.180	0.198	0.191	0.185	0.206	0.199	0.222	0.210	0.215	0.211	0.203	0.214
Mn	0.000	0.000	0.005	0.003	0.000	0.000	0.000	0.000	0.002	0.009	0.000	0.001	0.000	0.000	0.009	0.002	0.000
Mg	0.555	0.539	0.560	0.565	0.580	0.556	0.552	0.637	0.592	0.608	0.600	0.615	0.634	0.687	0.623	0.457	0.627
Ca	0.009	0.000	0.003	0.000	0.005	0.001	0.013	0.010	0.008	0.000	0.010	0.007	0.006	0.000	0.006	0.009	0.001
Na	0.209	0.228	0.220	0.246	0.210	0.218	0.172	0.212	0.142	0.181	0.127	0.093	0.140	0.149	0.105	0.237	0.137
K	1.633	1.580	1.617	1.609	1.603	1.635	1.631	1.639	1.660	1.649	1.697	1.680	1.673	1.666	1.687	1.662	1.649
P	0.010	0.000	0.000	0.000	0.000	0.000	0.000	0.000	0.004	0.000	0.000	0.000	0.000	0.000	0.000	0.011	0.001
S	0.007	0.000	0.002	0.000	0.010	0.005	0.007	0.001	0.000	0.000	0.000	0.007	0.000	0.000	0.000	0.009	0.000
Cr	0.022	0.002	0.008	0.014	0.021	0.010	0.008	0.008	0.002	0.000	0.000	0.010	0.000	0.006	0.000	0.000	0.002
Co	0.000	0.002	0.000	0.000	0.000	0.001	0.000	0.001	0.000	0.002	0.000	0.000	0.001	0.000	0.001	0.000	0.000
Ni	0.003	0.000	0.008	0.009	0.000	0.000	0.002	0.000	0.000	0.002	0.002	0.000	0.007	0.002	0.010	0.000	0.010
Total	13.942	13.968	13.945	13.956	13.924	13.939	13.911	13.966	13.910	13.915	13.911	13.893	13.913	13.937	13.897	13.980	13.890

Dudar Formation Detrital Muscovites Sample D2

	D2M5					D2 M6								
	Left on Fig.7.3----------Right													
SiO2	49.320	48.747	48.780	49.556	46.391	48.011	49.413	49.312	49.778	48.655	50.089	49.294	47.914	47.127
TiO2	0.558	0.509	0.495	0.450	0.485	0.495	0.583	0.439	0.507	0.515	0.404	0.397	0.469	0.361
Al2O3	30.790	31.286	31.430	30.696	30.165	32.464	32.301	30.902	30.151	29.336	28.534	28.536	29.230	30.595
FeO	1.839	1.696	1.655	1.819	1.573	1.622	1.660	1.719	1.892	1.808	1.906	1.788	1.690	1.798
MnO	0.000	0.000	0.000	0.000	0.000	0.000	0.008	0.044	0.000	0.067	0.040	0.000	0.031	0.028
MgO	2.938	2.179	2.357	2.957	2.157	2.095	2.031	2.627	2.785	2.709	3.097	3.019	2.656	2.364
CaO	0.072	0.007	0.064	0.114	0.055	0.049	0.060	0.063	0.031	0.000	0.022	0.069	0.054	0.056
Na2O	1.063	0.896	0.885	0.867	0.829	0.881	1.141	0.893	0.794	0.686	0.547	0.616	0.741	0.869
K2O	9.768	9.676	9.643	9.674	9.032	9.818	9.649	9.890	9.893	9.660	9.921	9.604	9.458	9.272
P2O5	0.000	0.000	0.000	0.058	0.075	0.000	0.108	0.000	0.000	0.000	0.000	0.069	0.000	0.000
SO	0.000	0.014	0.033	0.053	0.022	0.000	0.015	0.000	0.025	0.001	0.013	0.039	0.000	0.000
CrO2	0.102	0.000	0.000	0.030	0.102	0.006	0.053	0.021	0.062	0.035	0.072	0.190	0.053	0.094
CoO	0.010	0.001	0.002	0.000	0.023	0.001	0.000	0.020	0.008	0.000	0.000	0.001	0.000	0.006
NiO	0.000	0.000	0.000	0.134	0.140	0.000	0.090	0.033	0.005	0.000	0.065	0.091	0.000	0.000
Total	96.460	95.010	95.344	96.409	91.049	95.442	96.710	95.963	95.932	93.472	94.707	93.714	92.296	92.568
Si	6.485	6.487	6.469	6.511	6.442	6.370	6.413	6.511	6.574	6.590	6.698	6.656	6.568	6.445
Ti	0.055	0.051	0.049	0.044	0.051	0.049	0.057	0.044	0.050	0.052	0.041	0.040	0.048	0.037
Al	4.772	4.908	4.913	4.753	4.937	5.077	4.982	4.809	4.693	4.683	4.498	4.542	4.723	4.932
Fe	0.202	0.189	0.184	0.200	0.183	0.180	0.182	0.190	0.209	0.205	0.213	0.202	0.194	0.206
Mn	0.000	0.000	0.000	0.000	0.000	0.00	0.001	0.005	0.000	0.008	0.005	0.000	0.004	0.003
Mg	0.576	0.432	0.466	0.579	0.446	0.414	0.396	0.517	0.548	0.547	0.617	0.608	0.543	0.482
Ca	0.010	0.001	0.009	0.016	0.008	0.007	0.008	0.009	0.004	0.000	0.003	0.010	0.008	0.008
Na	0.271	0.231	0.228	0.221	0.223	0.227	0.290	0.229	0.203	0.180	0.142	0.161	0.197	0.230
K	1.639	1.643	1.632	1.621	1.600	1.662	1.611	1.669	1.667	1.669	1.693	1.655	1.654	1.618
P	0.000	0.000	0.000	0.006	0.009	0.000	0.012	0.000	0.000	0.000	0.000	0.008	0.000	0.000
S	0.000	0.002	0.005	0.009	0.004	0.000	0.002	0.000	0.004	0.000	0.002	0.007	0.000	0.000
Cr	0.011	0.000	0.000	0.003	0.011	0.001	0.005	0.002	0.006	0.004	0.008	0.020	0.006	0.010
Co	0.001	0.000	0.000	0.000	0.003	0.000	0.000	0.002	0.001	0.000	0.000	0.000	0.000	0.001
Ni	0.000	0.000	0.000	0.014	0.013	0.000	0.009	0.004	0.000	0.000	0.007	0.010	0.000	0.000
Total	14.023	13.945	13.955	13.978	13.932	13.986	13.968	13.987	13.961	13.939	13.926	13.918	13.944	13.971

Dudar Formation Detrital Muscovites Sample D2

	D2 M7																		
	Left (in Fig 7.3)----------right																		
SiO2	46.120	47.016	47.321	47.991	47.647	47.079	47.627	48.006	47.873	48.379	48.724	48.501	48.648	48.704	48.513	47.575	46.749	46.279	48.032
TiO2	0.567	0.484	0.593	0.527	0.577	0.493	0.474	0.549	0.526	0.500	0.519	0.475	0.457	0.414	0.526	0.599	0.597	0.525	0.582
Al2O3	31.770	32.190	31.713	32.415	31.753	32.401	31.350	30.946	30.675	31.065	30.694	30.420	30.223	30.177	30.563	30.279	30.360	30.270	30.850
FeO	1.389	1.497	1.464	1.558	1.563	1.464	1.641	1.695	1.762	1.824	1.807	1.860	1.763	1.832	1.691	1.682	1.588	1.617	1.494
MnO	0.067	0.021	0.000	0.028	0.000	0.000	0.000	0.000	0.014	0.005	0.000	0.022	0.007	0.017	0.026	0.000	0.003	0.000	0.000
MgO	1.776	1.791	1.964	2.077	1.953	1.881	2.316	2.255	2.566	2.390	2.558	2.515	2.706	2.562	2.571	2.337	2.248	2.267	2.119
CaO	0.045	0.042	0.000	0.014	0.044	0.076	0.100	0.000	0.036	0.053	0.035	0.028	0.043	0.031	0.000	0.035	0.019	0.017	0.050
Na2O	0.945	0.962	1.016	1.112	1.070	0.979	1.103	0.894	1.093	0.930	0.875	0.873	1.021	0.950	1.104	0.756	0.873	1.077	0.885
K2O	9.313	6.413	9.457	9.596	9.471	9.525	9.477	9.511	9.696	9.619	9.506	9.523	9.506	9.692	9.649	9.534	9.108	9.155	9.448
P2O5	0.076	0.000	0.000	0.000	0.000	0.000	0.075	0.017	0.000	0.086	0.036	0.021	0.000	0.000	0.037	0.000	0.010	0.000	0.060
SO	0.065	0.009	0.036	0.024	0.000	0.019	0.032	0.020	0.000	0.003	0.000	0.052	0.000	0.003	0.006	0.052	0.000	0.030	0.000
CrO2	0.189	0.036	0.082	0.037	0.132	0.023	0.128	0.141	0.032	0.062	0.043	0.000	0.009	0.054	0.058	0.094	0.000	0.027	0.096
CoO	0.000	0.019	0.020	0.000	0.000	0.023	0.000	0.000	0.000	0.008	0.000	0.014	0.000	0.006	0.005	0.000	0.015	0.003	0.008
NiO	0.059	0.028	0.070	0.115	0.000	0.050	0.087	0.000	0.000	0.013	0.000	0.000	0.056	0.00	0.044	0.000	0.041	0.004	0.020
Total	92.391	93.507	93.735	95.493	94.210	94.011	94.412	94.035	94.275	94.938	94.794	94.304	94.436	94.444	94.794	92.942	91.611	91.270	94.642
Si	6.319	6.358	6.387	6.365	6.399	6.338	6.394	6.460	6.445	6.454	6.501	6.510	6.523	6.535	6.486	6.481	6.448	6.421	6.410
Ti	0.058	0.049	0.060	0.053	0.058	0.050	0.048	0.056	0.053	0.050	0.052	0.048	0.046	0.042	0.053	0.061	0.062	0.055	0.058
Al	5.131	5.131	5.046	5.067	5.027	5.141	4.961	4.908	4.868	4.885	4.827	4.813	4.776	4.773	4.817	4.862	4.936	4.950	5.010
Fe	0.159	0.169	0.165	0.173	0.176	0.165	0.184	0.191	0.198	0.204	0.202	0.209	0.198	0.206	0.189	0.192	0.183	0.188	0.167
Mn	0.008	0.002	0.000	0.003	0.000	0.000	0.000	0.000	0.002	0.001	0.000	0.003	0.001	0.002	0.003	0.000	0.000	0.000	0.000
Mg	0.363	0.361	0.395	0.411	0.391	0.378	0.464	0.452	0.515	0.475	0.509	0.503	0.541	0.512	0.512	0.475	0.462	0.469	0.421
Ca	0.007	0.006	0.000	0.002	0.006	0.011	0.014	0.000	0.005	0.008	0.005	0.004	0.006	0.005	0.000	0.005	0.003	0.002	0.007
Na	0.253	0.252	0.266	0.286	0.279	0.256	0.287	0.233	0.285	0.240	0.226	0.227	0.265	0.247	0.286	0.200	0.233	0.290	0.229
K	1.628	1.624	1.629	1.624	1.623	1.636	1.623	1.633	1.665	1.637	1.618	1.631	1.626	1.659	1.646	1.657	1.603	1.620	1.608
P	0.009	0.000	0.000	0.000	0.000	0.000	0.009	0.002	0.000	0.010	0.004	0.002	0.000	0.000	0.004	0.000	0.001	0.000	0.007
S	0.011	0.002	0.006	0.004	0.000	0.003	0.005	0.003	0.000	0.000	0.000	0.009	0.000	0.001	0.001	0.009	0.000	0.005	0.000
Cr	0.021	0.004	0.009	0.004	0.014	0.002	0.014	0.015	0.003	0.007	0.005	0.000	0.001	0.006	0.006	0.010	0.000	0.003	0.010
Co	0.000	0.002	0.002	0.000	0.000	0.002	0.000	0.000	0.000	0.001	0.000	0.002	0.000	0.001	0.001	0.000	0.002	0.000	0.001
Ni	0.007	0.003	0.008	0.012	0.000	0.005	0.009	0.000	0.000	0.001	0.000	0.000	0.006	0.000	0.005	0.000	0.005	0.000	0.002
Total	13.974	13.964	13.973	14.002	13.973	13.987	14.013	13.953	14.041	13.974	13.947	13.961	13.989	13.987	14.009	13.950	13.938	14.003	13.930

Dudar Formation Detrital Muscovites Sample D2

D2 M8

	Left on (Fig. 7.3) ----------right										
SiO2	46.222	48.776	48.607	48.866	48.977	49.225	49.248	49.608	49.536	48.927	48.513
TiO2	0.379	0.376	0.353	0.362	0.443	0.349	0.388	0.398	0.257	0.345	0.391
Al2O3	31.709	30.028	29.763	29.938	29.693	29.537	29.245	29.386	29.279	29.119	28.706
FeO	1.609	1.807	1.913	1.887	1.771	1.808	1.686	1.802	1.958	1.795	1.829
MnO	0.014	0.000	0.000	0.000	0.048	0.057	0.000	0.020	0.128	0.000	0.052
MgO	1.686	2.665	2.680	2.752	2.743	2.785	2.919	2.775	2.847	2.631	2.846
CaO	0.091	0.000	0.030	0.010	0.025	0.000	0.058	0.041	0.105	0.075	0.000
Na2O	1.003	0.858	0.860	0.687	0.764	0.888	0.782	0.770	0.714	0.737	0.654
K2O	9.431	9.562	9.659	9.636	9.614	9.788	9.723	9.682	9.616	9.625	9.673
P2O5	0.000	0.000	0.000	0.027	0.000	0.000	0.000	0.000	0.000	0.000	0.000
SO	0.019	0.017	0.000	0.014	0.000	0.000	0.061	0.012	0.010	0.000	0.069
CrO2	0.000	0.099	0.069	0.037	0.004	0.041	0.099	0.035	0.000	0.073	0.000
CoO	0.000	0.005	0.000	0.000	0.022	0.000	0.000	0.019	0.000	0.007	0.000
NiO	0.000	0.010	0.000	0.042	0.032	0.012	0.000	0.097	0.000	0.008	0.041
Total	92.164	94.204	93.935	94.258	94.137	94.491	94.210	94.646	94.448	93.340	92.772
Si	6.353	6.552	6.558	6.561	6.583	6.600	6.616	6.633	6.638	6.632	6.625
Ti	0.039	0.038	0.036	0.037	0.045	0.035	0.039	0.040	0.026	0.035	0.040
Al	5.137	4.754	4.733	4.738	4.704	4.668	4.631	4.631	4.625	4.652	4.620
Fe	0.185	0.203	0.216	0.212	0.199	0.203	0.189	0.201	0.219	0.203	0.209
Mn	0.002	0.000	0.000	0.000	0.005	0.006	0.000	0.002	0.015	0.000	0.006
Mg	0.345	0.534	0.539	0.551	0.550	0.557	0.585	0.553	0.569	0.532	0.579
Ca	0.013	0.000	0.004	0.001	0.004	0.000	0.008	0.006	0.015	0.011	0.000
Na	0.267	0.223	0.225	0.179	0.199	0.231	0.204	0.200	0.186	0.194	0.173
K	1.654	1.639	1.662	1.650	1.649	1.674	1.666	1.651	1.644	1.664	1.685
P	0.000	0.000	0.000	0.003	0.000	0.000	0.000	0.000	0.000	0.000	0.000
S	0.003	0.003	0.000	0.002	0.000	0.000	0.010	0.002	0.002	0.000	0.012
Cr	0.000	0.011	0.007	0.004	0.000	0.004	0.011	0.004	0.000	0.008	0.000
Co	0.000	0.001	0.000	0.000	0.002	0.000	0.000	0.002	0.000	0.001	0.000
Ni	0.000	0.001	0.000	0.004	0.003	0.001	0.000	0.010	0.000	0.001	0.004
Total	13.999	13.958	13.980	13.942	13.944	13.981	13.959	13.936	13.938	13.932	13.954

Appendix 6 Petrographic Descriptions of Dated Samples

Below are presented descriptions of the conglomerate clast and in-situ basement lithologies chosen for isotopic dating. Mineralogy is listed, followed by a brief description of the petrography of the rock.

A6.1 Conglomerate Clasts

A 6.1.1 Dudar Formation Conglomerate clasts

D2:Garnet-Mica Schist

Medium/coarse grained schist. Muscovite, garnet, hornblende, sphene, feldspar, calcite. Calcite appears invasive and may replace some mineral species.

Source within the Mulhacen Unit

D3; Feldspar-Tourmaline Mylonite

Coarse grained augen gneiss. Large feldspar augen and brittley fractured tourmaline porphyroblasts. Quartz, muscovite, plagioclase, microcline, tourmaline. Stretched quartz fabric.

Source within the Mulhacen unit

D4: Garnet-Mica schist

Coarse grained schist. Quartz, muscovite, tourmaline, garnet, chlorite, calcite. Coarse crenulated muscovite foliations.

Source within the Mulhacen Unit

S1: Garnet-Mica-Chloritoid Schist.

Large boulder in Dudar formation above Pinos Genil. Top of coarsening upwards sequence. 1.5 m diameter. Provenance in Veleta unit of the Nevado Filabride complex.

Medium grained schist with crenulated foliation. Muscovite in schistocity with recrystallised quartz. Large Garnet porphyroblasts preserve an earlier deformation fabric recorded in straight quartz inclusion trails. Chloritoid is extensively developed aligned to the schistocity. 2-3% retrograde chlorite mainly on Chloritoid and in Muscovite. Graphitic.

C1B: Garnet-mica Schist

Quartz, muscovite, garnet, tourmaline, opaque oxides, rutile, chlorite. Coarse grained schist. Subhedral garnet porphyroblasts with chlorite alteration. Cracks developed with opaque oxide filling. Muscovite dominantly fresh, some affected by chlorite replacement. Minor euhedral olive green tourmaline.

Source in Mulhacen Unit.

***C1C:** Garnet-Mica Schist*

Quartz, muscovite, garnet, sphene, opaque oxides, calcite, chlorite. Coarse schist. Chlorite alteration of garnets and some micas, otherwise muscovite is very fresh. Garnets are small. Calcite appears associated with muscovites, and possibly replacive.

Source most likely in Veleta Unit.

***C1E:** Garnet-Mica Schist*

Quartz, muscovite, garnet, zoisite/epidote group mineral, tourmaline, calcite. Coarse grained schist. Recrystallised quartz, with poorly defined foliation picked out by fresh muscovites., surrounds euhedral garnets and minor tourmaline and rutile. Calcite appears to be invasive.

Source probably within the Mulhacen Unit.

***C8A:** Garnet-Mica schist.*

Quartz, muscovite, garnet, tourmaline, sphene, chlorite. Coarse grained schist with large garnet porphyroblasts with straight pre-tectonic inclusion trails. Garnets thinly mantled with retrogressive chlorite. Tourmaline present in small euhedral crystals. Minor Sphene is also present.

***C8C:** Garnet-Mica Schist*

Quartz, muscovite, garnet, tourmaline, chlorite. Coarse grained schist with prominent folded schistocity., defined by extensive foliated graphitic muscovite. Garnets and muscovites are slightly chloritised. Tourmaline is minor.

Source probably in the Veleta Unit.

***C11D:** Quartz-Mica-Amphibole schist*

Quartz, muscovite, hornblende, epidote, garnet, tourmaline, zoisite/clinozoisite, chlorite, calcite. Coarse grained schist with crenulated earlier foliation. Garnet porphyroblasts, muscovite altered in places to chlorite but mostly fresh. Calcite appears replacive in some areas, and spatially associated with quartz/feldspar vein.

Source within the Mulhacen units.

***C11B:** Garnet-Mica Schist*

Quartz, muscovite, garnet, chlorite, calcite, rutile. Medium to coarse grained schist with small subhedral garnets. Muscovite defining schistocity is largely fresh, but some is chlorite altered. Calcite possibly replacing earlier phases.

Sourced most probably from the Veleta unit.

***C19C:** Quartz-Mica Schist*

Quartz, muscovite, rare tourmaline, opaque oxides. Medium grained schist, with muscovite foliations, in straight schistocity, spaced by recrystallised quartz. Extremely fresh mineralogy, no alteration of muscovites.

A6.1.2 Pinos Genil Formation Clasts

SAF B: Garnet-Mica Schist

Quartz, muscovite, garnet, chlorite, tourmaline, sphene. Coarse grained schist. Large garnets concentrated in micaceous zones, both with slight chlorite alteration. Calcite is invasive and associated with some opaque oxide staining. Muscovite is dominantly fresh. Tourmaline is small, as is sphene.

Source most likely in the Mulhacen Unit.

SAF 1A: Garnet-Mica-Zoisite Schist

Quartz, muscovite, garnet, zoisite, rutile. Medium grained schist. Highly recrystallised polygonal quartz, with euhderal garnets and very fresh muscovite in the main foliation. Garnets show some chlorite alteration around rims.

Source within the Mulhacen Unit.

SAF 2E: Garnet-Mica Schist

Quartz, muscovite, garnet, tourmaline, sphene, chlorite.

Medium grained schist. Garnets small and euhedral, altering to chlorite around rims. Muscovite is dominantly fresh, though some is affected by chlorite alterations. Muscovite forms prominent foliation in this rock, evenly spaced, and a little graphitic. Tourmaline and rutile occur as small grains.

P2: Garnet-tourmaline-mica schist

Mica, quartz, garnet, tourmaline., sphene. Coarse grained schist, large garnet porphyroblasts with chlorite alteration.

A6.2 Basement / Source Rocks

A 6.2.1 Nevado Filabride

UTH 1 : Feldspar-Tourmaline Mylonite

Detachment zone within the Mulhacen complex, at approximately 2000m elevation.

Quartz, feldspar, tourmaline, zoisite/epidote group minerals, muscovite, sphene. Highly strained bands of quartz, with large alkali feldspar augen and deep blue tourmaline porphyroblasts. Zoisite/epidote type mineral occurs in discrete band within mylonitic foliation. Muscovite is rare, but other similar lithologies are more micaceous. This description is representative of conglomerate clast P2, which shares the same mineralogy, but a less extremely strained texture.

UTH3: Garnet-Mica-Epidote Schist.

In-situ Mulhacen group of the Nevado Filabride complex, at 2250m elevation in Sierra Nevada.

Medium grained with prominent schistocity defined by coarse muscovite and re crystallised quartz unaffected by later folding/crenulation. Large Garnet porphyroblasts have S shaped inclusion

trails recording syn-tectonic mineral growth. The inclusion fabric in some crystals merges at the edge of the crystal with the dominant fabric of the rock. Epidote is well developed aligned along the foliation occurring as lozenge shaped crystals. Minor tourmaline is present as small euhedral crystals again aligned in the foliation.

C2: Garnet-Amphibole-Mica Schist

In-situ from the Mulhacen group of the Nevado Filabride Complex.

A coarse grained schist with a moderately developed foliation. Large subhedral Garnet porphyroblasts contain pre-tectonic inclusion trails while a second later euhedral group contain no inclusions. Green amphibole is extensive and poikiolitic, enclosing quartz, mica and even Garnet. Tourmaline is present in small euhedral crystals. Very small grains of a dark brown mineral, possibly rutile or sphene are present also.

VE: Garnet-Mica Schist

From the Veleta Unit , at 2500m elevation in the Sierra Nevada.

Quartz, muscovite, garnet, chlorite, feldspar, tourmaline. Coarse grained schist. Prominent foliation defined by graphitic muscovite, suffering some alteration to brown oxides and chlorite. Garnets are small and altered to chlorite. Feldspar occurs as augen with opaque oxide rims and crack infills. Tourmaline is small and uncommon

A 6.2.2 Alpujarride Complex

UTH4: Mica-Schist

Within the Alpujarride Complex, around 1200m elevation in Sierra Nevada.

Quartz, muscovite, biotite, garnet, alkali feldspar. Fine grained schist. Single prominent foliation defined by equally spaced micas. Muscovite and biotite are very fresh.

QR1: Garnet-Mica-Staurolite Schist

'Black Schist' from top of Alpujarride beneath unconformity with the earliest sediments of the Granada Basin.

Quartz, feldspar, muscovite, biotite, staurolite, tourmaline. Crenulated schistocity defined by graphitic muscovite and biotite, surrounds garnets. Garnet is slightly altered and retrogressed. Staurolite occurs in pressure shadow areas near garnet porphyroblasts. Tourmaline is rare and very small.

ALP4:Phyllite

Low grade, fine grained quartz-mica schist cut by numerous quartz veins. Quartz recrystallised and sutured grain contacts.

References

Akkerman, J. H., G. Maier, and O. J. Simon, 1980, On the geology of the Alpujarride complex in the western Sierra de las Estancias (Betic Cordilleras, SE Spain): Geologie en Mijnbouw, v. 59, p. 363-374.

Allen, P. A., and J. R. Allen, 1990, Basin Analysis Principles and Applications, Blackwell Scientific Publications, 451 p.

Allen, P. A., P. Homewood, and G. D. Williams, 1986, Foreland basins: an introduction, *in* P. A. Allen, P. Homewood, and G. D. Williams, eds., Foreland Basins: Spec. Pub. Int. Ass. Sediment., p. 3-12.

Allerton, S., L. Longeran, J. P. Platt, E. S. Platzman, and E. McClelland, 1993, Palaeomagnetic rotations in the eastern Betic Cordillera, southern Spain: Earth and Planetary Science Letters, v. 119, p. 225-241.

Allerton, S., K. Reicherter, and J. P. Platt, 1994, A structural and palaeomagnetic study of a section through the eastern Subbetic, southern Spain: Journal of the Geological Society, London, v. 151, p. 659-668.

Allmendinger, R. W., T. A. Hauge, E. C. Hauser, C. J. Potter, and J. Oliver, 1987, Tectonic heredity and the layered lower crust in the Basin and Range Province, western United States, *in* M. P. Coward, J. F. Dewey, and P. L. Hancock, eds., Continental Extensional Tectonics: Geological Society Special Publication, p. 223-246.

Applegate, J. D. R., J. D. Walker, and K. V. Hodges, 1992, Late Cretaceous extensional unroofing in the Funeral Mountains metamorphic core complex: Geology, v. 20, p. 519-522.

Argast, S., and T. W. Donnelly, 1987, The chemical discrimination of clastic sedimentary components: Journal of Sedimentary Petrology, v. 57, p. 813-823.

Atwater, T., 1970, Implications of plate tectonics for the Cenozoic Tectonic evolution of western North America: Geological Society of America Bulletin, v. 81, p. 3513-3536.

Bluck., B.J., 1978, Sedimentation in a late orogenic basin: the Old Red Sandstone of the Midland Valley of Scotland, *in* D. R. Bowes, and B. E. Leake, eds., Crustal Evolution in Northwestern Britain and Adjacent Regions: Geol. Soc. Spec. Pub. No. 10, p. 249-278.

Bakker, H., 1991, The structural configuration of the eastern Sierra de los Filabres, SE Spain: Geologie en Mijnbouw, v. 70, p. 287-298.

Bakker, H. E., K. De Jong, H. Helmers, and C. Biermann, 1989, The geodynamic evolution of the Internal Zone of the Betic Cordilleras (south-east Spain): a model based on structural analysis and geothermobarometry: Journal of Metamorphic Geology, v. 7, p. 359-381.

Bally, A. W., and S. Snelson, 1980, Realms of subsidence, *in* A. D. Miall, ed., Facts and Principles of World Petroleum Occurrence: Mem. Can. Soc. Petrol. Geol., p. 9-75.

Banda, E., and J. Ansorge, 1980, Crustal structure under the central and eastern part of the Betic Cordillera: Geophysical Journal of the Royal Astronomical Society, v. 63, p. 515-532.

Banks, C. J., and J. Warburton, 1991, Mid-crustal detachment in the Betic system of southeast Spain: Tectonophysics, v. 191, p. 275-289.

Beaumont, C., 1981, Foreland basins: Geophysical Journal of the Royal Astronomical Society, v. 65, p. 291-329.

Bellon, H., P. Bordet, and C. Monenat, 1983, Chronologie du magmatisme neogene des Cordilleres Betiques (Espagne meridionale): Bull. Soc. geol. France, v. 7, p. 205-217.

Bhatia, M. R., 1983, Plate tectonics and geochemical composition of sandstones: Journal of Geology, v. 91, p. 611-627.

Bhatia, M. R., and A. W. Crook, 1986, Trace element characteristics of graywackes and tectonic setting discrimination of sedimentary basins: Contributions to Mineralogy and Petrology, v. 92, p. 181-193.

Blanco, M. J., and W. Spakman, 1993, The P-wave velocity structure of the mantle below the Iberian Peninsula- evidence for subducted lithosphere below southern Spain: Tectonophysics, v. 221, p. 13-34.

Blankenship, C. L., 1992, Structure and palaeogeography of the External Zone of the Betic Cordillera, southern Spain: Marine and Petroleum Geology, v. 9, p. 256-264.

Blankenship, C. L., 1993, Reply to "To balance or not?" by K. Reicherter: Marine and Petroleum Geology, v. 10, p. 515-516.

Blankenship, C. L., 1993, Reply to comments on "Structure and palaeogeography of the External Betic Cordillera, southern Spain" by Sanz de Galdeano *et. al.* and Molina and Ruiz-Ortiz: Marine and Petroleum Geology, v. 10, p. 521-522.

Bluck, B. J., 1980, Evolution of a strike-slip fault controlled basin, Upper Old Red Sandstone, Scotland: Special Publication of the International Association of Sedimentologists, p. 63-78.

Bluck, B. J., 1990, Terrane provenance and amalgamation: examples from the Caledonide: Philosophical Transactions of the Royal Society of London, v. 331, p. 599-609.

Bluck, B. J., and T. J. Dempster, 1991, Exotic metamorphic terranes in the Caledonides: Tectonic history of the Dalradian block, Scotland: Geology, v. 19, p. 1133-1136.

Bocaletti, M., R. Gelati, and A. C. Lopez-Garrido, 1987, Neogene-Quarternary sedimentary tectonic evolution of the Betic Cordillera: Acta Naturalia de lAteneo Parmense, v. 23, p. 179-200.

Bramlette, M. N., 1941, The Stability of Minerals in Sandstone: Journal of Sedimentary Petrology, v. 11, p. 610-625.

Brown, G. C., and A. E. Mussett, 1981, The Inaccessible Earth: London, George, Allen and Unwin, 235 p.

Brun, J., D. Sokoutis, and J. Van Den Driessche, 1994, Analogue modelling of detachment fault systems and core complexes: Geology, v. 22, p. 319-322.

Buck, W. R., 1988, Flexural rotation of normal faults: Tectonics, v. 7, p. 959-973.

Buforn, E., A. Udias, and M. A. Colombas, 1988, Siesmicity, source mechanisms and tectonics of the Azores-Gibraltar plate boundary: Tectonophysics, p. 89-118.

Cabrera, J., M. Sebrier, and J. L. Mercier, 1987, Active normal faulting in High Plateaus of Central Andes: the Cuzco Region (Peru): Annales Tectonicae, v. 1, p. 116-138.

Campillo, A. C., A. Maldonado, and A. Mauffret, 1992, Stratigraphic and Tectonic Evolution of the Western Alboran Sea: Late Miocene to Recent: Geo-Marine Letters, v. 12, p. 165-172.

Channell, J. E. T., 1986, Palaeomagnetism and continental collision in the Alpine Belt and the formation of late-tectonic extensional basins, *in* M. P. Coward, and A. C. Reis, eds., Collision Tectonics: Geological Society Special Publication, p. 261-284.

Chopin, C., and H. Maluski, 1980, $^{40}Ar/^{39}Ar$ Dating of High Pressure Metamorphic Micas From the Gran Paradiso Area (Western Alps): Evidence Against the Blocking Temperature Concept: Contributions to Mineralogy and Petrology, v. 74, p. 109-122.

Clauer, N., 1981, Strontium and argon isotopes in naturally weathered biotites, muscovites and feldspars: Chemical Geology, v. 31, p. 325-334.

Cliff, R. A., 1985, Isotopic dating in metamorphic belts: Journal of the Geological Society, London, v. 142, p. 97-110.

Coney, P. J., 1980, Cordilleran metamorphic core complexes: An overview, *in* M. P. Crittenden, P. J. Coney, and G. H. Davis, eds., Cordilleran Metamorphic Core Complexes: Geological Society of America Memoir 153, p. 7-13.

Coney, P. J., 1987, The regional tectonic setting and possible causes of Cenozoic extension in the North American Cordillera, *in* M. P. Coward, J. F. Dewey, and P. L. Hancock, eds., Continental Extensional Tectonics: Geological Society Special Publication.

Coney, P. J., and T. A. Harms, 1984, Cordilleran metamorphic core complexes: Cenozoic extensional relicts of Mesozoic compression: Geology, v. 12, p. 550-554.

Copeland, P., and T. M. Harrison, 1990, Episodic rapid uplift in the Himalaya revealed by $^{40}Ar/^{39}Ar$ analysis of detrital K-feldspar and muscovite, Bengal Fan: Geology, v. 18, p. 354-357.

Copeland, P., T. M. Harrison, and M. T. Heizler, 1990, $^{40}Ar/^{39}Ar$ single-crystal dating of detrital muscovite and K-feldspar from leg 116, southern Bengal Fan: implications for the uplift and erosion of the Himalayas: Proceedings of the Ocean Drilling Program, Scientific Results, v. 116, p. 93-114.

Copeland, P., T. M. Harrison, W. S. F. Kidd, X. Ronghua, and Z. Yuquan, 1987, Rapid early Miocene acceleration of uplift in the Gangdese Belt, Xizang (southern Tibet), and its bearing on accommodation mechanisms of the India-Asia collision: Earth and Planetary Science Letters, v. 86, p. 240-252.

Cox, A., and R. B. Hart, 1986, Plate Tectonics: How it works: Palo Alto California, Blackwell Scientific Publications, 392 p.

Cox, R., and D. R. Lowe, 1995, Compositional evolution of coarse clastic sediments in the southwestern United States from 1.8 to 0.2 Ga and implications for relationships between the development of crustal blocks and their sedimentary cover: Journal of Sedimentary Research, v. A65, p. 477-494.

Cronin, V. S., 1989, Structural Setting of the Skardu intermontane basin, Karkoram Himalaya, Pakistan: Geological Society of America Special Paper 232.

Crowell, J. C., 1974, Origin of Late Cenozoic basins in southern California, *in* W. R. Dickinson, ed., Tectonics and Sedimentation: Society of Economic Palaeontologists and Mineralogists Special Publication, p. 190-204.

Cullers, R. L., A. Bass, and L. J. Suttner, 1988, Geochemical signature of provenance in sand-size material in soils and stream sediments near the Tobacco Root, Montana, U.S.A.: Chemical Geology, v. 70, p. 335-348.

Cuthbert, S. J., 1991, Evolution of the Devonian Hornelen Basin, west Norway: new constraints from petrological studies of metamorphic clasts, *in* A. C. Morton, S. P. Todd, and P. D. W. Haughton, eds., Developments in Sedimentary Provenance Studies: Geological Society Special Publication, p. 343-360.

Dabrio, C. J., and J. Fernandez, 1986, Depositos de rios trenzados conglomeraticos Plio-Pleistocenicos de la depresion de Granada: Cuadernos Geologia Iberica, v. 10, p. 31-53.

Davis, G. H., and P. J. Coney, 1979, Geologic development of the Cordilleran metamorphic core complexes: Geology, v. 7, p. 120-124.

Davis, G. R., P. H. Nixon, D. G. Pearson, and M. Obata, 1993, Tectonic implications of graphitised diamonds from the Ronda peridotite massif, southern Spain: Geology, v. 21, p. 471-474.

De Jong, K., 1990, Alpine tectonics and rotation pole evolution of Iberia: Tectonophysics, v. 184, p. 279-296.

De Jong, K., and H. Bakker, 1991, The Mulhacen and Alpujarride Complex in the eastern Sierra de Los Filabres, SE Spain: Litho-stratigraphy: Geologie en Mijnbouw, v. 70, p. 93-103.

De Jong, K., J. R. Wijbrans, and G. Feraud, 1990, Exhumation and cooling of the Mulahcen HP/LT metamorphic complex, Betic Cordilleras, SE Spain: TERRA abstracts, v. 2.

De Jong, K., J. R. Wijbrans, and G. Feraud, 1992, Repeated thermal resetting of phengites in the Mulhacen Complex (Betic Zone, southeastern Spain) shown by $^{40}Ar/^{39}Ar$ step heating and single grain laser probe dating: Earth and Planetary Science Letters, v. 110, p. 173-191.

De Jong, K., H. P. Zeck, P. Monie, and I. M. Villa, 1992, Comment and Reply on "Very high rates of cooling and uplift in the Alpine belt of the Betic Cordilleras, southern Spain: Geology, v. 10, p. 1052-1054.

De Larouziere, F. D., J. Bolze, P. Bordet, J. Hernandez, C. Montenat, and P. Ott d'Estevou, 1988, The Betic segment of the lithospheric Trans-Alboran shear zone during the ALte Miocene: Tectonophysics, v. 152, p. 41-52.

Deer, W. A., R. A. Howie, and J. Zussman, 1966, An Introduction to the Rock-Forming Minerals, 528 p.

Dempster, T. J., 1985, Uplift patterns and orogenic evolution in the Scottish Dalradian: Journal of the Geological Society, London, v. 142, p. 111-128.

Dempster, T. J., and B. J. Bluck, 1989, The age and origin of boulders in the Highland Border Complex: constraints on terrane movements: Journal of the Geological Society, London, v. 146, p. 377-379.

Dempster, T. J., and B. J. Bluck, 1995, Regional metamorphism in transform zones during supercontinental breakup: Late Proterozoic events of the Scottish Highlands: Geology, v. 23, p. 991-994.

Dewey, J. F., 1988, Extensional Collapse of Orogens: Tectonics, p. 1123-1139.

Dewey, J. F., M. L. Helman, E. Turco, D. H. W. Hutton, and S. D. Knott, 1989, Kinematics of the western Mediterranean, *in* M. P. Coward, M. P. Dietrich, and R. G. Park, eds., Alpine Tectonics: Geological Society Special Publications, p. 265-283.

Diaz De Federico, A., R. L. Torres-Roldan, and E. Puga, 1990, The rock-series of the Betic substratum: Doc. et Trav. IGAL, v. 12-13, p. 19-29.

Dickinson, W. R., 1970, Interpreting detrital modes of graywacke and arkose: Journal of Sedimentary Petrology, v. 40, p. 695-707.

Dickinson, W. R., 1974, Plate Tectonics and Sedimentation, *in* W. R. Dickinson, ed., Tectonics and Sedimentation: Society of Economic Paleontologists and Mineralogists Special Publication, p. 1-27.

Dickinson, W. R., L. S. Beard, G. R. Brakenridge, J. L. Erjavec, R. C. Ferguson, K. F. Inman, R. A. Knepp, F. A. Lindberg, and P. T. Ryman, 1983, Provenance of North AMerican Phanerozoic sandstones in relation to tectonic setting: Geological Society of America Bulletin, v. 94, p. 222-235.

Dickinson, W. R., and C. A. Suczek, 1979, Plate tectonics and sandstone compositions: Bull. Am. Ass. Petrol. Geol., v. 63, p. 2164-2182.

Doblas, M., and R. Oyarzun, 1989, Neogene extensional collapse in the western Mediterranean (Betic-Rif Alpine orogenic belt): Implications for the genesis of the Gibraltar Arc and magmatic activity: Geology, v. 17, p. 430-433.

Dodson, M. H., 1973, Closure Temperature in Cooling Geochronological and Petrological Systems: Contributions to Mineralogy and Petrology, v. 40, p. 259-274.

Dorsey, R. J., 1988, Provenance evolution and unroofing history of a modern arc-continent collision: evidence from petrography of Plio-Pliestocene sandstones, eastern Tiawan: Journal of Sedimentary Petrology, v. 58, p. 208-218.

Dryden, L., and C. Dryden, 1946, Comparitive Rates of Weathering of Some Common Heavy Minerals: Journal of Sedimentary Petrology, v. 16, p. 91-96.

Dunham, R. J., 1962, Classification of carbonate rocks according to depositional texture, *in* W. E. Ham, ed., Classification of Carbonate Rocks: Memoir, American Association of Petroleum Geologists, No. 1, Tulsa.

Egeler, C. G., and O. J. Simon, 1969, Orogenic evolution of the Betic Zone (Betic Cordilleras, Spain), with emphasis on the Nappe Structures: Geologie en Mijnbouw, v. 48, p. 296-305.

El Fegi, M. S., 1989, Petrography and Geochemistry of Lower Paleozoic Sandstone Sequence, Girvan: Ph.D. thesis, University of Glasgow.

England, P. C., and S. W. Richardson, 1977, The influence of erosion upon the facies of rocks from different metamorphic environments: Journal of the Geological Society, London, v. 134, p. 201-213.

Fernandez, J., B. J. Bluck, and C. Viseras, 1991, A lacustrine fan-delta system in the Pliocene deposits of the Guadix Basin (Betic Cordilleras, South Spain): Cuadernos de Geologia Iberica, v. 15, p. 299-317.

Fernandez, J., and J. Rodrigiez-Fernandez, 1991, Facies evolution of nearshore marine clastic deposits during the Tortonian transgression-Granada Basin, Betic Cordilleras, Spain: Sedimentary Geology, v. 71, p. 5-21.

Fitch, F. J., J. A. Miller, and D. B. Thompson, 1966, The palaeogeoghraphic significance of isotopic age determinations on detrital micas from the Triassic of the Stockport-Macclesfield district, Cheshire, England: Palaeogeography, Palaeoclimatology, Palaeoecology, v. 2, p. 281-312.

Folk, R. L., 1962, Spectral subdivision of limestone types, *in* W. E. Ham, ed., Classification of Carbonate Rocks: Memoir, American Association of Petroleum Geologists, No. 1, Tulsa.

Friend, P. F., 1985, Molasse basins of Europe: a tectonic assessment: TRansactions of the Royal Society of Edinburgh: Earth Sciences, v. 76, p. 451-462.

Garcia-Hernandez, M., A. C. Lopez-Garrido, P. Rivas, C. Sanz de Galdeono, and J. A. Vera, 1980, Mesozoic palaeogeographic evolution of the External Zones of the Betic Cordillera: Geologie en Mijnbouw, v. 59, p. 155-168.

Gautier, P., and J. P. Brun, 1993, Structure and kinematics of Upper Cenozoic extensional detachment on Naxos and Paros (Cyclades Islands, Greece): Tectonics, v. 12, p. 1180-1194.

Girty, G. H., 1991, A note on the composition of plutoniclastic sand produced in deifferent climactic belts: Journal of Sedimentary Petrology, v. 61, p. 428-433.

Girty, G. H., B. J. Mossman, and S. D. Pincus, 1988, Petrology of Holocene sand, Peninsular Ranges, California and Baja Norte, Mexico: implications for provenance-discrimination models: Journal of Sedimentary Petrology, v. 58, p. 881-887.

Goldich, S. S., 1938, A study in rock weathering: Journal of Sedimentary Petrology, v. 4, p. 89-95.

Gomez-Pugnaire, M. T., J. Chacon, F. Mitrofanov, and V. Timofeev, 1982, First report on the Pre-Cambrian rocks in the graphite bearing series of the Nevado-Filabride complex (Betic Cordilleras, Spain): Neues Jahrb. Geol. Palaeontology Monash, v. 3, p. 176-180.

Gomez-Pugnaire, M. T., and J. M. Fernadez-Soler, 1987, Highe-pressure metamorphism in metabasites from the Betic Cordilleras (S.E. Spain) and its evolution during the Alpine Orogeny: Contributions to Mineralogy and Petrology, v. 95, p. 231-244.

Graham, J. R., J. P. Wrafte, J. S. Daly, and J. F. Menuge, 1991, A local source for the Ordivician Derryveeny Formation, western Ireland: implications for the Connemara Dalradian, *in* A. C. Morton, S. P. Todd, and P. D. W. Haughton, eds., Developments in Sedimentary Provenance Studies: Geological Society Special Publication, p. 199-213.

Graham, S. A., R. V. Ingersoll, and W. R. Dickinson, 1976, Common provenance for lithic grains in Carboniferous sandstones from Ouachita Mountains and Black Warrior Basin: Journal of Sedimentary Petrology, v. 46, p. 620-632.

Graham, S. A., R. B. Tolson, P. G. Decelles, R. V. Ingersoll, E. Bargar, M. Caldwell, W. Cavazza, D. P. Edwards, M. F. Follo, J. F. Handschy, L. Lemke, I. Moxon, R. Rice, G. A. Smith, and J. White, 1986, Provenance modelling as a technique for analysing source terrane evolution and controls on foreland basin sedimentation, Foreland Basins: Special Publication of the International Association of Sedimentologists, p. 425-436.

Grantham, J. H., and M. A. Velbel, 1988, The influence of climate and topography on rock-fragment abundance in modern fluvial sands of the southern Blue Ridge Mountains, North Carolina: Journal of Sedimentary Petrology, v. 58, p. 219-227.

Harland, W. B., R. L. Armstrong, V. A. Cox, L. E. Craig, A. G. Smith, and D. G. Smith, 1990, A geologic time scale, 263 p.

Harrison, T. M., 1983, Some observations on the interpretation of $^{40}Ar/^{39}Ar$ age spectra: Isotope Geoscience, v. 1, p. 319-338.

Haughton, P. D. W., 1988, A cryptic Caledonian Flysch terrane in Scotland: Journal of the Geological Society, London, v. 145, p. 685-703.

Haughton, P. D. W., and C. M. Farrow, 1989, Compositional variation in Lower Old Red Sandstone detrital garnets from the Midland Valley of Scotland and the Anglo-Welsh Basin: Geological Magazine, v. 126, p. 373-396.

Haughton, P. D. W., and A. N. Halliday, 1991, Significance of a late Caledonian igneous complex revealed by clasts in Lower Old Red Sandstone conglomerates: Geological Society of America Bulletin, v. 103, p. 1476-1492.

Haughton, P. D. W., S. P. Todd, and A. C. Morton, 1991, Sedimetary Provenance Studies, *in* A. C. Morton, S. P. Todd, and P. D. W. Haughton, eds., Developments in Sedimentary Provenance Studies: Geological Society Special Publication, p. 1-11.

Hebeda, E. H., N. A. I. M. Boelrijk, H. N. A. Priem, E. A. T. Verdurmen, and R. H. Verschure, 1980, Excess radiogenic Ar and undisturbed Rb-Sr systems in basic intrusives subjected to Alpine metamorphism in southeastern Spain: Earth and Planetary Science Letters, v. 47, p. 81-90.

Herron, M. M., 1987, Geochemical classification of terrigenous sands and shales from core or log data: Journal of Sedimentary Petrology, v. 58, p. 820-829.

Hill, E. J., S. L. Baldwin, and G. S. Lister, 1992, Unroofing of active metamorphic core complexes in the D'Entrecasteaux: Geology, v. 20, p. 907-910.

Hirst, J. P. P., and G. J. Nichols, 1986, Tectonic controls on Miocene alluvial distribution patterns, southern Pryrenees, *in* P. A. Allen, P. Homewood, and G. D. Williams, eds., Foreland Basins: Spec. Pub. Int. Ass. Sediment.

Holm, D. K., and R. K. Dokka, 1993, Interpretation and tectonic implications of cooling histories: An exampl from the Black Mountains, Death Valley extended terrane, California: Earth and Planetary Science Letters, v. 116, p. 63-80.

Houghton, H. F., 1980, Refined techniques for staining plagioclase and alkali feldspars in thin section: Journal of Sedimnetary Petrology, v. 50, p. 629-631.

Houghton, H. F., 1980, Refined techniques for staining plagioclase and alkali feldspars in thin section: Journal of Sedimentary Petrology, v. 50, p. 629-631.

Hurford, A. J., 1991, Uplift and cooling pathways derived from fission track analysis and mica dating: a review: Geologische Rundschau, v. 80, p. 349-368.

Ingersoll, R. V., 1988, Tectonics of sedimentary basins: Geological Society of America Bulletin, v. 100, p. 1704-1719.

Ingersoll, R. V., T. F. Bullard, R. L. Ford, J. P. Grimm, J. D. Pickle, and S. W. Sares, 1984, The effect of grain size on detrital modes: a test of the Gazzi-Dickinson point-counting method: Journal of Sedimentary Petrology, p. 103-116.

Ingersoll, R. V., and C. A. Suczek, 1979, Petrology and Provenance of Neogene sand from Nicobar and Bengal Fans, DSDP sites 211 and 218: Journal of Sedimentary Petrology, v. 51, p. 1247-1258.

Irwin, J. I., C. Kirschbaum, T. H. Lim, D. Powell, and W. E. Glassley, 1989, A laser-microprobe study of argon isotopes in deformed pegmatites from the Northern Highlands of Scotland, *in* J.

S. Daly, R. A. Cliff, and B. D. W. Yardley, eds., Evolution of Metamorphic Belts: Geological Society Special Publication, p. 149-160.

Johnson, K., 1994, Differentiating the tectonic and erosive components of denudation using fission track analysis: a case study from S.E. Spain: ICOG-8 Abstracts.

Jordan, T. E., 1981, Thrust loads and Foreland Basin evolution, Cretaceous western United States: Bull. Am. Ass. Petrol. Geol., v. 65, p. 2506-2520.

Kampschuur, W., and H. E. Rondeel, 1975, The origin of the Betic Orogen, southern Spain: Tectonophysics, v. 27, p. 39-56.

Karig, D. E., 1971, Origin and development of marginal basins in the western Pacific: Journal of Geophysical Research, v. 76, p. 2542-2561.

Keen, C. E., 1987, Some important consequences of lithospheric extension, *in* M. P. Coward, J. F. Dewey, and P. L. Hancock, eds., Continental Extensional Tectonics: Geol. Soc. Spec. Pub. No. 28, p. 67-74.

Kelly, S. P., and B. J. Bluck, 1989, Short paper: Detrital mineral ages from the Southern Uplands using $^{40}Ar/^{39}Ar$ laser probe: Journal of the Geological Society, London, v. 146, p. 401-403.

Kelly, S. P., and B. J. Bluck, 1992, Laser $^{40}Ar/^{39}Ar$ ages for individual detrital muscovites in the Southern Uplands of Scotland, U.K.: Chemical Geology (Isotope Geoscience Section), v. 101, p. 143-156.

KIngston, D. R., C. P. Dishroon, and P. A. Williams, 1983, Global Basin Classification System: The American ASsociation of Petroleum Geologists Bulletin, v. 67, p. 2175-2193.

Kingston, D. R., C. P. Dishroon, and P. A. Williams, 1983, Hydrocarbon Plays and Global Basin Classification: The American ASsociation of Petroleum Geologists Bulletin, v. 67, p. 2194-2198.

Klein, G. d., 1987, Current aspects of basin analysis: Sedimentary Geology, v. 50, p. 95-118.

Krynine, P. D., 1942, Provenanace Versus Mineral Stability as a Controlling Factor in the Composition of Sediments: Geological Society of America, Bulletin, v. 53, p. 1850-1851.

Krynine, P. D., 1946, The tourmaline group in sediments: The Journal of Geology, v. 54, p. 65-87.

Kuznir, N. J., and R. G. Park, 1987, The extensional strength of the continental lithosphere: its dependence on geothermal gradient and crustal composition and thickness, *in* M. P. Coward, J. F. Dewey, and P. L. Hancock, eds., Continental Extensional Tectonics: Geol. Soc. Spec. Pub. No. 28, p. 35-52.

Le Pichon, X., 1983, Land locked Oceanic basins and Continental Collision: the Eastern Mediterranean as a case example, *in* K. J. Hsu, ed., Mountain Building Processes, p. 201-212.

Lee, J., 1991, Incremental $^{40}Ar/^{39}Ar$ thermochronology of mylonitic rocks from the northern Snake Range, Nevada: Tectonics, v. 10, p. 77-100.

Lee, J. K. W., T. C. Onstott, K. V. Cashman, R. J. Cumbest, and D. Johnson, 1991, Incremental heating of hornblende in vacuo: implications for $^{40}Ar/^{39}Ar$ geochronology and the interpretation of thermal histories: Geology, v. 19, p. 872-876.

Leeder, M. R., and R. L. Gawthorpe, 1987, Sedimentary models for extensional tilt-block/half-graben basins, *in* M. P. Coward, J. F. Dewey, and P. L. Hancock, eds., Continental Extensional Tectonics: Geol. Soc. Spec. Pub. No. 28.

Lister, G. S., G. Banga, and A. Feenstra, 1984, Metamorphic core complexes of Corilleran type in the Cyclades, Aegean Sea, Greece: Geology, v. 12, p. 221-225.

Lister, G. S., and G. A. Davis, 1989, The origin of metamorphic core complexes and detachment faults formed during Tertiary continental extension in the northern Colorado River region, U.S.A.: Journal of Structural Geology, v. 11, p. 65-94.

Livaccari, R. F., J. W. Geissman, and S. J. Reynolds, 1993, Palaeomagnetic evidence for large-magnitude, low angle normal faulting in a metamorphic core complex: Nature, v. 361, p. 56-59.

Longeran, L., and M. A. Mange-Rajetzky, 1994, Evidence for Internal Zone unroofing from foreland basin sediments, Betic Cordillera, SE Spain: Journal of the Geological Society, London, v. 151, p. 515-529.

Loomis, T. P., 1975, Teriary mantle diaporism, orogeny, and plate tectonics east of the Strait of Gibraltar: American Jounal of Science, v. 275, p. 1-30.

Luepke, G., 1984, Stability of Heavy Minerals in Sediments, Benchmark Papers in Geology Series.

Mack, G. H., 1984, Exceptions to the relationship between Plate Tectonics and sandstone composition: Journal of Sedimentary Petrology, v. 54, p. 212-220.

Malavielle, J., 1993, Late orogenic extension in moutain belts: insights from the Basin and Range and the late Phanerozoic Variscan belt: Tectonics, v. 12, p. 1115-1130.

Malavielle, J., P. Guihot, S. Costa, J. M. Lardeaux, and V. Gardien, 1990, Collapse of thickened Variscan crust in the French Massif Central: Mont Pilat extensional shear zone and St. Etienne late Carboniferous basin: Tectonophysics, v. 177, p. 139-149.

Mange, M. A., and H. F. W. Maurer, 1992, Heavy Minerals in Colour, 147 p.

Maynard, J. B., R. Valloni, and H.-S. Yu, 1982, Composition of modern deep-sea sands from arc-related basins, *in* J. K. Leggett, ed., Trench-forearc geology: sedimentation and tectonics on modern and ancient active plate margins: Geological Society Special Publication, p. 551-561.

McDougall, I., and T. M. Harrison, 1988, Geochronology and Thermochronology by the 40Ar/39Ar Method: New York, Oxford University Press.

McKenzie, D., 1978, Some remarks on the development of sedimentary basins: Earth and Planetary Science Letters, v. 40, p. 12-32.

Miall, A. D., 1990, Principles of Sedimentary Basin Analysis, 668 p.

Middleton, G. V., 1960, Chemical compositionm of sandstones: Bulletin of the Geological Society of America, v. 71, p. 1011-1026.

Milliken, K. L., 1988, Loss of Provenance information through subsurface diagenesis in Plio-Pliestocene sandstones, Northern Gulf of Mexico: Jour. of Sed. Pet., v. 58, p. 992-1002.

Mitchell, J. G., and A. S. Taka, 1984, Potassium and argon loss patterns in weathered micas: implications for detrital mineral studies, with particular reference to the Triassic palaeogeography of the British Isles: Sedimentary Geology, v. 39, p. 27-52.

Molina, J. M., and P. A. Ruiz-Ortiz, 1993, DIscussion of "Stratigraphy and paleogeography of the External Betic Cordillera, southern Spain" by C.L. Blankenship: Marine and Petroleum Geology, v. 10, p. 516-518.

Molnar, P., and P. Tapponier, 1975, Cenozoic Tectonics of Asia: effects of a continental collision: Science, v. 189, p. 419-426.

Monie, P., J. Galindo-Zaldivar, F. Gonzalez Lodeiro, B. Goffe, and A. Jabaloy, 1991, $^{40}Ar/^{39}Ar$ geochronology of Alpine tectonism in the Betic Cordilleras (southern Spain): Journal of the Geological Society, London, v. 148, p. 289-297.

Monie, P., H. Maluski, A. Saadallah, and R. Caby, 1988, New 40Ar-39Ar ages of Hercynian and Alpine thermotectonic events in Grande Kabylie (Algeria): Tectonophysics, v. 152, p. 53-69.

Montenat, C., P. Ott D'Estevou, and P. Masse, 1987, Tectonic-sedimentary characters of the Betic Neogene basins evolving in a crustal transcurrent shear zone (SE Spain): Bull. Cent. Rech. Explor.-Prod Elf-Aquitaine, v. 11, p. 1-22.

Morton, A. C., 1979, Surface features of heavy mineral grains from Palaeocene sands of the central North Sea: Scotish Journal of Geology, v. 15, p. 293-300.

Morton, A. C., 1981, Stability of detrital heavy minerals in Tertiary sandstones from the North Sea Basins.: Clay Minerals, v. 19, p. 287-308.

Morton, A. C., 1985, A new approach to provenance studies: electron microprobe analysis of detrital garnets from Middle Jurassic sandstones of the northern North Sea: Sedimentology, v. 32, p. 553-566.

Morton, A. C., 1987, Influences of provenance and diagenesis on detrital garnet suites in the Paleocene Forties sandstone, cenral North Sea: Journal of Sedimentary Petrology, v. 57, p. 1027-1032.

Morton, A. C., 1991, Geochemical studies of detrital heavy minerals and their application to provenance research, *in* A. C. Morton, S. P. Todd, and P. D. W. Haughton, eds., Developments in Sedimentary Provenance Studies: Geological Society Special Publication, p. 31-45.

Munro, A., 1995, Soft sediment deformation associated with core-complex rise in the Sierra Nevada, Betic Cordillera, Southern Spain: M.Sc. Thesis, University of Glasgow.

Nelson, K. D., 1992, Are crustal thickness variations in old mountain belts like the Appalachians a consequence of lithospheric delamination: Geology, v. 20, p. 489-502.

Nesbitt, H. W., 1979, Mobility and fractionation of rare earth elements during weathering of a granodiorite: Science, v. 279, p. 206-210.

Nesbitt, H. W., N. D. MacRae, and B. I. Kronberg, 1990, Amazon deep-sea fan muds: light REE enriched products of extreme chemical weathering: Earth and Planetary Science Letters, v. 100, p. 118-123.

Nesbitt, H. W., and G. M. Young, 1989, Formation and diagenesis of weathering profiles: Journal of Geology, v. 97, p. 129-147.

Okonkwo, C. T., 1989, Geochemistry and sedimentology of the GRampian Group metasedimentary rocks, Upper Strathspey: Scottish Journal of Geology, v. 25, p. 239-248.

Parsons, T., and G. A. Thompson, 1993, Does magmatism influence low-angle normal faulting?: Geology, v. 21, p. 247-250.

Pettijihn, F. J., 1975, Sedimentary Rocks, 628 p.

Pettijohn, F. J., 1941, Persistence of Heavy Minerals in Sandstone: Journal of Geology, v. 46, p. 610-625.

Pettijohn, F. J., 1954, Classification of sandstones: Journal of Geology, v. 62, p. 360-365.

Pettijohn, F. J., P. E. Potter, and R. Siever, 1972, Sand and Sandstone, Springer-Verlag.

Platt, J. P., 1982, Emplacement of a fold-nappe, Betic orogen, southern Spain: Geology, v. 10, p. 97-102.

Platt, J. P., 1986, Dynamics of orogenic wedges and the uplift of high pressure metamorphic rocks: Geological Society of America Bulletin, v. 97, p. 1037-1053.

Platt, J. P., and R. L. M. Vissers, 1989, Extensional collapse of thickened continental lithosphere: A working hypothesis for the Alboran Sea and Gibraltar arc: Geology, v. 17, p. 540-543.

Platzman, E. S., 1992, Palaeomagnetic rotations and the kinematics of the Gibraltar arc: Geology, v. 20, p. 311-314.

Platzman, E. S., J. P. Platt, and P. Olivier, 1993, palaeomagnetic rotations and fault Kinematics in the Rif Arc of Morocco: Journal of the Geological Society, London, v. 150, p. 707-718.

Power, G. M., 1968, Chemical variation in tourmalines from south-west England: Mineralogical Magazine, v. 36, p. 1078-1089.

Priem, H. N. A., N. A. I. M. Boelrijk, E. H. Hebeda, I. S. Oen, E. A. T. Verdurmen, and R. H. Verschure, Isotopic dating of the emplacement of the ultramafic masses in the Serrania de Ronda, southern Spain: Contributions to Mineralogy and Petrology, v. 70, p. 103-109.

Priem, H. N. A., N. A. I. M. Boelrijk, E. H. Hebeda, and R. H. Verschure, 1966, Isotopic age determinations on tourmaline granite gneisses and a metagranite in the eastern Betic Cordillera (south-eastern Sierra de los Filabres), S.E. Spain: Geology en Mijnbouw, v. 45, p. 184-187.

Puga, E., A. Diaz de Federico, E. Fediukova, M. Bondi, and L. Morten, 1989, Petrology, geochemistry and metamorphic evolution of the ophiolitic eclogites and related rocks from the Sierra Nevada (Betic Cordillera, Southeastern Spain): Schweizerische Mineralogische und Petrographische Mitteilungen, v. 69, p. 435-455.

Purdy, J. W., and E. Jager, 1976, K-Ar ages on rock forming minerals from the central Alps: Mem. Ist. Geol. Min. Univ. Padova, v. 30, p. 31.

Reaside, J. D., 1959, Stability of Index Minerals in Soils with Particular Reference to Quartz, Zircon and Garnet: Journa of Sedimentary Petrology, v. 29, p. 493-502.

Reicherter, K., 1993, To balance or not? Comment on "Structure and palaeogeeography of the External BEtic Cordillera, southern Spain", by C.L. Blankenship: Marine and Petroleum Geology, v. 10, p. 514-515.

Rodriguez-Fernandez, J., C. Sanz de Geldeano, and J. Fernandez, 1989, Genesis and Evolution of the Granada Basin (Betic Cordillera, Spain): International Symposium on Intermontane Basins: Geology and Resources.

Roest, W. R., and S. P. Srivastava, 1991, Kinematics of the plate boundaries between Eurasia, Iberia, and Africa in the North Atlantic from the Late Cretaceous to the present: Geology, v. 19, p. 613-616.

Rogers, G., and R. J. Pankhurst, 1993, Unravelling dates through the ages: geochronology of the Scottish metamorphic complexes: Journal of the Geological Society, London, v. 150, p. 447-464.

Roser, B. P., and R. J. Korsch, 1986, Determination of tectonic setting of sandstone-mudstone suites using SiO_2 content and K_2O/Na_2O ratio: Journal of Geology, v. 94, p. 635-650.

Russell, R. D., 1937, Mineral Composition of Mississippi River sands: Bulletin of the Geological Society of America, v. 48, p. 1307-1348.

Samson, S. D., and E. C. Alexander, 1987, Calibration of the interlaboratory 40Ar-39Ar dating standard Mmhb-1: Chemical Geology (Isotope Geosience Section), v. 66, p. 27-34.

Sanz de Galdeano, C., A. Martin Algarra, J. A. Vera, and P. Rivas, 1993, Comments on "Structure and palaeogeography of the External Betic Cordillera, southern Spain" by C.L. Blankenship: Marine and Petroleum Geology, v. 10, p. 518-521.

Sanz de Galdeano, C., and J. A. Vera, 1992, Stratigraphic record and palaeogeographic context of the Neogene basins in the Betic Cordillera, Spain: Basin Research, v. 4, p. 21-36.

Sanz de Galdeono, C. S., 1990, Geological evolution of the Betic Cordilleras in the Western Mediterranean, Miocene to the present: Tectonophysics, v. 172, p. 107-119.

Schwab, F. L., 1975, Framework mineralogy and chemical composition of continental margin-type sandstone: Geology, v. 3, p. 487-490.

Schwab, F. L., 1986, Sedimentary "signatures" of foreland basin assemblages: real or counterfeit?, *in* P. A. Allen, P. Homewood, and G. D. Williams, eds., Foreland Basins: Spec. Pub. Int. Ass. Sediment., p. 395-410.

Scott, R. J., and G. S. Lister, 1992, Detachment faults: Evidence for a low-angle origin: Geology, v. 20, p. 833-836.

Seranne, M., 1992, Devonian extensional tectonics versus Carboniferous inversion in the northern Orcadian basin: Journal of the Geological Society, London, v. 149, p. 27-37.

Serrane, M., and M. Seguret, 1987, The Devonian basins of western Norway: tectonics and kinematics of an extending crust, *in* M. P. Coward, J. F. Dewey, and P. L. Hancock, eds., Continental Extensional Tectonics: Geol. Soc. Spec. Pub. No. 28, p. 537-550.

Srivastava, S. P., W. R. Roest, L. C. Kovacs, G. Oakley, S. Levesque, J. Verhoef, and R. Macnab, 1990, Motion of Iberia since the Late Jurassic: Results from detailed aeromagnetic measurements in the Newfoundland Basin: Tectonophysics, v. 184, p. 229-260.

Srivastava, S. P., H. Schouten, W. R. Roest, K. D. Klitgord, L. C. Kovacs, J. Verhoef, and R. Macnab, 1990, Iberian plate kinematics: a jumping plate boundary between Eurasia and Africa: Nature, v. 344, p. 756-759.

Steel, R., and T. G. Gloppen, 1980, Late Caledonian (Devonian) basin formation, western Norway: signs of strike-slip tectonics during infilling, Sedimentation in Oblique-Slip Mobile Zones: Spec. Pub. Int. Ass. Sedt. No.4, p. 79-104.

Stromberg, S. G. L., 1994, The Origin of the External Basins of the Betics, Southern Spain: Ph.D. thesis, University of Glasgow.

Suttner, L. J., and P. K. Dutta, 1986, Alluvial sandstone composition and paleoclimate, 1.Framework Mineralogy: Journal of Sedimentary Petrology, v. 56, p. 329-345.

Sylvester, A. G., 1988, Strike-slip faults: Geological Society of Americ Bulletin, v. 100, p. 1666-1703.

Thoulet, J., 1913, Notes sur lithologie sous-marins: Int. Oceanog. Monaco. Ann., v. 5, p. 1-14.

Torres-Roldan, R. L., 1979, The tectonic subdivision of the Betic zone (BEtic Cordilleras, southern Spain): its significance and one possible geotectonic scenario for the westernmost Alpine Belt: American Journal of Science, v. 279, p. 19-51.

Tubia, J. M., and J. I. Gil Ibarguchi, 1991, Eclogites of the Ojen nappe: a record of subduction in the Alpujarride complex (Betic Cordilleras, southern Spain): Journal of the Geological Society, London, v. 148, p. 801-804.

van de Kamp, P. C., and B. E. Leake, 1985, Petrography and geochemistry of feldspathic and mafic sediments of the northeastern Pacific margin: Trabsaction of the Royal Society of Edinburgh: Earth Sciences, v. 76, p. 411-449.

Van Der Plas, L., and A. C. Tobi, 1965, A Chart for Judging the Reliability of Point Counting Results: American Journal of Science, v. 263, p. 87-90.

van Wees, J. D., K. de Jong, and S. Cloetingh, 1992, Two-dimensional P-T-t modelling and the dynamics of extension and inversion in the Betic Zone (SE Spain): Tectonophysics, v. 203, p. 305-324.

Velbel, M. A., 1985, Mineralogically mature sandstones in accretionary prisms: Journal of Sedimentary Petrology, v. 55, p. 685-690.

Wagner, G. A., G. M. Reimer, and E. Jager, 1977, Cooling ages derived by apatite fission track mica Rb-Sr and K-Ar dating: the uplift and cooling history of the Central Alps: Memiors of the Institute of Geology and Petrology of the University of Padova, v. 30, p. 1-27.

Watts, A. B., J. P. Platt, and P. Buhl, 1993, Tectonic evolution of the Alboran Sea basin: Basin Research, v. 5, p. 153-177.

Weijermars, R., T. B. Roep, B. V. Van den Eeckhout, P. G., and K. Kleverlaan, 1985, Uplift history of a Betic fold nappe inferred from a Neogene-Quarternary sedimentation and tectonics (in the Sierra Alhamilla and Almeria, Sorbas and Tabernas Basins of the BEtic Cordilleras, S.E. Spain: Geologoe en Mijnbouw, v. 64, p. 397-411.

Wernicke, B., and G. J. Axen, 1988, On the role of isostasy in the evolution of normal fault systems.: Geology, v. 16, p. 848-851.

Windley, B. F., 1986, The Evolving Continents, John Wiley and Sons Ltd.

Wright, N., P. W. Layer, and D. York, 1991, New insights into thermal history from single grain $^{40}Ar/^{39}Ar$ analysis of biotite: Earth and Planetary Science Letters, v. 104, p. 70-79.

York, D., 1969, Least squares fitting of a straight line with correlated errors: Earth and Planetary Science Letters, v. 5, p. 320-324.

Zeck, H. P., F. Albat, B. T. Hansen, R. L. Torres-Roldan, A. Garcia-Casco, and A. Mirtin-Algarra, 1989, A 21±2 Ma age for the termination of the ductile Alpine deformation in the internal Zone of the Betic Cordilleras, South Spain: Tectonophysics, v. 169, p. 215-220.

Zeck, H. P., P. Monie, I. M. Villa, and B. T. Hansen, 1992, Very high rates of cooling and uplift in the Alpine belt of the Betic Cordilleras, southern Spain: Geology, v. 20, p. 79-82.

Zeitler, P. K., 1989, The geochronology of metamorphic processes, *in* J. S. Daly, R. A. Cliff, and B. D. W. Yardley, eds., Evolution of Metamorphic Belts: Geological Society Special Publication.

Zeitler, P. K., J. F. Sutter, I. S. Williams, R. Zartman, and R. A. K. Tahirkheli, 1989, Geochronology and temperature history of the Nanga Parbat-Haramosh Massif, Pakistan: Geological Society of America Special Paper 232.

Zuffa, G. G., 1980, Hybrid Arenites: their composition and classification: Journal of Sedimentary Petrology, v. 50, p. 21-29.

Zuffa, G. G., 1991, On the use of turbidite arenites in provenance studies: critical remarks, in A. C. Morton, S. P. Todd, and P. D. W. Haughton, eds., Developments in Sedimentary Provenance Studies: Geological Society Special Publication No. 57.